TOBER, 1949

8-304

dup#1

Journal of METALS

He finds trouble by ear

As this cableman runs his pickup coil along the cable, his ear tells him when he has hit the *exact spot* where unseen trouble is interfering with somebody's telephone service.

Trouble develops when water enters a cable sheath cracked perhaps by a bullet or a flying stone. With insulation damaged, currents stray from one wire to another or to the sheath. At the telephone office, electrical tests on the faulty wires tell a repairman approximately where to look for the damage.

A special "tracer" current, sent over the faulty wires, generates a magnetic field. Held against the sheath, an exploring coil picks up the distinctive tracer signal and sends it through an amplifier on the man's belt to headphones. A change in signal strength along the cable tells the exact location of the "fault."

Compact, light, simple to use, this test set makes it easier for repairmen to keep your line in order. It is another example of how Bell Laboratories research helps make Bell Telephone service the most dependable in the world.

BELL TELEPHONE LABORATORIES

Exploring and inventing, devising and perfecting, for continued improvements and economies in telephone service.

Journal of METALS

Published to provide a continuing, authoritative, and up-to-date record of technologic, engineering, and economic progress in all branches of the metals industry by the

Metals Branch
American Institute of Mining and Metallurgical Engineers, Inc.
29 West 39th Street, New York 18

o o o

T. W. LIPPERT
Manager of Publications
Editor, Journal of Metals

o o o

JAMES A. STANGARONE
Advertising Manager

o o o

WINIFRED D. GIFFORD, HAROLD N. UNDERHILL, ***Assistant Editors;*** **GRACE PUGSLEY,** ***Production Manager;*** **WALTER J. SEWING,** ***Assistant.***

o o o

OFFICERS, AIME

Lewis E. Young	*President*
A. B. Kinzel	*Vice President*
Philip Kraft	*Vice President*
R. W. Thomas	*Vice President*
C. H. Benedict	*Vice President*
D. H. McLaughlin	*Vice President*
Andrew Fletcher	*VP & Treasurer*

o o o

AIME STAFF

E. H. Robie	*Secretary*
H. A. Maloney	*Asst. Treasurer*
E. J. Kennedy, Jr.	*Asst. Secretary*
Ernest Kirkendall	*Asst. Secretary*
William H. Strang	*Asst. Secretary*
H. Newell Appleton	*Asst. to Secretary*

o o o

Technical Publications Committee

E. M. Wise	*Chairman*
E. J. Kennedy, Jr.	*Secretary*

o o o

Auxiliary Publications Committees

O. B. J. Fraser	*Chairman, IMD*
Michael Tenenbaum	*Chairman, ISD*
Carleton C. Long	*Chairman, EMD*

o o o

Publications Advisory Committee

J. B. Austin, F. N. Rhines, C. D. King, John D. Sullivan, Fred P. Peters, A. W. Schlechten, Frank T. Sisco, M. Tenenbaum, Felix Wormser

o o o

The AIME Also Publishes
Mining Engineering
and
Journal of Petroleum Technology

IN THIS ISSUE

VOL. 1, NO. 10 OCTOBER 1949

COVER

Another 250 lb of inoculated iron for Mack Truck valve inserts. Using a practice devised by International Nickel, chunks of aluminum-magnesium alloy (3.8 lb) are tossed into this heat of high-nickel (35 pct) iron in the Piston Ring Dept., Koppers Co., Baltimore, to impart higher strength and ductility.

FEATURES:

Journal of Metals REPORTER 9
It's Everyone's Business 10
Temperature Measurement in Basic Arc Furnace 12
Quality, Oxygen-Decarbonized Acid Electric Steel 18
Melting Control, Direct-Reading Spectrometer **28**
Analysis of Oxygen in Titanium 31

AIME NEWS

Drift of Things 36
Personals 39
Obituaries 45
Membership Proposals 47

TECHNICAL ARTICLES

Temperature Scale and Emissivity of Liquid Iron 665
by Miner N. Dastur and Nev A. Gokcen
Size Effects, Quenching High-Purity Precipitation-Hardenable Alloys 668
by W. L. Finley
Ternary System, Copper-Manganese-Zinc 675
by T. R. Graham, J. R. Long, C. E. Armentrout, A. H. Roberson
Discontinuous Crack Propagation—Further Studies 683
by L. D. Jaffe, E. L. Reed, H. C. Mann
Free Energy Changes, Martensite Transformation in Steels *by J. C. Fisher* 688
Kinetics of the Austenite→Martensite Transformation 691
by J. C. Fisher, J. H. Hollomon, D. Turnbull
Simultaneous Aging and Deformation in Metals *by J. D. Lubahn* 702
Transverse Bending of Single Crystals of Aluminum 710
by M. K. Yen, W. R. Hibbard, Jr.
Stages in Deformation of Monel Metal, Shown for Polarized Light 722
by D. H. Woodard
Influence of Temperature, Stress-Strain-Energy, for Cu and Ni-Cu Alloys 727
by D. J. McAdam, Jr.
Kinetics of Reactions of Titanium with O_2, and H_2 741
by E. A. Gulbransen, K. Andrew
Structure of Diborides of Ti, Zr, Cb, Ta and V 749
by J. T. Norton, H. Blumenthal, S. J. Sindeband
Diffusion and Solubility of Carbon in Alpha Iron *by J. K. Stanley* 752
Interface Energies in Some Al and Cu Alloys *by K. K. Ikeuye, C. B. Smith* 762
Preparation and Casting of Beryllium Melts 769
by J. G. Kura, J. H. Jackson, M. C. Udy, L. W. Eastwood
Metallographic Examination of Beryllium Alloys 779
by M. C. Udy, G. K. Manning, L. W. Eastwood

Technical Notes

Observations, Alpha Brass Single Crystals After Cutting and Polishing 700
by R. Maddin, W. R. Hibbard, Jr.
On the Problem of Grain Boundary Movement 708
by C. G. Dunn, F. W. Daniels, M. J. Bolton
High-Temperature Scaling of Cobalt *by C. R. Johns, W. M. Baldwin, Jr.* 720
Thermodynamic Treatment of Very Small Solid Solubilities 740
by Lester Guttman

Published the fifth day of each month by the American Institute of Mining and Metallurgical Engineers, Inc., 29 West 39th Street, New York 18, N. Y. Telephone: Pennsylvania 6-9220. Subscriptions $8 per year for non-AIME members in United States and North, South and Central America; $9, foreign; $6 for AIME members, or $4 in combination with a subscription to *Mining Engineering* or the *Journal of Petroleum Technology*. Single copies, 75 cents; special issues, $1.50 . . . The AIME is not responsible for any statement made or opinion expressed in its publications. . . . Copyright 1949 by the American Institute of Mining and Metallurgical Engineers, Inc. . . . Registered cable address, AIME New York . . . Indexed in Engineering Index, Industrial Arts Index and Chemical Abstracts . . . Reentered as second-class matter Sept. 21, 1949, at the post office at New York, N. Y., under the Act of March 3, 1879.

High Vacuum FURNACES

- HEAT TREATING
- SINTERING
- DEGASSING
- BRIGHT SOLDERING
- METAL DISTILLATION
- THERMAL REDUCTION
- MELTING and CASTING

PRODUCTION FURNACES — MELTING AND CASTING

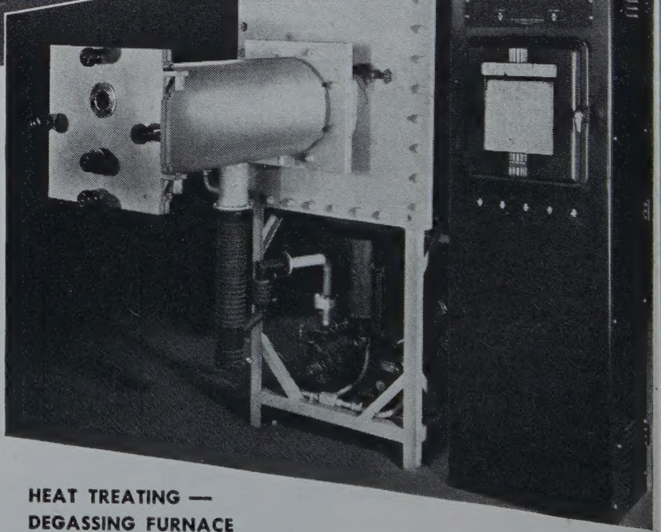

HEAT TREATING — DEGASSING FURNACE

High Vacuum Metallurgy is not new as laboratory technique. It *is* new as a practical industrial operation.

For the first time, National Research Corporation offers its services to design and build, to your requirements, furnaces which operate in the micron pressure range. Pressures run as low at 10^{-4} mm. Hg. absolute.

Six years' experience in the engineering and construction of High Vacuum metallurgical equipment is at your disposal. Write National Research Corporation.

Write to
VACUUM ENGINEERING DIVISION,
National Research Corporation,
Cambridge 42, Massachusetts

We supply a complete line of diffusion pumps, vacuum gauges, valves, seals, coating equipment, dehydration equipment and special high vacuum apparatus.

HIGH VACUUM FOR INDUSTRY
NATIONAL RESEARCH CORPORATION
Vacuum ENGINEERING DIVISION

Authors In This Issue

C. B. Post (p. 12): born in Clarksburg, W. Va. Graduated from West Virginia University, University of Pittsburgh, School of Chemistry and Physics, Pennsylvania State College with Ph.D. degree. Is a member of AIME and lives in Wyomissing, Pa. Has been connected with Weirton Steel Co. and at present with Carpenter Steel Co. Mr. Post has previously presented an AIME paper on Interaction of Liquid Steel with Ladle Refractories. . . . **D. G. Schoffstall** (p. 12): born Tower City, Pa., and attended Tower City high school. Graduated from Gettysburg College with B.S. degree. He is Metallurgist of the Carpenter Steel Co. and now lives in Reading, Pa. Mr. Schoffstall has previously presented an AIME paper as co-author on Determining the Hydrogen Content of Molten Steel by Vacuum Extraction. . . . **Clyde Wyman** (p. 18): born in Oshkosh, Wis., and attended Oshkosh high school and Marquette College. Is a member of AIME and now resides in Chicago. He has worked for Sivyer Steel Casting Co. as Melter and with Oklahoma Steel Casting Co. as Chief Metallurgist and Asst. Works Manager. Mr. Wyman has previously presented AIME papers on the Recovery of Vanadium and Other Alloys-Acid Elec. Furnace, and on the Use of High-Purity Oxygen For Decarbonization in 5-ton Acid Elec. Furnace. His major activities are fishing, golf, bowling, hunting. . . . **E. R. Vance** (p. 28): born in New Philadelphia, Ohio, and attended McKinley high school in Canton, Ohio. Attended Purdue University. Was Special Chemist for Timken Roller Bearing Co. in the Steel & Tube Div. for some years and now is Chief Chemist. Mr. Vance makes his home in Canton, Ohio. His hobbies are gun collecting, hunting and pistol shooting, enjoys fishing, golfing, motorboating and football. . . . **Gerhard Derge** (p. 31): born in Lincoln, Neb., and attended Warren Harding high school, Warren, Ohio. Graduated from Amherst College and Princeton University with B.A. and Ph.D. degrees. Is a member of AIME and lives in Pittsburgh. Mr. Derge is a member of the staff of the Metals Research Lab. and Dept. of Metallurgical Engineering at Carnegie Institute of Technology and is at present Professor of Metallurgy. Mr. Derge has previously presented AIME papers on Oxygen in Basic Electric Furnace Baths and Sampling and Analysis of Steel for Hydrogen. He enjoys tennis, fishing and general outdoor activities. . . . **W. L. Finley** (p. 668): born in Brooklyn and attended Brooklyn Preparatory School. He graduated from Lehigh University with degree of B.S.Ch.E. and from Yale University as D.Eng. He is a member of AIME and now lives in Fairfield, Conn. He has worked for Remington Arms Co., Inc., an affiliate of DuPont, and since 1939 has been Supervisor, Metals Research. His assignments have included lead base alloy development, wartime developments of designs and processes to adapt steel and aluminum alloys to small arms ammunition components and recently titanium alloy development. Mr. Finley has previously presented an AIME paper on Some Effects of Applied Stresses on Precipitation Phenomena. His chief interests are cycling, reading and listening to good music. . . . **A. H. Roberson** (p. 675): born in Carson, Iowa. Attended Mesa, Ariz., high school and University of Arizona, graduating with B.S. Chem. and M.S. Met. degrees. Now lives in Corvallis, Ore. He has worked for United Verde Copper Co. and the Magna Copper Co. in Arizona, and he is now with the U. S. Bureau of Mines doing research on Ti and Zr metals and alloys. Mr. Roberson has previously presented AIME papers. His hobbies are fishing and gun collecting. . . . **C. E. Armentrout** (p. 675): born in Torrington, Wyo. Attended South high school, Salt Lake City, graduating with B.S. degree. Now lives in College Park (Berwyn) Md. Is associated with U. S. Bureau of Mines as Metallurgist. Mr. Armentrout has previously presented an AIME paper as co-author on Alpha Solid Sol. Area of the Cu-Mn-Al System. His chief pleasures are hunting and fishing. . . . **E. L. Reed** (p. 683): born in Somerville, Mass., and attended Somerville high school. He graduated from Tufts College with degree of B.S. and D.Sc. from Harvard. Now lives in Arlington Heights,

C. Wyman

E. R. Vance

W. L. Finley

"C-RO"
POLISHING COMPOUND

"C-RO" is a relatively heavy, metallographic, polishing compound in which small, sharp uniform particles provide a fast, sure and flawless cutting action. It polishes without burnishing. Write for Bulletin 208.

53-585....."C-RO".....¼ lb.....$5.00

BURRELL
1942 FIFTH AVE
PITTSBURGH 19
PENNSYLVANIA

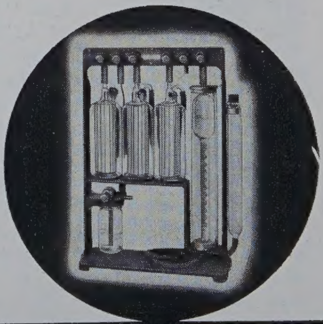

INDUSTRO
model B
GAS ANALYZER

Analyzers for the rapid control analysis of gas mixtures comprising any or all of the following: carbon monoxide, methane, oxygen, hydrogen, and nitrogen. Two models, B and C, for use in combustion control plus other applications. Write for Bulletin 213.

Model B		**$87.50**
Model C	**110 volts**	**$140.00**

BURRELL
1942 FIFTH AVE
PITTSBURGH 19
PENNSYLVANIA

Mass. He has worked as Metallurgist with Sauveur & Boylston, Cambridge, Mass., American Sheet & Tin Plate Co., Pittsburgh, and Watertown Arsenal, Watertown, Mass. Mr. Reed's hobbies are mountain climbing and stamp collecting. . . .

A. A. Roberson

L. D. Jaffe (p. 683): born in Brooklyn, and attended Abraham Lincoln high school. He graduated from M.I.T. with degree of M.S. and from Harvard with a Sc. D. degree. Is a member of AIME and now lives in Cambridge, Mass. He has been associated with the laboratories of Watertown Arsenal in the Specifications Unit and then as Chief of Phase Transformations Unit and now Chief, Physical Metallurgy Branch, Mr. Jaffe has presented a great many AIME papers. He enjoys sailing and mountain climbing. . . .

C. E. Armentrout

J. C. Fisher (p. 688): born in Ithaca, New York, and attended Ithaca high school. Graduated from Ohio State University with degree of B.A. and from M.I.T. with degree of D.Sc. He is a member of AIME and now lives in Schenectady. He has worked as research engineer on the staff of Battelle Memorial Institute, and since 1947 has been Research Associate at General Electric Research Lab. . . .

L. D. Jaffe

J. H. Hollomon (p. 691): born in Norfolk, Va., and attended Augusta Military Academy. He graduated from M.I.T. with B.S., and Ph.D. degrees. Is a member of AIME and now lives in Scotia, New York. He was Instructor at Harvard Graduate School and after service with the Army at Watertown Arsenal, became Asst. Head, Metallurgy Research at General Electric Co. Mr. Hollomon has presented many AIME papers. . . . **D. Turnbull** (p. 691): See September issue Journal of Metals. . . . **R. Maddin** (p. 700): See September issue Journal of Metals. . . . **W. R. Hibbard, Jr.** (pp. 700 and 710): See September issue Journal of Metals. . . .

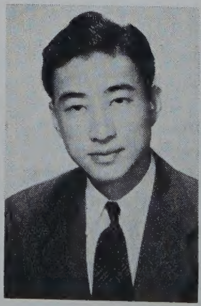
M. K. Yen

M. K. Yen (p. 710): born in Pei-ho-tian, Hopeh, China, and went to Wesley Middle School, Wachung, China. Attended National Central University, China, and graduated from Yale University with B.S. degree, subsequently M.Eng. and D. Eng. Worked as Associate Engineer, Bureau of Ind. Research, Chungking, China, and as Research Metallurgist, Research Dept. Chase Brass Co., Waterbury, Conn. Now is Research Associate, College of Engineering, N. Y. U., New York. Mr. Yen is a member of AIME and has previously presented several papers. He makes his home in New York City and his major activities are swimming, bridge and enjoys music. . . .

J. T. Norton

D. I. McAdam, Jr. (p. 727): born in Washington, Pa., and attended Washington & Jefferson College, Harvard, University of Pennsylvania, graduating with degrees of B.A., M.A., Ph.D., D.Sc. Mr. McAdam is a member of AIME and now lives in Washington, D. C. Was at one time Instructor at Lehigh University, and became Metallurgist at U. S. Naval Eng. Exper. Station, also with Bureau of Standards, and now Consulting Metallurgist. Mr. McAdam has presented several AIME papers and enjoys mountain climbing. . . .

S. J. Sindeband

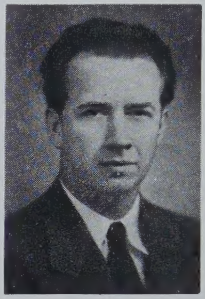
J. K. Stanley

J. T. Norton (p. 749): born in Medford, Mass., and attended Nashua High School. He graduated from M.I.T. with degree of Sc.D. Is a member of AIME and makes his home in Cambridge, Mass. Became Res. Assoc. Physics, M I T. and then Assoc. Prof., Metallurgy and now Full Professor of Metallurgy at that Institute. Prof. Norton has previously presented a great many AIME papers both as author and collaborator. . . .

C. S. Smith

S. J. Sindeband (p. 749): born in New York City and attended Townsend Harris high school. Graduated from School of Eng. Columbia University with B.A., B.S. and M.S. degrees. Is a member of AIME and lives in Chappaqua, N. Y. Worked for Consolidated Edison Co. and was on Active Duty, U. S. Navy, with rank Lt. Cmdr. in the Naval Ordnance Lab as assistant to Tech. Director at the end of the war. Is now Technical Director for American Electro Metal Corp. Mr. Sindeband has previously presented an AIME paper. His hobbies are amateur radio and gardening. . . .

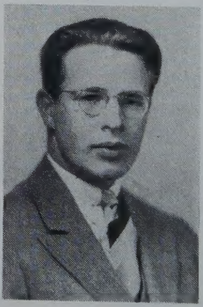
M. C. Udy

H. Blumenthal (p. 749): born in Marburg, Germany, and attended Marburg high school. He graduated with degree of Ph.D. in chemistry from the University of Marburg. Now lives in Brooklyn. Has worked in Nickel Alloy and Cadmium foundries as Chemist and at present is Research Chemist and Metallurgist. Mr. Blumenthal's hobbies are photography and hiking. . . .

L. W. Eastwood

J. K. Stanley (p. 752): born in Cleveland, Ohio, and attended East Technical high school. Graduated with degree of B.S. from Case Institute of Technology and from University of Pittsburgh with Ph.D. degree. Is a member of AIME and makes his home in Pennridge, outside of Pittsburgh. He has worked for National Smelting Co. as Metal-

Attention Authors

Mail your Annual Meeting papers to headquarters. The deadline for all IMD, ISD and EMD papers to be preprinted is Oct. 15.

G. K. Manning

lurgist and is at present with Westinghouse Electric Corp. as Research Metallurgist. Mr. Stanley has previously presented papers on Recrystallization, Orientation and Soft Magnetic Materials (Fe-Al, Fe-Co). Enjoys traveling, photography and music. . . . **K. K. Ikeuye** (p. 762): born in Stockton, Calif., and went to Porterville Union high school. Graduated from Missouri School of Mines with degree of B.S. in Met., presently at Illinois Inst. Tech., Chicago graduate school for M.S. Now lives in Chicago and on the staff of Institute for Study of Metals as Metallurgist. Mr. Ikeuye enjoys fishing, tennis and carpentry. . . . **C. S. Smith** (p. 762): born in Birmingham, England, and attended University of Birmingham graduating with degree of B.Sc., and M.I.T. with degree of D.Sc. Is a member of AIME and presented very many AIME papers. Now lives in Chicago. Was for sometime Res. Met. for American Brass Co., Res. Supervisor on War Metallurgy Committee, NDRC, Assoc. Div. Leader in Charge of Metallurgy, Los Alamos, and at present Professor of Metallurgy and Director of Institute for the Study of Metals, University of Chicago. Mr. Smith's major activity is mountain climbing, and is interested in the study of history of metallurgy. . . . **M. C. Udy** (p. 769): born in Farmington, Utah, and attended Niagara Falls high school. Graduated from Lehigh University with degree of B.S. and M.S. and from Ohio State with degrees of B.S. in Chem. Eng., M.S. in Met. Eng. and Ph.D. in Metallurgy. Is a member of AIME and now lives in Columbus, Ohio. Mr. Udy is on the staff of Battelle Memorial Institute as Research Metallurgist and has previously presented AIME papers on Low Temperature Gaseous Reductions of a Magnetite, and Boron in Certain Alloy Steels. Enjoys bowling, photography. . . . **L. W. Eastwood** (p. 769): born in Wiota, Wis., and went to Palloville high school. Graduated from University of Wisconsin with B.S., M.S., Ph.D. degrees. Is a member of AIME and now lives in Westerville, Ohio. Became Asst. Prof. Michigan College of Min. & Tech., Research Metallurgist Aluminum Co., and at present Supervisor Battelle Magnesium Foundry. Mr. Eastwood has presented several AIME papers. . . . **G. K. Manning** (p. 779): born in Anderson, Ind., and went to Anderson high school. Graduated from Franklin College, University of Michigan with B.A., and M.S.E. degrees. Is a member of AIME and lives in Columbus, Ohio. Worked with Republic Steel Corp., as Metallurgist, and at present Supervisor, Metallurgical Engineering, Battelle Memorial Institute. Mr. Manning has previously presented AIME papers on the Relationship Between Transformation at Constant Temperature and Transformation during Cooling, and The Cobalt-Chromium Binary System. His hobby is photography.

Engineering Societies Service

THE following employment items are made available to AIME members on a nonprofit basis by the Engineering Societies Personnel Service, Inc., operating in cooperation with the Four Founder Societies. Local offices of the Personnel Service are at 8 W. 40th St., **New York 18;** 100 Farnsworth Ave., **Detroit;** 57 Post St., **San Francisco;** 84 E. Randolph St., **Chicago 1.** Applicants should address all mail to the proper key numbers in care of the New York office, and include 6¢ in stamps for forwarding and returning application. The applicant agrees, if placed in a position by means of the Service to pay the placement fee listed by the Service. AIME members may secure a weekly bulletin of positions available for $3.50 a quarter or $12 a year.

POSITIONS OPEN

Metallurgists, two, 23-35, B.S. in metallurgy or mining; some practical experience necessary for one. In lieu of experience, a graduate who specialized in ore-dressing problems would be acceptable for one of the jobs. Duties will be to conduct ore-dressing investigations (mainly flotation tests and microscopic examinations) in the research laboratories and supervising special tests in the concentrators. Must be single. Salaries, $2700-$3900 a year. Location, South America. Y-798.

Process Metallurgist for process development and semi-works production of metals by chemical or electro-furnace reduction. Write stating qualifications, experience and salary expected. Location, New Jersey. Y-1646.

Physical Metallurgist, preferably with Doctor's degree, for research project concerned with the effect of environment on the properties of metals at elevated temperatures. Later may lead to a teaching position. Location, California. Y-2749.

ELECTRIC FURNACE CONFERENCE

Early indications are that the Seventh Annual Electric Furnace Steel Conference, to be held Thursday to Saturday, Dec. 8-10, at the William Penn Hotel, Pittsburgh, will break all past records. Certain papers to be presented at the Conference are currently appearing in the Journal of Metals. All those who plan to attend the Conference should make their reservations directly with the William Penn Hotel.

PROFESSIONAL SERVICES

Limited to A.I.M.E. members, or to companies that have at least one A.I.M.E. member on their staffs. Rates, hereafter, one inch only, for one year, $40.

R. S. DEAN LABORATORIES

Consulting, Research, Development
Chemistry, Electrochemistry, & Metallurgy
Laboratory Research on a Contract Basis

2005 K St., N. W. EX 5656
Washington 6, D. C.

MAX STERN
Consulting Engineer

Expert for Scrap Recovery and Shipwrecking—Modernization of Plants and Yards for Ferrous and Nonferrous Metal Scrap

150 Broadway New York 7, N. Y.

C. L. MANTELL
Consulting Engineer

Tin Metallurgy
Electrochemical Processes

451 Washington St., New York 13, N. Y.

LEWIS B. LINDEMUTH
Consulting Engineer

140 CEDAR STREET, NEW YORK 6, N. Y.

STEEL PRODUCTION
DESIGN · OPERATION · CONSTRUCTION · METALLURGY

HEAVY DUTY CRANKSHAFTS
cast in High Test
NICKEL ALLOY IRON

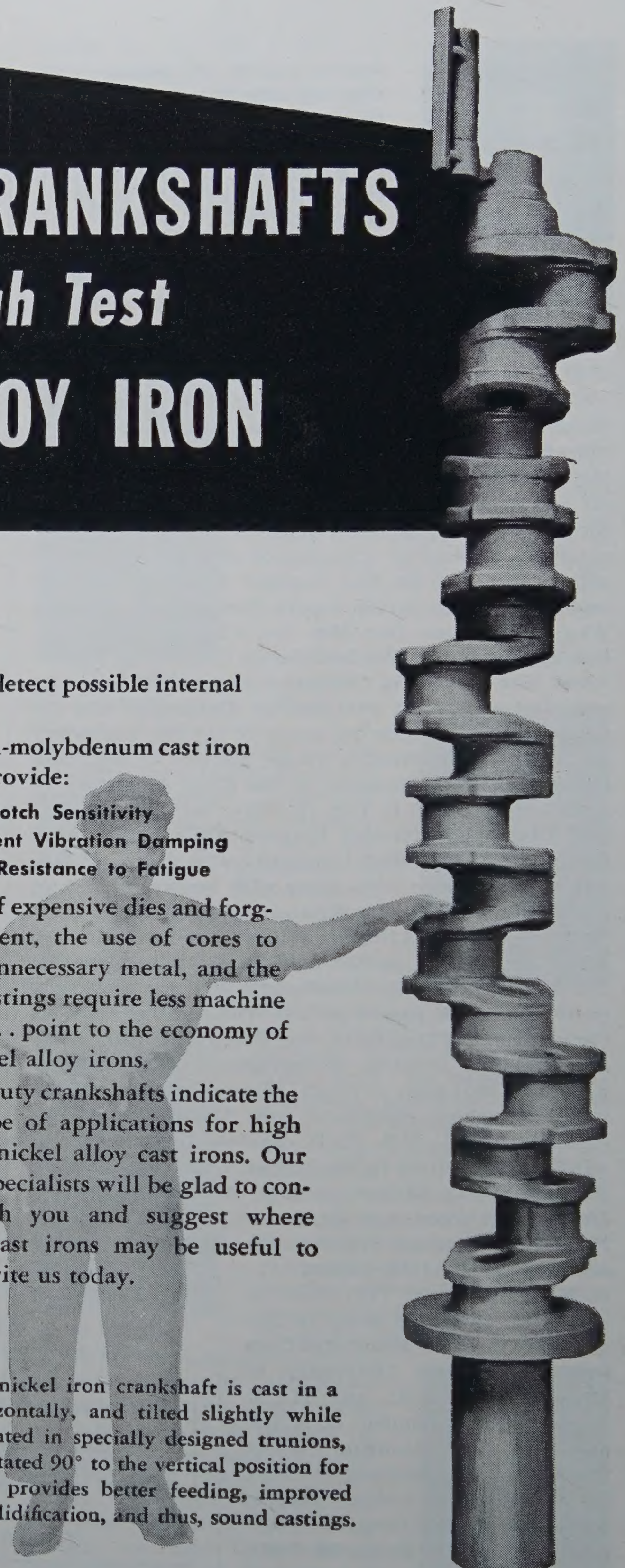

Crankshafts ranging from 800 to 4000 pounds in weight, and from 6 to 18 feet in length . . . for large Diesel engines in marine, locomotive, and stationary power plants . . . are now produced commercially by Pacific Car & Foundry Company's efficient new casting method.

The photograph shows an unmachined 8-throw unit that weighs 2105 pounds. It was cast in high strength nickel-molybdenum gray iron at Pacific's foundry in Renton, Washington.

This nickel alloy iron, produced as an inoculated iron in the basic electric furnace, consistently meets strength specifications of 60,000 to 75,000 p.s.i.

Each shaft is stress-relief annealed, and x-rayed to detect possible internal defects.

These nickel-molybdenum cast iron crankshafts provide:

- **Low Notch Sensitivity**
- **Excellent Vibration Damping**
- **High Resistance to Fatigue**

Avoidance of expensive dies and forging equipment, the use of cores to eliminate unnecessary metal, and the fact that castings require less machine tool time . . . point to the economy of using nickel alloy irons.

Heavy duty crankshafts indicate the wide scope of applications for high strength nickel alloy cast irons. Our casting specialists will be glad to consult with you and suggest where nickel cast irons may be useful to you. Write us today.

This high test nickel iron crankshaft is cast in a mold set horizontally, and tilted slightly while pouring. Mounted in specially designed trunions, the mold is rotated 90° to the vertical position for cooling. This provides better feeding, improved directional solidification, and thus, sound castings.

Don't Forget...

Jot down—"INCO Booth, No. 302'—in your memo book of companies to visit at the **NATIONAL METAL EXPOSITION,** at the Public Auditorium in Cleveland, Ohio, October 17th to 21st. Convenient facilities for discussing your problems with our metallurgists and foundry specialists will be available.

INCO
BOOTH
NO. 302

THE INTERNATIONAL NICKEL COMPANY, INC.

67 WALL STREET
NEW YORK 5, N.Y.

Journal of Metals REPORTER

* Accurate bath temperature readings in the basic electric furnaces may be obtained through the modification and application of the immersion Rayotube. C. B. Post and D. G. Schoffstall on p. 12 describe this rugged, accurate and low-cost method for consecutive bath readings.

* Manganese can be recovered and reused from openhearth slag by crushing, calcining, grinding, jigging and flotation. From this series of treatments an 80 pct manganese-iron alloy is recovered. A firm of consultants announced that $23 worth of manganese and iron per ton of slag can be recovered for an outlay of $13.

* What are the metallurgical factors influencing quality of oxygen decarbonized acid electric steel? The degree to which each variable in standard oxygen practice influences the physical properties of steel is described for the first time on page 18.

* Improvement in speed and accuracy in analytical control of high-grade electric furnace and openhearth heats seems to be promised by the direct-reading spectrometer. Timken reports on two years of experience (p. 28) involving over a million determinations. Less manpower is required than with a spectrograph, and the direct-reader is accurate, rugged and standardization is maintained even after long shutdowns.

* Armco has started building three 225-ton basic openhearths-- the initial construction on what will ultimately be an entirely new steel plant involving 12 openhearths. The same company has just completed a second continuous galvanizing unit which can coat 48-in. wide sheet up to 2 plus oz class coat at very high speed and very high adherence.

* Some of the technical men in Washington have devised the term "megabucks" as a monetary unit. The national debt expressed as 250,000 megabucks hardly seems impressive enough to cause much worry.

* Traces of lead in fluorspar will cause trouble in high-alloy steel, according to investigations now being carried out by Timken.

* Several operators of large door-charge electric furnaces are considering rebuilding to permit top charge of light scrap with heavy scrap as usual machine-charged through the door.

* A startling report has just been issued by the Steel Founders' (British) productivity team--the first sent to the United States by the Anglo-American Productivity Council. American productivity in steel founding is estimated as being 50 to 90 pct higher than British, in manhours per ton.

The British note that in America the exercise of skill has been taken from the shop floor into the pattern shop, the methods office and the brains of the supervisors. In America more machines are used, technical innovations are readily adopted, power is freely used and freely available. In America, in contrast to Britain, wage systems are simple and incentives are "crude, direct and powerful." In America, says the report, the rewards of productivity are shared by workers, technicians, investors and customers.

It's Everyone's Business

WITH summer's record heat tempered, the month of September was a potpourri of atomic bombs (Russian version), strike threats, Yanks, Dodgers, Red Sox, Cardinals, and a great scurrying of politicos in and out of Washington. Congressmen drifted into the hinterland at the slightest opportunity to rest their jangled nerves and mend fences. Out in Pittsburgh and Des Moines, the epicenters of labor and agriculture, Mr. Truman mounted his campaign charger and unfurled his battle-flag for 1952. He pridefully spoke of his record—not as tarnished as sometimes suggested—but made no attempt to gloss over failure to repeal the Taft-Hartley Labor Act. Meanwhile, the father of this Act, Senator Taft, also chose Labor Day to start visiting every county in Ohio in preparation for his trial by vote in 1950. If he is defeated next year the Republican conservative wing may be permanently crippled; if he wins he can hardly avoid being the strongest contender for standard bearer in 1952. And, also on Labor Day, General Eisenhower, speaking before the American Bar Association, gave every indication of willingness to grasp the same standard if the Republicans would care for a nice middle-of-the-road contender.

Meanwhile, confused and harried Britains and Canadians conferred with their American opposite numbers in Washington in an eleventh-hour effort to somehow resolve the desperate world dollar problem. What Mr. Bevin described as "perhaps the most momentous talks of all time" ended with a 3000-word statement from the finance ministers so bland and commonplace as to be a source of much puzzlement on both sides of the Atlantic. What concessions there were seemed to be all one way, from North America to Britain. But within a week the British paid the piper with a long-overdue, drastic and immediate devaluation of the pound sterling. Practically all the world's currencies then toppled in a mad rush to maintain pre-devaluation ratios.

By indulging in some highly optimistic flights of conjecture many attempts were made to translate all these moves into a tidy British "balance sheet" for 1952 to show an equalization between outgo and income. But there is little justification for regarding devaluation, even in conjunction with the other measures of agreement in the Washington talks, as any means of economic salvation, either in Britain or Western Europe. Devaluation, if it is to be other than a futile gesture, will have to be accompanied by unpleasant forms of retrenchment and energetic effort to achieve greater productivity.

The British worker will have to work longer and harder to send far more goods to the United States just to maintain current dollar sales. This means a further serious drop in the standard of living of Britain and Western Europe, and the political repercussions can well be quite violent. Even so, there can be some doubt as to whether in 1952 there will be a balance between what Europe needs from the dollar area and what Europe sells to the dollar area. The dollar sales in the Marshall group of countries have declined by 30 pct in the past six months (see graph), and if this drift is not halted the hunger and unemployment prophesied by the assembly at Strasbourg will not wait even until 1952.

Granted the British master all these difficulties, there is still another hurdle to cross in order to lift deliveries to the United States to near the calculated levels for 1952. The Washington talks promised a review of tariffs and customs procedure in the United States, but during the same week the relatively mild Reciprocal Trade Agreements Act just squeezed through Congress with the slimmest of margins. In short, Congress has never cared to pursue policies appropriate to a great creditor nation or to ease the way for repayment of the billions of dollars pumped out over the past several decades to subsidize exports.

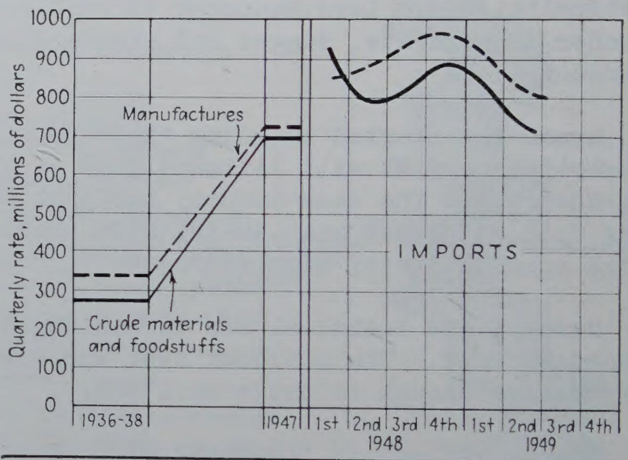

Americans keep advising Europeans to expand their exports to the United States. Even Mr. Hoffman has been guilty of some guile when he recently said that American tariffs are no higher than in 1914 and insinuated that they could hardly be a bar to greater imports. But in 1914 the United States was probably the most highly protected country in the world, and today its tariffs are quite high when viewed in the light of the country's record position as an exporter and creditor power. Today, duty on imports of machinery are 12½ pct, rising to 40 pct for textile machinery. On bicycles the duty rises to as high as 30 pct, cutlery pays up to 35 pct, glass up to 40 pct, boots and shoes 20 pct, hosiery 50 pct, and clocks in some cases up to ad valorem rates of over 200 pct. Superimposed on all this is a set of rules and regulations specifically designed to discourage or to delay. Many onerous restrictions stand in the way of foreign enterprise attempting to operate in the United States, of which the situation in shipping is the most notorious. All this is hardly likely to be changed without prolonged and anguished outcries from Congress. But the alternative is further outright gifts of money abroad, with no inclination or intention of accepting anything in return. It is a policy likely to make many a future historian's eyes bulge with disbelief.

The tide of recession in the United States shifted sharply in August, much to the pleased surprise of all pundits. September was everyone's favorite for the turn. The Federal Reserve Board's August index on industrial production rose all the seven points it had lost in July, this being the first upward movement since October 1948. The Census Bureau reported August unemployment down 400,000, and preliminary September figures show a further drop of 338,000. The labor picture is now 59,411,000 employed, 3,351,000 unemployed and 1,459,000 in the armed forces. But still some 2,000,000 persons continued to work part-time from necessity rather than choice. The impetus behind this improvement was partly seasonal and partly sparked by restocking to fill out inventories on a rising price curve. Preparations for the Christmas trade, particularly in the consumer goods, would normally carry this autumn upswing on through the turn of the year. But the entire labor situation is in such a turmoil as possibly to put a painful crimp in the curve of economic recovery.

Base metal prices (see graph) wallowed in a trough of indecision through most of September under the twin impacts of a rising industrial curve and a deteriorating labor situation. There has been the usual seasonal increase in buying activity, some cautious replenishment of depleted stocks, but prices in general show no real recovery from the unwarranted declines earlier in the year. In zinc, the galvanizers have been in the market regularly but diecasters came in for a little and are quickly out. Battery manufacturers are taking sizable quantities of lead and the demands for electrical equipment, which account for half the consumption of copper, have been well maintained and even show some recent improvement. Under the impact of industrial strife, copper continues to hold (Oct. 3) at 17.625¢ compared with 23.5¢ last March. Lead dropped back to 14.75¢ on Sept. 26, as against 21.5¢ in March; and zinc dropped from 10¢ down to 9.25¢ on Oct. 3, as compared with its first quarter peak of 17.50¢. As regards production, output from American mines has fallen off but world output continues to rise. There are no signs of surpluses, however, least of all in lead.

On the labor front Mr. Murray was in the downstage spot all month; Mr. Lewis carried on his independent show off in a corner, and Mr. Reuther, the rubber workers and a host of other unions, marked time in the wings awaiting their cues. The employers rallied in earnest for a real fight, with practically no defections in their ranks. The issue was security to be totally financed out of the yields of the risk-takers. Just how much room is left in the American economy for the worker to increase his share of business profits is probably something on which employer and employe will never agree, but for the first time in nine years there was no insatiable consumer demand to foster collusion between them and thus avoid the basic issue. Both sides brought up such a show of force that face-saving retreat became impossible—a test of strength on the picket line became the only alternative.

Even while the labor aristocrats drove for security, their lowly brethren were given a hand up early in September by Mr. Truman as he redeemed still another of his campaign pledges. (Others: Atlantic Pact, Wheat Agreement, Housing Act, stop-gap farm price legislation, Military Assistance Program.) The Senate, all in a hurry to get home for a six-day holiday, rushed through an advance in the national minimum wage from 40¢ to 75¢ an hr. This was the first change since a rather meaningless 40¢ was passed in 1938.

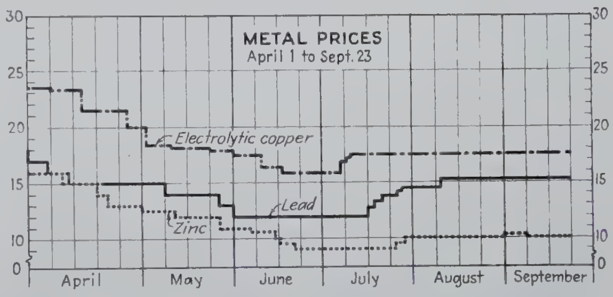

Almost forgotten amidst portentious happenings elsewhere in the economy are the limited geographic areas which continue to show such serious unemployment that the situation may become chronic without government help. Whereas the national average of unemployment is now less than 6 pct of the total labor force, there are eleven areas with over 12 pct unemployment, and a few smaller areas may soon be added to the list. In these limited areas unemployment compensation has so far acted as a buffer to the local economy, but from now on the benefit rights will begin steadily to run out.

With the exception of Knoxville, Tenn. and Muskegon, Mich., all the eleven distress areas are in the northeastern corner of the U. S. and six are in New England. In Lawrence, Mass., 37 pct of the labor force is out of work, and in the Providence area, which is tantamount to the whole state of Rhode Island, one out of every five workers is unemployed. The chief industries in these depressed areas are consumer goods, all early victims of the recession—textiles, shoes, jewelry, machine tools, electrical goods and so on.

The improvement in the general economy has already helped the textile and leather industries. Furthermore, Mr. John Steelman, the President's adviser, has instructed the ten chief government spending agencies to shift their procurement activities whenever possible to the eleven areas, and public works and other government activities already planned for these areas will be speeded up. It is expected that all these activities will pump some new life into these eleven areas by year's end. It's mostly a form of robbing Peter to bolster Paul, but so far no one has cared to suggest an optional course.

Temperature Measurement in

THE temperature of molten steel in the arc furnace is one of the most important variables in steelmaking. During the course of a heat, the temperature has a large influence on the extent of chemical reactions in the bath, and also between the bath and the slag. The temperature of the bath at tap determines to a large extent the resulting fluidity during the pouring of ingots, the occurrence of casting and ingot surface defects, and the porosity and segregation in the ingots and wrought products. In this respect, any device which enables the melter to know the temperature of the bath at any time during the course of the heat will enable him to pay that much more attention to the other factors involved in steelmaking, and is a welcome addition to the furnace controls.

This paper will be presented before the Seventh Annual Electric Furnace Steel Conference, Dec. 8-10, Pittsburgh.

C. B. Post is metallurgist and D. G. Schoffstall is meltshop metallurgist, Carpenter Steel Co., Reading, Pa.

The authors gratefully acknowledge the cooperation of C. C. Wilson, Melting Supt., Carpenter Steel Co., and Harold Mead, Leeds & Northrup Co., Philadelphia, and the encouragement of J. H. Parker, Chairman of the Board, F. R. Palmer, President, and B. H. DeLong, Vice President, Carpenter Steel Co., without which this work would not have been possible.

In presenting this paper, for subsequent discussion, temperature measurements in electric arc furnaces, the authors are aware that each shop presents its own particular practices; consequently, several different methods of measuring temperatures at the furnace are in use at the present time. Each method may have its advantages in any one shop, and whether any method is so universal in its scope to serve best in all shops is an open question. The most this paper can do is to summarize experience at Carpenter with the optical pyrometer (1926-1947), the immersion thermocouple (1946-1948) and the present standard method, the Leeds & Northrup immersion rayotube.

The Optical Pyrometer: The optical pyrometer has done valuable work for the steel industry for a number of years. In its present form it can still yield worthwhile temperature measurements in the hands of a competent operator. Its main use is at tap where a valuable, worthwhile reading can be obtained on the concave side of the stream. Provided the stream is clear and the operator is competent, and the instrument is in good calibration, a "relative" temperature can be recorded for the temperature of the heat. One of the main difficulties is to obtain an image of stream which is free from oxide streaks or films which will affect the readings, and it is here that the instrument requires considerable experience and discrimination on the part of the operator. Because of this large inherent error in the instrument and operator, correlations of tapping temperatures and some variable such as percent yield in prepared billets, or porosity, require a considerable number of heats to be averaged before a trend can be recognized on an average basis.

The optical pyrometer can be used to obtain temperatures before tap, but the method is of questionable use because of emissivity effects and the amount of labor involved. A large spoonful of metal, say 30 lb, is taken from the bath and several readings on the stream are taken with the pyrometer as the spoon is slowly poured on the floor. A stop-watch is used to time the operation from the time the spoon is taken through the door, or from the bath, and the time of each temperature reading is recorded. If the temperature readings are plotted against time, then an extrapolation to zero time will yield a reading for the temperature of the bath. This method has been used only on a few occasions, and its use on a routine basis would not be considered.

The instrument can hardly be called a control instrument because the most useful readings are obtained at tap when the heat is going into the ladle. The optical pyrometer makes no distinction between different optical emissivities of high-alloy steels compared to lower alloyed carbon steels; consequently, each grade of steel must be standardized from its own data, and different grades of higher alloyed steel cannot be used to indicate approximately correct tapping temperatures for a new grade. The optical pyrometer also leaves unanswered the now important question of what was the course of temperatures in the heat before tap. As is well known, a heat brought up to tapping temperature during the very last stages of the refining period will exhibit differences in fluidity, cleanness, etc., compared to a heat brought to tapping temperature about midway during the refining period and soaked at this temperature until tap.

The type of data obtained with the optical pyrometer readings at tap are illustrated in figs. 1, 2 and 3. These three figures are constructed from

Basic Arc Furnace

by C. B. Post and D. G. Schoffstall

A SUCCESSFUL method for giving the melter an accurate bath temperature reading at any time during the course of a heat enables him to master one of the most important variables in basic electric steelmaking. Here, the authors describe the modification and application of the immersion Rayotube, the result being a rugged, accurate and low-cost method for consecutive bath readings.

many heats, preferably 25 to 50. This averages out some of the variables and inherent errors in the optical pyrometer and operators.

Fig. 1 shows tapping temperatures plotted against percentage prepared billet yields (curve A), the expected percentage of heats showing dirty tops on disk inspection (curve B), and the expected percentage of heats showing pipe on disk inspection (curve C) for two grades of steel, SAE 6120 and 0.90C-1.75 pct Mn oil-hardening steel. Fig. 3 shows sculling temperature for low-alloy steels as dependent upon carbon content. In constructing figs. 1 and 2, the prepared yields, etc., were averaged for all the heats falling within a 10°C range, say 1570° to 1580°C, to get the charts. The data apply to 10 in. square, 1000 lb ingots. The heats were 10 tons, tap weight.

Platinum-Rhodium Thermocouple: In the last few years, considerable work has been done in trying to adapt the platinum-platinum rhodium thermocouple to determine the temperatures of the molten metal in basic electric arc furnace practice.[1] At Carpenter there had been some experience with a commercial version of this thermocouple equipment, although probably not as extensive as those shops using this method in a routine manner. The platinum-platinum rhodium thermocouple has been found to give reproducible results with an error of plus or minus 10°C.

The main reason for investigating the use of the thermocouple was to obtain readings before tap, so that the melter could come up to tap with a good deal of certainty that he would hit the correct tapping temperature and also follow a prescribed course of temperatures during the refining period. The platinum-platinum rhodium thermocouple was not found to answer to this requirement. In the way the instrument was used, the conviction grew that several operating features of this type of instrument made it difficult to take readings throughout the course of a heat for routine control.

In the first place, the head of the thermocouple is subjected to the full heat of the furnace for about 30 to 40 sec, which is a relatively long time for the thermocouple head refractories to stand up under this heat. There is considerable labor involved in keeping the thermocouple head calibrated and in repair. At the very least, the head will require replacement of the silica tube and adjustment of the platinum wire after each reading. Gen-

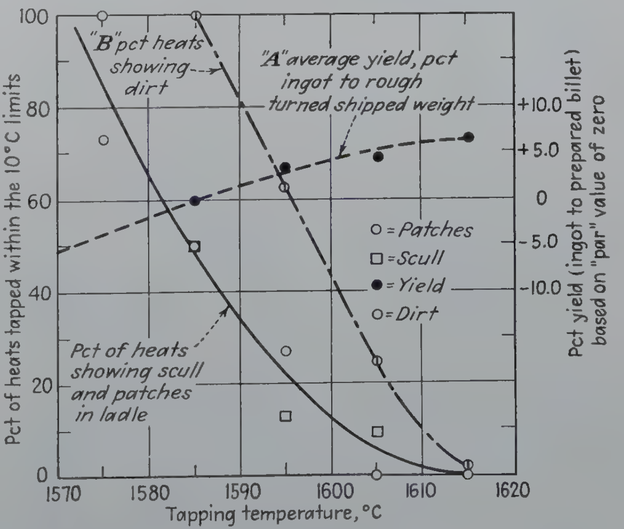

Fig. 1—Effect of tapping temperature on probable yield (ingot to billet weight) and occurrence of scull ladles and slag in disk inspection. SAE 6120.

---

[1] **"A Method for the Determination of Bath Temperatures," L. F. Weitzenkorn, AIME Electric Furnace Steel Proceedings, 1944.**

erally, only one reading was possible on each heat, at tap, because of the larger number of spare heads required if more than one reading per heat is attempted. It was estimated that six men would be kept busy repairing thermocouple heads around the clock if three readings were taken on each 12-ton heat from four electric arc furnaces, tapping on the average four heats per furnace per day.

Sufficient routine work with the immersion thermocouple lead to a realization of its inherent difficulties when more than one temperatuure reading is desired on each arc heat. There may be ways of overcoming some of the difficulties by modification of the above design of thermocouple and such methods would be of good value in the literature on this subject.

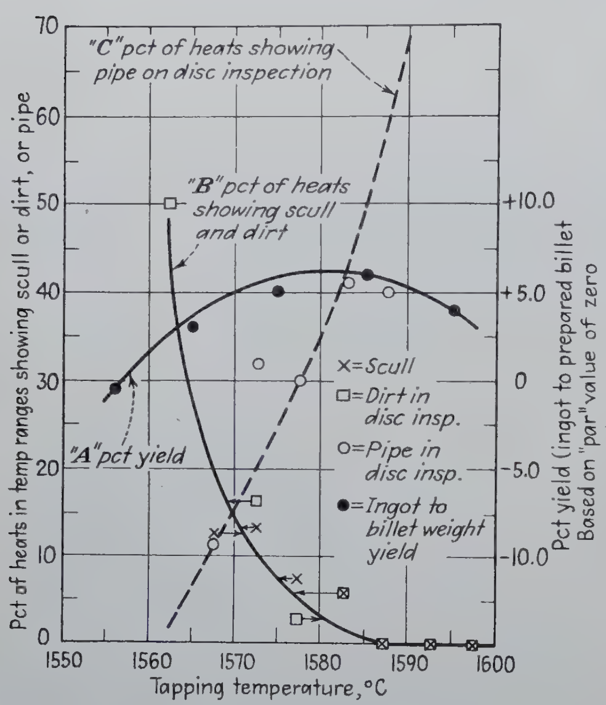

Fig. 2—Effect of tapping temperature on probable yield (ingot to billet weight) and occurrence of scull ladles, slag and pipe in disk inspection. Oil-hardening tool steel, 0.90 C and 1.75 Mn; 10-in. ingots.

The Immersion Rayotube: The "Immersion Rayotube," hereafter called the "blowpipe" has been used with success in the openhearth. Here the "wild" condition of the metal in the hearth enables the heavy-walled pipe to be plunged into the bath with no harm other than some adhering metal which is easily stripped from the tube. In the basic arc furnace, however, the highly deoxidized metal and the reducing slag cause severe erosion of the pipe and welding of the metal to the extent that considerable experimentation was necessary to adapt the blowpipe to electric arc melting.

These modifications of the blowpipe for use in basic electric arc melting and the comparison of the modified blowpipe against the platinum-platinum rhodium thermocouple temperatures will be described along with some brief notes on its use in basic electric furnace practice.

Description of Instrument: The Immersion Rayotubes[2] are the standard "blowpipes" of the Leeds & Northrup Co., described in detail elsewhere. A schematic sketch of the blowpipe and the method of using it is shown in fig. 4. The tube is used in conjunction with a Leeds & Northrup Speedomax recorder.

The Rayotube unit of the blowpipe is kept in standardization by means of a "checking" unit supplied by the Leeds & Northrup Co. The "checking" unit is a closely calibrated Rayotube assembly which, when clamped onto the "blowpipe" unit, allows the "blowpipe" to be brought into comparison with the "checking" unit. When the two instruments are "sighted" on the same hot body (furnace-wall, banks, or electrodes), the adjustment is such that any factor which will cause low readings on the immersion Rayotube (dirty window, etc.) will be compensated by increasing the voltage output of the Rayotube in the blowpipe when compared to the standard Rayotube sighted on the same body.

In the set-up at Carpenter, dry nitrogen is used instead of air as in most openhearth installations. Dry nitrogen gas was available at all arc furnaces for other purposes, and it was thought at the beginning that dry air would have some effect on the standardization of the instrument when high-alloy steels were compared to low-alloy due to exothermic reactions at the face of the "bubble." This was never substantiated in the case of air, but it is known that high and low-alloy steels all read virtually the same with dry nitrogen.

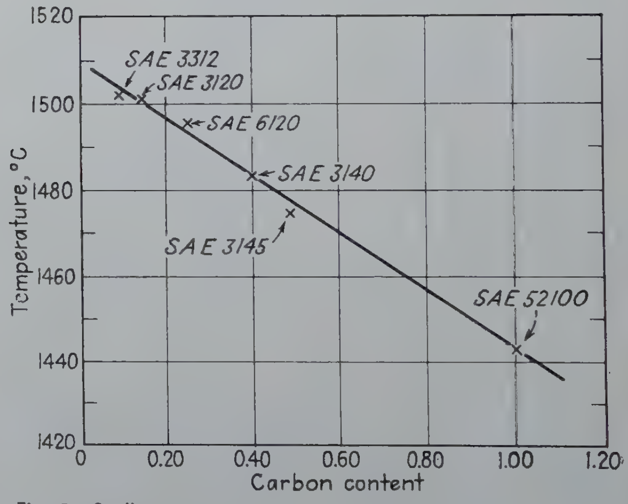

Fig. 3—Sculling point of alloy steels depending on carbon content determined by the optical pyrometer.

The amount of nitrogen consumed on each reading is about 70 cu ft. The nitrogen is brought to the furnace at 125 psi, in 1½-in. diam main line pipes. Trailers of dry nitrogen of 10,000 cu ft capacity at 2000 psi supply the main lines. Fig. 5 shows a schematic drawing of the nitrogen lines to the blowpipe unit at the arc furnaces. The flow regulator as supplied with the equipment will open wider if the incoming pressure drops, and will tend to keep a constant volume of nitrogen flowing into the blowpipe. A constant pressure regulator set at 80 psi is put in the line between the flow regulator and the shut-off valve on the 125-lb pressure line to prevent the flow regulator from bleeding the whole nitrogen system.

---

[2] **"A Radiation Pyrometer for Open Hearth Bath Measurements," H. T. Clark and S. Feigenbaum, Metals Technology, June, 1946, AIME.**

Protection of the end of the blowpipe in reduced baths: The main problem connected with the use of the blowpipe in basic electric arc furnaces is the protection of the pipe from the rapid cutting action of the highly deoxidized metal and the reducing slags.

The protection was first accomplished by using a heavy cardboard tube over the outside of the pipe as shown in fig. 6. The cardboard proved to be excellent protection for the tube except at the very end where "stickers" would frequently weld to the metal of the blowpipe.

Readings were made with the cardboard protection sheath. This practice, however, led to low results when compared to thermocouple readings. The reason for these low readings remained obscure for a considerable time. Persistent and detailed analysis of the situation led to the conclusion that smoke from the cardboard tube, which at that time projected over the end of the metal tube, was being blown into the "bubble" with the result that the rayotube was seeing a low temperature due to the fog.

Successful temperature readings were accomplished finally by using a graphite "head" on the blowpipe as shown in fig. 7. Good blowpipe v. thermocouple readings were obtained immediately when using a graphite-tipped pipe, the pipe still being protected by a heavy cardboard tube. Further, there was relief from the very serious problem of "stickers" since little or no molten metal adheres to the graphite.

The arrangement adopted is shown in fig. 7, illustrating the manner of machining the end of the blowpipe to receive the graphite insert which is screwed onto the pipe. The graphite section is 2¾ in. long, with the inner face threaded for 1 in., eight threads per inch. The contour of the inner surface of the blowpipe is maintained to close tolerances to provide a metal support for the insert. A detailed drawing is shown in fig. 8.

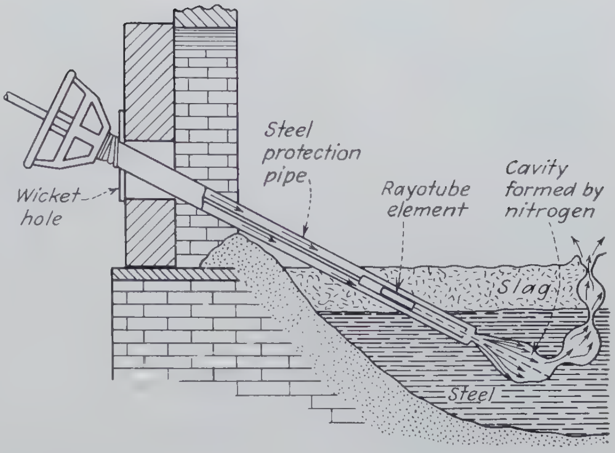

Fig. 4—Method of using the blowpipe.

Graphite heads are interchangeable on all blowpipes. The melter unscrews the graphite head after each reading and replaces it at once from a bank of about a dozen kept with each blowpipe. Care is taken to see that the outside cardboard tube does not come quite to the end of the graphite head. About 40 of these heads can be cleaned up and kept in condition in the course of several hours by one man who services the instruments. This repair work consists in removing globules of metal and coating the end of the heads with graphite cement.

When using the blowpipe, the pipe is inserted through a hole in a large plate suspended at the furnace door. In this manner, the operator is fully

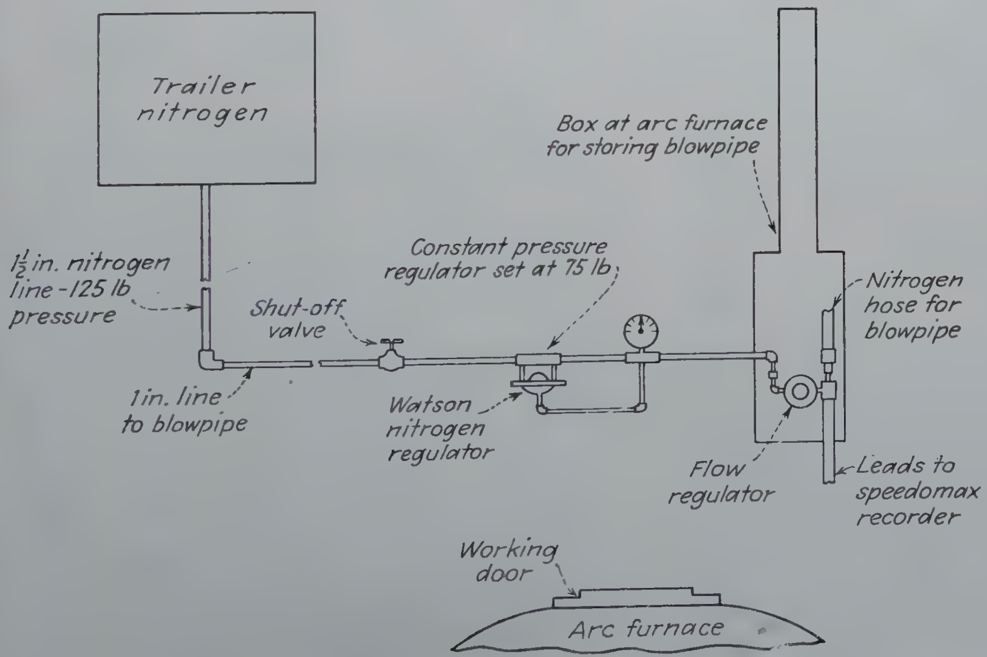
Trailer nitrogen
1½ in. nitrogen line-125 lb pressure
Shut-off valve
Constant pressure regulator set at 75 lb
Box at arc furnace for storing blowpipe
Nitrogen hose for blowpipe
1 in. line to blowpipe
Watson nitrogen regulator
Flow regulator
Leads to speedomax recorder
Working door
Arc furnace

Fig. 5—Method of running nitrogen lines to the Rayotube unit at the arm furnaces.

protected from splash, and he also has support for the pipe, the temperature being read much the same as through a wicket-hole in the openhearth furnace.

Calibration of immersion Rayotube with platinum-platinum-rhodium thermocouple: Immersion rayotube readings, followed directly by platinum-platinum-rhodium thermocouple readings, were used to check the calibration of the Rayotube. The thermocouple goes into the metal bath for a depth of approximately 8 in., closer to the electrodes than the banks. The bath was always rabbled before starting temperature readings, and care was taken to make all temperature readings at least ½ hr after any alloy addition and about 1½ hr after the ferrochromium addition to stainless steel.

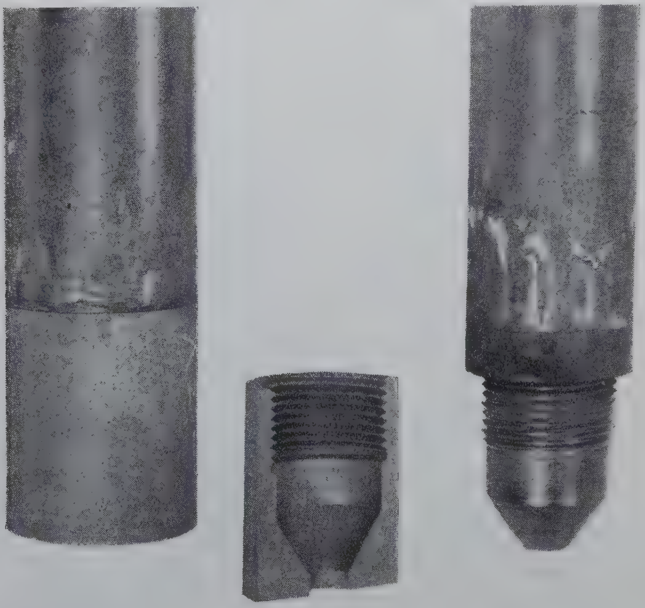
Fig. 7—Rayotube and graphite insert.

The distribution of temperature differences (°C Rayotube v. °C thermocouple) is shown in fig. 9. It is apparent that the spread between the blowpipe and the thermocouple is not greater than ±20°C. Actually, 62 pct of the readings (47 readings) fell within ±10°C deviation. The following table shows the distribution of the data in fig. 9.

Range of Deviation Blowpipe v Thermocouple	No. of Readings	Pct of Readings
0 to +10	14	30
+10 to +20	8	17
0 to −10	15	32
−10 to −20	10	21.5
	47	

No difference has been noticed when reading different types of alloys. The above data were obtained on low-alloy steels of various carbon contents, chrome-iron stainless and chrome-nickel stainless steels. When using nitrogen, the calibration setting on the Speedomax recorder is 100°C lower than when using air through the blowpipe.

When the blowpipe is equipped as described above, the instrument can be used to obtain consecutive readings on a heat of steel in such a manner that the melter can control his heat within prescribed limits. The type of information which can be obtained on individual heats is shown in figs. 10, 11, and 12.

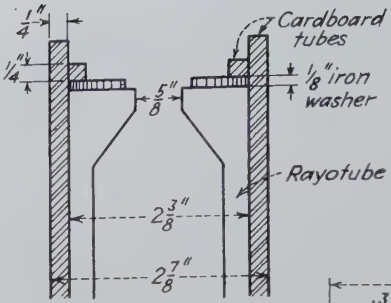

Fig. 6—(Left) Rayotube with cardboard tube protection.

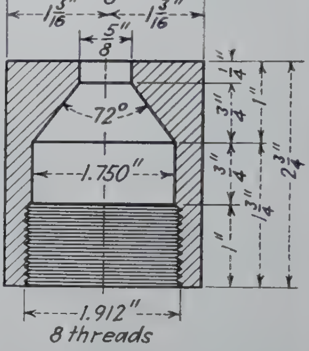

Fig. 8 — (Right) Details of graphite insert.

The reproduction of blowpipe readings in the same molten bath, and also the character of readings obtained on various types of steel, blowpipe v. thermocouple, are shown in the following table:

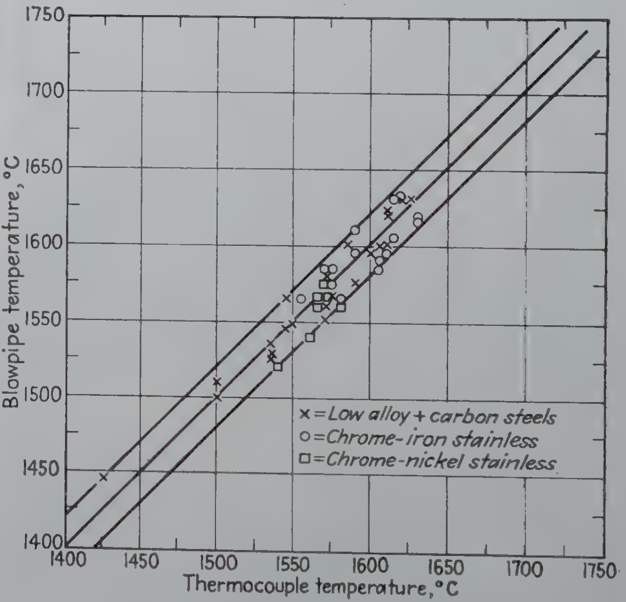

Fig. 9—Blowpipe v. thermocouple readings.

Stock	Blowpipe Readings	Thermocouple Readings	Optical
AISI 414	#1 Blowpipe 1631	1615	1615
	#2 Blowpipe 1632		
AISI 430	#1 Blowpipe 1595	1610	1624
	#2 Blowpipe 1593		
AISI 302	#1 Blowpipe 1558	1566	1615
	#2 Blowpipe 1564		
Vega Tool Steel	#1 Blowpipe 1560	1570	1579
	#2 Blowpipe 1550		
1.10 Pct C Tool Steel	#1 Blowpipe 1525	1537	1568
	#2 Blowpipe 1535		

Each group of readings was taken in the same bath within a 5-min period before tap and the optical readings were made at tap.

Figs. 10 and 11 show the log and temperature on two heats of 52100 alloy steels. It is apparent that here we have two heats of the same stock melted under widely different temperature conditions. The possibilities that are suggested in establishing melting controls in respect to time of heat, kilowatt consumption, and temperature control with its various metallurgical aspects are quite clear.

On 100 pct disk inspection, the two heats of figs. 10 and 11 showed the different characteristics as follows:

Heat A, fig. 10, 48 billets, 11 recuts, 8 billets scrapped on account of dirt, 77.3 pct billet yield.

Heat B, fig. 11, 46 billets, 3 recuts, all billets clean; 79.6 pct billet yield.

Fig. 12 shows the temperature and melting log for a heat of low-carbon, low-alloy steel in which a different magnitude of temperatures may be expected than on the previous type of alloy shown. In this type bath, it may or may not be desirable to melt down about 1600°C and maintain a high temperature throughout the heat, as is shown in the chart. It is on such problems as this that the blowpipe can be used to advantage for both experimentation and routine control.

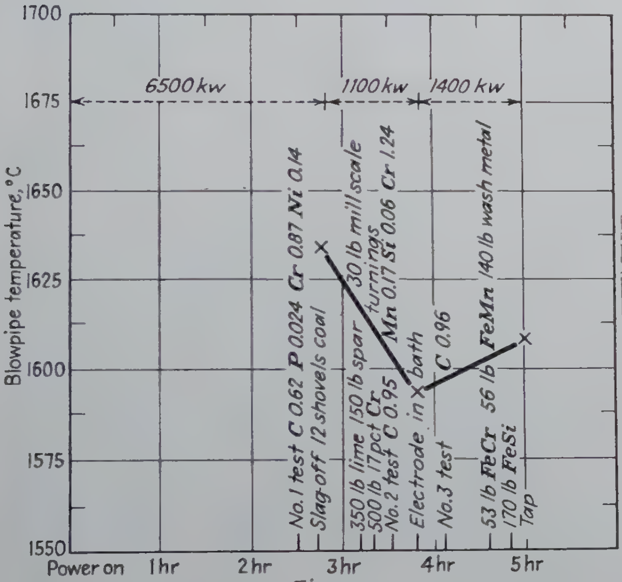

Fig. 11—Heat "B", 52100 alloy. Optical at tap = 1576°C.

Conclusions: The immersion Rayotube has been modified and applied to basic electric arc furnace melting. A graphite insert on the end of the blowpipe enables the instrument to be used for consecutive readings in the furnace bath without any unusual labor and maintenance.

The blowpipe has been calibrated with the immersion thermocouple to within ±20°C. The immersion thermocouple has an error of at least ±10°C. and this means that the blowpipe has an error at the greatest of ±10°C, and probably smaller. It has been shown that little, if any, difference exists when reading a wide range of alloys, and that dry nitrogen can be used in place of air if the recording device is compensated by −100°C.

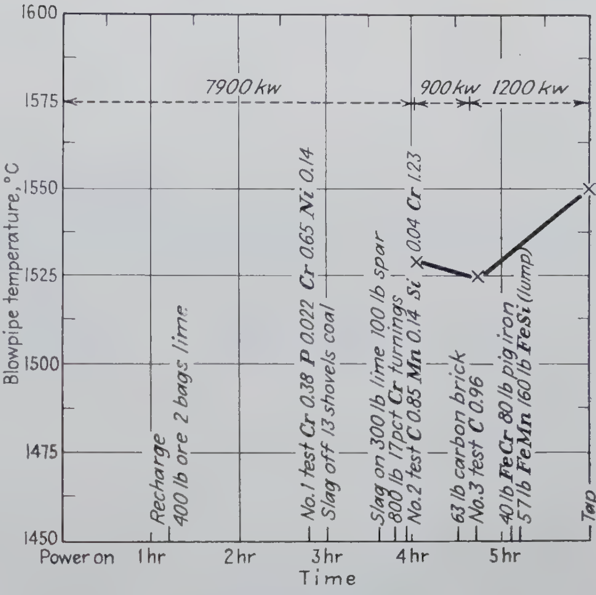

Fig. 10—Heat "A", 52100 steel. Optical at tap = 1573°C.

The instrument appears to be rugged and yet simple in application requiring no skilled personnel in its operation. The immersion rayotube is an instrument for temperature control in melting high-grade basic electric steels. The instrument enables any number of readings to be taken during the course of a heat by the melter with reproducible results.

The cost per reading when using the modified blowpipe in the arc furnace can be listed approximately as follows:

70 cu ft of nitrogen	=	46¢
One cardboard sleeve	=	08¢
Graphite head per reading (10 readings per head)	=	06¢
Total	=	60¢

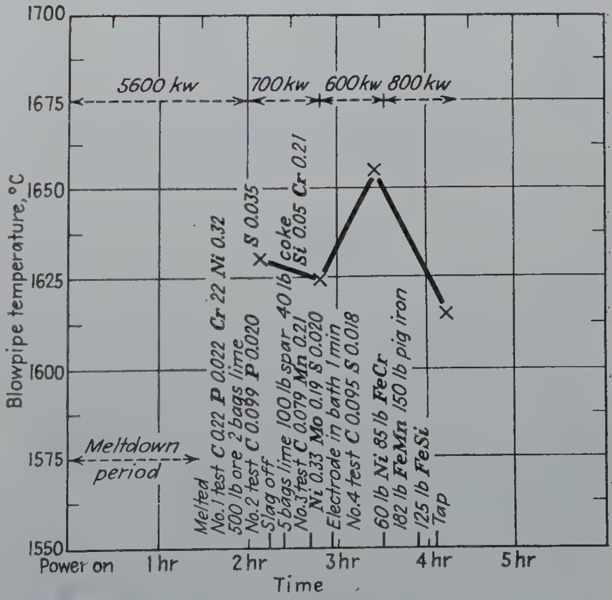

Fig. 12—Heat "C", NE-8720. Optical at tap = 1615°C.

Quality of

Oxygen-Decarbonized Acid Electric Steel

by Charles A. Faist
and
Clyde Wyman

THIS investigation is reported in an attempt to clarify and expand on a previous paper.[1] The use of high-purity oxygen for the purpose of decarbonization of heats of steel has been widely discussed in the past. For the most part, however, discussions have dealt chiefly with the economics of oxygen versus ore practices. Little has been said about the quality of oxygen-decarbonized steels because, no further thought has been given the subject once an oxygen practice has proved more economical than the former ore practice and has not adversely affected the quality of the steel as compared with that obtained by the old ore practice.

It is advantageous, however, to investigate the oxygen practice more fully once the initial practice has been made standard. Much thought should be given to closer control of the many variables in the furnace practice in an effort to analyze their effect on the quality of the finished heat.

Burnside Steel Foundry Co. proceeded along this line of reasoning shortly after a standard oxygen practice had been adopted in the spring of 1948. It was felt that much could be learned from determination of the degree to which each variable in standard practice influenced the physical properties of the steel. It was also thought that, should a correlation be found between various metallurgical factors and quality, a control of these variables could be instituted to provide for a greater uniformity in quality and saving in cost of the produced heat.

Primarily the investigation was formulated into two distinct phases. The first was to deal with the investigation of all individual variable factors of the heat, to determine whether or not each separate factor had any marked influence on the quality of the steel. The second phase was proposed to determine the effect of various additional factors that most markedly influenced the economics of the heat.

It was believed that, through correlation and analysis of the results of both phases of the investigation, a program could be worked out for quality control of oxygen-decarbonized heats.

Phase I — Investigation of Metallurgical Factors Affecting Quality: The investigation of factors influencing quality was begun by systematically collecting data on more than 600 oxygen-decarbonized heats of steel. These factors included concentrations of carbon, silicon, and manganese at meltdown as well as after oxygen injections; melting rate, charge weight, heat time, power consumption, injection time, oxygen volumetric rate, rates of carbon, manganese, and silicon removal, percentage FeO and MnO in meltdown and final slags, temperature of tap, physical, and chemical properties, and so forth.

Many of these data were constantly available from the standard furnace heat sheet or from chemical and physical laboratory records. In some instances certain phases of the investigation required special forms for accumulation of data.

Actual analysis of the effects of various metallurgical factors was begun by plotting average values of large numbers of heats. In each instance a single factor was systematically plotted against average values for all other factors involved in standard practice. Mass plot was used where the initial plot of averages showed no marked trend. (Mass-plot methods tend to strengthen an indistinct trend by creating, through density of points, a readily discernible band if such a trend exists.)

Insofar as degree of influence was concerned, it was very surprising to find that only a small percentage of the total number of factors investigated had a relatively pronounced effect on the general quality and economics of the heat and for graphs on which plotted points fell completely "out of bounds" these points were eliminated. In these instances, it was deduced that the nonconforming intercept

---

[1] Use of High-Purity Oxygen for Decarbonization in Five-Ton Acid Electric Furnaces, by Clyde Wyman, Charles A. Faist and Edmund J. Goehring, Proc. Electric Furnace Steel Conf. (1948) 154.

This paper will be presented at the Electric Furnace Steel Conference, Pittsburgh, Dec. 8-10, 1949.

Charles A. Faist is a research member under the direction of the metallurgy department, and Clyde Wyman is chief metallurgist, Burnside Steel Foundry Co., Chicago.

WHAT are the metallurgical factors influencing quality of oxygen-decarbonized acid electric steel? There have been many discussions of the economics of oxygen v. ore practices, but here is the first determination of the degree to which each variable in standard oxygen practice influences the physical properties of the steel. This paper may arouse some controversy, but thereby a great deal of free thinking can be stimulated.

points were due to the influence of factors other than those being plotted on the graph in question.

Analysis of Charts: From the initial graphical analysis, it was seen that the quality of the steel was largely influenced by the following principal factors

(1) Meltdown carbon concentration.
(2) Melting rate.
(3) Total points of carbon removal.
(4) Rate of carbon removal.
(5) Meltdown silicon concentration.
(6) Percentages of FeO, MnO and SiO_2 in final slag.
(7) Ratio of acid to basic constituents in final slag.
(8) Percentage residual aluminum (total)
(9) Percentage manganese recovery (based on additions).
(10) Time of heat (power on to power off).
(11) Tapping temperature.

The plotted coordinate points on the charts represent average values for large numbers of heats. Where only a few points are shown, each point represents some 50 or 60 heats. When many coordinate points are shown, each point represents an average value for four to six heats. No attempt was made to classify the factors according to specific types of heat analysis; a composite picture is presented for steel analyses in general. It must be remembered, in dealing with an analysis of any melting process, that all the innumerable variables constantly exert their influence on bath conditions. This must be borne in mind when studying the trends indicated on the graphs. Interest in specific values on these charts is not of so much importance as is the trend indicated, since in all instances the slope of any particular curve is influenced by the uncontrollable variables. If, however, a trend is discernible when plots are made, this trend must then be recognized as being the result of primary dependency of the two factors being plotted.

Fig. 1 shows the plot of meltdown carbon concentration versus P-value. P-value is defined as by the equation:

$$P = \frac{\left(\dfrac{\text{Tensile Strength} + 6\ \text{Red. Area}}{1000}\right)}{5}$$

The trend indicates that the P-value slowly decreases with increasing carbon concentration at meltdown. This trend is partially related to the melting rate. It is a known fact that melting rate increases with increased carbon content of the scrap because of the lower melting point of the latter. A correlation is derived by considering fig. 2 in conjunction with this curve.

Fig. 2 shows the relationship existing between melting rate and P-value. As the melting rate decreases, the P-value increases. Going back to fig. 1, it may be seen that higher carbon at meltdown adversely affects the quality because of the increased melting rate.

The effect of the total amount of carbon removed during the oxygen injection on the P-value is shown

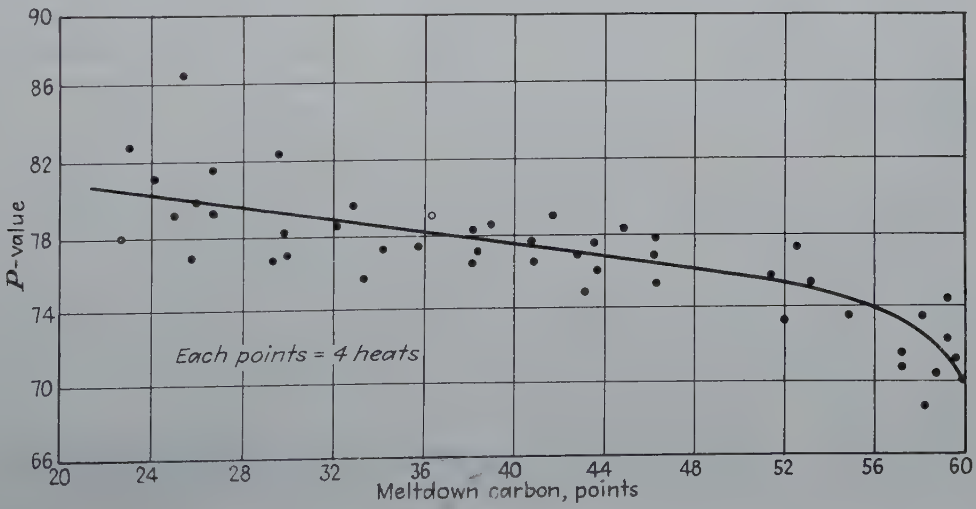

Fig. 1—Effect of meltdown carbon on P-value.

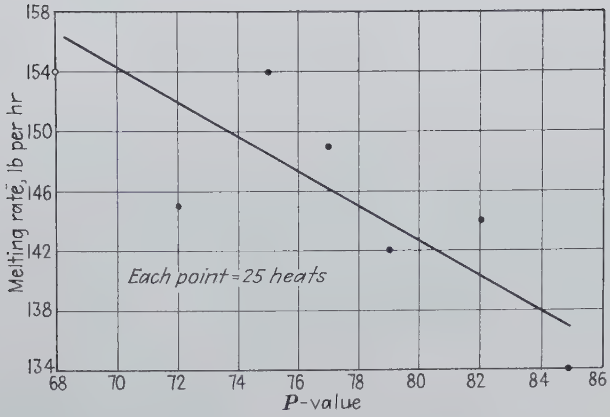

Fig. 2—Effect of melting rate on P-value.

on fig. 3. As the amount of carbon removed increases, the P-value decreases. Possible explanation of this trend might be: (1) the heats in which larger amounts of carbon are removed might possibly be those in which the finished heat has a higher finishing carbon, or, (2) the heats in which larger amounts of carbon are removed may be those that have higher carbon, manganese, and silicon concentration and, therefore, higher melting rates.

When rate of carbon removal is plotted against P-value, as shown on fig. 4, a trend is noted in which P-value gradually increases with increase in rate of carbon removal.

Since in oxygen practice the oxygen boil is the equivalent of the ore boil in ore practice, it would normally be expected that the rate of carbon removal would indicate the degree of the boil and the greater the carbon removal, the more mechanical "boiling" action, and, subsequently, the cleaner the steel.

Fig. 5 shows the influence of meltdown silicon on the P-value. In this, the P-value decreases rather abruptly as the meltdown silicon concentration increases up to approximately 10 points. Above this concentration, the slope of the curve lessens. The oxidation of increasing amounts of initial silicon is related to the build up of SiO_2 in the slag to higher values than would normally exist if this initial silicon concentration were lower. This graph confirms to some extent the melter's desire to melt in with a low silicon concentration. A graph showing effect of SiO_2 in slag as it affects P-value will be shown shortly.

Fig. 6 is very interesting because it does not follow in line with generally accepted concepts concerning the effect of FeO content of the final slag upon quality. This curve was double checked, however, and the trend indicated may be considered representative of the data accumulated.

P-value increases steadily from a minimum at around 8 pct. FeO to a maximum between 11 and 13 pct. FeO. After this maximum is reached, the P-value decreases steadily, with additional increase in FeO.

It is generally accepted that fairly high oxide content in steels results in the formation of type I inclusions. In this type the sulphides are globular because of their relatively low solubility. By increasing the oxide content of the steel a certain requisite amount during deoxidation, the solubility of the sulphide inclusion is increased to a point where the sulphides are eventually precipitated in the grain boundaries. This is the detrimental type II inclusion.

Addition of deoxidizing agent over and above that required to deoxidize the steel will result in the formation of complex, low-solubility sulphides known as type III. Since type III inclusions are angular and form within the grain, they are not detrimental. Just how this curve ties in with low P-value in the upper FeO ranges is not readily explained.

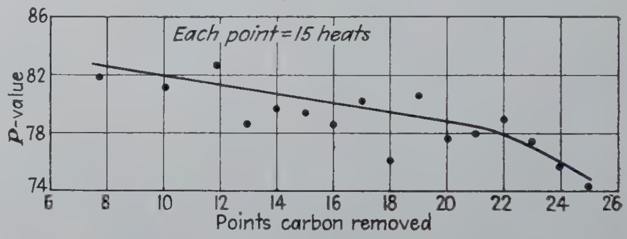

Fig. 3—Effect of carbon removal on P-value.

The next graph, fig. 7, shows the influence of SiO_2 and MnO contents of the final slag on the P-value of the steel. Although the curve shows that variation of SiO_2 content has very little influence, there is a very slight trend toward increase in P-value with decrease in SiO_2 concentration. There is, perhaps, a tendency for the higher SiO_2 content in the finishing slag to strive for attainment of equilibrium conditions should the FeO and MnO (the basic constituents) be abnormally low. This condition might manifest itself in subsequent reduction of silica followed by the return of silicon to the bath, particularly at the higher temperatures attained in finishing the heat.

The MnO curve shows a marked increase in P-

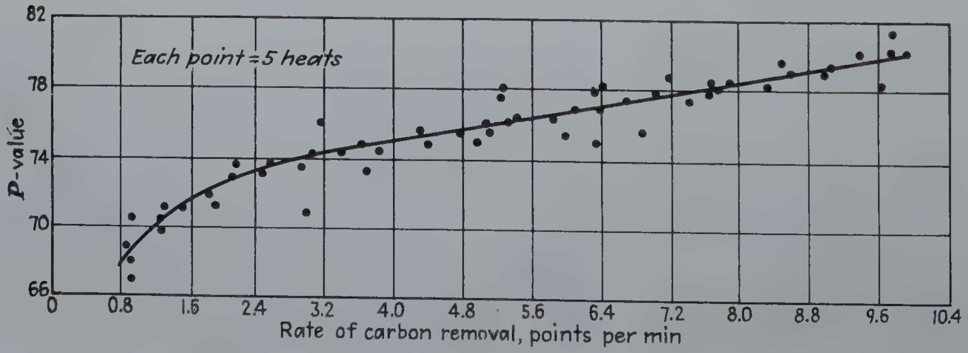

Fig. 4—Effect of rate of carbon removal on P-value.

value with a decrease in MnO content in the final slag. Lower MnO values appear to indicate that higher manganese recoveries should be expected, since MnO in the slag is an indication of manganese oxidation in the bath.

Since each of the slag constituents FeO, SiO_2 and MnO may be classified as acid or basic in nature, and since a trend was found to exist when each was separately plotted against P-value, it was thought that a ratio of acid to basic constituents could be plotted against P-value to further clarify the influence of slag acidity or basicity on quality.

Fig. 8 shows that with increase in the relative acidity ratio (defined: Relative Acidity $= \frac{\% SiO_2}{\% FeO + \% MnO}$) the P-value increases. CaO, also a basic constituent, was not considered, since its concentration in an acid slag is usually too small to have any effect on this ratio.

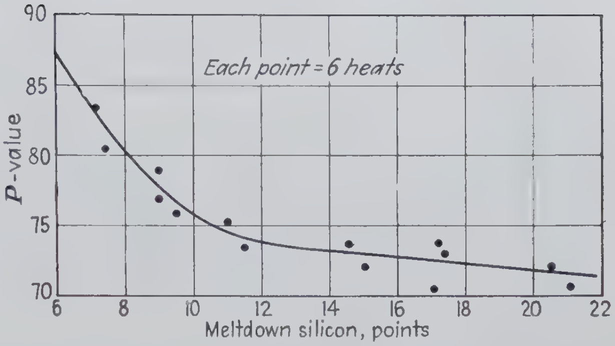

Fig. 5—Effect of meltdown silicon on P-value.

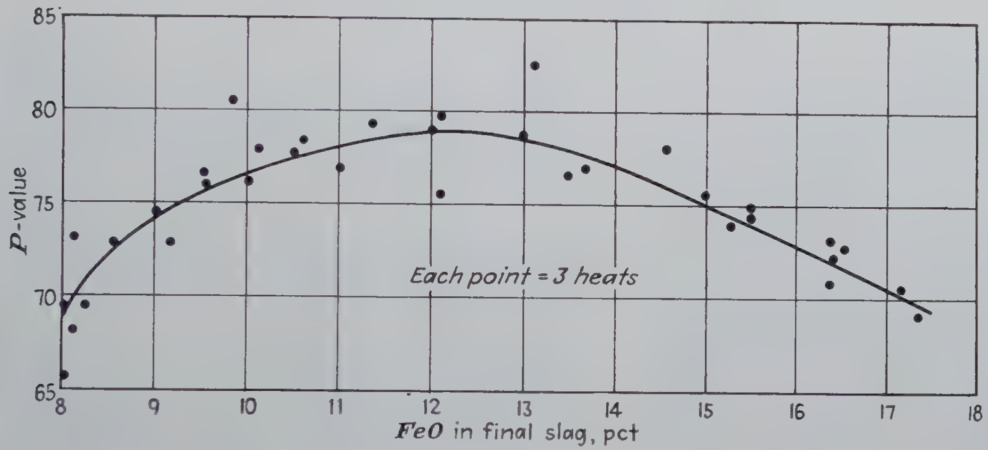

Fig. 6—Effect of FeO in final slag on P-value.

It appears that the P-value is highest for relative acidity values of about 3, since the curve levels off at that point.

Normally, there is a variation of approximately 15 to 20 pct. for SiO_2 during the heat. On the other hand, FeO changes markedly. MnO changes a moderate amount. The chief variable, however, is FeO.

On the basis of these slag curves, it would appear that proper slag control should go far in producing a heat of uniform quality and also of higher quality.

Fig. 9 shows that as percentage of manganese recovery increases the P-value also increases. (The term "manganese recovery" as used here is based on additions made; it is not calculated from initial manganese concentrations.) It appears that manganese recovery is related to the degree to which the processes of oxidation were carried out during refining, and also to the degree of deoxidation to which the bath was subjected.

By analysis of the curves for manganese recovery and percentage of MnO in the final slag, an indication of degree of oxidation and deoxidation during the heat should be found.

Fig. 10 shows that a trend is established wherein the percentage residual total aluminum in finished steel is plotted against P-value. With increased

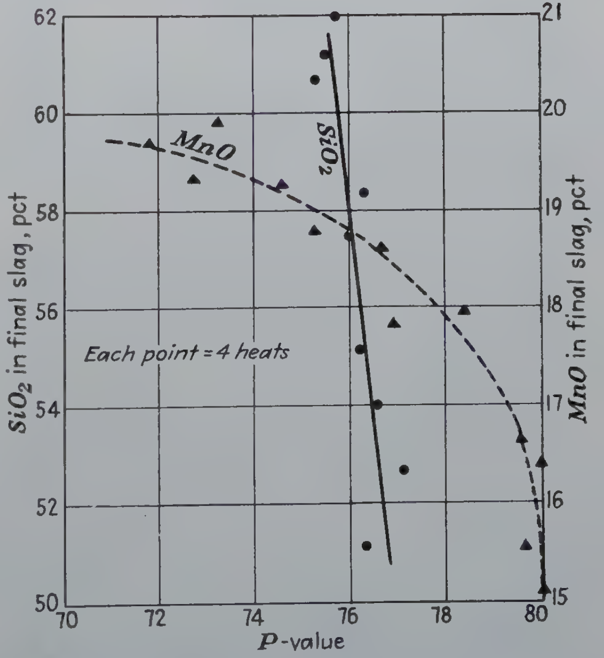

Fig. 7—Effect of percentages of SiO_2 and MnO of final slag on P-value.

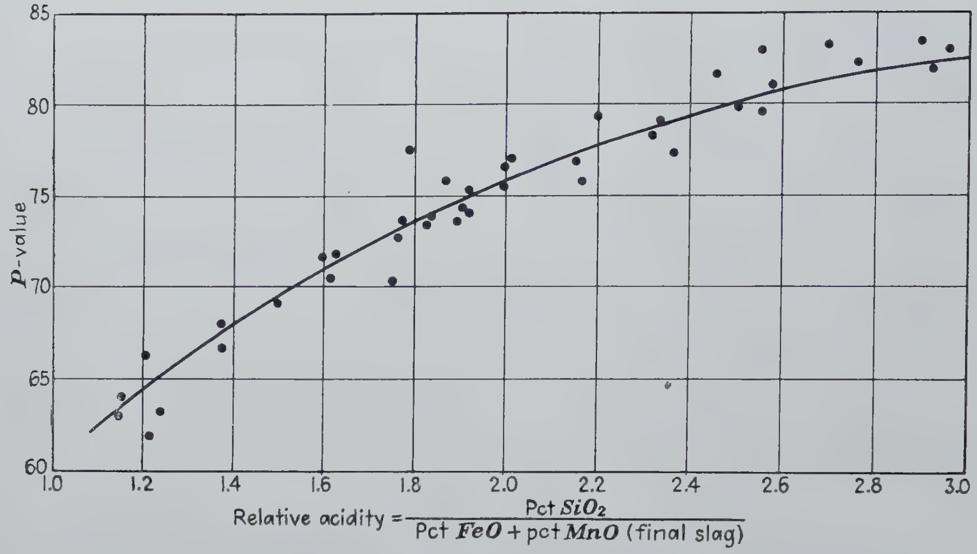

Fig. 8—Effect of relative acidity of final slag on P-value.

residual aluminum, an increase in P-value is established. It appears that the relationship is a straight-line function within the limits of this graph. Unfortunately, not enough heats were available to extend the extremes of the graph with any reasonable certainty that a correct plot would be made. It is apparent, however, that a more thorough deoxidation of the steel is found in the higher ranges of residual aluminum.

Fig. 11 shows that tapping temperature appears to have no appreciable influence on the P-value until temperatures above 3200°F are reached. After this temperature is exceeded, the P-value decreases sharply. All temperatures recorded on the data sheets for this graph were made using a Leeds-Northrup optical pyrometer and may have been slightly inaccurate. The variations should be averaged out, however, because of the large number of temperature readings taken, and the trend, therefore, should be representative.

Fig. 12 shows that with increase in the time of heat, a trend toward increase in P-value results. This appears as would normally be expected and probably follows from the fact that all variables are allowed time enough to approach conditions of optimum effectiveness and equilibrium.

Summary of Phase I: From the study of the variable factors as far as they affect the quality of the steel, the following summary is made. Graphic analysis of data indicates that P-value:

(1) Decreases with increase in meltdown carbon concentration.

(2) Increases as melting rate decreases.

(3) Increases as points of carbon removed decrease.

(4) Increase as rate of carbon removal increases.

(5) Decreases with increase in meltdown silicon concentration.

(6) Increases to maximum and then decreases with increase in percentage of FeO in final slag (Maximum between 11 and 13 pct.).

(7) Increases slightly with decrease in percentage of SiO_2 final slag; increases markedly with decrease in percentage of MnO final slag.

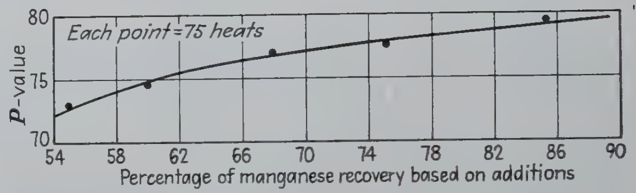

Fig. 9—Effect of percentage of manganese recovery on P-value.

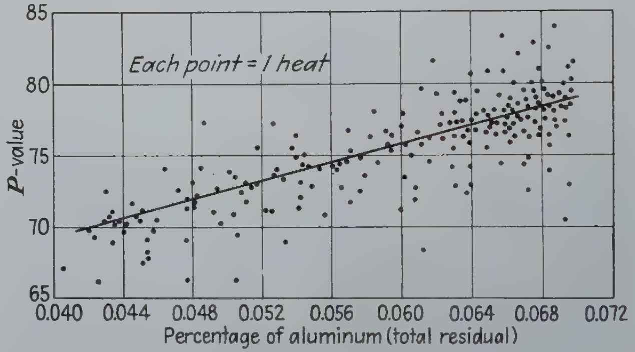

Fig. 10—Effect of percentage of residual aluminum on P-value.

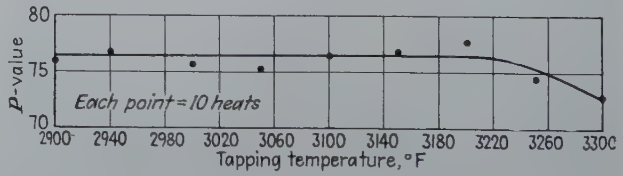

Fig. 11—Effect of tapping temperature on P-value. Temperature measured with L. and N. optical pyrometer.

(8) Increases with increase of relative acidity of final slag.

(9) Increases with increase in percentage of Mn recovery (based on addition).

(10) Increases with increase of residual total aluminum.

(11) Remains constant with increase in tapping temperature until 3200°F is reached, whereupon P-value decreases abruptly.

(12) Increases with increase in time of heat.

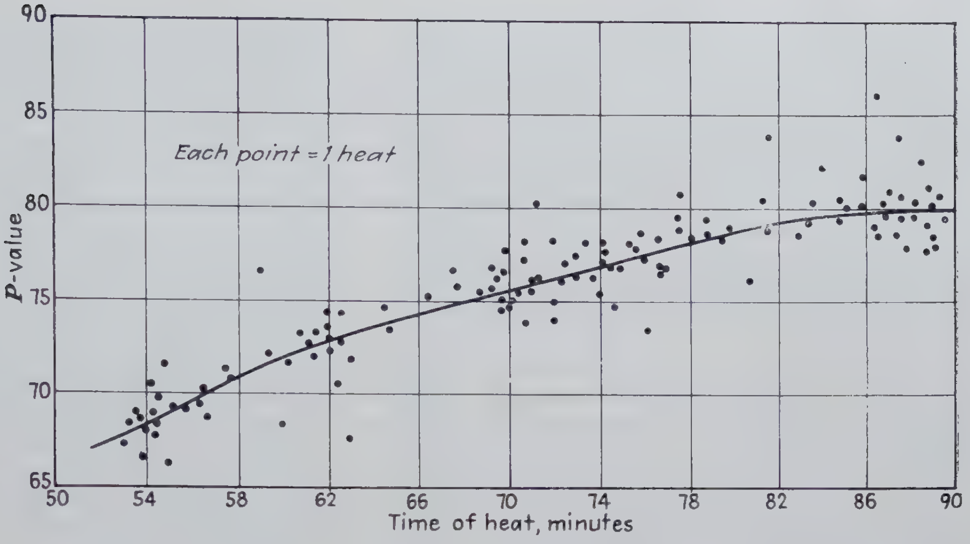

Fig. 12—Effect of time of heat on P-value.

Phase II—Investigation of Metallurgical Factors Affecting Economics of Heat: To further study the oxygen-decarbonized heat, it was decided to find a correlation between all metallurgical variables that would directly or indirectly influence the cost of the heat.

The major items of cost to be considered were power consumption and oxygen consumption. In normal practice and with proper control, the major factors involved in determining the power consumption would naturally be power necessary to completely melt and reduce elemental concentrations of the scrap to the point where the heat specifications could be made. The assumption is made that the furnace is operating with its optimum weight of charge and that the power circuit is efficient.

This being so, the meltdown concentrations of carbon, manganese, and silicon should be as fair indexes of the power consumption. In Burnside practice, the meltdown silicon concentration is low enough usually to be an incidental factor in consideration of power consumption.

The result of a plot of manganese and carbon concentrations at meltdown against power consumption per ton shown on fig. 13 indicates that power consumption decreases as manganese concentration increases. Since the oxidation of maganese is a strongly exothermic reaction, the heat generation on oxidation makes it possible to increase bath temperature to the point where less electrical energy is necessary to sustain or increase bath temperature.

The carbon curve shows that as carbon concentration at meltdown increases, the power consumption increases. The reason for this trend is not evident. It is possible that on every high meltdown-carbon heats the manganese and silicon concentrations are too low to provide sufficient heat to initiate the high-temperature carbon reaction, with the result that the eventual decarbonization takes place at a slower reaction rate. This retardation may require a longer decarbonization period—a period during which the power is off. Because of slow reaction rates, the heat of reaction may not be sufficient to make up for all the thermal losses during the power-off period and therefore might result in a lower temperature at the end of injection than would normally be expected with a higher rate of reaction. This temperature would have to be brought up through subsequent power input, thus increasing power consumption.

In analyzing the effect of various factors on cost of oxygen, it was proposed to plot the variables against oxygen consumption. The factors included a graphical study of meltdown carbon and manganese concentrations, percentage of FeO in meltdown slag, charge weight, effect of oxygen-gas

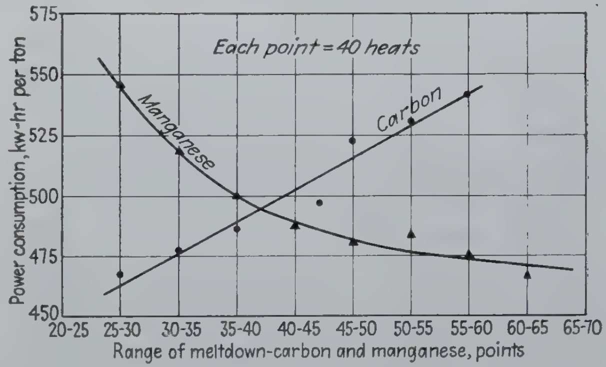

Fig. 13—Effect of meltdown carbon and manganese concentration on power consumption.

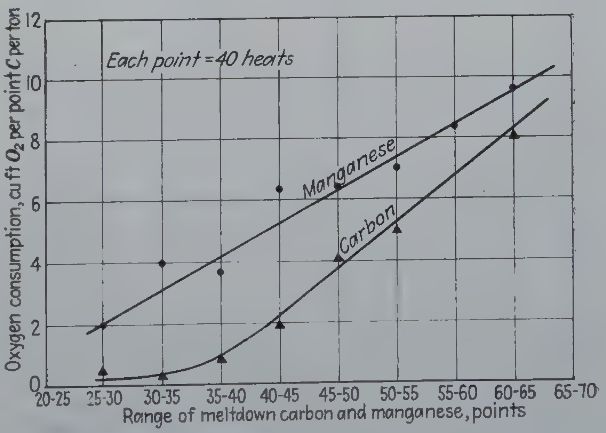

Fig. 14—Effect of meltdown carbon and manganese concentration on oxygen consumption.

velocity, effect of size of orifice in lance pipe, effect of meltdown carbon and manganese concentrations on the rate of carbon removal, and, lastly, the effect of reaction time on oxygen consumption.

When on fig. 14 meltdown carbon and manganese concentrations at meltdown are plotted against oxygen consumption, it can be seen that oxygen consumption increases with increases in both carbon and manganese concentrations. The carbon curve shows no appreciable increase in oxygen consumption until the rangs of 35 to 40 points of carbon is reached. Thereafter the consumption increases steadily. These curves appear logical, since it would be expected that more oxygen would be required the higher the initial concentration of these elements.

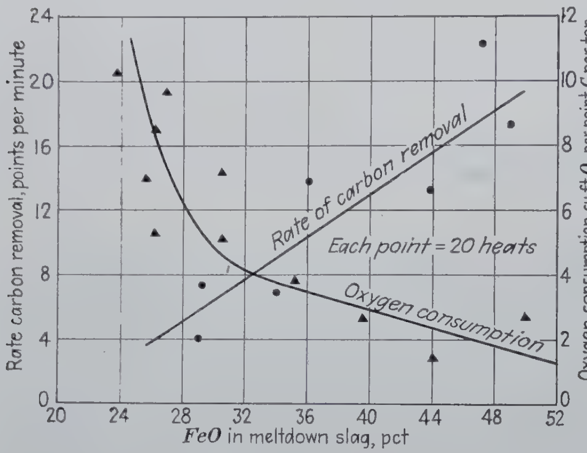

Fig. 15—Effect of FeO content in meltdown slag on rate of carbon removal and oxygen consumption.

When a graphical analysis is made on the FeO in the meltdown slag, as it affects the rate of carbon removal and oxygen consumption, the trends shown on fig. 15 are indicated.

Oxygen consumption decreases as meltdown FeO in the slag increases. As would be expected, the greater the oxidizing power of the slag, the less gaseous oxygen would be required to attain the requisite state of oxidizing power.

The rate of carbon removal increases rapidly with increase in FeO content of meltdown slag. This follows because the rate of carbon removal is a function of high temperature and readily available oxygen.

The trend taken by the curve in fig. 16 is very significant. The marked decrease of oxygen consumption with increase in weight of charge indicates the necessity of operating the furnace near its charge capacity if oxygen efficiency is desired. This curve is very similar to the trend taken by power consumption when plotted against weight of charge and is an important economic factor to be considered.

An important phase of the investigation covered the study of the effect of oxygen velocity and sizes of pipe orifice on the consumption of oxygen. These plots are shown on figs. 17 and 18.

The graph of lance-pipe orifice velocity versus oxygen consumption shows a trend of decreased consumption of oxygen with increased velocity. Undoubtedly this is due to the increased impingement of the oxygen gas against the steel. As in most chemical reactions, this increased impingement of one of the reactants should accelerate the reaction and thereby serve to make it more efficient. From the practical outlook, however, there are precautions to be taken when higher and higher velocities are used. For all furnaces, depending on the geometric shape of the interior and the bath depth, there is a critical velocity that cannot be exceeded without running into the danger of severe bottom or bank erosion or extreme roof splatter. In our practice, this critical velocity appeared to be in the neighborhood of 260 to 265 fps. Four days operation in this range caused severe gouging of the furnace bottom.

When the effect of various sizes of pipe diameters was studied, a plot showed that as lance-pipe orifice size increased the oxygen consumption increased (fig. 18). For various pipe diameters, a family of approximately paralled curves was obtained. This is, of course, another way of showing the data formerly shown on the velocity curve, since velocity is related to flowing pressure and orifice size.

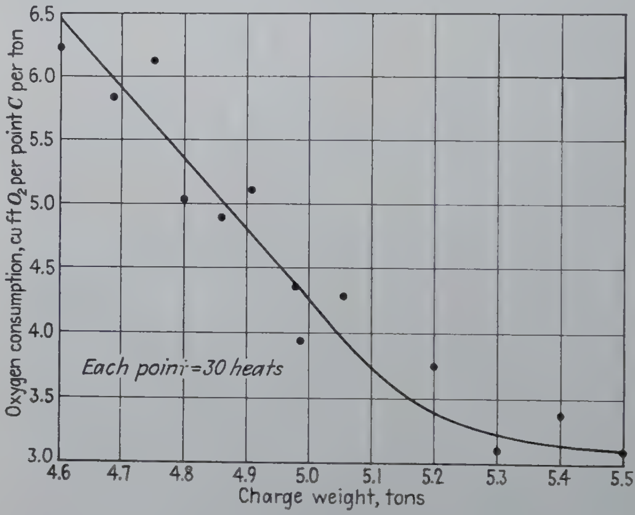

Fig. 16—Effect of charge weight on oxygen consumption.

Since it was observed in phase I of the investigation that the rate of carbon removal had a marked effect on the P-value, it was thought advisable to determine the effect of meltdown carbon and manganese concentrations on the rate of carbon removal. This is shown on fig. 19. It was observed from the graph that as carbon concentration increased the rate of carbon removal increased rapidly to a maximum and then leveled off.

As the meltdown manganese concentration increases, the rate of carbon removal decreases, since the manganese holds preference over carbon in normal order of oxidation, particularly at the lower temperatures encountered at the start of the oxygen injection. However, as the oxidation of manganese progresses, this strongly exothermic reaction actually accelerates the rate of carbon removal. Experience has shown that this beneficial effect is encountered when the manganese concentration reaches a range of from to 35 to 45 points of manganese. The carbon and manganese curves intersect each other within this range, thus locating the approximate optimum meltdown manganese and carbon concentration for the most desirable rate of carbon removal.

A good index for the efficiency of oxygen consumption is found in the visible carbon flame during the injection (fig. 20). Since the carbon flame is characteristic and distinct, it becomes relatively simple to observe during the injection. If the carbon flame appears very shortly after the start of oxygen injection, it indicates that favorable oxidizing conditions are present and that the bath temperature is high enough to initiate the carbon reaction. Slow-starting carbon flames indicate that oxidizing conditions are not favorable, or that the bath is too cold for an efficient oxidation of carbon.

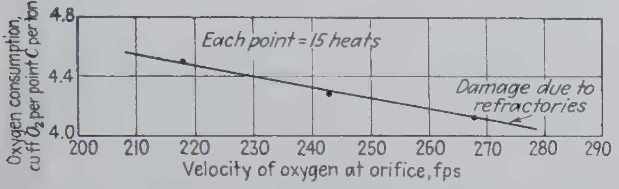

Fig. 17—Effect of oxygen impingement velocity on oxygen consumption at constant pressure and volumetric rates.

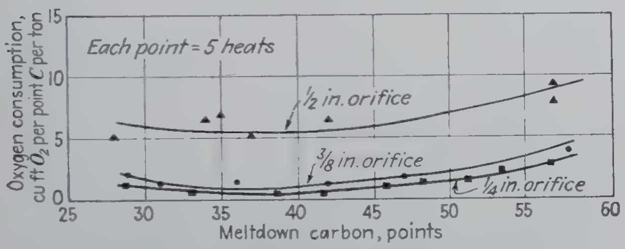

Fig. 18—Effect of pipe-orifice size on oxygen consumption, at constant volumetric rate.

By "unfavorable oxidizing conditions" is meant a deficiency of injected oxygen, too low an oxygen pressure (or velocity), too cold a bath, a low FeO content in slag and bath, or perhaps an abnormally high manganese concentration or silicon concentration at meltdown, or both.

If the percentage of the total injection time during which the characteristic carbon flame was observed is plotted against the amount of oxygen consumed, it is found that as the percentage of carbon flame time increases the oxygen consumption decreases and approaches the theoretical value of 100 pct oxygen efficiency. This value is 3.2 cu ft O_2 per ton-point carbon removal. This efficiency is not an easy mark to attain, since at any particular time elements other than carbon are being oxidized. Also, much of the O_2 comes from the FeO present prior to the injection of gaseous oxygen.

Summary of Phase II: A summary of the effects of variables on the economics of the heat can be made as follows:

(1) a—Power consumption increases as the meltdown carbon concentration increases.

b—Power consumption decreases as the meltdown manganese concentration increases.

(2) a—Oxygen consumption increases as meltdown carbon concentration increases.

b—Oxygen consumption increases as meltdown manganese concentration increases.

(3) a—Rate of carbon removal increases as percentage of FeO in meltdown slag increases.

b—Oxygen consumption decrease as percentage of FeO in meltdown slag increases.

(4) Oxygen consumption decreases as the weight of charge increases.

(5) a—Oxygen consumption decreases as the orifice velocity of O_2 increases.

b—Oxygen consumption increases as the orifice diameter increases.

(6) a—Rate of carbon removal increases as meltdown carbon concentration increases.

b—Rate of carbon removal decreases as meltdown manganese concentration increases.

(7) Oxygen consumption decreases with increase in percentage of total reaction time.

Analysis of Results of Investigation (Phases I and II: Before a summary of the results of the graphical analyses of phases I and II can be made, it must again be stressed that the results obtained are based entirely on the results of data accumulated. The charts are all representative of averages for 600 to 700 heats. Some of the plotted results indicate trends that are not in line with normally expected or established concepts and are not readily explainable in the light of present theories. It must be remembered that much is yet to be understood about the actual chemical actions and reactions going on during the making of a heat. This applies both to the bath and to the slag. No one theory satisfactorily explains all the phases of reaction and equilibrium conditions in the making of a heat.

The purpose of this paper is to portray the actual heat data in graphic form so that it may be considered for analysis in future control work. Just why some of the curves conform as they do is a job for the analyst. It is recognized also that controversy will be aroused, but if free thinking can be stimu-

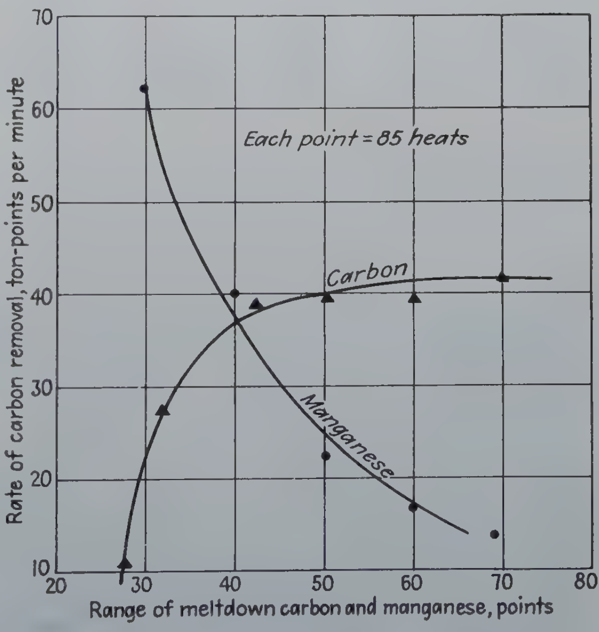

Fig. 19—Effect of meltdown carbon and manganese concentration on rate of carbon removal.

lated, this paper will have accomplished one of its secondary aims.

It must be recognized that an enormous number of data must be used in calculation in arriving at values to be plotted. In many instances, many man-hours were consumed in plotting innumerable coordinate points on graphs that when finished showed no correlation whatsoever and as a result could not be used.

In order to simplify the graphical analysis, a list of the various metallurgical factors is given below. For each factor an optimum value is finally given, which represents the best overall value when considering its influence on all other variables with which it has been correlated.

Influence of Meltdown Carbon Concentration:

(1) Optimium P-value requires meltdown carbon to be 50 points or lower.

(2) Optimum melting rate requires meltdown carbon to be less than 35 points.

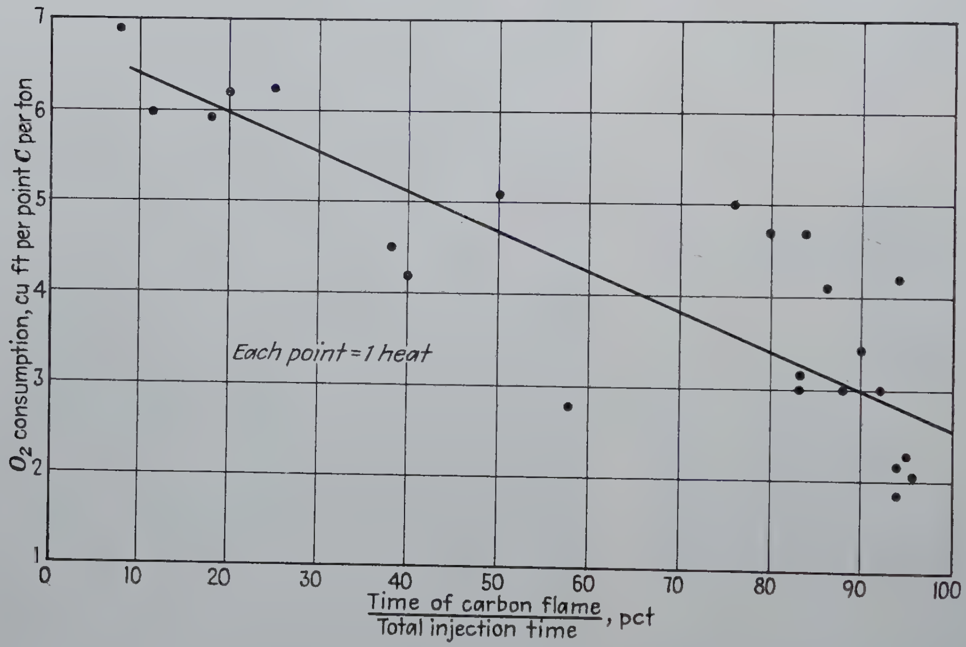

Fig. 20—Effect of observed carbon flame time on oxygen consumption.

(3) Optimum power consumption requires meltdown carbon to be 35 to 40 points.

(4) Optimum oxygen consumption requires meltdown carbon to be less than 50 points.

(5) Optimum rate of carbon removal requires meltdown carbon to be 40 to 50 points.

(6) Best overall value for carbon at meltdown is 35 to 45 points.

Influence of Meltdown Manganese Concentration:

(1) Optimum P-value—no correlation obtained.

(2) Optimum melting rate—no correlation obtained.

(3) Optimum power consumption requires meltdown manganese to be over 45 points.

(4) Optimum oxygen consumption requires meltdown manganese to be less than 45 points.

(5) Optimum rate of carbon removal requires meltdown manganese to be 25 to 35 points.

(6) Best overall value for manganese at meltdown is 40 points.

Influence of Meltdown Silicon Concentration:

(1) Optimum P-value requires silicon at meltdown to be less than 10 points.

(2) Best overall value for silicon at meltdown is minimum silicon.

(3) Best overall rate of carbon removal is 8 points per minute and over.

Influence of Meltdown FeO in Slag:

(1) Optimum rate of carbon removal requires FeO content in slag of 45 pct and over.

(2) Optimum oxygen consumption requires FeO content in slag of 45 pct and over.

(3) Best overall value of meltdown FeO in slag is 45 pct and over.

Influence of Final Slag Analysis:

(1) Optimum P-value requires SiO_2 of less than 55 pct.

(2) Optimum P-value requires MnO of less than 17 pct.

(3) Optimum P-value requires relative acidity greater than 2.5

(4) Best overall value for manganese recovery is 75 pct.

(5) Best overall value for tapping temperature is below 3200°F.

(6) Best overall value for total residual aluminum is above 0.06 pct.

(7) Best overall value for total heat time is above 75 min.

(8) Best overall value for weight of metallic charge is 4.9 tons and over.

(9) Best overall value for oxygen-lance pipe diameter is ¼ or ⅜ in.

(10) Best overall value for oxygen gas orifice velocity is the highest velocity that does not exceed the critical velocity, which in turn is dependent on furnace design.

These optimum values will vary somewhat, owing to the dependency of each factor on all other variables encountered during the melting cycle. However, these optimums indicate clearly that they may be used as starting points when an effort is being made to establish future controls.

It cannot be stressed too frequently that no attempt was made to obtain exacting values from any particular chart. Only an indication as to the degree to which each factor was influenced was sought.

Much work is yet to be done before some of the influences indicated graphically can be isolated to a higher degree and accurately analyzed.

Many questions arise from time to time in the making of an oxygen heat as to causes for some apparently unexplainable peculiarities during the melting cycle.

There are still phases of the investigation to be completed. At the present time, work is being done on the effect of cutting scale on the meltdown slag and bath conditioning. As is indicated on the graphs, a high meltdown FeO content in the slag is essential to a high rate of carbon removal; also, the bath temperature must be hot enough to initiate the oxidation of carbon reaction. In an attempt to raise the FeO content of the meltdown slag, conditioning of the slag with varying amounts of cutting scale was resorted to. A typical analysis of this scale shows approximately 53.3 pct FeO content.

To start with, 14 lb of scale was added to each heat just after meltdown and when the heat was still almost cold. It was noted that no appreciable action, or reaction, took place. Next 20 lb of scale was added per heat. It appeared that as the temperature of the bath increased a well-defined reaction began when the carbon oxidation temperature was reached. This reaction manifested itself in an intermittent bubbling (CO bubble) through the slag.

In this reaction an excellent yardstick for calculating the correct time for initial oxygen injection was found. If injection was started prior to this initial scale reaction, a delay was experienced before the carbon flame appeared. On the other hand, if the oxygen injection was begun shortly after the initial scale reaction had begun, it was discovered that the carbon flame arose immediately and continued to accelerate during the injection period.

It also appears that a more uniform boiling action results after scale addition, but this, of course, is merely a visual indication. Much work still remains to be done on this particular phase before any statistical information can be collected.

At present much thought is being given to investigation of temperature on various metallurgical factors and bath conditions. This phase would necessarily involve an accurate temperature-measuring device. It is believed that a combination of an immersion recording bath pyrometer and spiral fluidity tester should produce the requisite degree of accuracy for proper temperature-measurement technique. At the present time, Burnside Steel Foundry Co. is considering purchase of an immersion pyrometer for this purpose.

This investigation could possibly be expanded to include a study of heat balances in an attempt to clarify the degree and order of oxidation reactions.

Conclusion: This paper has attempted to bring out the effect of the many variables comprising acid electric practice as they influence the quality and economics of acid electric steel. Principally, the investigation concerned itself with the trends indicated by dependency of one factor on another. The exterior influence, on any particular graphical analysis, of variables other than the particular factors being plotted is fully recognized.

In any investigation carried out on commercial heats, it is impossible to eliminate these variables or to hold them constant to any great degree. Therefore, when a trend is discernible between two factors, the degree of influence of all other variables can only be surmised and theorized upon.

By careful analysis, however, all the trends can be evolved into a general pattern for control purposes.

As closer control of the various influential metallurgical factors is worked into a practice, a method is found that should ultimately reward the investigator with a higher quality of steel of greater uniformity at a more economical cost.

AT THE SOUTHERN OHIO OPENHEARTH MEETING

Following the Midyear Meeting of AIME, Columbus, Sept. 25-29, the Southern Ohio Section, National Openhearth Committee, had its regular sessions on operations, practice and quality. Shown here (left to right) are C. E. Sims, of Battelle; L. R. Berner, Inland Steel Co.; R. W. Lewry, Portsmouth Steel Co.; N. F. Tisdale, Molybdenum Corp. of America; and H. P. Gaw, Armco Steel Corp.

Melting Control with the

Direct-Reading Spectrometer

by Earl R. Vance

THE development of alloy steels and the application of the electric furnace to large-scale production of high-grade steels has made the question of analytical control and speed in analysis one of greatest importance. Without exaggeration it might be said that the chemical laboratory controls the electric steel industry—it is impossible to make good electric steel without close chemical control. In addition this control of the molten steel must be handled in an almost inconceivably short time. Yet an error in analysis may mean an "off heat," the rejection of hundreds or even thousands of dollars worth of materials.

Does it not seem remarkable that a furnace operator can remove a spoonful of metal from his furnace and in 30 min, often less, know accurately the percentage of carbon, manganese, phosphorus, sulfur, chrome, nickel, molybdenum, copper and tin? Yet this is being accomplished regularly in numerous electric steel plants in this country and abroad.

This is one of the lead-off papers for the forthcoming Seventh Annual Electric Furnace Steel Conference, Dec. 8-10, Pittsburgh.

Earl R. Vance is chief chemist, Timken Roller Bearing Co., Canton, Ohio.

This fast control analysis was brought about by constant effort on the laboratory's part to reduce the time necessary for a determination without sacrificing accuracy. Back in 1924, when molybdenum steels were first introduced, it required 5 hr for the determination of this element. Today, with improved methods, this element can be analyzed in 6 min. A combustion sulfur test can be run in 3 min as compared to the 45-min period necessary for the older evolution method.

The real value of savings possible through rapid control analysis is apparent since melt shop time can be calculated at approximately one dollar per minute. It is obvious that any gain in analytical time will effect quite a saving, especially when considered on an annual basis. Costly erosion of ceramic furnace linings may be reduced, for with rapid analysis the bath no longer has to be held at approximately 3000° F while waiting for preliminary analysis before adjusting the alloy content.

Most analyses obtained by the best wet chemical methods are slow and time consuming. The analysis of tin in alloy steels requires approximately 2½ hr while 8 to 12 hr are necessary to complete a determination for aluminum. In the usual steel mill control laboratory one analyst is required for each element so that time delays are held to a minimum. A laboratory of this type requires much valuable floor space.

While the spectrograph had been used for quite some time in other fields, the first instrument to be used successfully for ferrous melting control was set up in a foundry in 1935. Since that date many installations have appeared in the control laboratories of hot-metal industries.

A Baird Three Meter Grating Spectrograph was installed in the Timken laboratory in 1943 for the analysis of preliminary and ladle tests from the melt shop. Samples of spectrographic analysis are cast in the form of rods, 7/32 in. in diam, by pouring the molten metal into a mold or sucking it up

LARGE-SCALE production of high-grade electric-furnace steels demands quick and accurate analytical control. The spectrograph was an enormous improvement over the best wet chemical methods. Now, the direct-reading spectrometer may well be the last word in rapid control analysis. Here is the first report by the company that has used this new method for over two years.

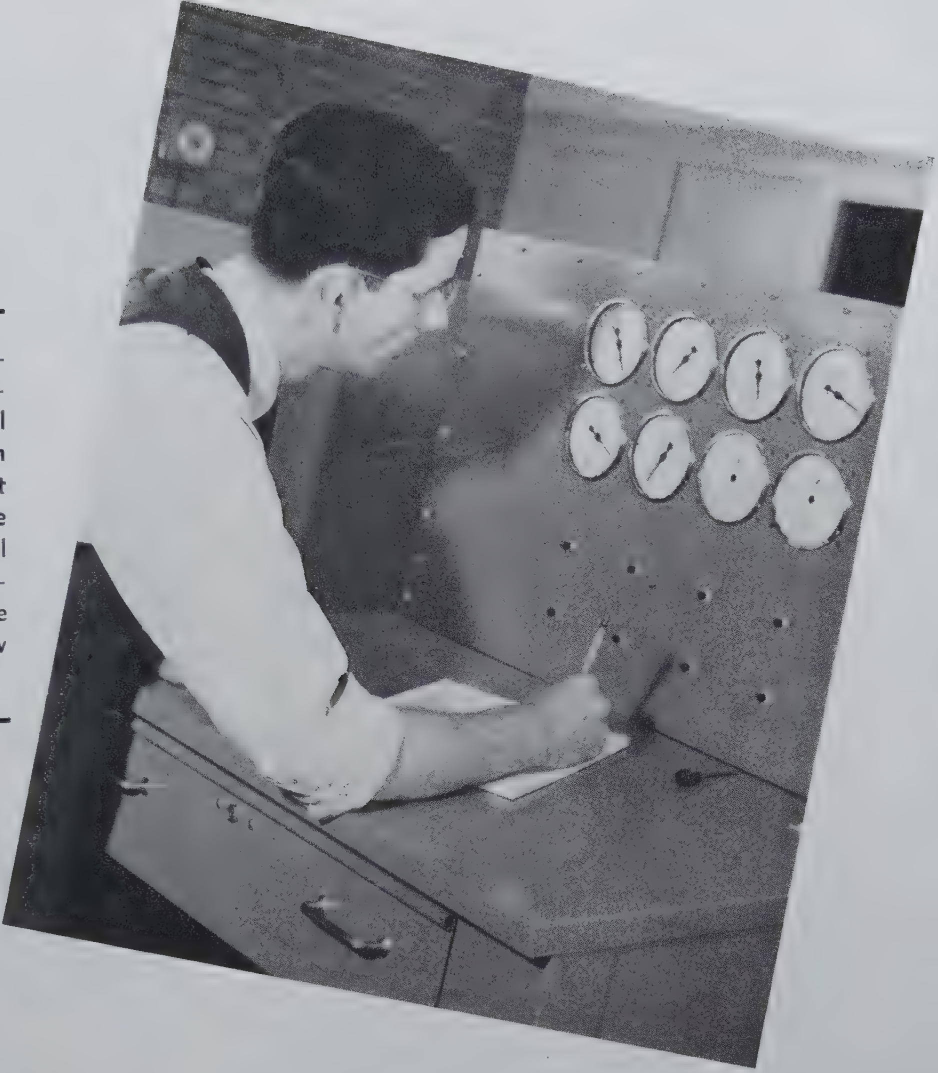

in a glass tube. The cast pins are sent to the laboratory by a pneumatic tube system, where they are carefully ground to a point and placed in the electrode holders which are connected to a power source. High voltage power is applied and light from the resulting arc is broken up into the various element lines which are photographed on film or photographic plates. The exposed emulsion is then developed, washed, dried and cooled to room temperature in a dark room. Element lines are selected, which vary in blackness or density as the percentage of the element changes in the steel. The density of the line for the element required is read on a densitometer and calculated to percent, after which it is reported by telautograph to the furnace operator.

The headaches caused by interfering elements in wet chemistry are largely eliminated and most of the chemical elements are photographed simultaneously. The use of a spectrograph avoids the necessity of waiting several hours for certain elements, as is the case when wet chemical methods are employed. It is reported that one large steel producer increased his tonnage approximately 30 pct after a spectrograph was installed, since heats could be diverted to other specifications prior to tapping, when the copper and tin contents were too high.

With the spectrograph there is a substantial saving in time over the wet chemical methods for special elements such as aluminum, but these elements are not usually requested for control analysis. Control elements are normally Mn, Cr, Ni, Mo V and Cu. Depending on the number of elements requested, a report of spectrographic analysis can be completed in from 10 to 25 min, which time is not too much better than a well organized wet chemical laboratory. Approximately the same number of employees are necessary, as in the chemical laboratory, if delays are to be held to a minimum.

The last word in rapid control analysis was realized with the development of the direct-reading spectrometer. In this instrument, the photographic stage has been entirely replaced by sensitive photo multiplier tubes, which pick up the emitted light from the elements, at the various wavelengths and report it as percentage on calibrated clock dials within 35 sec after a sample has been placed in the electrode holders.

The use of photo tubes eliminates all of the possible errors associated with plates or film, dark room developing and processing, densitometer readings and calculating boards.

A Baird Associates-Dow Direct-Reading Spectrometer was installed in the Timken control laboratory in May 1947 and was the first instrument of this type to be used in the steel industry. A simultaneous analysis of alloys is made; therefore, a total of eight chemical elements can be reported to the melt shop approximately 6 min after a sample has been delivered to the laboratory.

For over two years the direct reader has been used to furnish analyses of all types of steel, except the stainless grades, for elements in the following ranges:

Element	Calibration Range	Element	Calibration Range
Manganese	0.05-1.60	Copper	0.02 -1.20
Silicon	0.01-1.00	Vanadium	0.01 -0.30
Chrome	0.03-7.00	Tungsten	0.05 -5.40
Nickel	0.02-5.00	Aluminum	0.002-1.60
Molybdenum	0.01-1.00	Tin	0.007-0.10

Determination for carbon, phosphorus and sulfur are made in the wet chemical laboratory.

The direct reader is operated 24 hr a day, 7 days a week, with one operator on each 8-hr shift, instead of three, as with the spectrograph. The operator can very easily take care of the necessary elements, on the preliminary and ladle tests, from seven electric and three openhearth furnaces. Operators were selected from the chemical laboratory force, with the thought in mind that, since the number of chemists would be reduced when the spectrometer was installed, it would be essential that these operators could return to the chemical laboratory and carry on control analysis in case of a major spectrometer breakdown. To date this has not been necessary.

The spectrometer is located in an air-conditioned room, which is maintained at a temperature of 75° F and 50 pct relative humidity. It is felt that air conditioning is quite essential to good operation; that is, the atmosphere surrounding the analytical gap is held uniform, but more important, the insulation and fine windings in the electronic circuits are not subjected to absorbtion of moisture due to varying atmospheric conditions in the annual dry and rainy periods.

The instrument is well insulated against shock, the customary vibration found in steel and rolling mills causing no interference. The exit slits, which pass the emitted light from the grating to the photomultiplier tubes, are of the fixed or locked down type. In over 2 yr they have never been changed or adjusted, due to varying mechanical or physical changes in the spectrometer. In a recent check, it was found that the light from the element lines was still passing through the exact center of each exit slit, which is thought to be quite remarkable, since the light is reflected approximately 24 ft and the slightest movement will cause the light to miss these narrow slits which are from 50 to 200 microns, or 0.002 to 0.008 in. in width.

There are 65 electronic tubes used in the various circuits in the spectrometer, but to date there has never been a shutdown caused by a burned-out tube. During vacation period shutdowns the tubes are checked and weak tubes are replaced, even though they cause no trouble in operation. In the past year, five tubes have been replaced in this manner. Many of the original tubes are still in use, which indicates well-designed circuits.

The location of trouble has been simplified since a channel has been designed for each element and the circuits which control that channel are built into a drawer, which is easily replaced with a spare drawer in case of trouble. The troublesome drawer is then repaired by the operator and held as a spare for future use. Tube fatigue is practically unknown, as shown by experiments in which from 20 to 40 exposures are made in rapid succession.

In order to check the effect of a shutdown, the spectrometer was standardized before it was turned off for a recent three-week vacation period. At the conclusion of this time the power was turned on and the electronic circuits allowed to warm up for 20 min. The same standard pins were then sparked and the analyses for all elements were in excellent agreement with the results obtained before the shutdown.

An investigation was completed recently to determine if any gain in accuracy resulted from the use of the spectrometer as compared to the spectrograph. Twenty determinations were made on each instrument on the same day, using identical pins from type 4320 steel. The following table indicates the difference in accuracy of the two methods, reported as percent standard deviation.

		Pct. Standard Deviation		Extremes,
Elements	Chemical Analysis	Spectrograph	Spectrometer	Spectrometer
Manganese	0.55	1.82	1.35	0.54-0.56
Silicon	0.28	1.97	2.46	0.27-0.29
Chrome	0.45	1.92	2.06	0.44-0.47
Nickel	1.69	1.85	0.79	1.68-1.71
Molybdenum	0.215	2.66	1.68	0.21-0.22

In a recent survey of a 2-yr period, it was found that results from the spectrometer were used to control the melting of 14,184 heats of steel. This constituted a total of 951,207 tons, on which 75,470 tests were submitted, making a grand total of 1,021,250 determinations, reported by the aid of the direct-reader.

In addition to this tremendous task the instrument has been used to separate mixups of bars and billets in a few hours time that would have required several days to drill and analyze.

Much interest is evidenced by the numerous visitors from this country and abroad who have inspected the spectrometer. It is felt that in the near future this type of instrument will be used quite extensively. With the improvement in accuracy and the shorter period required to report analysis, it is felt that the direct-reading spectrometer is, by far, the greatest contribution that the control laboratory has ever made towards effecting a savings in the melting department.

Analysis of

Oxygen in Titanium

THE pace of titanium research has been retarded somewhat by the lack of a suitable method of determining oxygen content. Here, the author describes a reliable method of oxygen analysis by a modification of the vacuum fusion techniques which have become conventional for the analysis of gases in steel.

by Gerhard Derge

THE combination of attractive physical properties and abundance of raw materials has resulted in widespread interest in the metallurgy of titanium[1]. The fact that the molten metal reacts strongly with oxygen and the common oxide refractories has been one of the major obstacles in this development and this has in turn pointed to the necessity for the analysis of oxygen in titanium. This same reactivity of titanium with oxygen has made the analysis a difficult one and this article is presented because sufficient evidence is now available to indicate that reliable results can be obtained by suitable modification of the vacuum fusion techniques which have become conventional for the analysis of gases in steel. This information should be encouraging and useful to those who have been planning work in this field and debating the potentialties of various analytical methods.

Gerhard Derge is with the Metals Research Laboratory, Carnegie Institute of Technology, Pittsburgh.

Conventional vacuum fusion methods for the analysis of gases in steel are adequately described and appraised in good reviews in the Metals Handbook[2] and the publications of the British Committee on the Heterogeneity of Steel Ingots[3], both of which include excellent bibliographies. Successful special applications to alloy steels and ferro-alloys (many of which are not unlike titanium in their high reactivity with oxygen) have been included in the British work and similar applications have been described more recently in this country by Mallett[4]. Over a period of years the author has made many similar applications in this laboratory. Therefore, when the problem of titanium analysis was presented, since time was important, it seemed logical to extend this reliable, general procedure by suitable modification, rather than to develop an entirely new and untried method.

The apparatus and procedures used in this laboratory for steel analyses have already been published[5] and it is only necessary to describe the specific procedure adopted for titanium analysis. This procedure will be understood best if the guiding principles and objectives which determined it are outlined first. The exact procedure will then be described, and finally the analytical results obtained from specimens with established oxygen content will be presented.

Early experience with steels showed that if volatile and easily oxidized elements such as manganese are present they may lead to side reactions which give low oxygen results. The most effective means of combating this "manganese error" are to insure rapid pumping in the entire high vacuum zone and particularly that portion of it which is hot and to add small amounts of tin to the molten metal bath. In this laboratory these same precautions have been used successfully with other elements than manganese and it was anticipated that they would prove equally satisfactory for titanium.

In general, the ferro-alloys and non-ferrous metals have been analyzed by adding the sample to a bath of previously reduced iron and the temperature has been increased slowly from about 1200°C to whatever maximum is required to complete the extraction in a reasonable length of time. The temperature should be increased at a rate which prevents a sudden gas evolution which might ex-

In practice, temperatures are observed with an optical pyrometer through a Pyrex window and recorded without correction because changing conditions prevent accurate emissivity corrections.

ceed the capacity of the diffusion pump to maintain a low pressure in the hot zone above the crucible.

Based on the above principles, the following specific procedure has been adopted for titanium.

Materials: The only special materials required are a high purity commercial grade of tin and a reasonably pure iron saturated with carbon. For this purpose ingot iron is melted in air in a graphite crucible by induction heating. This preliminary preparation eliminates a large portion of the oxygen in the iron and saturates it with carbon so as to avoid excessive attack on the graphite crucible of the vacuum fusion apparatus.

Procedure: Standard vacuum fusion apparatus is used.[5] With a new crucible assembly, the iron, tin, and titanium are placed in the storage chamber before closing the apparatus. The system is then evacuated and the empty crucible assembly baked out at about 2100°C until a satisfactory blank is obtained at 1800°C. The crucible temperature is lowered to about 1200°C and 25 g of iron dropped into the crucible. The temperature is then raised to 1800°C within a few minutes and the bath held at that temperature until a satisfactory blank is again obtained. The temperature is then lowered to 1400°C, 5 g of tin added, and the temperature held constant until a satisfactory blank is reached. The titanium sample is then added and the temperature raised slowly to 1800°C. The increase of temperature after the titanium addition must be done with care to avoid objectionable spitting and sudden pressure increase above the crucible. The temperature range between 1600°C and 1650°C seems to be especially critical in this respect and ordinarily about two thirds of the total gas evolution has been completed by the time this range has been passed. It is not certain that the reaction would not complete itself near 1650°C, but the time required at this temperature would certainly be excessive. The reaction completes itself very rapidly at about 1800°C. The pertinent data from a typical run are shown in table I. The collected gas is then analyzed by conventional low-pressure, fractional freezing methods. Additional samples can be analyzed in the same crucible by repeating the addition of iron and tin before each sample.

Detailed discussion of the important but conventional features of blanks and blank corrections, gas analysis, and calculation of results will be omitted as they have been adequately described in the literature.[2, 3]

Results: A variety of iron-titanium samples containing up to 10 pct titanium have been analyzed by this general procedure, with appropriate changes in the amount of reduced iron required for the bath, with apparently satisfactory results. An experienced operator can judge the reliability of such an analysis by the ease with which blanks are obtained before and after the analysis and the condition of the crucible at the end of the work. However, the quantitative evidence that this procedure yields reliable results is based on the analysis of a series of carefully prepared samples of titanium with controlled oxygen composition (see acknowledgments). Regarding the preparation of these samples it will suffice to say that the titanium employed was the highest purity obtainable by the thermal decomposition of the tetraiodide on a hot titanium filament according to the method of Van Arkel.[6] This metal had an annealed hardness of 70-80 Vickers. Oxygen was added in the form of high purity titanium dioxide powder, which was placed

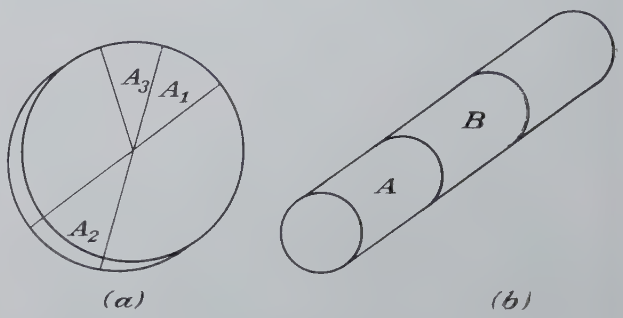

Fig. 1-a—Method of sectioning cast ingots; b—method of sectioning iodide rod.

TABLE I

Typical Record of Analysis

Room temperature = 24°C (Feb. 1, 1949); Iron (C saturated) for bath = 25 g (approx.); Tin for bath = 5 g (approx.); Titanium sample B_2 = 0.2788 g (based on a nominal expected oxygen of 0.5 pct).

Clock Time	Operation	Manometer Reading, cm.	Crucible Temp., Deg. C
12:00	add 25 g iron	......	1200
12:26		1.80 small volume	1800
12:53		2.77 small volume	1800
*	Pumped out some gas to keep readings on small volume		
1:21		2.00 small volume	1800
1:26		2.10 small volume	1800
1:31		2.16 small volume	1800
1:36		2.22 small volume	1800
1:42	Pumped out gas, lowered temperature add 5 g tin		1460
1:46		0.17 small volume	1380
1:48		0.19 small volume	1365
1:50		0.21 small volume	1390
1:54		0.22 small volume	1390
2:00	Pumped out gas add titanium sample B_2		1390
2:02		0.64 small volume	1380
2:05		0.76 small volume	1390
2:13		1.00 small volume	1500
2:18		1.22 small volume	1600
2:23		1.80 small volume	1620
2:25		2.60 medium volume**	1630
2:27		2.70 medium volume**	1630
2:31		2.75 medium volume**	1630
2:33		2.77 medium volume**	1630
2:35		2.78 medium volume**	1750
2:37		2.78 medium volume**	1780

Analyzed gas by fractional freezing.

* This part of the procedure is subject to great variation, depending upon previous treatment of crucible and choice of temperature.

** Medium volume reading X4.833 = small volume reading.

---

[1] B. W. Gonser, "Titanium," Jl. of Metals, vol. 1, p. 6, Jan. 1949.

[2] "The Determination of Oxygen, Nitrogen and Hydrogen in Ferrous Metals," Metals Handbook, A.S.M., 1948 Edition, pp. 408-11.

[3] Eight Report on the Heterogeneity of Steel Ingots, Iron and Steel Inst. (London), Special Rep. No. 25 (1939); Second Report of the Oxygen Subcommittee of the Committee on the Heterogeneity of Steel Ingots (1939); Third Report of the Oxygen Subcommittee (1941); Fourth Report of the Oxygen Subcommittee (1943).

[4] M. W. Mallett, "A Versatile Vacuum Fusion Apparatus," A.S.M. preprint No. 41, 1948.

[5] G. Derge, "Rapid Analysis of Oxygen in Molten Iron and Steel," Trans. AIME, vol. 154, 248 (1943); T. T. Omori and G. Derge, "Vacuum Fusion Analysis of Silicon Steels," Blast Furnace and Steel Plant, vol. 31, 888 (1943).

within holes drilled in the titanium rod. A small weight loss invariably occurred during the melting. This loss was assumed to be due entirely to the loss of some of the powdered compound in the blast of the electric arc, since no weight loss was experienced during the melting of the metal alone, and chemical analyses on titanium-nitrogen alloys made by the fusion of titanium and powdered titanium nitride check the calculated analyses when it was assumed that the entire loss during melting was due to the loss of titanium nitride powder. The high purity titanium-oxygen alloys prepared from these materials were cast in the form of twenty-five gram ingots which were melted in purified argon in an electric arc furnace on a cold hearth. Freezing of this small ingot is quite rapid and it is believed that this chill casting avoided any serious chemical segregation.

Analyses were made on pie shaped segments cut from the cast ingot as shown in fig. Ia. This method of cutting should average possible segregation so that A_1 and A_2 should be duplicate samples. The gas analysis includes values for nitrogen and hydrogen and all of the results are listed in table II, even though the principal interest is in oxygen. The table also includes analyses of cylinders cut as shown in fig. Ib from the original rod of iodide titanium used to prepare the other ingots. Samples X_1 and X_2 were from a cast ingot which had no intentional oxygen addition and represents the pick-up to be expected from the arc melting procedure. Fused ingots A and B had nominal intentional oxygen addition of 0.1 and 0.5 pct respectively and the total expected oxygen is determined by adding the average pick-up due to fusion of 0.031 pct shown by ingot X. These items are all listed in table II. The average analysis of ingot A is 1.5 pct greater than the total estimated value, while the average of ingot B is 3.6 pct less than the expected value. Such results are ordinarily regarded as quite satisfactory in vacuum fusion analysis of other metals, particularly steels, as will be seen by reference to the general reviews of the subject and the "Cooperative Study of Methods for the Determination of Oxygen in Steel" conducted by the United States Bureau of Standards[7]. The results for hydrogen show good checks for duplicate samples and indicate that the vacuum fusion method is also satisfactory for this element. The nitrogen results show a larger variation, partly because all analytical errors are cumulative in this value, and indicate that other methods may be preferred for this element.

TABLE II

Analytical Data

Sample Description		Sample Weight, G	Oxygen, Added as TiO_2	Total Estimated Oxygen	Weight, Pct Vacuum O	Fusion H	Analysis N
Iodide	a	1.129	0.00	.....	0.015	0.0036	0.0055
Titanium	b	1.230	0.00	.....	0.013	0.0038	0.0096
Fused ingot	X_1	0.7098	0.00	.....	0.035	0.0022	0.019
No addition	X_2	0.8460	0.00	.....	0.027	0.0033	0.012
				av.	0.031*		
Fused ingot A	A_1**	0.4192	0.105	0.136	0.203**	0.0024**	0.088**
TiO_2 added	A_2	0.3596	0.105	0.136	0.150	0.0018	0.043
	A_3	0.2112	0.105	0.136	0.126	0.0024	0.024
				av. of A_2, A_3	0.138		
Fused ingot B	B_2	0.2788	0.493	0.524	0.516	0.0037	0.059
TiO_2 added	B_3	0.1819	0.493	0.524	0.494	0.0020	0.045
				av.	0.505		

* This is considered as the normal oxygen pick up during fusion and is added to the intentional oxygen added as TiO_2 to determine the "total estimated oxygen."

** Sample A_1 was used as a trial run to determine emperature range, results should not be weighted equally with A_2 and A_3.

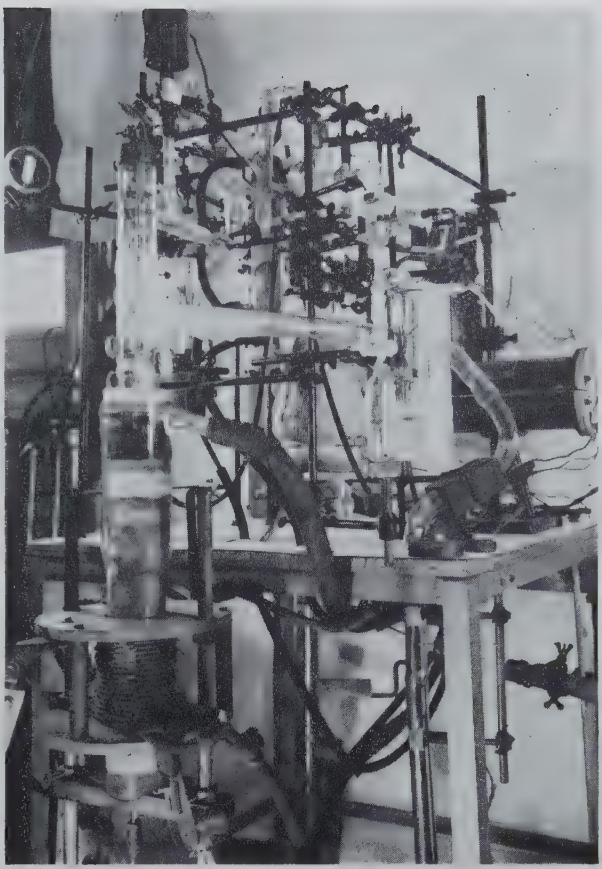

Equipment used for making analyses to determine oxygen in titanium-oxygen alloys up to 0.5 pct oxygen.

Conclusion: Proper modification of the vacuum fusion analytical procedure as ordinarily applied to steels has resulted in the satisfactory analysis of carefully prepared titanium-oxygen alloys containing up to 0.5 pct oxygen. It may be expected that more extensive work will lead to further improvements and refinements but these results are sufficient to indicate that the general principles involved in good vacuum fusion practice can be expected to yield correct results in titanium analysis.

Acknowledgments: The cooperation of Walter L. Finlay, Supervisor of Metals Research, Remington Arms Co., Inc., Bridgeport, Conn., who provided the titanium-oxygen alloys of known oxygen content, and the generous permission of this company to publish these results are gratefully recognized. The experimental work was conducted by Jack R. Shegog.

---

[6] **U. S. Patent No. 1, 671, 213, Van Arkel et al, 1928.**

[7] **J. G. Thompson, H. C. Vacher, H. A. Bright, Trans. AIME, Vol. 125, page 246 (1937).**

Openhearth and IMD Groups to Meet Pittsburgh, Oct. 28

Most of the programs have been completed for the annual meeting of the Pittsburgh Section, AIME, Oct. 28, according to chairman H. P. Greenwald of the Bureau of Mines. Openhearth and IMD sessions will be held in various 17th floor rooms of the William Penn Hotel, and for the most part will be off-the-record. A luncheon and dinner are planned, and after dinner the committee has arranged for the showing of two special motion pictures—the one furnished by Gulf Oil on airborne missles and the other an official film showing the defense of Antwerp during the Battle of the Bulge.

According to E. H. Hollingsworth of Alcoa, the Institute of Metals program will be as follows:

"Metallurgical Factors Influencing Flow Stress of Metals," by M. Manjoine, Westinghouse Electric Corp.

"Vibrational Damping Capacities of Some Plain Carbon Steels," by G. P. Chatterjee and G. R. Fitterer, University of Pittsburgh.

Movie on Metal Flow and Transfer.

Paper on stresses in nonferrous metals. Exact subject and authors to be announced.

Those attending this morning openhearth session in the Ballroom, Friday at 9:30 a.m. will hear E. G. Hill, Chairman of the National Open Hearth Committee and Director of Metallurgy and Development at Wheeling Steel, open up the meeting with "A Few Remarks on the Future Use of Oxygen." Following this there will be series of interesting discussions.

(1) Variation in Heat and Ingot Analysis.
  a—Variations in composition of heat during teeming.
    Factors affecting.
    Control.
    Methods of sampling and variation.
  b—Variation in composition of ingots.
    Effect of deoxidation and mold practice on variation of composition within the ingot.
(2) Sulphur in the Open Hearth Process.
  a—Loss of sulphur in transit.
  b—Copper-sulphur relationship.
  c—Handling of lower silicon higher sulphur iron.
  d—Sulphur in rusty scrap.
  e—Sulphur balance in the open hearth.
(3) Elimination of sulphur from the operators point of view.
(4) Furnace construction.

Refractories and Masonry

Ballroom, Friday 2:00 p.m.

(1) Tearing Down Open Hearth Furnaces—Procedures and Labor Saving Devices.
(2) Rebuilding Open Hearth Furnaces.
  a—Brick Handling to and on job.
(3) Open Hearth Furnace Roofs.
  a—Design, erection, patching, heating-up practice.
(4) Metal Mixer linings.
  a—Open hearth mixers and submarine type mixers.

Acid Open Hearth

Monongahela Room, Friday 2:00 p.m.

(1) Acid furnace maintenance and operation.
(2) Series of pro-con questions.
  a—Added silicon to the charge, regardless of pig iron or substitute source of carbon is necessary for bank protection in an acid furnace.
  b—Special deoxidizers are needed in the manufacture of high quality acid steels.
  c—Chromex, as a source of chromium gives as satisfactory product as does ferrochrome in the acid furnace.
(3) Open Hearth Combination Control.
  a—Importance and methods.
(4) A study of acid slags including cup tests and petrographic examination.

EXTRACTIVE METALLURGY SESSION IN COLUMBUS

As part of the Midyear Meeting of AIME, Columbus, Sept. 25-29, the Extractive Metallurgy Div. heard two papers, one on titanium and the other on the silver—silver-sulphide system. J. D. Sullivan, of Battelle, (right) officiated as chairman, and the co-chairmen were R. R. McNaughton (center) of Consolidated Mining & Smelting Co., and Bruce W. Gonser (left) of Battelle.

Southern California Section Fall Meeting

All divisions of the Southern California Section, including metals, mining and milling, industrial minerals, and petroleum, will participate in the fall meeting on Oct. 20 and 21. Los Angeles, of course, is the host town; metals division meetings are to be held at the new Institute of Aeronautical Science building, while the petroleum, industrial minerals, and mining and milling division meetings will be at the Elk's Club.

Two full days of technical sessions are scheduled for the petroleum group by general chairman John T. Thatcher, Jr. Thursday, the Town House will be host for the oil men's luncheon.

This year the industrial minerals, and mining and milling divisions will join together for a two-day session. Ian Campbell and George Dub have planned for numerous papers by good men on interesting subjects.

Four papers are listed for the metals division on Thursday afternoon and evening, with the meeting taking the form of a symposium on creep of metals. Fred Boericke is chairman.

The annual all-division luncheon of the Section will be on Oct. 21 at the Town House. In addition to other business, Student Awards will be presented.

The men responsible for the programs have spent a lot of time getting them ready for you so that you will be assured of an interesting and profitable time.

Walter Hull Aldridge, John Fritz Medalist for 1949

Announcement has just been made by the John Fritz Medal Board of Award of the award of the John Fritz Medal for 1949 to Walter Hull Aldridge, president of the Texas Gulf Sulphur Co., and recipient of the AIME Saunders Mining Medal in 1933. This board of award is composed of four representatives, all past presidents, from each of the four Founder Engineering Societies. The medal is called the "medal for medalists," regarded as the highest honor an engineer may attain.

Further details regarding the career and professional achievements of the Medalist will be published in a forthcoming issue of the journals.

The citation reads:

"WALTER HULL ALDRIDGE

As Engineer of Mines and Statesman of Industry who by his rare technical and administrative skills has importantly augmented the mineral production of our country and Canada, and who by giving unselfishly of his wisdom and vision has guided his professional colleagues to higher achievements."

AIME and ASME Joint Meeting

The final draft of the program for the twelfth joint meeting of the Coal Division, AIME, and the Fuels Division, ASME, to be held at French Lick Springs Hotel, Oct. 26 and 27, has been completed. It looks like a program which fuels men can't afford to miss. For a list of papers see page 51 of *Mining Engineering*. The banquet speaker is to be Philip Willkie, son of the late Wendell Willkie. A program is being prepared for the ladies which will include a visit to the French Lick Springs Hotel gardens, bridge, dancing, and a bus trip to the nearby Indiana State Park limestone cave.

Get on the ball, you fuels men, and your ladies; get your facts and fun at French Lick.

Pittsburgh Section Off-the-Record Meeting

The Pittsburgh Section has gone all-out to plan its Oct. 28 meeting to interest coal, petroleum, open-hearth, and metals men. Programs for each group are listed in the related journal but get to the meeting if you can possibly make it. You'll find it worthwhile.

The Coal Division sessions will be held in the Pittsburgh Room of the William Penn Hotel; all other sessions will be on the 17th floor. There will be a luncheon and dinner and at the latter, two special motion pictures will be shown, the first on air-borne missiles, and the second on the defense of Antwerp during the Battle of the Bulge.

Industrial Minerals Division Meets in Tampa

Tuesday, Nov. 8, is registration day for the annual fall regional meeting of the Industrial Minerals Division; the Tampa Terrace Hotel, needless to say in Tampa, Fla., will be headquarters from Nov. 8 to 12. Two days of technical sessions are scheduled for Wednesday and Thursday featuring papers on geology, mining, and milling of Florida phosphates and other mineral resources, and papers on industrial minerals in the southeastern states. A cocktail party and banquet wind up Thursday's affairs, but be up for the field trips on Friday and Saturday to a limestone quarry, a heavy mineral operation, and the phosphate producing areas. If you want to stay over Saturday evening, there's the University of Florida-University of Kentucky football game.

THE DRIFT OF THINGS

. . . as followed by **EDWARD H. ROBIE**

1950 Dues Bills

To expedite the recording and acknowledgment of remittances, the plan of staggering the mailing of dues notices is being continued this year. First to be sent out have been the bills to our members outside of the U. S. A., for these will require more time in transit, and often delay is incurred in securing American dollars. Mailing of all bills will be completed in late December. It is hoped that members will respond as promptly as they can, although dues do not actually become payable until January first.

Those who have found the dues bill more or less complicated in previous years will, we hope, find the current statement simpler and more acceptable. It is predicated on the assumption that a member will wish the same Branch journal or journals in 1950 that he has been receiving in the past. If he wishes to change his selection he should so state on the bill and correct it accordingly. Members are entitled to receive free, as part consideration for their dues, a 1950 subscription to one of the following: **Mining Engineering, Journal of Metals, or Journal of Petroleum Technology.** If two different journals are desired the additional charge is $4, or if all three are wanted the added charge is $8. Additional subscriptions to the **same** journal must be paid for at the nonmember price —$8 each for the Americas and $9 foreign.

The technical papers published by each of the three Branches of the Institute appear monthly in the respective journals. Enough extra copies of these technical papers are printed each month so that they can be bound together at the end of the year into Transactions volumes, supplied at cost to those who wish to have them. Such bound copies for members' libraries preserve a complete file, in permanent form, of the technical publications of the respective Branches of the Institute. Although one may try to keep individual copies of the journals, often one or more will become lost.

These three Transactions volumes will be published in January of each year, each containing all the technical papers, discussion, and an index, published by the respective Branches in the previous year, and nothing else. Members that have already requested one or more of these volumes to be published next January will find the appropriate charge therefor on their bills. Those that did not so specify on their publication selection slips last year, but now wish to have one, should add the item to their bill and enclose an additional $3.50 for each volume selected; so long as our limited supply lasts they will be accommodated.

We shall assume that members will wish to receive, early in 1951, the same bound volume or volumes, if any, that were selected in 1950 and shall govern our overrun printing accordingly, unless we are advised to the contrary. The price of the 1951 volumes cannot be set until their cost is known but it should not be greatly different from the current price of $3.50.

No Institute Directory was published in 1949 but the usual volume will be prepared in the spring of 1950. Members that have not already advised Institute headquarters of any desired change in their listing should do so in the next few months, for no special canvass will be made for Directory purposes.

Bills will be sent out in duplicate, one copy to be returned to the AIME with remittance and the other to be retained for the member's record. If payment is made through a bank or agent, they should be sent both copies with the request that one be returned to the Institute, or at least they should advise us of the member's name and ledger number when making payment, so that proper credit may be accorded. The ledger number is the number that appears opposite the name on the address stencil.

Student Associates again in 1950 will have the privilege of selecting one of the Branch journals if they pay $4.50 dues. If they do not wish to have an annual subscription to a journal their dues are $2. They will be billed according to the amount they paid in 1949 but of course have the privilege of changing their classification for 1950 if they wish.

Mudd Volumes for Junior Members

For years, all Junior Members of the AIME, at the time they attain that status, have been given several volumes thought to be of interest to them, through the Seeley W. Mudd Memorial Fund. A dozen or more titles have been distributed in all. Currently each Junior Member is receiving a copy of the Institute's 75th Anniversary volume plus a copy of the new ECPD book, "A Professional Guide for Junior Engineers." Also, he is given the privilege of selecting, as a third volume, one of several books that are in more limited supply and not of as wide professional interest.

The Mudd Fund Committee hopes, in the next year or so, to be able to supply books of special interest to young men in each of the ten Divisions of the Institute, as well as two or three volumes of general interest to all groups. Currently, for instance, no book is being offered of special interest to young petroleum engineers. Each Division is being asked to select the subject and potential author for such a book, and suggestions from the Junior Members themselves will be welcomed. The books should be concise and practical, preferably covering a subject of wide technical interest to Division members, and also preferably filling a gap in current technical literature. They may possibly take the form of a handbook. If they are of such a nature that they can be sold, to others than Junior Members who will get them free, so much the better for the Mudd Fund.

Steel and Coal

When this issue reaches its readers, they will know much more than we do now—on Sunday, Sept. 18th—whether or not a steel or coal strike is going on or is imminent. The report of President Truman's fact-finding board was a masterful compromise that satisfied neither side. Fortunately no general wage increase, for the steel or other industries, was recommended, and the amounts demanded for social insurance and pensions were reduced considerably below Mr. Murray's initial demands. The disagreement, bitter on both sides, is not on whether pensions are desirable — but whether workers should contribute to part of the cost.

The threatened coal strike has quite a different reason. The twenty-cent a ton royalty for miners' welfare seems never to have been adequate for the benefits paid, and certainly not after the three-day week reduced output from eleven to eight million tons. A group of Southern operators has refused to pay any royalty at all on coal mined since July 1, when the contract expired, the royalty agreement being a part of the contract. Mr. Lewis says this has made the miners boiling mad and they may quit work any time, which will mean still less money in the welfare fund.

To us, it seems unfortunate that social insurance and pensions ever should have become a matter for company-union negotiation. Had employers been more farsighted they would have urged more adequate payments under the Federal laws and thus perhaps have avoided individual company responsibilities in this regard. One bad feature of such plans from the economic standpoint, unless they are liberalized, is that they tie the employe to one company and thus do not promote a mobile labor supply in the country, a desirable factor for efficient production.

Sharing Our "Know How"

Point Four of President Truman's recommendations made to Congress last June has attracted considerable attention. It has to do with assistance to the peoples of economically undeveloped areas to raise their standards of living. The suggested aid falls into two categories: (1) technical, scientific, and managerial knowledge necessary to economic development; and (2) production goods — machinery and equipment — and financial assistance in the creation of productive enterprises. The President especially mentioned the fields of mining and metallurgy in referring to the need in underdeveloped countries for technicians and experts.

Assistance so far has been more in imparting American know-how to visitors from foreign countries than in sending American technologists abroad. More than 25,000 foreign students were enrolled in American universities in the college year just closed, and approximately 5100 of these were studying engineering. The ECA has just announced that fifty British engineers, with at least Master's degrees, will be brought to the United States this fall for one year of graduate training in practical applied science and technology, partly in schools and partly in plants. The cost will be about $3000 per man.

The Department of State hopes to send more technical men and teachers abroad in the future than in the past, but a start has already been made. For instance, George V. Allen, the State Department's Assistant Secretary for Public Affairs, who is intimately concerned with the project, recently cited the fact that two American mining engineers from the Bureau of Mines were now in Mexico assisting the Government in working out ore extraction processes. Also, many American geologists have been sent to Brazil in the last seven years to assist that country in locating and mapping its strategic minerals. The largest deposits of manganese in the Western Hemisphere have thus been discovered.

We feel that American firms in the mineral industry should cooperate to the fullest extent in these plans to promote world recovery, as many of them are now doing. Interested individual engineers should get in touch with the Department of State, Washington.

Arkansas Bonanza

Large mining companies have many offers of properties, and some of these offers are accompanied by reports that arouse the risibilities of the exploration engineers. Jack Baragwanath sends us a sample, a report of a mineral occurrence on a certain Arkansas farm which we will call the Smith farm, just to hide its identity and protect Freeport Sulphur from too much competition in securing an option:

"The starting point for the location of minerals is at the southeast corner of the Smith farm. The lead is located 1000 ft west of the said starting point and the vein runs thence northerly 1122 ft and averages 148 ft in width and about 25 ft thick. The ore is about 20-25 ft below the surface of the farm. The silver pocket is located 800 ft west of the starting point, thence north 300 ft to center of pour-out, thence north 200 ft to northerly edge of pocket. The pocket is 200 ft across at its widest part and about 38 ft thick. The ore is about 28 ft below the surface. There is a silver-copper vein about 15 ft wide through the pour-out at about 2000 ft down that runs the entire length of the Smith farm. The probable depth of the vein is about 1000 ft. [Then comes similar data about a copper pocket.]

"The Smith farm is one of the best that I have found in Ark. . . . There is a fortune in either of the three minerals. . . . The silver and copper were deposited in a molten form from a volcano and the lead was formed through filtration."

ITINERARY OF AIME SECRETARY

The Secretary of the Institute plans to be at the following places in the month of October:

Oct. 1. St. Louis and Rolla, Mo.
2. Baxter Springs, Kans.
3. Dallas
4. Austin
5-7. San Antonio (Petroleum Division)
8. Austin
10. Carlsbad, N. Mex.
11. El Paso
12. Silver City, N. Mex.
13. Morenci, Ariz.
14. Miami and Superior, Ariz.
15. Tucson
16. Tucson and Ajo, Ariz.
17. Ajo
18. La Jolla, Calif.
19-20. Los Angeles (Divisional Meeting)
21. Jerome, Ariz.
22. Albuquerque
24. Wichita
26. French Lick, Ind. (Fuels Conference)
27. La Fayette, Ind.
28. Chicago (ECPD Annual Meeting)

Mr. and Mrs. Robie are driving and are planning to visit as many Local Sections and Affiliated Student Societies as possible en route.

Fuels and Domestic Security

Fuels of the future, and their relationship to the domestic security of the United States will be discussed at the 29th annual meeting of the American Petroleum Institute in Chicago, Nov. 7 to 10. The fuels session will be held in the grand ballroom of the Stevens Hotel on Thursday morning, Nov. 10.

The forum will be opened with papers by W. M. Holaday of the Socony-Vacuum Oil Co., New York City, and W. G. Whitman of MIT. Holaday will discuss such questions as these: For maximum efficiency and conservation of our resources, should we use coal, liquid fuels, or gas? Which is best for power production, steam or internal combustion engines? What should be the fuel for steam power, coal, oil, or gas? What should be the fuel for internal combustion engines, Diesel fuel or gasoline?

Whitman will give his opinions on these questions: Who holds the responsibility for National Security? What about the fuel requirements for the next war?

Other Whitman questions revolve around these points: Timing of discovery and development—What is best for our country? Stockpiling versus imports—What should we do? Should we conserve our crude reserves and go the synthetic route, and if we do go the synthetic route what should we use in the production of synthetic fuels — gas, bunker oil, shale, or coal?

In Changing Your Address

When notifying AIME headquarters of a change of address, or of company position or affiliation, please mention the Branch of the Institute to which you belong—Mining, Metals, or Petroleum. This will make for a more expeditious handling of the change and will facilitate the preparation of various reports. A new Directory will be issued next spring; listings will be the same as in the 1948 Directory unless the Secretary's office has been notified of a change.

Gerow CIMM Secretary

Carlyle Gerow took office as secretary-treasurer of the Canadian Institute of Mining and Metallurgy on Oct. 1. The AIME wishes him every success in his new post and anticipates a continuation of the fine fraternal spirit and co-operation that has characterized relations between our two institutes.

PRESIDENT YOUNG ON TOUR

President Young has already visited the Oklahoma City, El Paso Metals, Southwestern New Mexico, Carlsbad Potash and San Juan Sections of the AIME. Members in the following areas will have a chance to meet him as he continues his tour:

Oct. 1. Colorado School of Mines
4. Southeast Section, Birmingham
5. Univ. of Alabama, Tuscaloosa
6. Petroleum Branch, San Antonio
10. New Mexico School of Mines, Socorro
11. Colorado Section, Denver
12. Utah Section, Salt Lake City
14. Montana Section, Butte
14. Columbia Section, Wallace
15. Univ. of Idaho and Washington State Student Chapters, Moscow
17. North Pacific Section, Seattle
19. CIMM meeting, Vancouver
20-21. Southern California Section, Los Angeles
26. Coal Division, French Lick
27. Illinois Inst. of Tech., forenoon.
27. Univ. of Wisconsin, afternoon
28. Michigan College of Mines, Houghton
29. Upper Peninsula Section, Ishpeming
Nov. 7. Boston Section
8. Tri-State Section, Joplin (Tentative)
9. Kansas Section, Wichita
14. Arizona Section, Tucson
17. Lehigh Valley Section Luncheon (Tentative)
Dec. 7. New York Section
15. Coal Mining Institute, Pittsburgh
Jan. 9. Delta Section
10. Gulf Coast Section
11. North Texas Section
16. East Texas Section
(Above Jan. dates tentative)
19. Ohio Valley Section

Personals

John Eliot Allen has joined the department of geology at the New Mexico School of Mines, Socorro. He had been at Penn State.

J. W. Allingham, 509 7th St., Calumet, Mich., is a geologist with the U. S. Geological Survey.

H. I. Altshuler has left Peru, where he was general manager of the Vanadium Corp. of America, to take the post of general manager for Frontino Gold Mines Ltd. in Colombia, now under the technical direction of the Gold Fields American Development Co., of London and New York. Mr. Altshuler's new address is care of Frontino Gold Mines Ltd., Segovia Antioquia, via Otu, Colombia.

Robert B. Anderson is on a year's leave of absence from the Inland Steel Co. to get a degree in electrical engineering at VPI.

Robert H. Arndt is a professor in the department of geology at the University of Arkansas, Fayetteville, Ark.

H. J. Ashe, recent graduate of the Colorado School of Mines, has a job with the Inspiration Copper Co. His address is Box 96, Inspiration, Ariz.

L. J. Barraclough, chief mining engineer to the 3,000 - ton - per - day Indian coal company, Messrs. Andrew, Yule & Co., visited the States on business and as the delegate of the Mining, Geological and Metallurgical Institute of India to the UN Conference on the Conservation and Utilization of Natural Resources in August. An authority on hydraulic stowage in Indian mines, he holds several government appointments.

Mr. Barraclough left New York on his way home early in September after visiting coal mining properties in Pennsylvania. He suggests that any AIME members wishing to visit India should get in touch with P. K. Ghosh, Honorary Secretary of the Mining and Geological Institute of India, care Geological Survey of India, Calcutta, who will arrange for a proper reception.

H. L. Batten, who for some years has been consulting engineer for Canadian Exploration, Ltd., and manager of the Emerald Tungsten Project, Salmo, B. C., has established an office at 704 Birks Bldg., Vancouver, B. C., and will carry on a general consulting practice specializing in development projects in British Columbia.

Jacob P. Berry for the past two years had been general superintendent of Moccasin Mines, Ltd., at Watson Lake, Yukon Territory. Recently he resigned this post to become manager of the United Mining and Dredging Co. operating in the Cariboo area of British Columbia.

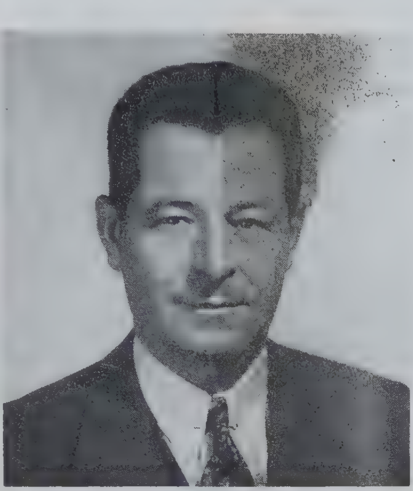
J. J. Kelleher

J. J. Kelleher has been made assistant sales manager, a newly created post, for the Hercules Powder Company's explosives department. For several years he was manager of the Company's contractors division. He has worked on some of the major construction jobs in the country.

Dwight L. Harris

Dwight L. Harris resigned as assistant professor of metallurgy in the School of Mines at Washington State to continue graduate work at MIT. A research assistantship at the Institute in radioactive tracer investigations has been granted him. He expects to complete work for a doctorate at the same time.

J. T. Boyd has an avocado grove near Carlsbad, Calif., and although somewhat slowed down by Parkinson's disease, has been making mine examinations in California, Nevada, and Mexico.

Walter W. Bradley married the former Mrs. John R. Roberts last April. While on a trip to the East Coast in August they stopped in at AIME headquarters.

Lloyd D. Brownson is assistant to the engineers of the U. S. Smelting Refining and Mining Co., at Lark, Utah.

E. L. Bruce, Miller Memorial professor and head of the department of geology at Queen's University, Kingston, Ont., has been elected vice-president of the Society of Economic Geologists for 1950.

R. D. Bradford, of San Francisco, has been named general manager of the Utah department of the American Smelting and Refining Co., succeeding **W. J. O'Connor,** who retired on May 1. Mr. O'Connor had served AS&R for 39 years, and spent 32 of them in Utah. Mr. Bradford joined the Company in 1926, and has worked in its New York, East Helena, Mont., and El Paso, Texas, operations.

J. Ross Clare, formerly with the Lamaque Mining Co., can now be reached in care of the Canadian Johns Manville Co., Matheson, Ont.

Frank A. Colbert is in Rancagua, Chile, working as junior mine shift boss for the Braden Copper Co.

W. A. Coster, formerly with the Demerara Bauxite Co., is carrying out an assignment for the Afghanistan Government.

Robert I. Davis is working for Cia. Minera Sta. Maria del Oro, Sta. Maria del Oro, Durango, Mexico.

Danford J. Dodds is employed by the Bagdad Copper Corp., Bagdad, Ariz., as assayer-chemist. Prospecting is good in that area and excitement growing over the recent discovery of U_3O_8 at the nearby Hillside mine.

Murl H. Gidel, chief geologist of the Anaconda Copper Mining Co., has been elected president of the Alumni Association of the Montana School of Mines for the ensuing year.

T. R. Goedicke has left Sherwin Kelly Geophysical Services to return to the University of North Carolina, Chapel Hill, where he is studying for his doctor's degree in geology.

Patrick Green, formerly general mine foreman for Patiño Mines and Enterprises, may be reached temporarily at home, where his address is Box 622, Cashmere, Wash.

Thomas A. Greene is now an assistant engineer with the Anaconda Copper Mining Co., and can be reached at 2601 Princeton Ave., Butte, Mont.

Wm. A. Griffith, having completed requirements for a master's degree at MIT, where he was an instructor, has taken a job with the New Jersey Zinc Co. at Palmerton, Pa.

Donald R. Haake, formerly in the production department of the Rochester & Pittsburgh Coal Co., has gone to Wheeling, W. Va., as industrial engineer for the Valley Camp Coal Co.

George R. Haataja can now be reached in care of the Braden Copper Co., Rancagua, Chile.

Coming Meetings

OCTOBER

3 Boston Section, AIME.
3-4 National Assn. of Corrosion Engineers, Adolphus Hotel, Dallas, Texas.
3-6 Assn. of Iron and Steel Engineers, William Penn Hotel, Pittsburgh.
5 Chicago Section, AIME. R. S. Archer on "Temper Brittleness in Steels."
5-7 Petroleum Branch, AIME, fall meeting, Plaza Hotel, San Antonio, Texas.
6 American Iron and Steel Institute, Drake Hotel, Chicago.
7 Columbia Section, AIME.
10-14 American Society for Testing Materials, Fairmont Hotel, San Francisco.
11 Delta Section, AIME. Discussions on company organization.
11 East Texas Section, AIME.
11-14 American Standards Assn., annual meeting, New York City.
12 El Paso Metals Section, AIME.
12 Southwestern New Mexico Section, AIME.
12 San Francisco Section, AIME.
13 New York Section, AIME. M. L. Haider on "Canadian Oil Developments."
13 ASME, Metropolitan Section Night.
13-14 Texas Mid-Continent Oil and Gas Association, annual meeting, Rice Hotel, Houston.
14 Eastern Section, Open Hearth Committee, Iron and Steel Division, annual all-day fall meeting, Warwick Hotel, Philadelphia.
14 Southwestern Section, Open Hearth Committee, Iron and Steel Division, Kansas City, Mo.
14 Rio de Janeiro Section, AIME.
17 Detroit Section, AIME.
17-19 Institute of Metals Division, AIME, fall meeting, Allerton Hotel, Cleveland.
17-21 National Metal Congress and National Metal Exposition, Public Auditorium, Cleveland, Ohio.
17-21 American Society for Metals, annual meeting, Cleveland, Ohio.
17-21 American Welding Society, annual meeting, Cleveland, Ohio.
17-23 AIEE, 1949 Mid-West meeting, Netherland Plaza, Cincinnati.
18 Gulf Coast Section, AIME.
18 Washington, D. C., Section, AIME.
19 Southwest Texas Section, AIME.
19-20 Society for Non-Destructive Testing, Cleveland, Ohio.
20 Carlsbad Potash Section, AIME.
20 Utah Section, AIME.
20-21 S. Calif. Section fall meeting, with Petroleum, Mining and Metals Branches, Los Angeles.
21 Oregon Section, AIME.
24-28 Thirty-seventh National Safety Congress and Exposition, Chicago.
25 Montana Section, AIME.
26-27 Joint Fuels Conference, ASME-AIME, French Lick Springs Hotel, French Lick, Ind.
28 Pittsburgh Section of Open Hearth Committee and Pittsburgh Section, AIME, annual fall meeting, William Penn Hotel, Pittsburgh.
28 Delta Section, AIME, Hallowe'en dance and buffet dinner, Metairie County Club, New Orleans.
28-29 ECPD, annual meeting, Edgewater Beach Hotel, Chicago.
31 Alaska Section, AIME.

NOVEMBER

1 Society for Applied Spectroscopy, New York City.
1-5 Pacific Chemical Exposition, California Section, American Chemical Society, San Francisco Civic Auditorium.
2 Chicago Section, AIME. Ladies Night. J. P. Skinner on "Synthetic Sapphire."
2-4 American Society of Civil Engineers, fall meeting, Washington, D. C.
4 Columbia Section, AIME.
7 Boston Section, AIME.
7-10 AIChE, annual meeting, Pittsburgh, Pa.
7-12 International congress on tunnel driving in rock formation, organized by the Societe de l'Industrie Minerale. Information on meeting available from French Mining Mission, 1322 18th St., N. W., Washington, D. C.
8 Delta Section, AIME. Problems of offshore drilling.
8 East Texas Section, AIME.
8-11 Industrial Minerals Division, AIME, Tampa, Fla.
9 El Paso Metals Section, AIME.
9 San Francisco Section, AIME.
9 New York Section, AIME. Ladies Night. C. Goodman on "Atomic Energy."
10-11 National Air Pollution Symposium, Huntington Hotel, Pasadena, Calif.
10-14 ASTM, first Pacific area national meeting, San Francisco, Calif.
11-12 Central Appalachian Section, AIME., and W. Va. Coal Mining Inst., Summit Hotel, Uniontown, Pa.
11 Rio de Janeiro Section, AIME.
12-14 Geological Society of America, annual meeting, Hotel Cortez, El Paso.
14 Arizona Section, AIME, annual meeting, Pioneer Hotel, Tucson.
15 Gulf Coast Section, AIME.
15 Washington, D. C., Section, AIME.
16 Southwest Texas Section, AIME.
16-18 Industrial Hygiene Foundation, 14th annual meeting, Mellon Institute, Pittsburgh.
16-18 Geological Society of America, annual meeting, Hotel Statler, Washington, D. C.
17 Carlsbad Potash Section, AIME.
17 Utah Section, AIME.
28-Dec. 3 22nd Exposition of Chemical Industries, New York City.

DECEMBER

4-7 AIChE, national meeting, Pittsburgh, Pa.
7 American Mining Congress, Annual Business Meeting, New York City.
7-9 Eighth Annual Conference, Electric Furnace Steel Committee, Iron and Steel Division, AIME, Hotel William Penn, Pittsburgh.
8-10 Seventh Annual Conference, Electric Furnace Steel Committee, Iron and Steel Division, AIME, Hotel William Penn, Pittsburgh.

JANUARY 1950

18-20 American Society of Civil Engineers, annual meeting, New York.
30 AIEE, winter meeting, New York.

FEBRUARY 1950

10 Southwestern Section, Open Hearth Steel Committee, Iron and Steel Division, St. Louis, Mo.
12-16 Annual Meeting, AIME, Statler Hotel, New York City.

APRIL 1950

4-7 Nat'l Assn. of Corrosion Engineers, St. Louis.
10-12 Open Hearth Conference, and Blast Furnace, Coke Oven and Raw Materials Conference, Netherlands Plaza Hotel, Cincinnati.
19-21 American Society of Civil Engineers, spring meeting, Los Angeles.
23-26 American Ceramic Society, annual meeting, New York City.
24-26 AMC Coal Convention, Netherlands Plaza Hotel, Cincinnati, Ohio.

DECEMBER 1950

7-9 Electric Furnace Steel Conference, Iron and Steel Div., Hotel William Penn, Pittsburgh.

APRIL 1951

2-4 Open Hearth and Blast Furnace, Coke Oven and Raw Materials, Conference, Iron and Steel Division, Statler Hotel, Cleveland, O.

Daniel A. Jones is employed by the Territory of Alaska as assayer and mining engineer at the Nome assay office. Most of the summer was spent in examinations and examining samples to assay during the winter. It is his job to help further in every way possible the mining industry in northwestern Alaska.

Peter Joralemon completed his studies at Harvard, receiving a doctor's degree in geology, and is now working as a geologist for Getchell Mine, Red House, Nev.

Lou D. Jordan, formerly general superintendent of the Consolidated Mines for the Benguet Consolidated Mining Co. in the Philippines, has returned to the Western Hemisphere to work for the San Francisco Mines of Mexico at San Francisco del Oro, Chihuahua.

Thomas F. Kearns was reelected last May as president of the Silver King Coalition Mines. At the same time, **James Ivers** became vice-president and general manager, and **M. G. Heitzman** took over as manager of operations.

L. Russell Kelce of Kansas City has been elected to serve as a director of the National Coal Association. Mr. Kelce recently became president of the Sinclair Coal Co., and has been with that Company since 1924.

John M. Kerr is now serving as general manager of the Berwind-White Coal Mining Co. in Windber, Pa., thus moving up from his former post as general superintendent.

Daniel N. Klemme can be reached at the Hancock Oil Co. of California, 2828 Junipero, Long Beach, Calif.

R. P. Kinkel has resigned as manager of Buffalo Ankerite Gold Mines, Ltd., S. Porcupine, Ont.

Mack C. Lake has been appointed consulting engineer exclusively for the Oliver Iron Mining Co. and other U. S. Steel Corp. subsidiaries. He will deal largely with the company's ore developments in foreign fields.

Stanley Lefond is working for the Mene Grande Oil Co., Apartado 234, Maracaibo, Venezuela.

W. D. Lowry, until recently a geologist with The Texas Co. in California, has joined the staff of Virginia Polytechnic Institute, Blacksburg, Va., as associate professor of geology.

Robert C. McCain is working for the Frontier Refining Co. as an assistant geologist. Mail reaches him at Box 574, Durango, Colo.

I. H. McLean has taken up an appointment as a mining engineer in India and is addressed care of Agent, Central Provinces Manganese Ore Co., Nagpur, C.P., India.

Morris M. Menzies received his degree in geological engineering from the University of British Columbia, Vancouver, last spring, worked as a junior geologist for the Hudson Bay Mining and Smelting Co., and returned to Vancouver for postgraduate work this fall.

Paul Klempner

Paul Klempner and his wife recently arrived from Johannesburg, South Africa, for an extended tour of the United States. Mr. Klempner is a consulting engineer and just prior to his departure from South Africa he designed and supervised the erection of an asbestos plant and completed a number of surveys including reports on manganese, chromium, tungsten, and gold deposits.

Charles S. Merriam has been appointed head of the Solid Fuels Branch of the Mining and Geology Division, Natural Resources Section, SCAP, replacing **Daniel J. Carroll,** who has been transferred to the Economic and Scientific Section of SCAP as supervisor of coal production. The two men will co-ordinate the efforts of the two sections to keep coal production up, as well as to improve coal cleaning and preparation, use of mechanical equipment so far as is possible and to better utilization in Japan.

Pomeroy C. Merrill has left his post with the Eastern Mining and Metals Co. in Malaya. An attack of pneumonia forced him to take the first boat back to the States. **Robert E. Tally, Jr.,** has taken over his job.

Hugh D. Miser, of the U. S. Geological Survey, nationally known expert on petroleum geology, received the degree of Doctor of Laws at the 75th commencement of the University of Arkansas. The citation read: "your devotion to science and your high standards of scholarship and research have been a constant source of inspiration. You have explored many unknown paths of knowledge."

James W. Morgan became vice-president and general manager of the Ayrshire Collieries Corp. on Sept. 1. Connected with the coal industry since he graduated from Lehigh in 1921, he worked for C. A. Hughes & Co. until accepting the post of assistant to the vice-president in charge of operations of Truax-Traer's Eastern mines in 1948.

Alexander R. Mutch, formerly a student at Otago School of Mines, has the job of assistant geologist on a coal survey with the New Zealand Geological Survey, Balclutha, N. Z.

E. N. Pennebaker expects to be in South Africa until the end of the year reviewing geological and exploration problems for the O'okiep Copper Co.

J. S. Peterson and his wife are on a round-the-world pleasure trip and will spend the remainder of the year in the States on business and vacation. Mr. Peterson is vice-president and assistant general manager of the Benguet Consolidated Mining Co., Baguio, P. I.

R. E. O'Brien, who had been with the Mountain City Copper Co., is working for the Anaconda Copper Mining Co. at Conda, Idaho.

H. Gordon Poole, who had a year's leave of absence from his post as professor of mining engineering at the University of Washington, is returning from Mexico City where he was attached to the American Embassy as a mining and metallurgical consultant of the Bureau of Mines to the Mexican Government.

H. N. Propp has been made assistant district manager, central territory, crusher and process machinery division, Nordberg Mfg. Co. He has transferred to Milwaukee, Wis., from the San Francisco district office where he served as sales engineer for the past year.

Norman Phillips recently joined the chemical laboratory staff of the research and development department of the Babcock & Wilcox Co. in Alliance, Ohio.

James Quigley has completed a month's study of the Marysvale, Utah, uranium district for the Centennial Development Co. **Harold B. Spencer** is president of Centennial and is in charge of the Company's shaft sinking and tunnel driving activities.

P. H. Reagan, consulting mining engineer of Hye, Texas, returned from Nicaragua and has gone to Western Australia. He expects to return to his office in December.

Robert St. Clair is employed by the Carnegie-Illinois Steel Co. at their

Ohio district works as a process engineer.

Raymond E. Salvati, operating vice-president of the Island Creek Coal Co., was elected president of the Boston, Mass., Company at the June meeting of the board.

H. Sano, who retired as professor of the College of Engineering at Tokyo Imperial University to act as director of the Coal Board, is now Emeritus Professor at the University. As director of the Coal Board he endeavored to increase coal production in Japan in co-operation with officials of the Allied Powers, among whom he found many AIME members.

Hans H. Schou can be reached at the Frontino Gold Mines, Ltd., Segovia, Antioquia, Colombia.

George P. Schubert, since the closing of the Copper Range Smelter, has taken over as professor in charge of shops and drawing at Michigan College of Mining and Technology.

Munshi Lal Sethi has been minerals adviser to the Government of Jaipur since February. Eighteen different Indian States have formed the new province of United States of Rajasthan, covering an area of about 125,000 sq mi. In June Mr. Sethi received appointment as director of mines and geology to this new province in addition to his duties as minerals adviser.

Joseph G. Sevick graduated from the Missouri School of Mines in May and has become associated with the research department of the zinc division of the St. Joseph Lead Co., Monaca 7, Pa. He lives at 1200 Penn Ave., New Brighton, Pa.

A. Ben Shallit has been appointed superintendent of Carbonate Mines, Inc., Bald Butte, Mont.

James C. Shields, II, since last November has been doing geological field work in Cuba, practically all in Oriente Province. He is resident geologist for Geological Engineering Consultants (Cuba), Inc., in Havana.

Carl W. Sinclair retired from the staff of John A. Roebling's Sons Co. on July 1. He can be reached now at the Galigher Co., 545 W. 8th S., Salt Lake City 8.

L. E. Sinclair has resigned from Mount Isa Mines, Ltd., to go to New Caledonia, where he will be in charge of Establissement Baelande's mining interests in that island.

James T. Smith, who had been studying at the University of British Columbia, can be reached in care of Roan Antelope Copper Mines, 64 East Rand, Luanshya, N. Rhodesia.

Francis B. Speaker has transferred to the New York City office of Hewitt-Robins, Inc. As field engineer he will work out of the New York office for both Robins conveyors division and Hewitt rubber division.

Carsten Steffens has resigned as assistant director of Stanford Research Institute to take the post of associate professor of chemistry at the University of New Mexico in Albuquerque.

A. George Stern, former chief of the western research division of the Westvaco Chlorine Products Corp., is Pacific Coast manager of the Heyden Chemical Corp., San Francisco. His home address is 764 Forest Ave., Palo Alto, Calif.

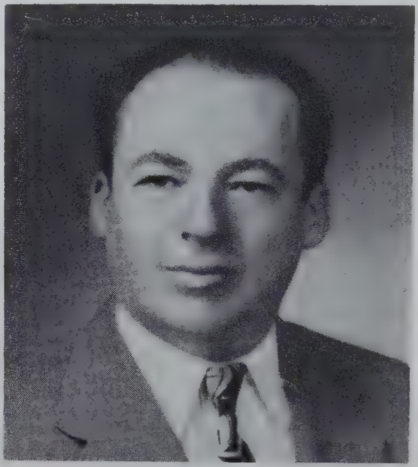

Edward M. Thomas

Edward M. Thomas heads the Bureau of Mines newly established roof-control section of the health and safety division; the section will further the attack on the No. 1 killer in the nation's coal mines, falling rock and coal. While a major project of the new section is the adaptation of suspension roof support to more general use in mining, it will attack all phases of the roof-control problem through education, investigation, and research.

John K. Stewart is an engineer in training with Hollinger Consolidated Gold Mines Ltd., Timmins, Ont. His address in Timmins is 11 James Ave.

H. W. Straley, III, consulting geological and geophysical engineer, after spending a year in eastern Oklahoma has moved his office from Friendship Station, D. C., to Box 68, Princeton, W. Va. Temporarily he may be reached at 1459 Cameron Terrace, Drury Hills, Atlanta, Ga.

H. S. Taylor, who has been general counsel and vice-president in charge of mining operations, is the new president of the 95-year old iron ore, coal, and lake shipping concern, Oglebay, Norton and Co. Mr. Taylor was engaged in law practice for several years before joining the Company and is active now in many associations.

Alberto J. Terrones L., after spending a 4½ month leave in Mexico visiting operations there, returned to the Cerro de Pasco Copper Co. and his new job of geologist of the Cerro de Pasco division.

Gustave W. Voelzel and his wife made a six week trip this summer through Canada and New England. They visited AIME headquarters in New York City and returned to El Paso, Texas, by way of Niagara Falls.

J. K. Whatmough was appointed mine manager of Starratt Olsen Gold Mines, Ltd., Madsen, Ont., on June 1.

J. A. Willcox has a job with the Polaris-Taku Mining Co. in Tulsequah, B. C.

Alexander N. Winchell, after an interesting year as visiting professor of geology at the University of Virginia, has returned to his home at 88 Vineyard Rd., New Haven, Conn., where he will resume his editorial and consulting work in the field of mineralogy and crystallography.

P. F. Yopes is employed as a mining engineer with the safety division of the Bureau of Mines, working out of the Seattle office.

—In the Metals Branch—

Edgar C. Bain, vice-president in charge of research and technology at the Carnegie-Illinois Steel Co., will have two medal-receiving days in October. On the 19th he will get the John Price, Wetherill Medal of the Franklin Institute of the State of Pennsylvania, awarded for discovery or invention in the physical sciences or for new and important combinations of principles or methods already known. On Oct. 20 he will receive the Gold Medal of the ASM (see September Personals).

C. G. Benson, who has been with General Electric since graduation from Harvard, helped set up the Company's new plant in Brockport, N. Y. The major portion of his work has been in manufacturing methods and plant layout, with some specializing in plastic molding.

John O. Cartledge recently was promoted from the post of shift superintendent to assistant works metallurgist at the Port Pirie works of the Broken Hill Associated Smelters Pty. Ltd.

R. H. Covington has changed his address from the American Zinc Co. of Illinois, Dumas, Texas, to the

American Zinc Oxide Co., P. O. Box 327, Columbus 16, Ohio.

H. R. Dahlberg has left his post as assistant professor of industrial engineering at Oregon State and has joined the Twin City Testing and Engineering Laboratory as supervisor in the mechanical and metallurgical department in St. Paul, Minn.

Reginald S. Dean, metallurgical engineer and consultant of Washington, D. C., has moved his offices to 6000 34th Place, N.W., Washington 15. Dr. Dean is also president of R. S. Dean Laboratories, which has just moved into its own laboratory and office building at 5810 47th Ave., Riverdale, Md., just outside Washington.

Robert A. Eastman has the job of chemist at the Great Falls reduction works of the Anaconda Copper Mining Co. He can be reached at 821 3rd Ave. S.W., Great Falls, Mont.

John E. Gaus has left the ranks of metallurgists to enter the broader field of the entire mineral industries as curator of the Mineral Industries Museum at Penn State.

Robert E. Hagen is working in the research laboratory of the Oliver Iron Mining Co. in Duluth, Minn.

E. Hartshorne has transferred to New Haven, Conn., where he is assistant director of research and development for Winchester Repeating Arms Co., division of Olin Industries.

Robert H. Jacoby is chief metallurgist of the Key Co., 2700 McCasland Ave., East St. Louis, Ill.

T. G. Johnston, Jr., after receiving his degree in metallurgical engineering from Purdue in June, accepted the job of junior metallurgist in the metallurgical department of the National Tube Co. in Lorain, Ohio.

Jerome W. Kaufman, a recent Lehigh graduate, has a job as metallurgist at the Naval Air Material Station, Johnsville, Pa.

William C. Leslie, who has been a student at Ohio State, is working in the research laboratory of the U. S. Steel Corp. at Kearny, N. J.

Francis F. Lucas has retired from the Bell Telephone Laboratories. He can be reached at his home, 245 Rutledge Ave., East Orange, N. J.

N. E. Nilsen has been promoted to chief general manager of the Emperor, Loloma and Dolphin Mining Companies, with headquarters in Melbourne, Australia. Former general manager of the companies' properties at Vatukoula, Fiji, he will spend about half his time there.

Elliott S. Nachtman has been named instructor in metallurgical engineering at the Illinois Institute of Technology. He had served as a chemist for the Harshaw Chemical Co. and held a similar job with the Argonne National Laboratory.

Donald M. Liddell catches up with the news; the man behind him is unknown.

Donald M. Liddell returned to New York City in August after a 2½ months' professional trip to England and the Continent, which included participation in the Empire Mining and Metallurgical Congress.

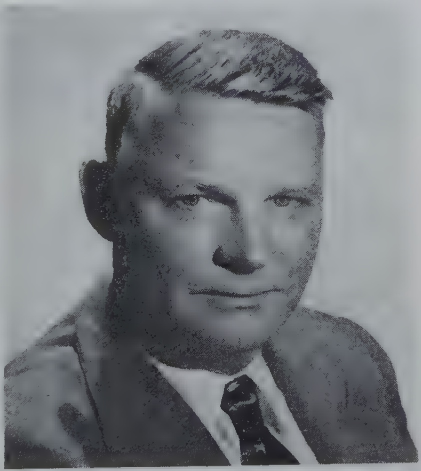

Eric G. Peterson

Eric G. Peterson has been appointed general manager of the Peabody Engineering Corp., New York City, and will continue as general sales manager of all the Company's products in all divisions. Already known as one of industry's leading designers of combustion equipment, Mr. Peterson's new duties will broaden his supervision and interest to include the activities and welfare of all the Peabody offices and subsidiaries throughout the world.

Fred D. Rosi, formerly at the Hammond Metallurgical Lab., Yale, is now reached at the Research Laboratories, Sylvania Center, Bayside, L. I., N. Y.

John W. Pugh is with the General Electric Co., Rm. 522, Bldg. 5, Schenectady, N. Y.

Waldemar P. Ruemmler has succeeded **G. E. Johnson** as manager of the East Chicago plant of the Eagle-Picher Co. He joined Eagle-Picher in 1948 and has been successively in charge of research and development, and acting superintendent at East Chicago. Prior to this affiliation he was associated with Battelle Memorial Institute.

Edgar Sengier, managing director and chairman of the executive committee of Union Miniere du Haut-Katanga, has been honored by the French Government with the order of Commander of the Legion of Honor. This high decoration, together with the U. S. Medal for Merit and the Commander of the British Empire previously conferred, are in recognition of the outstanding services rendered by Mr. Sengier during the war years to Belgium's three great allies.

Morris A. Steinberg has been made a member of the board of directors of Horizons, Inc., of Princeton, N. J., and Cleveland, Ohio. The war had interrupted his studies, but after receiving his doctorate in physical metallurgy in July of 1948 he joined Horizons, Inc., and in March 1949, was appointed head of the metallurgy division.

John E. Stukel, Jr., has joined the operating department of the Youngstown Sheet and Tube Co. as a development engineer. He was assistant professor at Carnegie Institute of Technology.

John M. Thomas, research associate at the University of Michigan, has a new address at 3147 Vassar St., Dearborn, Mich. He is metallurgical engineer with the Hoskins Mfg. Co., of Detroit.

George H. Thurston, formerly with American Smelting and Refining at Selby, Calif., is now metallurgist with the Hall-Scott motor division, ACF-Brill in Berkeley.

William V. Ward, who has been with the Division of Industrial Cooperation at MIT doing research work sponsored by the Atomic Energy Commission during the summer, plans this fall to enroll in the graduate school at MIT to start work towards the degree of science doctor in metallurgy. His wife and son accompanied him to Massachusetts from the University of Arizona with which he was connected in a student-instructor capacity. Their new address is 349 Westgate West, Cambridge, Mass.

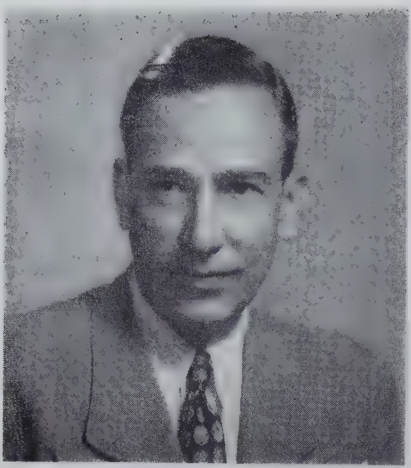

W. E. Mahin

W. E. Mahin, chairman of metals research at Armour Research Foundation of the Illinois Institute of Technology, has been named director of research. He heads a group of 411 scientists, engineers, and technicians who are working on 125 active research projects for industrial and government sponsors. For ten years previous to his joining the Research Foundation in 1947, Mr. Mahin was in charge of metallurgical engineering at the Westinghouse Electric Corp., Pittsburgh.

Ervin E. Underwood, after obtaining his B.S. degree in metallurgical engineering at Purdue, has moved to MIT for graduate work in their school of metallurgy.

B. H. Wadia has gone to Oroya, Peru, to work for the Cerro de Pasco Copper Co.

—In Petroleum Circles—

Roy F. Beery, Jr., formerly with the Shell Oil Co., has become division superintendent for the Danciger Oil and Refining Co., Norman, Okla.

George W. Burgess, junior exploitation engineer with the Shell Oil Co., can be reached in care of the Company, Box 488, Denver City, Texas.

Robert A. Coleman is a petroleum engineer trainee with the Gulf Oil Corp., with a mailing address at General Delivery, Kermit, Texas.

James Terry Duce is now residing in New York City, having moved from Washington, D. C., when executive offices of the Arabian American Oil Co., of which he is a vice-president, were established in the former city.

Thomas M. Esmond, who graduated from Texas Tech with a B.S. degree in petroleum geology last May, is employed by R. C. Lipscomb Oil Producer in San Antonio, Texas, as a geologist.

Martin Felsenthal joined the Continental Oil Co at Ponca City, Okla., on Aug. 1, to work as research engineer in the production laboratory of the Company's research and development department. Recently he received his M.S. degree in petroleum engineering from Penn State.

Lester S. Grant went into full retirement as vice-president of the Franco Wyoming Oil Co. and vice-president and manager of McElroy Ranch Co. on June 1. In July he and Mrs. Grant made a three week pleasure trip to Alaska and expect to attend the 75th anniversary of the Colorado School of Mines. He can be reached care of McElroy Ranch Co., Box 912, Midland, Texas.

Diego Henao-Lindoño is with the Servicio Geológico Nacional de Colombia, Bogota, as a geologist.

Herbert A. Koch

Herbert A. Koch, general sales engineer for Dowell Incorporated in Tulsa, has been appointed head of the Fort Worth, Texas, office. Sales co-ordinator in the Fort Worth-Dallas area, he will have special responsibilities throughout Texas, Louisiana, and New Mexico. An alumnus of the University of Oklahoma, Mr. Koch has been with Dowell since 1944 and has received special training with the Company in electric pilot services.

Bart W. Gillespie is general manager for the Mexican American Independent Co., Reforma No. 1, Despacho 204, Mexico, D.F., Mexico.

William R. Goodier, formerly associated with the Shell Oil Co. in Great Bend, Kans., is now employed by the Barnsdall Oil Co., Newhall, Calif., as a petroleum engineer.

J. T. Holten, Jr., recent graduate of the University of Oklahoma, is working as an engineer for the Mid-Continent Petroleum Corp., Seminole, Okla.

M. King Hubbert, associate director of research of the Shell Oil Co. exploration and production research laboratory, served as a U. S. delegate to the United Nations Scientific Conference on Conservation and Utilization of Resources held at Lake Success, N. Y., Aug. 17 to Sept. 6.

Robert K. James is working at Eunice, N. Mex., as a petroleum engineer trainee with the Magnolia Petroleum Co.

Howard F. Johnston, district geologist for the Quaker State Oil Refining Corp., has been transferred from Newark, Ohio, to the newly opened production offices at Parkersburg, W. Va.

Paul S. Johnston has taken the post of professor of petroleum engineering at Texas Technological College, Lubbock, Texas.

Norris Johnston has been named president of the consulting firm Petroleum Technologists, Inc., in Montebello, Calif. For the past ten years he had been chief physicist in charge of production research for the General Petroleum Corp. During this period he was assigned to Socony-Vacuum to set up their Dallas production research laboratories.

Gordon H. White recently resigned from the Shell Oil Co. to join the ranks of the independent operators. He has incorporated his own company under the name of the Niles Oil Co., with headquarters at 1406 M & W Tower Bldg., Dallas, Texas. His work with Shell had taken him to many of the oil producing areas of this country; in 1938 he was sent to the Hague, Holland, returning to the Houston office in mid-1939.

Gordon H. White

Eugene L. Davis, formerly general production superintendent for the Signal Oil and Gas Co., Los Angeles, has accepted the post of project manager of the Arctic Contractors,

Eugene L. Davis

Fairbanks, Alaska. The Arctic Contractors, under contract to the Navy, are conducting oil exploration activities in Naval Petroleum Reserve No. 4, Point Barrow, Alaska.

M. C. Leverett joined the NEPA (nuclear energy for the propulsion of aircraft) project at Oak Ridge, Tenn., as its technical director in June. The NEPA project is a division of the Fairchild Engine and Aircraft Corp. and its work is under the U. S. Air Forces. Mr. Leverett was formerly research associate with the Humble Oil and Refining Co.

Arthur Maddox has been transferred from the International Petroleum Co., Barcelona, Venezuela, to the Carter Oil Co. in Tulsa, Okla.

Melford F. Rabalais has changed his mailing address to Kerr-McGee Oil Industries, Inc., Sunray, Texas.

Glenn Nelle has joined the General Petroleum Corp. as assistant manager of Rocky Mountain operations. Mr. Nelle had been in Venezuela with Socony-Vacuum.

E. E. Rehn has announced his resignation as division geologist of the Western Division of the Sohio Petroleum Co., and is returning to Evansville, Ind., to open consulting geological offices at 308 Grein Bldg.

Bruce H. Sage, professor of chemical engineering at California Institute of Technology, was given the new $1,000 Precision Scientific Co. award in petroleum chemistry at the recent national meeting of the American Chemical Society. He is credited with having significantly enlarged the recoverable natural oil resources of the country during his nineteen years of research.

N. van Wingen, professor of petroleum engineering of the University of Oklahoma, has resigned to join, as vice-president, the consulting firm, Petroleum Technologists, Inc., in Montebello, Calif. Prior to joining the University staff, he had been associated for nine years with the Richfield Oil Corp.

Herbert N. Wade is with The Texas Co. in Buckeye, N. Mex., as an engineer trainee.

Theodore G. Ward, Jr., has taken the job of junior engineer with the Atlantic Refining Co., Dallas, Texas.

David B. Wilke, Jr., after graduation from the University of Kansas with a B.S. degree in petroleum engineering, was employed by the Skelly Oil Co. He is working in their New Mexico district and can be reached at Drawer D, Hobbs, N. Mex.

Walter L. Williams is an engineer trainee with American Republics Corp., Silsbee, Texas. His address there is P. O. Box 451.

Obituaries

Charles Worth Fowler, Jr. (Member 1942), president of United Oilwell Service, Caracas, Venezuela, died Sept. 30, 1948. He was 49 years old. Most of Mr. Fowler's career was spent in Mexico and South America; he had been with the Mexican Gulf Oil Co., Yacimientos Petroliferos Fiscales, Argentina, and the Pantepec Oil Co. of Venezuela. He was also a junior member of Brokaw, Dix, Garner & McKee.

Charles W. Fowler, Jr.

Paul Armitage (Member 1918), noted corporation lawyer and an expert in taxation practice, died on June 28. Mr. Armitage was a member of the law firm of Armitage and Holloway in New York City, which firm had been counsel to the Woolworth Estates, the United Verde Extension Mining Co., the G. R. Kinney Co., to name but a few. Mr. Armitage graduated from Columbia University in 1894 and from Columbia's Law School two years later. He was admitted to the bar in the same year, and, in 1905, admitted to practice before the U. S. Supreme Court.

Mr. Armitage, a champion figure skater in his youth, was a founder of the New York Skating Club. He was also a member of the Academy of Political Science, the American Bar Association, and a director of a number of firms.

Percy A. E. Armstrong (Member 1924), a leader in the development of stainless steel, died on Aug. 7 after a long illness. Born and educated in England, he came to this country 30 years ago. Nationally recognized for his work in metallurgy, he was an early developer of stainless steel and held more than 100 patents on steel alloys. Mr. Armstrong was a vice-president and general manager of the Allegheny Ludlum Steel Co.

William Albert Baueris (Member 1936), mining engineer of Seattle, Wash., died on Feb. 23 at the age of 65. Mr. Baueris had a long and varied career in exploration, mining, construction, and manufacturing. It began in 1900 when he worked for five years as a structural draftsman and field superintendent for the Chicago Bridge and Iron Works. In 1909, he graduated from the Missouri School of Mines, did some geological reconnaissance, worked in the Homestake mine for a year, and then spent twelve years with the Puget Sound Bridge & Dredging Co. in Seattle. From 1922 to 1925 his were various activities associated with gold mining, and 1936 found him examining Bonanza Creek and Ungalik River deposits in the Norton Sound area of Alaska. Later, he headed the Ungalik Syndicate, finally retiring in 1942.

William Bell (Member 1936), of Robinson, Ill., is dead. Mr. Bell, who was born in Franklin, Pa., on Aug. 29, 1874, had been an independent owner and operator of oil producing properties in Pennsylvania, West Virginia, Indiana, and Illinois, for the past 50 years.

Necrology

Date Elected	Name	Date of Death
1897	Thomas J. Barbour	Unknown
1914	Z. T. Crittenden	March 25, 1949
1946	Henry Davenport	Unknown
1933	Carl Erickson	June 28, 1949
1919	Charles T. Evans	May 13, 1949
1938	Dwight H. Fortine	Aug. 3, 1949
1944	Russell J. Parker	Sept. 9, 1949
1928	R. C. Patterson	April 3, 1949
1920	E. T. Stannard	Sept. 9, 1949
1926	Arthur D. Storke	Sept. 9, 1949
1939	W. W. Taylor	Unknown
1920	C. Erb Wuensch	Aug. 27, 1949

Walter Frederic Bart Berger (Member 1907), died on June 6. Born in Denver in 1877, he attended the Colorado School of Mines for a year after graduating from Yale. He spent some time in Japan for the Chipman Chemical Co. and upon his return opened an office in New York City. He later moved to Denver to form the partnership of Berger & Sayre, mining engineers, and subsequently practiced independently. In recent years his home was in Victoria, B. C.

Walton Ambrose Bishop (Member 1945), died on June 10. He was 73 years old. Mr. Bishop had been with the Pocahontas Fuel Co., in Pocahontas, Va., for the past 43 years, and when he died, was the firm's chief engineer. Mr. Bishop was born in Snowville, Va., and was familiar with "Snowville wood, iron, steel, textile and grain mill machinery, from childhood." He was, for two years, operating engineer for the Radford Light and Power Co., then worked as an electrical engineer with the Virginia Iron Coal and Coke Co. before joining Pocahontas, in 1901.

Thomas Clark Botterill (Member 1942), died on June 15, at the age of 56. Mr. Botterill was a Canadian citizen although he was born at Rock Springs, Wyo. He pursued various studies in civil and mining engineering, and began his career as a draftsman in 1907. The next 25 years found him working as an engineer or superintendent on 12 different Canadian mining properties, including the Brittania Mining and Smelting Co., the Pacific Construction Co. In 1932 he formed his own consulting business, and from 1932 until his death his activities included both consulting and management work for numerous firms in British Columbia. His last position was managing director for the Hedley-Monarch Gold Mines in Vancouver.

John R. Comstock (Member 1920), general superintendent of the Pittsburgh Coke & Chemical Co. since Dec. 20, 1943, died suddenly July 14, 1949, at the Neville Island plant of the Company.

Mr. Comstock's outstanding personality and long association in the Merchant Blast Furnace field had given him a host of admiring friends and a national reputation in blast furnace operation.

A graduate of Stevens Institute of Technology in 1911 with a mechanical engineering degree, Mr. Comstock started his steel experience with the Pennsylvania Steel Co. at Steelton, where he became assistant superintendent of blast furnaces. In 1921 he was made assistant general manager of the Hanna Furnace Co. at Cleveland, and served in that capacity until 1931. In 1933 he was appointed general superintendent of the Globe Iron Co. at Jackson, Ohio, until 1943 when he became associated with the Pittsburgh Coke & Chemical Co. He was 58 years old at the time of his death.

George Bradstreet Dodge (Member 1939), vice-president of the American Rubber Mfg. Co., San Francisco, died in 1948. Born in Waukeegan, Ill., in 1880, he held various posts in the East and in 1906 became vice-president of the Western Belting Hose Co., the Lightning Hose Rack Co. and American Rubber, which later absorbed Western and Lightning.

Louis W. Huber

Louis W. Huber (Member 1937), vice-president of the National Mine Service Co., died Aug. 17, 1949. The suddenness of his death was a distinct shock to his many friends and associates in many mining fields of the country.

Born in Paris, Ill., May 13, 1899, his mining experience began early in life when he was but 15 years of age. He did everything there was to do in the underground operation of a coal mine from trapping and driving mule, on through coal loading, timbering, undercutting, electrical and mechanical repairs, maintenance, to face bossing in order to pay his own way through high school and college. All this practical underground work stood him in good stead later in life.

For two years after graduating from the University of Illinois in mining engineering in 1921, Mr. Huber was engaged in research work on mine ventilation and part-time teaching at his Alma Mater. Then he took the job of mine ventilation engineer in the Midwest for the B. F. Sturtevant Co. The fall of 1924, he joined the faculty of Carnegie Institute of Technology to teach mining engineering in the department of mining and metallurgy.

Four years later he became associated with Mine Safety Appliances Co. as sales representative in Cincinnati, Ohio, and steadily progressed in his work and responsibilities to become district manager. His service with this company extended over a period of 20 years, from 1928 to 1948.

On May 1, 1948, Mr. Huber was elected vice-president of National Mine Service Co. in charge of its two divisions in Kentucky, and all field operations and representatives in the states of Kentucky, Tennessee, Illinois, and Indiana. His home and headquarters for many years were in Lexington, Ky.

A foremost authority on mine ventilation, his services as a consultant were widely sought. In safety work, he served untiringly, and he was known throughout the country for his active participation and leadership in rescue work following many mine disasters.

Tore Flygare (Member 1947), Swedish mining engineer, died in November, 1947. Mr. Flygare, who had an E.M. degree from the Royal University of Technology in Stockholm, had been with Philippine Iron Mines for four years. In 1941 he joined the International Engineering Corp. in Manila, and at the time of his death was working with the Boliden Mining Co. in Boliden, Sweden.

Emil Gathmann (Member 1913), president of the Gathmann Engineering Co., the Gathmann Research Laboratories, Cantonsville, Baltimore, Md., former head of the Bethlehem Steel Company's ordnance department, inventor of note, died on Aug. 23. Holder of more than 100 patents for various types of metal he developed, he had invented a type of depth bomb to be used against submarines; many of his patents related to naval ordnance, particularly for fuses. A native of Chicago, where he was born in 1874, Mr. Gathmann went to Baltimore in 1909 after starting an engineering firm in New York.

Virgil O. Harris (Member 1943) is dead. Born at Bison, Okla., in 1907, he took his B. S. degree from Oklahoma University. Following graduation he joined the staff of the Humble Oil and Refining Co., with which he was associated at the time of his death.

Joseph Samuel Henry (Member 1918), mining engineer of Castlemaine, Vic., Australia, died on March 26. He was 73 years old at the time of his death. He received his technical education in Australia, at the Technical College of Geelong in Victoria, worked for a time in London, and then was engaged in tin dredging operations in Siam and Australia. In recent years, before his retirement, he was a consulting engineer to the Austral Malay group and other companies "down under."

William D. Mark

An Appreciation By W. W. LYTZEN

William D. Mark (Member 1928), aged 44, mining engineer for the RFC, died suddenly of a heart attack on June 16 at his home in Chevy Chase, Md.

Bill joined the geological department of the Anaconda Copper Mining Co. at Butte, after graduating from the Idaho School of Mines, and in 1933 went to South America with the Cerro de Pasco Copper Co. as a geologist. Upon his return to this country he joined the RFC as field representative in Boise, Idaho, and Spokane, Washington, and for the past 13 years has been with the Washington Office of that Corporation.

Bill Mark was highly regarded, not only for his great personal integrity, but also for his integrity and ability in his profession. His sudden death came as a shock to his associates and many friends.

Walter Miller (Member 1918), of Ponca City, Okla., is dead. Mr. Miller was a vice-president of the Continental Oil Co. in that city. Born in Switzerland in 1881, Mr. Miller had little formal education and worked, until 1909, as a machine hand, blacksmith's helper, bookkeeper, and cost accountant, at which time he joined the Tidewater Oil Co. in Bayonne, N. J. He began there as a clerk, and within eight years had advanced to process superintendent. In 1919 he became a consulting refining engineer in Tulsa, and two years later joined the Marland Refining Co. in Ponca City, as manager of manufacturing. In 1930 he went with Continental Oil.

Clarence J. Peterson (Member 1916), died on May 8. Born in Honolulu, T. H., in 1885, Mr. Peterson received an A.B. degree in geology and mining from Leland Stanford Junior University in 1910, and spent the first six years of his career doing exploration work in Venezuela for the Bermudez Co. of Trinidad, and as an examining mining engineer for the Tonopah Mining Co. in Nevada. He then served as a geologist with such firms as the Empire Gas and Fuel Co. and the Cities Service Gas Co. until 1930, when he joined the Texoma Natural Gas Co. in Amarillo, Texas, as chief geologist. He held this position at the time of his death.

Victor H. Wilhelm (Member 1921), Captain USNR, died at the Long Beach Naval Hospital on July 7 after an illness of several months. He was 63 years of age, graduated as a geologist and mining engineer from Stanford University in 1907, and followed mining and oil all of his life. After some years spent in all of the western states, Mexico, Canada, and Alaska, he settled down in California and was one of the early petroleum engineers of the State, being well known as an engineer and deputy supervisor with the California State, Division of Oil and Gas, then known as the State Mining Bureau. He became chief petroleum engineer of the Old Petroleum Midway and California Petroleum Companies and continued as such when those companies became The Texas Co. He will be remembered by a host of friends as the sage of the local petroleum industry and for his friendliness, advice, and counsel given particularly to young geologists and engineers.

Victor H. Wilhelm

In February of 1941 he was called to active duty as Lieutenant Commander in the Naval Reserve in the Office of Inspector Naval Petroleum Reserves in California and rose to the rank of Captain. He remained on active duty at the close of the war and has been the Inspector of Naval Petroleum Reserves in California since 1944.

E. A. Cappelen Smith (Member 1904), noted expert on metal refining, and consulting metallurgical engineer with Guggenheim Brothers in New York City, died on June 25 at the age of 75. Mr. Smith originated the Guggenheim method of extracting nitrate from caliche, and an extraction process used at the Chiquicamata plant of the Chile Exploration Co. His development of a method of basic copper converting was instrumental in revolutionizing the copper-smelting industry.

Born in Trondheim, Norway, he graduated from the Technical College of Trondheim and came to the United States in 1893. He became a chemist for the Chicago Copper Refining Co., later served as superintendent of Anaconda's electrolytic copper refinery, metallurgical engineer for the Baltimore Copper Smelting and Rolling Co., and a consultant with ASARCO in New York. He joined the Guggenheim brothers in 1912. From 1925 to 1931 he served as president of the Anglo Chilean Nitrate Corp., managing 62 per cent of all Chilean nitrate production.

Mr. Smith was a director of the Chile Copper Co., and the Chile Exploration Co. He held patents on processes used in the development of selenium, tellurium, platinum, and palladium from electrolytic copper refining slimes. His distinguished work in hydrometallurgy earned for him the gold medal of the Mining and Metallurgical Society of America in 1920, the Norwegian decoration of Knight Commander with Star of the Order of St. Olaf, and Chile's highest civilian honor, Knight Commander of the Order "Al Merito."

Proposed for Membership

Total AIME membership on Aug. 31, 1949, was 15,870; in addition 4424 Student Associates were enrolled.

ADMISSIONS COMMITTEE

James L. Head, Chairman; Albert J. Phillips, Vice-Chairman; George B. Corless, T. B. Counselman, Ivan A. Given, Robert L. Hallett, Richard D. Mollison, and John Sherman.

Institute members are urged to review this list as soon as the issue is received and immediately to wire the Secretary's office, night message collect, if objection is offered to the admission of any applicant. Details of the objection should follow by air mail. The Institute desires to extend its privileges to every person to whom it can be of service but does not desire to admit persons unless they are qualified.

In the following list C/S means change of status; R, reinstatement; M, Member; J, Junior Member; AM, Associate Member; S, Student Associate; F, Junior Foreign Affiliate.

ALABAMA

Birmingham—DONOHO. CHARLES KERR. (C/S—J-M). Chief metallurgist, American Cast Iron Pipe Co.

ARIZONA

Hayden—ELROD, SAM D. (C/S—S-J). Junior engineer, Kennecott Copper Corp.

Superior—PELLETIER, JOHN DAVID. (R, C/S—S-J). Geologist, Magma Copper Co.

Tucson — MARVIN, THOMAS CROCKETT. (C/S—J-M).

ARKANSAS

Fayetteville—MATTHAEI, RICHARD. (C/S—J-M). General superintendent, Corona Silica Corp.

Malvern—SACKETT, EARL L. H. (C/S—J-M). Assistant division metallurgist, Baroid sales division, National Lead Co.

CALIFORNIA

Berkeley—SMITH, EMORY. (M). Supervising engineer, California State Division, Industrial Safety.

Chino—SHAFER, ROBERT ROY. (C/S—S-J). Engineer in training, Stanolind Oil and Gas Co.

Long Beach—O'NEILL, DONALD BAILEY. (C/S—S-J). Engineer trainee, Shell Oil Co.

Los Angeles—CROG, RICHARD STANLEY. (C/S—J-M). Research group leader, Union Oil Co. of California. HAYASE, MASASHI. (C/S—S-J). STERLING, MORTON ALAN. (C/S—S-J). Petroleum engineer, Eagle Oil and Refining Co.

North Hollywood—CABEEN, WILLIAM ROSS. (C/S—J-M). Owner, William Ross Cabeen and Associates.

Ojai — McENTEE, JAMES ROBERT. (C/S—J-M). Senior mechanical engineer, Shell Oil Co.

San Francisco—GRAY, EDWARD GORDON. (C/S—AM-M). Project engineer, Goldfield Consolidated Mines. VER PLANCK, WILLIAM EVERETT, JR. (C/S—J-AM). Junior mining geologist, California Division of Mines.

San Marino — HOPKINS, JOHN. (M). District manager, Kobe, Inc.

COLORADO

Climax — FROHLING, EDWARD SEBASTIAN. (C/S—S-J). Metallurgical testing engineer, Climax Molybdenum Co.

Denver—BAKER, CROSBY FRED, JR. (C/S—J-M). Chief chemist and metallurgist, American Smelting and Refining Co.

Ouray—GRIGSBY, HARRY GORDON. (C/S—S-M). Mill operator, Idarado Mining Co.

Sargents — DUNN, JAMES EDWARD. (C/S—J-M). Superintendent, Callahan Zinc-Lead Co.

Silverton — ARCHIBALD, JOHN ELLIS. (M). Partner and mine manager, Lead Carbonate Mines, Inc.

CONNECTICUT

Milford—SNYDER, JOHN ALDEN. (C/S—J-M). Research metallurgist, Remington Arms Co.

GEORGIA

Atlanta—COFER, HARLAND ELBERT, JR. (C/S—S-J). Teacher, Emory University.

IDAHO

Burke—POWERS, PHILIP PHINEAS. (C/S—S-AM). Surveyor, Hecla Mining Co.

Kellogg—HARDY, ROBERT MONROE. (AM). Assistant treasurer, Sunshine Mining Co.

ILLINOIS

Berwyn — HRADECKY, FRANK JOSEPH. (M). Chief draftsman, Open Hearth Combustion Co.

Brookfield — GRAY, VERNON MAX. (C/S—S-AM). Cast-house metallurgist, Reynolds Metals Co.

Chicago—HATCH, GERALD GORDON. (C/S—S-J). Research metallurgist, Armour Research Foundation.

Clarendon Hills—DUNN, RAY P. (C/S—J-M). Plant metallurgist, Doehler-Jarvis Corp.

Evanston—ANDERSON, WALTER WILLARD. (R, C/S—JA-M). Technical director, Western Division, Commercial Testing and Engineering Co.

Mt. Vernon—POMEROY, CHESTER MITCHELL. (C/S—J-M). Technical representative, explosives, E. I. du Pont de Nemours and Co.

INDIANA

Evansville — INGLE, WILLIAM DAVIDSON, JR. (C/S—J-AM). Combustion engineer, Ingle Coal Corp.

Gary — NAULT, WILLIAM ALFRED. (C/S—J-M). Metallurgist, Carnegie-Illinois Steel Corp.

Whiting—GRAVES, DONALD B. (C/S—J-M). Physical metallurgist, Federated Metals division, American Smelting and Refining Co.

KANSAS

Baxter Springs—HOCKER, RICHARD LESLIE. (C/S—S-J). Field engineer, Amerada Petroleum Corp.

Belleville—ARROWSMITH, MURRAY REX. (C/S—S-J). Mining geologist.

Burden—MORRIS, SAM J., JR. (C/S—S-J). Area engineer, The Texas Co.

Eureka — ARNOLD, EDWIN S. (C/S—J-M). Assistant district superintendent, Phillips Petroleum Co. WITHERSPOON, PAUL ADAMS, JR. (C/S—J-M). Reservoir engineer, Phillips Petroleum Co.

Gorham—EHLERS, PETER LEE. (J). Junior petroleum engineer, Stanolind Oil and Gas Co.

Independence — LEE, THOMAS WILLIAM. (M). Production superintendent, Union Gas System, Inc.

KENTUCKY

Lexington — ROLL, WILLIAM HAYDEN. (M). Mining engineer, Department of Mines and Minerals, Commonwealth of Kentucky.

Wheelwright—KURTYKA, JOHN CHESTER. (R, C/S—S-M). Engineer, Inland Steel Co.

LOUISIANA

Hackberry — SIMPSON, JOHN MILTON. (C/S—S-J). Petroleum engineer, Stanolind Oil and Gas Co.

New Orleans — GRAHAM, WILLIAM JOSEPH. (C/S—S-J). Petroleum engineer trainee, The Texas Co.

MARYLAND

Baltimore—HAYES, SELDEN C. (C/S—J-M). Superintendent, heat treating and pickling, rustless division, Armco Steel Corp.

MASSACHUSETTS

Waltham—CLEVENGER, GALEN WILLIAM. (C/S—J-M). Senior metallurgist, Division of Industrial Co-operation, MIT.

MICHIGAN

Ann Arbor—LANDES, KENNETH KNIGHT. (R, C/S—JA-M). Chairman, department of geology, University of Michigan.

Detroit — KLAPKA, KARL JEROME. (C/S—J-M). Field engineer, Wheel Trueing Tool Co.

Ishpeming—AHL, WAYNE JOHN. (C/S—S-J). Mining engineer, Inland Steel Co.

MINNESOTA

Duluth — WILLIAMS, MILTON FRIEL, JR. (C/S—J-M). Associate chemical engineer, Oliver Iron Mining Co.

Hibbing—SMITH, DAVID POST. (C/S—S-J). Mining engineer trainee, Oliver Iron Mining Co.

MISSISSIPPI

Durant—MOORE, JOHN P. (C/S—S-J). Junior exploitation engineer, Shell Oil Co.

MISSOURI

Flat River—MARR, CHARLES A. (C/S—S-J). Mining engineer, St. Joseph Lead Co.

NEW MEXICO

Albuquerque — GRISWOLD, GILBERT RIPLEY. (C/S—J-M). Mining engineer, George W. Potter.

Fierro—YOUNG, THOMAS WESLEY. (C/S—J-M). Foreman, U. S. Smelting Refining and Mining Co.

Los Alamos—CAMPBELL, GILBERT LEWIS. (C/S—J-AM). Project librarian, Los Alamos Scientific Laboratory. TIPTON, CLYDE RAYMOND, JR. (C/S—J-M). Physical metallurgist, University of California, Los Alamos Scientific Laboratory.

Monument — BRAKEY, ROBERT JAMES, JR. (C/S—S-J). Field engineer, Amerada Petroleum Corp.

Silver City — RICHMOND, KENNETH CLYDE. (R, C/S—S-M). Engineer-contractor, self-employed.

Vanadium—GLADSTONE, IRVIN. (C/S—J-M). Chief geologist, Bayard division, U. S. Smelting Refining and Mining Co.

NEW JERSEY

Morristown—FINE, MORRIS EUGENE. (C/S—J-M). Member, technical staff, Bell Telephone Laboratories.

Westfield — DAHLSTROM, ROY. (M). Technical director, Titanium division, National Lead Co. LAGERGREN, MILTON ANDY. (C/S—J-M). Design engineer, American Smelting and Refining Co.

NEW YORK

Bayside—RUBENSTEIN, HENRY S. (C/S—S-J). Research engineer, Sylvania Electric Products, Inc.

Brooklyn — MITILINEOS, JOHN DIMITRIOS. (C/S—S-J). Metallurgical engineer, American Platinum Works.

Flushing — ARNAUT, ARNOLD DOUGLAS. (C/S—S-J). Junior engineer, Sylvania Electric Products, Inc.

Hicksville — RACEK, EDWARD WILLIAM. (C/S—S-J). Petroleum engineer, Acme Well Supply Co.

Lewiston—EVANS, FRED LEROY. (C/S—J-M). Plant superintendent, U. S. Vanadium Corp.

Long Island City — LUTTER, FRANK WILLIAM. (C/S—S-AM). Service engineer, Hardinge Co.

New York—CAMPBELL, JOHN BARDO. (C/S—S-J). Associate editor, **"Materials and Methods,"** Reinhold Publishing Corp. FREUDENTHAL, ALFRED MARTIN. (M). Professor of civil engineering, Columbia University. MORGAN, DAVID E. (C/S—J-M). Consulting engineer; vice-president, International Manufacturing and Equipment Co.

Port Washington—DeVINCENTIS, HAROLD ANTHONY. (C/S—J-M). Project leader, Sylvania Electric Products, Inc.

NORTH CAROLINA

Asheville—HASH, LEWIS JACKSON. (C/S—S-J). Geologist, Tennessee Valley Authority.

OHIO

Ashtabula — MICKSCH, JOSEPH ERNEST. (C/S—S-J). Research engineer, Lake City Malleable, Inc.

Canton—ROWLAND, ELBERT S. (C/S—J-M). Research metallurgical engineer, Timken Roller Bearing Co.

St. Clairsville—JOSLIN, RICHARD EDWIN. (R, C/S—M-AM). Preparation, Hanna Coal Co.

Cleveland—BALDWIN, WILLIAM MARCH, JR. (C/S—J-M). Research professor, Case Institute of Technology.

Columbus — MILLER, CARL EDWARD. (M). Technical advisor, Battelle Memorial Institute.

Martins Ferry—BALCAR, FRANK A. (C/S—J-M). General manager, B. B. R. Drilling Co.

Springfield—HELMAN, DONALD DEANE. (C/S—S-J). Chief metallurgist, Ohio Steel Foundry Co.

West Middletown—WESTFALL, E. R. (M). Superintendent, masonry department, Armco Steel Corp.

Youngstown — STEIGNER, EDWARD SAMUEL. (M). Tubular products development engineer, Youngstown Sheet and Tube Co.

OKLAHOMA

Shidler—BENZ, LEWIS WALTER. (M). Assistant district superintendent, Phillips Petroleum Co.

Tulsa—HAMNER, FRANCIS MERRICK. (AM). Geological engineer, Schermerhorn Oil Corp. SHERMAN, HENRY ALVORD. (M). Production manager, Schermerhorn Oil Corp. WENGER, EVERETT SAMUEL. (C/S—J-M). Petroleum engineer, Amerada Petroleum Corp. WILSON, RALPH HERBERT. (C/S—J-M). Field laboratory supervisor, Shell Oil Co. WOLFF, PAUL ANTHONY. (M). Consulting engineer, Barnsdall Research Corp.

OREGON

Albany—DILLING, ELMER DONALD. (C/S—J-M). Metallurgist, U. S. Bureau of Mines.

Maupin—ROE, JOSEPH THOMAS. (C/S—J-M). Construction engineer, Dantore division, Dant and Russell, Inc.

PENNSYLVANIA

Allentown—CONSTANTIN, GASTON FRANCOIS. (C/S—J-M). Research engineer, Fuller Co.

Beaver Falls—SHEPPARD, RALPH EDGAR. (C/S—S-J). Research engineer, St. Joseph Lead Co.

Bridgeville—MARTIN, ROBERT EDWARD. (R, C/S—S-J). Demonstrator, Cardox Corp.

Clarksville—KING, THOMAS ANTHONY. (C/S—S-J). Section foreman, Westmoreland Mining Co.

Cornwall — SLEEMAN, ROBERT WARREN. (R, C/S—S-J). Head engineer, Bethlehem Steel Co.

Dalton — ROTH, WILLIAM BELFORD. (C/S—S-J). Student engineer, Hudson Coal Co.

Easton — BLANCO CARRANZA, NESTOR, (J). Junior field geologist, Socony- Vacuum Oil Co. of Colombia.

Lebanon — LAMBERT, KENNETH ALFRED, JR. (R, C/S—S-J). Engineer, Bethlehem Steel Co. PEETS, ROBERT G. (C/S—J-M). Chief mining engineer, Cornwall division, Bethlehem Steel Co.

New Kensington — HOLLINGSWORTH, ERNEST HOWARD. (C/S—J-M). Research metallurgist, aluminum research laboratories, Aluminum Co. of America.

Pittsburgh — EDDINGER, RALPH TRACY (C/S—S-M). Chemical engineer, Pittsburgh Consolidated Coal Co. MERRILL, TIMOTHY WARRINGTON. (C/S — J-M). Metallurgical engineer, Vanadium Corp. of America. PELLISSIER, GEORGE EDWARD. (C/S—J-M). Research associate, supervisor, physical and analytical methods, research laboratory, Carnegie-Illinois Steel Corp.

Pottsville—INGERSOLL, DALLAS EAST. (R—M). Division superintendent, Philadelphia & Reading Coal and Iron Co.

Scranton — FOSTER, RALPH KEELER. (R, C/S—S-J). Service engineer, Ingersoll-Rand Co.

State College — FREDRICKSON, JAY WARREN. (C/S — S-AM). Chief, division of metallurgy, School of Mineral Industries, Pennsylvania State College.

Washington — LUCAS, EUGENE FREDERICK. (C/S—S-J). Metallurgical engineer and chairman of works committee, Molybdenum Corp. of America.

SOUTH CAROLINA

Greenville—KELLEY, JOSEPH A. (C/S—J-AM). Division manager, Zonolite Co.

TENNESSEE

Memphis — PHELAN, STEPHEN RICE. (C/S—J-M). Geological and geophysical engineer, Stephen R. Phelan.

Rockwood — LUDWIG, ROBERT LEE. (J). Associate metallurgist, NEPA projects, Fairchild Engine and Airplane Corp.

TEXAS

Alice — CHILDRESS, CHARLES OTTO. (C/S—S-J). Petroleum engineer, Magnolia Petroleum Co.

Andrews — VOGEL, ALFRED J. (C/S—S-J). Assistant superintendent, Fuhrman Petroleum Corp.

Austin—BEAN, ERNEST F., JR. (C/S—J-AM). Student, University of Texas.

Beaumont — CHANEY, PRESTON EARL. (C/S—J-M). Research engineer, Sun Oil Co. DIBRELL, ETHERIDGE. (R, C/S—J-M). Reservoir engineer, Sun Oil Co.

Bellaire—OLIVE, MARION DOYLE. (J). Petroleum engineer, J. R. Butler and Co.

Brownfield — GOODWIN, GENE MERREL. (C/S—S-J). Production engineer, Magnolia Petroleum Co. RHOADS, BENJAMIN JUDSON, JR. (J). Junior petroleum engineer, Stanolind Oil and Gas Co. ROWE, MARTIN DECATUR, JR. (C/S—S-J). Petroleum engineer, Magnolia Petroleum Co.

Conroe—NORTON, CHARLES A. (C/S—J-M). Field foreman, The Texas Co.

Corpus Christi—ALDRIDGE, EDWIN ERNEST, JR. (C/S—J-M). Senior production engineer, Pan American Production Co. NEAL, LESLIE RALPH, JR. (C/S—S-J). Junior petroleum engineer, La Gloria Corp.

Dallas — ELFRINK, ELLIOTT BAIRD. (J). Senior research engineer, Magnolia Petroleum Co. GRAHAM, GORDON LLOYD. (C/S—J-M). Petroleum engineer, DeGolyer and MacNaughton. KIMBLER, OSCAR KAVANAH. (J). Assistant chemical engineer, Atlantic Refining Co. PREHN, WALTER LAWRENCE, JR. (J). Associate chemical engineer, Atlantic Refining Co.

El Paso—PONSFORD, REGINALD GEORGE. (R—M). Partner, Ponsford-Moos Equipment Co.

Galveston—MANNING, JOHN ALBERT, JR. (C/S—S-J). Research engineer, Tin Processing Corp.

Houston—KASTROP, JULIAN EDWARD. (C/S—J-M). District editor, **World Oil,** Gulf Publishing Co. MEERS, ROBERT J. (C/S—J-AM). Division superintendent of drilling and production, Union Oil Co. of California. SMITH, HORACE VERNON. (C/S—J-M). General manager, Rolo Mfg. Co.

Irving—HURD, RAY MERLE. (J). Associate chemist, Atlantic Refining Co.

Laredo — CALOHAN, WILLIAM FRANK. (C/S—J-M). Consulting geologist.

Midland—SIMON, GERALD DAVE. (R, C/S—S-J). Petroleum engineer, The Texas Co.

Overton — BYRD, LAWRENCE HERMAN. (C/S—J-M). Assistant district superintendent, Humble Oil and Refining Co.

San Antonio—STAPP, WILFORD

LEE. (C/S—J-M). Petroleum geologist, Sunray Oil Corp.
Texas City—GEYER, ALVIN AUSLEY. (C/S—S-J). Roustabout engineer, Pan American Gas Co.
Victoria—DAVIS, JOHN ODUS. (C/S—S-AM). Petroleum engineer, Jergins Oil Co. of Texas.
Wickett—DAVIS, CHARLES EDWARD. (C/S—S-J). Field geologist, North Ward-Estes field, Texas, production division, Gulf Oil Corp.

UTAH

Cedar City—MADDOX, ROBERT DAVID. (C/S — J-M). Assistant mine engineer, Columbia Iron Mining Co.

VIRGINIA

Austinville—MOULD, CHANNING BENNETT. (C/S—S-J). Mining engineer, New Jersey Zinc Co.
Dante—COPELAND, ALFRED EUGENE. (C/S—S-J). Quality control engineer, Clinchfield Coal Corp.

WASHINGTON

Seattle—BAUER, WOLF GUNTHER. (M). Consulting engineer.

WEST VIRGINIA

Morgantown—FOWLER, CLEON ROSCOE. (C/S—S-M). Assistant superintendent, Christopher Coal Co.

WISCONSIN

Milwaukee—HUFFAKER, RAY EUGENE. (C/S—S-J). Metallurgical engineer, Ladish Co. IRVING, GORDON ERNEST. (C/S—S-J). Ore testing engineer, Allis-Chalmers Mfg. Co. MITCHELL, WILL, JR. (C/S—J-M). Director, basic industries research laboratory, Allis-Chalmers Mfg. Co.
Neshkoro—CODDINGTON, SAMUEL LEE. (C/S—S-J). Engineering trainee, Link-Belt Co.

WYOMING

Rock Springs—QUAY, JACK H. (C/S — AM-M). Engineer, Union Pacific Coal Co.

ALASKA

Anchorage—ARNELL, EDWARD LLOYD. (AM). Law partner, Plummer and Arnell.
Fairbanks—SAUNDERS, ROBERT H. (C/S—J-M). Surveyor, U. S. Smelting Refining and Mining Co.

ALBERTA

Edmonton—DOWNING, JOHN ARTHUR. (C/S — S-AM). Geologist, Bear Oil Co. LAKE, HAROLD EDGAR. (C/S—J-M). Mine superintendent, Eldorado Mining and Refining Co.

BRITISH COLUMBIA

Trail—JOHNSON, ROBERT. (C/S—S-J). Engineer in training, Consolidated Mining and Smelting Co. of Canada.

ONTARIO

Ottawa—GOUDGE, MONSON FRASER. (M). Chief, industrial minerals section, Bureau of Mines. McDONALD, ROGER DUNCAN. (C/S — S-J). Junior metallurgist (physical), Bureau of Mines, Ottawa.
Toronto—BULLEN, ROBERT LAWRENCE. (C/S—J-M). General superintendent, blue lead division, Canada Metal Co.

QUEBEC

Montreal—STEVENS, ROBERT WILLIAM. (C/S—J-M). Mining engineer, Dominion Engineering Works, Ltd.

CHIHUAHUA

Parral—BAKER, WILLIAM DAVIS. (C/S—S-M). Shift boss, American Smelting and Refining Co.

SONORA

Cananea—AGETON, ROBERT WILLIAM. (C/S—J-M). Engineer, Cananea Consolidated Copper Co.

ARGENTINA

Buenos Aires—MORAN, THOMAS GRAYSON. (C/S—J-M). Chief geologist, Damon Dinerman y Cia.

BOLIVIA

Oruro—PFEIFFER, ULRICH PAUL. (M). Metallurgist and mill foreman, Empresa Minera San Jose.

BRASIL

Rio de Janiero—DA SILVA, JAIR CARVALHO. (J). Tin plate division, National Steel Co. of Brasil.

CHILE

Rancagua—COLBERT, FRANK ANTHONY. (C/S—S-AM). Junior mine shift boss, Braden Copper Co.

COLOMBIA

Antioquia—BREEDING, WILLIAM HENRY. (C/S—J-M). Chief engineer, Pato Consolidated Gold Dredge, Ltd.

VENEZUELA

Caracas—HALL, MERLE LEROY, JR. (R, C/S—S-J). Field petroleum engineer, Texas Petroleum Co. LANDRETH, THOMAS CHART. (C/S—J-AM). Field engineer, Socony-Vacuum Oil Co. of Venezuela. SLOAN, C. CARLETON, (M). Production foreman, Socony-Vacuum Oil Co. of Venezuela.

ENGLAND

Port Talbot—KESTERTON, ARTHUR JOHN. (C/S—JFA-AM). Melting shop manager, Steel Co. of Wales.
Southport—PARK, CYRIL JOHN. (C/S—JFA-M). Director, William Park and Co., Forgemasters, Ltd.
London—HARRIS, EDWARD PERCIVAL. (M). Director and technical manager, H. J. Enthoven and Sons, Ltd.

FINLAND

Outokumpu—HAKAPAA, ERKKI ANTERO. (M). Mine superintendent, Outokumpu Co. HEIKKINEN, TIMO HENRIK. (M). Mill superintendent, Outokumpu Co.

FRANCE

Paris—KIMLER, COURTNEY WARREN. (R, C/S—JA-M). Sales engineer, ECA-OSR.

NORWAY

Oslo—ENGZELIUS, JOHAN GUSTAF. (M). Manager, Folldal Verk.
Sulitjelma—LANGE, JOHAN JOERGEN. (C/S—J-M). Assistant mill superintendent, Sulitjelma Mines.

SWEDEN

Surahammar—FORNANDER, SVEN GUNDE EDVIN. (C/S—JFA-M). Manager of research, Surahammars Bruks AB.

SOUTH AFRICA

Transvaal—McNEIL, ARCHIBALD. (M). Manager, Tweefontein United Collieries, Ltd.

INDIA

Bihar—NARAYANAN, PYLORE ISWARIYER ANANTHA. (M). Assistant director (ore dressing), National Metallurgical Laboratory, Tatanagar.
Bombay—RAJAGOPALASWAMY, KURMA. (M). Chief geologist, Associated Cement Companies.
Katni, C. P.—WILKS, ALAN DUDLEY. (C/S—JFA-M). Superintendent, ordnance factory, Government of India.

QUEENSLAND

Mount Isa—BURGER, DIONYS. (AM). Staff geologist, Mount Isa Mines, Ltd. HOSKING, PETER KAY. (J). Junior metallurgist, Mount Isa Mines, Ltd. PIKE, ARTHUR STANTON. (C/S—J-M). Assistant smelter superintendent, Mount Isa Mines, Ltd.

VICTORIA

Essendon—RANKIN, RALPH IAN. (C/S—J-M). Tunnelling superintendent, State Electricity Commission of Victoria.

WESTERN AUSTRALIA

Chandler—FITZGERALD, MARTIN LAURENCE. (M). Manager, State (W.A.) Alumite Industry.

NEW ZEALAND

Dunedin—PICKERING, BRUCE RAYMOND. (C/S — S-J). Underground mine worker, Blackwater Mines, Ltd.
Huntly—MARSHALL, THOMAS. (C/S—S-J). Metallurgist, Dominion Laboratory, D. S. I. R.

STUDENT ASSOCIATES

Elected September—1949

Lawrence Adler	Columbia Univ.
Douglas Alexander	Otago Univ.
Robert C. Carruthers	MIT
Frank W. Cole	Univ. Okla.
Malcolm G. Coone	Univ. Texas
Albert B. Cowan	Univ. Texas
Jack P. Fly	Univ. Texas
Gene W. Hinds	Colo Sch. Mines
John P. Karshner	Colo. Sch. Mines
Philip L. McLaughlin	Univ. Texas
Fred M. Lynch	Univ. Texas
Francis L. Schulte	Univ. Texas
John E. Shelton	Univ. Texas
William S. Shropshire	Univ. Texas
Allen I. Swartz	MIT
Walter R. Williams	Univ. Texas

Optical Temperature Scale and Emissivity of Liquid Iron

MINU N. DASTUR[*] and NEV. A. GOKCEN[†]

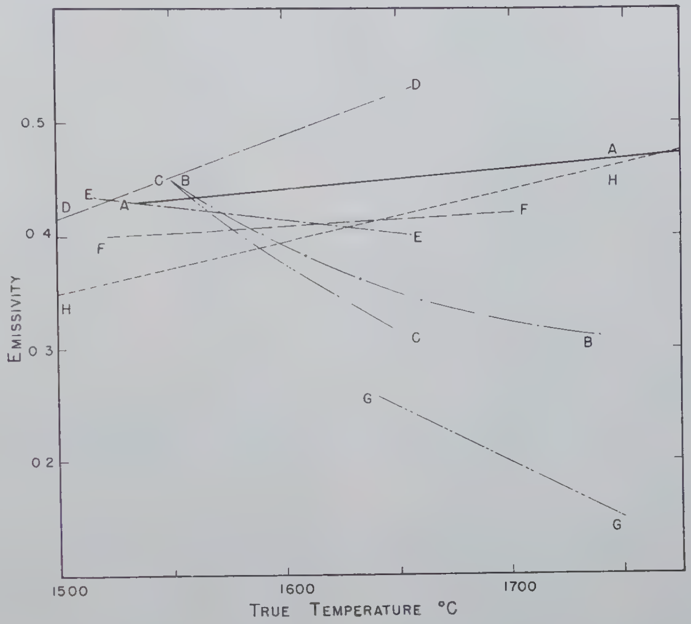

FIG 1—Results of observations of emissivity of pure iron and plain carbon steels by various investigators.

A. Present investigation, pure iron. B. Basic electric arc steel, *Naeser*. C. Small basic electric arc steels, *Guthmann*. D. Experimental basic high-frequency; steel, *Goller*. E. Experimental high-frequency furnace with sillimanite lining; steel, *Knowles and Sarjant*. F. Experimental high-frequency furnace with sillimanite lining; Armco iron, *Knowles and Sarjant*. G. Armco iron, *Naeser*. H. Iron, *Bidwell*.

In metallurgical process industries a knowledge of true melting and casting temperatures is very essential for increasing the operating efficiency as well as improving the quality of the finished product. Optical pyrometers are widely used for the purpose because of their cheapness and ease of operation. It is an unfortunate fact, however, that this mode of measuring temperature entails a source of severe error inasmuch as with all non-black bodies, the temperature observed is always below the true temperature owing to deficient emissive power. Hence, the need for emissivity correction arises.

In 1913 Bidwell[1] obtained emissivity values of 0.36–0.48 for a temperature range of 1520–1800°C. He measured the true temperature of molten iron by sighting into a carbon cavity immersed in the iron under an atmosphere of hydrogen. In 1914 Burgess[2] determined the emissivity of a smooth surface of liquid iron free from oxide to be 0.37 under an atmosphere of hydrogen. He claimed to have attained an accuracy of within 5°C at 1500°C with an optical pyrometer using monochromatic light. He reported that no difference appeared to exist between the emissivities of pure iron and of steels containing considerable percentages of carbon, nickel or manganese; nor was there any appreciable variation of emissivity with temperature from 1530 to 1571°C. Wensel and Roeser[3] found an emissivity value of 0.4 for temperatures above 1375°C for cast iron.

The average emissivity value for carbon steels reported by Leiber,[4] Todd,[5] Hase[6] and Umino[7] range from 0.4 to 0.45.

Knowles and Sarjant[8] made an extensive study of emissivity of molten iron and steel over a wide range of workshop and laboratory conditions. Observations of true temperature were made with immersion thermocouples, and correlated with apparent temperatures indicated by optical pyrometer readings taken on the pouring stream as it passed over the lip of the crucible. The emissivity of Armco iron was shown to be of the order of 0.4, rising slightly with increasing temperature. But for plain carbon steels containing up to 1.0 pct carbon the emissivity was shown to fall slightly with increasing temperatures. The results of their investigation are in agreement with those of Guthmann,[9] Naeser,[10] Spencer,[11] Todd[5] and Hase[6] in regard to the relation between emissivity and temperature for plain carbon steels. However, Goller[12] has found a rise of emissivity with increasing temperature for the same steels. Results of several investigations are given in Fig 1.

Measurement of True and Apparent Temperatures

The necessity for an accurate optical temperature scale for liquid iron in studies of gas-metal equilibria led to this investigation. Experimental measurements were carried out in the induction furnace used by Dastur and Chipman[13] in their studies of the reaction of hydrogen with oxygen in liquid iron. The furnace as modified for this work is shown in Fig 2. The atmosphere of the furnace was a mixture of purified argon with hydrogen containing a small controlled amount of water vapor. Gases were preheated by means of a platinum-10 pct rhodium resistance coil. The stream of hydrogen sweeping across the surface of molten iron vir-

New York Meeting, February 1950.
TP 2693 C. Discussion of this paper (2 copies) may be sent to *Transactions* AIME before April 1, 1950. Discussion is tentatively scheduled for publication in November, 1950.
Manuscript received May 12, 1949; revision received July 28, 1949.

[*] H. A. Brassert & Co., New York, N. Y.

[†] Graduate Student, Department of Metallurgy, Massachusetts Institute of Technology, Cambridge, Mass.

[1] References are at the end of the paper.

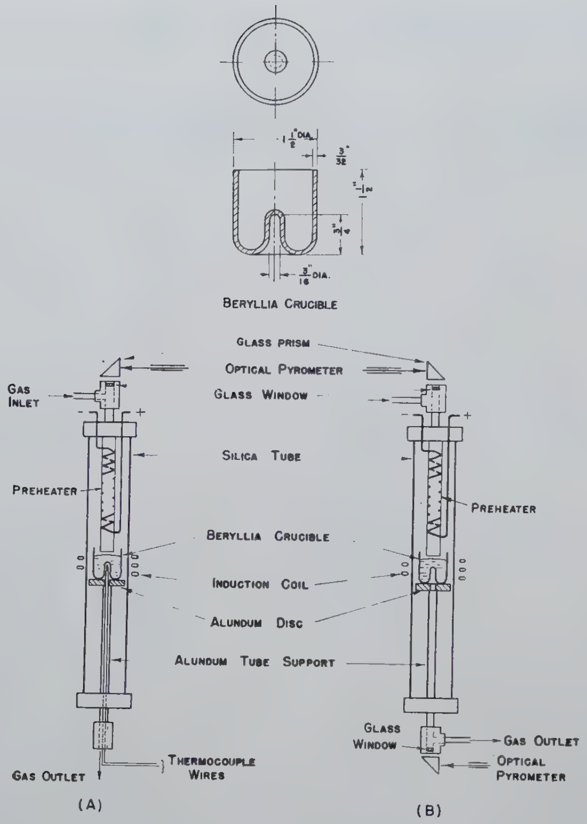

FIG 2—Furnace set-up for the determination of the true temperature scale and emissivity of liquid iron.

tually eliminates errors resulting from the presence of iron vapor except at temperatures approaching or above 1900°C. The charge consisting of about 90 g of pure iron was melted in a pure beryllia crucible especially designed for this purpose as shown in Fig 2.

Two sets of simultaneous temperature readings were obtained: (1) Optical top temperature reading by a sensitive optical pyrometer and bottom reading from a properly assembled thermocouple touching the top of the crucible cavity (see Fig 2A). (2) Top and bottom optical temperature readings by using the crucible cavity as a perfect black body for the bottom optical pyrometer (see Fig 2B).

After the charge was molten both the optical pyrometer and the thermocouple were frequently checked against the melting point of electrolytic iron in hydrogen which was taken as 1535°C. Thermocouples were also rechecked after each experimental run.

Optical temperature readings were taken when the gas preheating coil was hot and cold, and it was observed that the coil temperature has no effect upon temperature readings.

Each pair of simultaneous readings was taken when a constant and steady temperature had been obtained by adjusting the power input from a high-frequency source. Temperature measurements obtained by stepwise heating were in agreement with those of stepwise cooling, indicating the absence of temperature gradient between the molten metal and thermocouple.

THERMOCOUPLES

Calibrated platinum-platinum rhodium and tungsten-molybdenum thermocouples were used in this investigation for establishing the true temperature of liquid iron. Platinum-platinum rhodium thermocouples were used only up to 1660°C and tungsten-molybdenum thermocouples were used from 1650 to 1900°C.

Schulze[14] found that tungsten, molybdenum and tantalum were well suited for measuring high temperatures when the couples had been annealed at a higher temperature to assure constant thermal powers. The use of these thermocouples in liquid steel has been described by Taylor and Chipman.[15]

Schofield and Grace[16] in using platinum-platinum rhodium thermocouples reported that no effect was noticed in the thermocouple output from the field present in the induction furnace. The tungsten molybdenum thermocouples used in this investigation were from a batch calibrated and used by Potter[17] and were rechecked against the melting point of pure iron.

OPTICAL MEASUREMENTS

The optical systems at the top and bottom of the furnace contained identical sight glasses and prisms and two optical pyrometers which had previously been calibrated against a standard instrument from the Bureau of Standards. No temperature difference was observed upon interchanging pyrometers or sight glasses and prisms. Since the hollow tip in the center of the crucible was more than three times longer than its diameter, it presented a perfect black body condition for the measurement of the true temperature of melt, corrected for absorption and reflection from the intervening optical system and the gas column. After checking the melting point of iron, temperatures as high as 1900°C were recorded by taking simultaneous readings with optical pyrometers from top and bottom.

Results

The results of true and apparent (optical) temperature readings are plotted in Fig 3 which gives a calibration for the given experimental conditions. Such scales may lend themselves to the evaluation of transmissivity and emissivity values, as will be shown presently.

Transmissivity correction is obtained from the optical bottom temperature reading when emissivity is unity. For this purpose the melting point of electrolytic iron (1535°C) was used as reference temperature and the transmissivity evaluated by the Wien-Planck equation:

$$\ln (E\alpha) = \frac{c_2}{\lambda}\left(\frac{1}{T_t} - \frac{1}{T_a}\right)$$

E = Emissivity
α = Transmissivity
c_2 = Fundamental constant of Planck equation, 14,330 micron-degrees
λ = Wavelength of light used (0.65 micron)
T_t = True temperature °K
T_a = Apparent temperature °K

In the special case of the melting point of iron versus bottom optical reading the apparent temperature was 1748°K and the true melting point was

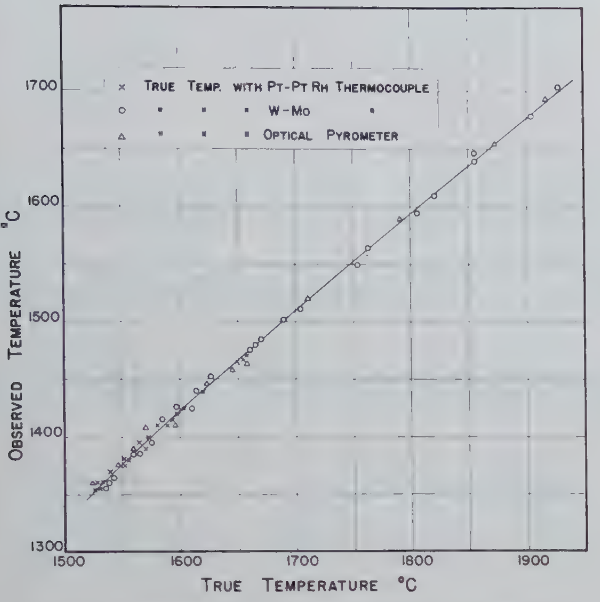

FIG 3—True temperature vs. observed (optical) temperature.

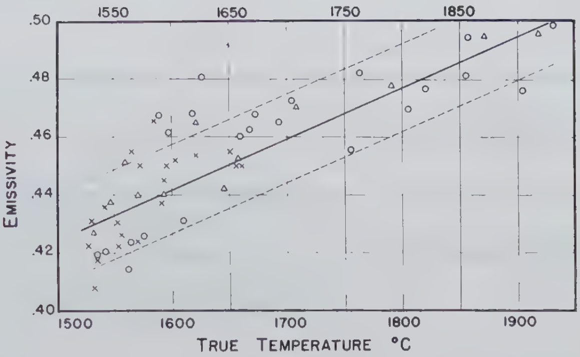

FIG 4—Emissivity of pure iron.

1808°K as measured by the platinum-rhodium couple. These values lead to a transmissivity of 0.65 which is considered constant within a temperature range of 1500–1900°C.

Once the transmissivity of the intervening optical system (sight glass and prism) was determined, the emissivity of liquid iron was calculated from observed top temperatures by the Wien-Planck equation using the experimental true and observed temperatures plotted in Fig 3. The scattering of the points in the emissivity plot of Fig 4 is of no great significance because even a slight error in the measurement of true or observed temperature will cause a relatively large change in the emissivity, since the logarithm of the emissivity is proportional to the difference in the reciprocal of the temperatures. An accuracy of ±5°C in observed temperature is equivalent to a change of ±0.017 in emissivity values at 1600°C. Variation of the effective wavelength (λ) with temperature introduces a negligible error in emissivity values.

The total change in the emissivity of liquid iron over the temperature range of 1540–1900°C is from 0.42 to 0.50. The result of this investigation is presented graphically with the results of previous investigators in Fig 1 showing the inconsistency of the reported emissivity values. Variation of the emissivity of steels with temperature, investigated under plant conditions and reported by Sosman[18] as 0.39 at 1425° and 0.50 at about 1650° agrees qualitatively with the present results. Any correlation between the plant data and the emissivity is often much less accurate because of the presence of atmospheric disturbing factors as investigated by Hall[19] and the surface condition of metal.[20]

The emissivity of molten iron also varies with the addition of alloying elements. The effects of several elements have been reported rather inconsistently in the available literature. The only such element investigated here was vanadium which was found to have no effect upon the emissivity at concentrations up to 2 pct.

Acknowledgments

The authors wish to thank Professor John Chipman for suggesting the experimental method, Mrs. Virginia Mahaday for making the beryllia crucibles and Hans Elvander for assistance in the temperature measurements. This investigation forms a part of a study of the physical chemistry of steelmaking sponsored by the Office of Naval Research under contract N5 ori-07816, Task Order XVI, NR-031-186.

References

1. C. C. Bidwell: *Phys. Rev.* (1913) **2,** 482.
2. G. K. Burgess: Temperature Measurements in Bessemer and Open-Hearth Practice. Bur. of Standards (1917) Tech. Paper No. 91.
3. H. T. Wensel and W. F. Roeser: Temperature Measurement of Molten Cast Iron. *Trans.* Amer. Foundrymen Ass'n. (1928) **36,** 191.
4. G. Leiber: Measurement of Temperature in Steel Bath of Basic Open-hearth Furnace. *Arch. f. d. Eissenhuttenwesen* (1937) **11,** 63.
5. W. J. Todd: High Temperature Measurement in a Steel Works. *Metal Treatment* (1939–40) **5,** 171.
6. R. Hase: Influence of Emissivity of Liquid Iron. *Arch. f. d. Eissenhuttenwesen* (1931) **4,** 261.
7. S. Umino: On the Emissivity of Substances in Steel Plants. *Tetsuto-Hagane* (July 25, 1937) **23,** 644.
8. D. Knowles and R. J. Sarjant: Emissivity of Molten Iron and Steel. *Jnl.* Iron and Steel Inst. (April 1947) **155,** 577.
9. K. Guthmann: Comparative Measurements of Temperature on Molten Pig Iron, Cast Iron and Steel. *Stahl und Eisen* (1937) **57,** 1245 and 1269.
10. G. Naeser: Reduction in Rejections with Radiation Measurements in Melting Practice Using Color-Intensity Pyrometer "Bioptrix." *Stahl und Eisen* (1939) **59,** 592.
11. W. H. Spencer: Discussion of paper by G. R. Fitterer, *Trans.* AIME (1936), **120,** 189.
12. G. N. Goller: Emissivity of Molten Stainless Steels. *Trans.* Amer. Soc. for Metals (1944) **32,** 239.
13. M. N. Dastur and J. Chipman: Equilibrium in the Reaction of Hydrogen with Oxygen in Liquid Iron. *Jnl. of Metals,* Aug. 1949, 441. AIME *Trans.* (1949) **185,** 441.
14. A. Schulze: Thermoelectric Properties of Tungsten, Molybdenum and Tantalum. *Ztsch. Metallkunde* (1932) **24,** 206.
15. C. R. Taylor and J. Chipman: Equilibria of Liquid Iron and Simple Basic and Acid Slags in a Rotating Induction Furnace. *Trans.* AIME (1943) **154,** 229.
16. F. H. Schofield and A. Grace: Quick Immersion Thermocouple for Measuring Temperature of Liquid Steel. Eighth Report on Heterogeneity of Steel Ingots, Iron and Steel Inst. Spec. Report No. 25 (1939).
17. R. D. Potter: Investigation of the Central Liquidus Surfaces and Phases of the Chromium-Molybdenum-Iron System. Sc. D. Thesis, M.I.T. (1949).
18. R. B. Sosman: Temperatures in the Open-hearth Furnace. *Trans.* AIME (1948) **176.** *Metals Tech.,* Aug. 1948.
19. J. A. Hall: Influence of Smoke and Atmospheric Absorption of Optical Pyrometry. *Jnl.* of Iron and Steel Inst.
20. J. A. Hall: Photographic Investigation of the Brightness Temperature of Liquid Steel Streams. *Jnl.* of Iron and Steel Inst., Jan. 1947, 55.

Size Effects in Quenching High-purity, Precipitation-hardenable Alloys[*]

WALTER L. FINLAY,[†] Member AIME

Introduction

Size effects in quenching steel are particularly prominent and well recognized because of the existence of a critical cooling rate separating nucleation and growth transformations, as exemplified by the formation of pearlite, from the shear type of transformation characterizing the martensite reaction. The absence of a similar, sharply demarcating cooling rate is characteristic of precipitation hardening systems and size effects in these are correspondingly less prominent. This paper is concerned with a size effect in high-purity, precipitation-hardenable alloys which appears not to have been recognized previously. This effect is believed to result from the thermal fluctuations which inevitably occur in quenching a specimen of finite size into a cooling liquid rather than from the existence of a critical cooling rate.

QUENCHING "ANOMALIES"

The precipitation hardening literature contains many references to so-called anomalous quenching and aging results. By "anomalous", investigators usually meant that their alloys did not consistently harden on aging after quenching according to some anticipated pattern; not infrequently virtually no age hardening occurred with compositions known to be precipitation-hardenable.

Perhaps the most prominent series of anomalies was reported over a 15-year period by Gayler and coworkers on aluminum-copper.[1,2,3,4] Working with silver-rich copper alloy, Cohen[5] secured some very interesting Rockwell F hardness changes of from 1–5 Rockwell points between the first peak and valley. Fink and Smith borrowed one of Cohen's specimens and, following his heat treatment and quenching practice to the letter, secured[6] very different results in which only one peak was obtained and in which the hardness level at the aging time of Cohen's first peak was 20 Rockwell F points higher.

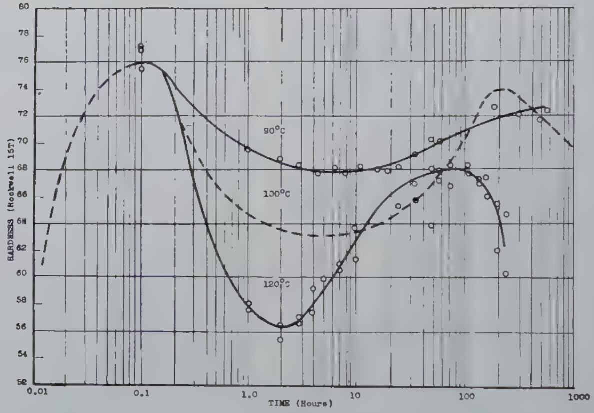

FIG 1—12 pct Al-Zn age hardening and retrogression.
Longitudinal specimens with 0.1 × 0.5 in. cross-section. 2 hr at 475°C; 10°C water jet quench.
Each point the average of five determinations.

Fink and Van Horn[7] encountered serious deviations in age-hardening high purity aluminum-zinc alloys. They stated that "the discrepancies were larger than might be expected from possible experimental errors in the Brinell readings."

Geisler, Barrett and Mehl[8] likewise encountered anomalous hardening results in aluminum-silver alloys, securing quite different age-hardening curves from two identical specimens. They stated that "the treatments of these samples had been the same, so that the different behaviors could be attributed only to accidental variations in the quenching practice."

Cleveland Meeting, October 1949.
TP 2694 E. Discussion of this paper (2 copies) may be sent to *Transactions* AIME before December 1, 1949. Discussion is tentatively scheduled for publication in May 1950.
Manuscript received April 29, 1949; revision received July 5, 1949.

[*] This paper is part of a dissertation presented by Walter L. Finlay to the Faculty of the Graduate Division of the School of Engineering of Yale University in partial fulfillment of the requirements of the degree of Doctor of Engineering, May, 1948.

[†] Supervisor, Metals Research, Remington Arms Co., Inc., Bridgeport, Conn.

[1] References are at the end of the paper.

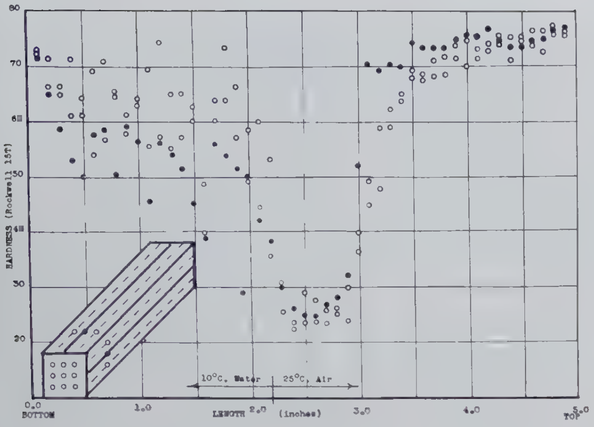

FIG 2A—12 pct Al-Zn partial immersion quenching.
Specimen with dimensions of 0.4 × 0.4 × 5.0 in. solution heat treated for 2 hr at 475°C; quickly placed vertically in quiet 10°C water with lower 2.2 in. immersed until entire specimen below 25°C. Each point a single hardness determination at locations sketched. Edge and midpoint hardnesses on one surface one hour after quenching.

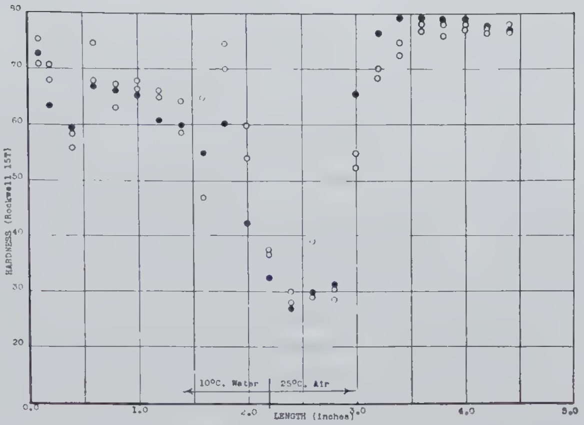

FIG 2B—Same as Fig 2A except:
Edge and midpoint hardnesses on adjacent surface 24 hr after quenching.

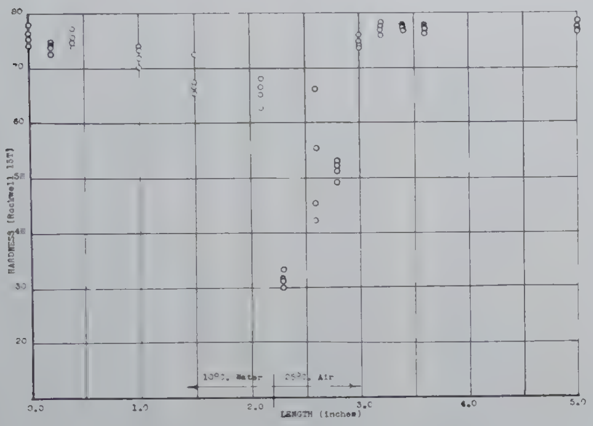

FIG 2C—Same as Fig 2A except:
Interior edge hardnesses.

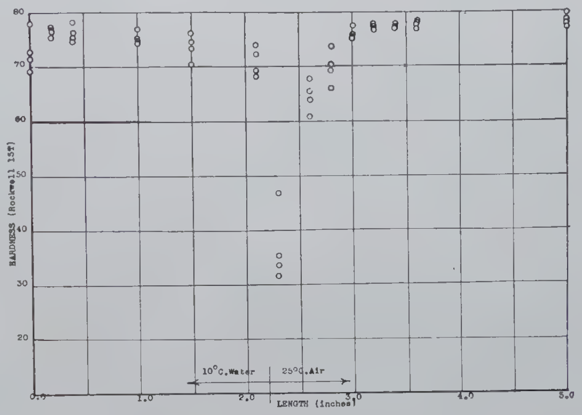

FIG 2D—Same as Fig 2A except:
Interior midpoint hardnesses.

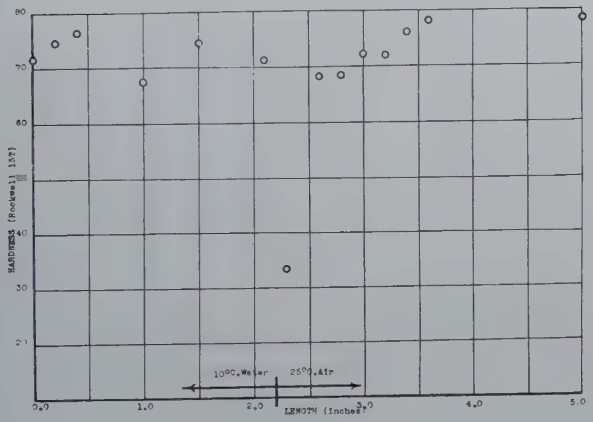

FIG 2E—Same as Fig 2A except:
Interior center hardness.

The present paper presents the view that these anomalies may be associated with retrogression effected by the thermal fluctuations accompanying quenching. Accordingly, the retrogression characteristics of the 12 pct aluminum-zinc alloy used in the investigation being reported are outlined in the following section.

RETROGRESSION

Retrogression is a term which has been applied[9] to the curious behavior of certain age-hardening alloys according to which a quenched alloy partially or completely aged at a lower temperature, at first softens appreciably before slowly hardening again at a higher temperature. Masing suggested[10] that the smaller of the precipitation particles which were stable at the lower temperature went back into solution at the higher temperature before additional precipitation could occur so that the observed weakening occurred. This explanation now appears to be generally accepted as valid.

A marked retrogression has been reported[11] for binary aluminum-rich aluminum-zinc alloys. The dashed curve in Fig 1 is a reproduction from Ref 11 for the 100°C retrogression of 12 pct aluminum-zinc; the 90 and 120°C retrogression curves also plotted in this figure present new data.

The 12 pct aluminum-zinc alloy was employed for a large part of the present investigation. Its pertinent behavior may, in terms of Rockwell 15T hardness, be summarized as follows: 1. It quenches to a hardness of 50–55. 2. At room temperature it ages to 76–78 in 0.1–0.2 hr, and stays unchanged at that level for at least 2 yr. 3. Retrogression from its room temperature peak of 76–78 has been shown from 70°C up to at least 120°C, and doubtless this behavior is even more marked at higher temperatures. Within the temperature range investigated, the bottom of the retrogression valley is reached in 1–10 hr, and extends to depths of 56–72, the higher the temperature the shorter the time to the valley and the greater its depth. As is characteristic of the retrogression reaction, the rise from the valley is much slower than the rate of initial precipitation hardening at room temperature even though the latter is lower.

The retrogression behavior of binary aluminum-copper alloys has been studied extensively and, in principle, is not dissimilar from that of aluminum-zinc, although it differs in details, principally in that longer times or higher temperatures are required for corresponding aging effects.

Commercially pure aluminum-base alloys also retrogress and industrial use is made of this.[17] In general, however, commercially pure alloys retrogress more reluctantly than their high purity counterparts.

Experimental Work

The following materials were employed in the investigation:

1. High purity 12 pct aluminum-zinc
2. High purity 4 pct aluminum-copper
3. Commercial purity 24S aluminum alloy
4. Commerical purity 75S aluminum alloy.

The preparation of the first two is described in Ref 11; the last two were purchased in the form of ⅞ in. diam rod from Alcoa.

QUENCHING DIFFICULTIES

Age-hardening anomalies of the kind mentioned in the introduction were encountered in attempting to precipitation-harden high-purity, 4 pct aluminum-copper and 12 pct aluminum-zinc creep specimens having a 0.4 in. diam by 7 in. gauge length, whereas ⅛ in. thick discs cut from these specimens and solution heat-treated and quenched together with the creep specimens gave consistent room temperature aging results. With the aluminum-zinc alloy, for example, a series of 10 individual Rockwell 15T hardnesses of 77 ±1 were common with the ⅛ in. thick discs. But individual Rockwell 15T hardnesses on either the surface or cross-section of 0.4 in. round specimens were almost always low and very erratic, a typical sequence of readings being 50–38–48–22–46.

Several different quenching procedures were tried in uniformly unsuccessful attempts to secure, in the 0.4 in. round specimens of 12 pct aluminum-zinc, the 76–78 Rockwell 15T hardness level very readily attained in ⅛ in. thick discs of the same material merely by dropping them into water. A special quenching unit was then built as the ultimate in quenching effectiveness. This quenching apparatus consisted of two parts: a vertical tube furnace for solution heat treating; and, axially aligned with the tube, a vertical quenching fixture into which the specimen dropped directly by gravity. A single specimen was suspended in the central portion of the vertical tube furnace by means of a wire. After a sufficient period of solution heat treating, the wire was cut and the specimen plunged directly into the jet quenching fixture. The latter consisted of a 1 in. id brass tube 10 in. long with approximately 200 holes 0.050 in. in diameter drilled into it in a uniform pattern with centers ⅜ in. apart and extending from one end of the fixture to the other. Water pressure of 60 psi gave rise to 200-odd jets which symmetrically struck the specimen as it dropped through the fixture. Jets were employed both submerged and not submerged.

The result of this ultimate effort in quenching 0.4 in. diam 12 pct aluminum-zinc was a Rockwell 15T hardness averaging in the neighborhood of 50—something of an improvement over air cooling, but still far short of the hardness obtained on thin disc specimens.

Several 0.4 in. diam, 4 pct aluminum-copper rounds and ⅛ in. thick discs were then jet quenched with similar results to those obtained on 12 pct aluminum-zinc, although, in the case of the 4 pct aluminum-copper, the rounds were not so markedly inferior to the discs.

The foregoing results definitely indicated a size effect. As a practical measure, therefore, all subsequent work on 12 pct aluminum-zinc and 4 pct aluminum-copper was done on specimens with a maximum thickness of 0.1 in. In order to gain some insight into the phenomena, however, a series of partial immersion quenching tests was conducted.

PARTIAL IMMERSION QUENCHING

Two rectangular bars, one with a square cross-section, 0.4 in. on a side, and another with a rectangular cross-section 0.1 in. thick and 0.4 in. wide, were employed in these tests. The specimens were solution heat treated in the standard manner and then were rapidly transferred to the quench where, in a vertical position their lower ends were immersed in the quenching medium. These experimental conditions were set up in order to secure, in one specimen, a wide range of both thermal gradients and a wide diversity of thermal fluctuations, since it was felt that the explanation for the puzzling phenomena encountered must be associated with failure, in a given region of the specimen, to maintain a uniform rate of temperature decrease during quenching.

The square cross-section bar, 0.4 × 0.4 × 5.0 in., was carefully machined with its bases precisely normal to the longitudinal axis. All surfaces were flat and were polished through No. 000 paper. A hole was then drilled through one end which thereafter became the top of the vertically-quenched specimen. Three specimens were made in this manner: one from high-purity 12 pct aluminum-zinc; one from commercial 75S; and one from commercial 24S. Each was individually placed in the vertical tube furnace and solution heat treated for 2 hr. It was then quickly placed vertically in quiet 10°C water with the lower end immersed until the entire specimen had cooled to a few degrees below room temperature. One hour after quenching, pencil lines were drawn on one side of the bar as shown in Fig 2A and hardnesses were determined at 0.1 in. intervals from bottom to top of the specimen at "edge" positions (0.1 in. in from the bar edge) and at the "midpoint" position (0.2 in. in from the bar edge). The specimen was then stored for 24 hr after quenching to 25°C and hardnesses were similarly determined on an adjacent side. The hardness patterns shown in Fig 2A and 2B were thereby obtained. Because of the care with which the specimen had been machined, it was possible to determine hardnesses on the bottom of the specimen in the nine positions sketched in Fig 2A.

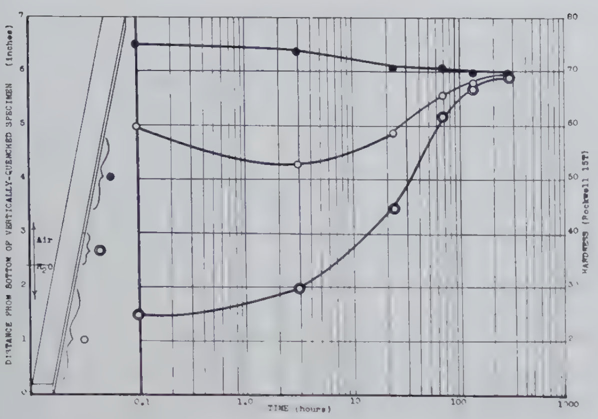

FIG 3—100°C aging of Fig 2 specimen.
After quenching as detailed on Fig 2, aged at 100°C.
Each point the average of 10 determinations on the surface in the region bracketed.

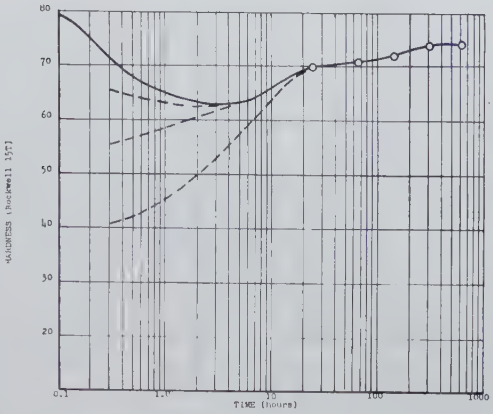

FIG 5—100°C aging of Fig 4 specimens.
After quenching as detailed on Fig 4, aged at 100°C.
It was found, regardless of quenching medium and location on specimen, that after 24 hr at 100°C all hardness values were within 3 Rockwell 15T points of each other.

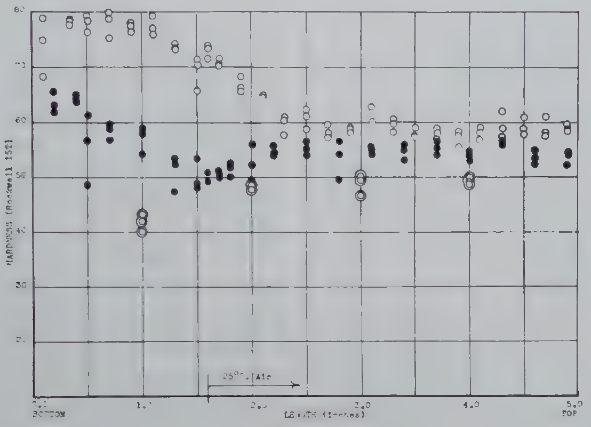

FIG 4—12 pct Al-Zn partial immersion quenching.
0.1 × 0.4 × 5 in. specimens; 2 hr at 475°C; quickly placed vertically for quenching—
⊙ Lower 1.6 in. in quiet 10°C water.
● Lower 1.6 in. in quiet 10°C oil.
(o) Entire specimen in still 25°C air.
Each point a single hardness determination.

Hardnesses throughout the interior of the bar were then obtained by the following procedure: the specimen was clamped gently into a small vise; a line was scratched 0.1 or 0.2 in. from the end; the vise and specimen were immersed in 10°C water; by slow sawing with a fine jeweler's hack saw, a 0.1 or 0.2 in. thick specimen was cut from the end of the bar; by means of slow strokes from a clean, sharp, small-toothed file, the end of the bar specimen was squared up with the longitudinal axis; and, finally, the specimen and vise were removed from the water, the specimen was removed and hardnesses were again determined at the nine locations sketched in Fig 2A. The results of this investigation are shown in Fig 2C, 2D, and 2E. There is an excellent general correlation between the surface and interior hardnesses indicating that the necessary machining operations to secure the interior hardnesses were carried out so that virtually no change in the actual hardnesses was effected by the machining operations. On the other hand, there are significant differences between the interior and surface hardnesses which fall into a consistent pattern when the data are analyzed from the standpoint of thermal-fluctuation-actuated retrogression and/or overaging.

The foregoing somewhat laborious procedure was carried out only on the 12 pct aluminum-zinc specimen since, as shown in Fig 6, the commercial aluminum alloys, 24S and 75S, were far less sensitive to whatever quenching variables were introduced by the test procedure and it was assumed that their interior hardnesses were the same as their surface hardnesses.

The data plotted in Fig 6 were determined one hour after quenching. Similar hardness determinations were made at intervals up to 500 hr after quenching, resulting—in the case of both 24S and 75S—in a hardness increase of approximately 5 Rockwell 15T points uniformly along the length of the bar. Subsequent elevated temperature aging (10 hr at 190°C for 24S and 24 hr at 120°C for 75S) likewise raised the hardness uniformly along the entire length of the bar.

In order to distinguish between the effect of thick and thin specimens, the series of partial immersion quench tests graphed in Fig 4 was run on 0.1 × 0.4 × 5.0 in. specimens of 12 pct aluminum-zinc.

SUBSEQUENT AGING OF PARTIAL-IMMERSION-QUENCHED SPECIMENS

There are very few investigating means available to determine, in a polycrystalline specimen during the early stages of precipitation hardening, at just what stage is a particular region in the course of age hardening, particularly when, as in the case under discussion, the thermal history is both widely variable within the specimen and known in only a speculative way. The simplest procedure which occurred to the writer was to age the various pieces of the Fig 2 specimen, as well as the Fig 4 specimens, at 100°C, since a very large background of data had been built up on the behavior of 12 pct aluminum-zinc aged at this temperature. Results of this aging analysis are plotted in Fig 3 and 5.

Discussion of Results

The outstanding feature of the results obtained from the partial immersion quenching test is the hardness of the region just above the quenching liquid level relative to the hardnesses of the other regions of the bar. From Fig 2, 4, and 6 the following broad details can be observed:

1. The high purity 12 pct aluminum-zinc shows a very sharp dip in hardness just above the quenching water level in the 0.4 in. square cross-section bar and the absence of any such dip in the 0.1 × 0.4 in. rectangular cross-section bar quenched in either oil or water.
2. The commercial purity 0.4 in. square cross-section bars of 24S and 75S show no dip.

The foregoing findings are the chief contribution which this paper offers to the experimental knowledge of the quenching operation. Unfortunately, time was not available to extend the investigation to other high purity systems than aluminum-zinc; but the previously-mentioned difficulties with 0.4 in. diam specimens of both high purity 4 pct aluminum-copper and 12 pct aluminum-zinc and the known lack of similar difficulties with commercial precipitation hardening aluminum alloys suggested that, in contrast to commercially pure alloys, high purity alloys may be vulnerable to unavoidable variables in even the best quenching practice. Among the possible explanations for this vulnerability and perhaps the most evident are:

1. *Critical cooling rate.* It might be assumed that a critical cooling rate exists, faster than that at which full hardening on aging subsequent to quenching is obtained and slower than that at which substantially full hardening during quenching to the temperature of the coolant is obtained. On this basis it might be argued that, after 0.1 hr at room temperature, 12 pct aluminum-zinc specimens cooled both above and below the critical cooling rate would be at approximately the same high hardness level; at about the critical cooling rate, such specimens would be soft, since very little precipitation would have occurred, yet room temperature precipitation could be very slow because the lattice defects present in volently quenched specimens would not be present to promote nucleation, despite the appreciable supersaturation.

2. *Quenching stresses.* Phillips and Brick suggested[12] that "quenching stresses are an important factor in accelerating and, perhaps, actually causing, age hardening."

3. *Thermal fluctuations.* Throughout the present paper the term "thermal fluctuations" is defined to comprise the momentary fluctuation which it is assumed would be observed if a continuous, instantaneous record could be kept of representative isotherms in a specimen being quenched. Such fluctuations would mean that, in a given small region affected (that is, a volume element several hundred atoms in diameter and larger), the temperature would first fall and then, momentarily, would rise before again falling. With slow, uniform cooling presumably an isotherm would contract uniformly without appreciable fluctuations occurring. With submerged jet-quenching of thin sections, perhaps such fluctuations would be minimized. With more massive specimens, however, the combination of fluctuating vapor zone surrounding the specimen being quenched, coolant convection currents, and an appreciable quantity of heat to be removed from the interior of the specimen, is assumed to give rise to thermal fluctuations of sufficient magnitude to cause the anomalous hardening results which have been reported.

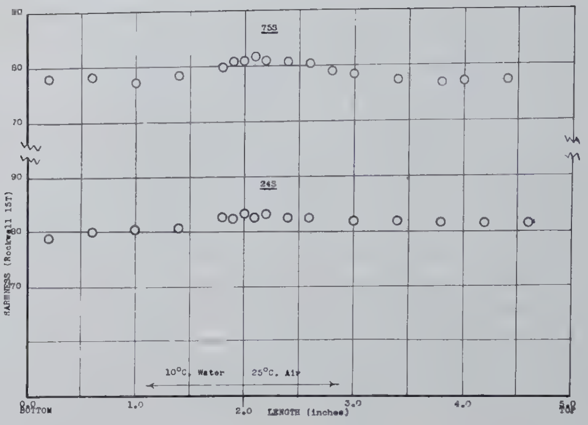

FIG 6—Commercial aluminum alloy partial immersion quenching.

24S and 75S bars with the same dimensions and heat treatment as Fig 2A. Each point the average of three determinations across the width of the specimen made one hour after quenching.

Table 1 . . . Data on Quenching Rates of 75S

75S Specimen and Coolant	Quenching Rate* (°F per Sec)
1/16 in. sheet—	
air	4
oil	128–1600
water	2500
3/4 in. diam, water quenched—	
center	830
4 in. diam, water quenched—	
1/8 in. from surface	280
center	42
2 in. diam; water quenched—	
1/8 in. from surface	430
center	135

* Average through the range 750–550°F.

In considering the critical cooling rate possibility, the excellent experimental work of Fink and Willey[13] is quite useful. These investigators established a "C" curve for 75ST, plotting as a function of time at isothermal quenching temperatures, the percentages of full 75ST properties attained. This work, in common with other published data by Fink and his collaborators on the precipitation hardening of high purity aluminum-copper and including the classic paper on double aging peaks,[6] was done with 0.064 in. thick specimens and thus, according to the findings of the present investigation, were quenched entirely satisfactorily. Fink and Willey also published[13] extensive quenching rates for 75S, a few pertinent data being given in Table 1.

From this tabulation it can be observed that, in aluminum alloys, air cooling is negligibly slow relative to the cooling effected by conduction through the aluminum to a water quenched surface. Additional pertinent information on quenching rates in aluminum alloys has also been given by Loring, Baer, and Carlton,[14] who employed a modified Jominy quench test specimen for their investigation. Extrapolating the Fink and Willey cooling rate data to the partial immersion quenching of the 0.1 and 0.4 in. thick specimens of the present investigation, one can conclude that, if a critical rate were of controlling importance, both these specimen thicknesses would have exhibited a sharp hardness dip if one did. The high purity 12 pct aluminum-zinc alloy showed a marked hardness dip in the 0.4 in. thickness but not in the 0.1 in. thickness. Hence it is concluded that the existence of a critical cooling rate does not explain the findings.

In developing their quenching stress thesis with high purity aluminum-copper alloys, Phillips and Brick used specimens from 0.0025 in. diam (filings) to 1.5 in. diam rod. Their many ingenious experiments established a very consistent trend in increasingly anomalous behavior with increasing specimen diameter. They concluded that the anomalies were related to and perhaps originated in the solution heat treatment and quench. It is perhaps significant, in light of the data reported by the present paper, that Phillips and Brick secured quite uniform results up to a specimen thickness of 0.125 in., but that from the next greater thickness (0.25 in.) investigated, results were increasingly anomalous. In a very worthwhile discussion of the Phillips and Brick investigation, Barrett estimated the magnitude of the quenching stresses existing on a radial element near to the surface of the specimens and concluded that they reached a maximum compressive stress of about 15,000 psi. More recent work by Finlay and Hibbard[11] investigated the effect of 100,000 psi hydrostatic pressure on the precipitation hardening of the 12 pct aluminum-zinc alloy. This hydrostatic pressure aging is of course a different situation from that obtaining in a quenched cylinder which has tangential tensile stress and radial compressive stress present. The hydrostatic pressure aging indicated that precipitation hardening was both accelerated and intensified relative to atmospheric-pressure-aged specimens, but the differences were by no means great enough to account for those shown by the present investigation. In any case, both the region of the sharp hardness dip and the region of the high hardness plateau at the upper end of the 0.4 in. thick, 12 pct aluminum-zinc specimen were above the water level and, therefore, were in locations where quenching stresses were much less than in the region below the water level and presumably were quite low. Accordingly, it does not appear that quenching stresses can explain the results obtained.

In considering the possible action of thermal fluctuations on a precipitation hardening system, one is led to the thought that they may—under proper combinations of time, temperature, and composition—effect retrogression. From Fig 3 and 4 it is seen that the various regions of the 12 pct aluminum-zinc alloy, whether of the 0.4 in. square or 0.1 × 0.4 in. rectangular cross-sections, and whether water, oil, or air quenched, do indeed exhibit a 100°C aging behavior which is consistent with the hypothesis that each has been retrogressed to a different degree depending upon the kind of thermal fluctuations to which it was subjected.

The element of retrogression which appears rather definitely to be present in the hardness dip region of the 0.4 in. square aluminum-zinc specimen is the existence of a supersaturated solid solution which is much less unstable than the same structure freshly quenched. This is evidenced by the relatively quite slow hardening rates at 100°C shown in Fig 3 compared to the much faster room temperature aging of the freshly quenched specimens shown in Fig 1. Similarly slow hardening rates are assumed in Fig 5, as shown by the dashed lines, since, unfortunately, data were not taken earlier than 22 hr on the 100°C aging of the Fig 5 specimens. Guinier's explanation[15] for the reduced hardening rate of the retrogressed structure assumes that the as-quenched matrix lattice is subjected to high internal stresses and, accordingly, has many lattice defects which promote nucleation of precipitate particles. Both the initial aging at room temperature and subsequent retrogression "anneal" at 100°C given the aluminum-zinc specimen tend to diffuse these defects away, so that the nucleation rate is reduced and, with it, the rate of hardening.

Evidence for the presence of the other element of retrogression—resolution of coherent precipitate particles—is not clear from the data obtained. It seems possible that both re-solution and overaging (that is, breaking away from coherency with the matrix) of precipitate particles are involved. Thus, in the case of the air quenched specimen of Fig 4, some precipitation must have occurred during the period of relatively slow cooling and subsequent room temperature aging of one hour's duration. The low hardness can be interpreted to indicate that some of the larger precipitate particles had broken away from coherency. Upon subsequent 100°C aging, some of these noncoherent particles may have redissolved in the aluminum matrix; others may have remained noncoherent; and possibly a number of coherent precipitate particles redissolved. In any case, the typical retrogression feature of a more perfect lattice and, consequently, a lower rate of nucleation are believed to have obtained and resulted in a reduced rate of hardening to the retrogression peak. This point of view is employed in the following paragraphs to examine the details of Fig 2 and 3:

1. The Fig 2 data show generally falling hardness from the bottom of the specimen to the water line. Below the latter it is pictured that the thermal fluctuations are quickly quieted by the rapid water quenching, the more rapid and effective the quenching (as in the bottom and edges) the less the thermal fluctuations. Thermal fluctuations, arising from heat coming from the interior, tend to begin to retrogress the outer portions so that they exhibit somewhat less than the expected room temperature hardness peak of 75–80 Rockwell 15T. Consistent with this, Fig 3 shows that on subsequent 100°C aging, retrogression continued and then recovery set in until the retrogression peak was attained. This viewpoint is consistent with the additional observations that: (*a*) the surface midpoint exhibits lower hardnesses than the surface edges; and (*b*) the surface has lower hardnesses than the interior.

2. Between the water line and 0.8 in. above the water line it is observed that (*a*) surface hardness is very low and does not change appreciably with distance but there is a noticeable tendency for the surface midpoints to become harder than the surface edges, and (*b*) like the surface, the interior hardness reaches a decided low at about the water line but, unlike the surface, the interior hardness recovers to higher values very quickly as the distance increases from the water line.

It is envisioned that because of the slower cooling just above the water line relative to that below the water line there are sufficient degree and duration of thermal fluctuations to soften the matrix to the retrogression valley. Fig 3 shows that subsequent 100°C aging raises this region out of the valley up to the retrogression peak. The interior is believed not to be subjected to as severe retrogression as the surface except at the water level and so it is generally harder but nevertheless at the retrogression valley.

3. Beyond approximately 1 in. above the water level, the hardnesses of all regions are at the highest levels attained and are matched only by the hardness at the very bottom of the specimen where presumably quenching was best. It is hypothesized that at the still slower cooling rate of this region, relative to that just above the water level, there is a longer period of severe thermal fluctuations capable of retrogressing the structure so that this region is retrogressed to the retrogression peak. Accordingly, on subsequent 100°C aging, as shown in Fig 3, the hardness falls off very slowly due to overaging.

4. From 0.8 to 1.8 in. above the water line it is observed that the surface midpoint is harder than the surface edge. This is just the opposite from the situation below the water line. Never-

theless, the thermal fluctuation retrogression theory gives a consistent explanation of the happenings. From its viewpoint it is believed that the edges both in the region under discussion and also below the water line are not retrogressed as much as the midpoints but, since in this case the hardness of the region is climbing out of the retrogression valley, the midpoints have reached the retrogression peak and are therefore harder than the edges which have not yet attained it. In the case of the region below the water the midpoints have also retrogressed more than the edges but there its advanced state meant that it had descended farther into the retrogression valley and hence was softer than the edges.

Fig 4 and 5 give the results of 0.1 in. thick bars as contrasted to the 0.4 in. thick bars of Fig 2 and 3. Similar, though less marked, results are shown in Fig 4 and 5 to those portrayed in Fig 2 and 3. The explanation for the data is also believed to be similar. No significant difference was found between the midpoints and the edges since there was not a sufficient thermal reservoir in the interior to give rise to it. For the same reason, a pronounced hardness valley was not developed just above the water line. The air-cooled specimen was discussed earlier. Subsequent aging of these specimens at 100°C resulted in the remarkably uniform hardness level characteristic of 12 pct aluminum-zinc overaging slowly from the retrogression peak.

Unlike the high-purity 12 pct aluminum-zinc, the commercial 75S and 24S bars with an 0.4 in. square cross-section did not exhibit a vulnerability to poor quenching practice. This is believed to be due to the fact that the commercial alloys have relatively very stable precipitates which resist retrogression and, indeed, this feature would appear to be a prerequisite to industrial use. As shown in Fig 6, the hardness curves, after partial immersion quenching of 75S and 24S, show no tendency whatever towards the hardness valley which is such a pronounced feature of the comparable 12 pct aluminum-zinc bar.

Summary and Conclusions

The high purity, binary, aluminum-zinc alloy containing 12 pct zinc was shown to exhibit marked retrogression at quite moderate temperatures. By means of a special testing technique, termed partial immersion quenching and aging, it was established that this alloy was quite vulnerable to the variables encountered during quenching, and this was ascribed to its ready retrogression, possibly in concert with overaging, as effected by thermal fluctuations; further, that this vulnerability dropped to negligible proportions when the specimen thickness was not greater than 0.1 in.; and, finally, that commercial purity alloys 24S and 75S are not at all similarly vulnerable. Smaller scale tests indicated that high purity 4 pct aluminum-copper exhibited a quenching and aging behavior similar to that of the high purity 12 pct aluminum-zinc alloy.

A selection from the extensive literature on the "anomalous" quenching and aging behavior shown by high purity, binary, precipitation hardening alloys was presented. Examination of these references shows the use of specimen thicknesses considerably greater than 0.1 in. The thicknesses employed included 3/16 in. for silver-aluminum;[5] 1/4 in. for aluminum-zinc;[7] 1/4 in. for aluminum-silver;[8] 5/32 in. for aluminum-copper;[1,2,3,4] and, quite recently, 1/2 in. for aluminum-copper.[16] The majority, and perhaps all, of these anomalies are perhaps explicable on the basis of the size effect postulated by this paper. Additional evidence supporting this view is given in Ref. 3 wherein, when some of the anomalous-hardening 5/32 in. thick specimens were forged to 1/8 in. thickness, good and consistent age hardening results were obtained.

Based on the foregoing, the generalization is tentatively put forward that many precipitation hardening systems, particularly those comprising high purity binary alloys, may, because of ready retrogression and overaging, exhibit quite erratic quenching and age hardening behavior when the specimen thickness exceeds some maximum in the neighborhood of 0.1 in., since greater thicknesses inevitably give rise to excessive thermal fluctuations upon being quenched into a liquid. Commercial precipitation hardening alloys are believed not to be subject to such retrogression and overaging, since considerable tolerance to a relatively wide range of quenching conditions is presumably one of the essential prerequisites determining the suitability of an alloy for industrial use. It would appear, therefore, that the research worker dealing with noncommercial alloys should consider the possibility of a significant size effect in many precipitation hardening systems and should employ some procedure such as the partial immersion quench test to insure that his quenching practice does not contain any uncontrolled variable which may invalidate his data, particularly in the early stages of aging.

Acknowledgment

Acknowledgment is made to the Remington Arms Co., Inc. for the use of equipment and facilities; and, for helpful discussions, to the writer's colleagues, M. B. Vordahl and D. R. Adessa, and to Professor W. R. Hibbard, Jr.

References

1. M. L. V. Gayler and G. D. Preston: *Jnl.* Inst. Met., (1932) **48, 197.**
2. M. L. V. Gayler: *Jnl.* Inst. Met., (1937) **60, 75.**
3. M. L. V. Gayler: *Jnl.* Inst. Met. (1938) **63, 67.**
4. M. L. V. Gayler and R. Parkhouse: *Jnl.* Inst. Met. (1940) **66,** 67–84.
5. M. Cohen: Aging Phenomena in a Silver-rich Copper Alloy. *Trans.* AIME (1937) **124,** 138–156.
6. W. L. Fink and D. W. Smith: Age-Hardening of Aluminum Alloys, III—Double Aging Peaks. *Trans.* AIME (1938) **128,** 223–233.
7. W. L. Fink and K. Van Horn: Equilibrium Relations in Aluminum-Zinc Alloys of High Purity. *Trans.* AIME (1932) **99,** 132–140.
8. A. H. Geisler, C. S. Barrett and R. F. Mehl: Aging in the Solid Solution of Silver in Aluminum. *Trans.* AIME (1943) **152,** 182–200.
9. R. F. Mehl and L. K. Jetter: The Mechanism of Precipitation from Solid Solution—The Theory of Age-Hardening. 1939 Symposium on Age-Hardening of Metals. Amer. Soc. for Metals, 342–417.
10. G. Masing: Present-Day Problems of Metallurgy. *Trans.* AIME (1933) **104,** 13–47.
11. W. L. Finlay and W. R. Hibbard, Jr.: Some Effects of Applied Stresses on Precipitation Phenomena. *Trans.* AIME **180,** 255. *Metals Tech.* Sept. 1948, TP 2470.
12. Arthur Phillips and R. M. Brick: Effect of Quenching Strains on Lattice Parameter and Hardness Values of High-purity Aluminum-Copper Alloys. *Trans.* AIME (1934) **111,** 94–112.
13. W. L. Fink and L. A. Willey: Quenching of 75S Aluminum Alloy. *Trans.* AIME (1947) **175,** *Metals Tech.*, Aug., 1947, TP 2225.
14. B. M. Loring, W. H. Baer, and G. M. Carlton: The Use of the Jominy Test in Studying Commercial Age-hardening Aluminum Alloys. *Trans.* AIME (1947), **175,** *Metals Tech.* Feb. 1948, TP 2337.
15. A. Guinier: Age-Hardening of Light Alloys. *Research* (1949) **2,** 6–11.
16. A. W. McReynolds: Plastic Deformation Waves in Aluminum. *Jnl.* Inst. Met. (1949) **1,** Sec. 3, 32–45.
17. U.S. Pat. #2,239,744 to D. W. Smith and W. L. Fink, issued on 4-29-41.

The Ternary System, Copper-manganese-zinc

T. R. GRAHAM,[*] J. R. LONG,[†] C. E. ARMANTROUT,[†] and A. H. ROBERSON[‡]

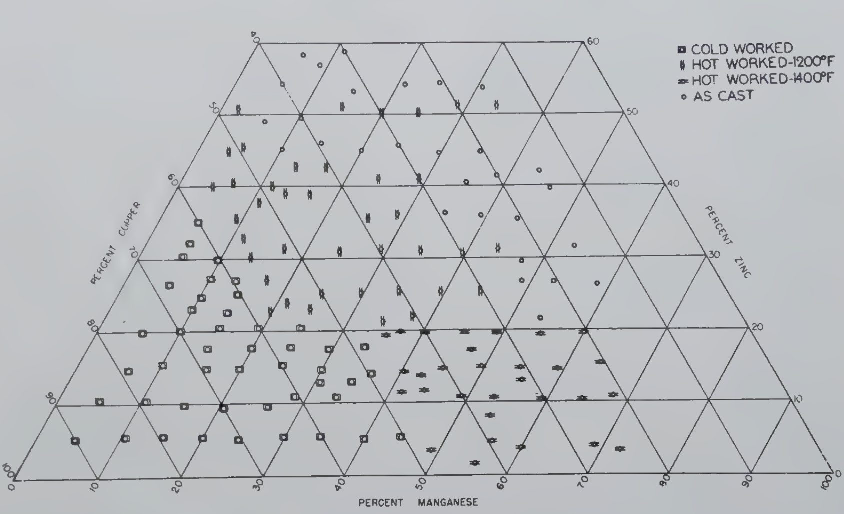

FIG 1—Condition of the alloys prior to thermal treatments used in this investigation.

Introduction

The preparation and fabrication of copper-manganese-zinc alloys and the evaluation of their engineering properties have for some time been an integral part of a research program of the Federal Bureau of Mines. In this project, the use of electrolytic manganese, along with high purity copper and zinc, has permitted the preparation of alloys which contain a minimum of impurities which are capable of producing detectable effects in the properties studied. The initial work on the physical properties of wrought alpha solid solution alloys and a general outline of the alpha solid solution area for alloys containing up to 40 pct manganese have been presented in previous reports.[1,2,3,4,5] The evidence accumulated in these investigations clearly showed that additions of manganese to the copper-zinc alloys improve the strength properties of the brasses without seriously reducing their characteristic ductility and that considerable quantities of manganese could be added to the copper-zinc alloys without exceeding the mutual solubilities of manganese and zinc in copper. In continuation of these studies, additional data have been obtained in a more extensive investigation of the phase relationships of the copper-manganese-zinc ternary system. The present report delineates the solid phase boundaries of the ternary system from the copper-zinc binary to the manganese-zinc binary for alloys containing up to 50 pct zinc.

Summary

The alloys used in this investigation were conditioned by working schedules designed to homogenize the structures prior to heat treatments required for the equilibrium phase study. The treated alloys were examined by metallographic methods including hardness and X ray data for confirmation.

The composite data of the investigation are summarily presented in a series of isothermal sections of the ternary system at 1100, 1200, 1300, 1400, and 1500°F. The salient features of the system as outlined by these data are: (1) the continuous alpha solid solution which extends across the diagram to the gamma-manganese phase of the manganese-zinc system at temperatures of 1200°F and higher, (2) the beta phase of the copper-zinc system similarly forms a continuous solid solution with its counterpart the beta field of the manganese-zinc binary, (3) at 1100°F (593°C) these alpha and beta fields are greatly restricted by complications arising from the allotropic transitions of manganese and the decreasing solubility of manganese in the alpha solid solution. The alpha + beta fields intersect the alpha + alpha manganese field to produce the beta + alpha manganese field and two adjacent three phase fields consisting of alpha + beta + alpha manganese and gamma + beta + alpha manganese.

Typical microstructures representative of the various phase areas at each temperature are also presented.

Review of Previous Work

The copper-manganese-zinc alloys have periodically been the subject of numerous investigations of both prac-

Cleveland Meeting, October 1949.
TP 2699 E. Discussion of this paper (2 copies) may be sent to *Transactions* AIME before December 1, 1949. Discussion is tentatively scheduled for publication in May, 1950.
Manuscript received April 29, 1949; revision received July 13, 1949.

Papers by authors of the U. S. Bureau of Mines staff are not subject to copyright.

[*] Metallurgist, Rolla Branch, Metallurgical Division, Bureau of Mines, Rolla, Mo.

[†] Metallurgist, College Park Branch, Metallurgical Division, Bureau of Mines, College Park, Md.

[‡] Metallurgist, Albany Branch, Metallurgical Division, Bureau of Mines, Albany, Ore.

[1] References are at the end of the paper.

tical and theoretical significance.[6] In a large measure, these studies have been concerned with the duplex, alpha + beta, alloys which constitute a commercially important group of engineering materials normally referred to as manganese bronzes. The actual manganese content of these alloys seldom exceeds 4 to 5 pct, and frequently is less than the total iron, nickel, tin and lead contents. Other investigations of the higher manganese compositions by Heusler,[7] Bauer and Hansen,[8] Guillet,[9] and Hieke and Ledebur[10] have been somewhat more extensive but are of limited value since their results were based on relatively impure alloys under admittedly nonequilibrium conditions. Reports by members of the Bureau's staff,[4,5] have discussed the characteristics of a large group of the copper-manganese-zinc alloys, but did not include alloys containing more than 40 pct manganese.

The binary systems involved have been thoroughly examined in numerous studies and the principal phase boundaries are well established. The copper-zinc system has recently been reviewed by Phillips and Brick.[11] The copper-manganese system was thoroughly examined in the early part of the Bureau's work on alloys of electrolytic manganese.[12] Potter and Huber[13] using powder metallurgy methods for the preparation of the alloys have determined the phase relationships of the manganese-zinc system for alloys containing up to 50 pct zinc by X ray diffraction and thermal analysis methods.

Experimental Materials and Methods

The alloys used in this investigation were prepared from electrolytic manganese, wire bar grade copper and 99.99+ zinc in substantially the same manner as described in the previous reports on these and similar alloys. It is perhaps also unnecessary to list the individual analyses for the 145 alloys examined but sufficient to point out that they were selected from some 500 heats of copper-manganese-zinc alloys which were made for a variety of experimental studies. These alloys were chosen on the basis of their suitability with due regard to their relative position in the ternary system and their low impurity content. The principal impurities present in the alloys are iron, silicon, and aluminum. Only four of the alloys contained greater than 0.020 pct iron and these contained less than 0.040 pct iron. The silicon content of all the alloys was reported as less than 0.005 pct. The residual aluminum from the intentionally added deoxidizer did not exceed 0.04 pct and in 96 of the alloys the aluminum content was less than 0.02 pct.

Since cast alloys are not ideally suited for the determination of phase relationship because of their inherent characteristics of segregation, porosity, tendency for grain boundary constituents, persistence of agglomerated precipitates, and others, efforts were made to give the alloys a substantial amount of working before the final thermal treatments. However, this was not possible in all cases and a fixed processing schedule which would suit all the alloys could not be devised.

In this investigation one group of the copper rich alloys has been hot and then cold worked. Another group containing higher manganese and zinc was hot worked only and still other compositions were examined in the as-cast condition. The metallurgical condition and composition of the individual alloys prior to heat treatment are denoted in Fig 1. Contrary to the general tradition that high manganese alloys are normally quite brittle and unworkable, this chart shows that a substantial proportion of the alloys was hot rolled or forged. With proper adjustment of temperature in accordance with the phase boundaries subsequently developed, no doubt many of the other compositions could have been hot and cold worked. In fact, in some later work, many of the alloys containing more than 50 pct manganese with 10 to 15 pct zinc were cold rolled 60 pct reduction in thickness after quenching from 1400°F (760°C) without difficulty.

The high copper alloys which were finished by cold working, Fig 1, had, in addition to some hot reduction, three anneals with cold reductions averaging 50 to 60 pct between anneals. The hot worked alloys were reduced approximately 80 pct from the as-cast size with intermittent soaking at 1200 or 1400°F (648 or 760°C). Examination of the hot worked alloys showed the cast structures were entirely destroyed and that homogeneous or uniform structures were produced.

Several of the alloys were not worked prior to heat treatment. These alloys were primarily those highest in zinc or manganese. The castings, which were chill cast in 1¼-in. diam ingots, were quite uniform and clearly defined in structure and without serious segregation.

Specimens of the individual alloys were heat treated for periods of 4, 8, 24, and 48 hr at 1300, 1400, and 1500°F (704, 760, and 815°C) and for 24, 48, and 200 hr at 1100 and 1200°F (593 and 648°C) in an atmosphere of helium, then quenched. In some of the highest manganese alloys slight demanganization occurred but seldom penetrated more than a few thousandths of an inch deep. All heat treated specimens were bisected so that an internal surface of one section could be used for metallographic study and the other was reserved for incidental hardness checks and X ray diffraction patterns as required for confirmation.

Approach to equilibrium conditions was determined by comparison of the structures obtained by various time periods at the same temperature. In general the structures differed but slightly and these differences were usually in amount of phases present. In a few instances, a phase was found to disappear in borderline compositions with longer heating periods. Structure of specimens held 24 and 48 hr at 1300, 1400, and 1500°F (704, 760, and 815°C) were unchanged by the longer time at temperature. Similarly structures of materials treated for 48 and 200 hr at 1100 and 1200°F (593 and 648°C) exhibit no change with the longer soaking time at temperature. The final observations from which the isothermal diagrams were drawn are based on the 48-hr treatment for 1300, 1400, and 1500°F (704, 760, and 815°C), while the 1100 and 1200°F (593 and 648°C) sections were based on 200-hr specimens.

Discussion of Results

The results of the investigation are graphically represented in Fig 2, 3, 4, 5, and 6 in which the isothermal sections for the ternary copper-manganese-zinc system at 1500, 1400, 1300, 1200, and 1100°F (815, 760, 704, 648, and 593°C) temperature levels have been drawn. In these drawings, the various phase boundaries have been extrapolated to the solubility values taken from the established copper-zinc, manganese-zinc, and copper-manganese diagrams. Where experimental observations permitted positive placement of the phase boundaries, solid lines have been drawn. Where the data are too incomplete for accurate placement of the phase boundary, but the trend of the field was known, dashed lines were used for the extension of the

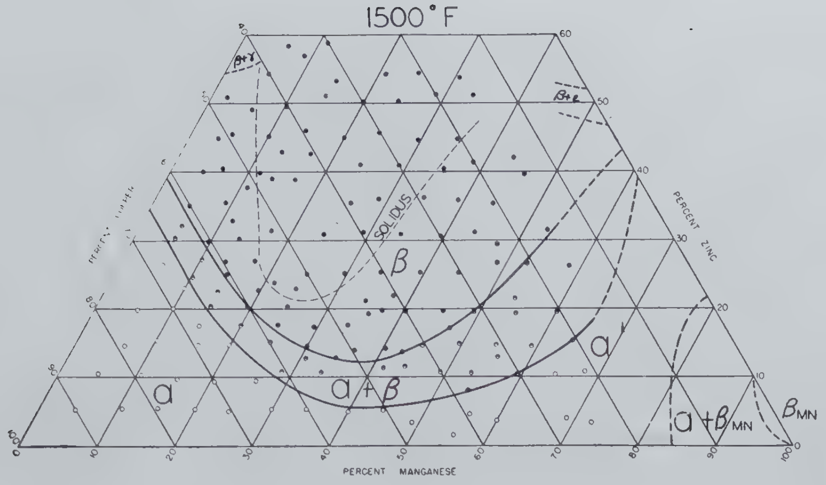

FIG 2—The isothermal section of the copper-manganese-zinc system at 1500°F (815°C).

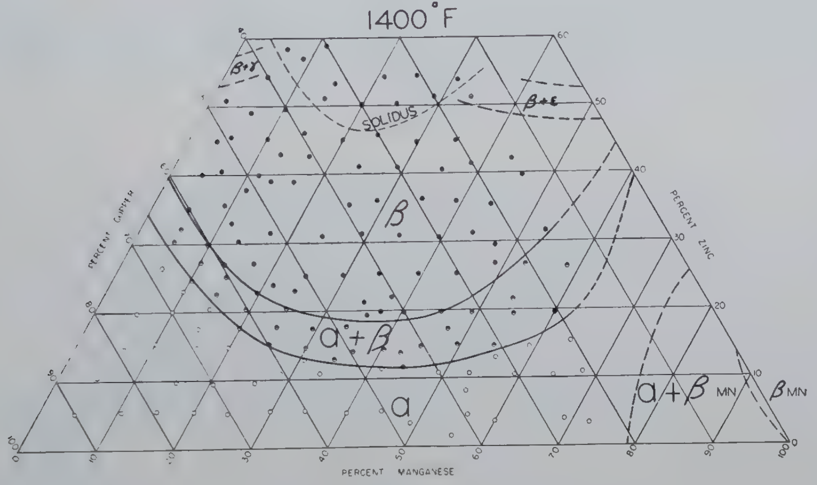

FIG 3—The isothermal section of the copper-manganese-zinc system at 1400°F (760°C).

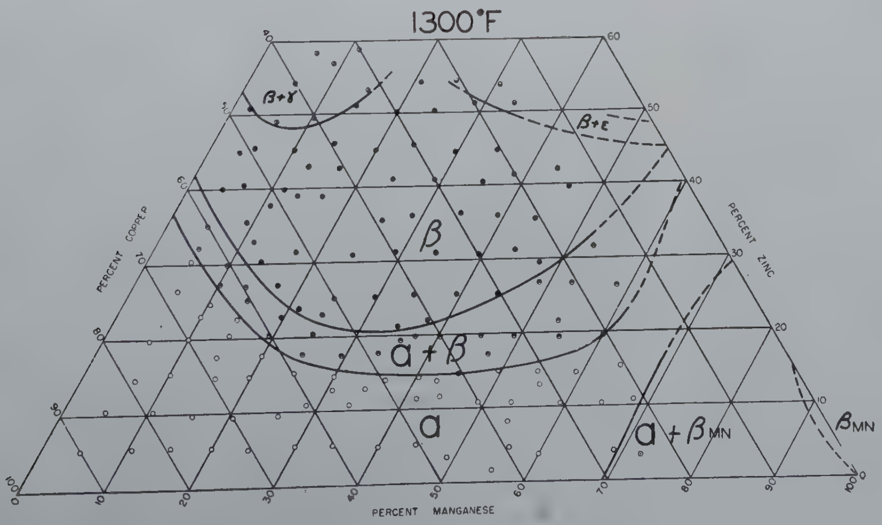

FIG 4—The isothermal section of the copper-manganese-zinc system at 1300°F (704°C).

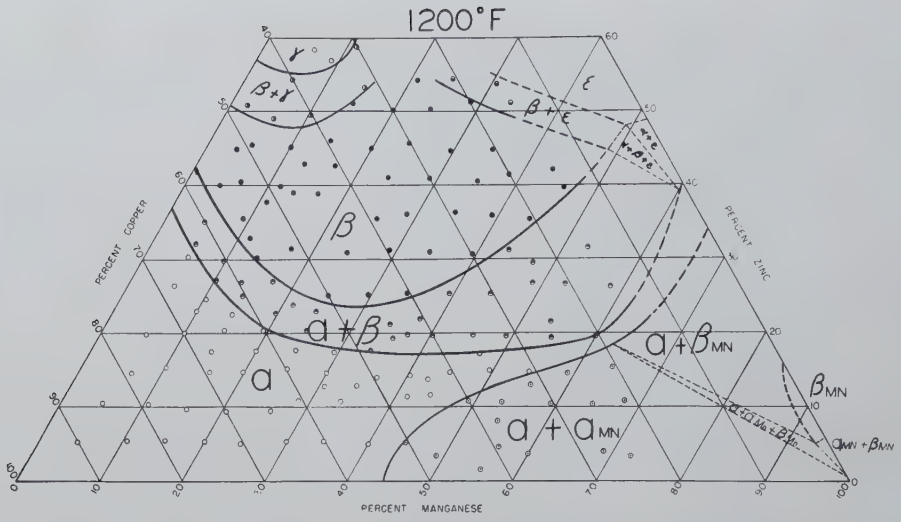

FIG 5—The isothermal section of the copper-manganese-zinc system at 1200°F (648°C).

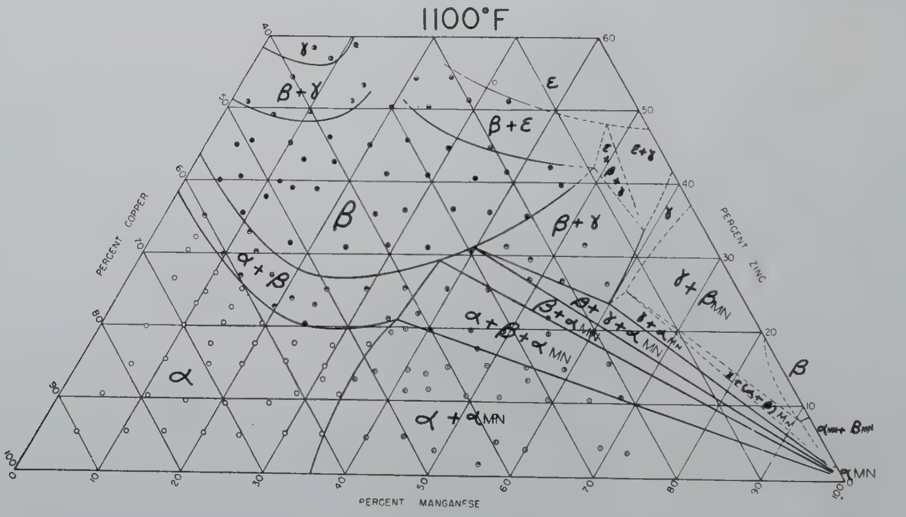

FIG 6—The isothermal section of the copper-manganese-zinc system at 1100°F (593°C).

boundary. In each of the isothermal sections, certain of the phase fields were not defined by the data but because they are necessary construction imposed by the binaries or by data in subsequent sections, dashed lines have been used to approximate their position.

At 1500°F (815°C), Fig 2, the alpha and beta solid solutions of the copper-zinc system extend uninterrupted to the manganese-zinc binary although the solubility of zinc in these phases decreases to a minimum at approximately 40 pct manganese then increases with larger amounts of manganese reaching a maximum solubility at the manganese-zinc binary. Some restriction in the alpha solid solution occurs near the manganese corner and a two phase field of alpha solid solution plus beta manganese has been estimated on the basis of the solubility data of the manganese-copper and manganese-zinc system. The solidus line which has been incorporated in the 1500°F (815°C) isotherm is not intended as an exact solidus but has been drawn primarily to differentiate between those alloys which showed evidence of melting and those which did not exhibit melting at this temperature.

Manganese decreases the solubility of zinc in the alpha phase of the copper-zinc system. The alpha and beta solubility lines are substantially parallel to one another and parallel to the lines of constant copper up to 15 to 20 pct manganese. In general, manganese and zinc act as equivalents. The present data show slightly less solubility of zinc in the alpha and beta phases in the range of 20 to 40 pct manganese than were previously recorded in work on the alpha solubility limits. Calculations by Hume-Rothery[14] on the earlier data, showed that manganese in small amounts affected the alpha-beta equilibrium as though it were a divalent element but departed from this simple relationship at rather low manganese contents. The solubility line of the present investigation indicates the solubility curves are comparable to the theoretical curve up to 15 to 20 pct manganese if equilibrium were determined by electron concentration alone and manganese possessed a valency of 2. As the concentration of manganese increases beyond 20 pct the alpha + beta phase field tends to widen and

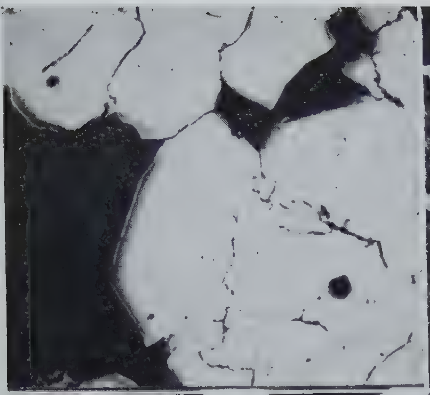

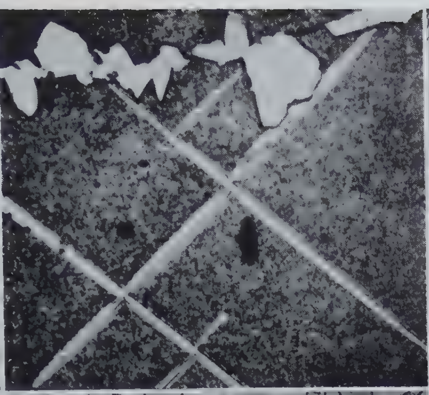

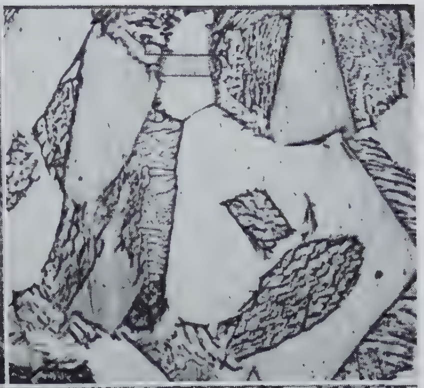

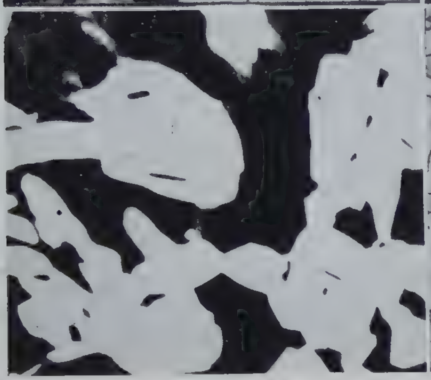

10

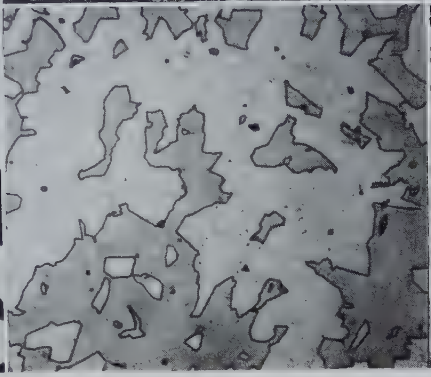

11

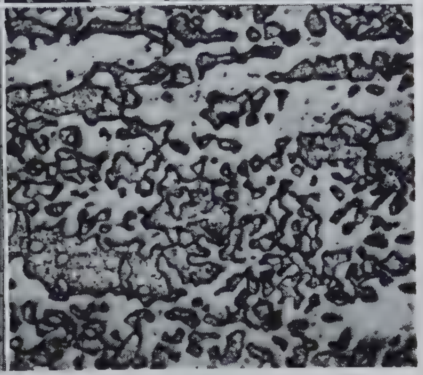

12

FIG 7—Alpha (light) and beta retained in the 58.0 Mn, 26.0 Zn alloy quenched from 1500°F.
× 250. ASTM copper etchant No. 11.

FIG 8—Beta (dark) and grain boundary alpha formed during cooling the 40.5 Mn, 14.2 Zn alloy from 1500°F.
× 250. ASTM copper etchant No. 11.

FIG 9—Alpha (light) and transformed beta (dark) in the 33.6 Mn 10.6 Zn alloy quenched from 1500°F.
× 250. ASTM copper etchant No. 11.

FIG 10—Alpha (light) and retained beta (dark) in the 58.0 Mn 26.0 Zn alloy quenched from 1400°F.
× 250. ASTM copper etchant No. 11.

FIG 11—Alpha (light) and beta (dark) structure of the 40.0 Mn 19.2 Zn alloy quenched from 1300°F.
× 250. ASTM zinc etchant No. 4.

FIG 12—Alpha (light) and beta manganese (dark) in the 72.1 Mn 3.2 Zn alloy quenched from 1300°F.
× 250. ASTM copper etchant No. 8 with 10 pct acetic acid added.

becomes more or less parallel to the copper-manganese binary at approximately 40 pct manganese. With larger amounts of manganese, the alpha + beta field continues to widen and the solubility of zinc in both the alpha and beta phases increases. These solubility curves are extrapolated from the 15 pct copper line to the manganese-zinc binary and decrease considerably in width with decreasing copper to correspond with the extent of this phase field in the binary system.

Similar trends of the alpha/alpha + beta and beta/alpha + beta solubility lines for the ternary system are shown in the 1400°F (760°C) isothermal section in Fig 3, although these curves are displaced to higher zinc concentrations. The solidus shifts rapidly as the temperature decreases from 1500 to 1400°F (815 to 760°C) and a rather large beta area is formed at the lower temperature. The projections of the beta + gamma field of the copper-zinc system and the beta + epsilon field of the manganese-zinc system are also introduced at 1400°F (760°C).

At 1300°F (704°C), Fig 4, the general shape and contour of the alpha and beta boundaries remain substantially the same as indicated for the higher temperatures. The alpha/alpha + beta and beta/alpha + beta lines are approximately parallel giving the field a spread of 5 to 6 pct as measured on lines of constant manganese for all compositions up to about 40 pct manganese. With increasing manganese the two phase field widens to a maximum at 60 pct manganese then decreases to the manganese-zinc binary values.

The metallographic structures of specimens treated at 1300, 1400, and 1500°F (704, 760, and 815°C) are in general quite similar to the characteristic alpha and beta structures of the copper-zinc system and are readily identified. Some exceptions, however, were encountered in the beta alloys which were immediately adjacent to the beta/alpha + beta boundary. These alloys, particularly in the low manganese range, often transform bodily to the alpha phase during the quench making it difficult to be positive of the high temperature structure. Characteristic micrographs of these structures as well as structures of the alpha and beta phases for alloys containing less than 30 pct manganese were presented in the report on the alpha solubility limits.[4] Phillips[15] has also described the mass transformation reactions for the binary copper-zinc alloys.

Representative structures for alloys containing more than 40 pct manganese and falling within the alpha + beta and beta fields are illustrated in Fig 7 to 11, inclusive. In these structures the beta phase appears as the dark or acicular constituent. In general, increasing manganese tends to stabilize the beta phase, but varying degrees of decomposition depending on composition and temperature were found to occur.

13

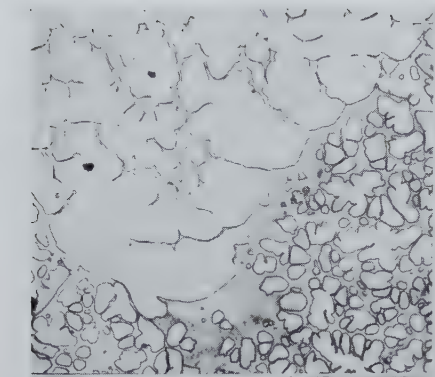

14

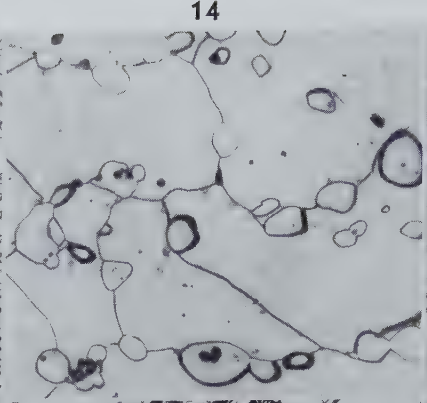

15

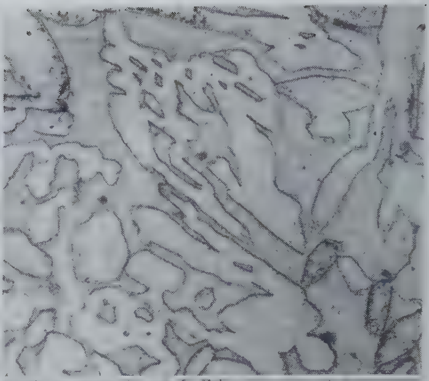

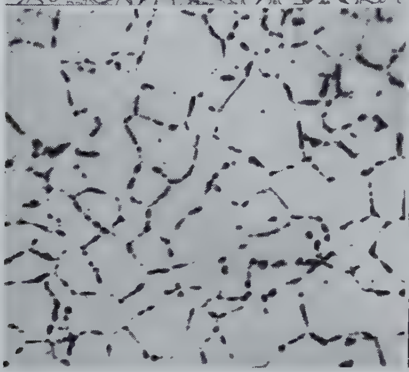

16

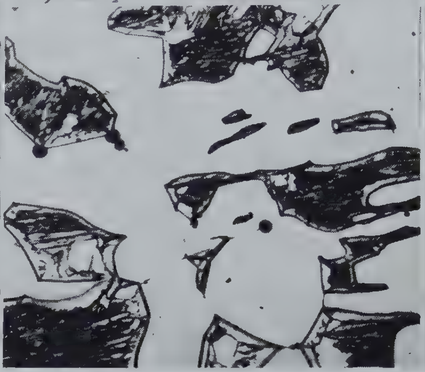

17

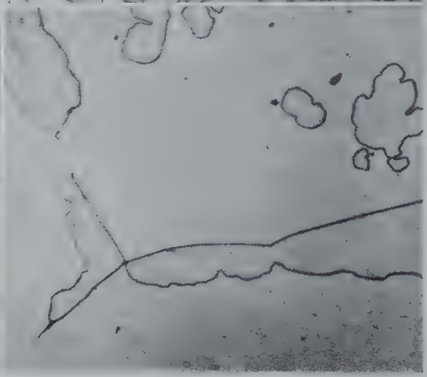

18

FIG 13—Beta and gamma phases in the 5.6 Mn 54.2 Zn alloy quenched from 1300°F.
× 250. ASTM copper etchant No. 11.

FIG 14—Alpha and beta structure of the 43.4 Mn 31.0 Zn alloy quenched from 1200°F.
× 250. ASTM zinc etchant No. 4.

FIG 15—Alpha and beta structure of the 37.5 Mn 22.0 Zn alloy quenched from 1200°F.
× 250. ASTM zinc etchant No. 4.

FIG 16—Alpha solid solution with alpha manganese in the 55.8 Mn 4.8 Zn alloy quenched from 1200°F.
× 250. ASTM zinc etchant No. 4.

FIG 17—Beta and epsilon structure of the 30.3 Mn 53.6 Zn alloy quenched from 1200°F.
× 250. ASTM zinc etchant No. 4.

FIG 18—Beta with a small amount of the gamma phase in the 1.75 Mn 50.8 Zn alloy quenched from 1100°F.
× 250. ASTM copper etchant No. 8 with 10 pct acetic acid added.

Fig 7 and 10 are characteristic alpha + beta structures obtained when there is little tendency for the beta phase to decompose. The formation of grain boundary and acicular alpha within the beta grain, Fig 8, occurs during the quench. Fig 9 illustrates an alpha + beta structure in which the beta phase is almost completely transformed during the cooling. In the micrograph of Fig 11, designated as an alpha + beta structure, it is quite probable that most of the alpha present was formed during the quench and that the beta/alpha + beta boundary could be lowered slightly at this point. However, evidence from the near-by compositions and the trends shown in pseudo-binary sections for higher and lower temperatures point to the position of the solubility line given.

The alpha + beta manganese structure is shown in Fig 12 for one of the alloys which falls within this field at 1300°F (704°C). The microstructure in Fig 13 is typical of the low manganese high zinc alloys in the beta + gamma field and are similar to the structures of beta + gamma brasses.

The beta solid solution field is slightly reduced by the beta + gamma and beta + epsilon fields at 1200°F (648°C), Fig 5, and the alpha + beta boundary has shifted to higher zinc concentrations. The eutectoid decomposition of the beta phase in the manganese-zinc system requires the formation of the three phase field alpha + beta + epsilon and the alpha + epsilon field which have been tentatively positioned in the isothermal section for this temperature.

The contour of the alpha solubility line has a decided bulge at 60 pct manganese and 20 pct zinc but the field of complete miscibility remains with a narrow corridor between the manganese solubility curve and the alpha/alpha + beta line. Since the gamma manganese phase of the manganese-zinc system, which has been treated as the alpha solid solution phase of the ternary system up to this point, remains stable at this temperature and none of the beta or alpha + beta alloys was found to contain manganese, it was assumed that these two boundaries have not joined at this temperature. It must be admitted, however, that only a limited number of alloys are positioned in this area. If a junction of the two lines did occur, it would necessarily be in the neighborhood of compositions containing less than 10 to 12 pct copper and alloys in the adjacent fields would contain precipitated manganese.

A new three phase field is introduced in the manganese rich corner of the diagram at 1200°F (648°C) based on the alpha to beta transition of manganese. Here again, the exact position of the alpha + alpha manganese + beta manganese field has been estimated, since all of the experimental compositions were found to contain only the alpha manganese phase. The beta manganese phase of the manganese-zinc system is stable at this temperature, therefore the three phase area must be placed at some intermediate position.

Microstructures representative of the

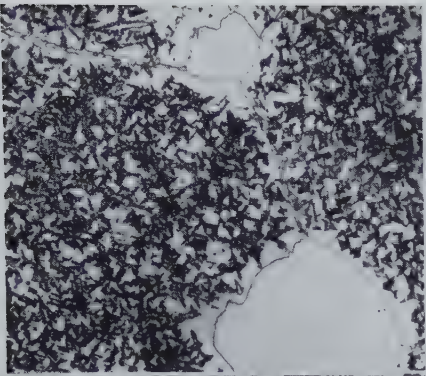

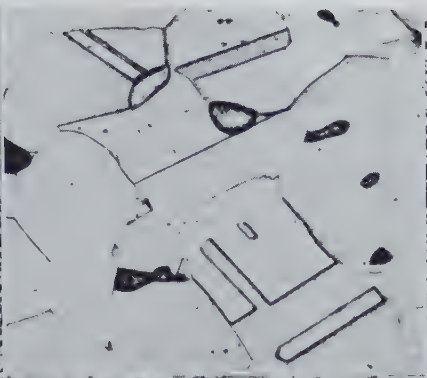

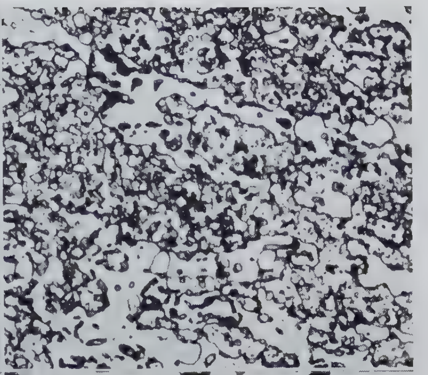

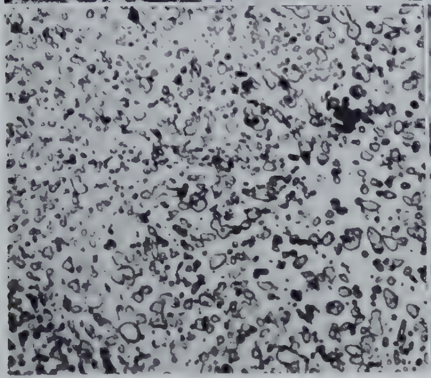

22

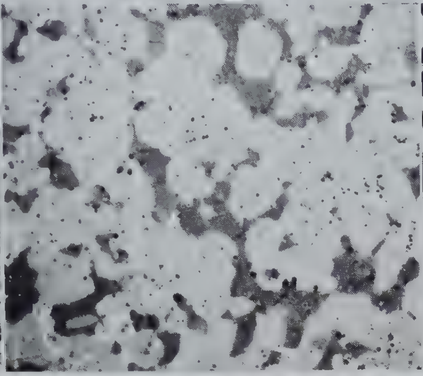

23

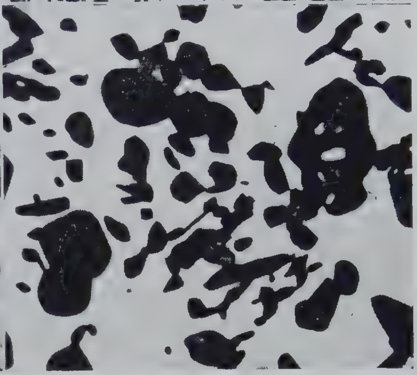

24

FIG 19—Transformed beta and gamma phases of the 10.2 Mn 49.6 Zn alloy quenched from 1100°F.
× 250. ASTM copper etchant No. 8 with 10 pct acetic acid added.

FIG 20—Alpha with traces of beta in the 19.7 Mn 22.2 Zn alloy quenched from 1100°F.
× 250. ASTM copper etchant No. 11.

FIG 21—Alpha + beta + alpha manganese structure in 54.5 Mn 19.2 Zn alloy quenched from 1100°F.
× 250. ASTM zinc etchant No. 4.

FIG 22—Beta solid solution with alpha manganese in the 53.2 Mn 21.2 Zn alloy quenched from 1100°F.
× 250. ASTM zinc etchant No. 4.

FIG 23—Beta (dark) + gamma of the manganese-zinc system (light) + alpha manganese (black) in the 48.4 Mn 26.4 Zn alloy quenched from 1100°F.
× 250. ASTM zinc etchant No. 4.

FIG 24—Beta (dark) and gamma of the manganese-zinc system (light) in the 47.2 Mn 29.3 Zn alloy quenched from 1100°F.
× 250. ASTM zinc etchant No. 4.

various phase fields at 1200°F (648°C) are shown in Fig 14 to 17, inclusive. Structures containing alpha and beta phases are shown in Fig 14 and 15. At this temperature, the high manganese beta phases are usually retained in the quench and do not transform or decompose. In Fig 14, the alpha phase is present in very minor amounts and the large grains of beta are restrained by the alpha. The alpha and beta structure in Fig 15 is representative of alloys which are more or less equidistant from the respective solubility limits. Fig 16 illustrates the alpha solid solution + alpha manganese alloys. Typical beta + epsilon structure is shown in Fig 17.

Sweeping changes occur in the copper-manganese-zinc ternary system as the temperature decreases to 1100°F (593°C). The construction given in Fig 6 is a complicated and radical departure from that of the isothermal section of Fig 5. The new fields are, however, dictated by positive metallographic and X ray evidence of the co-existence of the indicated phases in these areas. The absence of beta manganese in all experimental alloys at 1100°F (593°C) and 1200°F (648°C) and the negligible solubility of copper in both alpha and beta manganese ties these fields to the manganese corner.

The zinc content of the alpha + beta field has shifted to still higher values as the temperature decreased from 1200 to 1100°F (648 to 593°C), but the respective solubility lines of this field remain essentially parallel from the copper-zinc binary to the limit of this field at approximately 36 pct manganese.

Intersection of the alpha + alpha manganese and the alpha + beta fields creates a four phase invariant plane which at 1100°F (593°C) produces the two phase field, beta + alpha manganese, and the two adjacent three phase fields, alpha + beta + alpha manganese and gamma + beta + alpha manganese. Principal evidence to support this construction is the complete absence of beta manganese in any of the experimental alloys and the co-existence of only the beta and gamma phases without either alpha or beta manganese. The absence of beta manganese in the alloys indicates that the alpha manganese + beta manganese + alpha tentatively placed in Fig 5 must sweep toward the manganese-zinc binary before the alpha corridor is closed by the junction of the alpha + beta and alpha + alpha manganese fields. Were it otherwise, beta manganese and beta brass would be found to co-exist and this is not the case.

Representative microstructures for the two phase beta + gamma brasses are illustrated in Fig 18 and 19. Fig 18 shows the presence of a small amount of the gamma phase associated with retained beta. Transformed or decomposed beta and the gamma phase are present in Fig 19.

The microstructures observed for several of the ternary alloys containing less than 30 pct zinc annealed at 1100°F, (593°C) are reproduced in

25

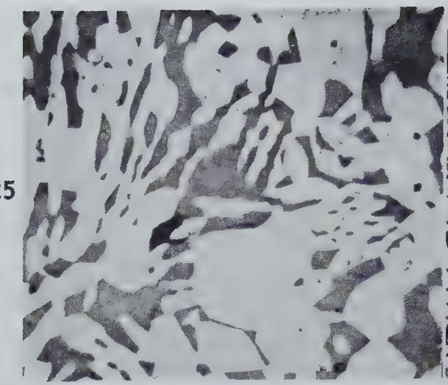

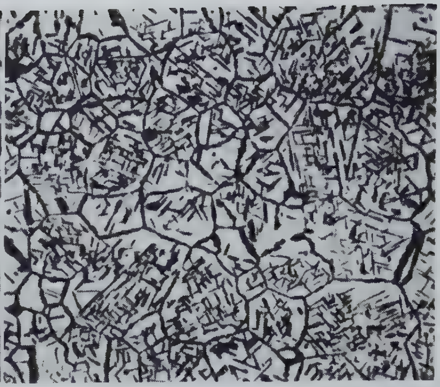

26

FIG 25—Beta (dark) and gamma of the manganese-zinc system (light) in the 52.6 Mn 26.3 Zn alloy quenched from 1100°F.
× 250. ASTM zinc etchant No. 4.

FIG 26—Alpha solid solution (light) and alpha manganese (dark) in the 55.4 Mn 13.0 Zn alloy quenched from 1100°F.
× 250. Unetched.

Fig 20 to 26. The copper rich alpha solid solution with traces of the beta phase is illustrated in Fig 20. The structure of Fig 21 is somewhat more complicated by the presence of alpha manganese along with the alpha and beta solid solution phases. With such structures relief polishing affords a rapid method for positive identification of the manganese constituent and subsequent etching reveals the beta and alpha phases, along with the manganese. Another characteristic of these alloys is the comparatively small grain size resulting from the presence of manganese which inhibits normal grain growth. The constituents in all specimens within this three phase area were also confirmed by X ray diffraction data. The precipitation of alpha manganese within the beta phase is shown in Fig 22. Only one specimen was found to fall within the narrow three phase field beta + gamma + alpha manganese. The microstructure of this alloy annealed at 1100°F (593°C) is given in Fig 23. Representative structures of alloys containing only the beta and gamma phases at 1100°F (593°C) are reproduced in Fig 24 and 25. These two micrographs clearly demonstrate the absence of a manganese phase. The presence of the gamma and beta constituents was confirmed by X ray diffraction. Fig 26 is characteristic of the alpha solid solution plus manganese alloys. The formation of alpha manganese in the grain boundaries and certain crystallographic planes within the grains is quite characteristic of alloys in this area.

Acknowledgments

The authors express appreciation for the valuable assistance of the various members of the metallurgical staff of the Bureau of Mines. Particular acknowledgment is due to the group at the Salt Lake City Laboratory where the experimental work of this investigation was conducted. The X ray investigations necessary for the identification of the various phases encountered in the microstructures were conducted by E. Vernon Potter and R. W. Huber of the Physics Section.

The final manuscript was prepared at the Rolla Station Laboratory at Rolla, Missouri.

References

1. J. R. Long and T. R. Graham: Physical Properties of a 65 Cu, 10 Mn, 25 Zn Alloy. *Trans.* AIME (1944) **156,** 222.
2. R. S. Dean, J. R. Long, T. R. Graham, and R. G. Feustel: Physical Properties of Cu-Mn-Zn Alloys Containing 60 Percent Cu and 5 to 25 Percent Mn. *Trans.* AIME (1946) **166,** 185. *Metals Tech.* Jan. 1946, TP 1956.
3. R. S. Dean, J. R. Long, T. R. Graham, and C. W. Matthews: A White High-Manganese Brass: *Trans.* AIME (1945) **161,** 244.
4. R. S. Dean, J. R. Long, T. R. Graham, and A. H. Roberson: The Alpha Solid Solution Field of the Copper-Manganese-Zinc System. *Trans.* AIME (1945) **161,** 232.
5. R. S. Dean, J. R. Long, and T. R. Graham: Copper-Manganese-Zinc Alloys—Physical Properties of Wrought Copper-Rich Alloys. *Trans.* AIME (1947) **171,** 105–118. *Metals Tech.* April 1947, TP 2183.
6. O. W. Ellis: Copper and Copper Alloys. Publ. by Amer. Soc. for Metals (1948), 127.
7. O. Heusler: The Ternary System Copper-Zinc-Manganese. *Ztsch: Anorg. Chem.* (1926) **159,** 37–54.
8. O. Bauer and M. Hansen: The Influence of a Third Metal on the Constitution of Brass Alloys. *Ztsch. Metallkunde* (1933) **25,** 17.
9. L. Guillet: *Rev. Met.* (1905) **2,** 105–111; (1906) **3,** 258–262.
10. W. Heike and K. Ledebur: The Alpha Plus Gamma Eutectoid of the Brasses. *Ztsch. Metallkunde* (1924) **16,** 380–381.
11. A. Phillips and R. M. Brick: Copper-Zinc Diagram. Metals Handbook A.S.M. 1948 Edition, 1206.
12. R. S. Dean, J. R. Long, T. R. Graham, and E. V. Potter: The Copper-Manganese Equilibrium System. A.S.M. (1945) **34,** 443–464.
13. E. V. Potter and R. Huber: The Manganese-Zinc Diagram from 0 to 50 Percent Zinc. A.S.M. Preprint No. 30 (Oct. 1948).
14. W. Hume-Rothery: The Effect of Manganese, Iron, and Nickel on the Alpha-Beta Brass Equilibrium. *Philosophical Mag.* (1948) Series 7, **39,** 89–97.
15. A. J. Phillips: The Alpha-Beta Transformation in Brass. *Trans.* AIME (1930) **89,** 194.

Discontinuous Crack Propagation—Further Studies[*]

L. D. JAFFE,[†] Junior Member AIME, E. L. REED,[†] and H. C. MANN[†]

The authors have recently published[1] evidence that brittle transgranular fracture of polycrystalline metals does *not* originate at a point and propagate continuously across the material, but rather develops at numerous related points, leading to a series of microcracks which subsequently link up. Series of related microcracks were observed in steel specimens broken in fatigue—specifically, at the central portions which broke during the final sudden fracture.

Microcracks of the type mentioned have also been reported by Baeyertz, Craig and Bumps[2] in steel broken under impact.[‡] Some micrographs published by Irwin[3] may possibly be interpreted as showing discontinuous brittle cracks. This paper presents additional observations of the authors on discontinuous crack propagation under various conditions.

Impact Test Specimens

The impact test specimens were cut longitudinally from a steel forging containing:

C	Mn	Si	P	S	Ni	V	Mo
0.24	0.50	0.15	0.034	0.027	1.52	0.03	0.33

The heat treatment consisted of oil quenching in a heavy section from 1600°F and tempering at 1260°F. The resulting yield strength was 78,000 psi, tensile strength 100,000 psi, elongation 20.0 pct in 2 in., and reduction of area 55.0 pct. Standard V-notch Charpy specimens were broken in a 217 ft-lb machine at a striking velocity of 16.8 fps. Energy absorption and fracture appearance of this material in the V-notch Charpy test are plotted as functions of temperature in Fig 1. After test, fractured halves of specimens appearing 0, 40, 80, and 100 pct fibrous (to the unaided eye) were electroplated with nickel, sectioned longitudinally (perpendicular to the notch at its midpoint), polished and etched with Cohen-Hurlich-Jacobson (C-H-J) reagent (picric acid plus Zephiran chloride in ethyl ether)[4] or with Vilella reagent (1 pct picric plus 5 pct hydrochloric acid in ethyl alcohol).[5]

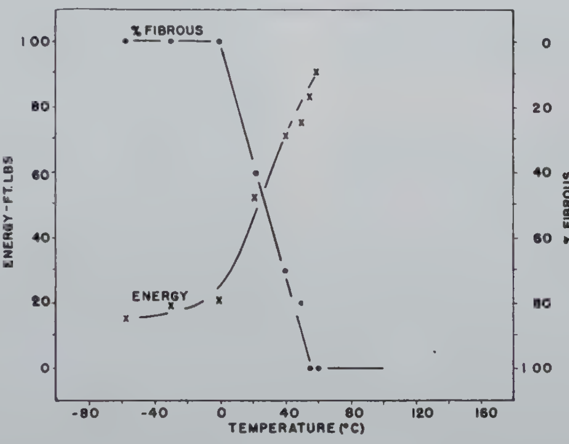

FIG 1—Impact transition curve. V-notch Charpy specimens.

Fig 2 and 3 show cracks near the path of final fracture in the specimen rated 0 pct fibrous. Many of the cracks terminate at the boundaries of ferrite grains, some at boundaries of pre-existing austenite grains.[*] A crack often starts near the end of another. Cracks within the same ferrite grains are parallel or approximately parallel in several cases. A large percentage of the cracks are branched.[†]

Fig 4 illustrated a group of cracks in the 40 pct fibrous specimen. Branching and parallelism are well marked. No more than three directions of crack have been observed on the polished surface in one ferrite grain. This is consistent with the evidence[6] that brittle fracture of ferrite takes place on the cube face crystallographic planes: the {100} planes. The appearance of some cracks suggests that they have passed around a projecting corner of a second ferrite grain by going outside the plane of polish.

In Fig 5 cracks in the 80 pct fibrous specimen may be observed. Some of

Cleveland Meeting, October 1949.
TP 2682 E. Discussion of this paper (2 copies) may be sent to *Transactions* AIME before December 1, 1949. Manuscript received May 2, 1949.
[*] Published by permission of the National Military Establishment.
[†] Watertown Arsenal Laboratory, Watertown, Mass.
[1] References are at the end of the paper.

[‡] Since preparing this article the authors have learned that Tipper[12] observed such microcracks near the fracture of mild steel plates. As the work of Baeyertz, Craig and Bumps was carried on simultaneously and independently of that of the authors, and apparently also without knowledge of Tipper's paper,[12] the microcracks have been found independently by three separate groups.

[*] By "ferrite" is not meant primary ferrite, but the body-centered cubic phase, within which carbide particles may or may not be dispersed.

[†] One of the cracks in Fig 3 seems to contain some particles. After lightly repolishing, without re-etching, hardly any of the particles could be found, but at higher magnification the edges of the crack appeared rough. It is thought that the particles are fragments torn from the edges and lodged in the crack during polishing.

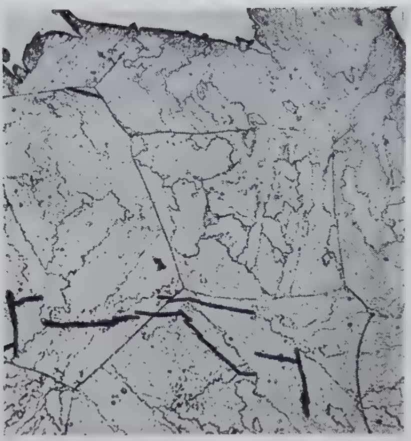

FIG 2—Microcracks near final fracture of Charpy bar rated 0 pct fibrous. Broken at −57°C, energy absorption 15 ft-lb.
× 500. Etched 1 min. in C-H-J reagent, repolished ½ min., re-etched 10 sec. Reduced approx. one half in reproduction

the cracks have a step-like path. In the area shown the final fracture appears transgranular and brittle ("crystalline"), with little if any evidence of deformation visible. The austenite and ferrite grains are equiaxed. Fig 6 shows an area where the final fracture appeared transgranular but ductile (fibrous), with evidence of local deformation near the break. The austenite and ferrite grains are not equiaxed and it appears that the material flowed in tension perpendicularly to the eventual path of fracture. No microcracks are evident in Fig 6. None was found near fibrous portions of the final fracture in the 40 pct or 80 pct fibrous specimens, or in any portion of the 100 pct fibrous bar. All cracks observed were within 0.01 in. of a brittle transgranular portion of a final fracture.

Service Fracture

A fracture was examined in a steel casting of this analysis:

C	Mn	S	P	Si	Cr	Mo	Ni
0.33	1.02	0.033	0.041	0.26	0.05	0.43	0.02

The casting had been normalized and drawn, giving a yield strength (0.1 pct offset) of 55–58,000 psi, tensile strength of 92–95,000 psi, 12–17 pct elongation in 2 in., and 13–28 pct reduction of area, in room temperature test. Sudden fracture occurred through a machined notch under service conditions of rapid loading at a temperature of −70°F. The fracture appeared to be almost completely brittle. It was prepared for examination in the same fashion as the impact test specimens, but a 4 pct picral etch was used.

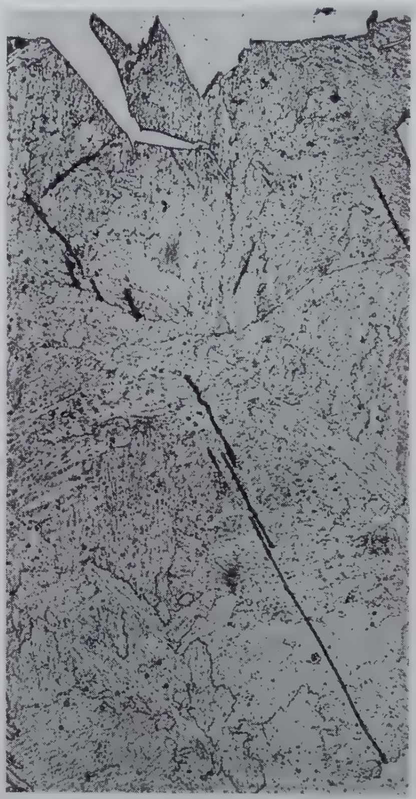

FIG 3—Microcracks very close to fracture in same Charpy bar as Fig 2.
× 500. Etched 1 min. in C-H-J reagent, repolished ½ min., re-etched 10 sec. Reduced approx. one half in reproduction

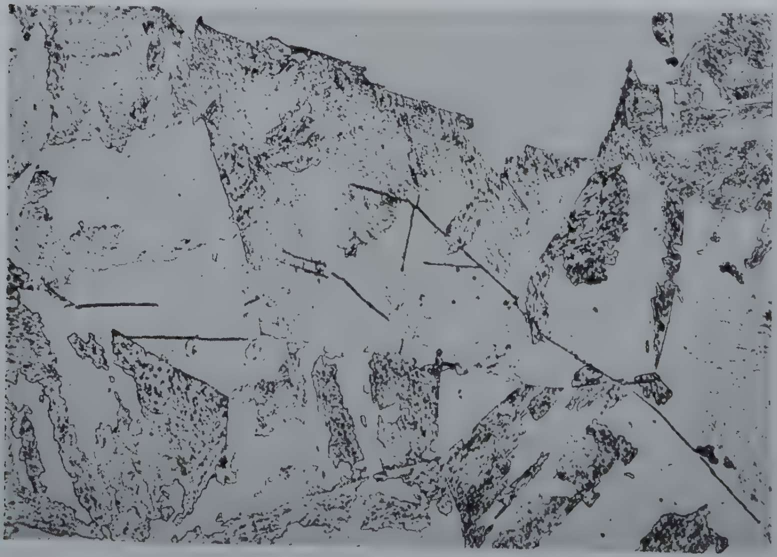

FIG 4—Group of microcracks in crystalline area near final fracture of Charpy bar rated 40 pct fibrous. Broken at +21½°C, energy absorption 52 ft-lb.
× 500. Etched in Vilella's reagent. Reduced approx. one half in reproduction

The crack in Fig 7 is "stepped" within a ferrite grain, the "treads" and "risers" appearing to lie along two sets of parallel planes. Neumann bands (deformation twins) may be seen in several ferrite grains. These twins are plainer in Fig 8. Cracks were distinguished from Neumann bands by repolishing the specimen lightly and examining without re-etching; cracks remained visible, the twins did not. Crack segments seem to be approximately parallel to Neumann bands within the same ferrite grain; some crack segments coincide with possible extensions of the bands. This suggests that microcracks have been nucleated at the stress concentrations surrounding the ends of twins, though the converse possibility that stress concentrations at the end of stopped cracks nucleated the twins cannot definitely be ruled out. Neumann bands in iron form along {112} crystallographic planes and not along the {100} planes.[7]

Fig 9 is of interest because it shows that microcracks within the metal parallel the path of the final complete fracture, when both are in the same ferrite grain. There is some evidence of this in Fig 4 also.

Micrographs discussed above have been at 500× magnification. Fig 10 shows at 1500× some of the cracks previously noted in Fig 9. A crack that might be thought "stepped" at the lower magnification is here seen to be discontinuous, at least in the plane of polish.

Fatigue Specimens

Fatigue specimens were cut transversely from a forging of the following composition:

C	Mn	P	S	Si	Cr	Mo	V
0.28	0.74	0.014	0.013	0.20	1.00	0.49	0.12

Heat treatment consisted of annealing

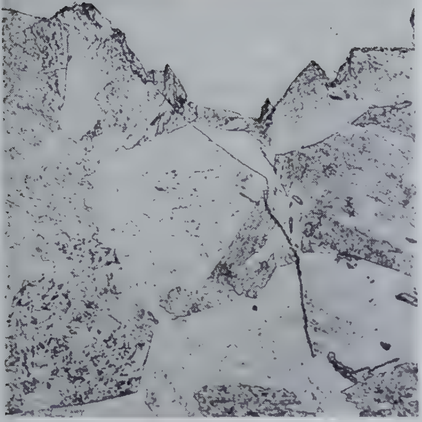

FIG 5—Some microcracks having a step-like path in crystalline area near final fracture of Charpy bar rated 80 pct fibrous. Broken at +50°C, energy absorption 75 ft-lb.
× 500. Etched in Vilella's reagent. Reduced approx. one half in reproduction.

from 1700°F, then holding 9 hr at 1675°F, water-quenching, holding 12 hr at 1150°F, and furnace-cooling. The material was heat-treated as a round approximately 8 in. in diam. The resulting yield strength (0.01 pct offset) was 105,000 psi, tensile strength 132,000 psi, elongation 15 pct, reduction of area 46 pct and V-notch Charpy impact energy 3–9 ft-lb at 70°F and 2 ft-lb at −40°F. The material was tested in rotating beam fatigue at 10,000 rpm as standard R. R. Moore specimens with 45° V-notch, having 0.015 in. radius at the base of the notch and a diameter across the notch of 0.220 in. All tests were at room temperature. The S-N curve is given as Fig 11.

Several specimens fractured at different stress levels were prepared for microexamination, as described for the impact bars. A micrograph of microcracks in a specimen broken under high stress has been published.[1] Fig 12 shows cracks in a specimen broken at the endurance limit: in 1,798,000 cycles at a nominal stress of 40,000 psi.* Microcracks were found in the fatigue specimens only near the path of final, complete, sudden fracture, where little or no evidence of deformation was observed, and never in the "battered" area where progressive fracture presumably took place over many cycles. No microcracks could be found below the notch in a specimen fatigued 40,880,000 cycles at 35,000 psi which did not fracture.

At the junction between the "battered" fracture and the final sudden brittle fracture, there was always observed a projection that appeared to have been highly deformed in longitudinal tension. An example is shown in Fig 13. The significance of this projection, as well as of the microcracks, will be discussed in the next section.

Discussion of Results

Microcracks have to date been observed by the authors every time they have been looked for in areas adjacent to a brittle transgranular fracture. An explanation of the microcracks in terms of a theory of discontinuous crack propagation was given in Ref. 1. Briefly, it is suggested that a crack propagates along a crystallographic plane, in a brittle fashion, until it is stopped by a grain boundary or by a particle of a second phase. New cracks are likely to start in the zone of stress concentration at the end of the stopped crack. The process then repeats, leading to discontinuous branching chains of microcracks. Cracks may also stop because

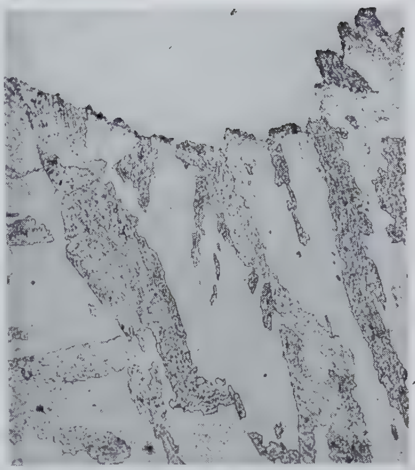

FIG 6—Local deformation in a fibrous area near final fracture of same Charpy bar as Fig 5.
× 500. Etched in Vilella's reagent. Reduced approx. one half in reproduction

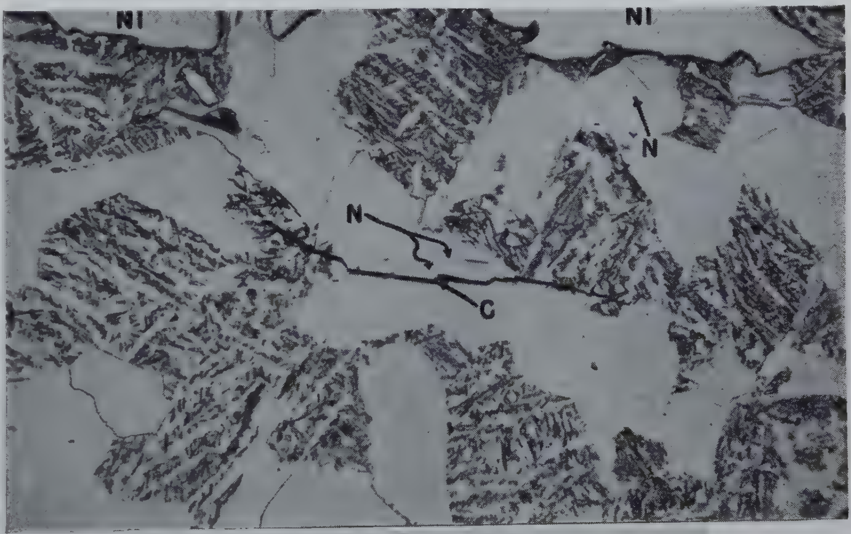

7

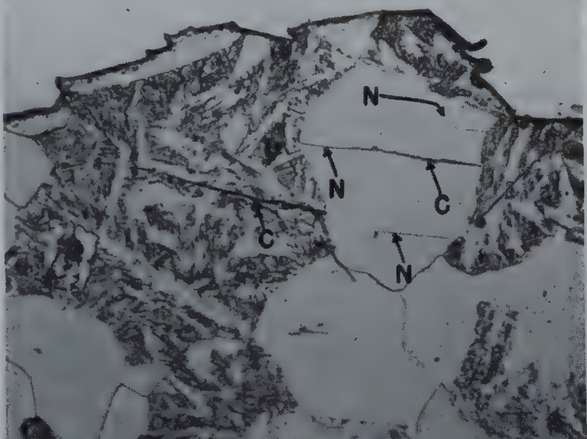

8

FIG 7 (above)—Step-like crack in ferrite grain near fracture of steel casting.
× 500. Etched in Picral. N = Neumann bands. C = Crack. Ni = Nickel electroplate. Reduced approx. one third in reproduction

FIG 8 (below)—Neumann bands and microcracks near fracture of steel casting.
× 500. Etched in Picral. N = Neumann bands. C = Cracks. Reduced approx. one third in reproduction.

---

* By nominal stress is meant maximum fiber stress calculated at the reduced section without considering stress concentration.

9

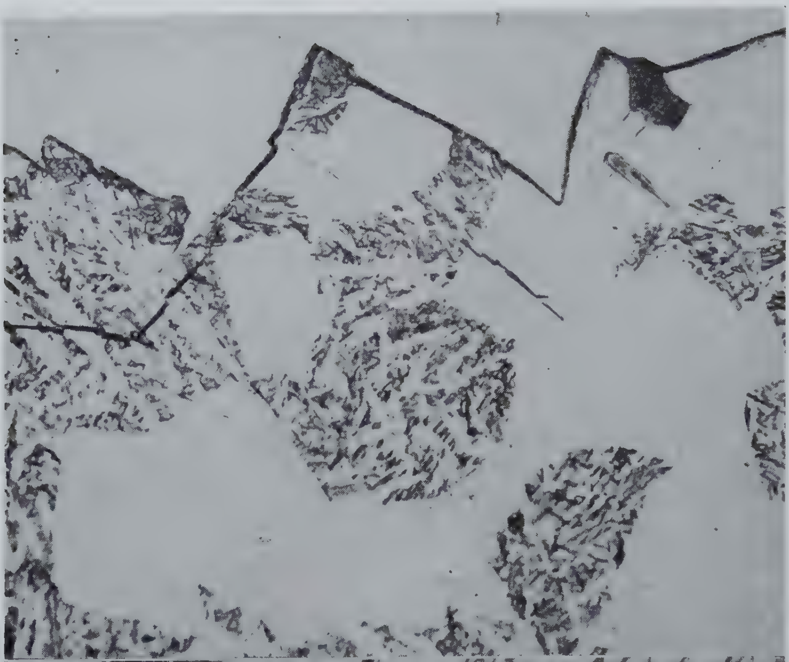

10

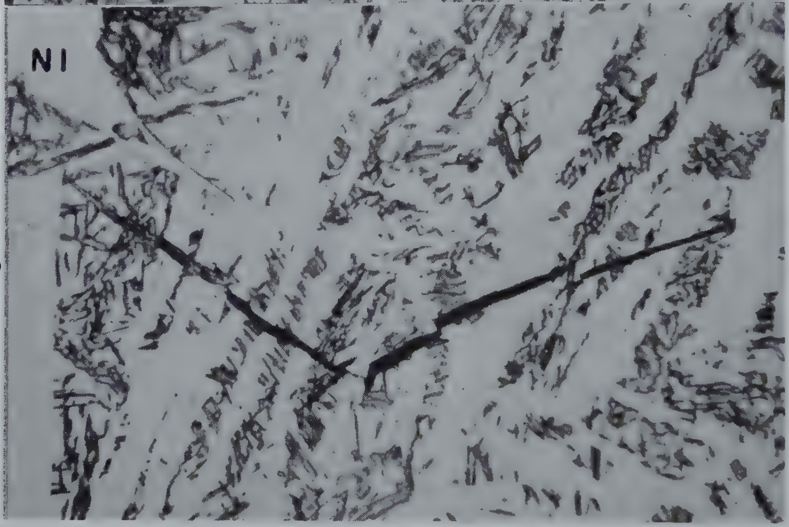

FIG 9—Microcracks near fracture of steel casting: 0.50 N.A.
× 500. Etched in Picral.

FIG 10—Same microcrack shown in Fig 9 at a higher magnification. View reversed left to right. 1.4 N.A.
× 1500. Etched in Picral. Ni = Nickel electroplate.

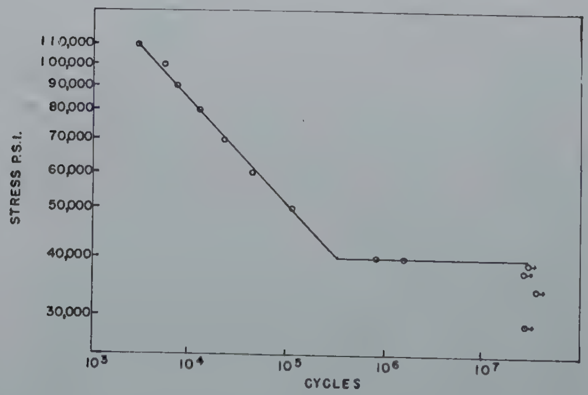

FIG 11—Fatigue test data. Notched R. R. Moore specimens.

the elastic energy released by their further spread would not be sufficient to propagate the crack (to form the new surfaces). In this last case, new cracks would have to be at orientations which would provide greater energy release.

The probability of further cracking near the ends of and within chains of microcracks will be much greater than elsewhere. The size of continuous crack will therefore tend to increase. This increase in size raises still further the probability of additional cracking in adjacent areas. When one continuous crack has traversed the specimen, macroscopic fracture has occurred. The brittle fractures which represent final severance of specimens or parts are series of linked microcracks.

Observation of microcracks in impact test specimens demonstrates that they are not associated with the repetitive loading which characterizes fatigue, and that series of microcracks can develop very rapidly (in the time of fracturing a brittle Charpy specimen, of the order of 10^{-5} sec).

The microcracks visible in the micrographs and discussed above are not identical with the Griffith defects,[8] sometimes also termed "microcracks," which are supposed to exist in the material prior to stressing.

The projection observed at the junction of the battered and the brittle regions in the fatigue specimens suggests that the material represented by the projection was deforming in tension while brittle cracking was occurring nearer the axis. The final brittle fracture presumably originated (a major series of brittle microcracks first developed) either close to the axis or a small distance below the tip of the progressively advancing "fatigue crack." Fracture originating close to the axis is analogous to fracture occurring in a tensile specimen after necking.[9] Fracture originating a small distance below the tip of the fatigue crack is analogous[10] to fracture originating a small distance below the tip of a machined notch, and might be expected because the stress there is triaxial tension, whereas at the crack or notch tip itself only biaxial stress can exist. (The stress system ahead of a fatigue crack cannot differ much from that under a sharp machined notch.[11]) In either case final fracture does not occur by propagation inward, in a brittle fashion, of the progressive fatigue crack.

Summary

Series of apparently discontinuous microcracks have been found adjacent to the path of final brittle failure in fatigue specimens, impact specimens, and a failed part, made from steel forgings and castings. These cracks

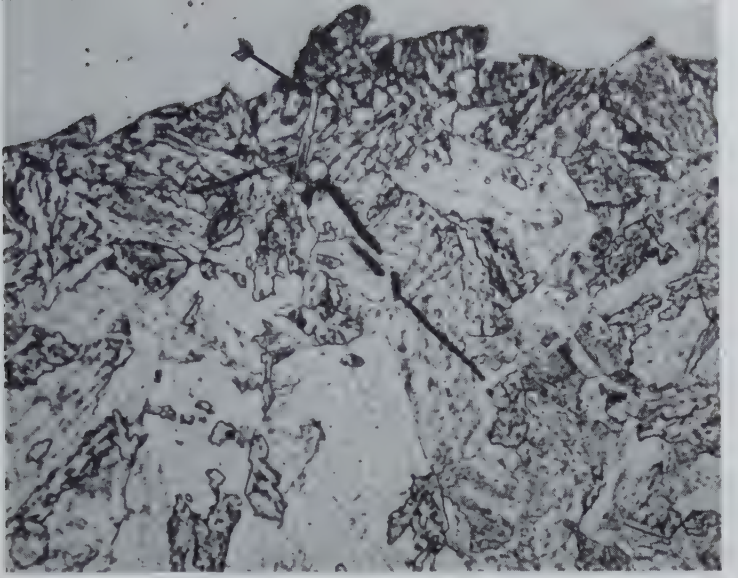

FIG 12—Microcracks near fracture of fatigue test specimen broken in 1,798,000 cycles at 40,000 psi.

White crack-like line indicated by arrow may be a crack which meets the surface outside the plane of polish and was partly filled with nickel electroplate. × 500. Etched in Vilella's reagent.

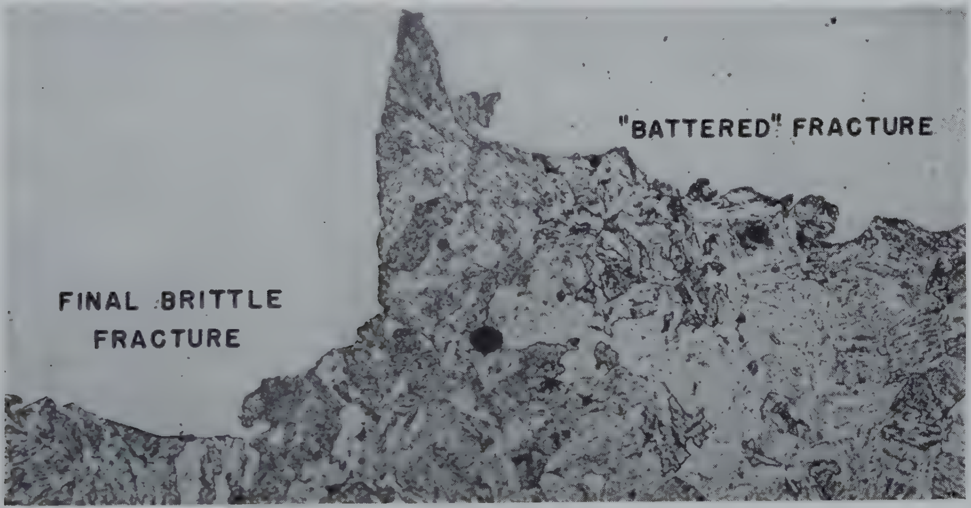

FIG 13—Projection at the junction of the "battered" (right) and final fracture (left).

Same fatigue specimen as shown in Fig 12. × 500. Etched in Vilella's reagent. Reduced approx. two-sevenths in reproduction.

have been observed every time they have been sought in areas close to a brittle transgranular fracture.

It is believed that the microcracks indicate that brittle transgranular fracture of polycrystalline metals does *not* originate at one point and propagate continuously across the material, but rather nucleates at numerous related points, leading to a series of microcracks which subsequently link up.

Microscopic evidence has also been found which is interpreted to mean that final fracture in a fatigue specimen does not occur by propagation inward, in a brittle fashion, of the progressive "fatigue crack." Rather, brittle fracture originates closer to the neutral axis and links with the fatigue crack subsequently.

References

1. L. D. Jaffe, E. L. Reed, and H. C. Mann: Discontinuous Crack Propagation. *Trans.* AIME **185**, 526; *Jnl. of Metals*, Aug. 1949. TN No. 16.
2. M. Baeyertz, W. Craig, and E. S. Bumps: A Metallographic Description of Fracture in Impact Specimens of a Structural Steel. *Trans.* AIME, **185**, 481; *Jnl. of Met.*, Aug. 1949.
3. G. Irwin: Fracture Dynamics, *Trans.* ASM (1948) **40A**, 147–166.
4. J. B. Cohen, A. Hurlich, and M. Jacobson: A Metallographic Etchant to Reveal Temper Brittleness in Steel. *Trans.* ASM (1947) **39**, 109–138.
5. J. R. Vilella: Metallographic Technique for Steel. Amer. Soc. for Metals, Cleveland. (1938) 40–45
6. F. Sauerwald, B. Schmidt, and G. Krämer: Uber den Sprödigkeitsbereich von Eisen bei Teifen Temperaturen. *Ztsch. Phys.* (1931) **67**, 179.
7. C. H. Mathewson and G. H. Edmunds: The Neumann Bands in Ferrite. *Trans.* AIME (1928) **80**, 311–333.
8. A. A. Griffith: The Phenomena of Rupture and Flow in Solids. *Trans.* Roy. Soc. (London) (1920) **A221**, 163–198.
9. P. Ludwik: Bestimmung der Reissfestigkeit aus der gleichmässigen Dehnung. *Ztsch. Metallkunde* (1926) **18**, 269–272.
10. E. Orowan. Private communication.
11. E. Orowan: Notch Brittleness and Ductile Fracture in Metals. *Trans.* Inst. of Eng. and Shipbuilders in Scotland (1946) **89**, 165–204.
12. C. F. Tipper: Brittle Fracture in Mild-Steel Plates—II. *Engineering* (1948) **165**, 594.

The Free Energy Change Accompanying the Martensite Transformation in Steels

J. C. FISHER*

Martensite transformations in steels and other alloys are characterized in part by the absence of composition changes during the growth of a new phase. Transformation occurs rapidly, and there is insufficient time for long range diffusion or partition of alloying elements to take place; martensite reactions in alloys thus are similar to phase transformations in single component systems.

A fundamental understanding of martensite transformations in steels is impossible without knowledge of the free energy change upon transforming austenite (face centered cubic iron containing alloying elements) to ferrite (body centered cubic iron containing alloying elements) of the same chemical composition. The present paper assembles the best information available concerning the influence of temperature and composition on this free energy change. Most of the material has been taken from the work of Johansson,[1] Mehl and Wells,[2] Zener[3,4] and Smith;[5] and indirectly, through these authors, from the work of Austin.[6]

In agreement with the generally accepted viewpoint, martensite is assumed to be an ordered solution of carbon in ferrite of the same composition as the parent austenite; only at high temperatures and low carbon concentrations is the carbon in ferrite distributed at random. The properties of the disordered solution are estimated by extrapolating the known properties of iron-carbon solid solutions into the range of supersaturation, and the free energy change associated with ordering is estimated from the theory developed by Zener. By incorporating Smith's recent thermodynamic measurements and Zener's theory of ordering, the present analysis modifies previous estimates of the free energy change associated with martensite transformations.

Consider a two component system consisting of a solvent A and a solute B. Let N_A and N_B represent mol fractions of A and B respectively, let $a_A = \gamma_A N_A$ and $a_B = \gamma_B N_B$ represent activities, and let superscripts 1 and 2 refer to phases 1 and 2. The partial molal free energies of A and B in phases 1 and 2 can be summarized as follows:

free energy	standard state
$\bar{F}_A{}^1 - \bar{F}_{A0}{}^1 = RT\ ln\ a_A{}^1$	pure A^1
$\bar{F}_A{}^2 - F_{A0}{}^2 = RT\ ln\ a_A{}^2$	pure A^2
$\bar{F}_B{}^1 - \bar{F}_{B0} = RT\ ln\ a_B{}^1$	pure B
$\bar{F}_B{}^2 - F_{B0} = RT\ ln\ a_B{}^2$	pure B.

The free energy of a gram atom of phase 1 is*

$$\Delta F^1 = N_A{}^1\bar{F}_A{}^1 + N_B{}^1\bar{F}_B{}^1$$

and that of phase 2 is

$$\Delta F^2 = N_A{}^2\bar{F}_A{}^2 + N_B{}^2\bar{F}_B{}^2.$$

A martensite transformation from phase 1 to phase 2 requires

$$N_A{}^1 = N_A{}^2 = N_A \text{ and } N_B{}^1 = N_B{}^2 = N_B,$$

and the free energy change per gram atom accompanying transformation is

$$\begin{aligned}\Delta F^{1\to 2} &= N_A(\bar{F}_A{}^2 - \bar{F}_A{}^1) + N_B(\bar{F}_B{}^2 - \bar{F}_B{}^1)\\ &= N_A[RT\ ln\ (a_A{}^2/a_A{}^1) + \Delta F_A{}^{1\to 2}] + N_B\ RT\ ln\ (a_B{}^2/a_B{}^1)\\ &= N_A[RT\ ln\ (\gamma_A{}^2/\gamma_A{}^1) + \Delta F_A{}^{1\to 2}] + N_B\ RT\ ln\ (\gamma_B{}^2/\gamma_B{}^1), \quad [1]\end{aligned}$$

where $\gamma_A{}^2$, $\gamma_A{}^1$, $\gamma_B{}^2$, $\gamma_B{}^1$ are activity coefficients, and where $\Delta F_A{}^{1\to 2}$ is the free energy change upon transforming a gram atom of pure A from phase 1 to phase 2 at the temperature in question.

For martensite transformations in plain carbon steels, A = iron (Fe), B = carbon (C), 1 = austenite (γ), 2 = ferrite (α), and Eq 1 is

$$\Delta F^{\gamma\to\alpha} = N_{Fe}[RT\ ln\ (\gamma_{Fe}{}^\alpha/\gamma_{Fe}{}^\gamma) + \Delta F_{Fe}{}^{\gamma\to\alpha}] + N_C\ RT\ ln\ (\gamma_C{}^\alpha/\gamma_C{}^\gamma). \quad [2]$$

Nothing is known concerning the values of $\gamma_{Fe}{}^\alpha$ and $\gamma_C{}^\alpha$ for carbon concentrations in excess of 0.025 pct. However, the approximation

$$\gamma_{Fe}{}^\gamma = \gamma_{Fe}{}^\alpha = 1$$

cannot be appreciably in error for small carbon concentrations, and Eq 2 reduces to

$$\Delta F^{\gamma\to\alpha} = N_{Fe}\Delta F_{Fe}{}^{\gamma\to\alpha} + N_C\ RT\ ln\ (\gamma_C{}^\alpha/\gamma_C{}^\gamma). \quad [3]$$

Johansson[1] and Zener[3] have calculated $\Delta F_{Fe}{}^{\gamma\to\alpha}$ from the specific heat measurements compiled by Austin.[6]* Their calculated values agree closely, and are summarized in Table 1.

The activity coefficients relative to graphite for carbon dissolved in iron vary with temperature according to the relationships

$$d\ ln\ \gamma_C{}^\gamma/d(1/T) = \Delta H_C{}^\gamma/R$$
$$d\ ln\ \gamma_C{}^\alpha/d(1/T) = \Delta H_C{}^\alpha/R$$

where $\Delta H_C{}^\gamma$ and $\Delta H_C{}^\alpha$ are the heats of solution of graphite in γ and α iron. Assuming the values of ΔH to be independent of carbon concentration and temperature,

$$ln\ \gamma_C{}^\gamma = \Delta H_C{}^\gamma/RT + I_1$$
$$ln\ \gamma_C{}^\alpha = \Delta H_C{}^\alpha/RT + I_2$$

Cleveland Meeting, October 1949.
TP 2704 E. Discussion of this paper (2 copies) may be sent to *Transactions* AIME before December 1, 1949. Discussion is tentatively scheduled for publication in May 1950
Manuscript received May 2, 1949.
* General Electric Co., Schenectady, N. Y.
[1] References are at the end of the paper.

---

* A gram atom of solution contains N_A gram atoms of component A, N_B gram atoms of component B, N_C gram atoms of component C, and so on.

* Johansson employed also specific heat measurements from several other sources.

where I_1 and I_2 are integration constants. The value of $RT\ ln\ (\gamma_C^\alpha/\gamma_C^\gamma)$ reduces to

$$RT\ ln\ (\gamma_C^\alpha/\gamma_C^\gamma) = \Delta H_C^\alpha - \Delta H_C^\gamma + RT\,\Delta I. \quad [4]$$

Smith[5] has determined quite accurately the value $\Delta H_C^\gamma = 10{,}000$ cal per g atom. ΔH_C^α is less accurately known, Smith having obtained a value 20,000 cal per g atom from his own experimental data, and a value 26,000 cal per g atom by making use of earlier data concerning δ-iron. The value $\Delta H_C^\alpha = 20{,}000$ appears to be the more reliable, particularly for use at low temperatures. Moreover, according to a recent theory of austenite decomposition,[10] $\Delta H_C^\alpha = 20{,}500$ cal per g atom gives the best agreement between calculated M_s temperatures and those determined by Lyman and Troiano[7] for a series of 3 pct chromium steels of varying carbon content. Therefore the value $\Delta H_C^\alpha = 20{,}500$ cal per g atom is assumed, and

$$RT\ ln\ (\gamma_C^\alpha/\gamma_C^\gamma) = 10{,}500 + RT\,\Delta I. \quad [5]$$

Consider the distribution of carbon at equilibrium in the two phase $\gamma + \alpha$ region. Then

$$\Delta \bar{F}_C^\gamma = \Delta F_C^\alpha,$$
$$RT\ ln\ \gamma_C^\gamma N_C^\gamma = RT\ ln\ \gamma_C^\alpha N_C^\alpha$$

and

$$\gamma_C^\alpha/\gamma_C^\gamma = N_C^\gamma/N_C^\alpha.$$

From the equilibrium boundaries of the iron-carbon phase diagram as determined by Mehl and Wells[2] and by Smith[5] the ratio N_C^γ/N_C^α is

$$N_C^\gamma/N_C^\alpha = 0.315/0.0128 = 24.6$$

at 800°C where the carbon concentrations are relatively low and both γ_C^γ and γ_C^α are practically independent of carbon concentration.[5] Therefore, at 800°C,

$$RT\ ln\ (\gamma_C^\alpha/\gamma_C^\gamma) = 6825. \quad [6]$$

It is assumed that γ_C^α and γ_C^γ vary similarly with carbon concentration, so that the ratio $\gamma_C^\alpha/\gamma_C^\gamma$ is independent of N_C.

According to Eq 4, 5, 6 the value of $N_C\ RT\ ln\ (\gamma_C^\alpha/\gamma_C^\gamma)$ is

$$N_C\ RT\ ln\ (\gamma_C^\alpha/\gamma_C^\gamma) = N_C(10{,}500 - 3.425\ T) \quad [7]$$

decreasing linearly from 10,500 N_C at absolute zero to 6825 N_C at 800°C. However, Eq 7 was obtained by an extrapolation that effectively assumes the solution of carbon in ferrite to remain random at low temperatures. Zener[4] has shown that spontaneous

Table 1 . . . The Free Energy Difference (calories per gram atom) Between γ-iron and α-iron

Johansson[1]		Zener[3]		Johansson[1]		Zener[3]	
°K	$-\Delta F_{Fe}^{\gamma\to\alpha}$	°K	$-\Delta F_{Fe}^{\gamma\to\alpha}$	°K	$-\Delta F_{Fe}^{\gamma\to\alpha}$	°K	$-\Delta F_{Fe}^{\gamma\to\alpha}$
300	997	273	1045	1050	46	1423	−22
350	938	373	924	1100	25	1473	−21
400	873	473	784	1150	+10	1523	−18
450	805	573	622	1179	0	1573	−14
500	735	673	487	1200	− 4	1623	− 7.5
550	664	773	342	1250	− 8	1673	0
600	595	873	209	1300	−15	1773	+32
650	523	923	147	1350	−18		
700	450	973	98	1400	−18		
750	379	1023	54	1450	−17		
800	310	1073	29	1500	−16		
850	247	1123	+14	1550	−13		
900	184	1183	0	1600	− 8		
950	121	1223	− 7	1650	− 2		
975	98	1273	−14	1674	0		
1000	73	1323	−18.5	1700	+ 1		
1033	54	1373	−21	1750	+ 6		

Mean Interpolated Values

°K	$-\Delta F_{Fe}^{\gamma\to\alpha}$	°K	$-\Delta F_{Fe}^{\gamma\to\alpha}$	°K	$-\Delta F_{Fe}^{\gamma\to\alpha}$	°K	$-\Delta F_{Fe}^{\gamma\to\alpha}$
200	1109	500	738	800	308	1100	22
210	1100	510	723	810	295	1120	16
220	1091	520	708	820	282	1140	11
230	1082	530	693	830	269	1160	+ 5
240	1072	540	678	840	256	1180	0
250	1062	550	663	850	243	1200	− 4
260	1051	560	648	860	230	1220	− 7
270	1040	570	634	870	218	1240	−10
280	1029	580	620	880	205	1260	−12
290	1018	590	605	890	192	1280	−14
300	1007	600	591	900	180	1300	−16
310	995	610	577	910	168	1320	−17
320	983	620	563	920	156	1340	−18
330	971	630	549	930	144	1360	−19
340	959	640	535	940	132	1380	−20
350	946	650	521	950	121	1400	−20
360	933	660	507	960	111	1420	−20
370	920	670	492	970	102	1440	−20
380	907	680	478	980	93	1460	−19
390	893	690	463	990	84	1480	−18
400	880	700	449	1000	75	1500	−18
410	866	710	435	1010	67	1520	−17
420	853	720	420	1020	60	1540	−15
430	839	730	405	1030	54	1560	−13
440	825	740	391	1040	48	1580	−11
450	811	750	377	1050	42	1600	− 9
460	797	760	363	1060	37	1620	− 6
470	782	770	349	1070	32	1640	− 3
480	767	780	335	1080	29	1660	− 1
490	753	790	321	1090	26	1680	+ 1
500	738	800	308	1100	22	1700	+ 4

Table 2 . . . Temperature Dependence of Zener's Order Parameter

T/T_C	z	T/T_C	z	T/T_C	z	T/T_C	z
1.000	0.377	0.99	0.502	0.90	0.742	0.70	0.924
0.999	0.418	0.98	0.551	0.88	0.770	0.65	0.947
0.998	0.434	0.97	0.588	0.86	0.795	0.60	0.964
0.997	0.446	0.96	0.619	0.84	0.818	0.55	0.978
0.996	0.457	0.95	0.645	0.82	0.838	0.50	0.987
0.995	0.466	0.94	0.668	0.80	0.856	0.45	0.993
0.994	0.474	0.93	0.689	0.78	0.873	0.40	0.997
0.993	0.482	0.92	0.708	0.76	0.888	0.35	0.999
0.992	0.489	0.91	0.726	0.74	0.901	0.30	1.000
0.991	0.496	0.90	0.742	0.72	0.913	0.25	1.000
0.990	0.502			0.70	0.924		

Let $\phi = 2(1 - z)\ ln\ (1 - z) + (1 + 2z)\ ln\ (1 + 2z)$.

T/T_C	ϕ	T/T_C	ϕ	T/T_C	ϕ	T/T_C	ϕ
1.000	0.396	0.99	0.698	0.90	1.559	0.70	2.590
0.999	0.484	0.98	0.843	0.88	1.693	0.65	2.764
0.998	0.523	0.97	0.962	0.86	1.819	0.60	2.911
0.997	0.553	0.96	1.067	0.84	1.936	0.55	3.032
0.996	0.579	0.95	1.162	0.82	2.046	0.50	3.126
0.995	0.603	0.94	1.251	0.80	2.150	0.45	3.197
0.994	0.624	0.93	1.333	0.78	2.249	0.40	3.246
0.993	0.644	0.92	1.412	0.76	2.342	0.35	3.275
0.992	0.663	0.91	1.488	0.74	2.429	0.30	3.289
0.991	0.681	0.90	1.559	0.72	2.512	0.25	3.295
0.990	0.698			0.70	2.590	0.20	3.296

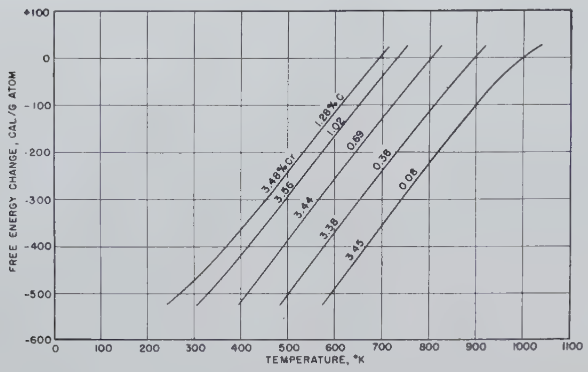

FIG 1—Variation of $\Delta F^{\gamma \rightarrow \alpha}$ with temperature for several 3.5 pct chromium steels of differing carbon content, according to Eq 12.

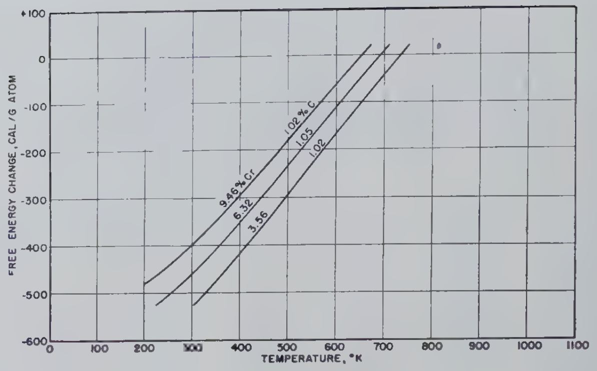

FIG 2—Variation of $\Delta F^{\gamma \rightarrow \alpha}$ with temperature for several 1.0 pct carbon steels of differing chromium content, according to Eq 12.

ordering of the carbon in ferrite takes place below the temperature

$$T_C \cong 28{,}000\ N_C \text{ (approximately)}$$

with a decrease in free energy that is not reflected in an extrapolation based upon high temperature properties; this free energy change must be added to the value of $N_C RT\ ln\ (\gamma_C{}^\alpha/\gamma_C{}^\gamma)$ that is given by Eq 7.

The decrease in free energy per unit volume on ordering can be derived from Zener's analysis, and is given by the expression

$$\Delta f_* = -\tfrac{1}{2}\,(\tfrac{2}{3}\,n_1\lambda z)^2\,E + \tfrac{1}{3}\,n_1 kT\,[2(1-z)\ ln\ (1-z) + (1+2z)\ ln\ (1+2z)] \qquad [8]$$

ergs per cc where

$n_1 = 6.03\ (10)^{23}\ N_C/N_S V_0$ carbon atoms per cc
$N_S =$ sum of mol fractions of all substitutional elements
$V_0 =$ volume corresponding to a mol of lattice sites
$\lambda = 1.68\ (10)^{-24}\ V_0$ strain per carbon atom
$z =$ Zener's order parameter
$E = 1.30\ (10)^{12}$ dynes per cm^2.

The value of the order parameter z depends only upon the temperature ratio T/T_C, as given in Table 2, where T_C is determined by the relationship

$$T_C = 3900\ V_0 N_C/N_S. \qquad [9]$$

When N_C is small, $N_S \cong 1$ and $V_0 \cong 7.2$, leading to the approximate relationship $T_C \cong 28{,}000\ N_C$. Changing to the appropriate units, the free energy change on ordering is

$$\Delta F_* = 2.39\ (10)^{-8}\ N_S V_0 \Delta f_* \qquad [10]$$

calories per gram atom.*

Combining Eq 3 and 7, and adding ΔF_* to the right hand member of Eq 7, the free energy change on transforming austenite to ferrite of the same carbon content is

$$\Delta F^{\gamma \rightarrow \alpha} = N_{Fe}\Delta F_{Fe}{}^{\gamma \rightarrow \alpha} + N_C\ (10{,}500 - 3.425\ T) + \Delta F_* \qquad [11]$$

cal per g atom for plain carbon steels.

Addition of an alloying element alters the value of $\Delta F^{\gamma \rightarrow \alpha}$ given in Eq 11 by the amount

$$N_i\ RT\ ln\ (\gamma_i{}^\alpha/\gamma_i{}^\gamma)$$

where the subscript i refers to a particular alloying element. Almost nothing is known concerning the ratio $\gamma_i{}^\alpha/\gamma_i{}^\gamma$ for alloying elements other than carbon; in the absence of adequate information, perhaps the simplest assumption that can be made is that $RT\ ln\ (\gamma_i{}^\alpha/\gamma_i{}^\gamma)$ is constant:

$$RT\ ln\ (\gamma_i{}^\alpha/\gamma_i{}^\gamma) = K_i.$$

With this assumption, Eq 11 becomes

$$\Delta F^{\gamma \rightarrow \alpha} = N_{Fe}\Delta F_{Fe}{}^{\gamma \rightarrow \alpha} + N_C\ (10{,}500 - 3.425\ T) + \Delta F_* + \Sigma N_i\ RT\ ln\ (\gamma_i{}^\alpha/\gamma_i{}^\gamma)$$

$$\cong N_{Fe}\Delta F_{Fe}{}^{\gamma \rightarrow \alpha} + N_C\ (10{,}500 - 3.425\ T) + \Delta F_* + \Sigma N_i K_i \qquad [12]$$

cal per g atom for the martensite transformation in alloy steels. The summation includes all alloying elements other than carbon.

Eq 12 is an estimate of the free energy change upon transforming austenite to martensite, obtained by extrapolating the properties of disordered iron-carbon solutions into the supersaturated range, and employing the theory of ordering developed by Zener. $\Delta F^{\gamma \rightarrow \alpha}$ values calculated from Eq 12 are used by Fisher, Hollomon, and Turnbull[10] in their analysis of austenite → martensite transformation kinetics. They suggest a value $K_{Cr} = 1200$ cal per g atom for chromium, leading to variation of $\Delta F^{\gamma \rightarrow \alpha}$ with temperature as shown in Fig 1 and 2 for a number of chromium steels.

References

1. C. H. Johansson: *Archiv f. d. Eisenhüttenwesen* (1937–38) **11,** 241.
2. R. F. Mehl and C. Wells: *Trans.* AIME (1937) **125,** 429.
3. C. Zener: *Trans.* AIME (1946) **167,** 513. *Metals Tech.* Jan. 1946. TP 1856.
4. C. Zener: *Trans.* AIME (1946) **167,** 550. *Metals Tech.* Jan. 1946. TP 1925.
5. R. P. Smith: *Jnl.* Am. Chem. Soc. (1946) **68,** 1163.
6. J. B. Austin: *Jnl. Ind. Eng. Chem.* (1932) **24,** 1225.
7. T. Lyman and A. R. Troiano: *Trans.* Am. Soc. Met. (1946) **37,** 402.
8. K. Honda and Z. Nishiyama: Sci. Repts. Sendai (1932) **21,** 299.
9. G. Kurdjumov and E. Kaminsky: *Ztsch. Phys.* (1929) **53,** 696.
10. J. C. Fisher, J. H. Hollomon, and D. Turnbull: Kinetics of the Austenite—Martensite Transformation. *Trans.* AIME (1949) **185,** 691. *Jnl. of Metals,* Oct. 1949.

---

* Zener's numerical values have been revised, following a more accurate calculation of the value of z at the critical temperature T_C (0.3772 vs. 0.33 as given by him), and assuming a martensite tetragonality ratio $r = 1.053$ for a completely ordered steel containing 1.28 pct carbon, as determined by Lyman and Troiano.[7] $r = 1.053$ falls between the values $r = 1.059$ and $r = 1.051$ determined by Honda and Nishiyama[8] and by Kurdjumov and Kaminsky[9] respectively. The strain corresponding to a tetragonality ratio r was assumed to be $e = (r-1)/(1+\nu)$ where $\nu = 0.3$ is Poisson's ratio. Assuming further that the density of iron is not altered by the addition of carbon, the volume of a gram atom of alloy is $V = N_S V_0$ cc, and the number of carbon atoms per cc is $n_1 = 6.03(10)^{23}\ N_C/N_S V_0$.

Although it was not so stated in his analysis, there must be, according to Zener's theory, a temperature region near the "critical temperature" T_C where ordered and disordered phases of differing carbon content coexist at equilibrium. Failure to consider the two phase region leads to errors in the value of Δf_*. However, the errors are small, and they are not considered further.

Kinetics of the Austenite→ Martensite Transformation

J. C. FISHER,* J. H. HOLLOMON,* Junior Member AIME, and D. TURNBULL*

Application of the concepts of nucleation and growth to the analysis of experimental transformation data has led to valuable descriptions of phase transformations, an outstanding example being the transformation austenite → pearlite which has been examined with particular care by Mehl and coworkers.[1–5] In addition to the pearlite transformation, the proeutectoid ferrite and proeutectoid carbide transformations are known to proceed by nucleation and growth. Martensite, on the contrary, until recently was thought to form by a mechanism involving neither nucleation nor growth; however, extension of standard nucleation theory[6] suggests that martensite, bainite, and the other products of austenite decomposition all grow from nuclei in the parent phase. The theory that martensite forms by nucleation and growth is strongly supported by recent experimental work of Kurdjumov and Maksimova.[7]

The concepts of nucleation and growth have been fruitful also in providing a sound basis for quantitative theoretical treatments of the kinetics of phase transformations. For example, Volmer and Weber[8] and Becker and Döring[9] developed the theory of nucleation from fundamental considerations to a point where excellent agreement was obtained with the results of experiments on the condensation of supercooled vapors. As a result of their analysis, the kinetics of vapor-liquid transformations now can be predicted. It seems probable that application of the theories of nucleation and growth to a quantitative study of austenite decomposition similarly will clarify the nature of the individual transformations involved, and will enable the calculation of austenite transformation kinetics.

In the present paper, the theories of nucleation and growth are applied to the austenite → martensite transformation in steels. The analysis begins with a discussion of nucleation in single component systems. Martensite appears to be coherent with the parent austenite, hence the nucleation theory is modified to include the effects of elastic distortion. Nucleation in the two component iron-carbon system then is discussed, for most steels are primarily alloys of these two elements. Finally, M_s temperatures and martensite transformation curves are calculated for each of several alloy steels of varying carbon and chromium content, and are compared with those determined experimentally by Lyman and Troiano[10] and Harris and Cohen.[11]

Nucleation Theory

NUCLEATION IN SINGLE COMPONENT SYSTEMS[6,12–14]

The work required for reversible formation of a region of phase β within the parent α phase is expressed conveniently as the sum of two terms: $W_1 = A\sigma$, the product of the area of the interface and the interfacial free energy, and $W_2 = V\Delta f$, the product of the volume of the region and the free energy increase per unit volume associated with the transformation. The total work is therefore $W = A\sigma + V\Delta f$.

When α is more stable than β, Δf is positive and W increases without limit as the volume increases. The transformation $\alpha \rightarrow \beta$ does not occur. It is nevertheless true that small regions of phase β enjoy temporary existence here and there in the α. The equilibrium number of β regions of given size is proportional to $exp(-W/kT)$ per unit volume of α, assuring that larger β regions occur with diminishing probability.

When α is less stable than β, Δf is negative and W passes through a maximum as V increases. Assuming for simplicity that regions of β are spherical, as is true when the interfacial tension is isotropic and there are no elastic strains,

$$W = 4\pi r^2\sigma + (4/3)\pi r^3\Delta f.$$

The maximum value of W is

$$W^* = 16\pi\sigma^3/3\Delta f^2 \qquad [1]$$

for regions with radius

$$r^* = -2\sigma/\Delta f. \qquad [2]$$

For single component condensed systems it has been shown[14] that the steady rate of nucleation of β per unit volume of untransformed α is nearly proportional to $exp[-(W^* + Q)/kT]$ where Q is the activation energy for the unit processes of adding or removing one atom from an embryo or nucleus. If T_0 is the temperature at which α and β are in equilibrium, the rate of nucleation is a maximum at a temperature $0 < T < T_0$ where $(W^* + Q)/kT$ is a minimum.

β regions smaller than critical size are called embryos; they tend to grow smaller and disappear, only exceptionally growing larger. Regions equal to or larger than critical size are called nuclei. A critical size nucleus may grow indefinitely large or may shrink back to α, either process decreasing the free energy of the region.

Cleveland Meeting, October 1949.
TP 2674 E. Discussion of this paper (2 copies) may be sent to *Transactions* AIME before December 1, 1949. Discussion is tentatively scheduled for publication in May 1950.
Manuscript received November 1, 1948; revision received May 24, 1949.

* Research Laboratory, General Electric Co., Schenectady, N. Y.

[1] References are at the end of the paper.

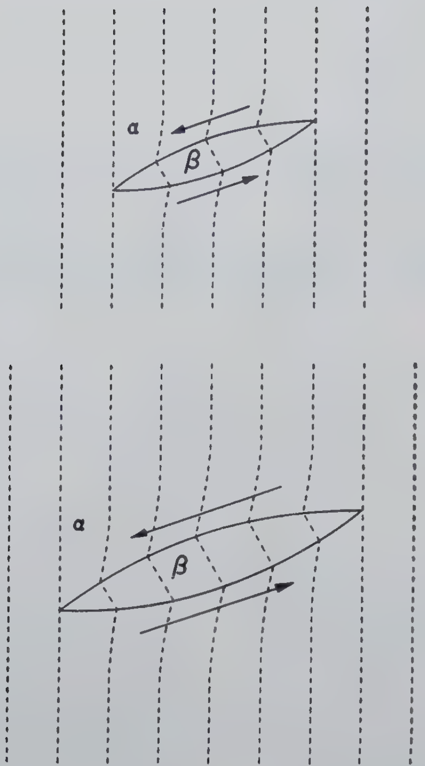

FIG 1—Growth of a martensite plate, schematic.

Arrows indicate direction of motion of parent phase.

It is important to recognize that embryos and nuclei do not suddenly appear full size in the parent phase.[12,13] They grow larger and smaller by a series of essentially bimolecular reactions,

$$\begin{array}{c} m\alpha \rightleftharpoons \beta_m \\ \beta_m + \alpha \rightleftharpoons \beta_{m+1} \\ \beta_{m+1} + \alpha \rightleftharpoons \beta_{m+2} \\ \cdot \\ \cdot \\ \cdot \\ \beta_{n-1} + \alpha \rightleftharpoons \beta_n \\ \cdot \\ \cdot \\ \cdot \end{array} \qquad [3]$$

where α represents a single atom or molecule of phase α, and β_i represents an i-atom region of phase β. β_m, where $m \cong 10$ for metals, represents the smallest possible region having the structure of β. For β_i smaller than critical size, the specific rate of decomposition of β_i is greater than that of formation. For β_i larger than critical size the converse is true.

The unit processes of adding or removing α atoms have activation energies, and occur in finite time. If the temperature of a sample of α is changed rapidly from equilibrium at $T_1 > T_0$ where α is stable, to $T_{-1} < T_0$ where β is stable, the embryos at T_1 may be retained at the new temperature; with rapid quenching there may be insufficient time for the set of reactions $\beta_{i-1} + \alpha \rightleftharpoons \beta_i$ to lead to appreciable change toward establishment of the steady state β_i—distribution characteristic of T_{-1}.

If T_{-1} is sufficiently below T_0, the larger embryos of β retained during quenching from T_1 will become nuclei during cooling as the critical size decreases. These nuclei then grow. The metamorphosis embryo → nucleus that takes place during cooling is independent of thermal motion in the sense that no additional α atoms need be activated and added to the β region. For this reason nucleation resulting from the decrease in r^* with falling temperature has been termed athermal nucleation, in contrast to thermal nucleation which takes place isothermally.

It may happen that W^*/kT_{-1} is so large that the steady rate of nucleation at T_{-1} is negligible. Transformation $\alpha \rightarrow \beta$ then is initiated entirely by athermal nucleation. If the growth rate of β regions is rapid, and the size of a β grain is limited by changes in α orientation that occur at α grain boundaries, β will be observed to form only upon cooling of the α. If cooling ceases, athermal nucleation and therefore transformation also ceases. If the cooling is continued, transformation continues.

Interrupted cooling can lead to "stabilization of the retained α" when retained embryos of nearly critical size grow smaller and decrease in number as the steady state distribution characteristic of the holding temperature is approached. Subsequent cooling then produces fewer athermal nuclei than would have been produced by direct cooling to the final temperature.

NUCLEATION OF COHERENT PHASES

The elastic distortion accompanying transformations in solids frequently is so large that it cannot be neglected in calculating nucleation rates. Consider for example a transformation that occurs by the mechanism sketched in Fig 1. The phases are coherent in the sense that lines and planes of atoms are continuous across interfaces. The habit plane, or α plane that is parallel to the plate of β, is not necessarily rational. The transformation is evidently a "shear type" transformation; however the figure suggests that the final dimensions of a β plate are attained by growth, not by homogeneous shear or shears throughout the volume to be transformed.

The idea that "shear type" transformations are accomplished by homogeneous shears seems questionable in view of the very high activation energy associated with an entire β-plate in the partly-sheared condition. No such difficulty arises when the configuration between β-nucleus and full size β-plate is recognized to be a growing plate of intermediate size. It is suggested below that martensite is a coherent precipitate. Martensite plates are assumed therefore to form by the mechanism of Fig 1, successive layers of atoms being deposited one atom at a time as the parent phase moves relative to the plates.

Assume a coherent embryo or nucleus of radius r and of thickness δ at the center, the two surfaces of the plate being portions of spheres of large radius. The volume of the embryo is

$$V = \pi r^2 \delta / 2 \qquad [4]$$

and its surface area is

$$A = 2\pi r^2 \qquad [5]$$

to a good approximation when $\delta \ll r$. The formation of a coherent β embryo in α requires (1) formation of a coherent α-β interface, (2) transformation of a volume of α to β, (3) concentration of elastic energy in the α (and to a lesser extent in the β).

Consider a sphere with center at the center of a thin coherent plate and with radius proportional to the radius of the plate. Select any point in the sphere (say on a line perpendicular to the plate at its center and at half the radius of the sphere). The elastic strain at the point is proportional to the ratio of the plate thickness to its radius,

$$e \sim \delta/r$$

as long as $\delta \ll r$. The strain energy per unit volume at the same location is proportional to the square of the strain,

$$E_v \sim (\delta/r)^2.$$

A similar proportionality holds at every point in the sphere; hence the total strain energy in the α is proportional to the product of $(\delta/r)^2$ and the volume of the sphere,

$$E = (3\theta/4)\,(\delta/r)^2\,(4\pi r^3/3) = \theta\pi r\delta^2. \qquad [6]$$

Here $3\theta/4$ is the proportionality constant.

The work associated with the reversible formation of an embryo of radius r and thickness δ is therefore

$$W = 2\pi r^2\sigma + \pi r^2\delta\Delta f/2 + \theta\pi r\delta^2. \qquad [7]$$

The most probable shape for an embryo of volume V is that for which W is a minimum. Minimizing W with the condition V = constant leads to the relationship

$$r = 3\theta\delta^2/4\sigma \qquad [8]$$

which relates r and δ for minimum free energy embryos.

Most embryos are minimum free energy embryos. The work associated with the reversible formation of an embryo of thickness δ is therefore

$$W = 15\pi\theta^2\delta^4/8\sigma + 9\pi\theta^2\delta^5\Delta f/32\sigma^2. \qquad [9]$$

W has a maximum

$$W^* = 8192\pi\theta^2\sigma^3/27\Delta f^4 \qquad [10]$$

for nuclei with thickness

$$\delta^* = -16\sigma/3\Delta f \qquad [11]$$

and volume

$$V^* = -32{,}768\pi\theta^2\sigma^3/27\Delta f^5. \qquad [12]$$

Coherent nuclei grow as plates that finally are stopped at the edges by α grain boundaries, particles of a second phase, or other crystal discontinuities. Each plate thickens until the value of W associated with its formation from the α is a minimum. The plate then is in equilibrium with the α and does not further thicken. Minimizing W at constant radius leads to the relationship

$$\delta/r = -\Delta f/4\theta \qquad [13]$$

for full size coherent plates.

The ratio δ^*/r^* for coherent nuclei of critical size is also $\delta/r = -\Delta f/4\theta$ and experimental observation that $\delta \ll r$ for fully grown coherent plates justifies the assumption that $\delta \ll r$ for the corresponding nuclei and embryos.

Martensite

It is generally agreed that martensite is ferrite supersaturated with carbon of the same concentration as the parent austenite. Large amounts of dissolved carbon slightly distort the body-centered cubic structure of ordinary ferrite to a body-centered tetragonal structure. Martensite forms in thin lens-shaped plates that have definite orientation and habit relationships with the parent austenite. Transformation takes place primarily during cooling, and the growth of individual plates is very rapid.

These observations concerning martensite formation suggest the identification of martensite as supersaturated ferrite that forms by rapid coherent growth of athermal nuclei.

Martensite embryos come into being at the austenitizing temperature. Although a particular embryo has only transient existence, there is a definite equilibrium concentration of embryos of any given size. During quenching, the largest embryos find themselves supercritical for coherent growth, and they grow rapidly to full-size martensite plates.

Although both coherent and noncoherent embryos are present at the austenitizing temperature, only noncoherent embryos can be retained during quenching. Even at cooling rates as great as 10,000°C per sec, about 0.1 sec is required to reach the martensite start temperature from the austenitizing temperature. Individual martensite plates are observed to form in times of the order of 10^{-4} sec, indicating that the rate of coherent growth of martensite is very great. The life of coherent embryos therefore must be less than 10^{-4} sec, and during a time as long as 0.1 sec a given embryo will disappear; further, the largest embryos do not reform, for at lower temperatures the steady concentration of coherent embryos decreases in proportion to $exp(-W/kT)$. Effectively, coherent embryos always are present in the equilibrium or steady state concentration, while only noncoherent embryos, which require relatively long times to grow or shrink, can be retained during quenching.

A non-coherent α-β interface differs from a coherent interface in that noncoherent α and β structures get out of step occasionally, producing essentially a series of dislocations spaced along the interface. When β consumes α by non-coherent growth, existing dislocations move with the interface, and new dislocations appear where the interfacial area increases. However, it is possible also for β to consume α by coherent growth, leaving behind in the β the dislocations that initially were present at the α-β interface. Coherent growth of martensite from non-coherent ferrite nuclei therefore presents no contradiction.

Most martensite plates nucleate at embryos that have the minimum free energy of formation consistent with becoming nuclei at the low temperature, for these embryos are present in the greatest numbers. Let the critical size V^* for coherent growth of supersaturated ferrite (martensite) at a low temperature be as sketched in Fig 2A for a given iron-carbon alloy. Fig 2 suggests possible configurations for the embryos that are primarily responsible for martensite nucleation upon cooling to the low temperature in question.

Embryo (B) is a non-coherent ferrite region of size V^*, having the same carbon content as the austenite. Embryo (C) is a non-coherent ferrite region of the same size, but with the equilibrium amount of carbon for ferrite in contact with austenite.† The free energy of forming embryo (C) evidently is less than that of forming embryo (B), hence embryos similar to (B) do not contribute significantly to the martensite transformation.

Embryo (D) is a carbon-free austenite region of size V^*, containing a small non-coherent ferrite region just large enough to nucleate coherent growth in pure γ-iron at the low temperature. Upon quenching, the ferrite region in embryo (D) becomes a nucleus for coherent growth in carbon-free austenite; it grows to the boundary of the carbon-free region. Then, however, it is supercritical for growth in austenite of average carbon concentration, and it continues its coherent growth. The free energy of forming

---

† The equilibrium concentration of carbon is so low that it is assumed to be zero.

Table 1 . . . Calculated Free Energy Change in Calories per Mol of Lattice Sites for the Austenite → Martensite Transformation in 12 Iron-Chromium-Carbon Alloys Studied by Lyman and Troiano[10,18] and Harris and Cohen[11]

Pct C	0.08	0.15	0.26	0.38	0.69	1.02	1.28	1.13	1.09	1.04	1.05	1.02
Pct Cr*	3.45	3.39	3.73	3.38	3.44	3.56	3.48	1.18	2.16	4.36	6.32	9.46
T°K	ΔF_m	ΔF_m	ΔF_m	ΔF_m	ΔF_m	ΔF_m	ΔF_m	ΔF_m	ΔF_m	ΔF_m	ΔF_m	ΔF_m
1020	+12											
1000	−2											
980	−18	+4										
960	−36	−13										
940	−56	−33	+8									
920	−79	−55	−14									
900	−102	−78	−36	+2								
880	−125	−102	−59	−21								
860	−150	−126	−83	−44								
840	−175	−150	−107	−68								
820	−200	−174	−131	−92	+19							
800	−224	−199	−155	−116	−5							
780	−250	−225	−180	−140	−29							
760	−277	−252	−205	−166	−54			+19				
740	−304	−279	−231	−192	−79	+11		−7	+2			
720	−331	−306	−259	−219	−106	−16		−34	−25	+3		
700	−358	−333	−286	−246	−133	−43	+7	−61	−51	−23	+13	
680	−386	−361	−313	−272	−160	−69	−19	−89	−79	−49	−13	
660	−413	−388	−340	−299	−187	−95	−46	−116	−106	−75	−38	+11
640	−440	−415	−366	−325	−212	−121	−72	−142	−132	−101	−63	−13
620	−467	−441	−391	−351	−238	−147	−97	−168	−158	−126	−89	−37
600		−467	−418	−377	−264	−172	−122	−195	−184	−152	−113	−61
580		−494	−445	−402	−291	−199	−148	−222	−210	−178	−139	−86
560		−521	−472	−428	−318	−225	−174	−248	−237	−204	−164	−110
540			−499	−456	−345	−253	−201	−276	−265	−231	−191	−135
520			−527	−484	−373	−280	−228	−305	−293	−259	−218	−161
500			−555	−511	−401	−308	−256	−333	−321	−286	−245	−187
480				−538	−428	−335	−283	−360	−348	−313	−270	−212
460				−566	−455	−362	−310	−387	−376	−339	−296	−237
440				−593	−481	−388	−336	−414	−403	−365	−321	−261
420				−618	−508	−414	−360	−441	−428	−391	−346	−285
400				−644	−533	−439	−385	−467	−453	−415	−370	−308
380				−669	−559	−463	−410	−492	−478	−440	−394	−331
360				−694	−583	−487	−433	−516	−503	−464	−417	−353
340				−718	−606	−510	−456	−540	−527	−487	−440	−375
320				−741	−629	−532	−478	−563	−549	−509	−461	−396
300				−762	−652	−554	−500	−585	−570	−530	−482	−416
280						−574	−520	−606	−591	−549	−502	−435
260						−595	−538	−626	−611	−569	−520	−454
240						−614	−556	−645	−630	−588	−538	−471
220							−574	−662	−647	−606	−555	−487
200							−590	−680	−664	−622	−571	−502

* P_1 pct manganese is counted as $2P_1$ pct chromium, and P_2 pct silicon as P_2 pct iron.

embryo (D) is less than that of forming embryo (C), for embryo (C) requires a larger ferrite region with greater area of interface and greater volume of the unstable phase.

Although embryo (E), with carbon concentration increasing from zero at the boundary of the ferrite region to the average value at the boundary of the volume V^* has a free energy of formation somewhat smaller than does embryo (D), it is assumed, for ease of calculation in the following analysis, that martensite nucleates from embryos similar to embryo (D).

The free energy of formation of embryo (D) is the sum of two free energies; (1) that required to clear the carbon from a volume V^*, and (2) that associated with formation of the small ferrite region. It is assumed that the free energy required for formation of the small ferrite region is small in comparison with that required to clear the carbon from volume V^*.

The free energy change accompanying the reaction

$$\text{Fe (solution of iron and carbon)} \rightarrow \text{Fe} \quad [14]$$

corresponds to a transfer of all carbon from one gram atom of iron in austenite of initial carbon concentration N_C to a large reservoir of austenite of carbon concentration N_C. The activity constant for the reaction is

$$K = a_{Fe}/a_{Fe(C)} = 1/a_{Fe(C)}$$

taking the activity of pure iron as unity. The corresponding free energy change is

$$\Delta F - \Delta F_0 = RT \ ln \ K = -RT \ ln \ a_{Fe(C)}.$$

The standard free energy change ΔF_0 is zero, hence

$$\Delta F = -RT \ ln \ a \quad [15]$$

cal per g atom of iron where the subscript has been dropped and *ln a* represents the logarithm of the activity of iron in an iron-carbon alloy.[15]

The activity of iron in austenite has been determined by Smith.[16] He shows that the relationship

$$-ln \ a = N_C/N_s + [6.5 - 6 \ exp \ (-1500/RT)] \ (N_C/N_s)^2 \quad [16]$$

gives satisfactory agreement with the experimental values over the entire temperature and composition range investigated. N_C is the mol fraction of carbon, and N_s is the mol fraction of iron. It is assumed in the following analysis that Eq 15 and 16 hold for steels of arbitrary composition when N_s is taken as the sum of the mol fractions of all substitutional elements.

The free energy change upon removing the carbon from a small region containing only n interstitial positions is

$$\Delta f_n = -(n/N) \ RT \ ln \ a = -nkT \ ln \ a. \quad [17]$$

The equilibrium number n_0 of carbon-free regions containing n lattice sites is proportional to $exp \ (-\Delta f_n/kT) = exp \ (n \ ln \ a)$. Assuming ideal mixing of carbon-free regions and the remaining iron atoms the proportionality factor is N per mol of lattice sites,[6] giving

$$n_0 = N \ exp(n \ ln \ a). \quad [18]$$

The number of regions larger than a critical size n^* is

$$n_r = \int_{n = n^*}^{\infty} n_0 dn = -(N/ln \ a) \ exp(n^* \ ln \ a) \quad [19]$$

per mol of lattice sites.

CALCULATION OF M_s TEMPERATURES

Fisher[17] has assembled information concerning the free energy change upon transforming austenite to martensite. The free energy change is

$$\Delta F_m{}' = N_{Fe}\Delta F_{Fe} + N_C \ (10{,}500 - 3.425T) + \Delta F_* + N_{Cr}RT \ ln \ (\gamma_{Cr}{}^{\alpha}/\gamma_{Cr}{}^{\gamma}) \quad [20]$$

cal per g atom for iron-chromium-carbon alloys,† where the symbols have the following meanings:

$\Delta F_m{}'$ = free energy change upon transforming a gram atom of austenite to martensite (in the absence of elastic distortion associated with coherency).

ΔF_{Fe} = free energy change upon transforming a gram atom of γ-iron to α-iron.

ΔF_* = free energy change accom-

---

† A gram atom of iron-chromium-carbon alloy contains N_{Fe}, N_{Cr} and N_C mols of iron, chromium and carbon.

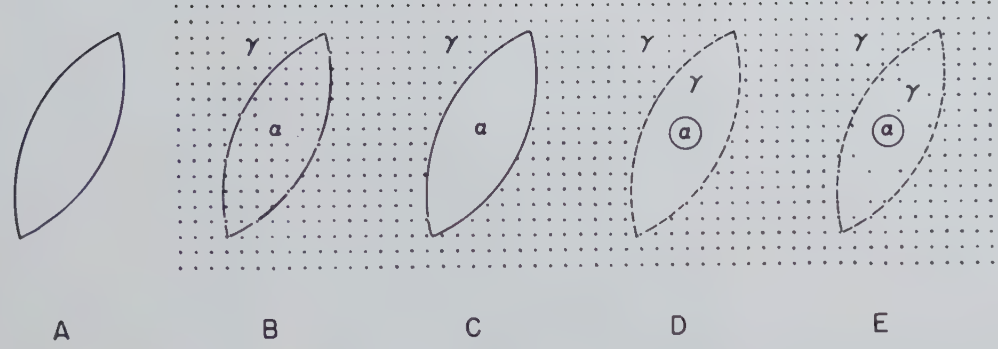

FIG 2—(A) Critical size for martensite growth. (B-E) Possible martensite embryos, schematic.
Dots represent carbon atoms.

panying the disordered-carbon → ordered-carbon transformation in a gram atom of martensite.
N_{Fe} = mol fraction iron.
N_C = mol fraction carbon.
N_{Cr} = mol fraction chromium.
R = gas constant, 1.986 cal per mol °K.
T = temperature, °K.
γ_{Cr}^{α} = activity coefficient for chromium in α phase.
γ_{Cr}^{γ} = activity coefficient for chromium in γ phase.

As very little is known concerning γ_{Cr}^{α} and γ_{Cr}^{γ}, the approximation $RT \ln (\gamma_{Cr}^{\alpha}/\gamma_{Cr}^{\gamma}) = K_{Cr}$ is made, where K_{Cr} is a constant.[17]

Let N_s be the sum of the mol fractions of all substitutional elements. The free energy change per mol of lattice sites is then

$$\Delta F_m = (N_{Fe}/N_s)\Delta F_{Fe} + (N_C/N_s)(10{,}500 - 3.425T) + \Delta F_*/N_s + (N_{Cr}/N_s)(1200). \quad [21]$$

The choice K_{Cr} = 1200 cal per g atom is justified in the following analysis. ΔF_m enters naturally into nucleation theory, for the free energy change per mol of lattice sites is very nearly proportional to the free energy change per unit volume. Table 1 gives values of ΔF_m vs. temperature for the 12 steels of interest in the present report.

It has been suggested that martensite nuclei form in carbon-poor austenite regions, and that the number of martensite plates that form on cooling to a given temperature is equal to the number of carbon-free regions in the austenite that exceed the critical size for coherent growth of martensite nuclei in austenite of average carbon concentration.

According to this interpretation there is no sharply defined M_s temperature above which martensite does not form. However, there is a definite temperature, the experimental M_s temperature, at which the probability of finding a martensite plate during microscopic examination of a given specimen area is say 0.5. This temperature corresponds to a definite number of martensite plates per unit volume of iron. An equation for the experi-

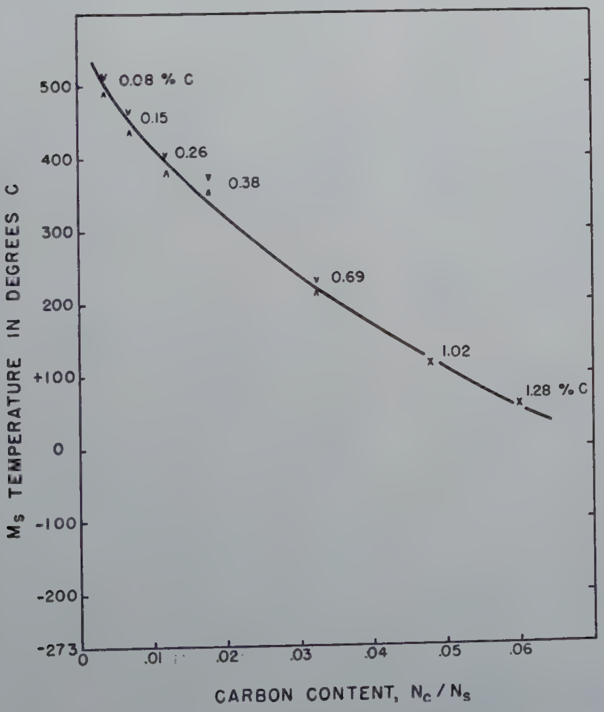

FIG 3—M_s temperature for 3 pct chromium steels as a function of carbon content.
Experimental values determined by Lyman and Troiano,[10] and (0.38 pct C only) by Klier and Lyman.[25] Curve calculated from Eq 25.

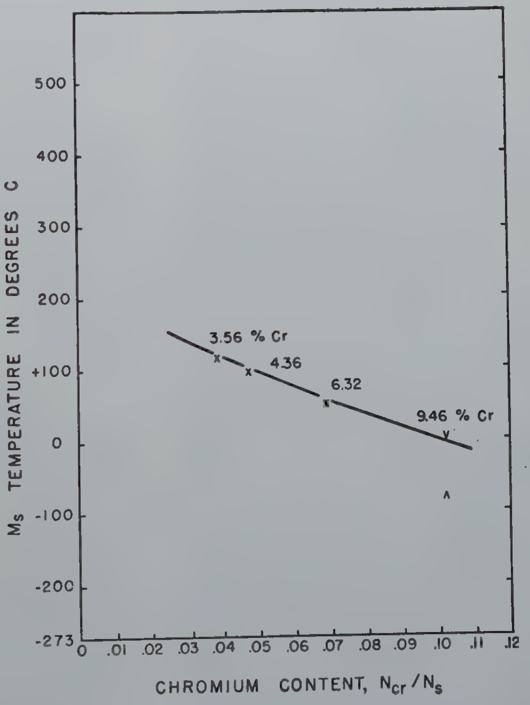

FIG 4—M_s temperature for 1 pct carbon steels as a function of chromium content.
Experimental values determined by Lyman and Troiano.[18] Curve calculated from Eq 25.

mental M_s temperature can be obtained therefore by setting the expression for the number of martensite nuclei (that is, the number of carbon-free austenite regions as large or larger than the volume of a critical size martensite nucleus) per mol of lattice sites equal to a constant,

$$n_r = -(N/ln\ a)\ exp(n^*\ ln\ a) = K_1. \quad [22]$$

Since the order of magnitude of $ln\ a$ is the same for all steels for which M_s is determined, the above condition is practically equivalent to stating that the exponent $n^*\ ln\ a$ is constant,

$$n^*\ ln\ a = K_2. \quad [23]$$

The number n^* of lattice sites in a critical size martensite nucleus is proportional to its volume V^* which is in turn proportional to ΔF_m^{-5} (see Eq 12). Here $\Delta F_m \sim \Delta f$ is the free energy change in calories per mol of lattice sites for transformation to supersaturated ferrite. The equation for the M_s temperature is therefore

$$\Delta F_m = K_3(-ln\ a)^{1/5} \quad [24]$$

or substituting the value $K_3 = -800$ which was found to give the best agreement with the data of Lyman and Troiano,[10]

$$\Delta F_m + 800(-ln\ a)^{1/5} = 0. \quad [25]$$

M_s temperatures calculated from Eq 25 are compared in Fig 3 with the experimental values determined by Lyman and Troiano[10] for seven 3 pct chromium steels containing from 0.08 to 1.28 pct carbon. Values of ΔF_m and $-ln\ a$ required for the calculation are given in Table 1 and Eq 16.

M_s temperatures calculated for four 1 pct carbon steels of varying chromium content are compared with the experimental values of Lyman and Troiano[18] in Fig 4. The value $K_{Cr} = 1200$ cal per g atom was selected to give agreement between Eq 25 and these experimental data.

MARTENSITE TRANSFORMATION CURVES

A martensite transformation curve gives the fraction of martensite, or the remaining fraction of untransformed austenite, as a function of quenching bath temperature for specimens cooled as rapidly as possible from the austenitizing temperature. The growth of individual martensite plates is stopped by austenite grain boundaries, previously formed martensite plates, and other crystal discontinuities that do not allow coherent growth across an interface. The size of the first few martensite plates that form in a specimen of austenite containing no undissolved carbides is determined, therefore, by the austenite grain size. The size of later martensite plates is determined by the size of the pockets of untransformed austenite remaining among previously formed martensite plates. Calculation of martensite transformation curves requires an estimate of the size of these austenite pockets as a function of austenite grain size and number of martensite plates.

Let V_0 be the volume of a mol of lattice sites, let qV_0 be the volume of a single austenite grain, and let mqV_0 be the volume of an average martensite plate that forms near M_s.

After n plates have formed, the mol of lattice sites is cut up into chunks about $qV_0/(qn + 1)$ cc in size. Let V_m be the volume of martensite formed. Slightly below M_s, $dV_m/dn = mqV_0/(qn + 1)$ is the volume rate of transformation per martensite plate. A better approximation to dV_m/dn is

$$dV_m/dn = mq(V_0 - V_m)/(qn + 1) \quad [26]$$

where V_0 has been replaced by $V_0 - V_m = V_a$, the remaining volume of untransformed austenite.

Integrating, $-ln\ (V_0 - V_m) = m\ ln\ [c(qn + 1)]$ where c is the integration constant. $V_m = 0$ when $n = 0$, hence $-ln\ V_0 = m\ ln\ c$ and

$$1 - V_m/V_0 = V_a/V_0 = (qn + 1)^{-m}. \quad [27]$$

Let n_0 be the number of martensite nuclei that would have appeared in the absence of nucleus growth. n, the actual number of martensite plates, is related to n_0 by the equation

$$dn/dn_0 = V_a/V_0 = (qn + 1)^{-m}. \quad [28]$$

Integrating,

$$(qn + 1)^{m+1}/(m + 1) = qn_0 + c_2.$$

The value of c_2 is $1/(m + 1)$, giving

$$(qn + 1)^{m+1} = (m + 1)qn_0 + 1$$

or

$$\begin{aligned}(qn + 1)^{-m} &= [(m + 1)qn_0 + 1]^{-m/(m+1)}\\ &\cong (qn_0 + 1)^{-m} \quad [29]\end{aligned}$$

since $m \ll 1$.

Therefore, the fraction of retained austenite is

$$V_a/V_0 = (qn_0 + 1)^{-m} \quad [30]$$

where

$$\begin{aligned}n_0 &= -(N/ln\ a)\ exp(n^*\ ln\ a)\\ &= -(N/ln\ a)\ exp(V^*\ ln\ a/v_0) \quad [31]\end{aligned}$$

is the number of martensite nuclei, q is the reciprocal of the number of austenite grains per mol of lattice sites, v_0 is the volume per lattice site, and $m \ll 1$ is a function of the shape of the martensite plate.

Let the ASTM grain size be g. There are then 2^{g-1} grains per sq in. visible at 100 diam, or $10^4 2^{g-1}$ grains per sq in. The area of an average spherical grain cut at random is $A = 2\pi r_g^2/3$, hence the radius of a typical grain follows from the relationship

$$10^4 2^{g-1}(2\pi r_g^2/3) = 1$$

giving

$$\begin{aligned}r_g &= 10^{-2} 2^{-g/2} \text{ in.}\\ &= 2.5(10)^{-2} 2^{-g/2} \text{ cm.}\end{aligned}$$

The volume per austenite grain is

$$V_1 = 4\pi r_g^3/3 = 65(10)^{-6} 2^{-3g/2} \text{ cc},$$

and the number of austenite grains per mol of lattice sites is V_0/V_1 where $V_0 = 7.2$ cc is the volume occupied by a gram atom of iron. The value of q is therefore

$$q = V_1/7.2 = 9.0(10)^{-6} 2^{-3g/2} \quad [32]$$

mol of lattice sites per austenite grain.

The volume of the average austenite grain is

$$4\pi r_g^3/3 = qV_0,$$

and the volume of the average martensite plate that forms in such a grain is

$$3(\delta/r)\pi^2 r_g^3/32 = mqV_0$$

where δ/r is the thickness to radius ratio for martensite plates. The ratio of plate volume to grain volume is

$$m = 9\pi(\delta/r)/128,$$

or

$$m = -9\pi\Delta f/512\theta = -\mu\Delta F_m \quad [33]$$

taking $\delta/r = -\Delta f/4\theta$ as given in Eq 13. μ is the constant of proportionality between m and ΔF_m.

Martensite transformation curves now can be calculated by means of Eq 30, where n_0 is given by Eq 31, q by Eq 32, and m by Eq 33. The coefficient μ in Eq 33 is the only unknown parameter. The best agreement between calculated transformation curves and those determined experimentally by Harris and Cohen[11] is obtained when

$$\mu = 7(10)^{-5}. \quad [34]$$

Fig 5 and 6 compare calculated and experimental curves for a 1.1 pct carbon steel and a 1.1 pct carbon, 1.5 pct

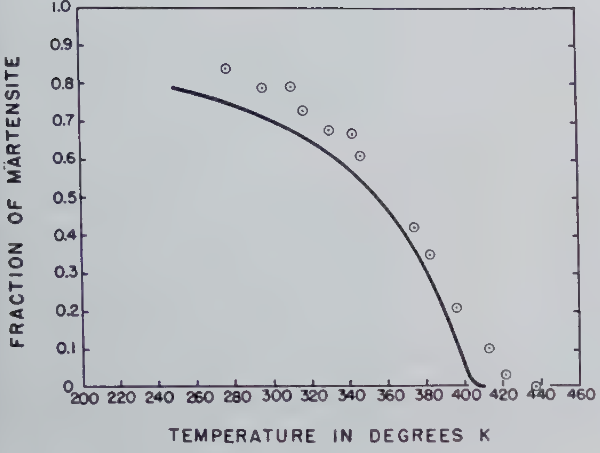

FIG 5—Martensite transformation curve for 1.1 pct carbon steel.

Experimental points determined by Harris and Cohen.[11] Curve calculated from Eq 30.

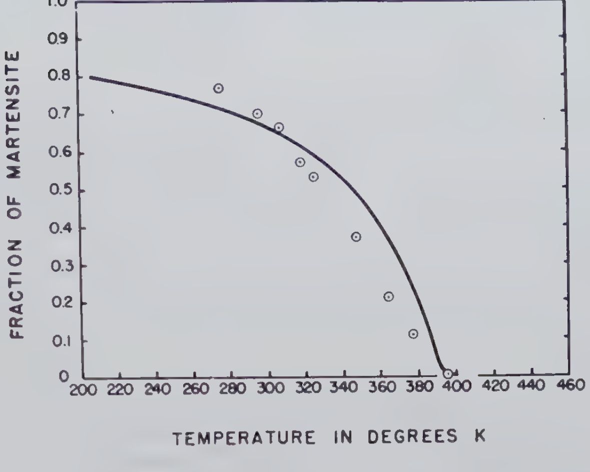

FIG 6—Martensite transformation curve for 1.1 pct carbon, 1.5 pct chromium steel.

Experimental points determined by Harris and Cohen.[11] Curve calculated from Eq 30.

chromium steel.

Two important effects have been neglected in calculating martensite transformation curves. It is observed frequently that the growth of one martensite nucleus immediately sets off the growth of several others in the strained austenite adjacent to the first martensite plate. Elastic strains set up by the first plate presumably have altered the critical size for growth of otherwise subcritical nuclei, so that a few of them become supercritical and grow. Further, when a significant fraction of austenite is transformed, interaction of the stress fields around neighboring martensite plates allows them to thicken considerably in comparison with the equilibrium thickness for an isolated plate. Both the multiplication effect and the thickening effect lead to increased transformation over that given by Eq 30, the discrepancy becoming large when a significant amount of martensite is present.

Significance of the Agreement between Theory and Experiment

M_s temperatures and martensite transformation curves have been calculated from the basic assumptions that martensite and austenite are coherent, and that martensite grows by the mechanism sketched in Fig 1. Agreement between theory and experiment, summarized in Fig 3–6, is satisfactory, although it can be contended that the significance of this agreement is diminished by the arbitrary choice of values for the two parameters θ (the coefficient of the strain energy term in the equation for the work of forming a coherent embryo) and σ (the coherent interfacial free energy).

Certainly, however, the significance of the agreement will be increased if it can be shown that the value of θ required for calculation of martensite transformation curves is that given by elasticity theory, and if it can be shown that the value of σ required for calculation of M_s temperatures is reasonable in comparison with known surface and interfacial free energies.

THE SHAPE OF A MARTENSITE PLATE

The strain energy associated with a martensite plate of thickness δ and radius r is $E = \theta\pi r\delta^2$ according to Eq 6. The value of the coefficient θ can be roughly estimated by assuming that the strain in the austenite surrounding a martensite plate is uniform throughout a circumscribed sphere of radius r. The shear strain is approximately $\gamma = \phi\delta/2r$ where ϕ is the "homogeneous shear" angle of the martensite. The energy per unit volume is

$$E_v = G\gamma^2/2 = \phi^2G(\delta/r)^2/8$$

and the total strain energy is

$$E = (4/3)\pi r^3[\phi^2G(\delta/r)^2/8] = (\pi/6)\phi^2Gr\delta^2,$$

whence

$$\theta = \phi^2G/6. \qquad [35]$$

Taking $\phi = 0.34$ corresponding to the Nishiyami[19] orientation relationship between martensite and austenite, and $G = 8(10)^{11}$ dynes per cm² (the value for ferrite) as an approximation for austenite, the value of θ is

$$\theta_1 = 1.54(10)^{10} \text{ dynes per cm}^2. \qquad [36]$$

This approximate value of θ may be compared with the value assumed in the analysis of martensite transformation curves. Eq 33 and 34 give

$$m = -9\pi\Delta f/512\theta = -7(10)^{-5}\Delta F_m$$

whence

$$\theta = 0.46(10)^{10} \text{ dynes per cm}^2, \qquad [37]$$

in satisfactory agreement with θ_1 in view of the approximations in the elastic analysis and in the assumption that austenite pockets remaining in partially transformed steel are spherical.

The thickness to radius ratio δ/r for martensite plates can be calculated from the relationship

$$\delta/r = -\Delta f/4\theta = -3.2(10)^{-4}\Delta F_m. \qquad [38]$$

At the M_s temperature, the ratio δ/r calculated for 3 pct chromium steels varies from 0.084 to 0.151 as the carbon content varies from 0.08 to 1.28 pct.

THE COHERENT α-γ INTERFACIAL FREE ENERGY

The experimental martensite start temperature corresponds to the presence of a definite number of martensite plates in a quenched sample of austenite of given grain size. A reasonable estimate of the number of plates needed to provide one visible plate per microscope field suggests that there are about 10^6 martensite plates per mol of lattice sites at the M_s temperature.

Substituting the value 10^6 for the number of martensite nuclei, Eq 22 becomes

$$10^6 = n_r = -(N/\ln a)\exp(n^* \ln a) = -(N/\ln a)\exp(V^* \ln a/v_0). \qquad [39]$$

For ordinary values of N_C/N_s, Eq 39 fixes the value of $V^* \ln a/v_0$ to be

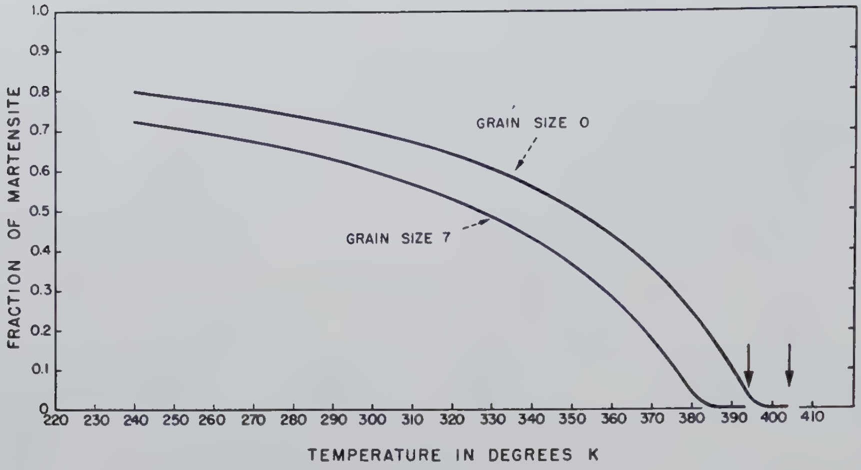

FIG 7—Calculated martensite transformation curves for 1 pct C, 3 pct Cr steel with ASTM grain sizes 0 and 7.
Arrows indicate temperatures for 0.01 pct transformation.

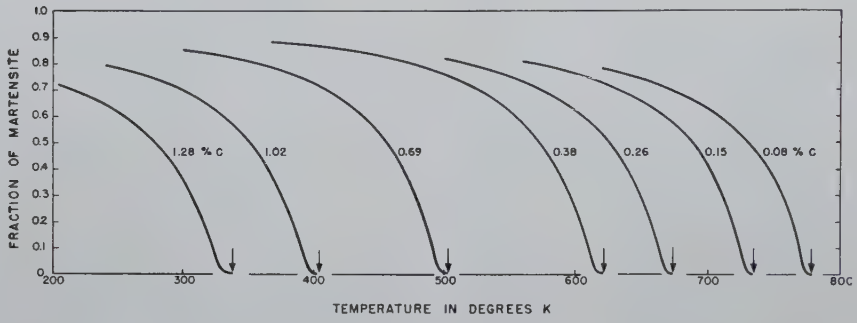

FIG 8—Calculated martensite transformation curves for 3 pct chromium steels of differing carbon content.
Arrows indicate temperatures for 0.01 pct transformation.

$$V^* \ln \cong a/v_0 - 45. \qquad [40]$$

Substituting the value of V^* from Eq 12,

$$32.768\,\pi\,\theta^2\,\sigma^3 \ln a/27\,v_0\,\Delta f^5 = 45. \qquad [41]$$

Taking $[-\ln a]^{1/5}/\Delta F_m = -1/800$ and $\theta = 0.46(10)^{10}$ from Eq 25 and 37, Eq 41 can be solved for the coherent α-γ interfacial free energy σ,

$$\sigma = 24 \text{ ergs per cm}^2. \qquad [42]$$

The value $\sigma = 24$ ergs per cm^2 that must be assumed in calculating M_s temperatures can be compared with the surface and interfacial free energies of solid copper, which should not differ markedly from those of iron:

$\sigma_1 \cong 1400$ ergs per cm^2
(surface tension of copper[20]
$\sigma_2 \cong 150$ ergs per cm^2
(non-coherent copper-copper interface[21]
$\sigma_3 \cong 5$ ergs per cm^2, very approximately (twin boundary[21]).

It is encouraging to note that the coherent α-γ interfacial free energy and the twin boundary free energy in copper agree as to order of magnitude.

It appears that the values of the parameters θ and σ, arbitrarily chosen to give agreement between theory and experiment, are close to the values expected from independent considerations. Within the error of an approximate calculation, θ is correctly given by a purely geometrical elastic analysis. The value of σ is reasonable in the light of what is known concerning coherent interfacial free energies of solids.

Influence of Austenite Grain Size and Other Variables

The M_s temperature and the extent of martensite transformation are dependent upon the austenitic grain size. Whenever nuclei form at random in the parent phase, and rapid growth of the new phase ceases at grain boundaries of the parent phase, each transformed particle is restricted to a single parent grain. The amount of transformation is the product of the number of nuclei and the size of each transformed region. The number of nuclei is independent of grain size, and the volume of a typical transformed region is proportional to d^3 where d is the mean grain diameter, leading to the relationship

$$(\text{pct transformation}) \sim d^3 \qquad [43]$$

during the early stages of transformation. A ten-fold decrease in grain diameter decreases the volume transformed to martensite by a factor of a thousand, thereby lowering the experimental M_s temperature.

Eq 30 gives the variation in the martensite transformation curve with grain size for all stages of transformation,

$$V_a/V_0 = (qn_0 + 1)^{-m},$$

where q is the number of mols of lattice sites per austenite grain. Fig 7 compares the calculated martensite transformation curves for two specimens of 1 pct C, 3 pct Cr steel with ASTM grain sizes 0 and 7, representing approximately a ten-fold change in grain diameter. The M_s temperature is 10–13°C lower (depending upon the method of measurement) in the fine grained material, and a comparable degree of transformation is achieved in a longer temperature interval.

INFLUENCE OF COMPOSITION ON THE SHAPE OF MARTENSITE TRANSFORMATION CURVES

Consider steels of varying chromium content and fixed carbon content. For these steels the free energy change ΔF_m on transforming austenite to martensite depends to a first approximation only upon the amount of subcooling below M_s. Hence n_0 and m in the relationship $V_a/V_0 = (qn_0 + 1)^{-m}$ are the same functions of the temperature interval below M_s for all steels of a particular carbon content, and the shape of the M_s transformation curve is independent of chromium content.

Steels with different carbon contents do not have quite the same shape, however, as shown in Fig 8 where calculated curves are compared for several 3 pct chromium steels of varying carbon content. The variation in shape with carbon content is in qualitative agreement with the observations of Grange and Stewart.[22]

Although grain size and carbon content influence the shape of martensite transformation curves, examination of Fig 7 and 8 indicates that for the usual grain sizes and carbon contents that are employed in commercial steels, the shape of the martensite transformation curve is relatively insensitive to these variables. The fraction of austenite transformed depends primarily upon the temperature interval below M_s, in agreement with the observations of Harris and Cohen.[11]

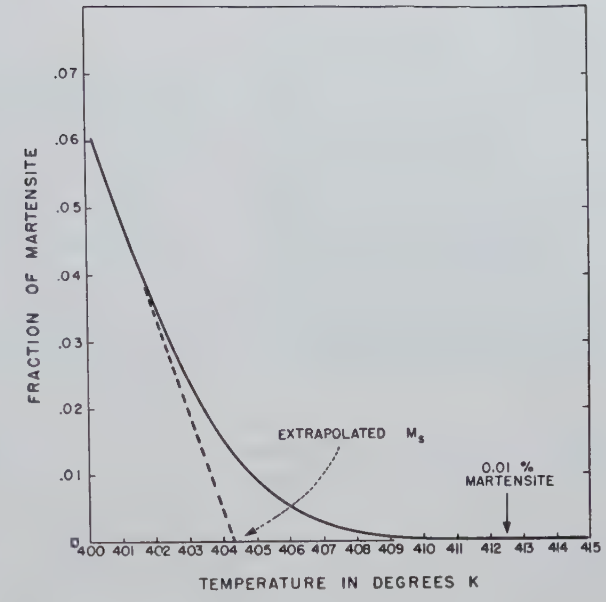

FIG 9—Shape of calculated martensite transformation curve near M_s.

EXTRAPOLATED M_s TEMPERATURES

The extrapolated M_s temperature is that at which the nearly linear portion of the martensite transformation curve intersects the axis of zero martensite. It lies a few degrees below the M_s temperature corresponding to the first plates visible during microscopic examination, as shown in Fig 9, where the shape of a calculated martensite transformation curve is given in detail near the M_s temperature.

Averaging data from 12 martensite transformation curves determined by Harris and Cohen[11] the extrapolated M_s temperature was found to lie about 6°C below the highest temperature of martensite observation for steels with M_s temperatures in the range $350 < M_s < 500$°K. This value compares favorably with the calculated value of about 9°C.

STABILIZATION

Consider a specimen of austenite that transforms partially to martensite upon quenching to a temperature T_{-2}. It frequently is found that holding the specimen for a time at $T_{-1} > T_{-2}$ decreases the amount of martensite formed on subsequent cooling to T_{-2}, the maximum amount of martensite corresponding to direct quenching to T_{-2}.[11] This process is termed stabilization.

A mechanism for stabilization in single component systems has been described in the first section on nucleation. When embryos that would have become athermal nuclei upon further cooling are present in excess of their steady state concentration at a holding temperature T_{-1}, they decrease in number with time. Subsequent cooling to $T_{-2} < T_{-1}$ then produces fewer athermal nuclei and less additional transformation. In general, stabilization requires that subcritical embryos of the new phase somehow be eliminated while the specimen is held at T_{-1}. In single component systems, only embryos that grow smaller are eliminated. In the iron-carbon system, martensite embryos perhaps may be eliminated by processes that involve the diffusion of carbon.

Harris and Cohen[11] have shown that stabilization does not occur at temperatures above a critical temperature σ_s, dependent upon composition, and that the amount of stabilization increases as the holding temperature decreases below σ_s. The σ_s temperature has both theoretical and practical significance, and a complete analysis of austenite decomposition should provide means for explaining and predicting its existence. However, the mechanism of stabilization appears to be more complex than that of the austenite → martensite transformation, and lies beyond the scope of the present analysis.

RATE OF GROWTH OF MARTENSITE PLATES

Coherent growth of martensite is very rapid, for each atom need move only about 0.34 of an atomic spacing to join the new lattice. The activation energy q^* for the unit process during this sort of "diffusion" is approximately $(0.34)^2$ times that for moving an atom a full atomic spacing. The latter value is estimated by Huntington and Seitz[23] to be about 0.36 times the activation energy for self-diffusion, the remaining 0.64 of the activation energy corresponding to the formation of a lattice vacancy. Birchenall and Mehl[24] report the activation energy for self-diffusion in γ-iron to be 48,000 cal per g atom, hence

$$q^* \cong 0.36\,(0.34)^2\,(48{,}000) = 2000 \quad [44]$$

cal per g atom (very approximately) is the activation energy for coherent growth.

The value $q^* = 2000$ cal per g atom is in excellent agreement with the experimental activation energy $q^* = 1600$ cal per g atom observed by Kurdjumov and Maksimova for isothermal transformation of austenite to martensite in the temperature range $79 \leq T \leq 173$°K where the rate of transformation is measurably slow,[7] although these authors assumed that q^* was associated with nucleation, rather than growth, of martensite plates. The very important work of Kurdjumov and Maksimova proves that the austenite → martensite transformation proceeds isothermally with a rate that approaches zero at the absolute zero of temperature, and is evidence strongly in favor of the nucleation and growth hypothesis of martensite formation.

Conclusions

Martensite start temperatures and martensite transformation curves have been calculated from the basic assumption that the austenite → martensite transformation proceeds by nucleation and growth. Martensite is identified as coherent supersaturated ferrite, and martensite nuclei are identified as small carbon-free austenite regions retained from the austenitizing temperature.

Agreement between experiment and theory is satisfactory, and there is reason to believe that adequate thermodynamic data will allow accurate calculation of M_s temperatures and martensite transformation curves for steels of arbitrary composition and heat treatment.

Acknowledgment

The authors' viewpoint concerning the austenite → martensite transformation has been influenced through study of Professor C. Zener's thought provoking article on the kinetics of austenite decomposition.[26] The authors are indebted to Professor M. Cohen, to Professor R. F. Mehl, and to members of the Metallurgy Division of the General Electric Research Laboratory for stimulating conversations and helpful criticism.

References

1. R. F. Mehl: *Trans.* Am. Soc. Met. (1941) **29,** 813.
2. F. C. Hull, R. A. Colton, and R. F. Mehl: *Trans.* AIME (1942) **150,** 185.
3. G. E. Roberts and R. F. Mehl: *Trans.* AIME (1943) **154,** 318.
4. F. C. Hull and R. F. Mehl: *Trans.* Am. Soc. Met. (1942) **30,** 381.
5. R. F. Mehl: *Jnl.* Iron and Steel Inst. (1948) **159(2),** 113.
6. J. C. Fisher, J. H. Hollomon, and D. Turnbull: *Jnl. App. Phys.* (1948) **19,** 775.
7. G. V. Kurdjumov and O. P. Maksimova: *Doklady Akad. Nauk SSSR* (1948) **61,** No. 1, 83.
8. M. Volmer and A. Weber: *Ztsch. Phys. Chem.* (1925) **119,** 277.
9. R. Becker and W. Döring: *Ann. Physik* [5] (1935) **24,** 719.
10. T. Lyman and A. R. Troiano: *Trans.* Am. Soc. Met. (1946) **37,** 402.
11. W. J. Harris, Jr. and M. Cohen: *Trans.* AIME (1949) **180,** 447, *Metals Tech.* Sept. 1948, TP 2446.
12. J. B. Zeldovich: *Acta Physicochim. URSS* (1943) **18,** 1.
13. D. Turnbull: *Trans.* AIME (1948) **175,** 774, *Metals Tech.* June 1948, TP 2365.
14. D. Turnbull and J. C. Fisher: *Jnl. Chem. Phys.* (1949) **17,** 71.
15. G. N. Lewis and M. Randall: Thermodynamics. McGraw-Hill, New York (1923).
16. R. P. Smith: *Jnl.* Am. Chem. Soc. (1946) **68,** 1163.
17. J. C. Fisher: *Jnl. of Metals* Oct. 1949.
18. T. Lyman and A. R. Troiano: *Trans.* AIME (1945) **162,** 196.
19. Z. Nishiyami: *Sci. Repts. Tokyo Imp. Univ.* (1934) **23,** 637.
20. H. Udin, A. J. Shaler and J. Wulff: *Jnl. of Metals* Feb. 1949, 186.
21. G. W. Sears: unpublished research.
22. R. A. Grange and H. M. Stewart: *Trans.* AIME (1946) **167,** 467. *Metals Tech.* June, 1946. TP 1996.
23. H. B. Huntington and F. Seitz: *Phys. Rev.* (1942) **61,** 315.
24. C. E. Birchenall and R. F. Mehl: *Jnl. Appl. Phys.* (1948) **19,** 217.
25. E. P. Klier and T. Lyman: *Trans.* AIME (1944) **158,** 394.
26. C. Zener: *Trans.* AIME (1946) **167,** 550. *Metals Tech.* Jan. 1946. TP 1925.

Some Observations in the Structure of Alpha Brass Single Crystals after Cutting and Polishing

ROBERT MADDIN,* Junior Member, and WALTER R. HIBBARD, JR.,† Member AIME

A series of X ray experiments conducted by G. I. Taylor[1] in 1927 and later substantiated in 1939 by J. A. Collins[2] both on axially strained aluminum single crystals, revealed evidence that during single slip crystallite rotation occurs in such a manner that "all parts of the material rotated about the transverse direction in the plane of slip."[1]

The actual method of preparing the specimens for X ray examination is not discussed in detail by Taylor except to say that "this specimen was cut parallel to the plane of slip, as calculated from measurements of marks in the surface of the specimen. It was ground and etched till the effect of the new cuts had disappeared. This was verified by applying the same treatment to an undistorted specimen. The X ray reflections[‡] in this case were perfect ones."[1]

Collins, on the other hand, cut his crystals in a mechanical shaper. These surfaces were polished on No. 1, No. 1/0, No. 2/0 and No. 3/0 papers and on a broadcloth lap using No. 600 alundum as a polishing medium. "Finally, the surface was deeply etched in Tucker's reagent. An undeformed crystal was prepared in the manner described and X rayed to determine whether or not the machining and polishing operations had produced any strain or distortion in the crystal. The Laue spots all seem to be sharp, free from tails and streaks indicating no detectable strains had been introduced in the crystals."[2]

Taylor's X ray technique involved the use of "homogeneous X rays from an iron anti-cathode"; whereas Collins used K_α radiation of copper at 31kv and 20 milliamperes.

Glancing angle X ray photograms were taken (1) with the axis of rotation of the spectrometer table in the plane of slip and at right angles to the slip direction, and (2) with the axis of the spectrometer table lying along the slip direction.

However, eight minute exposures were used in each case and the angle setting of the spectrometer table was increased by one degree for each exposure.

With the discovery of the action of three slip systems[3] in the plastic deformation of single crystalline alpha brass where, formerly, only one had

TN 23 E. Manuscript received June 24, 1949.

[*] Formerly Research Fellow in Metallurgy, Yale University, New Haven, Conn.; now Assistant Professor of Mechanical Engineering, The Johns Hopkins University, Baltimore, Md.

[†] Assistant Professor of Metallurgy, Yale University.

[‡] Presumably Laue back-reflection photograms.

[1] References are at the end of the paper.

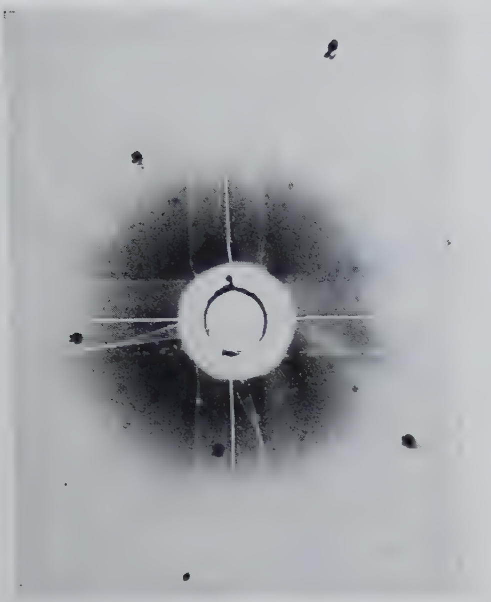

FIG 1—Laue photogram of {111} section from crystal showing absence of streaks or tails.

FIG 2—Glancing angle photogram of the crystal showing spread in orientation of the {111} plane.
$\theta = 21° 30'$; monochromatic radiation; eight hour exposure.

been considered to have operated, C. H. Mathewson suggested that the experiments of Taylor and Collins be repeated in order to examine critically the possible effects of the deformation process in terms of pole rotations introduced by the action of more than one slip system.

Consequently, the orientation of an undeformed single crystal of alpha brass was determined by the Laue back-reflection method. A disk, with its flat surfaces parallel to a convenient (111) plane, was carefully cut from the crystal with a No. 14B jeweler's saw in a goniometric miter box. The disk was polished carefully by hand on a series of fine files followed by No. 1/0, No. 2/0 and No. 3/0 metallographic papers. The disk was next etched in 1:1 HNO_3 so as to remove at least 0.125 in. from the cut surface. The (111) plane was within one degree of being parallel to the surface as determined by a Laue back-reflection photogram. The effects of cutting and polishing were seemingly removed as adjudged by the condition of the Laue spots shown in Fig 1. Although these spots are multiple indicating lineage imperfections somewhat less than 2° in magnitude, they are sharp and free from tails or streaks as they appeared in first photogram orienting the specimen.

The disk was mounted on a goniometer head set at the proper θ angle (21°30′) for primary octahedral reflections. Intense monochromatic copper K radiation was obtained by reflection from the C-cleavage surface of a suitably oriented pentaerythritol crystal. The tube was operated at 31kv and 11 milliamperes. The crystal reflected beam passed through a collimator 2 in. long containing a 1 mm bore. A 1.75 in. specimen to film distance was used. Satisfactory photograms were obtained using 8-hr exposures, Fig 2.

A spread of at least 35° may be seen in Fig 2. This spread in orientation may be interpreted as indicating that mechanically cutting a single crystal affects its structure throughout a considerable thickness. Changing the θ angle to 30° (an increase of 8°30′) resulted in a very weak 8° spread after 10 hr exposure.

The depth to which surface preparation disturbances can be detected in single crystals has been considered by Lacombe and Chaudron.[4] However, their disturbed structures were measured as less than 100 microns dependent upon the material. In the present investigations a minimum of 0.125 in. was removed after mechanical cutting and polishing and yet a disturbed structure was apparent, when investigated with directed characteristic radiation.

Since the present investigation made use of monochromatic X rays rather than white radiation to detect these disturbances and the exposures were considerably longer than those of Taylor and Collins, it would appear that they may not have removed with all certainty the mechanically disturbed surface by their treatments and the method of detection used. This suggests a reinvestigation of their findings, which is under way.

The authors would like to acknowledge the assistance of Mr. Marritt L. Kronberg of this Laboratory for setting up the monochrometer.

References

1. G. I. Taylor: Resistance to Shear in Metal Crystals. Cohesion and Related Problems. The Faraday Soc., Nov. 1927, 121.
2. J. A. Collins: Yale Univ., Ph.D. Dissertation, 1939, (cf also Collins and Mathewson, *Trans.* AIME (1940) TP 1145).
3. R. Maddin, C. H. Mathewson, W. R. Hibbard, Jr.: The Active Slip Systems in the Simple Axial Extension of Single Crystalline Alpha Brass. AIME *Trans.* **185**, 527 *Jnl. of Metals*, Aug. 1949. TP 2658.
4. P. Lacombe and G. Chaudron: Disc. to R. Maddin: Anomalies in the Appearance of Glide Ellipses. *Trans.* AIME (1948) **175**, 355.

Simultaneous Aging and Deformation in Metals

J. D. LUBAHN*

The influence of precipitation from solid solution on the subsequent deformation resistance of alloys is well known. However, the influence of precipitation or aging that occurs simultaneously with deformation may be entirely different and of considerable importance. It is thought[1] that the presence or absence of a yield point jog in impure iron at room temperature and the presence or absence of discontinuous flow at higher temperatures may be directly related to aging phenomena, particularly since the yield point jog is absent when the carbon and nitrogen are sufficiently removed.[2]

As a preliminary attack on the problem of simultaneous aging and deformation, three kinds of tests—constant strain rate tensile tests, constant load creep tests, and variable strain rate tensile tests—were carried out on an age hardenable aluminum alloy.

Constant Strain Rate Tensile Tests

Stress-strain curves at a strain rate of about 0.001 min^{-1} were obtained for specimens of 61S that had been quenched into liquid nitrogen after a one-hour solution treatment at 521°C, then aged at room temperature 10 min., 20 min., 4 hr, and 26.5 hr before testing. Strain-time curves were obtained on the same chart with the stress-strain curve by means of an auxiliary pen, driven parallel to the axis of the chart drum at constant speed by a synchronous motor and gear chain. The angle of rotation of the chart drum was proportional to strain. The strain rates reported are the measured slopes of the strain time curves. Constant strain rate was approximated (within a factor of 2) by manual adjustment of the oil inlet valve of the hydraulic testing machine in such a way that the course of the recorder pen was parallel to pre-drawn strain-time lines of the desired slope.

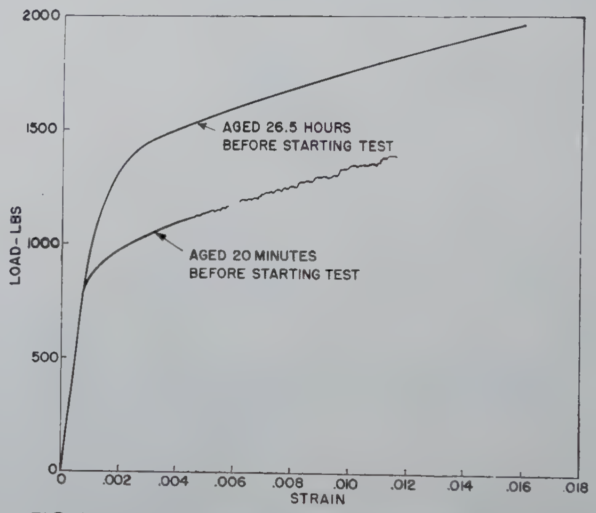

FIG 1—Effect of amount of prior room-temperature aging on the room-temperature stress-strain curve of solution treated 61S. Strain rate = 0.0013 min.$^{-1}$

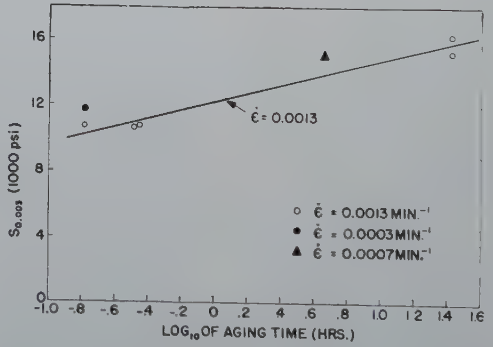

FIG 2—Effect of strain rate and prior room temperature aging on the flow stress at 0.003 plastic strain.

The specimens were machined from $\frac{9}{16}$ in. rod. The cylindrical portion was 0.357 in. in diam by $1\frac{3}{4}$ in. long and

Cleveland Meeting, October 1949.
TP 2697 E. Discussion of this paper (2 copies) may be sent to *Transactions* AIME before Dec. 1, 1949. Discussion is tentatively scheduled for publication in May 1950.
Manuscript received May 2, 1949; revision received July 25, 1949.

---

* General Electric Co., Schenectady, N. Y.

[1] References are at the end of the paper.

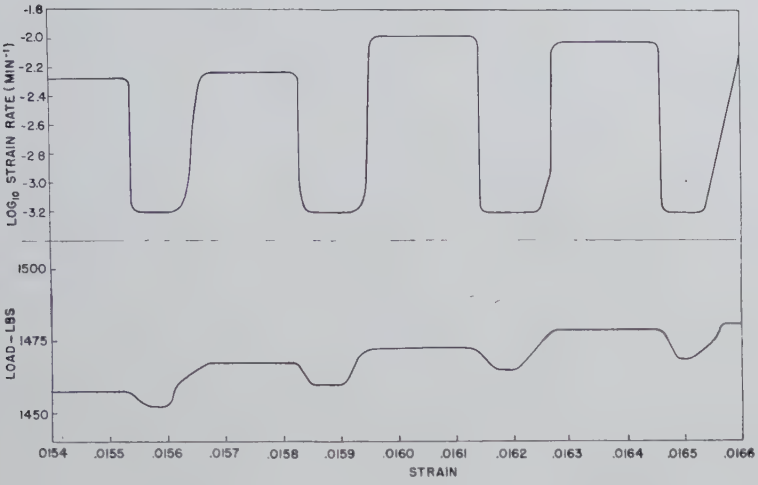

FIG 3—Discontinuous flow in 61S aged 10 min. at room temperature before room temperature testing at 0.00075 min^{-1} (or equivalent rate of head separation during discontinuous flow).

smoothed into the ½ in. —13 threaded ends by ¼ in. fillets. Strain was measured by an averaging Baldwin-Southwark microformer-type strain gauge with a 1.4 in. ga. length between conical points, used in conjunction with a Baldwin-Southwark stress-strain recorder and tensile testing machine.

As expected, the resulting stress-strain curves, two of which are plotted in Fig 1, show that for a given strain rate the flow stress is higher the longer the period of aging preceding the test. The entire stress-strain curve is smooth only for specimens aged for sufficiently long periods of time before testing. Although the early portions of the other curves also are smooth, the later portions exhibit discontinuous flow.*

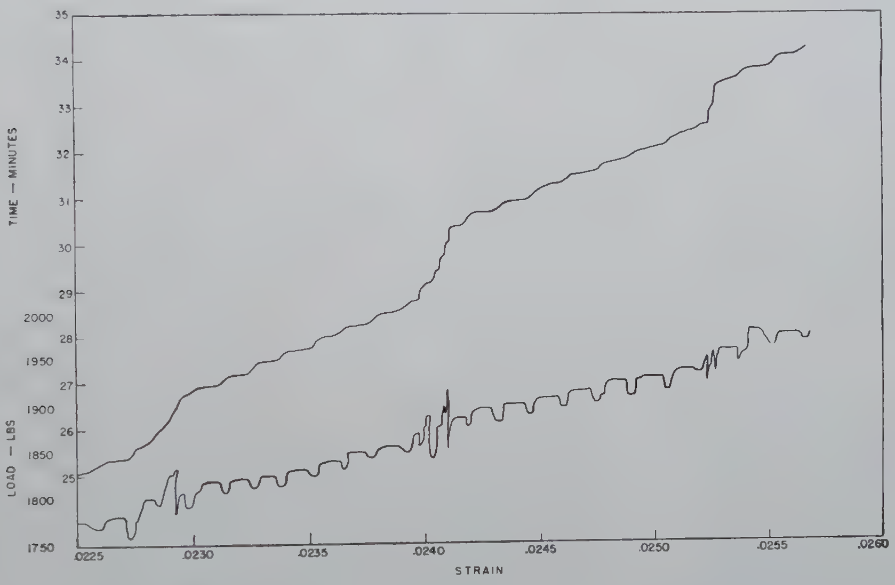

FIG 4—Discontinuous flow in 61S aged 10 min. at room temperature before room-temperature testing at 0.00075 min.$^{-1}$ (or equivalent rate of head separation during discontinuous flow).

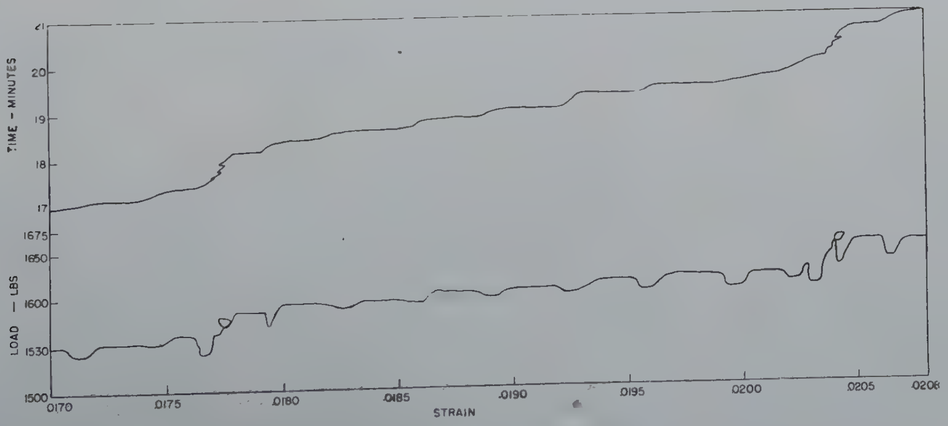

FIG 5—Discontinuous flow in 61S aged 10 min. at room temperature before room-temperature testing at 0.00075 min.$^{-1}$ (or equivalent rate of head separation during discontinuous flow).

---

* The term "discontinuous flow" will be used to designate any failure of the metal to follow a smooth stress-strain curve or strain-time curve.

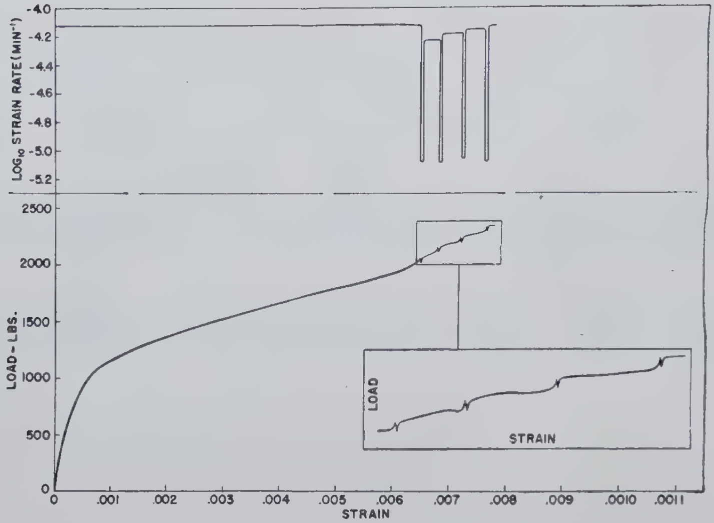

FIG 6—Discontinuous flow in 61S aged 10 min. at room temperature before testing at 0.0003 min.$^{-1}$ (or equivalent rate of head separation during discontinuous flow).

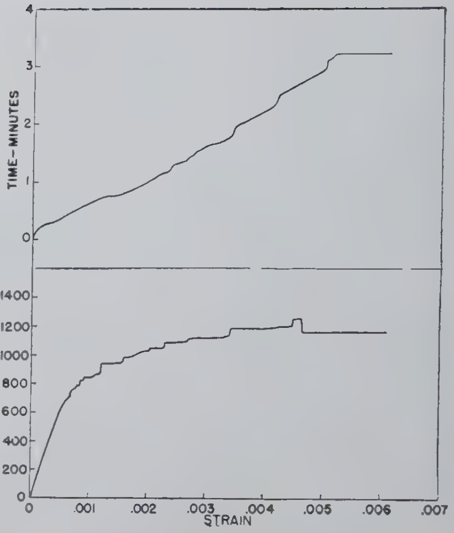

FIG 7—Discontinuous flow in 61S aged 2 min. at room temperature before room-temperature testing at 0.0008 min.$^{-1}$ (or equivalent rate of head separation during discontinuous flow).

For aging times that are not too short, flow stress values can be obtained from the early, smooth portion of each stress-strain curve. Flow stress values at a plastic strain of 0.003 increase with aging time for tests at a given strain rate (Fig 2), and a few tests indicate that a slower strain rate produces a higher flow stress (for a given initial condition of aging). This reverse rate effect will be discussed in connection with another type of test to be described below.

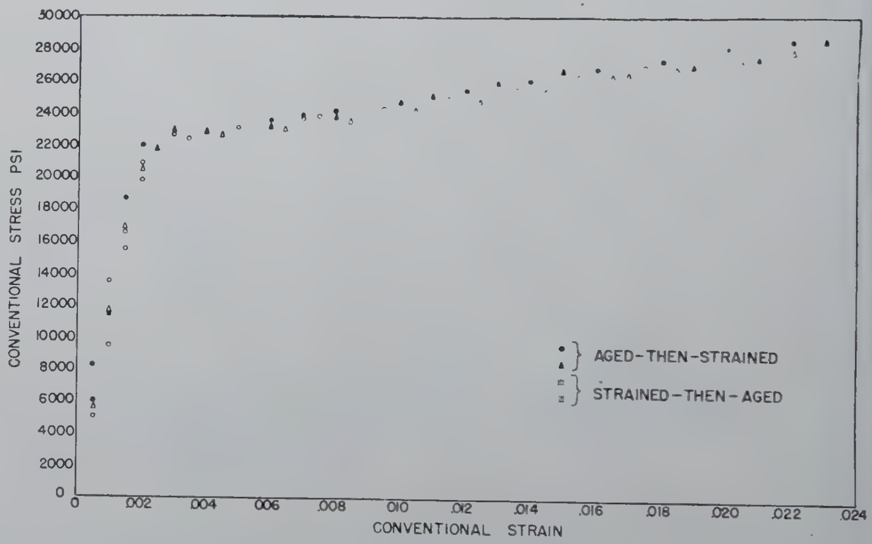

FIG 8—Creep curve for 61ST at room temperature and 41,900 psi initial stress (tested several months after aging).

After discontinuous flow began, a constant rate of head separation* was maintained, for it was no longer possible to keep the strain rate constant. The discontinuous flow exhibited different characteristics under different conditions of strain rate, amount of strain, and prior aging treatment. Usually there was a characteristic periodicity of rising and falling load, with slow extension prevailing during each period of falling and rising load and with sudden extension at the maximum load (Fig 3). This periodic flow sometimes was superimposed on a second kind of periodic disturbance (with a longer period) where groups of load variations occurred at regular intervals of strain (Fig 4), or where alternate lengthening and shortening combined with rising and falling load actually produced loops in the stress-strain curve (Fig 5).

At a smaller rate of head separation, smooth sections of normal stress-strain curve were separated by comparatively short, uniformly-spaced, strain intervals where a very pronounced rising and falling of load accompanied unusually slow extension (Fig 6). When a specimen was tested almost immediately upon warming to room temperature from the liquid nitrogen quenching bath, discontinuous flow began immediately; and under these conditions almost square steps were observed in the stress-strain curve (Fig 7). Similar periodic flow has been observed by McReynolds[3] during extension of specimens of several aluminum alloys. He employed a very soft tensile machine designed to produce a constant rate of increase of stress, rather than a constant strain rate.

Creep Tests

61ST was subjected to constant-load creep tests at room temperature. The load was applied through an 18:1 lever with three hardened steel knife edges. The knife edges were all in the same plane. The strain time curve was obtained with the same device employed for determining strain rates in tensile tests. The gear train for the time-drive was arranged so that quick changes in speed of 30:1 could be made as required

---

* The Baldwin-Southwark testing machine had a pump control that provided a constant rate of oil flow for a given position of the inlet valve, regardless of the load. Thus a constant rate of head separation was obtained by keeping a constant opening of the inlet valve. Such a procedure will not produce a constant elongation rate of the gauge length if the load is changing, however, for some of the head motion is used up in fixture deflection. Variations in elongation rate as great as 20 to 1 may be expected for a constant inlet valve setting.

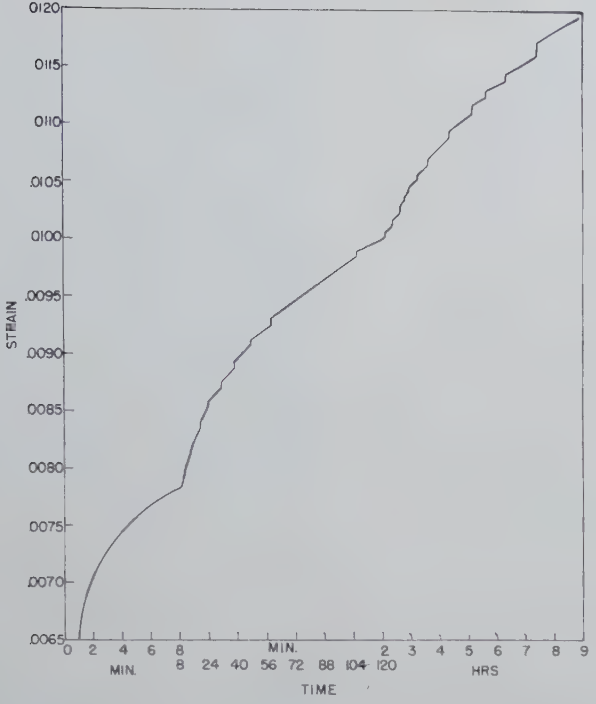

FIG 9—Creep curve for 61ST at room temperature and 42,300 psi initial stress (tested within a few hours after aging).

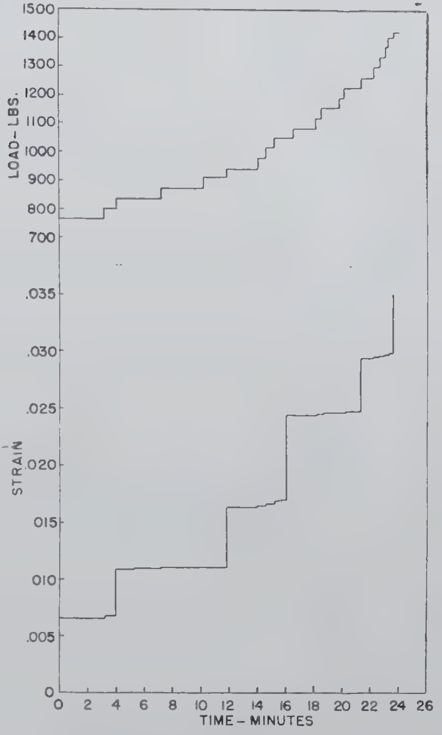

FIG 10—Room-temperature creep behavior at successively higher loads for 61S aged 10 min. at room temperature before beginning the test.

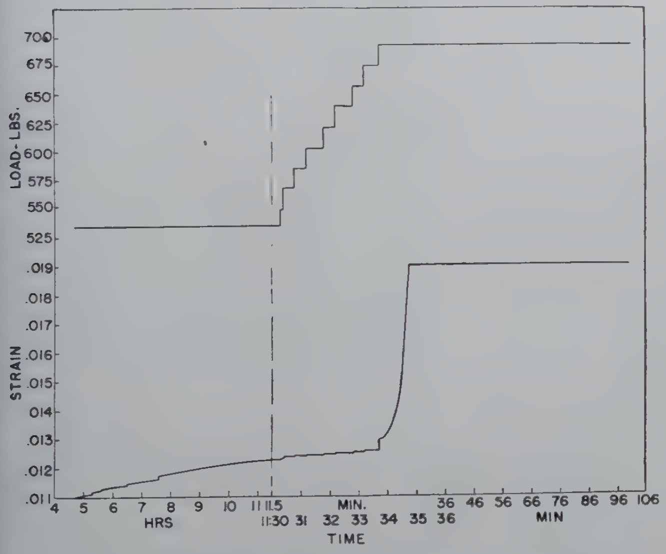

FIG 11—Creep curve for 61ST at room temperature and 42,300 psi initial stress. Tested within a few hours after aging (continuation of the test shown in Fig 9).

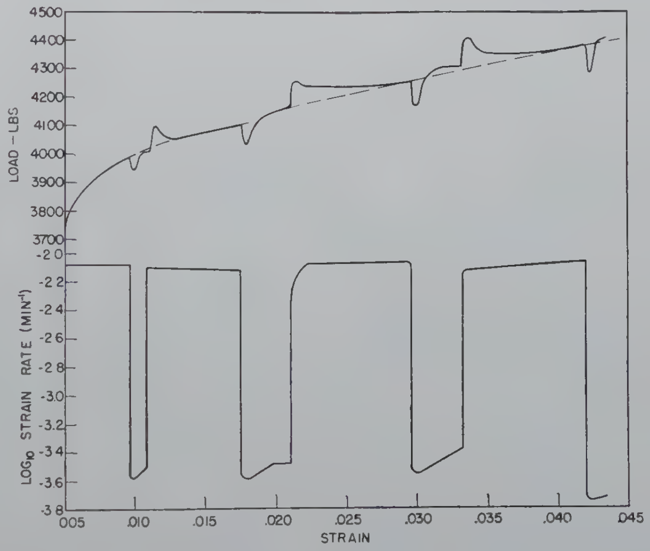

FIG 12—Transient effects in a tensile test on 61ST at room temperature.

to avoid a strain-time curve that was too nearly axial or circumferential for accurate slope measurements. 61ST tested in creep at room temperature several months after commercial aging (8 hr at 350°F) exhibited smooth strain-time curves as shown in Fig 8. On the other hand, 61ST tested within a few hours after the commercial aging treatment exhibited sudden periodic extensions superimposed on a smooth strain-time curve, as shown in Fig 9. Similar behavior has been observed with copper.[4] The difference in behavior between 61ST freshly aged at 350°F and that tested long after aging suggests that the freshly aged material had the greater capacity for change at room temperature.

A material that is aging rapidly during deformation ought to exhibit a very pronounced departure from the behavior of pure metals and other nonaging materials. To check this point, a creep test was made on 61S aged 20 min. at room temperature after quenching into liquid nitrogen from 521°C. Fig 10 shows that a large plastic extension* occurred upon application of the load, after which the material did not elongate further. Furthermore, suc-

---

* The extension was too rapid for the recorder to follow.

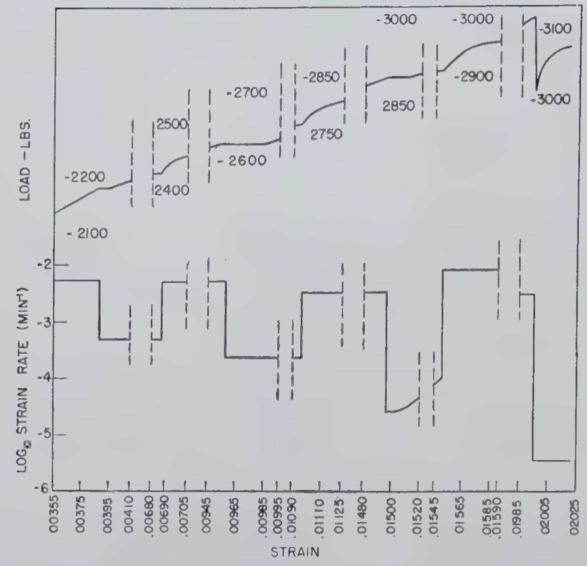

FIG 13—Tensile transients for OFHC copper at room temperature.

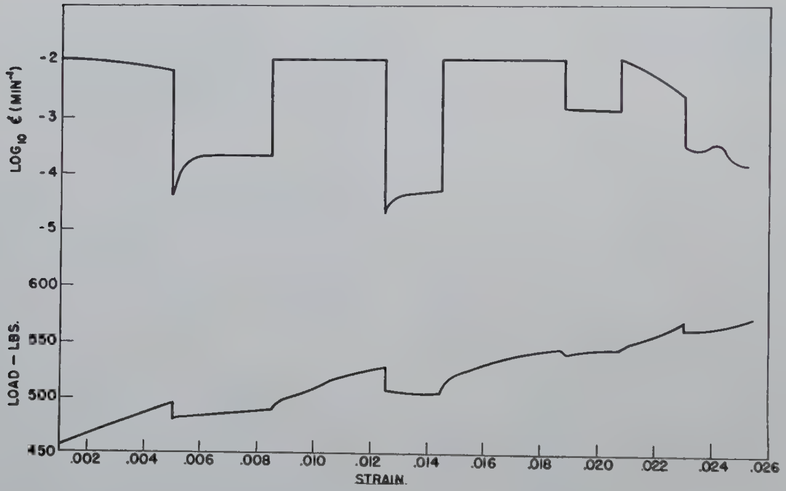

FIG 14—Tensile transients for pure (99.996 pct) aluminum at room temperature.

cessive additions of small load increments never caused gradual straining. After each load increment, either sudden plastic extension occurred or the specimen remained elastic.

The peculiar behavior observed upon successive application of small load increments to a currently aging metal was attributed to the fact that aging was proceeding during the test. If, as suggested above, the deformation behavior of recently aged 61S (61ST) can be affected by further room-temperature aging, then it might be expected that 61ST would exhibit creep behavior similar to that shown in Fig 10 for solution treated 61S. This expectation was realized (Fig 11).

Variable Strain Rate Tensile Tests

In these tensile tests the strain rate was changed suddenly from one constant value to another. When such a change is made, an immediate shift from a stress-strain curve characteristic of one rate to a second curve characteristic of the other rate might be expected. Actually, however, there is usually a period immediately following a rate change where the behavior conforms to neither curve, with rigorous conformity to the new curve being approached later. The temporary disturbance following a rate change has been called a "transient."[5*]

A peculiar transient is observed for 61ST tested at room temperature. Fig 12 shows that after changing the

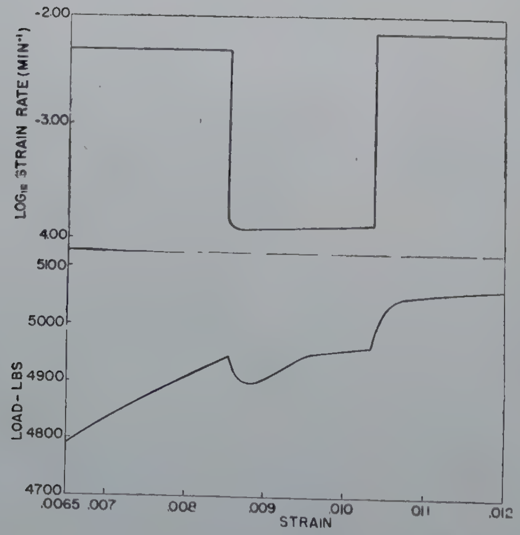

FIG 15—Transient effects in a tensile test on 61ST at the temperature of liquid nitrogen.

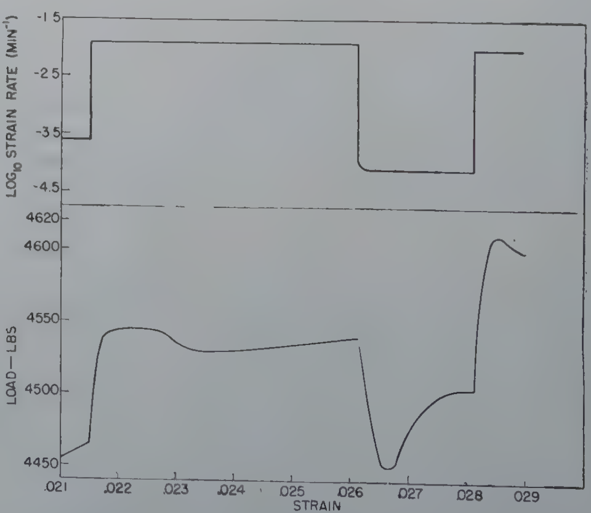

FIG 16—Transient effects in a tensile test on 61ST at the temperature of dry ice.

---

* The experimental equipment and procedure for measuring tensile transients are described in ref 5.

strain rate a new stress-strain curve appears to be approached; but then the stress changes in the opposite direction and approaches that corresponding to the curve preceding the rate change. This lack of rate effect for steady deformation (that is, after the dying-out of the transient) of 61ST at room temperature is surprising, for OFHC copper (Fig 13) and pure aluminum (Fig 14) both show a definite (though small) rate effect at room temperature.

The creep tests described above suggested that aging at room temperature could significantly affect the deformation of 61ST; it is possible that aging is responsible also for the peculiar transients and the lack of rate effect in 61ST tested at room temperature. To investigate this possibility, tensile transient tests were made at a series of temperatures At liquid nitrogen temperature (−194°C) a definite rate effect was observed (Fig 15) and the transient consisted only of a gradual shift from one curve to another, as is observed for non-aging metals (see Fig 14). This behavior would be expected if no aging occurred at −194°C. At the temperature of dry ice (−78°C) there was still a definite rate effect, although overshooting* was observed during the transient (Fig 16). In ice water (0°C) the overshooting during the transient was more pronounced and the rate effect (though small) was in the opposite direction to that observed at lower temperatures; upon increasing the rate, a lower stress-strain curve was approached than that preceding the rate change, and conversely (Fig 17). At 93°C the rate effect was large and in the expected direction, as shown in Fig 18.

The quantity $n = (\log S_2/S_1)/(\log \dot{\epsilon}_2/\dot{\epsilon}_1)$† was used as a measure of the rate effect. It was found to be roughly constant regardless of the change in rate, as illustrated in Fig 19. The influence of testing temperature on the rate effect is summarized in Fig 20, which shows n to have a pronounced minimum in the neighborhood of room temperature. It might be inferred that the rate effect in 61ST is a combination of an inherent rate effect (that observed in non-aging metals, where higher rates produce higher stresses) and a superimposed, inverse rate effect, due to aging, for which lower rates produce higher stresses. Fig 20 shows that the contribution of the aging to the overall rate effect is at a maximum near room temperature and disappears in the vicinity of −150°C.

According to the above viewpoint, transients are caused by a disturbance in the balance between two rate effects. Any disturbance of the balance between the inherent rate effect and the rate effect due to aging, such as a temporary pause in the plastic straining, might cause an unusual transient. An experiment on 61ST at room temperature in which a tensile test was

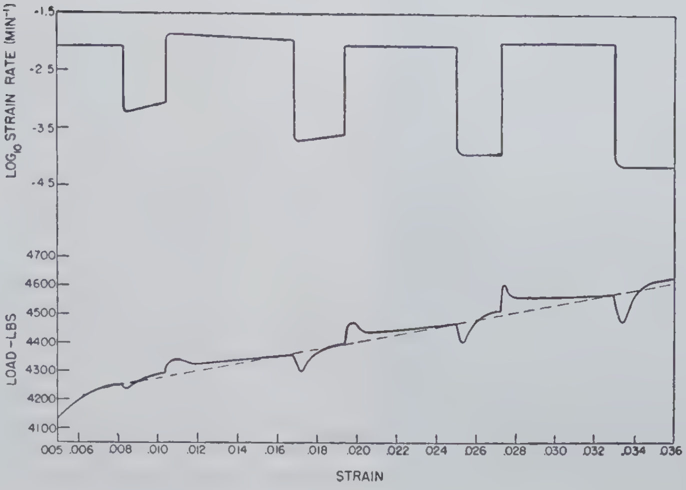

FIG 17—Transient effects in a tensile test on 61ST at 0°C.

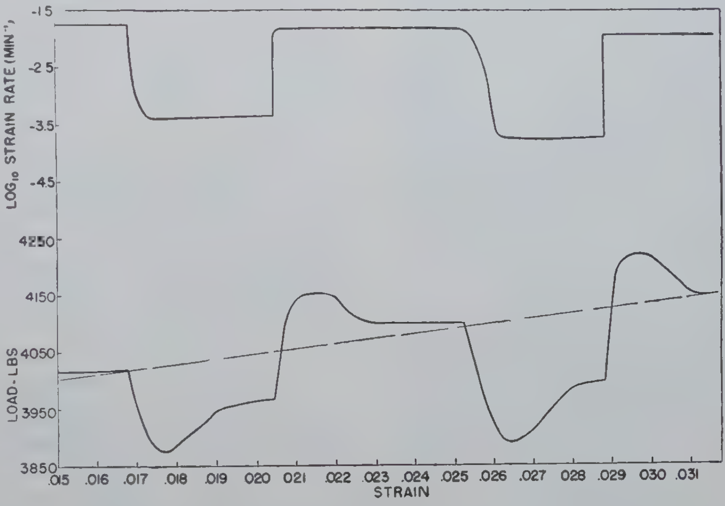

FIG 18—Transient effects in a tensile test on 61ST at 93°C.

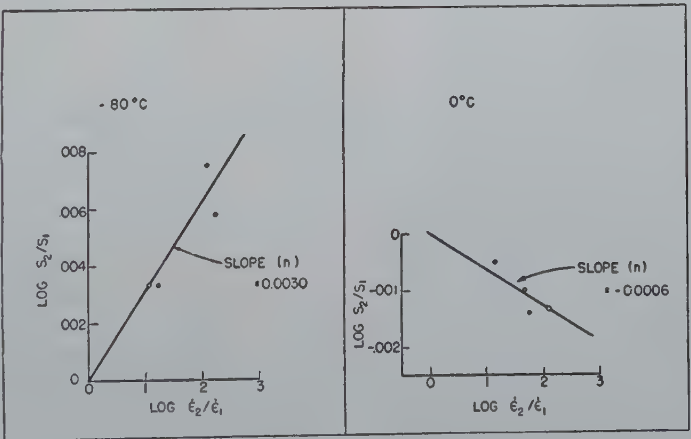

FIG 19—Determination of n values (rate effect) illustrated for two temperatures. Derived from data of Fig 16 and 17.

---

* Overshooting means that the stress changes to a value beyond that characteristic of the new strain rate, then slowly returns.

† The symbol $\dot{\epsilon}$ denotes strain rate.

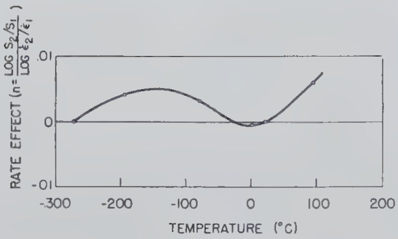

FIG 20—Effect of testing temperature on the rate effect for 61ST.

temporarily interrupted by a sojourn at a slightly lower load yielded such a transient following the interruption, even though the strain rate was the same before and after the interruption (Fig 21).

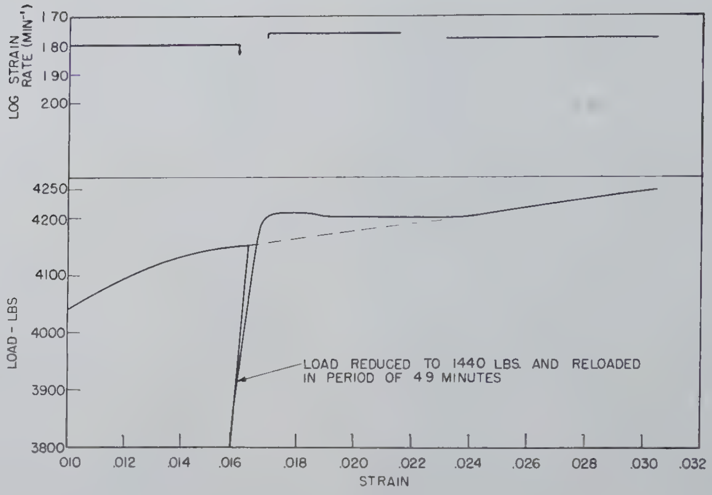

FIG 21—Transient effects at room temperature in 61ST caused by interrupting a constant strain rate tensile test.

Conclusions

If a metal is aging while it is being plastically deformed, it may show unusual deformation characteristics as follows:

1. Discontinuous yielding in a tensile test.
2. Periodic sudden extensions in a constant load creep test.
3. Failure ever to undergo gradual extension at constant load.
4. Unexpected transients following a sudden rate change.
5. An inverse rate effect, where an increase in flow stress (beyond the transient) is required to maintain a smaller strain rate.

Acknowledgment

The careful work of Miss Helen Lequear in performing the experiments is gratefully acknowledged

References

1. P. Ludwik and R. Scheu: The Yield Point of Electrolytic Iron and Mild Steel. *Ber. Fachausschusse Ver. Deut. Eisenhuttenleute* (1925) **5**, 1.
2. J. R. Low, Jr., and M. Gensamer: Aging and the Yield Point in Steel. *Trans.* AIME (1944) **158**, 207.
3. A. W. McReynolds: Plastic Deformation Waves in Aluminum. *Trans.* AIME **185**, 32: *Jnl. of Met.*, Jan. 1949.
4. E. N. da C. Andrade: On the Viscous Flow in Metals, and Allied Phenomena. *Proc.* Roy. Soc. (1910) **84**, 1.
5. R. P. Carreker, J. G. Leschen, and J. D. Lubahn: Transient Plastic Deformation. *Trans.* AIME (1949) **180**. *Metals Tech.*, Oct. 1948. TP 2477.

On the Problem of Grain Boundary Movement

C. G. DUNN,* Member AIME, F. W. DANIELS,* and M. J. BOLTON*

Recent observations on grain boundary movements in silicon iron have indicated the possibility of studying grain growth phenomena in two-grain specimens in which several variables affecting growth are readily controlled. These variables are (1) the energy per unit area (γ) in the grain boundary, (2) the orientation relationship of the two grains, and (3) the radius of curvature (τ) of the moving boundary.

Ideally, one grain *A* should be a narrow rectangular parallelepiped adjacent to a second grain *B* as shown two dimensionally in Fig 1. Such a two-grain group becomes unstable when one end of grain *A* is shaped according to the dotted line. Since the width *w* of grain *A* remains constant during growth of grain *B*, τ should also remain constant. The other variables mentioned above can be controlled in the preparation of each two-grain specimen.[1,2,3] For a particular orientation of each grain, γ is not necessarily fixed; γ may also depend on the orientation of the grain boundary, but this may be controlled to some degree.

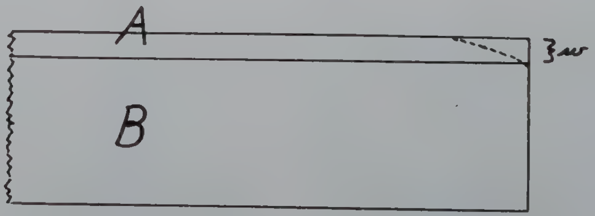

FIG 1—Schematic diagram of two grain-group for studying growth.

The energy relationships for the growth of grain *B* may be derived from the more simple arrangement of two grains *A′* and *B′* shown schematically in Fig 2. Here *B′* largely surrounds *A′*. Assume these grains are oriented with a common plane parallel with the flat

Technical Note No. 25 E. Manuscript received July 1, 1949.

* Research Physicist, and Metallurgists respectively, General Electric Co., Pittsfield, Mass.

[1] References are at the end of the paper.

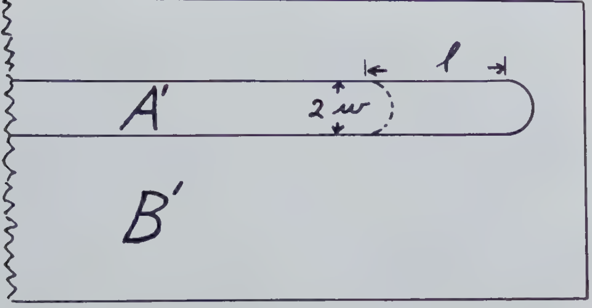

FIG 2—Schematic diagram of two grains A′ and B′.

portion of the specimen. Consider equal lengths l of grains A' and A. The total grain boundary energy for A' is twice that for A. Therefore, the width of A' will be taken equal to $2w$ so that both grains have the same grain boundary energy for transfering a unit volume of metal from A to B or A' to B'. When a volume V–that is, $2wlt$, where t is the thickness of the flat specimen*—transfers to B or B', the energy E released is obviously given by the following equation:

$$\frac{E}{V} = \frac{\gamma}{w} \qquad [1]$$

Thickness of the specimen does not enter this equation. Consequently, growth in such two-grain specimens should be independent of thickness. If γ is independent of grain boundary orientation, the shape of the active part of the grain boundary should reasonably approach a semicircle. When this occurs, w becomes identical with the radius of curvature τ of the advancing part of the boundary and Eq 1 then expresses the usual driving force for grain growth.[4] If γ varies with grain boundary orientation, γ in Eq 1 applies to the straight part of the boundary.

In the application of Eq 1 to grains A and B, it is assumed that the edge of grain A does not introduce an energy term. If a surface energy is involved, Eq 1 should be modified. It is also believed that w and τ may be different merely because a groove tends to form at the open end of the curved grain boundary. The term to use in Eq 1, therefore, is w rather than τ.

The present technique permits a time-temperature investigation at constant curvature to be made. Also, the rate of grain boundary movement can be measured as a function of temperature alone and the results used to calculate activation energies.

That the above method is experimentally feasible is indicated by the following example from our preliminary work. Silicon iron specimens capable of supporting exaggerated grain growth were prepared in the form of long strips 0.025 in. thick. Using a controlled grain growth technique,[1] one strip was converted into a suitable two-grain specimen with the common grain boundary lying parallel to the long dimension. The (110) planes of both grains were in the plane of the strip, and the [001] directions were 25° apart.

A 1 in. length cut from this specimen was annealed 4 hr at 1400°C in pure dry argon to eliminate boundary irregularities and to reveal the position of the boundary by thermal etching.[5] A final small two-grain specimen was prepared from the annealed piece and given an anneal of 10 hr at 1400°C in pure dry argon.

A photograph of the specimen in the as annealed condition is shown in Fig 3. The old boundary position extends across the length of the specimen. The new boundary (one end indicated by arrow) is curved along the advancing portion and coincides with the old boundary for a short distance. Observing these thermally etched boundaries at about 300 diam magnification, the old boundary appears as a "ghost line" whereas the new boundary is well defined. Reality of the new boundary was also confirmed by an X ray Laue photograph.

The specimen was then annealed an additional 48 hr at 140°C. No movement of the grain boundary occurred. It appears that the advancement was stopped by inclusions during the first anneal.

An estimate of the available energy for growth is of interest. With γ equal to 500 ergs per cm^2 approximately[6,7] and w equal to 1.3 mm, Eq 1 gives, on changing units, a driving energy of 0.00009 cal per cm^3. This energy may be contrasted with the value 9 cal per cm^3 reported for cold worked iron.[8] Larger values of γ/w could be obtained using smaller values of w.

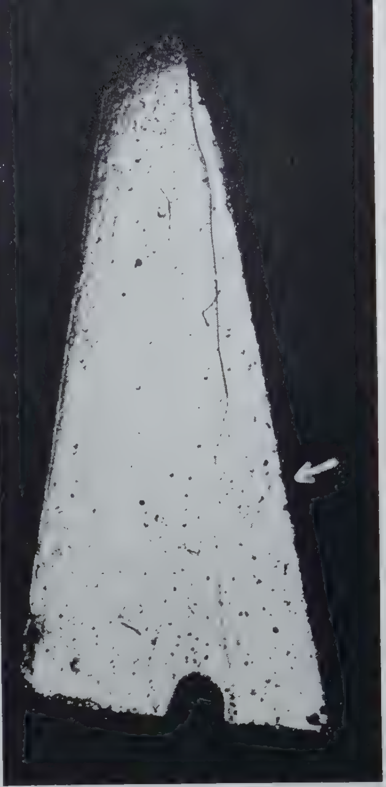

FIG 3—Photograph of a two-grain specimen showing growth of one grain.
Thermal etch. × 10.

More information using the present technique is anticipated from investigations now under way at this laboratory. It is hoped that results may be reported in the near future.

References

1. C. G. Dunn: Controlled Grain Growth Applied to the Problem of Grain Boundary Energy Measurements. *Trans.* AIME **185,** 72: *Jnl. of Met.*, Jan. 1949, T.N. No. 9.
2. C. G. Dunn and F. Lionetti: The Effect of Orientation Difference on Grain Boundary Energies. *Trans.* AIME **185,** 125: *Jnl. of Met.*, Jan. 1949.
3. T. S. Tiedema: To be published in *Cryst. Acta.* See also W. G. Burgers: Discussion TP2517E *Trans.* AIME, to be published in *Jnl. of Met.*
4. C. S. Smith: Grains, Phases and Interfaces: An Interpretation of Microstructures. (See reference to work of Zener.) *Trans.* AIME (1948) **175.** *Metals Tech.* June 1948, TP2387.
5. B. Chalmers, R. King, and R. Shuttleworth: The Thermal Etching of Silver. *Proc.* Roy. Soc. (1948) **A 193,** 465.
6. E. Orowan: Polycrystalline Metals and the Effect of Cold Work. (Discussion), *Proc.* Phys. Soc. (1940) **52,** 136.
7. W. Shockley and W. T. Read: Quantitative Predictions from Dislocation Models of Crystal Grain Boundaries. *Phys. Rev.* (1949) **75,** 692.
8. H. Quinney and G. I. Taylor: The Emission of the Latent Energy Due to Previous Cold Working When a Metal is Heated. *Proc.* Roy. Soc. (1937) **163,** 157.

---

* The value of t at the boundary is assumed to be essentially the same as the value of t everywhere else.

The Transverse Bending of Single Crystals of Aluminum*

M. K. YEN† and W. R. HIBBARD, JR.,‡ Junior Members AIME

Previous studies of plastic deformation of metals have emphasized the important role of bending and constraints during strain under relatively pure stresses.[1–5] Some new phenomena such as early conjugate slip[6] and polygonization[7] are intimately concerned with the relief of bending stresses, the former by slip and the latter by a process analogous to recrystallization. However, few analyses of the bending deformation of single crystals were found in the literature, and those[8,9] are sufficiently previous to the modern interpretations of slip to invite further investigation in this area.

The transverse bending mode of testing, using the two-point loading method, was selected because the center portion of the specimen may be considered as under a theoretically pure bending stress with a uniform bending moment. Considerable attention was given to both the lattice distortion and flow characteristics of the crystals during deformation.

Experimental Procedure

A specimen under the action of equal and opposite couples at both ends is said to undergo pure bending. The shear and moment diagrams of a specimen under the two-point loading method of transverse bending are shown in Fig 1. The moment over the middle-third of the span is equal to PL/6, and the vertical shear is zero. Fig 2(A) illustrates the stress distribution in the elastic range on a plane across the middle of the specimen. It can be seen that the normal stress has a maximum value at the extreme surfaces on the tension and compression sides, and decreases proportionately to zero as it approaches the neutral plane.

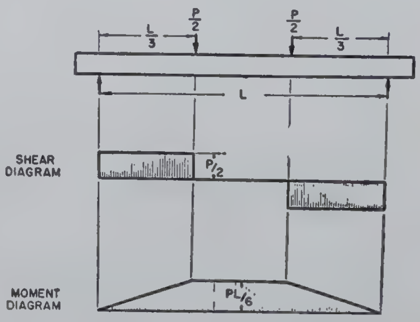

FIG 1—Shear and moment diagrams of a beam under transverse bending by the two-point loading method.

However, when the plastic range is reached, the stress distribution is no longer a straight line relation, but changes in a manner which can be best illustrated as shown in Fig 2(B). The following calculation and stress analysis are mainly in accordance with the works reported by Timoshenko[10] and Kochendörfer.[9]

From the simple beam formula, the maximum normal stress will occur at the surface of the specimen. For a round specimen with a radius r and for a rectangular specimen with a height $2h$ and width $2b$, the maximum normal stress, S_n, will be given by the following formulas:

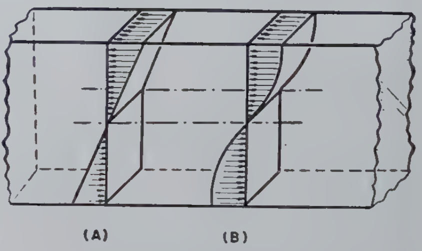

FIG 2—Stress-distribution in a beam for (A) elastic range and (B) plastic range.

For round specimen:

$$S_n = \frac{2PL}{3\pi r^3} \qquad [1]$$

For rectangular specimen:

$$S_n = \frac{PL}{8bh^2} \qquad [2]$$

Since it is reasonable to consider that slip takes place under the same conditions as in uniaxial loading, the resolved shear stress S_s, along the operative slip direction will be as follows:

For round specimen:

$$S_s = \frac{2PL}{3\pi r^3} \sin \chi \cos \lambda \qquad [3]$$

For rectangular specimen:

$$S_s = \frac{PL}{8bh^2} \sin \chi \cos \lambda \qquad [4]$$

where λ is the angle between the specimen axis and the slip direction and χ, the angle between the specimen axis and the major axis of the glide ellipse.

It was also reported by Kochendörfer[9] that the critical bending moment, that is, the bending moment exerted on the specimen to initiate slip, should be higher than the value given by the equations stated above. Based

---

Cleveland Meeting, October 1949.
TP 2687 E. Discussion of this paper (2 copies) may be sent to *Transactions* AIME before December 1, 1949. Discussion is tentatively scheduled for publication in May 1950. Manuscript received May 2, 1949; revision received July 1, 1949.

* A part of a Dissertation presented by M. K. Yen to the Faculty of the School of Engineering, Yale University in Candidacy for the Degree of Doctor of Engineering, May 1949.

† Research Associate, College of Engineering, New York Univ., New York City.

‡ Assistant Professor of Metallurgy, Yale University, New Haven, Conn.

[1] References are at the end of the paper.

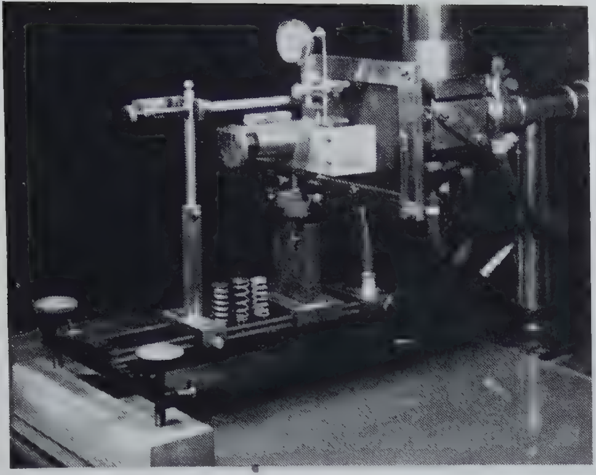

FIG 3—Bending apparatus assembly at X ray tube.

upon his analysis, the critical shear stress observed in bending may be 1.5 to 1.7 times greater than that in uniaxial loading for rectangular and round specimens respectively.

A special bending device to apply a transverse load by the two-point loading method used in this investigation consisted of three major parts: 1. Back-reflection camera with demountable pin-hole system. 2. Bending fixture with load-measuring device. 3. Deflectometer with a dial indicator.

The assembled equipment is shown in Fig 3. The back-reflection X ray camera had two interchangeable collimating pin-hole systems, 1.0 and 0.5 mm in diam.

In the bending device, the specimen was supported by two steel knife-edges with a span of exactly 3 in. The load was transmitted to the specimen through two knife-edges one inch apart which were mounted on a sliding steel plate bearing against a calibrated spring. The load was measured by reading the deflection of the compressed spring on the scale attached. The deflectometer consisted of a pivoted lever which was mounted so that the lower end contacted the center of the back side of the specimen. The upper end of the lever was attached to the stem of a dial indicator whose scale could be estimated to one ten-thousandth of an inch.

Two different types of specimens were made from high-purity aluminum rod having the following chemical compositions:

Pct	
99.975	Aluminum
0.006	Silicon
0.015	Copper
0.006	Iron

Round specimens, ¼ in. in diameter and 4 in. in length were prepared by Found[11] using a modified Bridgman method. Flat specimens were produced by a strain-annealing method comparable to that reported by Carpenter and Elam.[12]

The round specimens, used for preliminary work, were carefully metallographically polished by hand and etched with 2 pct hydrofluoric acid. Back-reflection Laue photograms were used to insure complete removal of any distortion.

The flat specimens were cut from strain-annealed pieces mounted in a special fixture which was used as a guide for a No. 8 jeweler's saw to cut along the longitudinal axis. After the sawing was accomplished, the specimen was then alternately polished and etched using 2 pct hydrofluoric acid and emery paper down to No. 000. Subsequent wet-polishing with alumina on a slow-speed wheel provided a smooth surface ready for the final electrolytic polishing.

The electrolytic polishing process used a dilute solution of fluoboric acid with low current density. Any smudge on the surface could be removed by immersing for about one minute in a hot solution containing 35 cc of 85 pct phosphoric acid and 20 g of chromic acid per liter. A subsequent rinsing with distilled water and alcohol and a final drying operation were then necessary.

After the specimen had been prepared according to this method, a one-inch gauge length was scribed on its center portion. A scratch was also made on the end of the specimen to serve as a reference mark for aligning purposes. The specimen was then placed carefully on the bending device and adjusted in such a manner that the two gauge marks coincided with the two knife edges for load application, and the reference mark was in a vertical position.

The back-reflection Laue method described by Greninger[13] was used for the determination of crystal orientation.

By suitably arranging a mirror with a binocular microscope, the front and top surfaces of the specimen could be observed concurrently during loading.

The load on the specimen was applied by gradually turning the knob on the back of the compressive spring which pushed the two knife edges forward against the specimen. The compression of the spring as well as the corresponding deflection of the specimen were recorded simultaneously so that the load-deflection curve could be made. X ray photograms and micrographs were taken at successive deflections of about 50 thousandths of an inch, in addition, to analyze the various surface markings.

Discussion of Results

Ten crystals, four round specimens and six flat ones, were investigated. The round specimens, approximately ¼ in. in diam, were used for preliminary work. Flat specimens A-10, A-11, and A-12 were bent after electrolytic polishing. Flat specimens A-13, A-14, A-15 were tested after mechanical polishing and etching with a dilute solution of hydrofluoric acid. The designations, dimensions and initial orientations for all specimens are shown in Table 1. In order to simplify the description of different positions on the specimen, the following designations are used: The "front" and "back" are the convex and concave sides on the bent specimen. The symbols "Top-T" and "Top-C" indicate

Table 1 . . . Dimensions and Initial Orientations of Round and Rectangular Specimens

Specimen		Dimension, In.	Area of Cross-section Sq In	Initial Orientation		
				χ	λ	$\cos\chi \sin\lambda$
Round	A-2	0.218 diam	0.0374	43°	36°	0.431
	A-3	0.243 diam	0.0464	38°	31°	0.406
	A-4	0.242 diam	0.0461	52°	42°	0.412
	A-5	0.241 diam	0.0456	40°	50°	0.509
Rectangular	A-10	0.132 × 0.221	0.0292	49°	44°	0.456
	A-11	0.132 × 0.223	0.0294	49°	44°	0.456
	A-12	0.129 × 0.224	0.0289	42°	41°	0.497
	A-13	0.128 × 0.239	0.0303	42°	41°	0.497
	A-14	0.132 × 0.227	0.0300	41°	44°	0.525
	A-15	0.132 × 0.225	0.0297	41°	44°	0.525

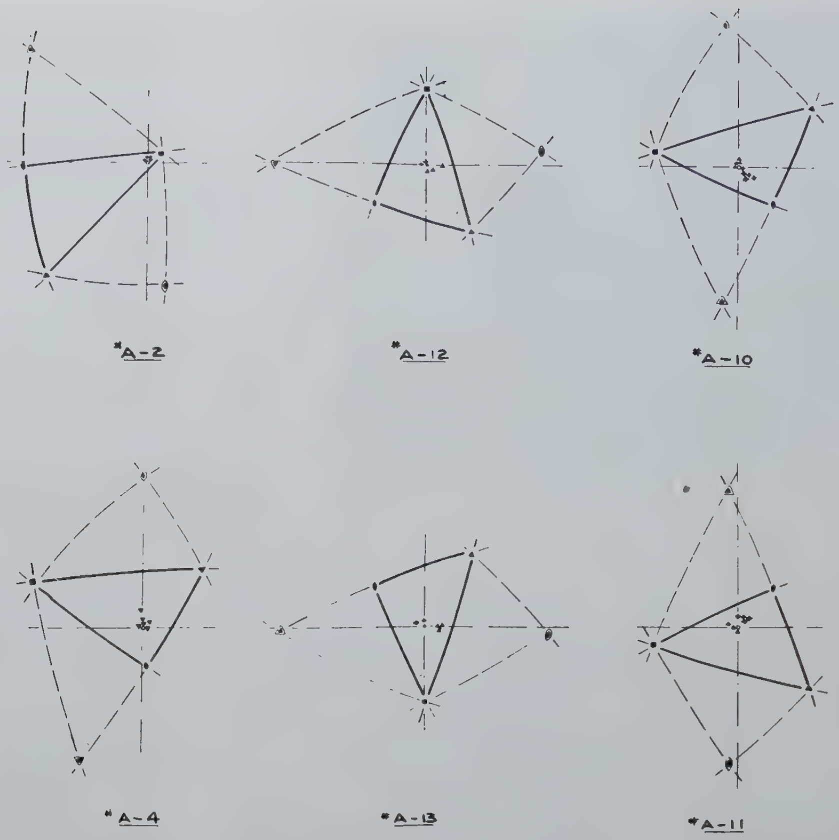

FIG 4—Axis rotations of bending specimens.
(▲) tension side and (+) compression side.

the regions on the top surface near the tension and compression edges respectively. For round specimens, only the symbols "front" and "back" are applicable. Unless otherwise noted, photograms and micrographs are taken with the stress axis horizontal and in the plane of the page.

Lattice Rotation in Bending

Axis orientations for the unstrained crystals and after various amounts of bending are shown in Fig 4. The axis of the unstrained crystal is designated by the small circle (o) at the center of the projection. The axes determined at the front and back side of the specimen after bending are represented by the triangle (▼) and cross (+) respectively. Thus the movement of the specimen axis relative to the axis of the unstrained crystal was observed.

For a single crystal subjected to tensile loading, the lattice rotation takes place in such a way that the slip direction gradually approaches the stress axis. For compression, the slip plane rotates toward a position parallel to the plane of compression. In the case of f.c.c. metals, the specimen axis during simple slip moves toward [110] and [111] for tensile and compressive stresses, respectively, whereas in duplex slip the end positions are [112] and [110] for tension and compression respectively.[14,15] Referring to Fig 4, it can be seen that when aluminum crystals were subjected to bending stress, the stress axis on the tension side of all specimens appeared to follow generally the Taylor and Elam rotation[14] toward the active slip direction. However, in the compression side, the change of orientation deviated from the path toward the (111) pole to a certain extent. In specimens A-10 and A-11, the axis on the compression side appeared to rotate toward a (110) pole instead of the (111) pole. This deviation could be ascribed to the restriction of flow in bending and possibly the presence of a secondary slip system.

Micrographic Observations

Round specimens A-2, A-3, A-4, and A-5 were prepared by polishing and deep-etching. It was noted that both the interlineage boundaries and a slight cored structure, similar to that in copper crystals observed by Hibbard,[16] were developed. However, the interdendritic spacing of the cored structure was considerably smaller than that of copper. A considerable number of slip lines were observed on the front and back surfaces even at very low deflection. The slip lines were localized in character but were gradually propagated toward the neutral plane as the load increased. The density of the lines also increased with an increase of load, but approached a constant value of approximately 1200 per inch at higher deformation. The lines generally appeared fairly equally spaced but slightly wavy in appearance.

Flat specimens A-10, A-11, and A-12 were prepared by mechanical polishing followed by the electrolytic polishing. Fig 5 and 6 show two photographs of specimen A-10 after a total deflection of 0.554 in. It was found that the surface markings on the top surface started at the edges of the specimen and moved toward the neutral plane with an increase in deformation. The density of lines increased with the degree of deformation but decreased as they approached the neutral plane. Considerable shift of the neutral axis toward the compression side was observed at higher deformation. This can be ascribed to the difference in specimen thickness between the tension and

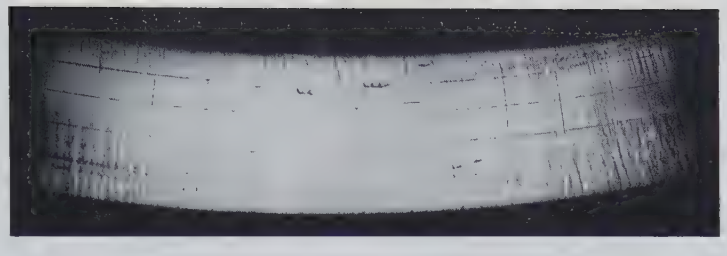

FIG 5—Specimen A-10. Top surface after 0.554 in. deflection. 4 ×.

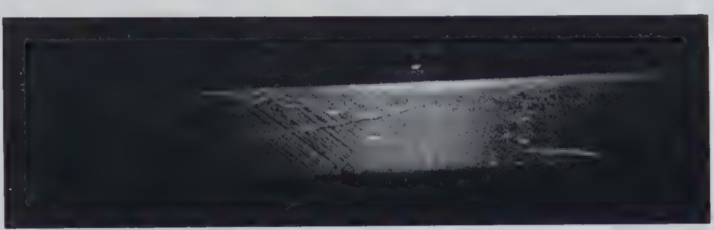

FIG 6—Specimen A-10. Front surface after 0.554 in. deflection. 4 ×.

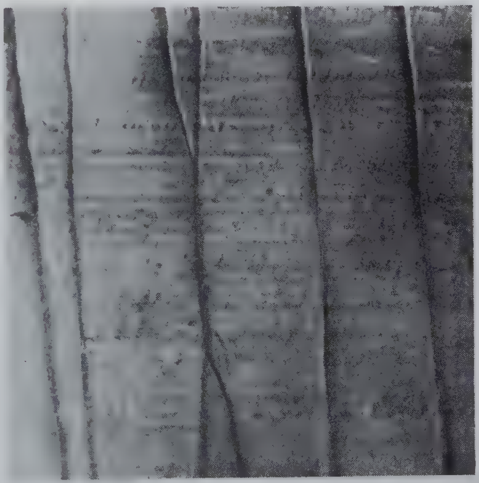

FIG 7—Specimen A-10. Surface Top-T after 0.250 in. deflection. 1000 ×.

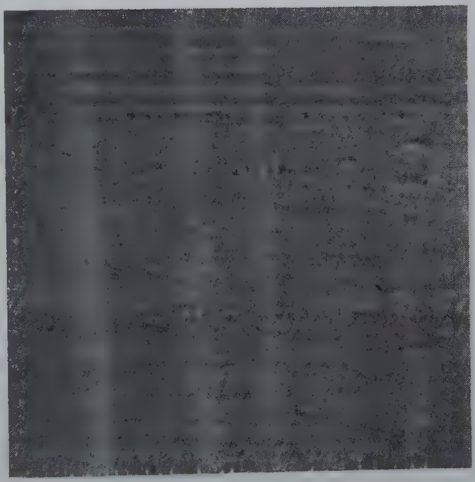

FIG 8—Specimen A-10. Surface Top-C after 0.250 in. deflection. 1000 ×.

compression sides caused by plastic flow and the resulting change in the stress distribution.

At first glance, no marked difference in the microscopic appearance of the markings on the tension and compression sides was observable at a magnification of 100 ×. However the microstructures at high magnification exhibit a rather distinctive aspect shown in Fig 7 and 8. Parallel narrow dark lines could be resolved on the tension side, but poorly defined light-colored bands with considerable width were observed on the compression side.

The development of markings on the front surface of these specimens started with equally spaced parallel lines (see Fig 9). The density of lines increased two fold as the deflection increased from 80.5 to 250.0 thousandths of an inch. Another set of markings inclined 45° to the specimen axis then appeared during further bending. The 45° lines appeared discontinuous in nature and were displaced where they met the vertical ones (see Fig 10). It was found that the lines inclined at 45° were the expected octahedral traces, whereas the vertical ones were thought to be cubic traces at an early stage of the investigation. In Fig 11 the crystal orientation of specimen A-10 is plotted on a stereographic projection with the pole of the front surface located at the center of the primitive circle. The traces of the markings on both the front and the top surfaces are sketched in the upper-left corner of the drawing. The loci of the poles of traces Top-I and Front-I intersect at a pole of an octahedral plane which was found to be the primary operative slip-plane having the maximum value of resolved shear stress. Trace Front-III was found only with slight oblique illumination at low magnification. (See Fig 6.) It appears as a band-like structure which makes an angle of about 90° with the octahedral traces. This band-like structure could not be resolved at higher magnification and may be regarded as evidence of a type of rotation of crystallites about an axis normal to the slip plane described by previous investigators.[17,18]

The trace Front II, which made an angle of about 90° with the specimen axis, was a somewhat confusing one. Referring back to Fig 11, the most probable plane in the zone of the axis is a cubic or a (100) plane. Since cubic slip does occur in aluminum at high temperatures, it led to the possibility that the cubic plane might slip under a rather complicated stress introduced by bending. Similar results were also found in specimens A-11 and A-12. The orientation of specimen A-11 is shown in Fig 12. By further study of specimen A-11 vertical traces Front II and Top I were established as continuous traces from the same plane. Referring to Fig

12, the pole of these two vertical traces Front II and Top I must be in the neighborhood of the specimen axis, but no significant plane could be found in that region of the projection. It appears therefore, that a possible explanation is that these lines are strain markings or cracks in the anodic coating left from electrolytic polishing. Further experiments on the specimens prepared by mechanical polishing and etching substantiate this finding.

When the specimens A-10 and A-12 were subjected to bending with a deflection of a tenth of an inch, a second set of slip markings (Top Trace II) was revealed at the Top-C surface of the specimens. From the analysis of the surface markings shown by Fig 11, it can be seen that these were the traces of a secondary octahedral plane. This was found to be in the (111) plane which had the second highest resolved shear stress among the twelve (111) [110] systems. The early occurrence of the secondary slip system may be ascribed to the restriction of flow at the compression side which varies from the condition for a crystal under pure compression and thus forces the secondary system into operation. Referring back to the projections showing lattice rotation, Fig 4, it can be seen that the rotation on the compression side is different from that in uniaxial loading in that the specimen axis was rotated toward the (110) direction and not toward the pole of the slip plane as in pure compression. This appeared to collaborate the microscopic observation of double slip since it is known that the [110] direction is usually the end position of the duplex slip for face-centered cubic crystals under compression.

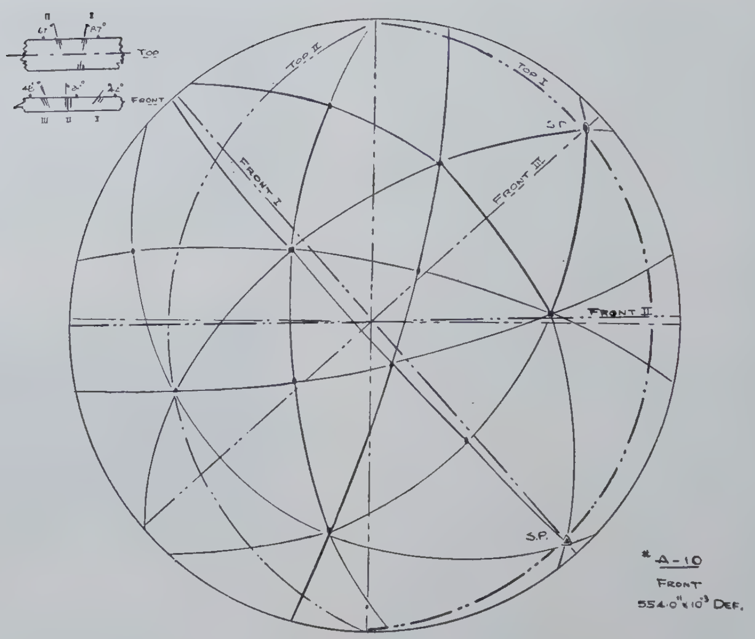

FIG 11—Stereographic profection of specimen A-10 after 0.554 in. deflection with front surface parallel to the plane of the projection.

In order to eliminate the uncertainty in the surface condition introduced by electrolytic polishing, specimens A-13, A-14, and A-15 were subjected only to mechanical polishing with fine alumina followed by etching with diulte HF solution. No appreciable difference was noticed in microscopic appearance of surface markings at low magnification between specimens with or without electrolytic polishing. The band-like structure found in specimen A-15 was comparable to that in Fig 6 of specimen A-10. In addition, a similar type of band structure both parallel and perpendicular to the traces of the operative slip plane of specimen A-13 was found.

However, at high magnification only traces of the theoretically predicted octahedral plane were observed. Except at Top-C surface of specimen A-13, a secondary set of slip markings was found to be the traces of the octahedral plane having the second highest resolved shear stress among all twelve possible slip systems. The slip markings generally appeared to be fairly straight and equally spaced. It was found, however, in the neighborhood of the region where the slip direction intersected the specimen surface that the markings ap-

FIG 9—Specimen A-10. Front surface after 0.081 in. deflection. 500 ×.

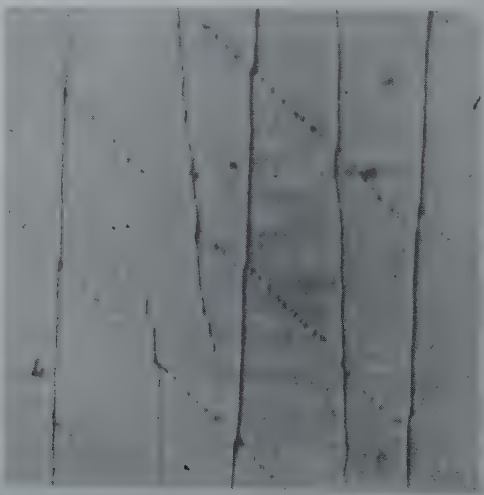

FIG 10—Specimen A-10. Front surface after 0.554 in. deflection. 1000 ×.

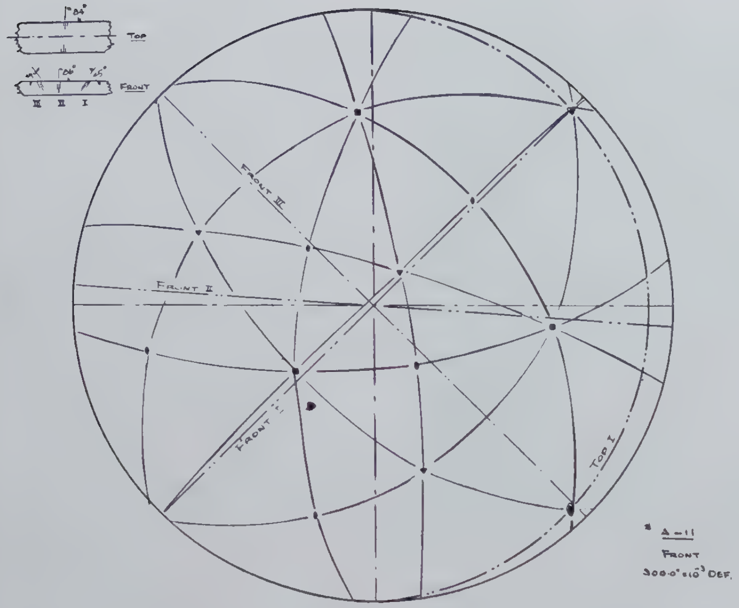

FIG 12—Stereographic projection of specimen A-11 after 0.300 in. deflection with front surface parallel to the plane of the projection.

peared to be either step-like or discontinuous in nature. Fig 13 shows slip markings on the Top-T surface and front surface of specimen A-15. The markings appeared to be straight and had an average distance between them of from 5 to 10 microns. The closest approach distance was in the order of one micron. Fig 14 shows slip markings on the front surface of specimen A-13 at × 1000 magnification. The pictures were taken on the surface where it is intersected by the direction of slip. The short step-like markings appeared not to follow any definite crystallographic angle as reported in alpha brass.[19] This may be due to the more complicated stress condition in bending where these steps were probably too small to be identified with any particular planes. Similar results were also found in specimen A-15 on the Top-T surface where it was intersected by the direction of slip (Fig 13). Regions showing the discontinuity of markings were also observed in both specimens A-13 and A-15. These markings were similar to those reported by Crussard[20] in aluminum crystals as well as by Andrade[21] in deformed lead crystals. They generally lost their width accompanied by a great decrease in their intensities as they passed each other. It is also interesting to note that the phenomenon of bending of the glide-lamellae did take place in specimen A-15 as shown in the upper edge of Fig 13.

Slip markings of specimen A-15 under oblique illumination are shown in Fig 15, and appear to be dark and light bands on the tension and compression sides respectively. The regions free from any resolvable slip markings are close to the neutral plane, at which the stress should be theoretically zero. The density of the markings on both sides increased from the inside outward and gradually approached a constant value at the edges of the specimen.

Asterism

When a crystal is deformed by uniaxial loading, distortion generally occurs by rotation of the crystallites about an axis lying in the slip plane normal to the slip direction. This type of rotation was more or less confirmed by analysis of the Laue spots obtained from deformed crystals.[2–5] Recently it was found that in addition there is also a relocation of glide-lamellae by a twisting distortion around the polar axis of the slip plane.[17,18] However, in the present investigation, the asterism of Laue spots in the X ray photograms did not appear to follow either of these types of distortion. The change of the Laue spots always exhibited the same

FIG 13—Specimen A-15. Top-T surface after 0.389 in. deflection. 1000 ×.

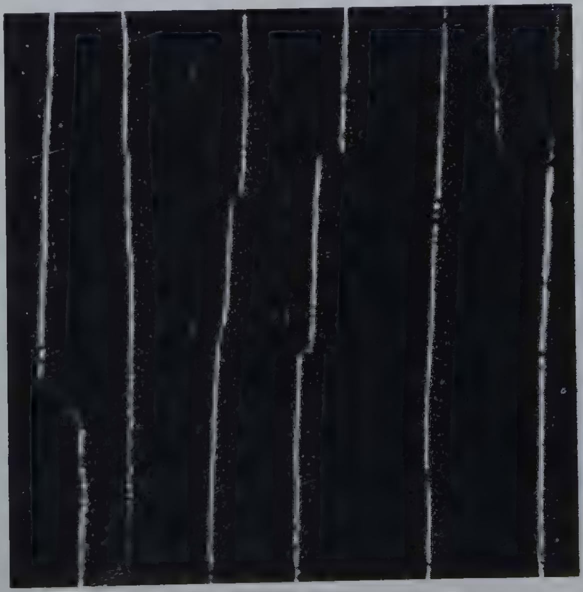

FIG 14—Specimen A-13. Front surface after 0.300 in. deflection. 1000 ×.

pattern regardless of the initial orientation or the orientation of the operative slip plane with respect to the stress axis. In general, the Laue spots on the photograms taken from the Front surface were elongated in the direction parallel to the specimen axis, whereas those from the Back surface were distorted so as to become elongated in the direction 90° to the former ones. However, no appreciable change in the shape of Laue spots on either the Top-T or Top-C surface was noticeable.

Fig 16 shows the change in shape of Laue spots on the Front surface of specimen A-10 with an increase in deflection. It can be seen that the elongation of spots did not occur until the specimen was subjected to bending far beyond the elastic range. This may be regarded as evidence in favor of the idea that asterism does not indicate the existence of elastic strain, but rather plastic deformation resulting from bending.

Fig 17 shows the types of Laue spots obtained from the Front, Top-T and Back surfaces of two other crystals, A-11 and A-15, with different initial orientations. It is apparent that all the specimens exhibited the same type of distortion as far as the nature of the asterism is concerned. It appears that the axis of rotation causing the asterism on the tension side is in vertical direction while that on the compression side is horizontal. The fact of no appreciable change of Laue spots from the top surface of the specimen further confirms these rotation axes.

FIG 15—Slip markings on the top surface of specimen A-15 near the neutral plane. The dark markings are near the tension side and the white ones are near the compression side. 50 X.

Reduced one-half in reproduction.

Furthermore, it was also found that in specimens A-12 and A-13 the Laue spots were not only elongated but also divided into small individual areas as shown in Fig 18 and 19. The traces of the active slip plane are indicated in the left corner of the photogram. It can be seen that the fragments of the spots appear to be aligned in a specific pattern, divided into two groups, one roughly parallel to the traces and the other normal to it. This break-up of the Laue spots in deformed crystals after annealing was observed by Collins and Mathewson[17] in aluminum and by Andrade and Tsien[22] in potassium and sodium. Very recently, Cahn[7] in a study of bent zinc crystals suggested "the deformation leads to elastic bending of glide-lamellae; when the crystal is annealed, the lamellae undergo 'polygonization.' The orientation of each new grain is the same as that of the part of the original crystal from which it grew but the elastic strain has vanished." In addition, the break-up of the Laue spots was also reported even in deformed aluminum crystals by Crussard.[20] It appears that the discrete asterisms in specimens A-12 and A-13 may be rationalized as a process of fragmentation occurring during deformation at room temperature. In Fig 18 and 21, the fragments of the Laue spots parallel to the traces of the operative slip plane as shown at left-upper corner may be regarded as a rotation of crystallites about an axis parallel to the slip plane. The fragments oriented normal to the traces may be rationalized as a break-up of crystallites due to the torsional rota-

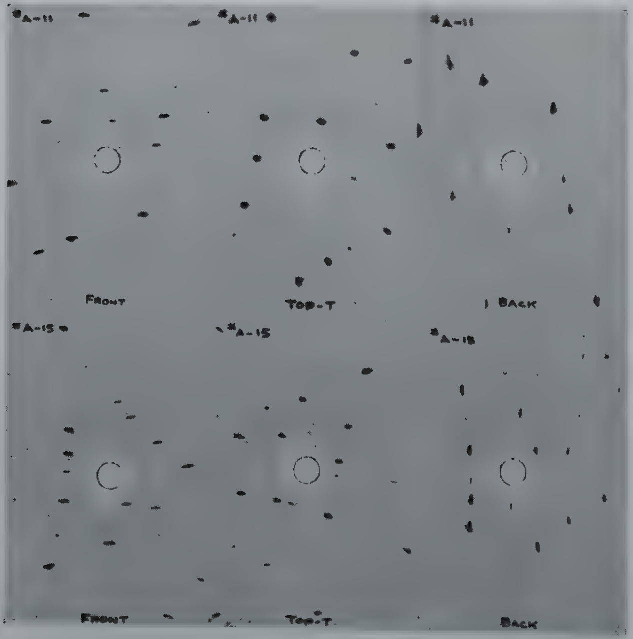

FIG 16—Laue photograms of specimen A-10 after various amounts of deflection as indicated.

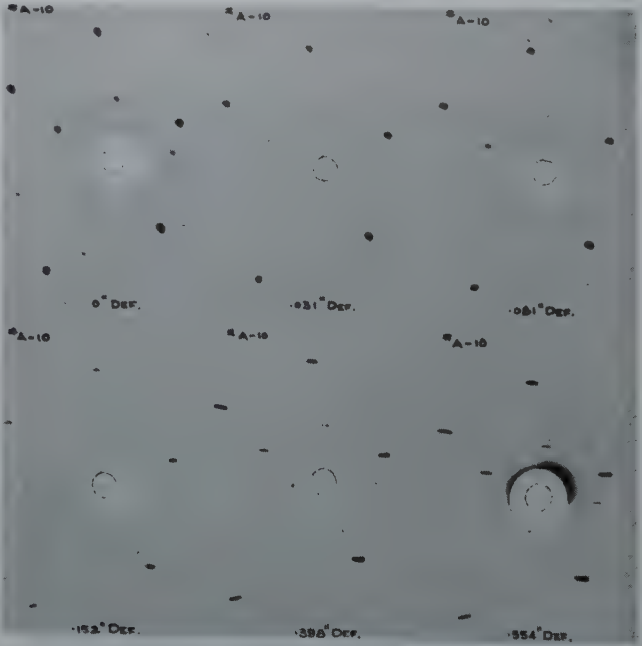

FIG 17—Laue photograms of specimens A-11 and A-15 after deflections of 0.300 and 0.266 in., respectively.

Reduced approximately one-third in reproduction.

tion around the pole of the slip plane.[17,23] The latter was reported recently by Heidenreich and Shockley[18] from a study of Laue spots and Kikuchi lines produced on electron diffraction patterns of extended aluminum crystals.

Load-deflection Diagrams

The load-deflection curves for aluminum crystals under bending were found to resemble the load-elongation curves reported for the crystals under tension. A definite yield point at a total load of several pounds was usually observed. The curve then gradually flattened with an increase in deflection. The load-deflection curves for flat specimens were quite consistent with each other. The yield point was in the neighborhood of 3 lb which resulted in a normal stress on the extreme surface of the specimen of about 1150 psi with a corresponding resolved shear stress in the neighborhood of 500 psi. Fig 20 shows the data recorded for specimens A-10, A-12, and A-14 having different initial orientations. The yield point and the rate of strain-hardening indicated by the load-deflection curves did not appear to vary significantly for different orientations. This agrees with the results of shear tests in aluminum crystals reported by Burgers and Lebbink.[24] They stated that slip in aluminum crystals deformed in shear may be found along lattice planes and directions differing from the usual slip system, (111) [110], and no appreciable variation on the shear stress required for different combinations of planes and directions was observed.

Flow-pattern in Bending

In order to understand the unique characteristics of flow in bending, two auxiliary experiments were performed. The first one was made on a study of the stress distribution pattern over the surface of a specimen by means of the commercial Stresscoat manufactured by Magnaflux Corporation, Chicago, Ill. It was found that the pattern produced by Stresscoat was practically the same as that found on specimens A-10 and A-11 prepared electrolytically and thus having an oxide coating. This may be regarded as confirmation that the anomalies in the surface markings of the electrolytically polished specimens resulted from surface cracks or strain markings in the anodic coating. It is believed that the major axis of the strain ellipsoid on the tension side lay parallel to the specimen axis whereas that on the compression side was normal to it. A similar analysis was also reported by Yamaguchi and Tagino[25] who found that fissures produced in a thin oxide layer during creep tests were oriented in the direction perpendicular to the major axis of the strain ellipsoid on the tensile specimen.

The second auxiliary experiment was the study of the flow pattern of bent specimens made of paraffin. The specimens were cast in a metallic mold hav-

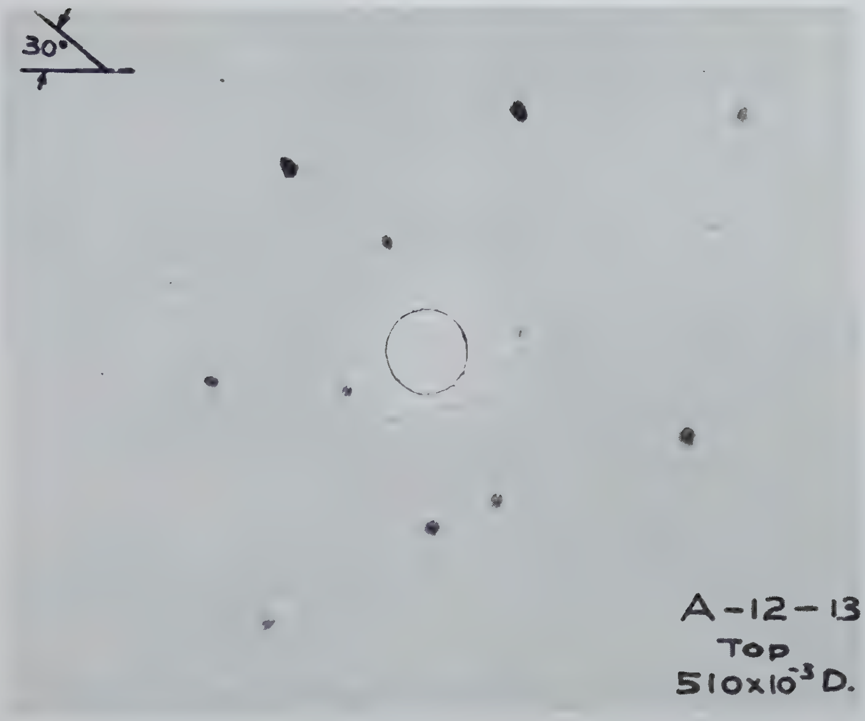

FIG 18—Laue photogram of specimen A-12, Top-T surface, after 0.510 in. deflection. 2 X.
Reduced approximately one-third in reproduction.

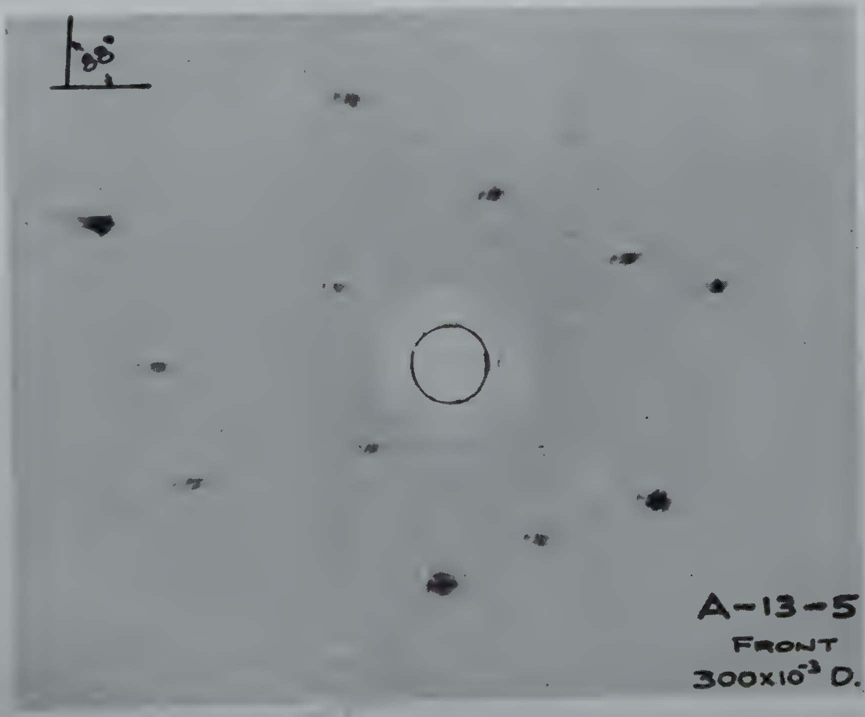

FIG 19—Laue photogram of specimen A-13, front surface, after 0.300 in. deflection. 2 X.
Reduced one-third in reproduction.

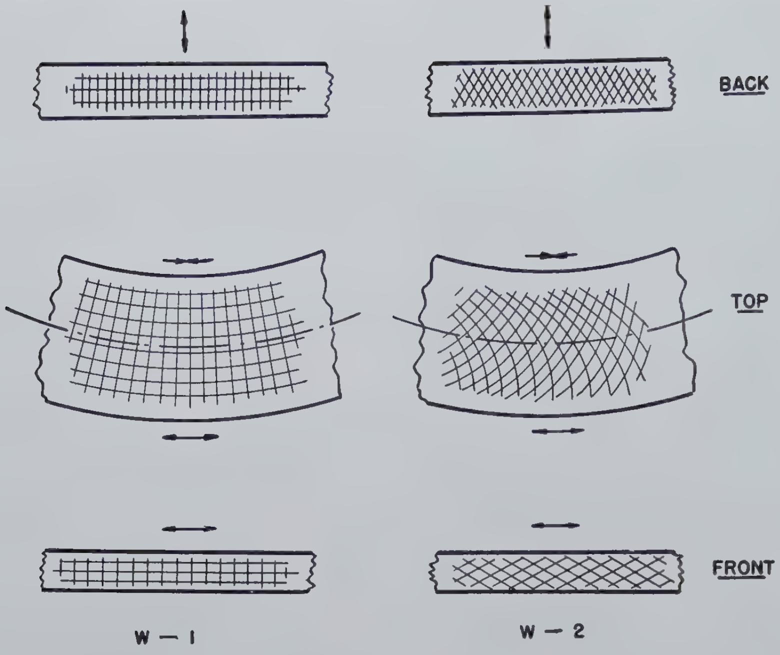

FIG 21—Schematic diagrams of flow patterns on bent wax specimens W-1 and W-2.

ing a rectangular cross-section of approximately ¼ by ½ in. Two sets of cross-lines, one at an angle of 0° and 90° and the other at 45° with the axis of the specimen, were carefully drawn on the various surfaces of specimens W-1 and W-2. The specimens were then bent, after being warmed slightly on a gas flame, to a deflection of about ¾ in. The originally square grid was distorted to a greater or less extent at the various positions of the specimen as shown schematically in Fig 21. The arrows indicate the direction of flow derived from the flow pattern on the paraffin specimens W-1 and W-2.

Mechanism of Deformation by Bending

A most significant characteristic of the process of plastic deformation by bending is that slip does not occur across the entire crystal but is restricted to a limited area. Slip markings appear to progress from the higher stressed toward the lower stressed region, gradually losing both intensity and width as the stress diminishes. The development of slip markings was found to consist of two different stages. At first a band-like structure was readily seen by unaided visual examination, then distinct slip markings appeared in the bands. These well-defined markings progressed toward a lower stress region with an increasing deformation. The line density was increased by the formation of new markings which appeared between the old ones under further loading. It is believed that the slip process in bending consists of an elastic bending followed by a plastic distortion, probably similar to the fragmentation processes described by Mark, Polanyi and Schmid,[1] Burgers[4] and others.[2,3,5] A schematic diagram of the distortion in two adjacent glide-lamellae under different stress conditions is shown in Fig 22. If the two undistorted glide-lamellae, shown in Fig 22A, were subjected to a pure shear, the lamellae would be deformed as illustrated in Fig 22B. Based upon this mechanism, the shear stress is about a thousand times larger than the observed critical shearing stress. However, it was found in this investigation that macroscopic bending of glide-lamellae did occur so that the stress distribution on the entire slip plane would be different from that produced by pure shear. This is shown schematically in Fig 22 C, D and E, that is, elastic bending, bending and plastic shear, and bending and fragmentation. It can be seen that under such conditions the slip process is composed of the successive glidings of a group of atoms at a time. The external force required to produce such a slip should be much less than the value required for an entire plane as a unit. The shear strain at the left end of the bending lamellae (Fig 22 C, D, and E) is practically equal to zero and increases gradually to a maximum value at the right end.

Furthermore, it is noteworthy that this mechanism of bending of glide-lamellae can be employed to interpret satisfactorily the asterism on Laue photograms of deformed aluminum crystals reported by Yamaguchi.[2] These results were criticized by Komar and Machalov[5] who suggested that the bending of the glide-lamellae is macroscopic rather than microscopic. They found that the length of the asterism on the Laue photograms of extended magnesium crystals decreased as the surface of the crystal was etched off successively. However, referring to the

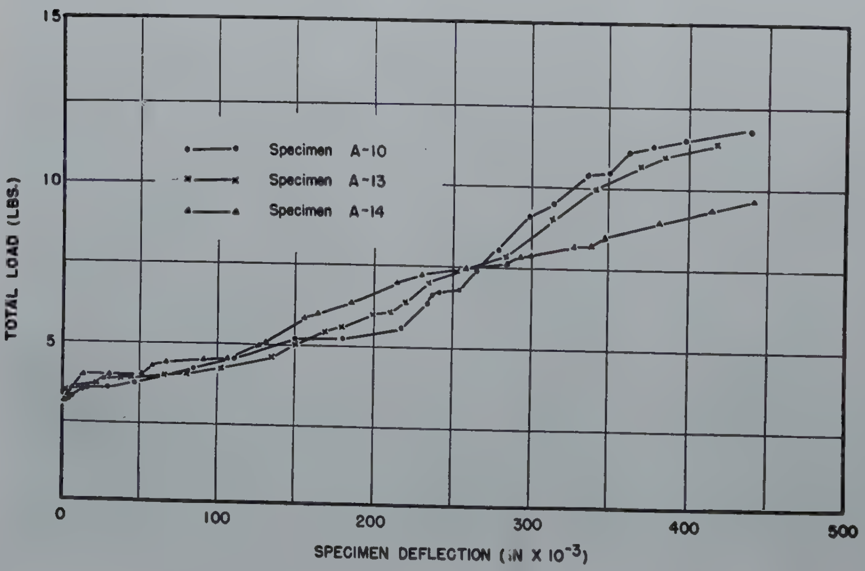

FIG 20—Load-deflection diagram of flat specimens A-10, A-13, and A-14.

mechanism of bending described in this paper, the phenomena of a decrease in the length of asterism as the outer layers of the crystal are removed by etching would be adequately explained, since the bending in the material between slip markings approaches a maximum at the outermost layer of the specimen and a greater distortion in Laue spots on X ray photograms would be expected there.

Flow Characteristics in Bending

Two different types of flow were observed on the tension and compression sides of the bent specimens. It appeared that the crystal acted as if it were divided into two parts separated by the neutral plane. The tension and compression sides experienced unusual types of axial loading where the flow of metal was restricted in a direction perpendicular to the neutral plane. There a stress-gradient existed such that the maximum stress occurred at the outermost layer of both the tension and compression sides and diminished gradually in the direction of the neutral plane. Thus the flow direction on the tension side was along the specimen axis whereas that on the compression side was in the direction roughly perpendicular to the top surface. It was found that the rectangular cross-section of all flat specimens became approximately trapezoidal during deformation, in good agreement with the characteristics of flow in a bent crystal as discussed above. The ideal flow characteristics in bending may be represented by the schematic diagram shown in Fig 23. The arrows illustrate the variation of strain introduced by the stress-gradient in a bent crystal. Sections of the undeformed crystal, shown by the dotted line, will gradually deform to those contours indicated by the solid lines during bending. Based upon this picture, the asterism on Laue photograms of a bent crystal may be interpreted as on overall bending of crystallites resulting from the process of fragmentation. Since the flow in bending is restricted in certain directions, the crystallites could not follow the type of rotation found in uniaxial loading. Instead of the usual type of rotation about an axis lying in the slip plane normal to the slip direction, the different shapes of Laue spots seem to indicate that the crystallites were bent about an axis in the slip plane and perpendicular to the direction of flow.

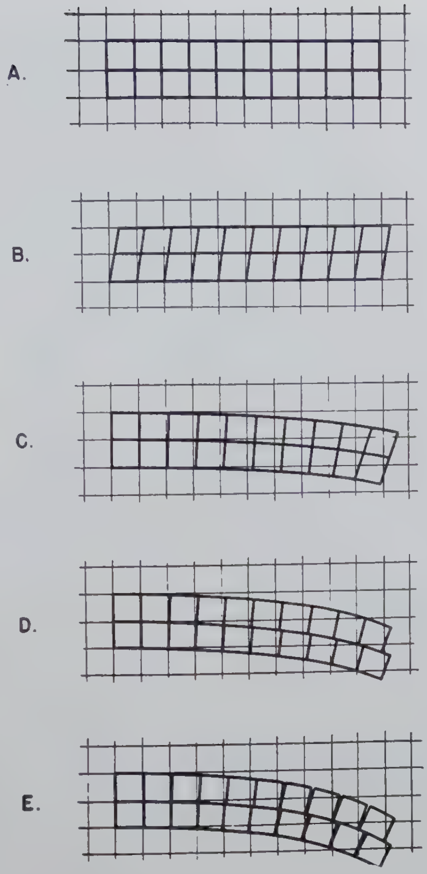

FIG 22—Schematic diagrams of slip mechanism.
(A) Undeformed, (B) Pure shear, (C) Elastic bending, (D) Bending and plastic shear and (E) Bending and fragmentation.

Summary

1. When an aluminum crystal is subjected to a bending stress, the major operative slip system is the same as for uniaxial loading. That is to say, the slip occurs on the octahedral plane which has the maximum resolved shear stress given by the equation $S_s = S_n \cos\lambda \sin\chi$, where S_n is the normal stress calculated by the simple beam formula.

2. The change of orientation on the tension and compression sides of a crystal during bending resembles closely that of two separate crystals deforming under tension and compression loading respectively. In general they appear to follow the Taylor and Elam rotation, that is, the stress axis rotates toward a [110] slip direction on the tension side and toward (111), the pole of active slip plane, on the compression side. However, a certain amount of deviation was observed. This may be due to the complication introduced by the restriction of flow during bending and consequently requiring the early operation of a secondary slip system.

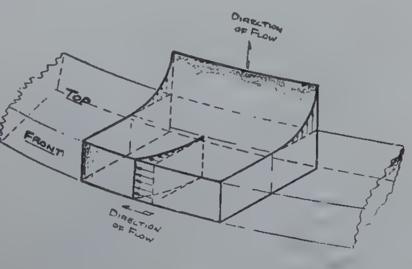

FIG 23—Schematic diagram of characteristics of flow in bending.

3. The anomalous surface markings on the electrolytically polished specimens may be attributed to the strain-markings or cracks on the anodic coating of the surface layer. It was found that these markings were analogous to the cracks produced on a deformed specimen treated with Stresscoat. The absence of these markings on mechanically polished and etched specimens further substantiated this interpretation.

4. "Cross-slip" or the step-like appearance of slip lines was observed on specimen surfaces intersected by the slip direction. However, no definite cross-slip plane could be identified. This may be due to the complicated stress distribution in the bending where these steps might be too small to permit the resolution of a particular plane.

5. The phenomena of slip over local regions of the specimen was noticeable in all the bending specimens. The growth of slip markings appears to undergo a process such that the slip markings occur initially at a higher stress region and move toward a lower stressed matrix, gradually losing both their intensity and width as the stress diminishes. The macroscopic bending of glide lamellae was also found.

6. From the study of the flow characteristics and the Laue spots on the X ray photograms of various bent specimens, it was found that the cause of subdividing of spots may be regarded as a result of crystallite fragmentation. The fragmentation appeared to take place by rotating the crystallites in the glide lamellae about an axis normal to the slip plane in addition to the usual type of bending about an axis lying in the slip plane perpendicular to the direction of slip. Following the rotation of crystallites, the elongation or asterism of Laue spots may be rationalized as an overall bending taking place about an axis in the slip plane and normal to the direction of flow.

Acknowledgments

The authors wish to thank Professor C. H. Mathewson for his interest and advice concerning this work, and to acknowledge the assistance of members of Hammond Metallurgical Laboratory, Yale University, and the Research Department of Chase Brass and Copper Co. The M-B Manufacturing Co., New Haven, Conn., kindly supplied the Stresscoat equipment.

References

1. H. Mark, M. Polanyi, and E. Schmid: *Ztsch. Phys.* (1922) **12,** 58.
2. K. Yamaguchi: Sci. Papers IPCR (Tokyo) (1928) **8,** 289; (1929) **11,** 151, 223.
3. G. I. Taylor: *Proc.* Roy. Soc. (London) (1927) **A116,** 39.
4. W. G. Burgers and P. C. Louwerse: *Ztsch. Phys.* (1931) **67,** 605.
5. A. Komar and M. Machalov: *Phys. Z. Sowjetunion* (1936) **9,** 613.
6. R. Maddin, C. H. Mathewson, and W. R. Hibbard, Jr.: Paper submitted to AIME in March 1949.
7. R. W. Cahn: Discussion on paper by W. G. Burgers in 1947. Bristol Conference on Strength of Solids (1948) 136.
8. Y. Kidani and S. Tagino: Bull. IPCR (Tokyo) (1929) **8,** 118.
9. A. Kochendörfer: Plastishe Eigenschaften von Kristallen und Metallischen Werkstoffen. J. Springer (1941) 151.
10. S. Timoshenko: Strength of Materials. (1940) **1,** 88, Nostrand.
11. G. Found: Yale Dissertation (1944).
12. H. C. H. Carpenter and C. F. Elam: *Proc.* Roy. Soc. (London) (1921) **A100,** 329.
13. A. B. Greninger: *Trans.* AIME (1935) **117,** 61.
14. G. I. Taylor and C. F. Elam: *Proc.* Roy. Soc. (London) (1925) **A108,** 28.
15. G. I. Taylor and W. S. Farren: *Proc.* Roy. Soc. (London) (1926) **A111,** 529.
16. W. R. Hibbard, Jr.: *Trans.* AIME (1948) **175,** 66. *Met. Tech.* Sept. 1947, TP 2244.
17. J. A. Collins and C. H. Mathewson: *Trans.* AIME (1940) **137,** 150.
18. R. D. Heidenreich and W. Shockley: *Jnl. Appl. Phys.* (1947) **18,** 1029.
19. R. Maddin, C. H. Mathewson and W. R. Hibbard, Jr.: *Trans.* AIME (1948) **175,** 86. *Met. Tech.* Feb. 1948, TP 2331.
20. M. C. Crussard: *Rev. Met.* (1944) **41,** 111,133; (1945) **42,** 286, 321.
21. E. N. daC. Andrade: Discussion of "Deviations of Real Crystals from the Ideal Lattice Structure." Int. Conf. on Phys. II (1934) 173.
22. E. N. daC. Andrade and L. C. Tsien: *Proc.* Roy. Soc. (London) (1937) **A163,** 1.
23. C. H. Mathewson: *Trans.* ASM (1944) **32,** 28.
24. W. G. Burgers and F. J. Lebbink: *Rec. Trav. Chim. Pays. Bas.* (1945) **64,** 321.
25. K. Yamaguchi and S. Tagino: Sci. Pap. IPCR (Tokyo) (1929) **9,** 277.

High Temperature Scaling of Cobalt*

CHARLEY R. JOHNS† and WILLIAM MARSH BALDWIN, JR.,‡ Junior Member AIME

Introduction

Cobalt is reported[1,2] to scale in accordance with the Pilling and Bedworth[3] parabolic law:

$$w^2 = Kt \quad [1]$$

where w = weight increase per unit surface area
K = constant
t = time

The reported values of the parabolic oxidation constant, K, in the temperature range 600 to 1100°C follow an Arrhenius type of equation as inspection of Fig 1 shows. According to Valensi's theory[5] on the scaling of metals where multiple-layered scales (for example, MeX, MeX_2, and others) are possible, this fact could be construed as indicating that a single oxide only is formed on cobalt in this temperature range. Since the single straight line extends above 920°C where only CoO is stable in air (see Fig 2) it might be inferred that this is the only oxide formed on scaling.

Arkharov and Voroshilova[10] have studied the scales formed when cobalt is heated in air in the temperature range 385 to 800°C and report that CoO is indeed found in the scale but that Co_3O_4 is also found as an overlay and in increasing amounts in the lower temperature ranges. No quantitative data regarding the relative proportions of the two oxides were reported. Again in the light of Valensi's theory this would indicate that the straight line in Fig 1 would be expected to undergo an inflection at some point in the temperature range 385 to 800°C.

Chauvenet[2] has studied the oxidation rates of CoO to Co_3O_4 and has found this reaction to proceed parabolically with time but reports parabolic scaling rates which are considerably (about ten times) larger than the scaling rates of cobalt metal itself.

This is difficult to explain in terms of Valensi's theory although a full discussion of the possible discrepancy cannot be made in view of the lack of sufficient data.

These points made an investigation of the scaling behavior of cobalt in air an attractive study.

Discussion of Results

Relatively large (approximately 95 sq cm of surface area) samples of 0.020 in. thick electrolytic cobalt strip,* sanded with 2/0 paper, were heated in air in a cyclone type furnace. The samples were weighed before and after the scaling treatment. The weight increases so observed obeyed the Pilling and Bedworth parabolic law at all temperatures studied. The parabolic scaling constants when plotted on a logarithmic scale as a function of absolute temperature are reproduced

---

These authors also state that a thin exterior veneer of Co_2O. may have formed also but was too thin to identify with X rays. In view of the instability of Co_2O_3 in air above 400°C (see Fig 2) this is unlikely.

Technical Note No. 24 E. Manuscript received June 21, 1949.

* Abstracted from a thesis submitted by C. R. Johns to the Department of Metallurgical Engineering, Case Institute of Technology, in partial fulfillment of the degree of Master of Science in Physical Metallurgy.

† Production Metallurgist, Thompson Products, Inc.

‡ Research Professor, Case Institute of Technology.

[1] References are at the end of the note.

* Supplied through the kindness of Dr. O. C. Ralston, Acting Chief of the Bureau of Mines, Metallurgical Div., Washington, D. C. A qualitative spectographic analysis showed only traces of nickel, copper, cadmium, iron, magnesium, chromium and manganese.

in Fig 1. Here it may be seen that in the higher temperature ranges the present data coincide quite well with the previously reported data. There is, however, a definite inflection in the data at around 625°C, the data for the temperature range below this point showing a slope that is roughly ½ that of the straight line drawn through the data above this point. This inflection would be expected on the basis of the reasoning presented above. If the straight line in the lower temperature range is due to the exclusive formation of Co_3O_4, the oxidation rate of CoO to Co_3O_4 in this temperature range should follow a straight line parallel to the lower branch of the cobalt curve and lying at a value ¼ that of the aforementioned lower branch. This is, of course, at complete variance with the experimental results of Chauvenet on the oxidation of CoO and illustrates in quantitative terms how her data cannot be reconciled with the requirements of Valensi's theory. In an attempt to resolve this discrepancy, samples of cobalt were oxidized to CoO at temperatures above which none of the other oxides is stable thermodynamically (around 920°C) and then subsequently oxidized in the temperature range in which Co_3O_4 was stable. These results are entered in Fig 1. In the present case the data parallel those of Chauvenet's (and incidentally, the scaling data for straight cobalt in the temperature range above 625°C) but do not behave in accordance with Valensi's theory. It must be admitted that the present data are of the proper order of magnitude to fit Valensi's requirements, and it may be that experimental errors prevent the data from exactly duplicating the values required by his theory, but for the present we must regard the case of the scaling of cobalt in air as being still unsettled.

An internal check on the data and on Valensi's theory could have been obtained if the proportions of CoO and Co_3O_4 in the scale could have been determined quantitatively in the temperature ranges between 500 and 800°C, but the absolute thickness of the scales formed in this temperature range are extremely small compared with other metals in which such quantitative determinations have been made (for instance, copper,[5] iron[11],) indicating the necessity of developing special techniques for such determinations.

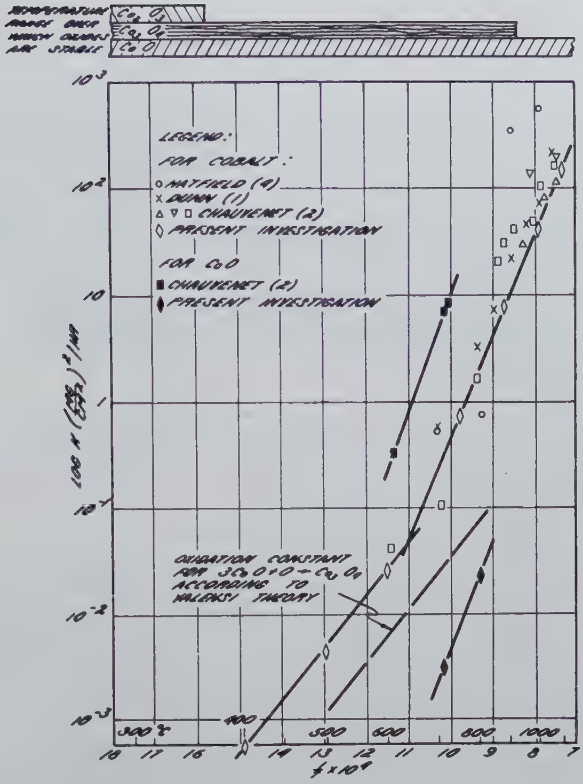

FIG 1—Relationship between the parabolic scaling constant for cobalt and CoO and temperature.

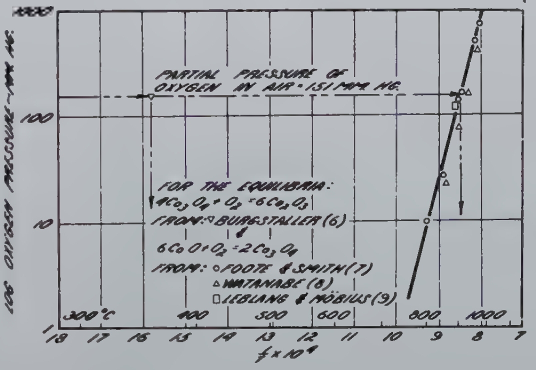

FIG 2—Dissociation pressures of various cobalt oxides as a function of reciprocal absolute temperature.

References

1. J. S. Dunn quoted by J. S. Dunn and F. J. Wilkins in "Review of Oxidation and Scaling of Heated Metals." H. M. Stationery Office (London) (1935) Sect. 4, "The Oxidation of Non-Ferrous Metals," p. 67–80.
2. G. Chauvenet: Doctor's Thesis, Univ. of Caen (1942) Order No. 34.
3. N. P. Pilling and R. E. Bedworth: The Oxidation of Metals at High Temperatures. *Jnl.* Inst. Metals (1923) **29,** 529–582.
4. W. H. Hatfield: Heat Resisting Steels. *Jnl.* Iron and Steel Inst. (1927) **115,** p. 483–508.
5. G. Valensi: Theoretical and Experimental Investigations about Conjugated Formation of Several Layers in Dry Corrosion. Pittsburgh International Conf. on Surface Reactions. Corrosion Publ. Co., Pittsburgh, Pa. (1948) p. 156–164.
6. S. Burgstaller: Untersuchungen über die Beständigkeit der Kobaltoxyde im Intervalle von Co_2O_3 bis CoO. *Abh. Deut. Nat. Schaft. Med. Ver. Böhmen "Lotos"* in Prag. (1912) **3,** 83–143.
7. H. W. Foote and E. K. Smith: On the Dissociation Pressures of Certain Oxides of Copper, Cobalt, Nickel and Antimony. *Jnl.* Amer. Chem. Soc. (1908) **30,** 1344–1350.
8. M. Watanabe: On the Equilibrium in the Reduction of Cobaltous Oxide by Carbon Monoxide. Sci. Rep., Tohoku Imp. Univ. (1933) **22,** 892–901.
9. M. LeBlanc and E. Mobius: Undersuchungen uber Kobaltoxyde und deren Systeme mit Sauerstoff. *Ztsch. Phys. Chem.* (1929) **A-142,** 151–176.
10. V. I. Arkharov and Z. A. Voroshilova: X-Ray Investigation on the High Temperature Oxidation of Cobalt. *Zhur. Techn. Fiziki* (1936) **6,** No. 5, 781–782.
11. A. O. Tesche: *Trans.* ASM (1950) (in print).

Stages in the Deformation of Monel Metal as Shown by Polarized Light

D. H. WOODARD,* Associate Member AIME

Introduction

One of the principal uses of polarized light in metallurgy is to show the granular structure of metals by contrasting reflections. This use is confined largely to anisotropic metals, such as beryllium, tin, magnesium, and the like.[1] Recently, Hone and Pearson[2] have extended the use of polarized light to include the isotropic metal aluminum. This was made possible by the formation of an anodic film that was optically anisotropic and that had a fixed and reproducible structural relationship to the grains in the substrata. With their method, it was possible to indicate localized textures in annealed aluminum sheet. In the course of an investigation of plastic deformation at the National Bureau of Standards, it was found that the isotropic single phase alloy Monel could be made optically anisotropic by treatment with the usual Monel contrast etchant. Experiments soon showed that differences in orientation could be detected easily.

Previous investigations involving the use of polarized light have been restricted to annealed metals. In this paper it will be shown that inhomogeneous plastic deformation which results in lattice bending and development of deformation bands experienced by individual grains in polycrystalline Monel, is revealed in the microstructure. This interpretation of the microstructure was confirmed by a study of slip lines formed after prior plastic strain.

Materials and Procedure

The material used was Monel, the chemical composition of which was C—0.17 pct, Mn—1.28 pct, Fe—1.61 pct, S—0.009 pct, Si—0.17 pct, Cu—30.70 pct, Ni—66.04 pct. The material was divided into 2 lots which were treated as follows: Lot A was heated at 1700°F for 3 hr to produce a fully annealed, coarse grained structure. Lot B was heated at 1400°F for 1 hr to produce a close approximation of a fully annealed structure without appreciable increase in the grain size of the original material. After each of these heat treatments the material was cooled in air.

Samples for metallographic examination were cut from tensile and compression test specimens and were prepared by grinding on lead-tin laps, followed by electrolytic polishing.† Etching and the development of ridges were avoided by keeping the voltage above 3.8 and by preventing contamination of the polishing solution with water.

Monel, when polished and treated with most etchants, is optically isotropic. However, when given a light etch for about 4 sec with the Monel contrast solution‡ the surface of the metal becomes optically active. The microstructure when observed under crossed nicols* appears different from that viewed by ordinary light. This is shown by a comparison of micrographs made of the same area of a plastically deformed specimen using polarized light (Fig 1*a*) and white light (Fig 1*b*).

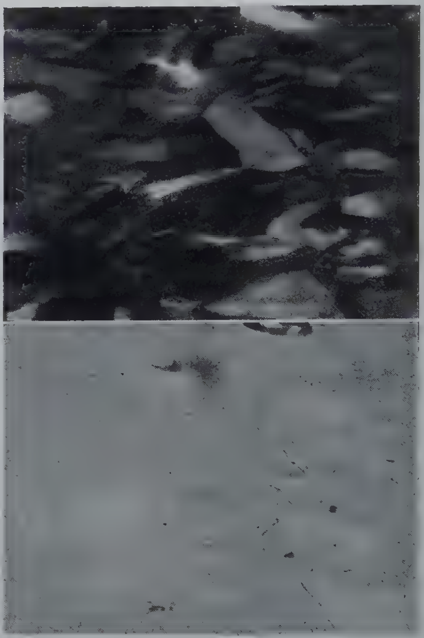

FIG 1—Appearance of the same area of plastically deformed Monel metal B under (*a*) (*above*) **polarized light and** (*b*) (*below*) **ordinary light.**

× 750. Reduced one half in reproduction.

If Monel, which has been lightly treated with the contrast etchant, is slightly deformed by compression, rectangular figures are apparent over the specimen. However, within too short a period to be photographed, these rectangles become circular, probably because of surface tension effects within the etched film. The two observations,

Cleveland Meeting, October 1949.
TP 2696 E. Discussion of this paper (2 copies) may be sent to *Transactions* AIME before December 1, 1949. Discussion is tentatively scheduled for publication in May 1950.
Manuscript received May 2, 1949; revision received July 11, 1949.

---

* General Physical Scientist, National Bureau of Standards.

[1] References are at the end of the paper.

† The electrolyte was a solution of nitric acid—1 part, methyl alcohol—2 parts.

‡ The etchant used consisted of chromic acid—3 g, nitric acid (conc.)—10 cc, ammonium chloride—5 g, water—90 cc.

* The expression "crossed nicols" employed in this paper conforms to the usages of optical crystallography. It does not mean that *Nicol prisms* are employed but merely that polarizing elements in the incident and reflected beams are crossed with respect to each other. The less explicit term "polarized light" is used in places where no ambiguity would result.

the rectangular figures becoming circular and the failure of the unetched surfaces to reflect polarized light, suggest that the Monel contrast etchant forms a film which is anisotropic.

Unless otherwise specified, all micrographs were made on a Bausch and Lomb Metallographic Research Microscope, equipped with a Foster vertical illuminator prism[3] which acts also as polarizer and analyzer fixed in the crossed position. Measurements of the intensity of the reflected resolved polarized light were made at the bellows eyepiece with a specially constructed photometer, which consisted essentially of a photo-multiplier tube, RCA-931, a bank of dry cells arranged to have 90 volts across each dynode, and a microammeter. As the current coming from this photo-multiplier is proportional to the intensity of the incident light, all light intensity values are expressed in microamperes.

Differences in Orientation Shown by Polarized Light

ANNEALED MONEL

It has been shown by many investigators that the orientation of fully annealed single phase alloys is uniform from point to point in individual grains and that the orientation varies from grain to grain in a more or less random manner. For fully annealed Monel, the intensity of the reflected polarized light is uniform over the entire area of each individual grain as illustrated by the micrographs of Fig 2. It should be noted, however, that in the case of Monel, the annealing must be complete and grain growth started before uniform reflection, that is, uniform orientation over individual grains, is obtained

The micrographs in Fig 2 show that each grain undergoes a half cycle of intensity from maximum to minimum for a 45° rotation of the plane of polarization, although the angle for maximum reflection varies from one grain to the next. It was noted that the difference in intensity between the maximum and the minimum of the reflected light may vary from one grain to another. It is, therefore, possible for two grains to be at different stages in their 90° cycle and yet reflect light with the same intensity. While the same intensity for different grains may mean different orientations, it is obvious that for any fixed direction of the planes of polarization, a difference in intensity must mean a difference in orientation. It is on this basis that polarized light is used in this study of plastic deformation.

INDIVIDUAL GRAINS IN PLASTICALLY DEFORMED MONEL

Fig 3 shows the microstructure of Monel after extensions of 2, 14, 30, and 38 pct, when deformed at a rate of 2½ pct every 5 min. These micrographs, like others photographed under crossed nicols, are referred to as intensity patterns because the areas of extinction can be changed to areas of brightness or vice versa, although the outlines in the pattern remain the same. Obviously, plastic deformation has caused nonuniform reflections from individual grains. If differences in intensity denote differences in orientation, then it follows that plastic deformation has caused inhomogeneous distortions in the lattice structure. This is in agreement with results obtained by Barrett and Levenson[4] who showed, by means of X rays and etch pits, that plastic deformation caused areas of nonuniform orientation over the individual grains. After a study of the intensity patterns shown in Fig 3 and other similar patterns, it was possible to classify the nonuniformities of reflection into four types shown by grains *A*, *B*, *C*, and *D*. These will be discussed under *Results*.

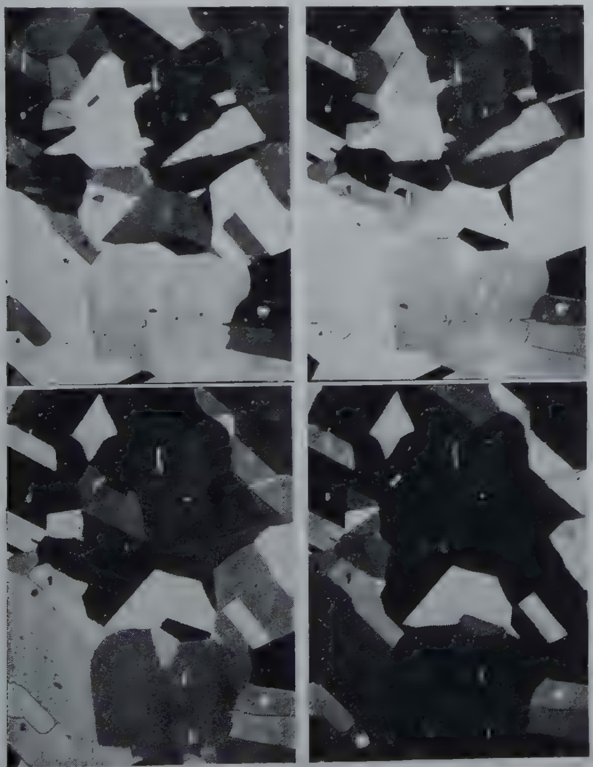

FIG 2—Variations in intensity patterns after successive rotations with respect to the plane of polarization, as indicated, of a specimen of annealed Monel metal A.
× 250. Reduced one half in reproduction.

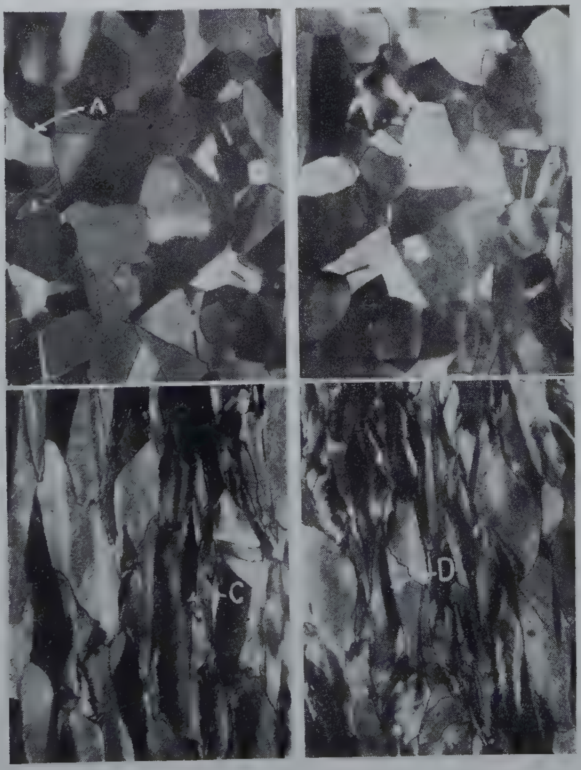

FIG 3—Variations in intensity patterns within individual grains in Monel metal B after plastic deformation in tension as indicated.
The axis of tension is in the vertical direction for all specimens.
× 750. Reduced one half in reproduction

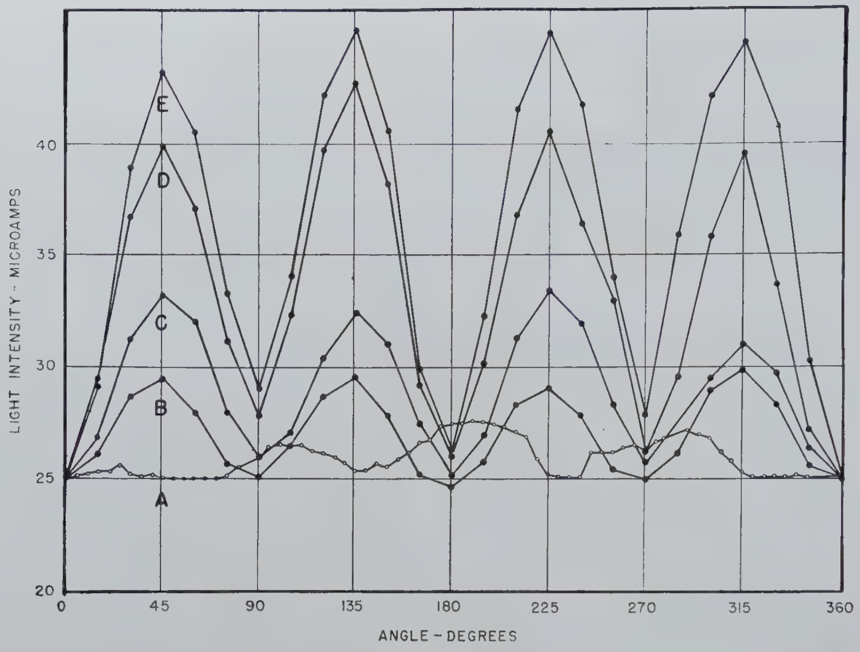

FIG 4—Effect of plastic deformation and angular rotation of crossed nicols on the overall intensity of light reflected from Monel metal B.

Curves A, B, C, D, and E represent specimens extended 0, 14, 33, and 38 pct respectively.

CORRELATION OF INTEGRATED INTENSITIES WITH DEGREE OF DEFORMATION

It was observed, in examining plastically deformed specimens, that the overall intensity of the reflected polarized light with crossed nicols changed as the plane of polarization or the specimen was rotated. These changes were measured by the photometer at regular angular intervals and the results are shown in Fig 4. The data for curve *A*, obtained from a transverse section of a fully annealed specimen, represents a condition of random or nearly random orientation. It is evident that plastic deformation results in the formation of four peaks in each curve and that increasing plastic deformation, from 0 to 38 pct, causes the amplitude to increase.

Since any orientation of an individual grain goes through four intensity cycles, it is apparent that the integrated intensity of many grains will show four peaks as more and more grains approach a common alignment. Any such directional deviation from the original state must be considered as a development of preferred orientation. X ray studies have shown that a progressive increase in preferred orientation results when polycrystalline metals are deformed plastically in tension. There is apparently a relationship between the degree of preferred orientation and the variation in integrated intensity, where preferred orientation appears under crossed nicols before its development can be detected by X rays.

In this connection, it is interesting to note that Mebs and McAdam[5] have interpreted variations of Poisson's ratio as showing the anisotropy of this same heat of Monel after 4 pct reduction of area. Hill[6] has shown that the development of preferred orientation accompanies anisotropy.

If plastic deformation, accompanied by a bending of the lattice, occurred in such a manner as to permit extension in the direction of flow, a plane cutting the specimen in this direction should show more areas of certain specific planes than would be observed in the case of a purely random orientation. The development of the peaks of Fig 5 is attributed to such a phenomenon. At present, there is very little information available on the intensity of the reflection from specific planes or on the number or orientations of the planes which combine to show this preferred orientation.

EVIDENCE OF BENT LATTICE STRUCTURE

Thin straight parallel lines usually seen on polished and etched surfaces of annealed metals after slight compression are considered to be traces of crystallographic planes, that is, the intersection of these planes with the surface of the metal. Sometimes however, these lines are curved and the question has been raised as to whether a set of such curved lines represents traces of a set of crystallographic planes which are bent, or the traces of several sets of parallel crystallographic planes which remain straight but which combine to give the effect of curved lines. The ability of polarized light to show changes in orientation along the length of a line furnishes an answer to this question and thereby yields information as to a mode of deformation.

Deformed Monel specimens were sectioned, polished, etched, and then deformed further to form traces, some of which are curved. It can be readily seen in Fig 5*a* and *d* that the slip lines bend as they go from one orientation to the other as evidenced by changes in the intensity pattern. The bends are not abrupt, as is the case at the grain boundaries, but have measurable radii of curvatures. In such cases, the intensity patterns show a gradual change in orientation which indicates a gradual change in position of the crystallographic axes. This bending of the slip lines, therefore, is interpreted as being due to a bending of the crystallographic planes of which these lines are traces. In a metal, such as Monel, which has a face-centered cubic structure, these slip lines are assumed to be traces of octahedral planes. There are four sets of these planes, each set inclined to each of the other sets at an angle of 70°.

Fig 5*b*, *c* and *d* show the microstructure of two specimens that had less prior strain than did the specimen whose microstructure is shown in Fig 5*a*. In Fig 5*b*, there are two sets of traces in the central grain, one set about horizontal, the other inclined about 30° to it. As the orientation changes, there is no change in direction of the horizontal set, but there is a change in the ends of the traces of the other set. The case of having two sets of traces, one straight and the other bent while going through a region of changing orientation, can be explained as follows: During the process of plastic deformation the lattice may be bent around an axis parallel to the surface in such a manner that the metal surface cuts off a longitudinal section of the cylinder. Then an octahedral plane at right angles to the axis of bending would intersect the surface of the metal in a straight line regardless of the amount of lattice bending. If the octahedral plane is at any other angle, the intersection of that plane with the specimen surface should show a change of direction with a change of orientation. The further the octahedral plane inclines toward the axis of bending, the greater is the curvature of the slip line with change in orientation. This is shown in the main grain of Fig 5*c*, where the traces go through the main grain with practically no change in direction with change in orientation. However, when they go through the twin, where an octahedral plane is inclined at the twin angle, the straight lines become curved with changes in orientation. This is clearly seen in Fig 5*d* which is an enlargement of the twinned region.

From a study of many orientation patterns, and the slip lines formed on the surface by further plastic deformation, it appears that initial bending occurs around axes nearly perpendicular to the octahedral planes and that the slip lines run approximately perpendicular to these axes of bending. The similarity of the microstructures of Fig 3 (deformed before polishing) and of Fig 5 (deformed both before and after polishing) indicates that the curvature of the traces and the accompanying changes in intensity were not due to a rumpling of the surface.

It was found that the number of slip lines formed on a specimen initially annealed, polished, and etched increased and their spacing became more irregular as the amount of plastic deformation increased. As can be seen in Fig 5*a* and *b*, the intensity pattern of the individual grains indicates that the strain was inhomogeneous and this resulted in the irregular spacing of the slip lines. A series of annealed specimens, compressed 4, 14, 32, and 36 pct before being sectioned and polished, were etched and then given 2 pct further compression. Examination showed that the 32 pct and 36 pct specimens had fewer slip lines present than the 4 pct and 14 pct. This showed that it is more difficult to develop slip lines on specimens that had a large amount of prior compression than on those that had a lesser amount. However, the greater the deformation before sectioning, polishing, etching, and deforming further, the deeper, wider, and more irregular become the slip lines.

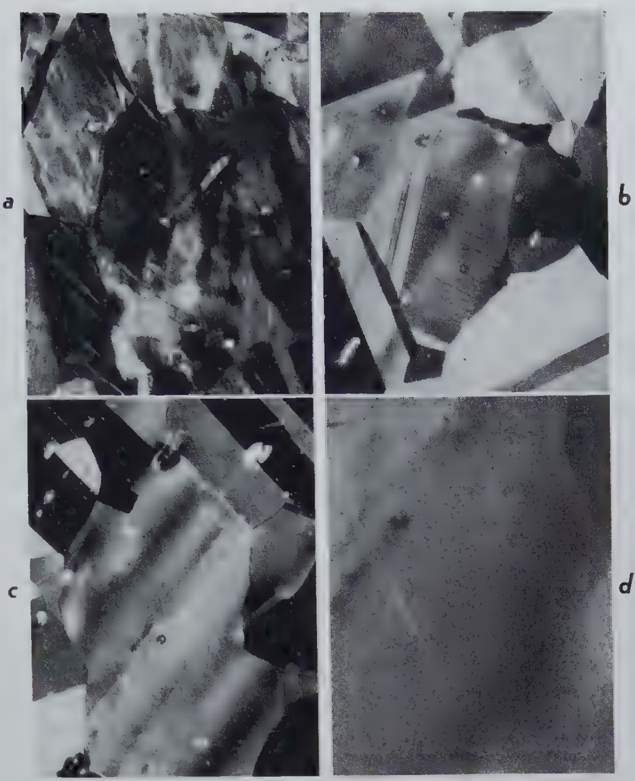

FIG 5—Effect of prior plastic deformation on the development of slip lines in Monel metal A.

(*a*) compressed 28 pct, (*b*), (*c*), and (*d*) compressed 2 pct. (*a*), (*b*), and (*c*) × 250. (*d*) × 750. Reduced one half in reproduction.

Discussion of Results

TYPES OF LATTICE BENDING

The concept of deformation by lattice bending has been presented by many investigators. Polanyi[7] related the elongation of Laue spots from zinc crystals with bending of the slip plane (*Biegegleitung*). Sun and Chu[8] interpreted Laue photographs of rock-salt crystals as showing that the first deformation occurs by a simple bending of the lattice around a fixed axis; as the crystal deforms further, bending begins around one or more new axes. Single crystals of cadmium, when oriented so that the glide plane is nearly parallel to the axis of compression, deform by a mechanism which Orowan[9] terms "kinking." Hess and Barrett[10] have shown that the kink bands described by Orowan are a special form of deformation bands and result from a bending of the lattice.

When the intensity patterns of Fig 4 are interpreted in terms of lattice bending, four types of deformation can be seen:

1. Broad diffuse bands of brightness and extinction, as typified by grain A: These represent lattice bending around an axis which is nearly parallel to the surface. These appear on specimens that have been sectioned longitudinally after slight plastic deformation.
2. Areas of brightness surrounded by areas of extinction, as typified by grain B: These are typical of a dome type of lattice bending wherein the crystallographic planes have been bent so that they are no longer flat planes, but are wrinkled into the shape of a dome.
3. Bands of brightness and extinction with the bands ending in areas of extinction and brightness respectively, as shown in grain C: Here the change in orientation at the end of the band shows that the deformation is of the twisted or screw type.
4. Bands of brightness or extinction sharply outlined in more or less irregular shapes and mainly extending in the direction of flow as shown by grain D: Bands of this type represent fully formed deformation bends and usually appear after severe necking of the specimen.

Examination of many intensity patterns shows that initial plastic deformation occurs through the bending of the lattice around a single axis and that, as the amount of deformation increases, lattice bending takes place around several axes.

From the extreme irregularity of the intensity patterns, it is evident that directions of flow can vary within small areas and that the deformation is by no means uniform or regular as would be the case for twinning.

DEVELOPMENT OF DEFORMATION BANDS

In the early stages of plastic deformation, the changes in orientation are gradual, as seen in Fig 3*a* and *b*. As deformation increases, the changes in orientation become gradually sharper and more distinct in more or less irregular areas. After severe plastic deformation, these areas of changed orientation become elongated and sharply outlined. They are clearly seen in Fig 3*d* and 6*a* and *b*. As their development is a gradual process, it is quite evident that

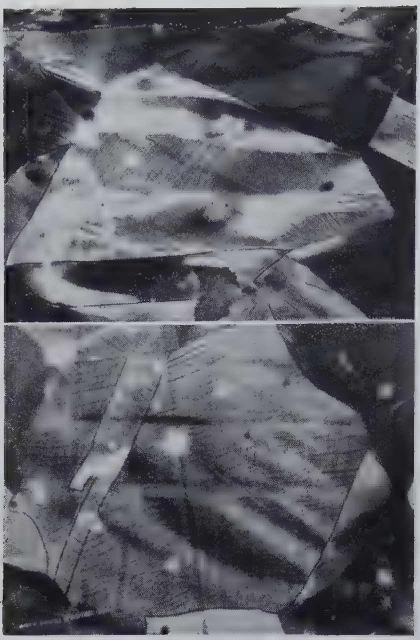

FIG 6—Inhomogeneous deformation within individual grains in severely deformed specimens of Monel metal A.

After prior compression of 36 pct for 6(*a*), 28 pct for 6(*b*), (*a*) (*above*) × 500, (*b*) (*below*) × 250. Reduced one half in reproduction.

these areas are deformation bands and not deformation twins.

As these deformation bands are formed, the area bounding them becomes thinner and more distinct until, with severe plastic deformation, they become grain boundaries. Frequently, a well-defined grain boundary was seen to end in a deformation band boundary which became gradually wide and diffuse. Such a condition could exist if, due to inhomogeneous plastic flow, there is, as postulated by Mott,[11] a shearing action along the orientation boundary (band boundary). With severe distortion, and its accompanying shear along the newly formed orientation boundary, this orientation boundary becomes a grain boundary. Further deformation is then a unique and distinct process within each orientation. In this way, a grain can be fragmented into smaller grains by plastic deformation.

CONTINUANCE OF DEFORMATION BANDS ACROSS GRAIN BOUNDARIES

Boas and Hargreaves[12] concluded from hardness measurements that the distortion in a grain is confined largely to the areas adjacent to the grain boundaries and is transmitted to a neighboring grain along its boundaries. However, Hibbard,[13] by means of X ray determinations of orientation, showed that deformation was not restricted to any particular area of the grain. Examination of many intensity patterns, such as those in Fig 3, show that differences in orientation do not occur more frequently near the grain boundaries than in the center of the grain. While many areas were observed, similar to Fig 6*a*, in which deformation bands in one grain are adjacent to deformation bands in the next, the proportion of such areas is small. From a consideration of the intensity patterns, it is evident that the transmission of deformation across a grain boundary is dependent upon the relationship of the two adjacent orientations. The response of a grain to the deforming stress is affected not only by the orientation of the grain itself but by the restricting action of adjacent grains of different orientation.

EFFECT OF LATTICE BENDING ON THE MECHANISM OF PLASTIC DEFORMATION

If deformation of Monel is to occur through lattice bending, then the concept of deformation by slip must permit gradual changes in lattice orientation, such as are seen in Fig 3*a* and *b*, and must account for the relative proportions of deformation by lattice bending and by slip. It is quite evident that slip did not occur through the distortion of layered regions which would leave the rest of the lattice undisturbed.

It is evident that when the lattice is bent, the lattice constants on the concave side would differ from those on the convex side. In such a case, there are limitations as to the amount that the lattice can be bent elastically without deforming plastically. The plastic deformation, or atomic readjustment, could occur through the motion of dislocations, where the nonuniform stresses set up by the bending of the lattice serve as the trigger mechanism to start the dislocations into motion. It is hoped that more quantitative information will be obtained from a program now underway which will coordinate the results obtained from polarized light with those obtained from other methods.

The current widespread interest in orientation changes during plastic deformation and the inability of other methods to present these changes visually has resulted in the publication of this paper at this time.

Summary

The microstructure of Monel can be revealed, when viewed under crossed nicols, as an intensity contrast pattern when a polished specimen has been etched with the ordinary contrast etching reagent. Differences in the intensity of the reflections were interpreted as differences in crystalline orientation. On the basis of this hypothesis, variations in crystalline orientation were shown to be present in individual grains in plastically deformed specimens. A study of these variations led to the conclusion that the individual grains were deformed in an extremely irregular flow pattern, some of the irregularity resulting from the restrictive action of neighboring grains.

A study of the microstructure of specimens that had been deformed plastically, sectioned, polished, etched, and then deformed further indicated that curved slip lines are the traces of crystallographic planes which had become bent as a result of the prior plastic deformation. Changes in lattice orientation are attributed to a bending of the lattice and are shown to become sharper and more distinct as the amount of plastic deformation is increased. These changes lead to the formation of deformation bands and to fragmentation of the grains.

It was shown that the integrated intensities of reflections from many grains varied as the specimen was rotated with respect to the plane of polarization of the incident light. The integrated intensity increased with an increase in the degree of deformation, thereby indicating that polarized light can be used to detect preferred orientation.

References

1. R. W. Drayton: *Trans.* AIME (1935) **117,** 119.
2. A. Hone and E. C. Pearson: *Metal Progress* (1948) **53,** 363.
3. L. V. Foster: *Jnl.* Opt. Soc. Am. (1938) **28,** 124.
4. C. S. Barrett and L. H. Levenson: *Trans.* AIME (1940) **137,** 112.
5. R. W. Mebs and D. J. McAdam, Jr.: Nat'l. Adv. Comm. for Aeronautics Tech. Note No. 1100.
6. R. Hill: *Proc.* Roy. Soc. (London) (1948) **A-193,** 281.
7. M. Polanyi: *F. Krist* (1925) **61,** 49.
8. Te-Yen Sun and Sheng-Lin Chu: *Acta Cryst.,* 135 (July 1948).
9. E. Orowan: *Nature* (1942) **149,** 643.
10. J. B. Hess and C. S. Barrett: Eleventh Quarterly Report, The Inst. for the Study of Metals, 70.
11. N. F. Mott: *Proc.* Phys. Soc., 391 (April 1, 1948).
12. W. Boas and M. E. Hargreaves: *Proc.* Roy. Soc. (London) (1948) **A-193,** 89.
13. W. R. Hibbard: *Trans.* AIME (1949) **180.** *Metals Tech.* Sept. 1948. TP 2469.

Influence of Temperature on the Stress-strain-energy Relationship for Copper and Nickel-copper Alloy

D. J. McADAM, JR.,* Member AIME

Introduction

In a series of papers the author and associates have discussed the influence of temperature on the tensile properties of metals.[11–18] These papers present much information about the influence of temperature and the stress system on the conventional indices of mechanical properties, with special attention to the fracture stress. A recent study of the data, however, has revealed much additional information about the influence of temperature on the fundamental factors involved in the flow of metals. The present paper presents results of this study. Attention will be confined almost entirely to results derived from tension tests of unnotched cylindrical specimens at strain rates a little slower than those used in ordinary tension tests.

According to a concept first presented by Ludwik and elaborated in recent papers by others,[8,9,22,23] the mechanical state of a metal depends on the total plastic strain, but not on the temperature during straining, provided that the only structural changes are those essential to plastic deformation. In the summer of 1948, however, the author made the previously mentioned study of results of a general investigation by the author and associates and reached the conclusion that the mechanical state depends not only on the total strain, but also on the temperature during the straining. A number of diagrams were then prepared. These conclusions were presented without diagrams in a discussion last October of a paper by Dorn, Goldberg and Tietz.[2]

The metals used in the investigation on which this paper is based were Monel and oxygen-free copper. The Monel was supplied by the International Nickel Co. through the courtesy of Dr. W. A. Mudge. The copper was supplied by the Scomet Engineering Co. through the courtesy of Dr. Sidney Rolle. The data to be presented are based on results of tests at temperatures ranging between 165 and −188°C. Description of the apparatus and methods of test are given in previous papers.[10,11,12]

The present paper is the first part of the general discussion of the influence to temperature on the stress-strain-energy relationship for metals. The next paper will deal with metals that are subject to structural changes other than those induced solely by plastic deformation.

Influence of Temperature and Plastic Strain on the Flow Stress of Monel and Copper

For a study of the influence of temperature on the stress-strain relationship, flow-stress curves obtained with annealed metals at various temperatures will be compared with curves obtained with the same metals after cold drawing or cold rolling at room temperature. Diagrams thus obtained with Monel and copper are shown in Fig 1 to 8. Fig 1 to 7 show the variation of the flow stress with temperature and plastic strain; Fig 8 is a diagram of a different type, derived from Fig 4 to 7. In Fig 1 to 7 strain is expressed in terms of A_0/A, in which A_0 and A represent the initial and current areas of cross-section. Since values of A_0/A are represented on a logarithmic scale, abscissas are proportional to true strains; moreover, the true strains representing prior plastic deformation and those representing subsequent strain during a tension test are directly additive.

Fig 1 shows flow-stress curves obtained with annealed Monel. Five of the curves are based on results of tension tests. Between yield and the maximum load, the flow was under longitudinal tensile stress; between the maximum load and fracture, the local contraction induced transverse radial tensile stress. The portions of curves designated F, therefore, represent flow with increasing radial stress ratio, the ratio of the transverse stress S_3 to the longitudinal stress S_1. Curve F_0 is based on the ultimate stresses of specimens taken from bars that had been cold drawn various amounts.[17] Since the tensile stress at the maximum load is unidirectional, curve F_0 represents the course that a flow-stress curve would take if the stress during an entire tension test could be kept unidirectional.

The flow-stress curve F obtained at room temperature (Fig 1) has been established accurately by numerous measurements of the diameter of the specimen during the extension from yield to fracture.[17] At the time of the experiments, however, no apparatus was available for measuring the diameter during tension tests at low temperatures. Nevertheless, curves have been established to represent with sufficient accuracy the flow at low temperatures. Each flow-stress curve must be tangent to a curve U, which starts at a point representing the ultimate stress of annealed metal. Since the ultimate stress is based on the area of

Cleveland Meeting, October 1949.
TP 2703 E. Discussion of this paper (2 copies) may be sent to *Transactions* AIME before December 1, 1949. Discussion is tentatively scheduled for publication in May 1950.
Manuscript received May 2, 1949.

---

* Chairman of Sect., Nat'l. Bur. of Standards.

[11] References are at the end of the paper.

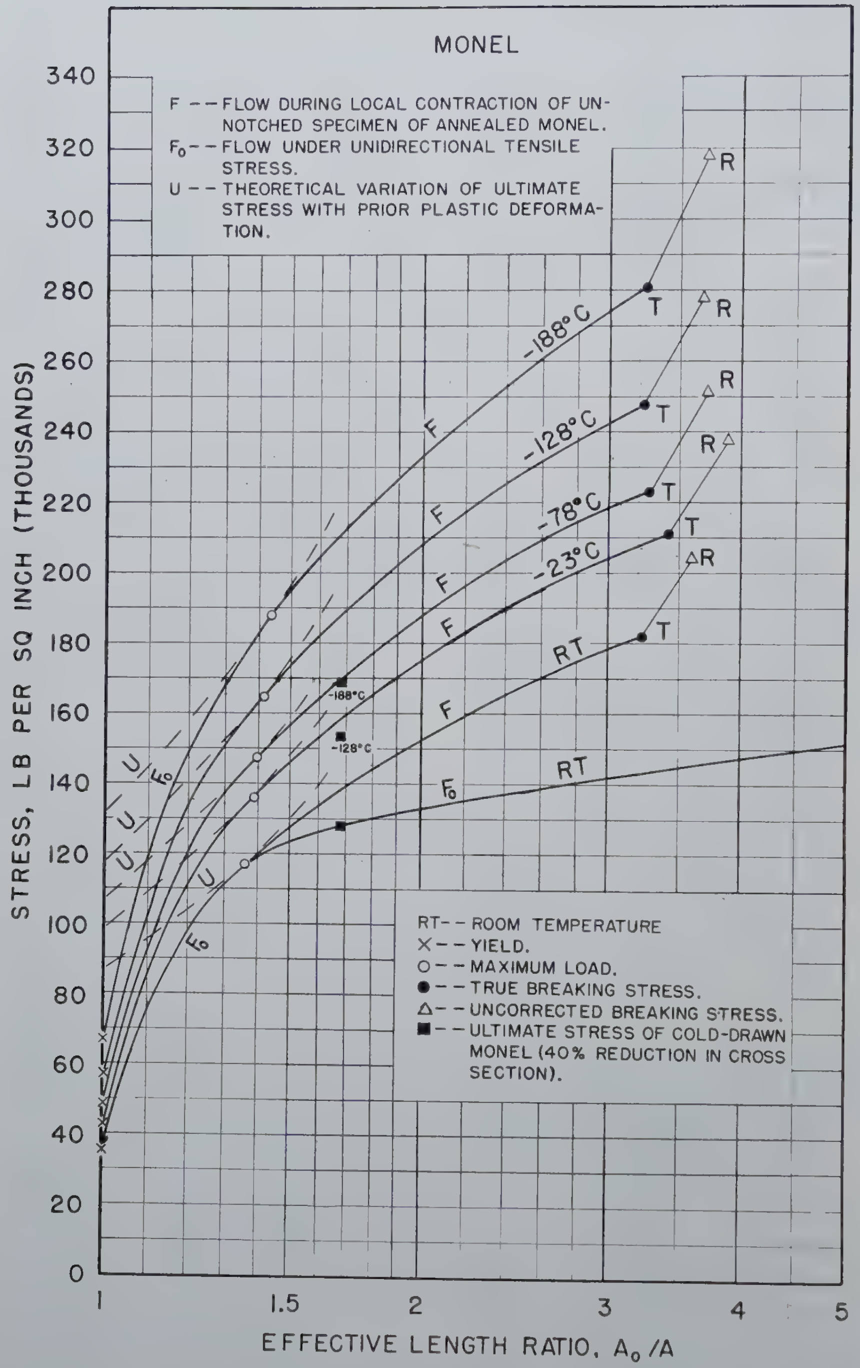

FIG 1—Flow of annealed Monel and ultimate stress of cold-worked Monel at various temperatures.

cross-section at the beginning of a tension test, this strength index varies with the amount of prior plastic deformation of the bar from which the specimen was taken. The variation is linear with L/L_0 or with A_0/A, until the load reaches a maximum and local contraction begins.* However, when A_0/A is represented on a logarithmic scale, the theoretical variation of the ultimate stress with prior plastic strain is represented by a curve *U*. To each curve *U*, the corresponding flow-stress curve must be tangent at a point representing the true stress at the maximum load. Except in some of the earliest of the tension tests by the author and associates, the extension at the maximum load was determined by means of an automatic diagram, and the point of tangency of the flow-stress curve with curve *U* can thus be established accurately. However, since the flow-stress curve and the tangent curve generally are close together for a considerable distance on each side of the point of tangency, the course of the flow-stress curve in this region can be established with sufficient accuracy, even when the extension at the maximum load has not been measured. Moreover, an additional check for the point of tangency is available when the extension at the maximum load has been determined at room temperature; for Monel, the extension at the maximum load increases slightly with decrease of temperature, as illustrated in Fig 1. Between the points representing yield and maximum load, the flow-stress curves for Monel at low temperature have been constructed so as to be in proper correlation with each other and with the accurately established curve representing flow at room temperature.

In order to extend the curves beyond the points of tangency with curves *U*, it is necessary to establish at least approximately the points representing the beginning of fracture. Points *R* in Fig 1 represent breaking stresses obtained by dividing the load at beginning fracture by the cross-sectional area determined after fracture. However, because plastic deformation of a ductile metal generally continues at the rim of the cross-section while the fracture is extending from the axis to the periphery, the area of cross-section generally decreases during fracture. The breaking-stress values indicated by points *R*, therefore, are too high. At room temperature, the transverse measurements during flow have made it possible to determine accurately the true fracture stress, the stress when the flow-stress curve reaches a maximum and fracture begins. This stress is represented by point *T*. Although transverse measurements were not made during flow at low temperatures, approximate values of the true fracture stresses have been estimated on certain assumptions and are indicated by points *T*. These points must be on the nearly straight lines extending downward from points *R* at such a slope that percent decreases in stress are equal to percent decreases in A_0/A*. Points *T* on these lines have been located on the assumption that the percent decrease in coordinates from *R* to *T* should be the same for low temperatures as for room temperature. The flow-stress curves between the points representing maximum load and beginning fracture have been constructed so as to be in proper correlation with each other and with the curve obtained at room temperature.

---

* L_0 and L represent the initial and current lengths.

* The lines are not quite straight because the scale is semilogarithmic.

The curves thus constructed are sufficiently accurate for use in a study of the influence of temperature and plastic strain on the flow stress. The first part of this study will be a comparison of these curves with the three points representing ultimate stresses of cold-drawn Monel. Since this metal had been reduced 40 pct in cross-section by cold drawing, and since ultimate stresses of severely cold drawn metal are practically the same as flow stresses at the maximum load, the three points representing ultimate stresses in Fig 1 have been placed at an abscissa representing a value of 1.67 for A_0/A. The point representing the ultimate stress at room temperature thus coincides with curve F_0.

If the flow stress (for a constant strain rate) were merely a function of temperature and total strain, the points representing ultimate stresses of cold-drawn Monel at −128 and −188°C would be much higher than they are in relation to the corresponding flow-stress curves. They would be below these curves, because the curves to the right of the points representing the beginning of local contraction are affected by the increasing radial stress ratio (S_3/S_1), but they would be higher than the corresponding points representing flow of annealed Monel at the maximum load. As shown in Fig 1, however, the points representing ultimate stresses of cold-drawn Monel at low temperatures are much lower in the diagram than the corresponding points representing the flow stresses of annealed Monel at the maximum load. The evidence, therefore, indicates that the flow stress at any instant depends not only on the temperature and total strain at that instant, but also on any prior changes in temperature during the flow.

For a thorough study of the influence of temperature and strain on the flow stress it is necessary to compare curves representing flow at various temperatures, but with the same stress system. Such a comparison is not made in Fig 1. The ideal stress system for this purpose is unidirectional tensile stress ($S_3/S_1 = 0$). As shown in Fig 1, a complete curve (F_0) has been derived to represent flow under this stress system at room temperature.[17] In Fig 2, this curve and other curves of Fig 1 have been reproduced for comparison with curves representing flow under unidirectional tensile stress at low temperatures. Fig 2 also contains flow-stress curves for cold-drawn Monel.

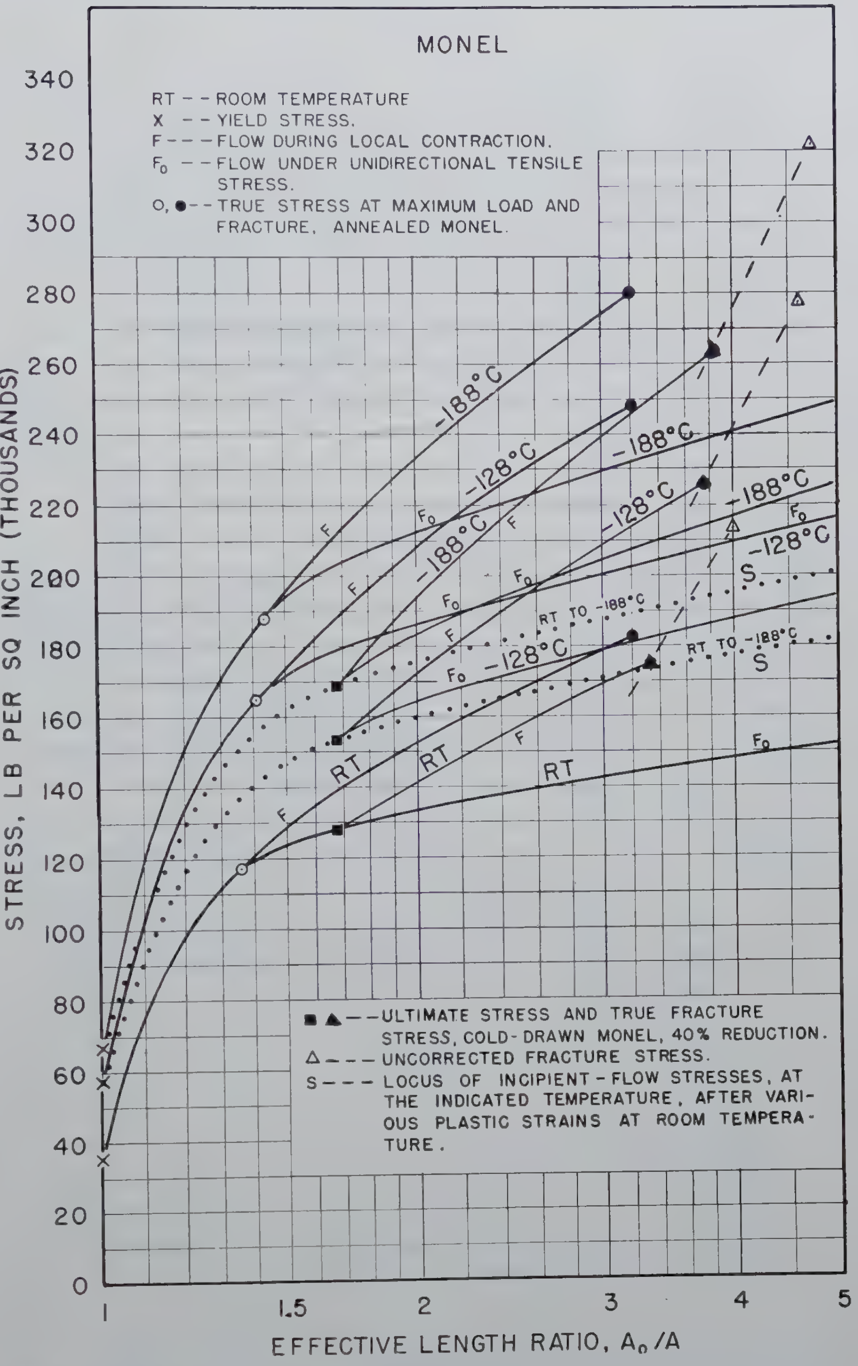

FIG 2—Influence of temperature on the flow of Monel under unidirectional tensile stress.

Curve F for cold-drawn Monel at room temperature is based on frequent transverse measurements during flow, and thus the point representing the beginning of fracture has been accurately established.[17] The F curves for cold-drawn Monel at low temperatures have been established approximately by the method used in establishing the F curves of Fig 1. The F_0 curves representing flow at low temperatures are not based directly on results of experiment; experiments to extend such a curve beyond the point representing the maximum load in a tension test would involve cold drawing or cold rolling at the low temperature. However, each of these curves in Fig 2 has been constructed with proper divergence from the corresponding F curve. Since the same amount of local contraction would cause about the same increase in the radial stress ratio (S_3/S_1) at low temperatures as at room temperature, the ratio of ordinates of corresponding F_0 and F curves at the same abscissa has been made about the same for low temperatures as for room temperature.

The junctions of the F and F_0 curves for cold-drawn Monel at low temperatures represent incipient flow at these

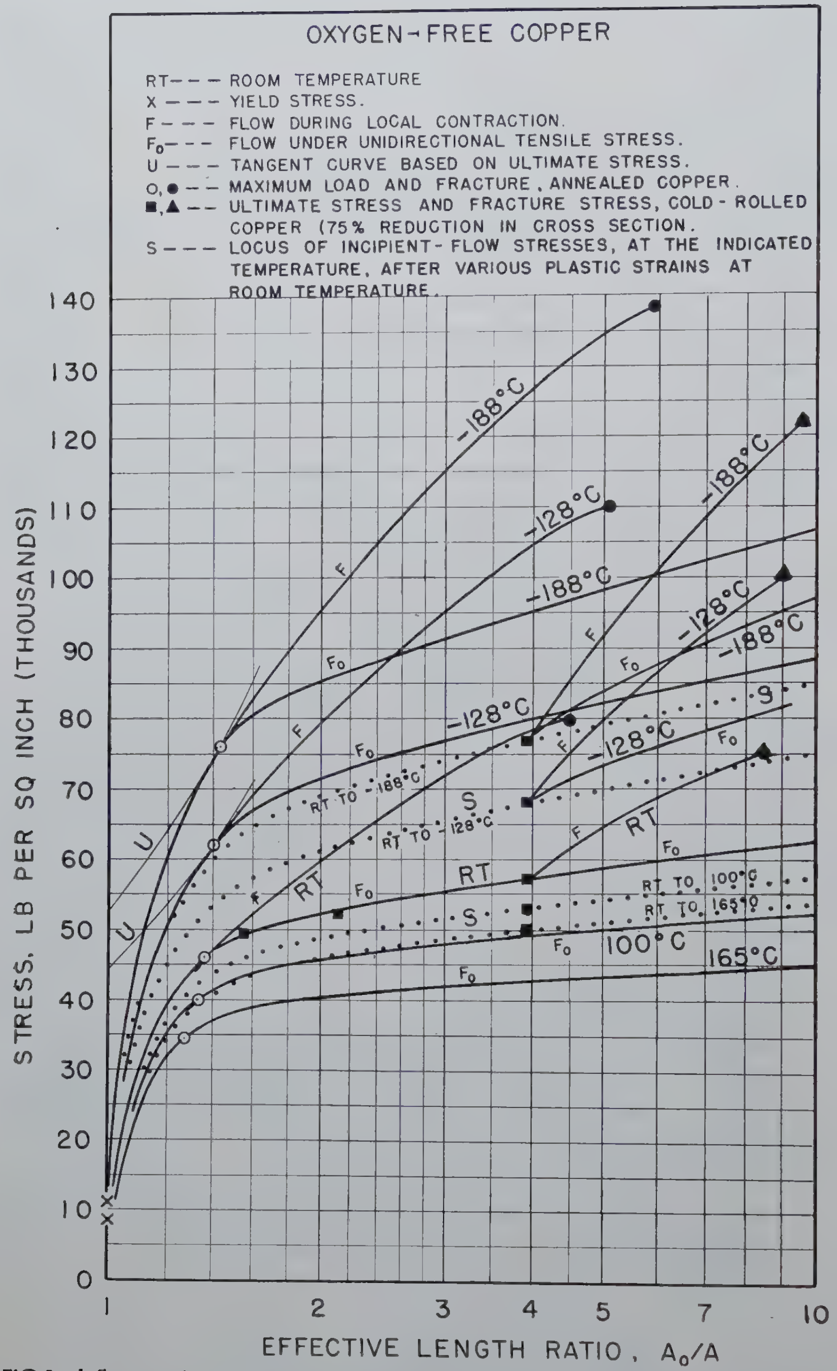

FIG 3—Influence of temperature on the flow of copper under unidirectional tensile stress.

temperatures after the indicated strain at room temperature. The dotted curve *S* passing through each of these junctions represents approximately the locus of incipient-flow stresses at the indicated temperature after various strains at room temperature. Such curves, although they do not represent continuous flow, will be termed "secondary flow-stress curves" to distinguish them from the primary curves from which they are derived. For accurate determination, such a curve should be based on results of tests of specimens that had been extended various amounts at room temperature. However, when a single point has been established far out on a secondary flow-stress curve, the curve can be constructed in proper correlation with the primary curves, so as to be accurate enough for a study of the influence of temperature and strain on the flow stress. Each secondary curve begins at the origin of the corresponding primary curve; it diverges continuously downward from that curve and upward from the F_0 curve for annealed Monel at room temperature. Beyond the points representing ultimate stresses of cold-drawn Monel, the ratios of corresponding ordinates of the three F_0 curves increase very little. Comparison of the primary and secondary F_0 curves in Fig 2 shows that the mechanical state depends not only on the total strain, but also on the temperature during the strain.

Fig 3 shows results of tests of annealed copper rod and of rod that had been plastically deformed three different amounts before the tension tests. Two lots of the copper rod had been cold drawn to 40 and 54 pct reduction in cross-section, and one lot had been cold rolled to 75 pct reduction. The points representing ultimate stresses and the corresponding strains of the cold-worked copper coincide exactly with F_0 curve for annealed copper at room temperature; this curve is based on numerous ultimate stress values for cold-drawn wire and cold-rolled strip.[17] However, Fig 3 is based almost entirely on results obtained with the annealed rod and severely cold-rolled rod, which were tested at room temperature and at low temperatures.

Curves *F* for annealed copper and severely cold-rolled copper have been established accurately by numerous transverse measurements of the diameter of the specimen during flow.[17] The true fracture stresses thus have been determined accurately. Although transverse measurements were not made during flow at low temperatures, the curves representing flow at these temperatures have been established by proper correlation with curves *U*, with the F_0 and *F* curves for room temperature, and with the points representing fracture at room temperature. Since the points representing ultimate stresses of the severely cold-rolled copper are far out along the secondary flow-stress curves *S*, the divergence of these curves from their origins must be approximately as indicated in the figure.

Comparison of the *S* curves with the F_0 curves from which they diverge gives additional evidence that the mechanical state of a metal depends not only on the total strain, but also on the temperature during the strain. Since "mechanical state" involves both strength and ductility, and since attention is being confined to resistance to flow, the term "strength state" will be used instead of "mechanical state," with the understanding that "strength" here means resistance to flow, not resistance to fracture. In general use, the word "strength" designates a property that varies with the temperature, as indicated by the variation of the hardness and flow stress. In the term "strength state," however, the word "strength" implies a condition of the metal, a property independent of temperature. In future discussion, the term "intrinsic strength" will be used with the same significance as "strength state."

The lower the temperature, the more rapid is the increase of the intrinsic strength with strain. The intrinsic strength or strength state is unchanged when the temperature is changed without change in the total strain. In Fig 2 and 3 for example, points at the same abscissa on the F_0 curve for room temperature and the two secondary flow-stress curves represent the same strength state, although they represent very different flow stresses. The effect of temperature on the flow stress evidently involves two factors: (1) a direct effect; (2) an effect of temperature on the rate of increase of the intrinsic strength with strain. The direct effect is illustrated by the vertical distance between the F_0 curve for room temperature and the corresponding S curve; the effect of temperature on the rate of increase of the intrinsic strength with strain is illustrated by the divergence of the primary and secondary curves for the same temperature. For a comparison of strength states by means of flow stresses, the flow-stresses must be determined at the same temperature.

From a set of F_0 curves and secondary flow-stress curves, such as those in Fig 2 and 3, the relationship between the direct temperature factor and the intrinsic strength factor can be determined. By the use of these factors, other locus curves may be developed, each representing incipient-flow stresses at one temperature after various strains at any other temperature, higher or lower, within the range represented in the diagram. These derived curves can be established in exact correlation with the primary and secondary curves, and extended throughout the strain range of curves from which they are derived. For a systematic study of the stress-strain-temperature relationship, three groups of these derived curves should be available. In Fig 4 and 5, three groups of these curves for Monel have been assembled together with the F_0 curves and S curves, which have been reproduced from Fig 2. In Fig 6 and 7 three similar groups of curves for copper have been assembled together with the F_0 curves and S curves, which have been reproduced from Fig 3. These derived curves will be termed "tertiary flow-stress curves." Like the secondary curves, they do not represent continuous flow.

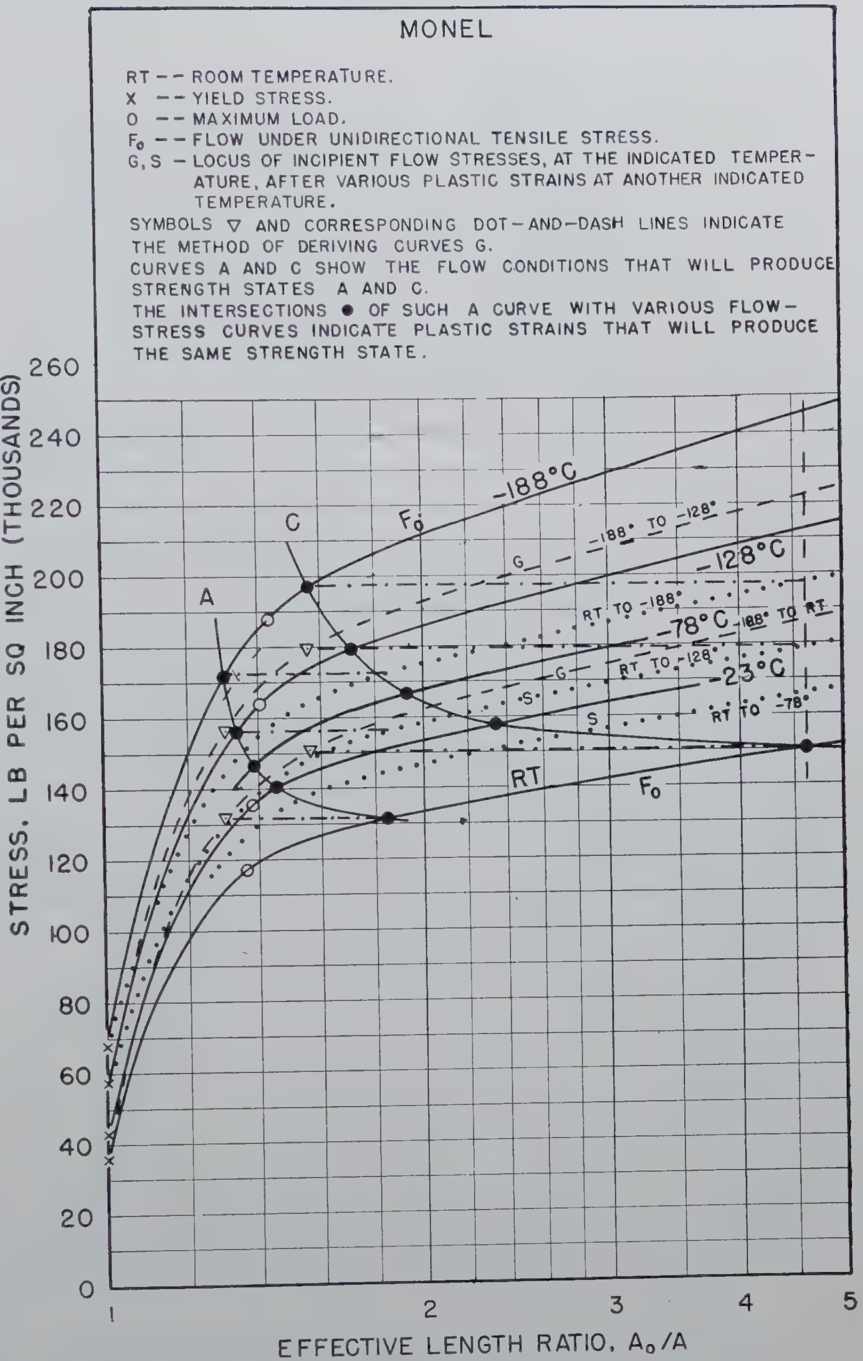

FIG 4—The flow stress of Monel as affected by temperature and total strain.

Before further consideration of the tertiary curves, attention will be given to curves of another type, the curves designated A to C in Fig 4 to 7. Each of these curves shows the influence of temperature on the strain that will produce the same strength state. These constant-state curves have been derived from the primary and secondary flow-stress curves by applying the following principles: (1) Varying the temperature without varying the plastic strain causes no change in the strength state. (2) Two specimens of the same metal, whatever their strain history, are in the same strength state if their flow stresses are the same at the same temperature. The first principle implies that points at the same abscissa on the F_0 curve for room temperature and the S curves represent the same strength state. The second principle implies that a horizontal line drawn between a primary and a secondary curve representing flow at the same temperature will intersect these curves at points representing the same strength state.

For an example of the use of these principles in deriving a constant-state curve, reference may be made to curve C in Fig 4. A point on the F_0 curve for room temperature has been selected

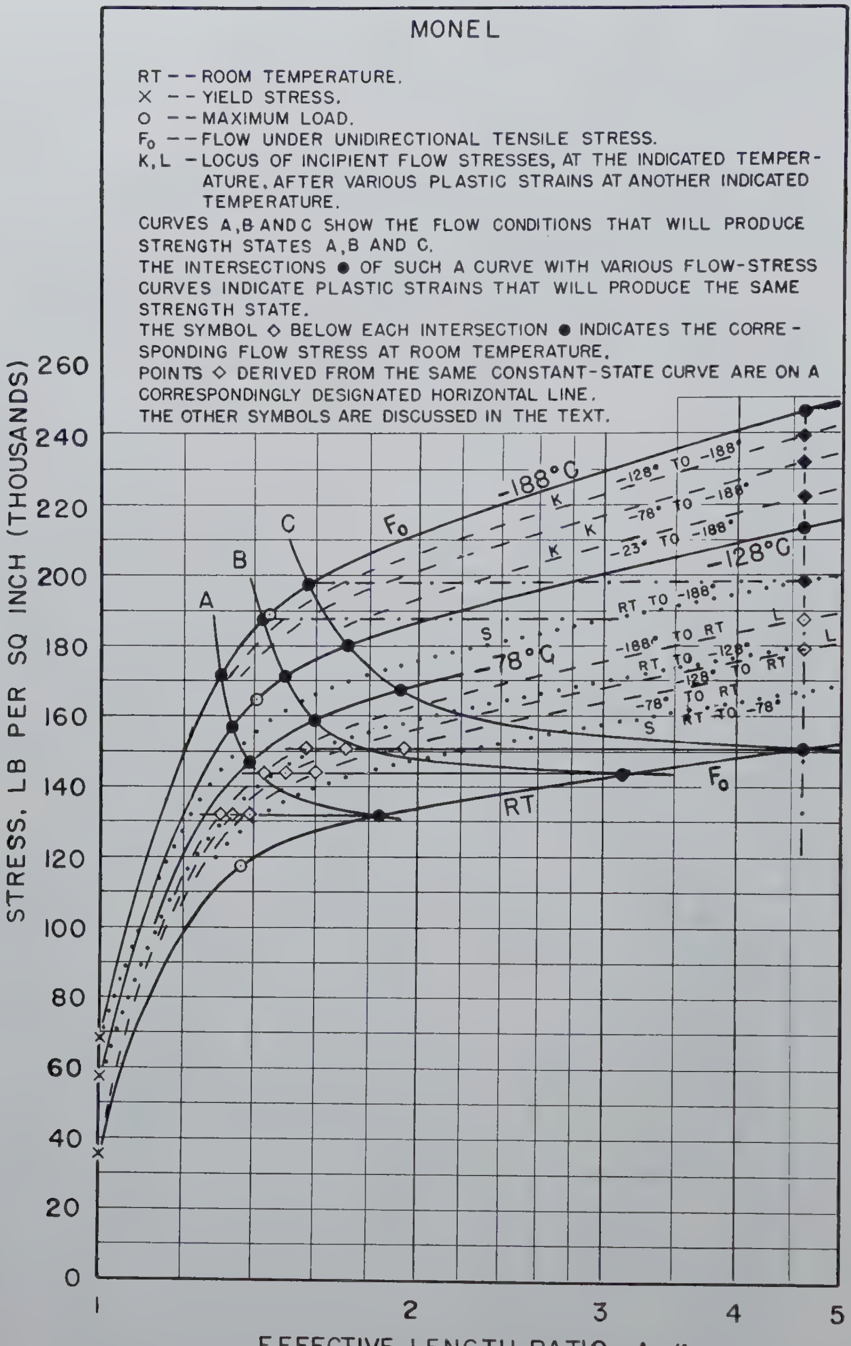

FIG 5—The flow stress of Monel as affected by temperature and total strain.

to represent state *C*. According to principle (1), the vertical line drawn through this point intersects the secondary flow-stress curves *S* at points representing the same strength state. According to principle (2), horizontal lines drawn from these intersections will intersect the corresponding F_0 curves at points representing the same strength state. The positions represented by the black circles have thus been established, and curve *C* drawn through these points represents a constant strength state. This method has been used in constructing all the constant-state curves in Fig 4 to 7.

Although a constant-state curve represents constant intrinsic strength, it does not represent constant ductility. With decrease in temperature, the strain to produce constant intrinsic strength decreases, while the total ductility of Monel and copper increases. The residual ductility thus increases as the temperature is lowered. Consequently, since "constant mechanical state" implies constant strength and ductility, it is not possible to produce such a state by varying the plastic strain with the temperature. Moreover, although a constant *strength* state may be produced by varying the strain with the temperature, the *structural* state is not constant. With decrease in temperature, the strengthening effect of plastic strain of Monel and copper increases, but the damaging effect[17] does not.

Attention will now be given to the three previously mentioned groups of tertiary flow-stress curves. One of the groups obtained with Monel is in Fig 4 and the other two are in Fig 5; one of the groups obtained with copper is in Fig 6 and the other two are in Fig 7. In deriving these curves, the points represented by inverted triangles have been established by a graphical method similar to the method of establishing the constant-state curves. Beyond these triangles, the tertiary curves have been extended by an arithmetical method involving the use of a direct temperature factor and an intrinsic strength factor. This method will be discussed later.

For an illustration of the graphical method, reference may be made to the inverted triangles on the *G* curves of Fig 4. Each of these curves represents the locus of incipient-flow stresses at the indicated temperature, after various strains at −188°C. In establishing a point on such a curve, this point should be placed at the proper distance directly below a selected point on the F_0 curve representing strain at −188°C. For convenience in establishing the two triangles on each of the *G* curves, the two specific strains selected are those represented by the black circles on the uppermost F_0 curve; these are the strains that will produce strength states *A* and *C*. If two specimens be strained these amounts at −188°C and then heated to room temperature, the points representing the incipient-flow stresses will be directly below the black circles on the F_0 curve. Moreover, since the two specimens will still be in states *A* and *C*, the incipient-flow stresses at room temperature should be the same as if the specimens had been strained to these states at room temperature. The two triangles on the lowest *G* curve, therefore, have been placed on the horizontal lines extending from the black circles on the F_0 curve for room temperature. From points directly above these two circles and on the secondary flow-stress curve *S* for −128°C, horizontal lines have been drawn to establish the two triangles on the *G* curve representing incipient-flow at −128°C. The same graphical method has been used to locate the triangles on all the tertiary flow-stress curves of Fig 5, 6 and 7.

The method of establishing these tertiary curves involves the assumption that, within the temperature range represented, there are no structural changes other than those essential to plastic deformation. It also involves the assumption that, if the flow stresses of two specimens of the same metal with different temperature-strain histories are equal at one temperature, they will be equal at any other temperature within the range represented. This assumption implies that the direct effect of temperature on the flow stress is the same for two specimens with the same intrinsic strength, whatever may be the difference in the temperature-strain history. If this assumption were incorrect, the concept of intrinsic strength would be as untenable as the concept of absolute velocity. However, the concept of intrinsic strength is supported by scattered evidence in the literature. Moreover, it receives additional support from the results of a study of the influence of temperature on strain energy.

In Fig 4, the group of *G* curves is similar in one respect to the group of secondary flow-stress curves *S*. In each group, the curves represent incipient-flow stresses at several indicated temperatures after strains at *one temperature*. By comparison of ordinates of either group with the associated F_0 curve, information may be obtained about the direct effect of temperature on the flow stress. Similar groups of curves are shown in Fig 6. Fig 5 and 7, however, each contain two groups of a different type from those in Fig 4 and 6. The curves in each group in Fig 5 and 7 represent incipient-flow stresses at *one temperature* after strains at several indicated temperatures. Attention will be confined almost entirely to Fig 5, although the discussion would apply as well to Fig 7. The upper group, comprising the *K* curves, shows results of straining at several temperatures followed by determination of the incipient-flow stresses at −188°C. Since the uppermost F_0 curve represents flow at −188°C, it belongs in the same group with the *K* curves. The lowest curve in this group is the secondary flow-stress curve *S* for −188°C. All the curves of the upper group have the same origin, the point representing yield at −188°C. The lower group in Fig 5, comprising the *L* curves and the F_0 curve for room temperature, shows results of straining at several temperatures followed by determination of the incipient-flow stresses at room temperature. All the curves of this group have their origin at the point representing yield at room temperature.

Since the ordinates in each of these groups represent incipient flow stresses at the same temperature, the ordinates at constant strain are proportional to the intrinsic strengths, and a horizontal line drawn through either of the two groups would intersect the curves at points representing the same intrinsic strength. In the lower group of curves in Fig 5, horizontal lines have been drawn to intersect the lowest F_0 curve at points representing strength states *A*, *B* and *C*. These horizontal lines intersect the tertiary flow-stress curves *L* at the indicated points, which are directly below corresponding circles on curves *A*, *B* and *C*. The strength states represented by horizontal lines *A*, *B* and *C*, therefore, are the same as those represented by curves *A*, *B* and *C*. The flow stresses represented by curves *A*, *B* and *C*, however, are primary flow stresses; the flow stresses represented by the horizontal lines are incipient-flow stresses after change to room temperature.

If ordinates in the curves of either the upper or lower group of Fig 5 be compared at the same abscissa, the ordinates will be proportional to the intrinsic strengths produced by the same strain at the indicated temperatures. Since the temperatures of pri-

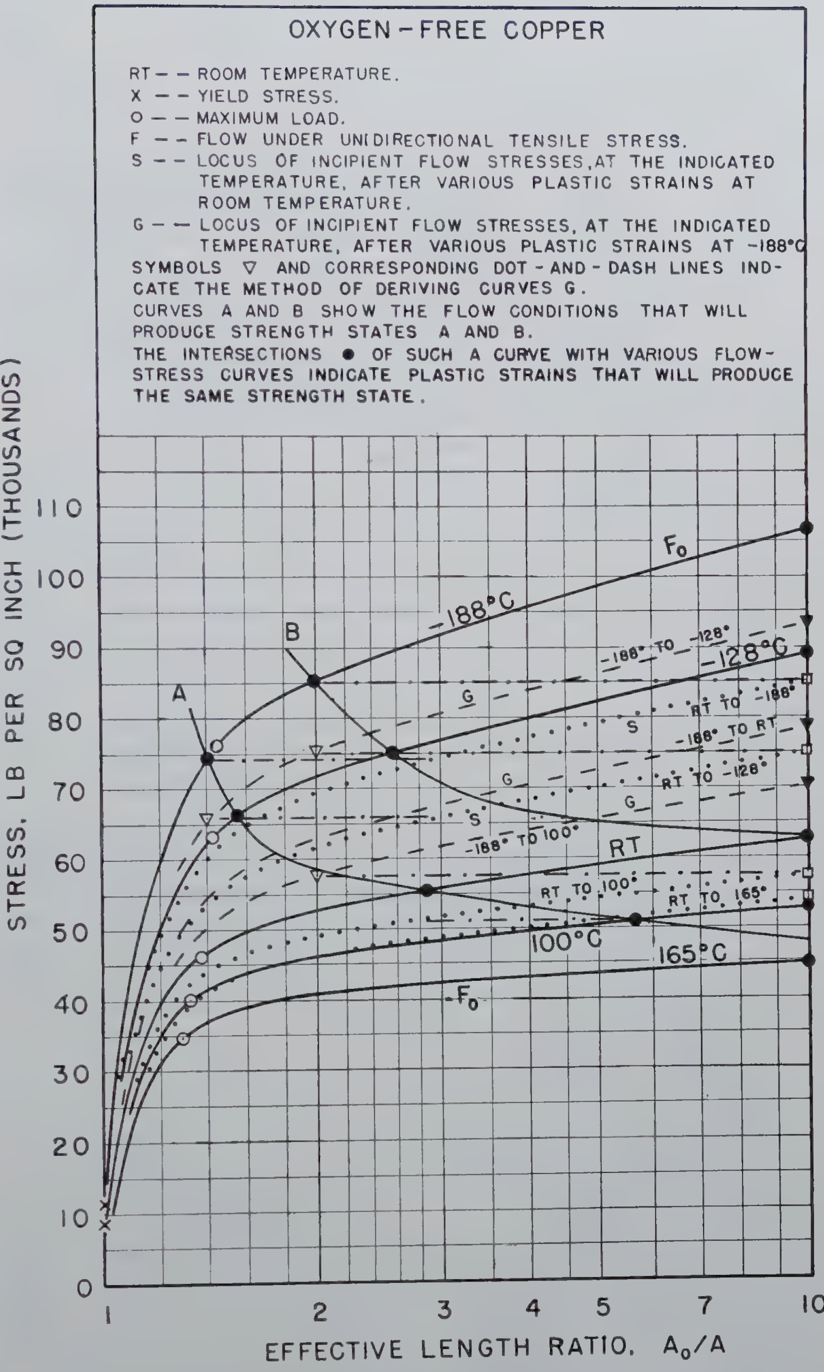

FIG 6—The flow stress of copper as affected by temperature and total strain.

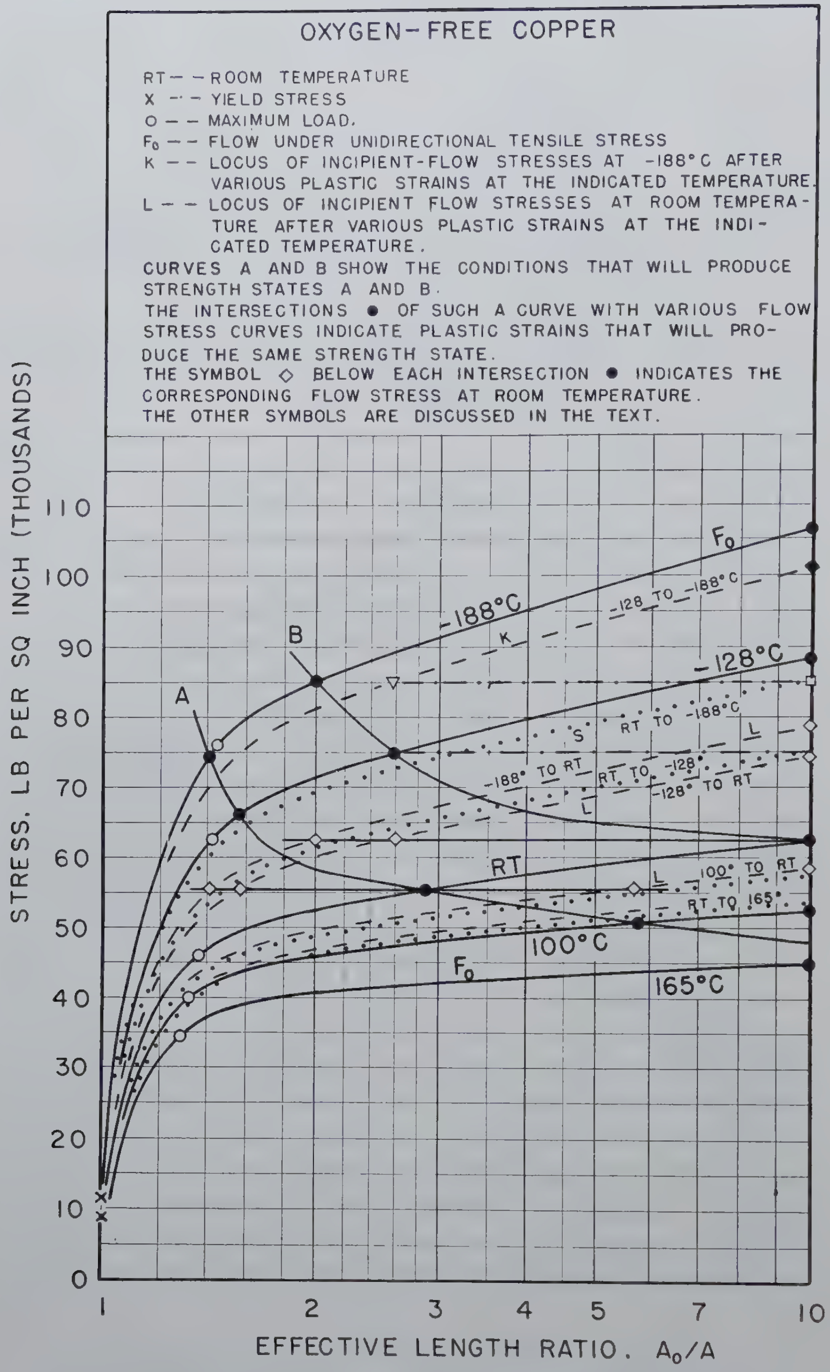

FIG 7—The flow stress of copper as affected by temperature and total strain.

mary flow were the same for both the upper and lower groups, the intrinsic strengths produced by the same strain should be in the same proportion for each group. Consequently, although the incipient-flow stresses represented by the curves of the upper and lower groups differ greatly, the ordinates at the same abscissa should be in the same proportion in each group. As will be shown in the discussion of Fig 8, the ordinates in each of the groups in Fig 5 and 7 are in correct proportion.

The effects of the difference between room temperature and −188°C are represented in Fig 5 by five ordinate ranges. The extreme ordinate range, the range between the highest and lowest F_0 curves, represents the effect of this temperature difference on the primary flow stress. Within this ordinate range are four other significant ranges. The ordinate ranges of the upper and lower groups of curves represent the effect of the above-mentioned temperature difference on the intrinsic strength. The range below the upper group of curves and the range above the lower group of curves, each represent the *direct* effect of the same temperature difference on the flow stress. Thus there are two ordinate ranges representing the effect of the same temperature difference on the intrinsic strength, and two ordinate ranges representing the direct effect of this temperature difference on the flow stress. However, when the effects of this temperature difference are expressed in terms of ordinate ratios instead of ordinate differences, a single ordinate ratio will represent the effect on the intrinsic strength and a single ordinate ratio will represent the *direct* effect on the flow stress. The product of these two ratios is the ordinate ratio for the highest and lowest F_0 curves in Fig 5. The effect of a temperature difference on the primary flow stress, therefore, should be expressed as the product of two flow-stress ratios, one of which will be called the intrinsic strength ratio and the other the direct temperature factor.

Plastic strain has very different effects on these two factors. Since the curves in each group from which intrinsic strength ratios are derived diverge from the corresponding point representing yield (Fig 5 and 7), the intrinsic strength ratio at yield is 1.0 and the ratio increases continuously with plastic strain. The direct temperature factor, for a change between room temperature and −188°C, is represented by the ordinate ratio for the uppermost secondary flow stress curve *S* and the F_0 curve for room temperature. For copper, this ratio is about 1.3 at yield, and changes little with plastic strain (Fig 7). For Monel, the ratio is about 1.9 at yield, but the ratio decreases rapidly with strain until it is about the same as for copper; thereafter the ratio changes very little.

Diagrams of a different type have been derived from Fig 4 to 7 and are shown in Fig 8. In this figure temperatures are plotted as abscissas. The temperature scale is the same that has been used in previous papers by the author and associates.[11–16,19] Temperatures in degrees K are plotted on a logarithmic scale. Since abscissas are proportional to the logarithm of the degrees Kelvin, the scale is the same in principle as Kelvin's original thermodynamic scale. This scale has been used because, within the range from room temperature −188°C, it gives a nearly linear relationship between temperature and conventional strength indices for various metals. Ordinates in the upper division of Fig 8 represent flow stresses; in the lower division ordinates represent flow-stress ratios.

Attention will be given first to the curves in the upper division. In this division, there are three groups of five curves, and two curves representing the influence of temperature on the yield stress. Each group of five curves represents variations of the flow stress when the plastic strain is constant at the amount indicated by the value of A_0/A. Each of these groups has been derived from corresponding groups of flow-stress curves in Fig 4 to 7 by using flow-stress values represented by the ordinates at the indicated value of A_0/A. To simplify the correlation between the curves in Fig 8 and the curves from which they are derived, the same letters have been used to designate the curves in Fig 8 and the corresponding curves in Fig 4 to 7. Moreover, the same symbols that designate established points on the curves in Fig 8 have been inserted at corresponding points on the vertical dot-and dash lines of Fig 5, 6, and 7.

In each group of five curves in Fig 8, the F_0 curve and the *S* curve are derived from corresponding primary and secondary flow-stress curves; the other three curves in the group are derived from tertiary flow-stress curves. The *S* curve and the *G* curve have similar meaning. The *S* curve represents the variation of the incipient-flow stress with temperature, after the indicated strain at room temperature; the *G* curve represents the variation of the incipient-flow stress with temperature after strain at −188°C. Each of these curves, therefore, represents constant intrinsic strength, and hence it represents the direct effect of temperature on the flow stress. The *K* curve and the *L* curve also have similar meaning. The *K* curve represents the effect of constant strain at various temperatures on the incipient-flow stress at −188°C; the *L* curve represents the effect of constant strain at various temperatures on the incipient flow stress at room temperature. The flow-stress variation represented by each of these curves, therefore, is proportional to the variation of the intrinsic strength with temperature.

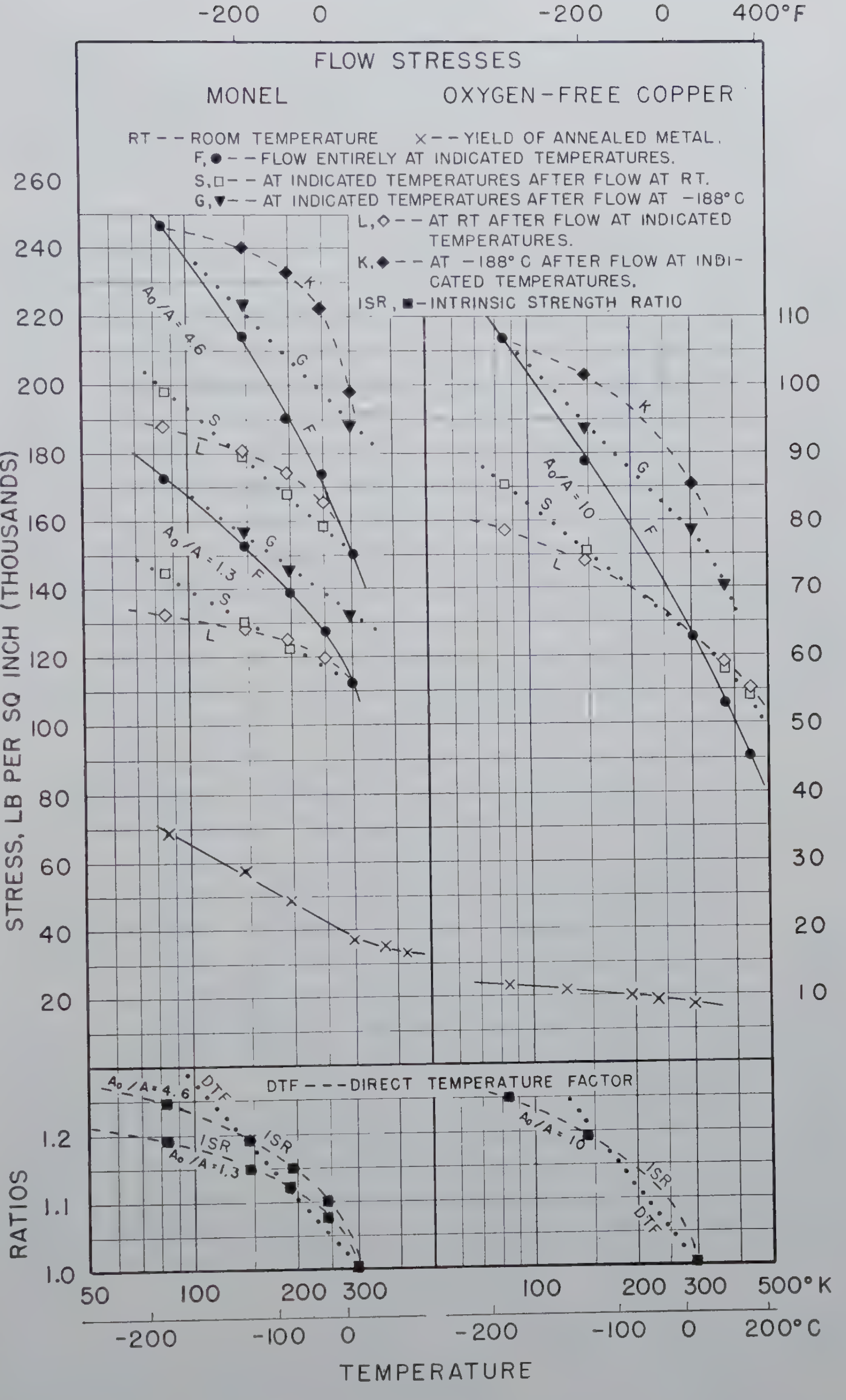

FIG 8—Influence of temperature on the flow stress of Monel and copper at constant strain.

As indicated by the *S* curves in Fig 8, the direct effect of temperature on the flow stress is nearly linear between room temperature and −188°C, on this temperature scale. The linear relationship is found not only at severe strains corresponding to A_0/A values of 4.6 for Monel and 10 for copper, but also at values of 1.3 for Monel and 4 for copper, abscissas at which the secondary flow-stress curves (Fig 2 and 3) are most accurately established. The linear relationship, however, probably ends a little above room temperature. The downward bending of the *S* curves for copper in Fig 8 possibly is due to the softening effect of "relaxation." If the *S* curves for Monel were extended above room temperature, they probably would turn upward because of strain aging.[11] Between room temperature and −188°C neither Monel nor copper shows evidence of either strain aging or relaxation. There is some doubt that the linear relationship persists below −188°C. Continuation of the linear relationship on this temperature scale, between −188°C and the temperature of liquid hydrogen (−252.8°C) would require about 35 pct increase in the flow stress. Results of tension tests by DeHaas and Hadfield[1] and by Kostenetz[7] indicate that the increase in the flow stress between −188°C and −252.8°C for most of the metals tested would be not more than about 20 pct. However, results obtained by Kos-

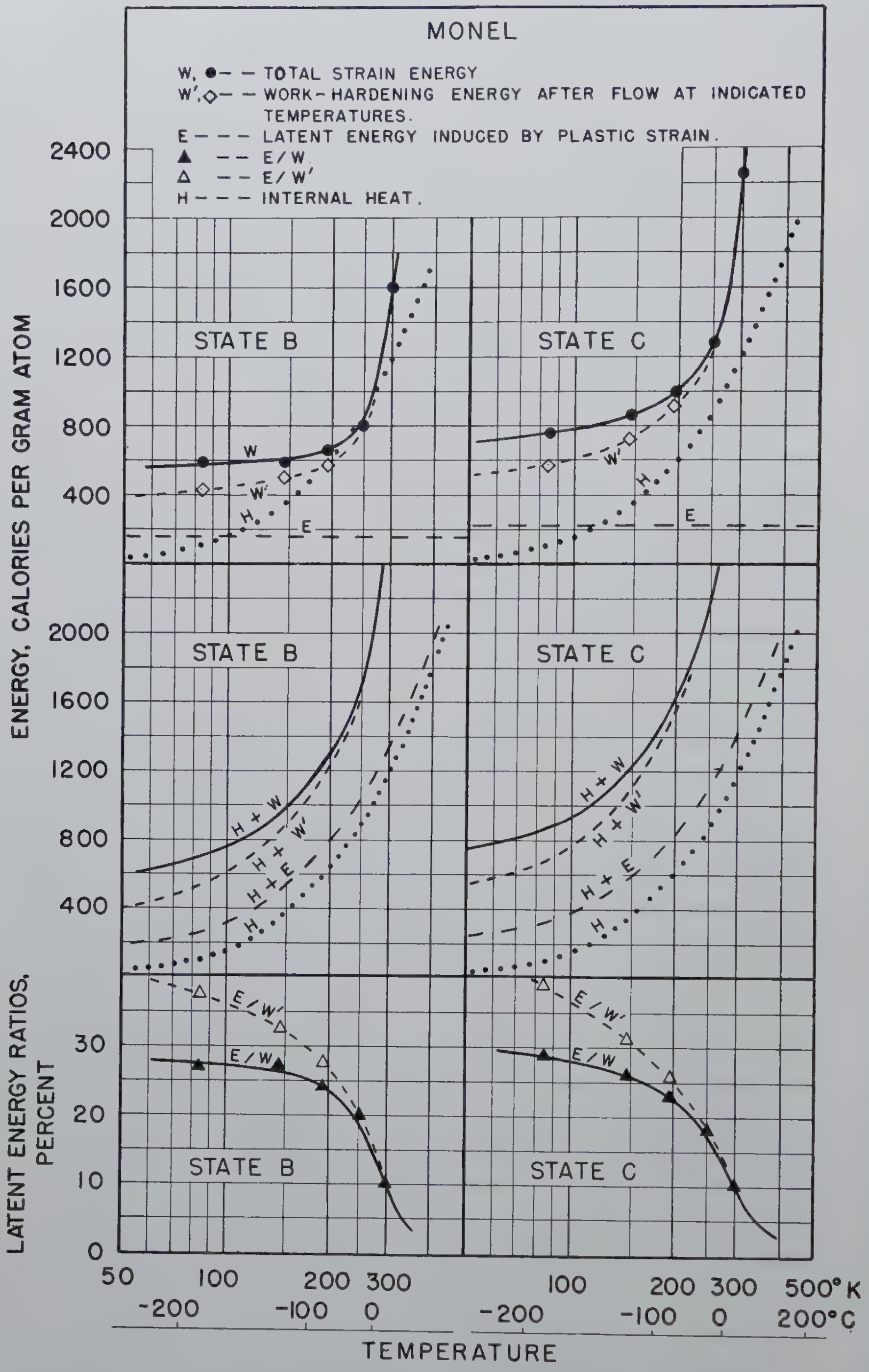

FIG 9—Influence of temperature on the strain energy of Monel for constant intrinsic strength

tenetz with some steels indicate an increase of about 35 pct, and his results for aluminum indicate an increase of 67 pct. The evidence based on these tests, therefore, is inconclusive. It appears probable, however, that the *S* lines for Monel and copper should be slightly curved if extended below −188°C; the curvature would be qualitatively similar to that of the F_0 curves in Fig 8.

The F_0 curve, even in the absence of strain aging, probably would reverse its curvature if extended far enough above room temperature. If extended over a sufficient temperature range, the curve would thus be similar in form to a curve representing the influence of temperature on the ultimate stress. Below the point of reversal the curvature is due largely to the influence of temperature on the intrinsic strength factor, as illustrated by curves *K* and *L* in Fig 8.

In each group of five curves in Fig 8, two curves represent the direct effect of the same range of temperature on the flow stress, and two curves represent the effect of the same range of temperature on the variation of the flow stress with the intrinsic strength. However, when the effect of this range of temperature on each of these four curves is expressed in terms of flow-stress ratios instead of flow-stress differences, only one curve is obtained to represent the *direct* effect of temperature, and only one curve is obtained to represent the effect of temperature on the intrinsic strength ratio. Curves so obtained are shown in the lower division of Fig 8. Lines *DTF* represent the variation of the direct temperature factor with temperature, and curves *ISR* represent the variation of the intrinsic strength ratio. Ratios are expressed in terms of the flow stress at the indicated strain at room temperature. Lines *DTF* are based on averages of closely agreeing ratios derived from lines *S* and *G*; curves *ISR* are based on closely agreeing ratios derived from curves *K* and *L*. However, there is another way in which the *ISR* curves can be derived. From a pair of F_0 and *S* curves in Fig 8 intrinsic strength ratios can be derived by calculating ratios of corresponding ordinates. Since the *S* curve represents the effect of lowering the temperature without change of intrinsic strength, any point on this curve represents the intrinsic strength produced by the indicated strain at room temperature. The ratio of ordinates of the F_0 and *S* curves at the same abscissa, therefore, is the ratio between the intrinsic strength produced by straining at the indicated temperature and the intrinsic strength produced by the same strain at room temperature. Ratios thus obtained from the F_0 and *S* curves are identical with those obtained at the same abscissas from curves *K* and *L*.

The fundamental factors involved in the effect of temperature on the flow stress, therefore, can be derived directly from corresponding F_0 and *S* curves. These factors could then be used to establish curves *G*, *K*, *L*, *DTF* and *ISR* in Fig 8 without the use of the tertiary flow-stress curves in Fig 4 to 7. Moreover, the same arithmetical method can be used, in conjunction with the graphical method, to derive the tertiary flow-stress curves in Fig 4 to 7 from the F_0 and *S* curves.

As indicated by the *ISR* curves in Fig 8, the influence of temperature on the intrinsic strength factor gradually becomes less prominent as the temperature is lowered between room temperature and −188°C. However, if the *ISR* curves were extended to some point above room temperature the steepness probably would begin to decrease, even in the absence of strain aging. The influence of prior plastic strain on the steepness of the *ISR* curve is illustrated by the relation between the two *ISR* curves for Monel. With decrease in the prior plastic strain, the steepness of the *ISR* curve decreases. At yield, the curve would become a horizontal line, and the influence of temperature on the flow stress would depend entirely on the direct temperature factor.

Influence of Temperature on the Strain Energy of Monel and Copper

The energy applied in the plastic deformation of metals is converted partly into heat and partly into latent energy. The conversion into latent energy is associated with the work-hardening, that is, the increase of intrinsic strength with strain. Since the strain energy is a function of the area beneath a flow-stress curve, the evidence in Fig 4 to 7 indicates that both the total strain energy and the latent energy vary with the temperature at which the metal is strained. The flow-stress curves in Fig 4 to 7, therefore, have been used to develop diagrams representing the influence of temperature on the strain energy of Monel and copper. The diagrams thus obtained are shown in Fig 9, 10 and 11. The energy values represented in these figures have been derived from the areas beneath flow-stress curves in Fig 4 to 7. The areas were determined by the use of original unreduced diagrams (20 in. wide) which were on coordinate paper with fine subdivisions. Since abscissas in these diagrams are proportional to true strains, the area beneath a flow-stress curve is proportional to the strain energy per unit volume of the *flowing* metal, even when this volume is decreasing because of local contraction. In calculating energy values per unit volume from the areas, a factor was used to convert abscissas to natural strains, and other factors were used so as to determine the energy equivalent of unit area in calories per gram atom.

Fig 9 and 10 show the energy relations for constant strength state; Fig 11 shows the energy relations for constant strain. Attention will be given first to the relations for constant state. States B and C represented by curves *W* in Fig 9 are the same as those represented by curves *B* and *C* in Fig 5; states A and B represented by curves *W* in Fig 10 are the same as those represented by curves *A* and *B* in Fig 7. The circles on the *W* curves in Fig 9 and 10 correspond to circles on the constant-state curves in Fig 5 and 7. Just as curve *C* in Fig 5 represents the effect of temperature on the *strain* that will produce state C, so curve *W* on the right side of Fig 9 represents the effect of temperature on the *strain energy* that will produce the same strength state. The similarity in form between the *W* curves in Fig 9 and 10 and the constant state curves in Fig 5 and 7 indicates that, for constant state, the variation of the strain energy with temperature is similar to the variation of the plastic strain.

Curves *W* in Fig 9 and 10 represent the influence of temperature on the *total* strain energy. However, just as the influence of temperature on the flow stress involves a direct tempera-

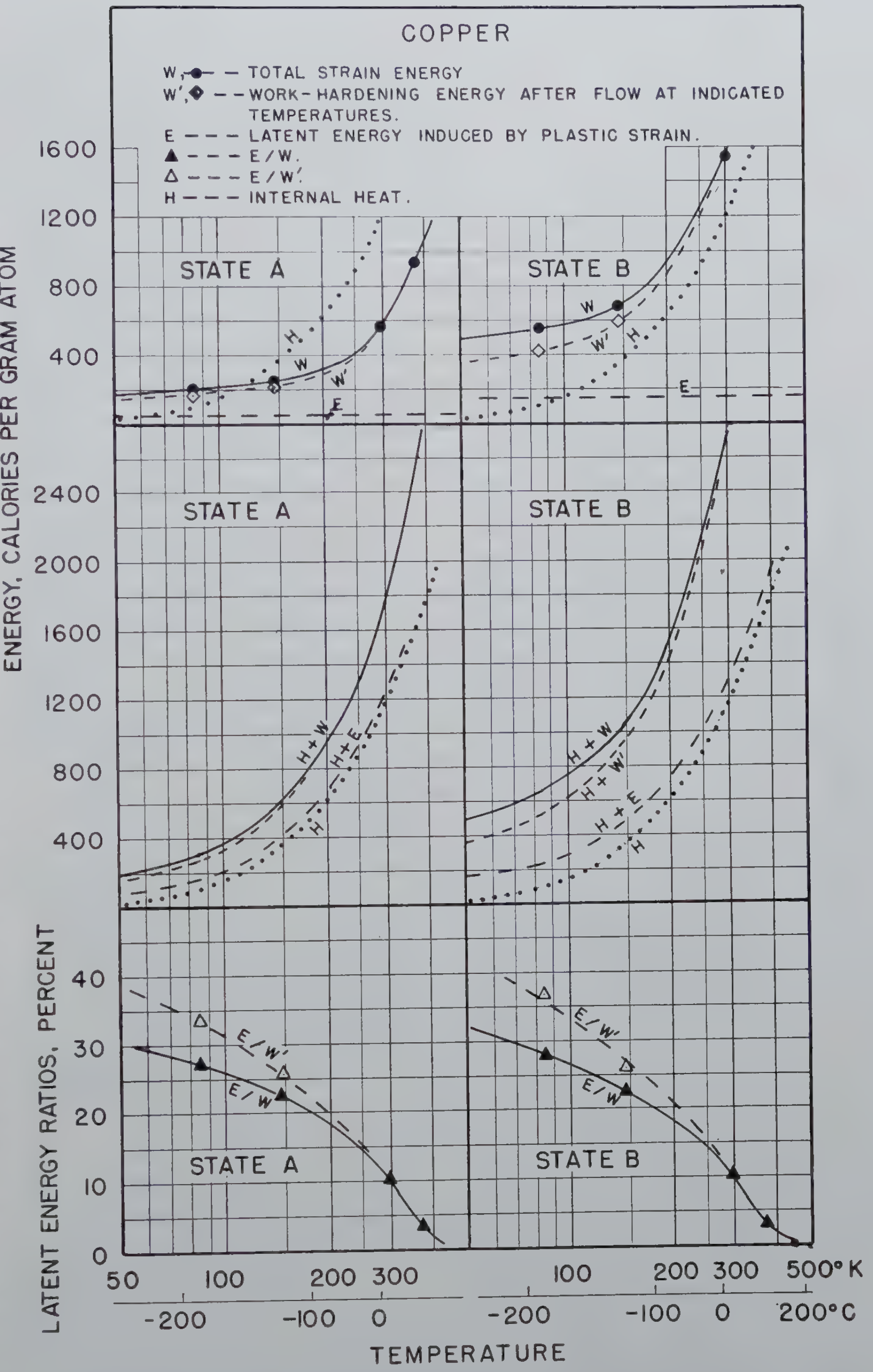

FIG 10—Influence of temperature on the strain energy of copper for constant intrinsic strength.

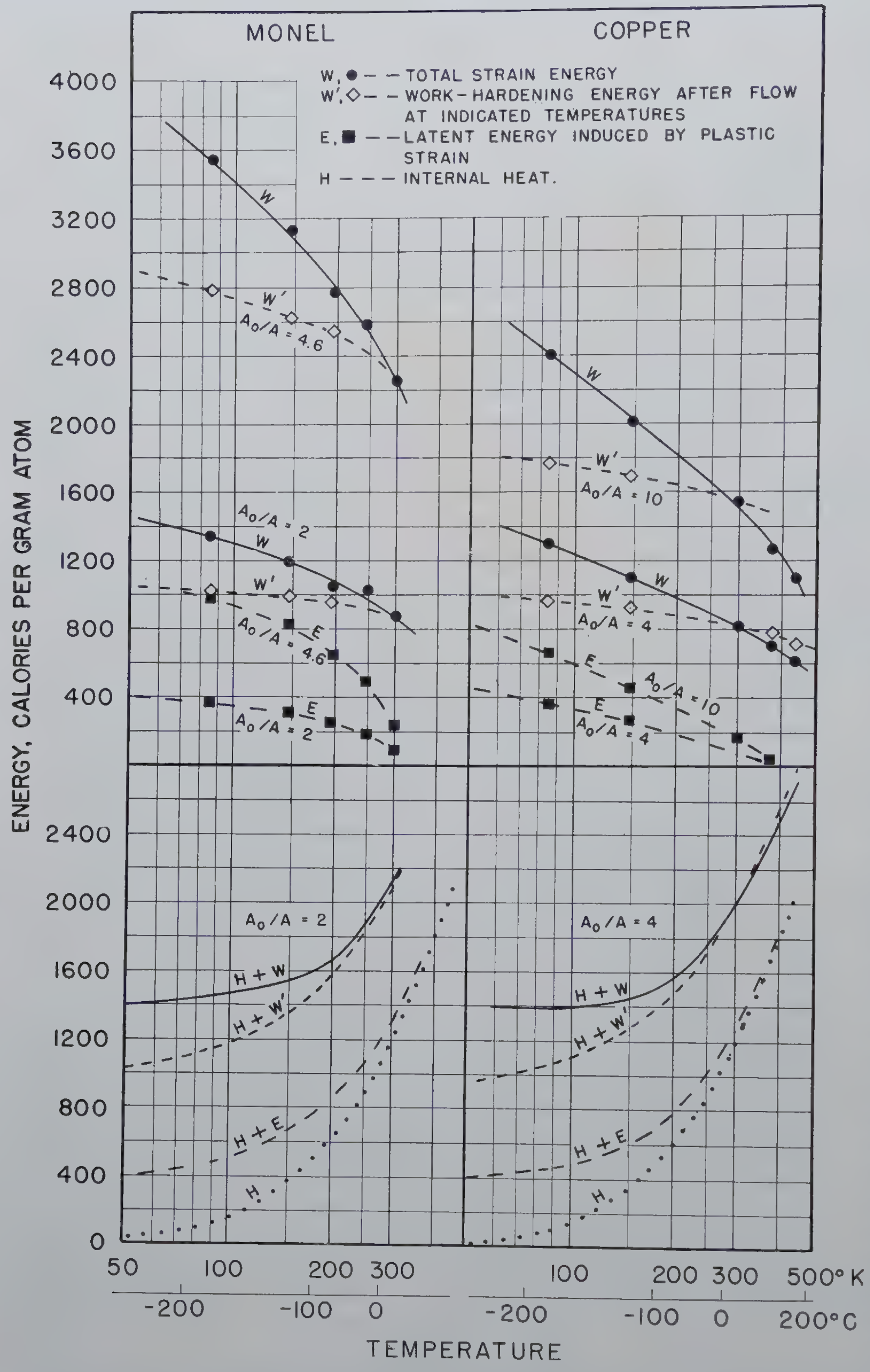

FIG 11—Influence of the temperature of Monel and copper on the strain energy for constant strain.

ture factor and an intrinsic strength factor, so the influence of temperature on the strain energy involves the same two factors. The relative influence of the two factors varies greatly with the metal. When the yield stress varies greatly with temperature, the influence of the direct temperature factor is most prominent. Curves *W′* have been developed to represent the influence of temperature on the work-hardening energy, the energy that remains after allowance for the influence of the direct temperature factor. Although partial allowance for this factor may be made by utilizing only part of the area beneath a flow-stress curve, the part above the point representing the yield stress, the allowance thus made is incomplete. Complete allowance can be made by the method now to be described. Whereas curves *W* in Fig 9 are derived from the areas beneath F_0 curves in Fig 5, curves *W′* in Fig 9 are derived from areas beneath the *L* curves in Fig 5. The strain energy values represented by the symbols on curves *W′* in Fig 9 correspond to the strain values indicated by symbols of the same kind on the horizontal lines representing strength states B and C in Fig. 5. Curves *W′*, therefore, represent strain energy values derived from curves representing incipient flow at *one temperature* after strain at various temperatures. It should be emphasized that curves *L* in Fig 5 and 7 do not represent continuous flow. The ordinates of curves *W′* in Fig 9 and 10, therefore, do not represent strain energies for continuous flow at room temperature. They represent merely the energy values obtained by making allowance for the influence of the direct-temperature factor on the strain energy, and thus obtaining values for what may be called work-hardening energy. Since the values for work-hardening energy represented by a *W′* curve are relative to the total strain energy at room temperature, curve *W″* crosses curve *W* at the abscissa representing room temperature (300°K). The values represented by a *W′* curve thus are merely relative values. They have been desired for use in the following study of the relation between applied energy and latent energy.

The relation between the total strain energy and the latent energy induced by plastic strain has been investigated by Taylor and Farren[20] and by Taylor and Quinney.[21] The metals used in their experiments were copper, annealed mild steel, and annealed decarburized mild steel. For various stages during plastic deformation of these metals the increments of applied energy and latent energy were determined. With copper, the ratio of these increments (latent energy ratio) was about 9 pct throughout a wide range of plastic strain, but eventually decreased rapidly to about 4 pct. With the mild steel, the ratio decreased continuously from about 13 to about 7 pct. With the decarburized steel, the ratio decreased from about 10 to about 3 pct. With all three metals, however, the ratio of the total latent energy to the total applied energy changed very little throughout a wide range of plastic strain, a range which was much greater for copper than for the steels. For a qualitative study of the influence of temperature of the latent energy ratio, it has seemed best to assume a ratio of 10 pct for Monel and copper at room temperature. This ratio, therefore, has been used in Fig 9 and 10.

Since each of the four *W* curves of Fig 9 and 10 represents the strain energy relation for constant intrinsic strength, a reasonable assumption is that each curve also represents the strain energy relation for constant latent energy. Beneath each of the W curves, therefore, a horizontal line E has been drawn to represent the influence of temperature on the latent energy E. The constant ordinate of line E is one-tenth the ordinate of curve W at room temperature. Comparison of corresponding ordinates of line E and curves W and W' shows that the latent energy ratios E/W and E/W' increase greatly with decrease in temperature. The variation of these ratios with temperature is represented directly by the curves in the lower division of Fig 9 and 10. The influence of temperature on these ratios evidently is nearly the same for both Monel and copper in each strength state. Moreover, comparison of these curves with the curves in the lower division of Fig 8 shows that the variation of the latent energy ratio with temperature is similar to the variation of the intrinsic strength ratio. The evidence indicates that the E/W ratio at −188°C is nearly three times the ratio at room temperature. If the ratio curves were extended to a point above room temperature, the steepness probably would begin to decrease. Moreover, above a certain temperature, the latent energy ratio would be affected by relaxation, and the influence of the strain rate on the ratio would become prominent.

Curves H in Fig 9 and 10 represent the total heat per gram atom, that is, the integral of the variation of the atomic heat with temperature. This will be termed "internal heat" to distinguish it from the part of the strain energy that is evolved as heat. Comparison of curves W and W' with curve H shows that the effect of temperature on the strain energy, for constant intrinsic strength, is qualitatively similar to the effect of temperature on the internal heat. The greater the internal heat, the greater is the total strain energy required to produce constant intrinsic strength, and the greater is the outflow of energy as heat. In the middle division of Fig 9 and 10, the total strain energy, work hardening energy, and latent energy are represented as superimposed on the internal heat.

Fig 11 shows the influence of temperature on the energy relations for constant strain. Curves W and W' in this figure have been derived from areas extending to the indicated abscissas beneath curves F_0 and L in Fig 5 and 7. Curves W and W' in Fig 11 are similar in form to curves F_0 and L of Fig 8. This similarity would be expected since each curve represents results obtained with constant strain, and since the curves in both figures are derived from the F_0 and L curves of Fig 5 and 7. For constant plastic strain, therefore, the variation of the strain energy with temperature would be similar to the variation of the flow stress. Curves E in Fig 11 have been derived from the corresponding W curves by making the ordinate ratios for the two curves the same as the corresponding values of the latent energy ratio E/W, as represented by ordinates of the curves in the lower division of Fig 9 and 10. Curves E in Fig 11, therefore, are similar in form to curves E/W in Fig 9 and 10. They also are similar to the curves *ISR* of variation of the intrinsic strength ratio (Fig 8).

In the lower division of Fig 11, the total strain energy, work hardening energy, and latent energy for constant strain are represented as superimposed on the internal heat. The curves thus obtained should be compared with the curves representing the superimposed energies for constant intrinsic strength (Fig 8).

The diagrams in Fig 1 to 11 present various pictures of the influence of temperature on the stress-strain-energy relationship for metals that are practically free from structural changes or relaxation within the range from room temperature to −188°C.

Conclusions

1. The mechanical state of a metal depends not only on the total strain, but also on the temperature during the straining.

2. With decrease in temperature the total strain required to produce a constant strength state decreases, while the ductility of many metals increases. By "strength state" or "intrinsic strength" is meant a condition of the metal, a property independent of temperature.

3. The mechanical state which involves both strength and ductility cannot be held constant by varying the total strain with the temperature.

4. The influence of temperature on the flow stress involves two factors: (1) A direct temperature effect; (2) the influence of temperature on the rate of increase of intrinsic strength with strain. The lower the temperature, the more rapid is the increase of intrinsic strength with strain.

5. The effects of the direct temperature factor and the intrinsic strength factor on the flow stress should be expressed in terms of flow-stress ratios rather than flow-stress differences. The ratio of the flow stresses for the same total strain at two different temperatures is the product of two flow-stress ratios, one representing the direct temperature factor and the other representing the intrinsic strength ratio.

6. Both these factors can be determined from a set of primary flow-stress curves and a corresponding set of secondary curves, each representing the locus of incipient-flow stresses at a given temperature after various plastic strains at room temperature.

7. By the use of the two factors so obtained other (tertiary) locus curves can be obtained, each representing incipient-flow stresses at one temperature after various plastic strains at another temperature, either higher or lower.

8. With plastic strain the intrinsic strength ratio increases continuously, but there is not much change in the direct temperature factor.

9. The variation of the total strain energy with temperature involves the same two factors that affect the flowstress. By making allowance for the influence of the direct temperature factor it is possible to determine the influence of temperature on the work-hardening energy.

10. The ratio of the latent energy induced by plastic strain to either the total strain energy or the work-hardening energy increases with decrease in temperature. The variation of the latent energy ratio with temperature is similar to the variation of the intrinsic strength ratio.

11. For constant intrinsic strength (constant latent energy) the variation of either the total strain energy or the work-hardening energy with temperature is qualitatively similar to the variation of the internal heat per gram atom, the integral of the variation of the atomic heat with temperature. The greater the internal heat, the greater is the total strain energy necessary to produce constant intrinsic strength, and the greater is the ouflow of energy as heat.

References

1. W. J. DeHaas and R. Hadfield: The Effect of the Temperature of Liquid Hydrogen on the Tensile Properties of Forty-one Specimens of Metals. *Phil. Trans.* Roy. Soc. (1933–34) A, **232**, 297–332.
2. J. E. Dorn, A. Goldberg, and T. E.

Tietz: The Effect of Thermomechanical History on the Strain Hardening of Metals. *Trans.* AIME **180,** *Metals Tech.*, Sept., 1948, TP 2445. Discussion, *Trans. Jnl. of Metals* (May, 1949) 325.

3. Dushman, Dunbar and Huthsteiner: Creep of Metals. *Jnl. Appl. Phys.* (1944) **15,** 108–124.
4. J. H. Holloman and C. Zener: Conditions of Fracture of Steel. *Metals Tech.* Dec. 1944. TP 1782.
5. J. H. Hollomon and J. D. Lubahn: Plastic Flow of Metals. *Phys. Rev.* (1946) **70,** Nov. 1 and 15, p. 775.
6. J. H. Holloman: The Mechanical Equation of State. *Trans.* AIME (1947) **171,** 535–543; *Metals Tech.*, Sept., 1946, TP 2034.
7. V. J. Kostanetz: Mechanical Properties of Metals and Alloys in Tension at Low Temperatures. *Jnl. Tech. Phys.* (U.S.S.R.) (1946) **16,** No. 5, 515–554.
8. C. W. MacGregor and J. C. Fisher: Tension Tests at Constant True Strain Rates, *Jnl. Appl. Mech.*, Dec. 1945, **12,** A217–A227.
9. C. W. MacGregor and J. C. Fisher: A Velocity-Modified Temperature for the Plastic Flow of Metals. *Trans.* ASME 1946, **68,** A11–A16.
10. D. J. McAdam, Jr. and R. W. Mebs: An Investigation of the Technical Cohesive Strength of Metals. *Trans.* AIME (1945) **162,** 474–536.
11. D. J. McAdam, Jr. and R. W. Mebs: The Technical Cohesive Strength and Other Mechanical Properties of Metals at Low Temperatures. *Proc.* Am. Soc. Test. Materials (1943) **43,** 661–703.
12. D. J. McAdam, Jr., R. W. Mebs, and G. W. Geil: The Technical Cohesive Strength of Some Steels and Light Alloys at Low Temperatures. *Proc.* Am. Soc. Test. Materials (1944) **44,** 593–644.
13. D. J. McAdam, Jr.: The Technical Cohesive Strength of Metals in Terms of the Principal Stresses. *Trans.* AIME (1945) **162,** 542–568.
14. D. J. McAdam, Jr., G. W. Geil, and R. W. Mebs: The Effect of Combined Stresses on the Mechanical Properties of Steels between Room Temperature and −188°C. *Proc.* ASTM (1945) **45.**
15. D. J. McAdam, Jr., G. W. Geil and R. W. Mebs: Effects of Combined Stresses on the Mechanical Properties of Some Nonferrous Metals. *Trans.* ASM (1946) **37,** 497–536.
16. D. J. McAdam, Jr., G. W. Geil, and R. W. Mebs: Influence of Plastic Deformation, Combined Stresses and Low Temperature on the Breaking Stress of Ferritic Steels. *Trans.* AIME (1947) **172.** *Metals Tech.* Aug. 1947, TP 2220.
17. D. J. McAdam, Jr., G. W. Geil and Frances Jane Cromwell: Flow, Fracture and Ductility of Metals. Trans. AIME **175,** 306. *Metals Tech.* Jan. 1948. TP 2296.
18. D. J. McAdam, Jr., G. W. Geil, and W. D. Jenkins: Influence of Strain Aging on the Fracture Stress of Low-carbon Steel. *Trans.* AIME (1948) **175.** *Metals Tech.* Jan. 1948. TP 2318.
19. D. J. McAdam, Jr., G. W. Geil and F. J. Cromwell: Influence of Low Temperatures on the Mechanical Properties of 18:8 Chromium-nickel Steel. *Trans.* ASM (1949) **41,** 609–645.
20. G. I. Taylor and W. S. Farren: Heat Developed during Plastic Extension of Metals. *Proc.* Roy. Soc. (1925) **A-107,** 425–451.
21. G. I. Taylor and H. Quinney: The Latent Energy Remaining in a Metal after Cold Working. *Proc.* Roy. Soc. (1934) **A-143,** 307–326.
22. C. Zener and J. H. Holloman: Plastic Flow and Rupture of Metals. *Trans.* Am. Soc. Metals (1943) **33,** 163–215.
23. C. Zener and J. H. Holloman: Problems in Non-elastic Deformation of Metals. *Jnl. Appl. Phys.* Feb. 1946, **17,** 68–87.

The Thermodynamical Treatment of Very Small Solid Solubilities

LESTER GUTTMAN*

The question of whether classical thermodynamics alone imposes any lower limit to solid solubilities was raised during a discussion among various members† of the Institute for the Study of Metals. Although our conclusions are not new,[1] they may be worth reiterating, since confusion on this subject seems to persist.

In a binary system (A,B), the conditions for equilibrium, at constant pressure and temperature, between a solid solution and a liquid solution are

$$\mu_A{}^S = \mu_A{}^l \qquad [1a]$$

$$\mu_B{}^S = \mu_B{}^l \qquad [1b]$$

Here μ denotes the chemical potential either of component A or B, as shown by the subscripts, and the superscripts s and l refer to the solid and liquid solutions, respectively. These two conditions are just sufficient to determine the compositions of both phases. Suppose, however, that the solid phase is found experimentally not to contain any of component B; then we cannot evaluate $\mu_B{}^S$, which is defined by

$$\mu_B{}^S = \left(\frac{\partial F^s}{\partial n_B{}^s}\right)_{n_A{}^s,P,T}$$

Here $n_A{}^S$ and $n_B{}^S$ are the number of mols of A and B, respectively, in the solid, whose free energy is F^S. Eq 1b cannot be used, but it is no longer needed: we stated at the outset that the solid has the composition "pure A," and only the liquid composition need now be determined, from Eq 1a. All the equilibrium properties of the system can be derived from Eq 1a rigorously and simply. Hence there is no purely thermodynamic reason to exclude phase diagrams which show precisely zero solid solubility. Marsh[2] has objected to such diagrams as implying that even the transformation of pure A begins at the eutectic temperature. In any case, the user of the diagram must have a certain minimum knowledge of how to interpret it, and it would seem simpler to remember the general rule that eutectic temperatures have no significance for pure components, rather than to show, say, by broken lines, on a scale which will often be exaggerated, a hypothetical solid-solubility about which we know only that it is less than a certain amount.

The case of an intermetallic compound in equilibrium with a binary liquid solution does not require a separate treatment since nothing in the foregoing was dependent on the nature of the components. Therefore, thermodynamics alone does not exclude the possibility that (intermetallic) compounds may exist with compositions always precisely those given by their chemical formulas.

With the aid of *extra*-thermodynamic methods, one may conclude that the solubility of one solid in another is never exactly zero. On the other hand, one would generally expect that the solubility will be small unless the components resemble one another (as do the metals), or form weakly-bound crystals. Therefore, it is useful to know that when there is no direct evidence for solid-solubility, one may neglect it without violating thermodynamic principles.

Technical Note No. 22 E. Manuscript received June 28, 1949.

* Institute for the Study of Metals, Univ. of Chicago, Chicago, Ill.

† J. W. Stout, L. Meyer, W. Band, T. Rosenqvist, O. J. Kleppa, the writer, and others.

[1] W. Hume-Rothery: *Jnl.* Inst. Metals (1926) XXXV, 295–307.

[2] J. S. Marsh: Principles of Phase Diagrams. McGraw-Hill Book Co., N. Y., 1935. pp. 93–4.

Kinetics of the Reactions of Titanium with O_2, N_2 and H_2

EARL A. GULBRANSEN* and KENNETH F. ANDREW*

Introduction

In a recent communication[14] we have reported on the kinetics of the reactions of zirconium with O_2, N_2 and H_2 as a function of the time, temperature and pressure variables. A systematic study was made and the results correlated with fundamental theories of gas-metal reactions. This paper will present a similar study for titanium.

Titanium and zirconium are members of the IV group of the periodic table and possess many similar physical and chemical properties as a result of their similar electronic configuration for the outer electrons. The two metals are relatively inert to both gas and liquid phase corrosion at room temperature. However, at moderate temperatures the metals become active and react readily with the common gases including O_2, N_2 and H_2 which are of interest in this study.

A study of the kinetics of these gas-metal reactions is of interest for three reasons: (1) to understand the rate of reaction of titanium and its role in the behavior of high temperature alloys; (2) to understand the practical difficulties of the reduction, refining and working of titanium; and (3) to correlate the data with fundamental theories of gas-metal reactions and crystal structure predictions.

Literature Survey

Several review papers[8] and books[42,43] exist on the preparation and properties of titanium and its alloys.

THE METAL

Titanium has, at room temperature, a hexagonal lattice of the zinc type. Hägg[19] gives a value of 2.953Å for the (*a*) axis, a value of 4.729 for the (*c*) axis and a density of 4.427 at 20°C. Burgers and Jacobs[5] have observed the transformation of the hexagonal to the body-centered cubic structure at 880°C and have established a value of 3.31 for the cube edge and a density of 4.31.

TITANIUM-OXYGEN

Carpenter and Reavell[6] using a pressure change method have studied the reaction at temperatures of 742° and 1000°C and for a pressure of one-fifth of an atmosphere. The probabilities for reaction are calculated from kinetic theory and they report a value of 10^{-5} for O_2 at 1000°C and 10^{-6} at 740°C.

The titanium-oxygen system has been investigated by Ehrlich.[10,11] Five phases are observed. Between (TiO_2 and $TiO_{1.90}$) an alpha-phase, consisting of a rutile lattice, is found. A beta-phase is observed between ($TiO_{1.80}$ and $TiO_{1.70}$). A gamma-phase is homogeneous between ($TiO_{1.56}$ and $TiO_{1.46}$) and has a structure of the corundum type. The delta-phase exists between $TiO_{1.25}$ and $TiO_{0.6}$ and has a sodium chloride structure. From $TiO_{0.42}$ to Ti the metal structure is observed.

The surface oxide films have been studied by Hickman and Gulbransen.[20] The rutile structure is observed in the temperature range studied, 300 to 700°C.

Cleveland Meeting, October 1949.
TP 2684 E. Discussion of this paper (2 copies) may be sent to *Transactions* AIME before Dec. 1, 1949. Discussion is tentatively scheduled for publication in May 1950.
Manuscript received April 22, 1949; revision received July 22, 1949.

* Westinghouse Research Laboratories, East Pittsburgh, Pa.

[14] References are at the end of the paper.

Three crystalline modifications of TiO_2 exist: rutile and anatase which are tetragonal and brookite which has an orthorhombic structure. Anatase is reported[36] to exist in two forms: I and II. Anatase II changes to anatase I at 642°C. Anatase I is stable up to 915°C where rutile becomes the stable modification. At 1300°C rutile transforms to brookite which melts at 1900°C. The monoxide, TiO, may be prepared from the dioxide by high temperature reduction with carbon or magnesium. Its melting point is 1750°C.

TITANIUM-NITROGEN

Carpenter and Reavell[6] report that at 1000°C a linear rate law is observed. The probability of reaction is given as 10^{-8} at 1000°C. Fast[12] has studied the solubility of nitrogen and its effect on the mechanical properties of the metal.

The crystal structure of TiN has been shown by several workers[2,21,44] to follow the sodium chloride structure. However, the calculated density is found to differ from the pycnometric value. This is studied by Brager[3,4] in detail. He has suggested that the titanium sites in the lattice are only partially filled at low temperatures. As the temperature of preparation is raised the vacant sites become occupied which expands the lattice and increases the hardness and density. An (*a*) value of 4.22Å is given for room temperature.

TITANIUM-HYDROGEN

The solubility and the crystal structures observed in this system have been reviewed in a recent book by Smith.[40]

Table 1 . . . Equilibrium Calculations on Titanium Reactions

Reaction	Literature References
(1) $Ti(s) + O_2(g) \rightleftarrows TiO_2(s)$	24, 25, 26, 32, 35, 37
(2) $2Ti(s) + CO_2(g) \rightleftarrows TiO_2(s) + TiC(s)$	CO_2 from 35
(3) $Ti(s) + \frac{1}{2}N_2(g) \rightleftarrows TiN(s)$	24, 26, 27, 38
(4) $3Ti(s) + 2CO(g) \rightleftarrows TiO_2(s) + 2TiC(s)$	CO from 35
(5) $Ti(s) + 2H_2O(g) \rightleftarrows TiO_2(s) + 2H_2(g)$	H_2O from 35
(6) $Ti(s) + 2CO_2(g) \rightleftarrows TiO_2(s) + 2CO(g)$	CO_2 and CO from 35
(7) $Ti(s) + C(s) \rightleftarrows TiC(s)$	24, 25, 26, 27, 35, 38

	(1)	(2)	(3)	(4)	(5)	(6)	(7)
t°C	$-\log p_{O_2}$	$-\log p_{CO_2}$	$-\log pN_2$	$-\log p_{CO}$	$-\log p \frac{H_2O}{H_2}$	$-\log p \frac{CO_2}{CO}$	$+\log K$
25	155.7	128.7	107.6	94.9	37.8	32.8	41.3
200	95.5	78.2	65.2	57.2	23.4	21.1	26.4
400	64.8	52.8	43.7	37.9	16.1	15.0	18.8
600	48.3	39.1	32.1	27.3	12.2	11.8	14.5
800	38.0	30.9	24.8	22.1	9.8	9.8	12.2

Systematic studies of the adsorption have been made by Huber, Kirschfeld and Sieverts[22] and by Kirschfeld and Sieverts[29] up to temperatures of 1000°C and at various pressures. The results show the formation of two phases of variable composition, an alpha and a beta phase. Hägg[19] has made an X ray crystal structure investigation of this system. The alpha phase is found to have the same structure as titanium and is homogeneous up to 33 at. pct of hydrogen. The beta phase is homogeneous from 50 at. pct to 66.7 and has a face-centered cubic structure.

Equilibria Calculations on the Reactions of Titanium with Gases

Titanium reacts with many of the common gases, with the exception of the inert gases, to form stable compounds. The chemical equilibria of these reactions may be calculated when the reaction products are TiO_2, TiN or TiC. Data on the free energy of formation of the hydride are not available.

Table I shows the reactions which are considered in this work together with the results and the literature references for each reaction.

The logarithms of the gas pressure or pressure ratios are tabulated as a function of the temperature in °C for the several reactions. For the reaction to form TiC the equilibrium constant K is tabulated.

The results show the following: (1) TiO_2, TiN and TiC are stable at all temperatures calculated in this study and from a thermodynamic point of view titanium will remove O_2, N_2, CO and CO_2 at the lowest pressures used in modern vacuum technology; (2) the reaction of water and carbon dioxide to form the oxide and hydrogen and carbon monoxide respectively are possible up to 800°C and perhaps higher in vacuums of the order of 10^{-7} mm of Hg.

Apparatus and Method

BALANCE

The vacuum microbalance and auxiliary equipment used for all of the kinetic measurements have been described.[15,16] The sensitivity of the balance is 0.86 divisions per microgram and the weight change can be estimated to 0.3×10^{-6} g. The balance zero point is constant and the instrument is insensitive to pressure and small changes in the temperature of the surroundings.

VACUUM SYSTEM AND FURNACE TUBE

The vacuum system and furnace tube have been described.[15,17] The system is constructed of all glass and ceramic materials. The furnace tube is double walled and is made from synthetic zircon. Vacua of McLeod gauge pressures of 10^{-6} mm or lower can be achieved with these tubes at temperatures of 1175°C and perhaps higher. The difficulties associated with and methods for the measurement of pressure in furnace tubes at high temperatures have been considered in another work.[17]

GAS PURIFICATION

The purification of the oxygen, nitrogen and hydrogen is the same as previously described.[15] The source of nitrogen is specially purified nitrogen and is obtained from our Bloomfield Lamp Works. A mass spectrometer analyses of the gases used for the nitriding experiments showed oxygen to be present to about 0.01 pct (the limit of the sensitivity of the mass spectrometer for the gas sample and pressure used).

Method

The methods used have been previously described.[14,15,16,17]

SAMPLES

Two types of titanium samples are used for the measurements: commercial titanium of approximately 99 pct purity with 0.77 pct of carbon, and iodide titanium. Both samples were obtained from the Remington Arms Co. Although no detailed analysis of the iodide titanium is available it is probably of a high degree of purity. A spectrographic analysis of the commercial titanium showed impurities of silicon and of iron. No quantitative spectrographic information is possible for these impurities since standards of known analysis are not available.

The specimens are cut from 15 mil sheets of the metal and weigh 0.6840 g. They have surface areas of 9 to 10 cm². The specimens, unless otherwise noted, were abraded starting with number one grit and finishing with 4/0 paper. The last two stages of the abrading are carried out under purified kerosene to minimize formation of oxide films.

Discussion of Results

HIGH VACUUM REACTION

The reaction of titanium in high vacua must be carefully considered if the metal is to be maintained in an essentially film free condition. This problem has been discussed in a previous paper for the case of the zirconium reaction.[14] Titanium like zirconium acts as a getter for many gases at low pressures and elevated temperatures. This behavior makes the problem a difficult one.

Due to the thermodynamic stability of TiO_2 it is impossible to reduce the oxide by hydrogen. Thus, the practical solution to maintaining the titanium in a film free condition is the use of the best high vacua possible.

A number of studies show that titanium can be heated to the reaction temperature without formation of further oxide or other films. If iodide titanium is heated, for example, in a vacuum of 10^{-6} mm of Hg or lower no weight change of any kind is observed until a temperature of 550°C is reached. Above this temperature the specimen loses weight and at a temperature near 1000°C the rate of weight loss increases rapidly. This behavior is quite different from that observed for zirconium.[14] We conclude that titanium is not as efficient a getter as zirconium and that the metal can be heated without further film formation.

REACTION WITH OXYGEN

The reaction is studied as a function of the time, temperature and pressure and the results are presented in Fig 1, 2, 3 and 4. The weight gain in micrograms per cm^2 is plotted against the time in minutes. Assuming the ratio of real to measured area to be unity and the oxide to be TiO_2,[20] the thickness of the film in Angstroms is 58.5 times the weight gain in micrograms per cm^2. A scale of 1000Å is marked on the curves.

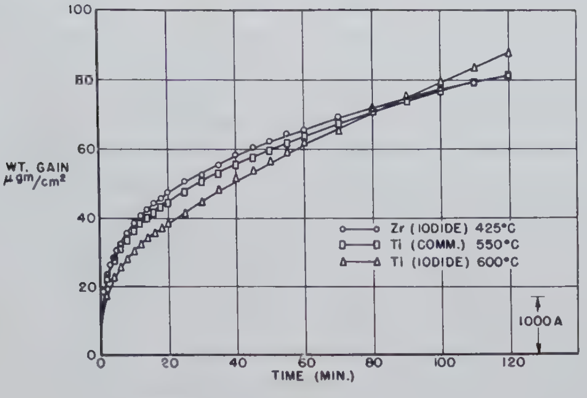

FIG 1—Reaction of Ti and Zr with O_2 7.6 cm O_2.

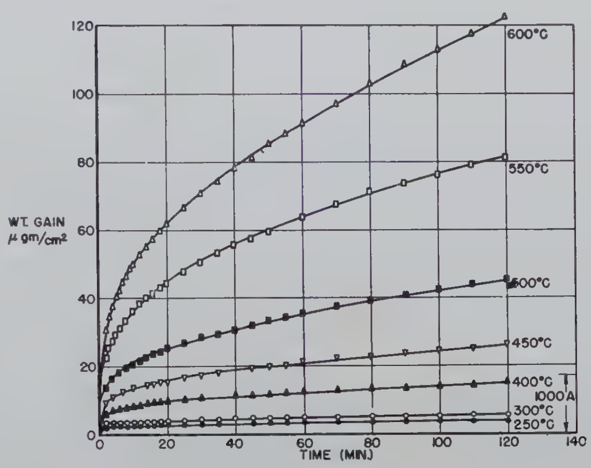

FIG 2—Reaction of Ti with O_2. Effect of temp. 250–600°C.

Time

Fig 1 shows the time course of two oxidation experiments on commercial and iodide titanium at 550 and 600° respectively. A comparison is made with the oxidation reaction of iodide zirconium at 425°C. The oxygen pressure is 7.6 cm for all experiments. The iodide titanium reacts at a lower rate than commercial titanium. The comparison with zirconium shows that titanium is less reactive at these temperatures.

The shapes of the oxidation curves are similar to those observed for other metals. A rapid reaction rate is observed in the early stages of the reaction which gradually decreases as the film thickens. In this sense the oxide film has protective properties.

Time and Temperature

Fig 2 shows the effect of temperature on the reaction over the temperature range of 250 to 600°C. A comparison of the 250°C curve with the 600°C curve shows a film thickness of 210Å after 2 hr of reaction at 250°C and a film of 7300Å at 600°C.

The effect of temperature on the reaction rate is very marked and appears to follow an exponential law.

Time and Temperature Equations

Three equations have been used extensively to explain the time variation of the oxidation rate. These are:

(1) the parabolic law[33,34,39,46]
$$W^2 = Kt + C$$
(2) the logarithmic law[41]
$$t = \beta(e^{w/\alpha} - 1) \text{ and}$$
(3) the linear law
$$W = K't + C$$

In the above equation W refers to the weight gain, t the time and K', K, C, α and β are constants.

In order to explain the temperature coefficient of the reaction rate Dunn[9] has applied the Arrhenius equation to the parabolic rate law constant K. Mott[33] has interpreted the physical significance of the activation energy for the various types of diffusion process of ions and electrons through an oxide film. To further understand the significance of the temperature dependence one of the authors[18] has applied the transition state theory[13] of chemical reactions and diffusion processes to the oxidation reaction. The parabolic rate law constant is given by the equation:

$$K = \frac{2kT}{h}\lambda^2 e^{\Delta S^*/R} e^{-E/RT}$$

ΔS^* and E are the entropy and energy of activation, λ, the interatomic distance between diffusional states, k is Boltzman's constant and h is Planck's constant. The equation is useful since both ΔS^* and E can be calculated. ΔS^* is the probability or steric factor for a given reaction.

Time and Temperature Correlation

Plots of the weight gain vs. the logarithm of the time show smooth curves of increasing slopes and indicate that the logarithmic law does not hold. A study of Fig 2 shows that the linear rate law is not applicable for the conditions studied.

Parabolic rate law plots are made for all of the data. In general the data deviate from the straight line during the initial stages of the reaction. However, good agreement is observed after 20 min. reaction time. This type of deviation has been predicted by Mott.[34]

Temperature Dependence and Activation Energy

The temperature coefficient of the reaction rate is one of the most important quantities to evaluate. If the reaction can be related to a mechanism it is possible to correlate the temperature coefficient of the reaction with an energy of activation. For the oxidation of titanium it is possible to calculate diffusion constants and an energy and entropy of activation since the data can be fitted to the parabolic rate law during a large part of the reaction.

Fig 3 shows the parabolic rate law

constants K in units of cm² per sec plotted against $\frac{1}{T}$. These parabolic rate law constants vary from 2.8×10^{-16} cm² per sec at 250°C to 6.27×10^{-13} at 600°C. In terms of Angstroms of film thickness, the above rates correspond to 1.7Å per sec at 250°C to about 80Å per sec at 600°C. The slopes are evaluated for the time range of 60 to 120 min.

Both commercial and iodide titanium experiments are included in Fig 3. Each group appears to fit a straight line relationship. The iodide titanium reacts at a slower rate. Below 350°C the data are scattered and the straight line relationship is no longer obeyed. An energy of activation of 26,000 cal per mol is calculated from the plot and the temperature independent factor $e^{\Delta S^*/R}$ evaluated from the expression derived for the parabolic rate law constant by the transition state theory.

Table 2 shows the values for the parabolic rate law constants and diffusion constants and the entropies, energies and free energies of activation of the rate determining process. The K values are related to thickness by the use of the density of the oxide and the stoichiometric ratio of oxygen in the oxide. A surface roughness ratio of 1 is assumed.

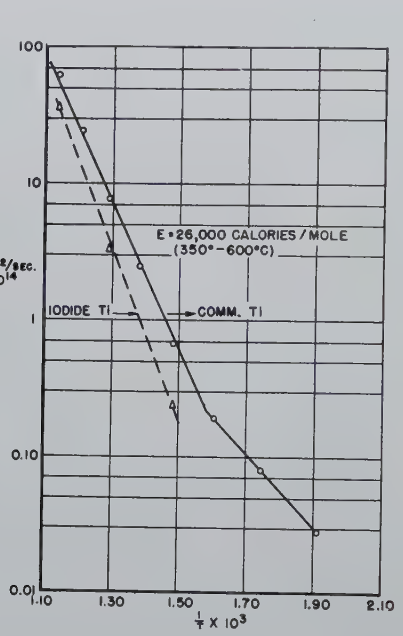

FIG 3—Reaction of Ti with O_2 log K vs $\frac{1}{T}$ 250–600°C.

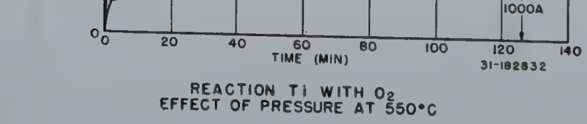

FIG 4—Reaction of Ti with O_2. Effect of pressure at 550°C.

Table 2 . . . Parabolic Rate Constants and Diffusion Constants Entropies, Energies and Free Energies of Activation for the Oxidation Process

t°C	K, cm² per sec	D_0, cm² per sec	ΔS* Cal per mol °C	E Cal per mol	TΔS* Cal per mol	ΔF* Cal per mol
350	0.190×10^{-14}	1.34×10^{-6}	−18.0	26,000	−11,200	37,200
400	0.667×10^{-14}	0.98×10^{-6}	−18.8	26,000	−12,100	38,100
450	2.43×10^{-14}	0.921×10^{-6}	−19.0	26,000	−13,700	39,700
500	7.70×10^{-14}	0.925×10^{-6}	−19.1	26,000	−14,800	40,800
550	24.73×10^{-14}	1.048×10^{-6}	−19.0	26,000	−15,600	41,600
600	62.7×10^{-14}	1.048×10^{-6}	−19.1	26,000	−16,700	42,700

The energy of activation of 26,000 cal per mol is higher than the value observed for the oxidation of zirconium,[14] namely 18,200. The entropies of activation are less negative than those observed for the oxidation of zirconium. ΔS^* varies from −18.0 to −19.1 cal per mol per °C for titanium oxidation while values of −23.1 to −25.2 are obtained for the zirconium reaction.

A comparison of the reaction rate at 400°C shows a parabolic rate constant K of 0.667×10^{-14} cm² per sec for the titanium oxidation and a K of 13.20×10^{-14} cm² per sec for the zirconium reaction. Iron at the same temperature has a K value of 0.409×10^{-14} cm² per sec or roughly equivalent to the titanium rate.

Calculation of Diffusion Constants

Let us assume with Wagner[47] and Mott[33] that the metal ions are diffusing through the oxide lattice together with electrons by one mechanism or another. If this is done we can calculate the diffusion constant K from the parabolic rate law constants of the expression, $D = K/2$. Thus, at 400°C, the value of D is calculated to be 0.334×10^{-14} cm² per sec and at 600°C a value of 3.14×10^{-13} cm² per sec. These values represent the coefficient of self diffusion of titanium in its oxide.

The mechanisms for self diffusion of titanium are as follows: (1) formation and diffusion of interstitial titanium ions and (2) formation and diffusion of titanium defects (absence of titanium ion in lattice). Calculations by Huntington and Seitz[23] have shown that for copper the diffusion of lattice defects is the more probable process. It is at present difficult to choose between the above mechanisms for titanium oxide since calculations have not been made for systems closely analogous to this one. However, the activation energy must be associated with the formation and diffusion of either interstitial ions or lattice defects.

Pressure Effect

The effect of pressure on the reaction at 550°C is shown in Fig 4. The pressure is varied by a factor of 100 from 7.6 cm to 0.76 cm of oxygen. The effect is largest for the thin film range. No simple relationship with the pressure has been determined. We conclude that the effect of pressure on the reaction rate is minor for the temperature and pressure range studied. This small effect is in agreement with the mechanism of metal ion diffusion. If oxygen atoms or ions diffuse through the film one might expect the rate to follow a square root function of the pressure for some pressure and temperature conditions.

REACTION WITH NITROGEN

The difficulties associated with the study of the kinetics of the nitrogen reaction on zirconium have been discussed in a previous paper.[14] These difficulties are the prevention of the high vacuum reaction with oxygen, water vapor, and others, and the prevention of secondary reactions by elimination of the impurities such as oxygen, hydrogen, and others in the nitrogen.

In this section the reactions of commercial titanium with purified lamp grade of nitrogen are studied in detail as a function of time, temperature and pressure.

The results are shown in Fig 5–8 and discussed in the following subsections. In all of the figures the weight gain in micrograms per cm² is plotted against the time and, where necessary, the temperature is given at the top of the graph.

Comparison of Nitrogen Reaction on Titanium and Zirconium

Fig 5 shows a comparison of the nitrogen reactions of the two preparations of titanium with the corresponding reaction for zirconium. The time course of the reactions for the iodide preparations of the two metals are practically identical at 600°C. The commercial preparation of titanium reacts at a greater rate. A purified lamp grade of nitrogen is used.

Time and Temperature

Fig 6 shows the time course of the reaction of commercial titanium with pure nitrogen for several temperatures. The reaction rate decreases as the reaction proceeds. The effect of temperature on the reaction rate is uniform and the rate of reaction appears to be an exponential function of the temperature. At 850°C a total reaction of 158 micrograms per cm² is found after 2 hr of reaction while at 550°C a total reaction of 6 micrograms per cm² is observed.

The shapes of the time curves are very similar to what one observes for the oxidation reaction. This leads one to apply the parabolic rate law expression to the nitride data. A plot of the square of the weight gain shows a straight line over the complete thickness range and indicates that the rate law $W^2 = Kt$ explains empirically the time course of the reaction. It is of interest to see if this rate law can be placed on a reasonable physical basis.

Van Liempt[45] in a study of the degassing of metals has solved the diffusion equation using an approximation method. The same method may be used for the reverse adsorption process. Van Liempt's equation is $Q/Q_0 = \frac{8}{d}\sqrt{\frac{Dt,}{\pi}}$ where Q is the quantity of gas evolved or taken up at any time t, Q_0, the original quantity of gas in the metal, and D, the diffusion coefficient. This expression gives the parabolic rate law, $\frac{W}{W_0} = K\sqrt{t}$. The temperature is involved in the solubility W_0 and in K which involves the diffusion constant D. Since both W_0 and K are temperature dependent it is impossible until

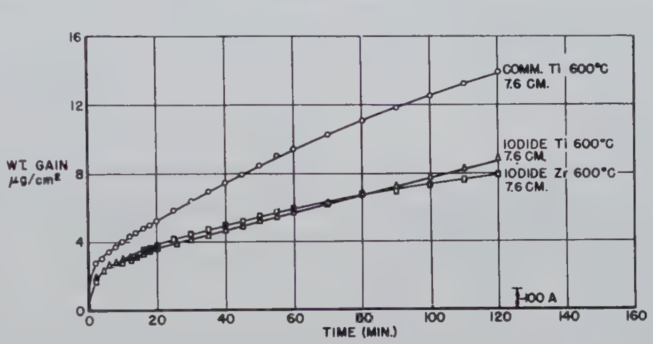

FIG 5—Reaction of Ti and Zr with pure N_2 600°C.

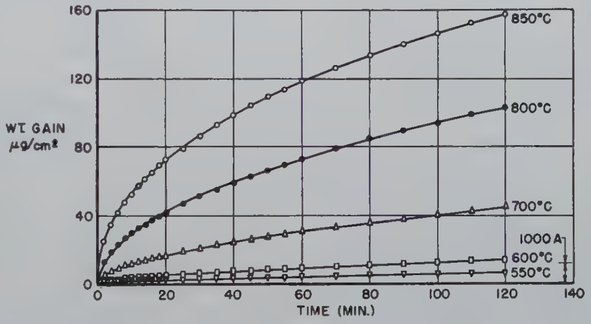

FIG 6—Reaction of Ti with pure N_2 550–850°C.

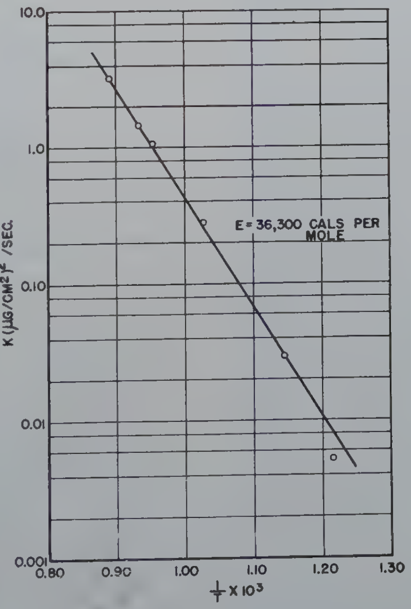

FIG 7—Reaction of Ti with pure N_2 log K vs. $\frac{1}{T}$.

data on W_0 are available to calculate D and the energy of activation E although an empirical energy of activation may be calculated.

Table 3 shows the values of the parabolic rate law constants for the temperature range of 550 to 850°C and Fig 7 shows a logarithmic plot of the parabolic rate law constant against $\frac{1}{T}$. A straight line is found for the temperature range of 550 to 850°C. An empirical energy of activation of 36,300 cal per mol is calculated. This can be compared to a value of 39,200 cal per mol obtained for the corresponding reaction with zirconium. This value is considerably higher than the energies of activation found for the oxidation process on most metals.

Table 3 . . . Parabolic Rate Law Constants Reaction Comm. Titanium with Nitrogen

t°C	T°K	$\frac{1}{T} \times 10^3$	$\frac{k}{2}$ (g per cm²) per sec.
550	823	1.2151	5.28×10^{-15}
600	873	1.1453	2.97×10^{-14}
700	973	1.0276	2.78×10^{-13}
775	1048	0.9542	1.08×10^{-12}
800	1073	0.9329	1.460×10^{-12}
850	1123	0.8904	3.2×10^{-12}

E = 36,300 cal per mol

Pressure

Fig 8 shows the effect of pressure on the time course of the nitride reaction at a temperature of 800°C. The pressure is varied from 7.6 cm to 0.076 cm, or by a factor of 100. Although the rate of reaction does vary with pressure the overall effect is small when compared to the predictions of the linear or square root law.

The influence of pressure on the permeability of metals to gases has been discussed by Barrer[1] and by the authors in a previous paper.[14] Two possible permeation rate-pressure equations have been used to explain the data. These are: (1) the linear rate law which is based on a mechanism of activated diffusion without dissociation and (2) the square root law which is based on a mechanism of activated diffusion with dissociation. The second type usually accounts for the permeation of gases through metals.

The pressure dependence of the reaction rate is not explained by either of the rate expressions. This indicates that the solubility term W_0 is not pressure dependent. A similar result is found for the nitrogen reaction on zirconium.[14] One explanation is that a nitride film is formed on the metal and that this film dissolves into the metal, the thickness of this film depending upon the relative rates of reaction and solution. This nitride film is not observed by visual and electron diffraction studies after removing the nitrogen and cooling at room temperature. The presence of the nitride film prevents the gas pressure from exerting its normal effect on the solubility.

REACTION WITH HYDROGEN

The reaction is studied as a function of time, temperature and pressure and a comparison is made with the hydrogen reaction on zirconium. The stability of the reaction product is studied as a function of the temperature under high vacuum conditions. Fig 9 to 14 show the results. The hydrogen is prepared by diffusion through a palladium tube after a preliminary purification.

Fig 9 shows a preliminary study of the reaction of commercial titanium with hydrogen at 2.0 cm pressure as a function of the temperature. The reaction appears to start at a temperature of about 290°C and the rate of reaction increases rapidly with temperature. Visual and electron diffraction analyses of the specimen showed no evidence of a surface film after cooling and it is assumed that the hydrogen is dissolving in the metal to form a compound or stable complex. The specimen loses weight on evacuating the hydrogen atmosphere. This indicates that the reaction product is unstable to a vacuum of 10^{-6} mm of Hg at a temperature of 400°C. This will be discussed in more detail later.

Time and Temperature

It is of interest to examine the time behavior of the reaction rate. Typical

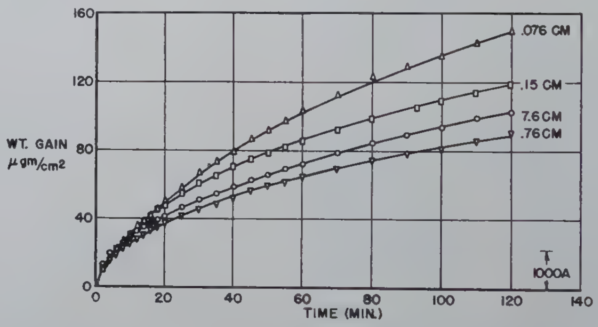

FIG 8—Reaction of Ti with pure N_2. Effect of pressure 800°C.

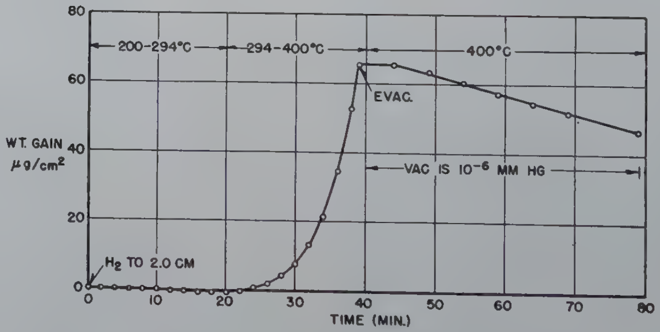

FIG 9—Reaction of Ti with H_2 and stability of hydride.

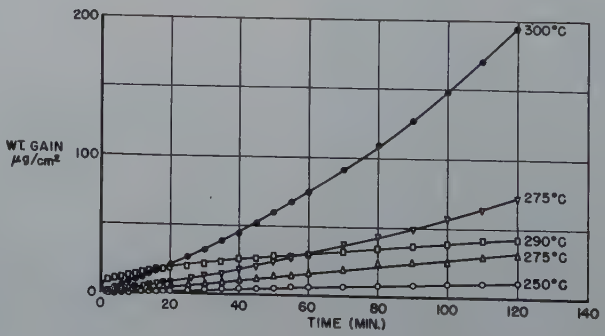

FIG 10—Reaction of Ti with H_2. Effect of temperature.

curves are shown for commercial titanium in Fig 10 for temperatures of 250 to 300°C. At temperatures of 250°C the reaction rate $\frac{dW}{dt}$ is constant with time. At a temperature of 300°C the reaction rate $\frac{dW}{dt}$ increases with the time. Some difficulty is observed in obtaining reproducible results. This may be due to the high sensitivity of the hydrogen type of reaction to impurities in the metal, to the presence of surface film, and to the lack of uniform metal specimens.

The shape of the time curves indicate that the reaction does not obey the parabolic rate law which is predicted by the equation of van Liempt[45] and discussed on p. 745. If it is considered that cracks and blisters are forming in the metal during reaction, the time course of the reaction cannot be expected to follow the parabolic law.

The 300°C curve after 2 hr of reaction shows a hydrogen uptake corresponding to the formula $TiH_{0.13}$. Hägg[19] has shown that titanium will take up hydrogen to 66.7 at. pct or to a formula TiH_2. We have not attemped to check this value.

A comparison of the reactions of titanium and zirconium with hydrogen is shown in Fig 11. Both the iodide and commercial forms of titanium react more rapidly than the iodide form of zirconium. The shapes of the curves are different in the sense that $\frac{dW}{dt}$ decreases with time in the zirconium reaction and increases in the titanium reaction. In regard to the hydrogen reaction titanium appears to react more rapidly on a simple weight gain basis than zirconium.

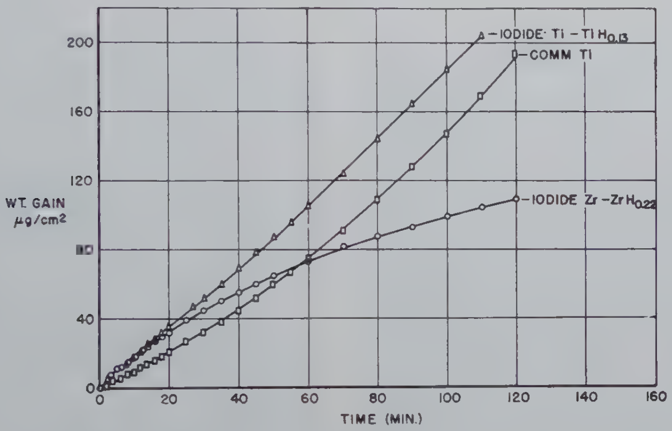

FIG 11—Reaction of Ti and Zr with H_2 300°C 2.1 cm H_2.

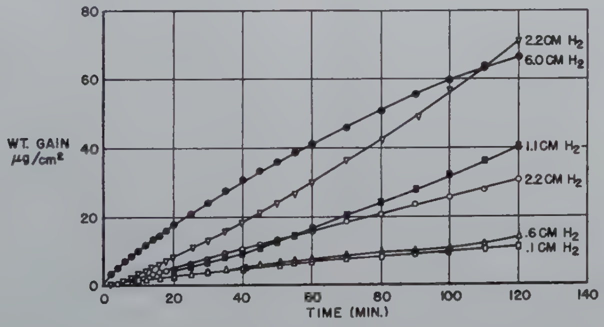

FIG 12—Reaction of Ti with H_2. Effect of pressure.

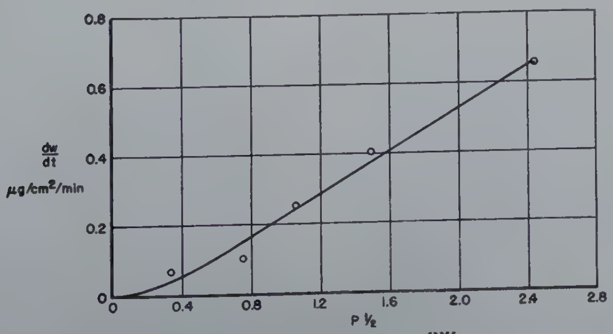

FIG 13—Reaction of Ti with H_2. Plot of $\frac{dW}{dt}$ vs $P^{1/2}$ 275°C.

Temperature

A study of the reaction with hydrogen as a function of the temperature is necessary if the details of the reaction mechanism are to be worked out. However, the data are not of sufficient reproducibility to give a good value for the temperature coefficient. Qualitatively, very little reaction occurs at 250°C while at 300°C a very rapid reaction is observed.

Pressure

The permeation of gases through metals has been summarized by Barrer[1] and discussed briefly here, under "Reaction with Nitrogen." If the reaction is limited by a process involving activated diffusion with dissociation of the hydrogen molecules the reaction rate may be expressed by the following:

$$\frac{dW}{dt} = kp^{1/2} e^{-b/T}.$$

This formula predicts that at constant temperature the reaction rate should follow the expression:

$$\frac{dW}{dt} = Ap^{1/2}.$$

Fig 12 shows the effect of pressure on the reaction rate at 275°C for a pressure range of 6.0 cm to 0.1 cm of H_2. The reaction is very sensitive to pressure although the 2.2 cm experiments are in disagreement with each other. The pressure effect for the hydrogen reaction is very different from the pressure effect in the nitrogen reaction.

Fig 13 shows a plot of the initial reaction rates $\frac{dW}{dt}$ as a function of the square root of the pressure. The two values of $\frac{dW}{dt}$ for the 2.2 cm pressure are averaged and included in the plot. Fair agreement with the square root law is found. This correlation shows that the diffusion of hydrogen into the metal is mainly by atoms of hydrogen rather than molecules and confirms the square root law.

Stability

Fig 14 shows the stability of the hydrogen complex with titanium as a function of temperature in a vacuum

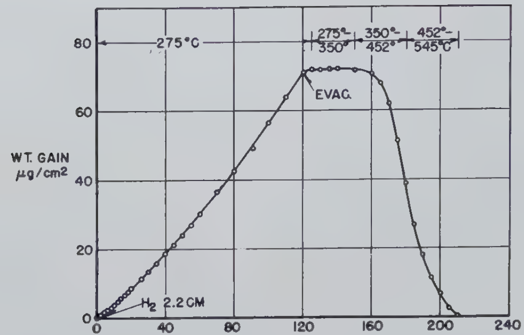

FIG 14—Reaction of Ti with H_2 275°C 2.2 cm H_2 stability curve.

of 10^{-6} mm of Hg. Hydrogen is added to titanium at a temperature of 275°C and a pressure of 2.2 cm of H_2. The reaction product is stable at 275°C in a vacuum of 10^{-6} mm of Hg. The temperature is gradually raised. At a temperature of about 350°C the hydrogen starts to be evolved. All of the hydrogen is removed from the metal if the heating is continued. This experiment confirms the results shown in Fig 9. At 400°C in this experiment the hydrogen is evolved at an appreciable rate. A comparison may be made with the stability of the zirconium-hydrogen reaction product.[14] In that case hydrogen started to be evolved at a temperature of about 435°C. This indicates that the titanium-hydrogen complex is less stable than the corresponding zirconium-hydrogen complex.

Conclusions

A study of the thermodynamic equilibria of the several gas phase reactions of titanium with oxygen, nitrogen, water vapor, carbon monoxide and carbon dioxide show the following results: (1) TiO_2, TiN and TiC are stable at all temperatures up to the transition temperature calculated in this study; (2) from a thermodynamic point of view titanium will remove O_2, N_2, CO and CO_2 at the lowest pressures used in high vacuum technique; and (3) the reactions of water and carbon dioxide to form the oxide and hydrogen and carbon monoxide respectively are possible up to 800°C and perhaps higher in vacuums of the order of 10^{-7} mm of Hg.

The oxidation reaction follows a modified parabolic rate law. An energy of activation of 26,000 cal per mol is calculated from the temperature dependence of the parabolic rate law constants. Diffusion coefficients and entropies of activation for the reaction process are calculated. The oxygen reaction is found to be insensitive to pressure.

The nitrogen reaction is of special interest. The time course of the reaction can be fitted empirically to a parabolic rate law. The temperature dependence of the parabolic rate law constants is used to calculate an empirical energy of activation of 36,300 cal per mol. The effect of pressure is small. The nature of the reaction is believed to be one involving the solution of nitride into the metal under the conditions of a nitride film present on the surface. The nitride is found to be stable to temperatures of at least 900°C.

The reaction with hydrogen obeys the square root of pressure law. In contrast to the nitrogen reaction a film is not formed during the reaction and it is shown that hydrogen is probably diffusing into the titanium lattice as atoms. The hydrogen reaction product is stable in a vacuum of 10^{-6} mm of Hg to a temperature of about 350°C.

References

1. R. M. Barrer: Diffusion In and Through Solids: University Press, Cambridge, England, 1941.
2. K. Becker and F. Ebert: *Ztsch. f. Phys.* (1925) **31**, 268–272.
3. A. Brager: *Acta physicochimica* U.R.S.S. (1939) **10**, 593–600.
4. A. Brager: *Acta physicochimica* U.R.S.S. (1939) **11**, 616–632.
5. W. G. Burgers, and F. M. Jacobs: *Ztsch. Kristallogr.* (1936) **A 94**, 299.
6. L. G. Carpenter and F. R. Reavell: *Metallurgia* (1948) **39**, 63–65.
7. P. Chevenard and X. Wache: *Rev. de Metall.*, May/June 1948, p. 121–128.
8. R. S. Dean and B. Silkes: Information Circular Metallic Titanium and Its Alloys. U. S. Bur. of Mines I.C. 7381 Nov. 1946.
9. J. S. Dunn: *Jnl.* Chem. Soc. (1929) 1149–1150.
10. P. Ehrlich: *Ztsch. Elektrochem.* (1939) **45**, 362.
11. P. Ehrlich: *Ztsch. anorg. allgem. Chem.* (1941) **247**, 53–64.
12. J. D. Fast: *Metallwirtschaft* (1938) **17**, 641–644.
13. Glasstone, Laidler and Eyring: The Theory of Rate Processes. McGraw Hill (1941).
14. E. A. Gulbransen and K. Andrew: AIME *Trans.* **185**, *Jnl. of Metals*, Aug. 1949, 515.
15. E. A. Gulbransen: *Trans.* Electrochem. Soc. (1942) **81**, 187–197.
16. E. A. Gulbransen: *Rev. Sci. Instr.* (1944) **15**, 201–204.
17. E. A. Gulbransen and K. Andrew: *Jnl. of Phys. and Coll. Chem.* (1949) **53**, 690–711.
18. E. A. Gulbransen: *Trans.* Electrochem. Soc. (1943) **83**, 301–313.
19. G. Hägg: *Ztsch. phys. Chem.* (1930) **B 11**, 433–454.
20. J. W. Hickman and E. A. Gulbransen: *Jnl. Anal. Chem.* (1948) **20**, 158–165.
21. W. Hofman and A. Schroeder: *Arch. Eisenhuttenwesen* (1936) **10**, **65**.
22. H. Huber, L. Kirschfeld and A. Sieverts: *Ber. Deutsch. chem. Ges.* (1926) **59**, 2891–2896.
23. H. B. Huntington and F. Seitz: *Phys. Rev.* (1942) **61**, 315, 325.
24. F. M. Jaeger, E. Rosenbohm and R. Fonteyne: *Proc.* Acad. Sci. Amsterdam (1936) **39**, 442–452.
25. K. K. Kelley: Bur. of Mines Bull. No. 371 (1934) Washington.
26. K. K. Kelley: I and E. C. (1944) **36**, 865–866.
27. K. K. Kelley: Bur. of Mines Bull. No. 407 (1937) Washington.
28. K. K. Kelley: Bur. of Mines Bull. No. 434 (1941) Washington.
29. L. Kirschfeld and A. Sieverts: *Ztsch. phys. Chem.* (1929) **A, 145**, 227–240.
30. B. Lustman: *Trans.* Electrochem. Soc. (1943) **83**, 301–313.
31. B. Lustman: Private Communication.
32. H. J. McDonald and H. Seltz: *Jnl. Am. Chem. Soc.* (1939) **61**, 2405–2407.
33. N. F. Mott: *Trans.* Faraday Soc. (1940) **36**, 472.
34. N. F. Mott: *Jnl.* Inst. Metals (1946) **72**, 367–380.
35. Nat'l Bur. of Standards Tables of Selected Values of Thermodynamic Properties, Washington.
36. Nat'l Res. Council, Bull. 107 (June 1943).
37. B. F. Naylor: *Jnl. Am. Chem. Soc.* (1946) **68**, 1077–1078.
38. B. F. Naylor: *Jnl. Am. Chem. Soc.* (1946) **68**, 370–371.
39. N. B. Pilling, and R. E. Bedworth: *Jnl.* Inst. Metals (1923) **29**, 529–582.
40. D. P. Smith: Hydrogen in Metals. Univ. of Chic. Press, Chicago, Ill. (1948).
41. G. Tammann and W. Köster: *Ztsch. anorg. Allgem. Chem.* (1922) **123**, 196.
42. W. M. Thornton: Titanium. The Chem. Catalog Co. Inc., N. Y., 1927.
43. A. E. van Arkel: Reine Metalle. Julius Springer, Berlin, 1939.
44. A. E. van Arkel: *Physica* (1924) **4**, 286–301.
45. J. van Liempt: Quoted by Barrer (Ref. 1).
46. C. Wagner and K. Grünewald: *Ztsch. phys. Chem.* (1938) **40 B**, 455.
47. C. Wagner: *Ztsch. f. Elektrochem.* (1941) **47**, 696–704.
48. C. Wagner: Private Communication.

Structure of Diborides of Titanium, Zirconium, Columbium, Tantalum and Vanadium[*]

JOHN T. NORTON,[†] Member AIME, H. BLUMENTHAL,[‡] and S. J. SINDEBAND,[‡] Member AIME

The interstitial phases formed by the transition elements with carbon, nitrogen and boron constitute a unique class of substances which are of considerable technical interest because of their well developed metallic properties and their high hardness and melting points. They are also of interest from the point of view of structure.

It was pointed out by Hägg[1] some years ago that the principal factor determining these structures was the relative sizes of metal and metalloid atoms. He predicted that if the ratio of the radii of metalloid to metal atoms was less than 0.59, the metal atoms would be arranged in a close-packed fashion of relatively simple type. This prediction has been amply confirmed. It appears, however, that this specification applies most generally to those structures in which the metalloid atoms occupy isolated positions in the lattice and there is no tendency for strong binding between the metalloid atoms themselves. The series of borides of the type MeB_2 formed from the transition elements of the fourth (Ti, Zr) and fifth (V, Cb, Ta) groups of the periodic table provide an opportunity to investigate this situation further. If one takes as a basis the radius of 0.87 Å for the boron radius and the Goldschmidt values for the metal atoms in 12 coordination, then the radius ratio varies from 0.54 for zirconium to 0.64 for vanadium, which latter is considerably greater than Hägg's limit of 0.59. It was of interest, therefore, to see if these five elements would form borides of the MeB_2 type and have simple isomorphous structures.

When this investigation was initiated, relatively little information had been published on the structure of this group of borides. McKenna[2] reported the preparation of ZrB_2 by a carbon reduction process. Its structure was hexagonal and the approximate lattice constants were given as $a = 3.15$ Å, $c = 3.53$ Å. Ehrlich[3] reported the structure of TiB_2 as being of the C 32 type with $a = 3.02$, $c = 3.21$ and $c/a = 1.06$ Å. Recently, Kiessling[4] published the results on ZrB_2, showing it to be one in which the metal atoms are arranged in a simple hexagonal lattice with the boron atoms in flat sheets, midway between the layers of metal atoms. The structure is C 32 type with $a = 3.169$, $c = 3.530$ and an axial ratio $= 1.11$ Å. He also states that CbB_2 and TaB_2 are isomorphous with ZrB_2.

Preparation of Borides

The borides of titanium, zirconium, columbium and tantalum were made by the electrolysis of fused salt baths after the method described by Andrieux.[5] The bath, totalling about 6500 g in each case had the following general composition: Metal Oxide + B_2O_3 + CaO + CaF_2. The actual proportions of the ingredients were determined for each individual case.

Although Andrieux reports the preparation of vanadium boride by the same electrolytic method, several attempts proved unsuccessful. However, it was possible to prepare VB_2 by the carbon reduction method used by McKenna to produce ZrB_2. The mixture consisted of $V_2O_5 + 6\,B_2O_3 + 11\,C$ and the reduction was carried out in an induction heated graphite crucible. This method proved satisfactory for ZrB_2 and TiB_2 and undoubtedly the others could be made in the same way.

The borides, which were all in the form of fine gray metallic crystals from the electrolytic bath or gray powders from the reduction process, were carefully separated from other constituents and analyzed chemically for metal and boron content. The densities of the boride powders were measured using a standard 10 cc pycnometer at 18°C and ethyl benzene proved to be the most satisfactory liquid for this purpose.

X Ray Technique

The boride crystals, as prepared, were too small for single crystal examination so that powder techniques were employed. Patterns of the finely ground borides were prepared, using the Norelco recording X ray spectrometer. The lines on these patterns were indexed with the aid of Hull-Davy charts and the approximate dimensions

---

Cleveland Meeting, October 1949.
TP 2689 E. Discussion of this paper (2 copies) may be sent to *Transactions* AIME before Dec. 1, 1949. Manuscript received May 2, 1949.

[*] Carried out under auspices of Office of Naval Research Contract N6-ONR-256 Task Order No. 1.

[†] Professor of Metallurgy, Massachusetts Institute of Technology, Cambridge, Mass.

[‡] American Electro Metal Corporation, Yonkers, N.Y.

[1] References are at the end of the paper.

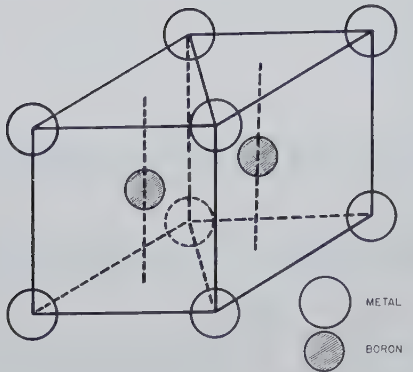

FIG 1—The unit cell of MeB_2 (C 32 type).
The open circles are metal atoms and the shaded circles are boron.

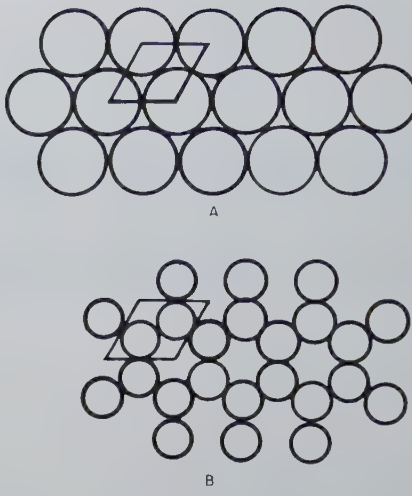

FIG 2—Sheets of metal atoms (A) and boron atoms (B) in the MeB_2 crystal.
In each case the unit cell is outlined.

of the unit cell obtained. Patterns were also made on the Phragmen focussing camera covering the angular range from 50 to 85°. It was found possible to index these lines readily and the cell constants were calculated more accurately. In order to prove the assumed structure, the density was calculated from the X ray data and compared with the measured density. Also, the diffraction line intensities were calculated and compared with those measured from the spectrometer records.

All lattice dimensions are reported in true Angstrom units and are considered correct within ±0.002 Å. Copper K alpha radiation was used throughout and the wavelengths used in the calculations were:

$$\alpha_1 = 1.54050 \text{ Å}$$
$$\alpha_2 = 1.54434 \text{ Å}$$

In calculating densities, the expression

$$\rho = 1.66020 \frac{\Sigma A}{V}$$

was used, where

ρ = density
ΣA = sum of at. wt of atoms in unit cell
V = volume of unit cell in Å^3

Results

The borides of titanium and zirconium proved to be quite pure, possibly because there was a considerable background of experience in their preparation and they were made in considerable quantities. The other three borides were somewhat less pure as indicated by a few faint extra lines in the diffraction patterns and by the chemical analysis. These impurities consisted of graphite and constituents of the electrolytic bath and it was difficult to make a complete separation. The diffraction lines of ZrB_2, TiB_2 and VB_2 were sharp but those of CbB_2 and TaB_2 were somewhat diffuse. Further work is necessary in order to decide whether or not this is an indication of a range of homogeneity.

Table 1 . . . Chemical Composition of Borides, Wt Pct

Substance	By Analysis		Theoretical for MeB_2	
	Me	B	Me	B
ZrB_2	80.0	18.9	80.7	19.4
CbB_2	81.3	16.9	81.2	18.8
TaB_2	89.2	10.5	89.4	10.6
TiB_2	68.9	30.1	68.9	31.1
VB_2	68.9	25.3	70.2	29.8

Table 2 . . . Lattice Constants and Density of Borides

Substance	Lattice Constants, Å			Density, G per Cm^2	
	a	c	c/a	Calc.	Obs.
ZrB_2	3.170	3.533	1.114	6.09	6.17
CbB_2	3.086	3.306	1.071	7.21	6.60
TaB_2	3.088	3.241	1.074	12.60	11.70
TiB_2	3.028	3.228	1.064	4.52	4.52
VB_2	2.998	3.057	1.020	5.10	4.61

The chemical analyses given in Table 1 show clearly, however, that the borides correspond to the formula MeB_2. The X ray diffraction data for all five borides is in complete agreement with a structure in which the metal atoms are arranged in a simple hexagonal lattice having an axial ratio slightly greater than unity. The lattice constants decrease with decreasing atom size and the axial ratio also decreases slightly. The lattice constants and densities are given in Table 2. The structure, therefore, corresponds to space group D^1_{6h} — C6/mmm with metal atoms at $0, 0, 0$; and boron atoms at ⅓, ⅔, ½; and ⅔, ⅓, ½. This is in agreement with Kiessling's results and shows that the five borides are indeed isomorphous.

Discussion of Results

From the structure as shown in Fig 1 it will be seen that the fundamental unit is a triangular prism of metal atoms with a boron atom at the center and that the prisms are packed together so as to share faces. From another point of view, the metal atoms are arranged in layers, parallel to the basal plane with the atoms in each layer having a close-packed arrangement, each metal atom with six equidistant neighbors in the plane and two neighbors, above and below, at slightly greater distance. The boron atoms are also arranged in flat sheets midway between the metal atom layers and each boron atom has three close neighbors. This is indicated in Fig 2. It thus appears that there would be strong boron-boron binding in such a structure.

From the point of view of close-packed interstitial structures, it is of interest to observe how the lattice dimensions change with metal atom

Table 3 . . . Calculated Lattice Dimensions in Å

Substance	Metal to Metal in Sheet	Boron to Boron in Sheet	Metal to Boron	Separation of Sheets	Metal to Metal in Pure Metal
ZrB_2	3.17	1.83	2.54	3.53	3.17
CbB_2	3.09	1.79	2.43	3.31	2.85
TaB_2	3.09	1.79	2.41	3.24	2.85
TiB_2	3.03	1.75	2.38	3.23	2.92
VB_2	3.00	1.73	2.31	3.06	2.63

size and these values, given in Table 3, afford some basis for speculation. All of these dimensions decrease with decreasing metal atom size. Perhaps it is simplest to consider the two extreme cases. In ZrB_2, the distance of closest approach (D.C.A.) of the metal atoms in the metal atom sheet is the same as is the case in metallic zirconium. The hole in which the boron atom is placed is limited in size both by the neighboring boron atoms and by the metal atoms. This hole is larger than the normal boron radius of 0.87 Å but it appears that the boron atom must fill it, first because this is generally true in interstitial phases and secondly because the separation of the metal atom sheets is considerably greater than would be expected from the metal atoms alone. A boron radius of about 0.92 Å is consistent with this structure. The metal atoms are in contact with one another in the sheet and the boron atoms are in contact with one another and with their metal neighbors giving a close packed arrangement.

On the other hand, in VB_2 the D.C.A. of the vanadium atoms in the metal sheet is considerably greater than in vanadium metal. If the metal sheet is close packed, the boron hole is limited by the metal atoms to a radius of about 0.81 Å which probably is too small. If the vanadium atoms are not closely packed and have the same size as in the metal, then the boron hole is limited to a radius of 0.87 Å by the boron neighbors and by the metal neighbors to about 0.91 Å. Thus it seems again as if the boron atoms are essentially in contact with both metal and boron neighbors but that the packing in the metal sheets has been loosened and as a result, the separation of the metal sheets has decreased. Kiessling[4] has reported that CrB_2 is isomorphous with the borides discussed here and it would be very interesting to know the lattice constants, for chromium is considerably smaller than vanadium and the radius ratio is 0.68.

Table 4 . . . Electrical and Thermal Properties of Borides

Substance	Electrical Resistivity Microhm-cm	Thermal Conductivity Cal per Cm per Sec °C at 200°C Avg	Wiedemann-Franz Ratio × 10^8
ZrB_2	38.8	0.0550	213
TiB_2	28.4	0.0624	179

The results show that there is no discontinuity in the series as the critical value of 0.59 for the radius ratio is exceeded and emphasizes the fact that this limiting value should be considered specific only for phases in which the metalloid atoms are in isolated positions. That the radius ratio is not the only factor controlling structure is shown by the fact that tungsten and molybdenum, as shown by Kiessling,[6] do not form borides which are isomorphous with the series discussed here although the radius ratio has a value of 0.62. A similar situation exists in the monocarbides.

In view of the apparent boron to boron binding, it might be expected that the borides would be less metallic than, for instance, the carbides. However, this does not appear to be the case. Electrical and thermal conductivity measurements were made on ZrB_2 and TiB_2 in the form of bars sintered without binder to about 85 pct of theoretical density. The values are given in Table 4. It will be observed that the properties are excellent and in fact compare favorably with the pure metals themselves. Also, the Wiedemann-Franz ratio is quite normal. This indicates that normal metallic linkages predominate. When sufficient quantities of the other pure borides are available, these experiments will be extended.

Another interesting aspect of the borides is the possibility of metal atom replacement to form solid solutions. On the basis of limited experiments on the series ZrB_2-TiB_2 it appears that a continuous series of solid solutions can be formed, when the borides are mixed and heated together and that the lattice constants deviate only slightly in a negative direction from Vegard's Law. These experiments are also being extended.

Summary

1. The borides of Ti, Zr, V, Cb and Ta corresponding to the formula MeB_2 have isomorphous crystal structures with the metal atoms arranged in a simple hexagonal lattice having an axial ratio slightly greater than unity.
2. The structure is of the C 32 type, space group D^1_{6h} – C6 mmm, with metal atoms at *0, 0, 0* and boron atoms at ⅓, ⅔, ½ and ⅔, ⅓, ½.
3. The unit cell contains one molecule of MeB_2.
4. This structure corresponds to alternate layers of metal and boron atoms, parallel to the basal plane of the lattice.
5. As the metal atom size increases, both *a* and *c* dimensions of the lattice increase and the axial ratio also increases slightly.
6. The borides have well developed metallic properties.

Acknowledgments

The authors wish to express their appreciation to the Office of Naval Research for the support of this investigation and permission to publish the results. They also gratefully acknowledge the important assistance of Mr. A. S. Cohan of the American Electro Metal Corporation and Mr. Albert Mahfuz of the Department of Metallurgy, Massachusetts Institute of Technology.

References

1. G. Hägg: *Ztsch. Phys. Chem.* (1929) **B6**, 221.
   Ibid. (1931) **12**, 33.
2. P. McKenna: *Ind. and Eng. Chem.* (1936) **28**, 767.
3. P. Ehrlich: *Angew. Chem.* (1947) **59**, 163.
4. R. Kiessling: *Acta Chem. Scand.* (1949) **3**, 90.
5. L. Andrieux: *Ann. Chim.* (1929) **12**, 423.
   Comptes Rendus (1929) **189**, 1279.
6. R. Kiessling: *Acta Chem. Scand.* (1947) **1**; 893.

The Diffusion and Solubility of Carbon in Alpha Iron*

JAMES K. STANLEY,† Member AIME

Introduction

Knowledge of the diffusivity of carbon in the low temperature form of iron (alpha iron existing below 910°C) is at the moment of considerable interest in the study of the decomposition of austenite and martensite, the elastic after-effect,[1,2,3] the magnetic after-effect[4] and the decarburization of steel below 910°C. Information on the solubility of carbon in iron, and to a lesser extent its diffusion, is also important in consideration of such phenomena as blue-brittleness, temper-brittleness, "magnetic" aging, quench-aging, strain-aging, and possibly the yield point. In order to obtain more information on these subjects more fundamental knowledge is necessary. It is the purpose of this work to present data on the diffusion and solubility of carbon in the alpha iron.

The high temperature form of iron (gamma; face-centered cubic) existing above 910°C is capable of dissolving relatively large amounts of carbon, up to 1.7 pct at 1130°C, while the low temperature form (alpha, body-centered cubic) existing below 910° dissolves only a limited maximum amount of less than 0.02 pct carbon at 725°C, according to data obtained here. Since the solubility of carbon in the face-centered or gamma iron is large, relatively speaking, no great analytical difficulties have been encountered in the determination of the solubility lines[5] or of the diffusion of carbon.[6] The limited solubility of carbon in alpha iron offers difficulties because experimental procedures and analytical methods for low carbon contents below say 0.01 pct have to be more refined than techniques used for work with gamma iron. Because of the difficulties of applying conventional methods to the determination of the diffusion of carbon in alpha iron, virtually no work has been done on this subject. However, by proper refinement of the analytical method for small amounts of carbon, the determination of the diffusion coefficient can be made readily using modified procedures.

The solubility of carbon in alpha iron has been determined over a temperature range by various investigators, but the agreement among them is poor. The present investigation establishes the limits quite accurately. Information of this kind is useful in establishing the correctness of equilibrium diagrams but, more significantly, such information on maximum solubilities, especially when extended to alloyed ferrites, should be extremely important in the study of aging and related phenomena.

Literature

The literature existing on the diffusion, in particular, and on the solubility of carbon in alpha iron is not extensive. The data which exist are not of a high order of accuracy, much of them being in the realm of conjecture.

THE DIFFUSION OF CARBON IN ALPHA IRON

Whiteley[7] made the qualitative observation, using metallographic techniques, that the rate of diffusion of carbon at the A_1 (725°C) point was very rapid and that its diffusion was still rapid at 550°C.

Snoek,[4] studying the magnetic after-effect in high purity iron, arrived at the conclusion that the after-effect could be explained by the presence of small amounts of carbon diffusing under the influence of magnetostrictive strain (lattice distortion due to magnetic interaction).

In later work, Snoek[8] made an estimate of the ratio of carbon diffusion in alpha to its diffusion in gamma iron, and concluded that for a temperature of 910°C the ratio of D_α/D_γ was 2600. Polder,[9] basing his calculations of D on relaxation phenomena in the elastic after-effect, estimated that D_α is about $\frac{1}{3}$ of D_γ at 910°C (1183°K) and is about $\frac{1}{12}$ of D_γ at 727°C (1000°K). Polder's equation for the diffusion of carbon in alpha iron was calculated to be

$$D = 5.2 \times 10^{-4} e - \frac{18000}{RT} \text{ cm}^2 \text{ per sec}$$

Ham[10] obtained data for the diffusion and solid solubility of carbon in alpha iron at two temperatures by using one technique similar to that employed in this study. He found a D of 8.0×10^{-7} cm² per sec at 702°C and of 2.7×10^{-7} at 648°C.

THE SOLUBILITY OF CARBON IN ALPHA IRON

Although pearlite is absent in steels containing 0.06 pct,[11] 0.05 pct,[12] or 0.045 pct C,[13] it appears that the carbon in these steels cannot be in solution in ferrite. The solubility of carbon at the A_1 (725°C) point was first determined by Scott[14] on the basis of cooling curves, and was found to be between 0.03 and 0.04 pct C.

Tamura[15] by interpolating between the solubility of carbon in delta iron at 1400°C and in alpha at room temperature (assuming zero solubility) ar-

Cleveland Meeting, October 1949

TP 2679 E. Discussion of this paper (2 copies) may be sent to *Transactions* AIME before December 1, 1949. Discussion of Fall Meeting papers is tentatively scheduled for publication in May, 1950. Manuscript received April 4, 1949; revision received July 7, 1949.

---

* This paper is taken from a thesis submitted by James K. Stanley in September 1948 in partial fulfillment for the degree of Doctor of Philosophy in Metallurgical Engineering at the University of Pittsburgh.

† Research Metallurgist, Research Laboratories, Westinghouse Electric Corporation, East Pittsburgh, Pennsylvania.

[1] References are at the end of the paper.

rived at a solubility of carbon in alpha iron of 0.034 pct at 720°C. Whiteley[7] using the Eggertz (colorometric) test and metallography placed the limit of solid solubility at about 0.03 pct at 720°C. Koster[16] on the basis of the Eggertz (colorometric) test placed the maximum solubility of carbon in alpha iron at 0.04 pct at the A_1 and gave the variation of carbon solubility with temperature.

Dickie,[17] using electrical resistivity measurements, made estimates of the solid solubility of carbon in Armco iron and several alloy steels by measuring the change in resistivity between the quenched and tempered states. Assuming a change of one microohm-centimeter being equivalent to 0.053 pct carbon, a calculation from his data gives the following solubility in Armco iron: 500°C, 0.008 pct; 625°C, 0.0172 pct; 710°C, 0.0194 pct; 750°C, 0.0199 pct and at 850°, 0.0204 pct.

Whiteley[18] on the basis of metallographic work on Armco iron, pure iron, and electrolytic iron, concluded that the solubility of carbon was relatively constant to about 550°C, and then increased to the A_1. The line connecting the A_3 and A_1, he suggested, should be convex and gave one point (0.02 pct C at 870°C) to support this idea.

Smith,[19] using a carburizing technique, arrived at the solid solubility of 0.02 pct at 750°C and 0.0128 pct at 800°C. The unpublished work of Ham[10] has been mentioned; he found a solubility of 0.0185 pct at 702°C and 0.011 pct at 648°C.

In a recent work, Pennington[20] using a decarburizing technique, arrived at values of solid solubility of 0.025 pct C at 760°C, 0.02 pct at 790°C and 0.014 pct at 815°C.

Dijkstra,[21] making internal friction measurements on high purity iron, arrived at the following set of solubilities at the indicated temperatures:

°C	250	400	450	500	550	600	650	700	710
Pct	0.001	0.002	0.003	0.004	0.007	0.01	0.012	0.016	0.02

Ziegler[22] indicates that the presence of oxygen decreases the solubility of carbon.

MAGNITUDE OF THE *A* AND *Q* VALUES IN THE DIFFUSION EQUATION

A knowledge of the magnitude of the frequency factor, A, in cm² per sec and the activation energy, Q, in gram-cal per gram-atom, are of importance in the study of variation of the diffusion coefficient with temperature.

Estimates of the Q values for the diffusion of carbon, other than those mentioned by Snoek[8] and Polder,[10] have been made. On the basis of spheroidization rates of cementite in pearlite Bailey[23] assigned a value to Q of 66,000 but this is more likely the heat of activation for spheroidization than for the diffusion of carbon. Richter[24,25] found an activation energy Q of about 20,000 in his work on the magnetic and elastic after-effects; Snoek[4] attributed his activation energy to the diffusion of carbon.

Ham[10] by actual, though limited, experiments found A and Q values of 165 cm² per sec and 37,000 gram-cal per gram-atom, respectively.

Experimental

Two methods were used in determining the diffusion of carbon in alpha iron. The first or Van Orstrand-Dewey[26] method consisted of diffusing carbon from a saturated "well" into an essentially carbon-free sample. The other or Grube[27] method consisted of diffusing carbon from a higher carbon to a lower carbon sample with both materials being in the entirely ferritic phase. Both methods are indicated schematically in Fig 1.

THE VAN ORSTRAND-DEWEY METHOD

The Van Orstrand-Dewey method can be used successfully to determine the diffusion coefficient below 725°C in the following manner (above 725°C this method no longer applies for reasons cited):

Two cylinders, one of high carbon corresponding to a composition close to the eutectoid, and the other essentially carbon-free, were welded together into what is called a diffusion couple. This diffusion couple is then annealed to diffuse the carbon across the weld or interface. After the diffusion anneal, the distribution of carbon with respect to the interface is determined, the concentration-penetration curve is plotted, and the curve is analyzed mathematically for the diffusion coefficient.

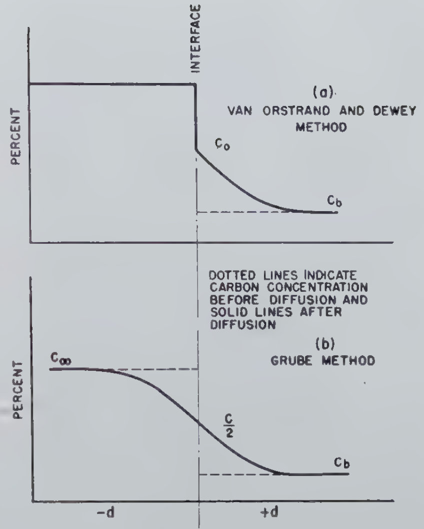
INTERFACE
PERCENT
(a)
VAN ORSTRAND AND DEWEY METHOD
C_o
C_b
DOTTED LINES INDICATE CARBON CONCENTRATION BEFORE DIFFUSION AND SOLID LINES AFTER DIFFUSION
(b)
GRUBE METHOD
PERCENT
C_∞
$\frac{C}{2}$
C_b
-d
+d

FIG 1—Schematic representation of penetration curves from which the diffusion coefficient is calculated.

Below a temperature of 725°C, the high carbon side of the couple corresponds metallographically to fine pearlite in which the carbon is available in large concentration in carbides and which can be rapidly transmitted to the diffusion interface due to the high rate of diffusion of carbon in the ferrite lamallae. This diffusion of carbon, as shall be seen subsequently, is of the order of a hundred times faster in ferrite than it is in austenite. In this case the solution of the diffusion equation is assumed to apply because the carbon-rich side behaves as if the carbon concentration on that side of the couple were constant.

Above 725°C the Van Orstrand-Dewey solution cannot be applied because the carbon concentration on the high carbon side is not constant. Actually the diffusion of carbon in austenite is considerably slower than that in alpha iron and hence the carbon is depleted from the austenite at the interface giving rise to a gradient; also the position of the interface probably changes. For these reasons the boundary conditions which satisfy the differential equation applicable to the Van Orstrand-Dewey no longer apply.

THE GRUBE METHOD

This method, used so frequently in diffusion studies, depends on the diffusion of solute atoms in high concentration across an interface into a sample of lower concentration. In the present case one depends upon the diffusion of carbon from a high-carbon ferrite, ("high" being used advisedly since the maximum carbon is about 0.02 pct at 725°C decreasing above and below this temperature) into a carbon-free ferrite. If the carbon in the high-carbon

Table 1 . . . Materials Used for Specimens

Material	C	O_2*	Si	Al	Cu	Mn	S	P	Others	Remarks
1	0.003–0.004	0.029	0.25	0.012	0.007	0.014	0.008	0.002		Deoxidized with Si and Al
2	0.005	0.013	0.01	0.092	0.009	0.003	0.009	0.002		Deoxidized with Al
3	0.005	0.055	0.006	0.005	0.008	0.005	0.001	0.002	0.048 Ni	Deoxidized with Al
4	0.001	0.038	0.007	0.006	0.003	0.013	0.006	0.001	0.38 Co	Vacuum melted; no deoxidation
5	0.006	0.03	0.21	0.010	0.007		0.008	0.002		Deoxidized with Si and Al
6	0.001	0.041	0.005				0.005	0.001		Air melted; no deoxidation
7	0.0044	0.030	0.007	0.008			0.006	0.002		Deoxidized with Si and Al
8	0.68	0.011	0.15				0.010	0.002		Deoxidized with Si
9	0.0054		0.004	0.009		0.023	0.008	0.001		Deoxidized with Al
10	0.001		0.004	0.001		0.011	0.005	0.002		Air melted; no deoxidation
11	0.43		0.06				0.007	0.002		Deoxidized with CaSi
12	0.0081		0.004	0.004	0.007	0.001				Air melted; no deoxidation

* Oxygen determined by the vacuum fusion method.

ferrite is purposely kept lower than the maximum solubility the diffusion can be checked above (this is an important advantage) and below 725°C.

SOLUBILITY OF CARBON IN ALPHA IRON

Information on solubility of carbon in alpha iron can be obtained by the Van Orstrand-Dewey method. As soon as the diffusion couple is annealed, there begins to be released at the interface from the high-carbon sample into the carbon-free sample a small amount of carbon which is assumed to be a measure of the carbon solubility at the diffusion temperature. This assumption appears to be valid. *Apriori*, it would seem that the carbon from a saturated "well" of carbon in iron should be released into a carbon-free ferrite at a concentration corresponding to its solubility limit, certainly at and below 725°C. Above that temperature the saturated "well" does not exist. A similar situation exists in the case of the diffusion of zinc in alpha-brass;[28] it has been shown that as zinc diffuses from α-brass into copper, it forms β-brass and at the α-β interface the zinc concentration is that corresponding to the limit of solid solubility given in the Cu-Zn diagram; for example, at 655°C the zinc released to the copper is 36.5 pct.

The solubility of carbon in alpha iron above 725°C can be studied by a decarburization method. In an early work Pennington[29] makes the statement that no carbon concentration gradient could be found in ferrite layers formed on the surface of 0.85 pct C steel decarburized between 725 and 910°C. This did not appear probable to the author who felt that a carbon gradient from zero at the immediate surface to the limit of solid solubility at the decarburization temperature must exist in the ferrite layer. If this were not the case one would have to look for another mechanism of decarburization.[30] The assumed lack of a gradient through the ferrite layer appeared to offer to Pennington a method of determining the solid solubility of carbon in ferrite. One could determine the solubility by analyzing the ferrite layer formed on decarburization assuming, of course, that the ferrite is saturated with carbon. Recently Pennington[20] used this method to determine the solubility at several temperatures.

Decarburization experiments were conducted to check Pennington's idea and it was found that if a high carbon alloy were decarburized and quenched from the decarburization temperature a carbon gradient in the ferrite layer existed. Even if the sample is slowly (furnace) cooled the carbon does not redistribute itself to give a uniform carbon distribution throughout the ferrite layer. The possibility exists that Pennington's analytical methods were not sensitive enough. His assumption that the carbon content of the ferrite layer should be a measure of the solid solubility cannot be considered valid. In the experiments performed by the author the limit of solid solubility by the decarburization method is the carbon concentration existing at the intersection of the decarburization curve in the ferrite with the carbon concentration in the austenitic region. Typical decarburization curves are given under *Results*.

COMPOSITION OF MATERIALS

Several materials were used for the diffusion and solubility studies. The basic material was electrolytic iron.

Ingots 12–15 lb were melted in an induction furnace and were either undeoxidized or deoxidized with silicon or aluminum or both. The high carbon materials for diffusion and decarburization were prepared by the addition of graphite to a silicon-killed melt. The materials were deoxidized for two reasons. One was that according to Ziegler[22] the carbon solubility was affected by oxygen in solution and the other was that an aluminum addition was desirable to prevent grain growth. Several series of ingots were prepared, analyzed, and the desired composition was then selected for samples. Analysis was carried out on drillings taken from the top and bottom of the ingots. When desirable compositions were found, the ingots were homogenized by heating to 950°C, holding about 15 hr and furnace cooling. The ingots were then forged at 850–900°C to one inch rounds. Sections of the rounds were analyzed at about one foot lengths and if the carbon contents of the ends of the round were in agreement, the section was used for samples. Table 1 gives the analysis of the materials used.

The possible effect of nitrogen on the diffusion of carbon was not investigated. The nitrogen content of sample 1, which was used extensively for the diffusion study, was 0.004 pct.

PREPARATION OF SPECIMENS

Cylinders of the various materials were machined, from forgings, to one-inch lengths and 0.75 in. diam and the ends were ground on a precision grinder.

Prior to the welding of the cylinders one of the faces of each was ground on several grades of metallographic paper finishing with 3/0. The cylinders were then welded on a welding machine in a hydrogen atmosphere, using 1500 lb load and 50 pulses of current (9000 amp). The welding conditions were kept as constant as possible to give identical samples. The region of the weld interface was probably heated to about 1000°C.

After the cylinders were welded they were cooled in hydrogen till black and were removed and quenched in water. The first couple welded by this procedure was tested for sufficiency of the weld. The one end of the sample was placed in a large vise and the other end was struck with a sledge hammer. The sample did not break but merely bent

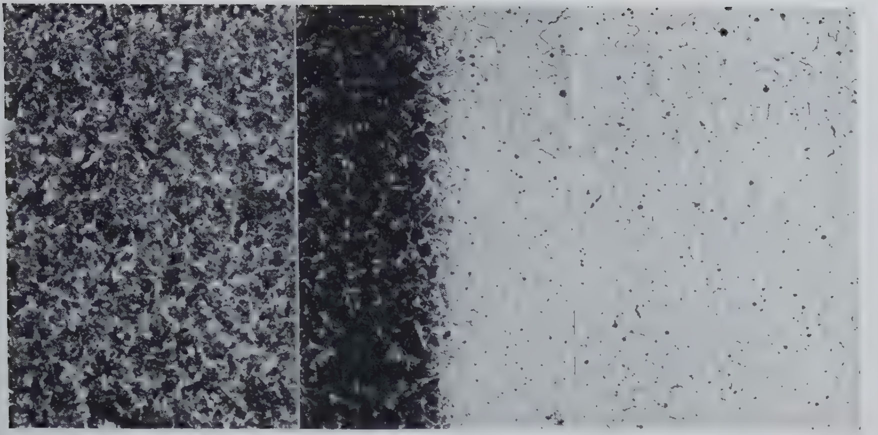

FIG 2—Diffusion weld between high-carbon and carbon-free iron.
Magnification × 100. Nital etch. Reduced one-half in reproduction.

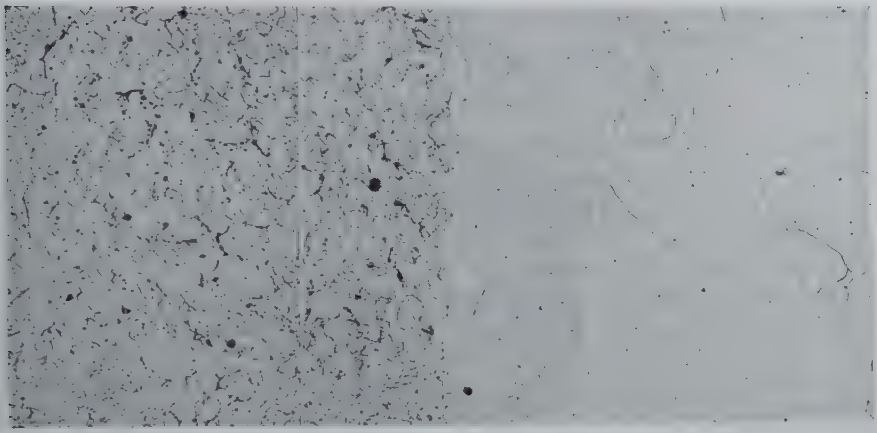

FIG 3—Diffusion weld between ferrite of different carbon contents.
(Left) 0.009 pct C and (right) 0.001 pct C. Magnification × 100. Nital etch. Reduced one-half in reproduction.

under the strokes. This indicated that the fusion was satisfactory. Examination of the weld zone was also made microscopically. Fig 2 shows the zone and the region near it in a high and low carbon sample; Fig 3 shows the zone and the region near it in a sample entirely in the ferritic state.

A variation in the preparation of the diffusion sample was carried out in the following manner: A small cylinder of high carbon (0.75 in. diam by 0.25 in.) was placed between two low carbon cylinders (0.75 in. diam by 0.875 in. long) and the three pieces were welded together in sandwich fashion. Such specimens (called double couples) were used when comparisons on grain size and oxygen were desired. Fig 4 shows a macrograph of a double couple. It illustrates how the grain size of the material changes, depending on the composition, when the couples are welded. There is, in the case of undeoxidized samples (No. 4 and 6), a pronounced coarsening of the grain structure; very large elongated grains are formed. In the case of deoxidized samples (No. 2 and 3), there may be little change in structure and sometimes even a definite refinement.

Specimens for decarburization were in the form of spools because it was desirable to have the decarburizing atmosphere (moist hydrogen) bathe the entire reduced section. The spools were 1¼ in. long; the ends of the spools were 1 in. in diam and ⅛ in. wide and the central portion was 0.75 in. in diam and 1 in. long.

THE DIFFUSION ANNEAL

Since this study involves changes in carbon of low concentration, the diffusion anneals were carried out in a vacuum because it was felt that risks should not be taken with gases such as hydrogen, nitrogen, helium or argon which might be decarburizing in the presence of small amounts of oxygen or moisture.

A quartz tube vacuum furnace was used. The furnace was made so that it could slide over the quartz tube. In this way a vacuum could be obtained while the furnace was being brought to temperature. When the desired vacuum was obtained, the preheated furnace was pulled over the quartz tube. When the anneal was completed, the furnace was pulled away from the quartz tube.

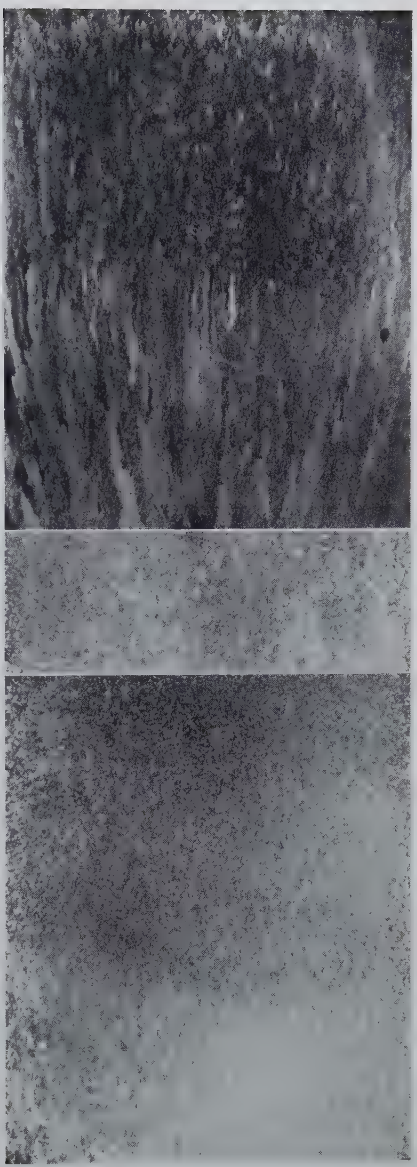

FIG 4—Grain structures in the diffusion specimens.
(Top) Deoxidized Iron. Sample No. 2.
(Middle) High carbon sample 0.68 pct C.
(Bottom) Undeoxidized iron. Sample No. 6.
(Magnification × 5).
Reduced one-third in reproduction.

The vacuum system consisted of a Cenco Hyper-Vac pump in series with two mercury pumps. A liquid nitrogen trap was placed between the mechanical and mercury pumps. Pressures were measured with thermocouple and ionization gauges. Even with the furnace heated to 700 or 800°C the pressures were of the order of 5×10^{-5} mm of Hg.

The furnace was wound in three sections with nichrome wire and resistors were inserted between the sections to improve the temperature distribution. An arrangement was worked out so

Table 2 . . . Details of the Diffusion and Decarburization Anneals

Experiment	Method	Temperature °C			Annealing Time		High Carbon Cylinder			Low Carbon Cylinder		
		Average	Standard Deviation σ*	Variation r†	Hours	Seconds	No	C	Grain Size‡	No	C	Grain Size‡
1	V.O.-D.	514.3	2.0	±1.3	134.8	4.85×10^5	8	0.68	See Fig 3	7	0.0044	4 to 5
2	V.O.-D.	606.1	1.2	±0.8	47.8	1.72×10^5	8	0.68	See Fig 3	1	0.004	5.8
3	V.O.-D.	672.1	1.0	±0.7	48.0	1.73×10^5	8	0.68	See Fig 3	5	0.006	4 to 5
4	V.O.-D. double	700	1.0	±0.7	21.3	7.67×10^4	8	0.68	See Fig 3	2	0.005	5.9
5	V.O.-D. couple	700	1.0	±0.7	21.3	7.67×10^4	8	0.68	See Fig 3	6	0.001	§
6	V.O.-D. double	700	1.0	±0.7	21.3	7.67×10^4	8	0.68	See Fig 3	3	0.005	5.0
7	V.O.-D. couple	700	1.0	±0.7	21.3	7.67×10^4	8	0.68	See Fig 3	4	0.001	§§
8	V.O.-D.	723.5	2.5	±1.7	30.3	1.09×10^5	8	0.68	See Fig 3	5	0.006	4 to 5
9	Grube	718.8	1.7	±1.1	48.3	1.74×10^5	12	0.0081	5–6	1	0.003	5.8
10	Grube	761.0	1.1	±0.7	40.08	1.44×10^5	9	0.0054	5–6	10	0.0008	About 1
11	Grube	786.0	2.5	±1.7	23.63	8.52×10^4	9	0.0057	5–6	10	0.0013	About 1
12	Decarburization	750 ± 4			24.5	8.82×10^4	11	0.43			0.016	(C in ferrite layer)
13	Decarburization	775			66	2.38×10^5	11	0.43			0.014	(C in ferrite layer)
14	Decarburization	800			19.5	7.02×10^4	11	0.43			0.012	(C in ferrite layer)
15	Decarburization	825			16	5.76×10^4	11	0.43			0.0095	(C in ferrite layer)
16	Decarburization	850			24	8.65×10^4	11	0.43			0.0065	(C in ferrite layer)
17	Decarburization	875			46.5	1.67×10^5	11	0.43			0.004	(C in ferrite layer)

* Standard deviation from probability plot.
† Error, r, $= \sigma \times 0.6745$.
‡ Grain size; ASTM estimate; intercept method.
§ Large elongated grains in the weld zone; see figure lower portion of Fig 5.
§§ Large elongated grains in the weld zone; similar to Fig 5.

that a uniform (better than ±0.25°) hot zone was maintained over a distance of 3-in.

Temperature control was obtained by using a Micromax controller-recorder in conjunction with a constant voltage transformer and an anticipator.[31] Temperatures were measured accurately to 0.1 of a degree. The variation in temperature was from ±0.6 to ±1.70°. The temperature of the anneal was obtained by plotting readings on probability paper and determining the standard deviation from the average, which when multiplied by 0.6745 gives the ± error.

Before the diffusion anneals were started, coils of chromel and alumel wire (24 gauge) were calibrated against a Bureau of Standards's platinum-platinum: rhodium secondary standard. This was done by placing the standard thermocouple and thermocouples prepared from each end of the coils into a 1 in. diam nickel-plated copper cylinder in which three holes had been drilled. The cylinder containing the three thermocouples was placed in the uniform temperature zone of the furnace and the readings of the thermocouples were obtained on a type K Leeds and Northrup potentiometer, using a Leeds and Northrup thermocouple selector switch. Slight differences between the ends of the chromel and alumel were noted. These were averaged and charts were prepared for the chromel-alumel thermocouples correlating millivolts and temperature. New thermocouples were used for each diffusion-anneal.

The thermocouples were placed into the low carbon end of the diffusion couple by drilling a hole sufficiently large for the thermocouple bead and then peening over the edge of the hole to keep the thermocouple from coming out. Connection was made between the thermocouple and the potentiometer by chromel and alumel lead-in wires joined to the furnace by a kovar-glass seal.

The diffusion anneal was carried out as follows: The furnace, drawn away from the quartz tube, was heated to the required temperature. The diffusion couple was placed into the cold quartz tube and connections were made to the potentiometer. The quartz tube was closed and was pumped down to the desired vacuum. The hot furnace was then pulled over the quartz tube containing the specimen.

Table 2 gives the details of the diffusion anneals reported upon in this investigation.

DECARBURIZATION ANNEAL

Samples used for decarburization were annealed in a conventional Globar Type furnace with a quartz tube as a furnace chamber. No extraordinary effort was exercised to obtain a fine temperature control, and hence the temperature varied ±4° of the desired temperature. The gas used was hydrogen saturated with moisture at room temperature (3.1 pct moisture by volume at 25°C). When the anneal was completed the samples were quenched in water.

MACHINING OF SAMPLES

After the diffusion anneal, the couples were machined to approximately 0.7 in. diam to remove possible decarburized layers and to get a uniform diameter couple. The region of the interface was polished with emery cloth and metallographic papers of increasing fineness. The samples were etched in 10 pct nital to bring out the interface. With the specimen properly centered in the lathe, layers about 0.02 in. were machined off near the interface and the thickness was then progressively increased to 0.04 in. at a distance of a centimeter from the weld. The length of the specimen after each cut was measured to the thousandth of an inch and estimated to the ten thousandth.

On the spools used for decarburization, turnings were taken on layers about 0.005 in. thick. In general, machining was continued until martensitic areas were reached.

CARBON ANALYSIS

Before the carbon analyses were made, the chips were screened on a 100-mesh screen to remove very fine particles which experience has shown can be relatively high in carbon presumably because of tool wear. After screening, the chips were washed in acetone and were dried over a small flame.

The carbon analysis was carried out by the method described by Stanley and Yensen.[32] The method is a modification of the conventional combustion method, employing the use of vacuum and liquid nitrogen.

The agreement between the present, also known as the Yensen, method and the conventional combustion one is reasonable. Various investigators[33,34] using the Yensen method have

Table 3 . . . Carbon Analysis of Standard Sample

Certified Analysis 0.014 pct C

Investigators	55a
Stanley and Yensen[32].....	0.0104 ± 0.0002 pct
Wooten and Guldner[33]....	0.0108 ± 0.0001 pct
Naughton and Uhlig[34].....	0.0105 ± 0.0003*
	0.0108 ± 0.0003
	0.0108 ± 0.0003

* Naughton and Uhlig used two variations of the low pressure combustion method.

analyzed the Bureau of Standard's sample 55*a* and have found it somewhat lower than the certified value which was determined by conventional combustion methods. See Table 3. The differences in the two methods have been considered by Naughton and Uhlig.[34]

ERRORS

There are certain errors in the diffusion experiment that are to be considered in obtaining the error of the diffusion coefficient. The main sources of error are those due to carbon analysis, temperature and measurement of layers. Other errors affecting *D* are due to: diffusion occurring during the welding of the diffusion couples, the diffusion occurring while the specimens were coming to and cooling from the diffusing temperature, and the change in dimensions due to thermal expansion.

The errors in carbon analysis and temperature can be estimated, the other errors are not readily treated. The diffusion in the welding operation is small (about 0.06 mm) as can be seen from Fig 2 but no corrections for this diffusion were made. The error due to heating up and cooling down of the diffusion couples was difficult even to approximate; however if the heating and cooling times were short compared to the time of the diffusion anneal, it was felt that no serious error was introduced. After the diffusion anneal the samples were furnace-cooled to about 500° and were then quenched. Corrections for thermal expansion can be made but were not made here because of the uncertainty of the temperature coefficient of iron in the range studied. The *D* values, if the expansion corrections were approximated, would be increased only by about 1 pct. It is believed that the diffusion data are good to ±10 pct.

Results

After the carbon analyses had been made they were plotted in relation to the distance from the interface on probability paper. From the best straight line obtained on the probability plot, curves were redrawn using rectangular coordinates. The types of penetration curves obtained by the Van Orstrand-Dewey method are illustrated in Fig 5 to 12 and for the Grube method in the ferritic state in Fig 13 to 15.

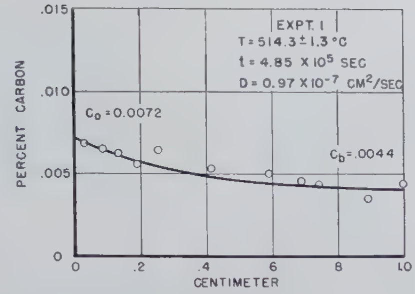

FIG 5—Carbon penetration at 514°C.

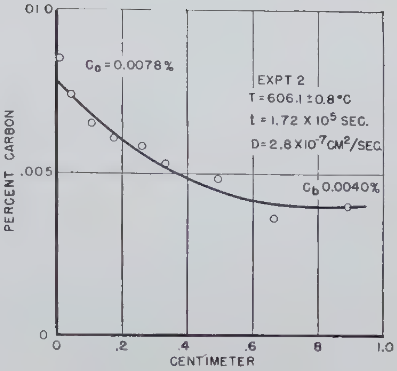

FIG 6—Carbon penetration at 606°C.

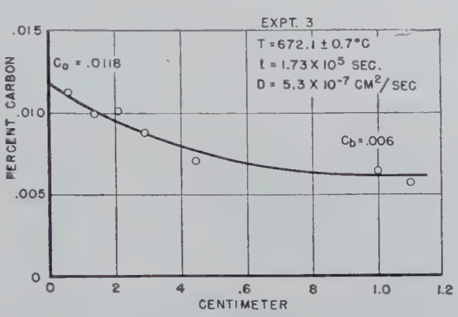

FIG 7—Carbon penetration at 672°C.

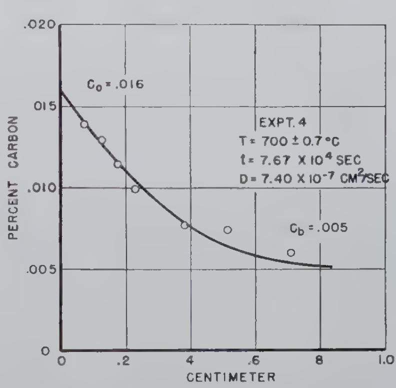

FIG 8—Carbon penetration at 700°C.

The *D* values for the curves were derived from Fick's law* of diffusion.

The differential form of Fick's equation is:

$$\frac{dC}{dt} = D\frac{d^2C}{dx^2}$$

The solution to the differential equation for the specific boundary conditions of the Van Orstrand-Dewey method is:

$$\frac{C_x - C_b}{C_o - C_b} = 1 - \phi\left(\frac{x}{2\sqrt{Dt}}\right)$$

where, using the *cgs* system,

C_x is the carbon at distance x in centimeters

C_b is the base or initial carbon content of the low carbon samples in per cent.

C_o is the carbon on the high side of the couple or the limit of solid solubility at the temperature.

D is the diffusion coefficient in centimeters squared per second.

t is the time in seconds.

ϕ is the Gauss error function.

The solution for the Grube method is:

$$\frac{2(C_x - C_b)}{C_\infty - C_b} = 1 - \phi\left(\frac{x}{2\sqrt{Dt}}\right)$$

where C_∞ is the carbon at infinity in the high carbon side of the couple and all other symbols remain as before.

The diffusion coefficients calculated by both methods are given in Table 4. In Fig 16, log *D* is plotted against the reciprocal of the absolute temperature. The agreement between points obtained by the two methods is gratifying.

The diffusion of carbon in alpha iron as a function of temperature can be represented by the equation:

$$D = 7.9 \times 10^{-3}\, e - \frac{18100}{RT}$$

No significant difference exists in *D* values between deoxidized, fine-grained samples and undeoxidized, coarse-grained samples. The diffusion coefficient at 700°C calculated for deoxidized, fine-grained samples (experiments 1, 2, 3, 4, 6) using the Van Orstrand-Dewey method samples gave a value of 6.4 × 10⁻⁷ cm² per sec. The experimental *D* value at 700 for an undeoxidized large elongated grain sample (experiment 5) gave a value of 6.75 × 10⁻⁷; experiment 7 also on an undeoxidized sample should not be compared with

---

* Discussions of Fick's law and the various solutions for limiting boundary conditions can be found in Jost[35] and Mehl.[36]

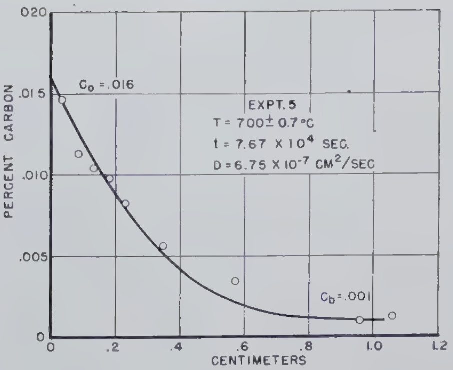

FIG 9—Carbon penetration at 700°C.

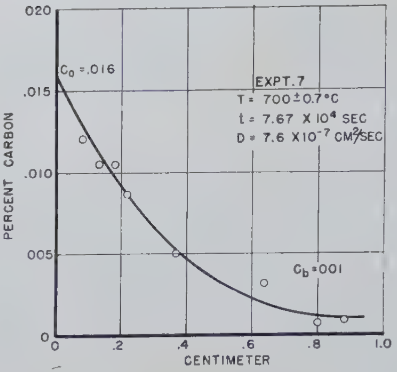

FIG 10—Carbon penetration at 700°C.

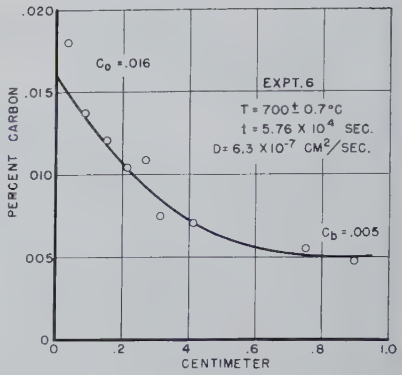

FIG 11—Carbon penetration at 700°C.

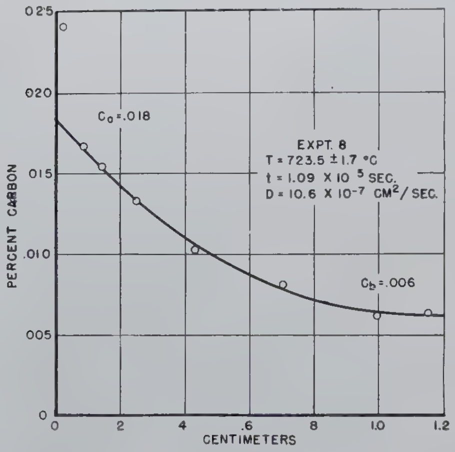

FIG 12—Carbon penetration at 723.5°C.

experiment 5 since the sample contained 0.38 pct cobalt. Reference to experiments 9, 10, 11 employing the Grube method indicates that no anomalies were observed due to differences in grain size (See Fig 3 for example).

Silicon up to 0.25 pct and cobalt up to 0.38 does not appear to affect the diffusion coefficient although it must be emphasized that the data are very meager and more work is necessary to establish the effect of these elements unequivocally. In the case of silicon (experiment 2) the calculation of *D* from the exponential relation derived from all the points gives a value of 2.7 × 10⁻⁷ at 606°C as against the experimental value of 2.8 × 10⁻⁷. In the case of cobalt (experiment 7) the calculation of *D* from the exponential relation gives a value of 7.2 × 10⁻⁷ at 700°C as against the experimental value of 7.6 × 10⁻⁷. These variations are both within 10 pct and no greater accuracy than this is claimed.

It has not been possible, as may be evident, to determine whether *D* varies with concentration as it does in the case of gamma iron.[6]

THE SOLUBILITY OF CARBON IN ALPHA IRON

The data on the solubility of carbon in alpha iron are given in Table 5. They have been obtained as the intercept carbon, C_0, from the carbon penetration curves obtained by the Van-Orstrand-Dewey method (experiments 1–8), Fig 5 to 12, and from the concentration of carbon at the ferrite-austenite interface, C_i, as is obtained in ferrite layers by the decarburization of a medium carbon steel (experiments 12–17); typical decarburization curves are given in Fig 17 and 18 for 750°C and 875°C, respectively. The data are plotted in Fig 19 together with data obtained by other investigators. The maximum solubility of carbon in alpha iron was found to be 0.019 pct at 725°C. The lines joining the carbon solubilities obtained by the Van-Orstrand-Dewey method and the decarburization method intersect nicely at the same point indicating that both methods are complementary and that the assumptions made regarding them are justified.

Discussion

The diffusion of carbon atoms in alpha iron as well as in gamma iron is interstitial and hence one need not concern himself with the mechanism of the process as one does for the diffusion of atoms in substitutional solid solutions.

The diffusion of carbon in alpha iron, however, is much more rapid than in gamma iron. Wells and Mehl[6] report the diffusion of carbon (in the range of 0.01 pct) in gamma iron as

$$D_\gamma = 0.07e - \frac{32{,}000}{RT}$$

Using their equation and the one found here for alpha iron, comparisons in the $\frac{D_\alpha}{D_\gamma}$ ratios at various temperatures can be made. Snoek[8] and Polder[9] predicted that at 910°C the ratio should be 2600 and 3, respectively. Actually the ratio at 910°C is 39. At 725°C the ratio increases to 126 and at 500°C it is 835.

It should be pointed out that the activation energy of the diffusion process in alpha iron is 18,100 gram-cal per gram-mol or about half the energy for diffusion in gamma iron, that is, 32,000. This value of 18,100 is identical (18,000) with that obtained by Snoek[8] from the theory of the magnetic after-effect and by Polder[9] from the theory of the elastic after-effect.

THE SOLUBILITY OF CARBON IN ALPHA IRON

The solubility of carbon in alpha iron has been established between 535 and 910°C with the maximum solubility of

Table 4 . . . Summary of D Values

Experiment	Method	Temperature °C	*D* cm² per sec Observed	*D* cm² per sec Calculated*	Percent Deviation from Calculated D
1	V.O.-D.	514.3	0.97 × 10⁻⁷	0.80 × 10⁻⁷	+21.0
2	V.O.-D.	606.1	2.8	2.7	+ 3.7
3	V.O.-D.	672.1	5.3	5.5	− 3.6
4	V.O.-D.	700.0	7.4	7.2	+ 2.8
5	V.O.-D.	700.0	6.75	7.2	− 6.2
6	V.O.-D.	700.0	6.3	7.2	−12.5
7	V.O.-D.	700.0	7.6	7.2	+ 5.5
8	V.O.-D.	723.5	10.6	8.9	+19.0
9	Grube	718.8	9.35	9.7	− 3.6
10	Grube	761.1	12.1	12.5	− 3.2
11	Grube	786.0	17.6	15.3	+15.0
				Average Deviation	±8.7

* Calculated from the equation of the straight line for data in Fig 16.

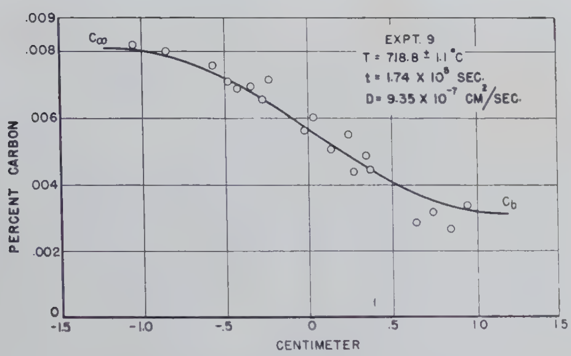

FIG 13—Carbon penetration at 719°C.

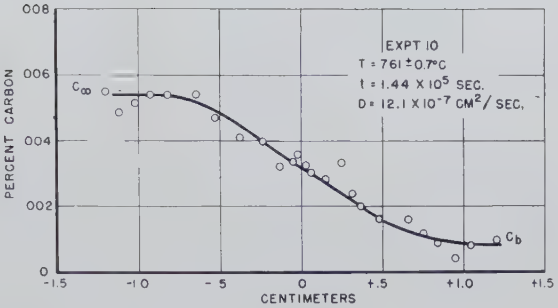

FIG 14—Carbon penetration at 761°C.

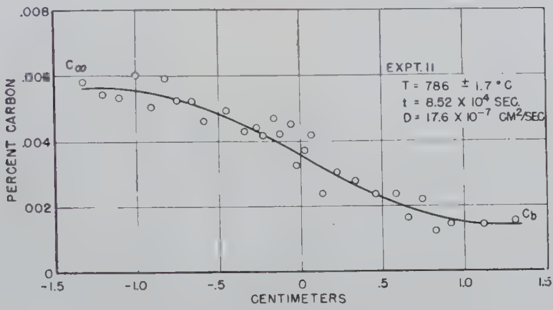

FIG 15—Carbon penetration at 786°C.

Table 5 . . . Solubility of Carbon in Alpha Iron

Experiment	Temperature, °C	Solubility, Pct	Method
1	514.3	0.0072	V.O.-D.
2	606.1	0.0078	V.O.-D.
3	672.1	0.0118	V.O.-D.
4	700.0	0.016	V.O.-D.
5	700.0	0.016	V.O.-D.
6	700.0	0.016	V.O.-D.
7	700.0	0.016	V.O.-D.
8	700.0	0.018	V.O.-D.
12	750	0.016	Decarburization
13	775	0.014	Decarburization
14	800	0.012	Decarburization
15	825	0.0095	Decarburization
16	850	0.0065	Decarburization
17	875	0.004	Decarburization

0.019 pct occurring at 725°C. The maximum solubility and the solubilities near it have been determined by several investigators. The present investigation is in agreement with Smith,[19] Ham,[10] and Dijkstra;[21] all other determinations have tended to be high. Fig 19 gives the data of the present experiments and the data of other investigators.

The limit of solubility below 725°C is rather important because it may serve as a base line for subsequent work which is needed to determine the effect of alloying elements on solubility. Such basic information is required if progress is to be made in the study of such phenomena as quench, strain, and "magnetic" aging as well as temper and blue-brittleness.

Summary

The diffusion of carbon in alpha iron was determined by two methods. One, the Van Orstrand-Dewey method, consisted of diffusing the carbon from a high carbon iron containing 0.68 pct C—corresponding to fine pearlite—into an essentially carbon-free iron. The other or Grube method consisted of diffusing carbon from a "high" carbon ferrite into a low-carbon ferrite. The first method could be used only below 725°C (eutectoid temperature) but the second could be used above and below 725°C. Both methods gave equivalent results.

The diffusion of carbon in alpha iron can be represented by the equation:

$$D_\alpha = 7.9 \times 10^{-3} e^{\frac{-18{,}100}{RT}}$$

The diffusion of carbon does not appear to be affected by grain size, deoxidation or small additions of silicon and cobalt. The present methods did not lend themselves toward determining if D varied with concentration.

At 725°C the diffusion of carbon is over 100 times as fast as it is in gamma iron.

The solubility of carbon in alpha iron below 725°C was determined by the Van Orstrand-Dewey method since the carbon leaving the pearlitic iron at the diffusion temperature corresponds to the carbon solid solubility. The solubility above 725°C was determined by a decarburization method, the solubility being the carbon concentration where the carbon gradient in the ferrite intersects the carbon gradient of the austenite-ferrite region. Both methods of determining solubility gave lines meeting at the same point to give a maximum solubility of 0.019 pct carbon at 725°C. The solubility lines between 514 and 910°C were obtained.

Acknowledgment

The writer is most appreciative of the University of Pittsburgh-Westinghouse Electric Corporation Graduate Study Program through which this study was made possible. It was a privilege to be associated with such personalities as Dr. G. R. Fitterer, Head of the Department of Metallurgy, University of Pittsburgh, and Dr. T. D. Yensen, Westinghouse Research Laboratories; both were most helpful in the carrying out of this work.

The writer wishes to acknowledge the assistance of the following: Messrs. Julius Heuschkel (welding), R. Anderson (metallography), R. Darby (machining), and Miss Joan Von Hoene for assisting with the numerous carbon analyses.

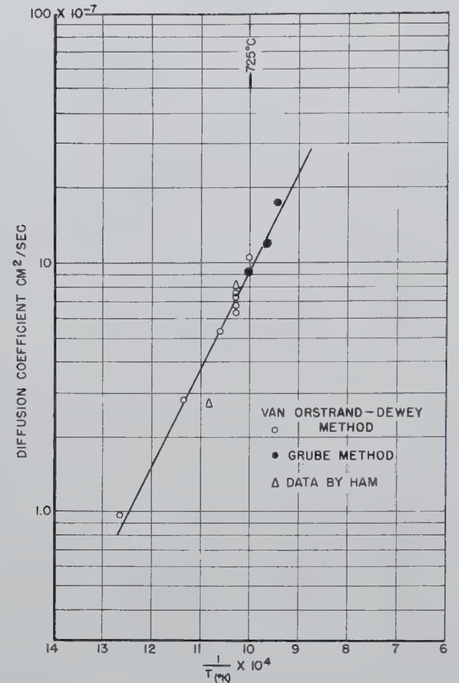

FIG 16—Plot of log D vs T.

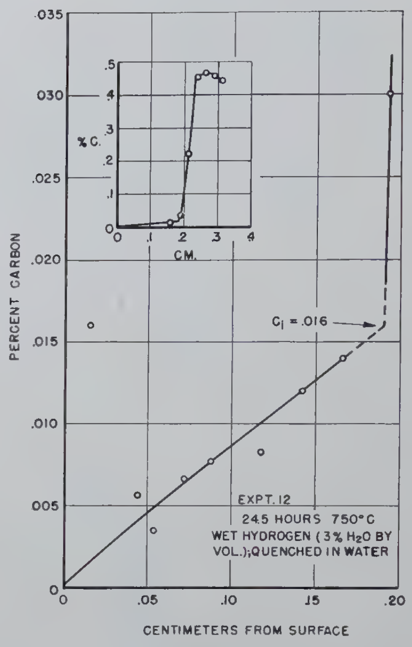

FIG 17—Decarburization curve at 750°C.

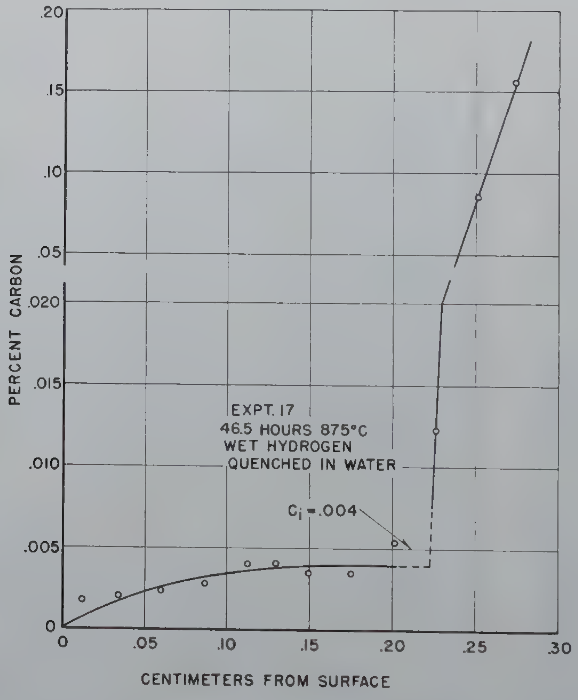

FIG 18—Decarburization curve at 875°C.

The writer also wishes to thank the following for graciously discussing the first draft of this paper: Drs. R. F. Mehl, Cyril Wells and R. Smoluchowski, Metals Research Laboratory, Carnegie Institute of Technology; Mr. F. E. Harris, Buick Motor Division, General Motors Corporation; Mr. J. L. Ham, Climax Molybdenum Corporation of America; Dr. C. Zener, Institute of Metals, University of Chicago; and Dr. J. L. Snoek, Eindhoven, Netherlands.

References

1. J. L. Snoek: Mechanical After-effect and Chemical Composition. *Physica* (1939) **6**, 591.
2. C. Zener: Anelasticity of Metals. *Trans.* AIME (1946) **167**, 155. *Metals Tech.* Aug. 1946, TP 1992.
3. J. L. Snoek: Effect of Small Quantities of Carbon and Nitrogen on the Elastic and Plastic Properties of Iron. *Physica* (1941) **8**, 711.
4. J. L. Snoek: Magnetic After-Effect and Chemical Constitution. *Phys-*

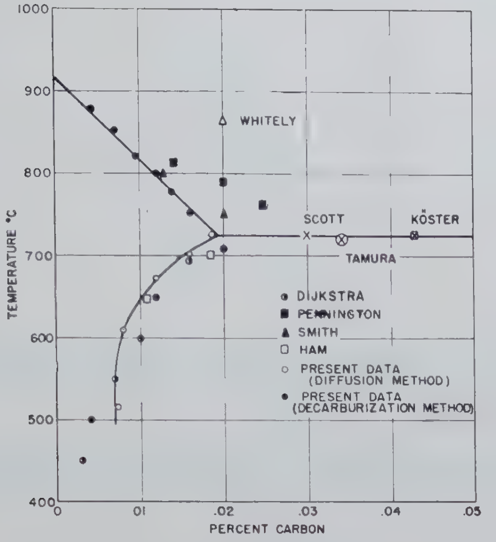

FIG 19—Solubility of carbon in alpha iron.

ica (1939) **6,** 161.

5. S. Epstein: Alloys of Iron and Carbon. McGraw-Hill Co., N.Y., 1936.
6. C. Wells and R. F. Mehl: Rate of Diffusion of Carbon in Austenite in Plain Carbon, in Nickel and in Manganese Steels. *Trans.* AIME (1941) **145,** 279.
7. J. H. Whiteley: The Solution of Cementite in Alpha Iron and Its Precipitation. Jnl. Iron and Steel Inst. (1927) **116,** 293.
8. J. L. Snoek: On the Decarburization of Steel and Related Questions. *Physica*. (1941) **8,** 734.
9. D. Polder: Theory of the Elastic After-effect and Diffusion of Carbon in α-Iron. *Philips Research Reports* (1941) **1,** 5.
10. Private communication from John L. Ham, Climax Molybdenum Co., dated Dec. 1, 1947 which referred to correspondence dated Oct. 21, 1946 to R. F. Mehl, Carnegie Institute of Technology.
11. A. Sauveur and V. N. Krivobok: Dendritic Segregation in Iron-Carbon Alloys. Iron and Steel Inst. (1925) **112,** 313
12. W. H. Hatfield: Discussion of Paper by A. L. Field on "Physica-Chemical Phenomena from Melt to Ingot." *Trans.* Faraday Soc. (1925) **21,** 272.
13. A. Bramley and F. W. Haywood: Cementation of Iron and Steel. Iron and Steel Inst., C.S.M. (1928) **17,** 67.
14. H. Scott: What is Steel? *Chem. and Met. Eng.* (1922) **27,** 1156.
15. S. Tamura: Pseudo-Twinning in Ferrite and Solubility of Carbon in α-iron at the A_1. *Jnl.* Iron and Steel Inst. (1927) **115,** 747.
16. W. Koster: Influence of Heat Treatment below the A_1 Point on the Properties of Technical Iron *Arch. f. d. Eisenhutt.* (1929) **2,** 29 (503).
17. H. A. Dickie: The Solubility of Carbide in Ferrite. *Jnl.* Iron and Steel Inst. (1929) **120,** 161.
18. J. H. Whiteley: A Survey of the Iron-Carbon Diagram Near Zero Carbon (Below 1000°C). *Jnl.* Iron and Steel Inst. (1936) **133,** 377.
19. R. R. Smith: Equilibrium of Iron-Carbon Alloys with Mixtures of CO/CO_2 and CH_4/H_2. *Jnl.* Am. Chem. Soc. (1946) **68,** 1163–1175.
20. W. A. Pennington: Thermodynamics in the Decarburization of Steel with Mill Scales. ASM 1948 Preprint No. 38.
21. L. J. Dijkstra: Precipitation Phenomena in the Solid Solutions of Nitrogen and Carbon in α-iron below the Eutectoid Temperature. Ninth Quarterly Report to ONR on Deformation of Metals, Inst. for the Study of Metals, Univ. of Chicago, May–July 1948.
22. N. A. Ziegler: The Solubility of Oxygen in Solid Iron. A.S.M. (1932) **20,** 73.
23. R. W. Bailey: Testing of Materials for Service in High Temperature Steam-Plant. *Proc.* Inst. Mech. Eng. (1932) **122,** 209.
24. G. Richter: Uber die Magnetische Nachwirkung um Carbonyleisen. *Ann. Phys.* (Leipzig) (1937) **29,** 605.
25. G. Richter: Uber die Mechanische und die magnetische Nachwirkung des Carbonyleisens. *Ann. Phys.* (Leipzig) (1938) **32,** 683.
26. C. E. Van Orstrand and F. P. Dewey: Preliminary Report on the Diffusion of Solids. U.S. Geol. Survey, Prof. Paper 45-G (1915) 83–96.
27. G. Grube and A. Jedele: Die Diffusion of Metalle in Festen Zustand. *Ztsch. f. Elektrochemie* (1932) **38,** 799.
28. E. Kirkendall, L. Thomassen and C. Upthegrove: Rates of Diffusion of Copper and Zinc in Alpha Brass. *Trans.* AIME (1939) **133,** 186.
29. W. A. Pennington: A Mechanism of the Surface Decarburization of Steel. A.S.M. (1946) **37,** 48.
30. J. K. Stanley: Fundamentals of Carburization and Decarburization. *Steel* (1947) **120,** 92.
31. M. J. Manjoine: An Anticipatory Method for Improving Automatic Temperature Control. *Instruments* (1945) **18,** 454.
32. J. K. Stanley and T. D. Yensen: A Rapid Method of Determining Minute Amounts of Carbon in Metals. *Ind. Eng. Chem.* (Anal. Ed.) (1945) **17,** 699.
33. L. A. Wooten and W. G. Guldner: Determination of Carbon in Low-Carbon Steel. *Ind. Eng. Chem.,* (Anal. Ed.) (1944) **16,** 248.
34. J. J. Naughton and H. H. Uhlig: Determination of Small Amounts of Carbon in Steel. *Anal. Chem.* (1948) **20,** 477.
35. W. Jost: Diffusion Und Chemische Reaction im Festen Stoffen. Theo. Steinkopf, 1937.
36. R. F. Mehl: Diffusion in Metals. *Trans.* AIME (1936) **122,** 11.

Studies of Interface Energies in Some Aluminum and Copper Alloys

K. K. IKEUYE* and CYRIL STANLEY SMITH,* Member AIME

In an earlier paper[1] one of the authors called attention to the significance of the relative free energies of grain boundaries and interphase boundaries in alloys in determining the shape and distribution of micro-constituents.

The ratio of the interphase and intercrystalline boundary energies (that is, $\frac{\gamma_{12}}{\gamma_{11}}$, where γ_{12} is the energy of the interface between a crystal of phase 1 and a crystal of phase 2, and γ_{11} is the energy of the boundary between two crystals of phase 1) will be denoted by Γ. It is this ratio that determines, by the simple triangle of forces relation,† the dihedral angle, θ, of phase 2 where it adjoins a boundary between two grains of phase 1. On a metallographic sample various angles are actually obtained because of the random orientation of the plane of observation, but the statistically most frequent angle is the true one. These basic principles were discussed in detail in the earlier paper.

The experiments described below show the effect of both composition and temperature on θ and Γ for some alloys containing a liquid phase, and provide data on the rate of approach to the equilibrium angles in both solid and liquid phases.

Experimental Procedure

All the alloys were melted in a graphite crucible and cast into ingots ¾ by 1⅛ in. cross-section. Some of the aluminum alloys consisted of two immiscible liquids from which uniform castings could not be obtained. The amount of liquid phase varied locally to a considerable extent and the analyses were meaningless. Nevertheless, the composition of the liquid would not differ from that in an alloy of the intended gross composition, and the synthetic composition of the alloys was therefore used in considering the surface energy results. The ingots were given initial deformation by cold-rolling to 50 pct reduction, annealed, and given a second 50 pct reduction prior to cutting into small samples for heat treatment at the times and temperatures subsequently reported. The resulting micro-samples were carefully prepared metallographically and examined at magnifications of 650, 1280, or 2500. The objectives used were 21X, 0.40 NA (dry); 41X, 0.65 NA (dry); and 80X, 1.40 NA (oil emulsion). The appropriate angles were measured by rotation of the stage of a Bausch and Lomb metallograph to align the appropriate boundaries successively with a cross-hair in a micrometer eyepiece. About 250 angles were measured on each phase. Though the angles were read to 1°, the accuracy is probably not above 3°, because of uncertainty in setting the cross-hair tangent to the sometimes curved boundary. The corners of very small particles, particularly in early stages of adjustment after cold-rolling, were difficult to measure and the results were slightly dependent on the magnification used (compare Fig 1-C and 1-D). With particles of larger size and more nearly equilibrium shape, magnification made no difference (*vide* Fig 1-F and 1-G). The measured angles were grouped in 10° intervals (5° if θ was less than 20°) and plotted in bar

Cleveland Meeting, October 1949.
TP 2691 E. Discussion of this paper (2 copies) may be sent to *Transactions* AIME before December 1, 1949. Discussion is tentatively scheduled for publication in May 1950. Manuscript received May 2, 1949; revision received July 11, 1949.

* Institute for the Study of Metals, Univ. of Chicago.

This research was done in part under contract with the Office of Naval Research.

[1] References are at the end of the paper.

† $\Gamma = \frac{\gamma_{12}}{\gamma_{11}} = \frac{1}{2\cos\frac{\theta}{2}}$. Note that θ will be zero for $\Gamma = 0.5$ and all values below. True values for Γ can not be obtained by direct microscopic means when $\frac{\gamma_{12}}{\gamma_{11}} < 0.5$.

graphs, of which Fig 1 is an example. The most probable angle was estimated and taken to be the true dihedral angle.

The frequency curves of even well-annealed alloys showed a greater spread of angle than that resulting from random sectioning alone, which indicates that the energies of all interphase boundaries are not identical, but vary slightly, supposedly as a result of differing orientation between the grains. Though this is of great interest and importance, it is a minor factor as far as general microscopic features are concerned and, for the present, is ignored.

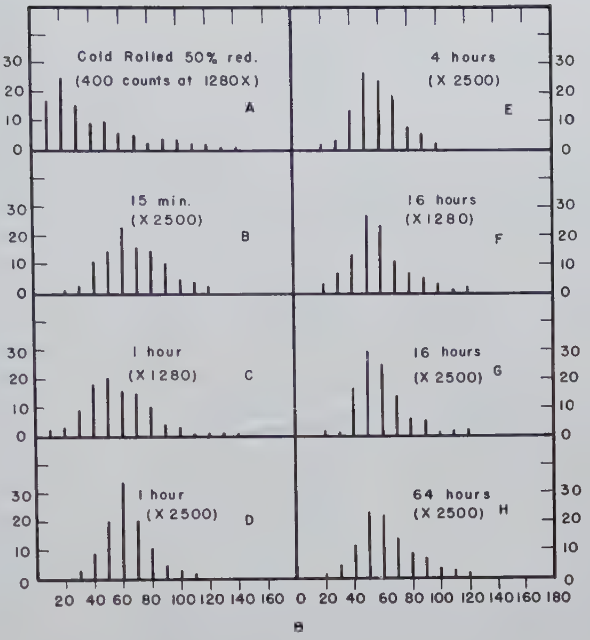

FIG 1—Distribution of measured angles in tin-rich liquid phase in longitudinal sections of 95-5 Al-Sn alloy, cold-rolled and annealed for varying times at 350°C.

250 angles measured for each sample, at 2500 ×, except where otherwise noted.

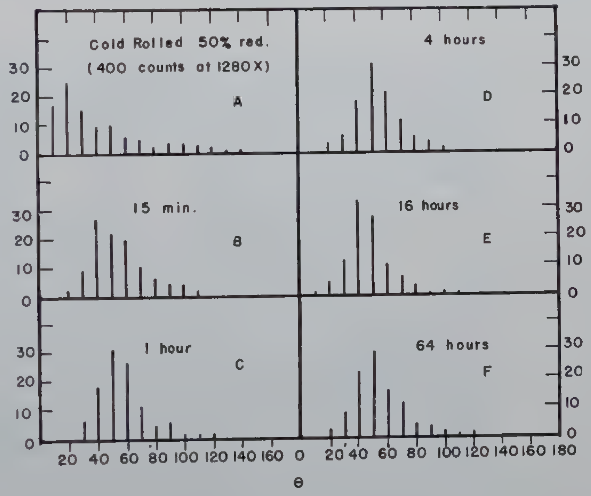

FIG 2—Distribution of measured angles of tin-rich phase in longitudinal sections of 95-5 Al-Sn alloy, cold-rolled and annealed for varying times at 450°C.

250 angles measured for each sample, at 2500 ×, except where otherwise noted.

Rate of Approach to Equilibrium

The distribution of dihedral angles for the liquid tin-rich phase in an aluminum-tin alloy with 5 pct tin, cold-rolled and subsequently annealed for various times at 350 and at 450°C, is shown in Fig 1 and 2. In all of these alloys, the structure consists of nearly pure aluminum grains with a tin-rich liquid dispersed as a continuous prism-like network along the edges of the three-dimensional grains. In the two-dimensional metallographic section, the tin-rich phase (solid, of course, after quenching) appears most frequently as triangles at the junction of three grains of aluminum. In the annealed samples, these triangles are essentially equilateral and equiangular, but cold-rolling distorts them considerably, resulting in a much wider spread of angles; annealing causes rapid restoration of the angles to the values determined by surface tension equilibrium. Fig 3 shows the same data as Fig 1 (that is, from the 350°C anneal) grouped according to the orientation of the apices in relation to the direction of rolling. In the rolled alloy most of the angles in the quadrants lying in the direction of rolling are smaller than the equilibrium value, while normal to this the particles have been flattened out and the angles increased. Annealing for 15 min. at 350°C gives a well-defined angle-distribution curve with a maximum at the equilibrium value, although the abnormally large spread of angles has not entirely disappeared. Annealing for 1 hr at 350°C gives liquid areas showing no anisotropy of angles, and further annealing causes no change. At 450°C (Fig 4) even the 15 min. anneal gives a structure that does not subsequently change, except for the size of the liquid particles.

In the solid state, restoration of distorted grain junctions to equilibrium configuration would be expected to occur at a slower rate than for a liquid phase and to be highly dependent on temperature. Tests were made on an alpha/beta bronze containing 16 pct tin at 650°C, a normal commercial annealing temperature. Annealing was done in a salt bath. Fig 5 to 8 show the microstructures obtained, while Fig 9 is a plot of the distribution of the corner angles of the beta grains after various times of heat treatment. The grains of beta had been flattened out by rolling, and in the initial condition there is a large number of small angles in the quadrant parallel to rolling, while the normal quadrants contain larger angles than the equilibrium value. After annealing for 4 min., as can be seen from Fig 6, the alloy has completely recrystallized and the beta phase has developed apices, each one meeting a contiguous alpha boundary. The angles still show considerable spread from the equilibrium values and the strong curvature imposed on local

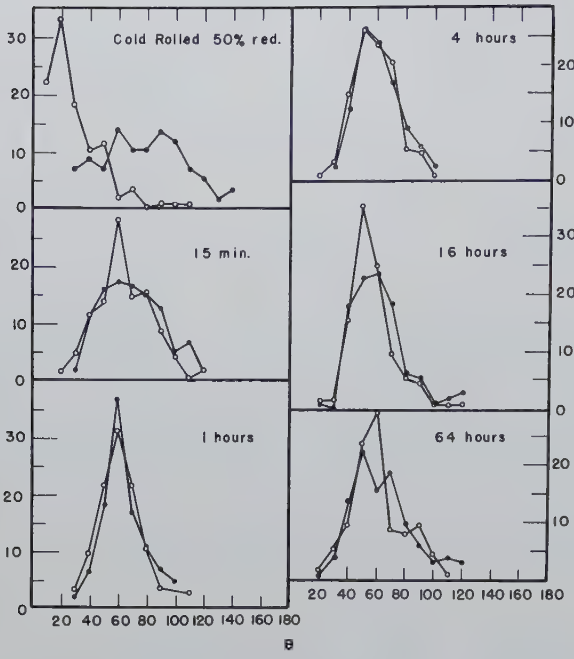

FIG 3—Same data as Fig 1, grouped in quadrants related to the rolling direction.

0 R = angles whose bisectors fall in quadrants 135–225° and 315–45° from rolling direction.

● N = angles whose bisectors fall in quadrants 45–135° and 225–315° from rolling direction.

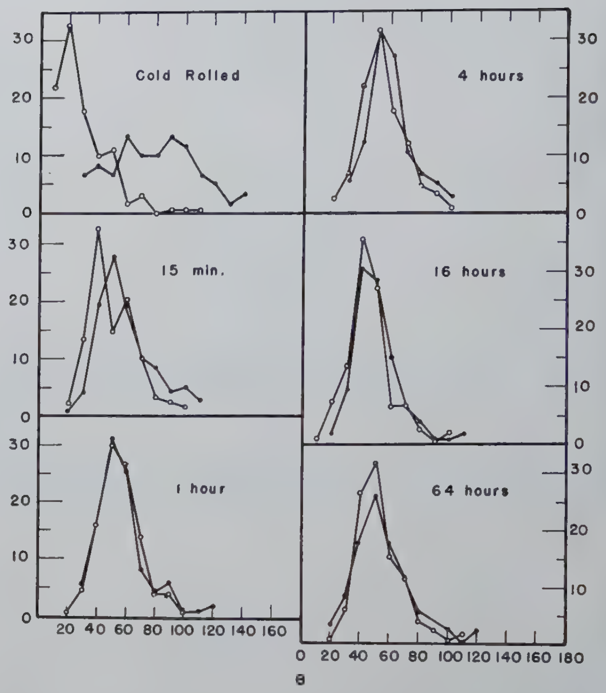

FIG 4—Same data as Fig 2, grouped in quadrants related to rolling direction.

See Fig 3 for definition of N and R quadrants.

5

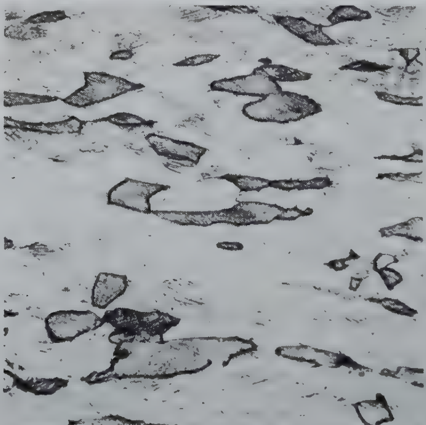

6

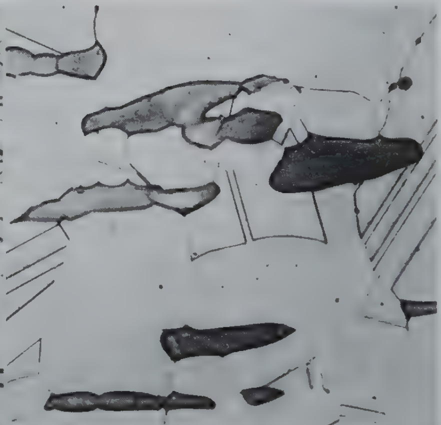

7

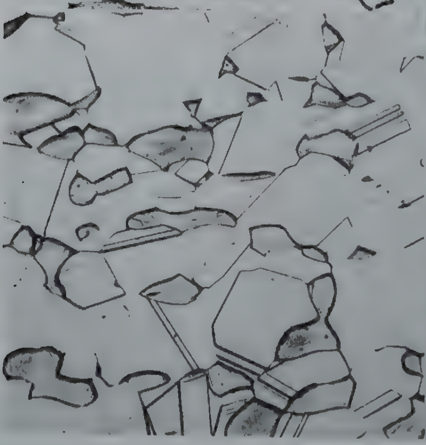

8

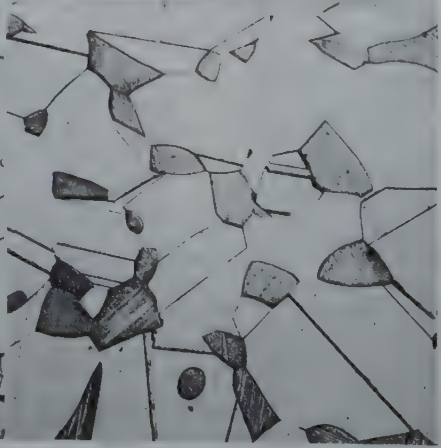

FIG 5—Microstructure of α/β bronze (16 pct Sn) as cold-rolled 50 pct reduction following 650° anneal.

Etched with potassium dichromate, followed by ferric chloride. 250 ×.

FIG 6—Same alloy as Fig 5, annealed 4 min at 650°C.

500 ×.

FIG 7—Same alloy as Fig 5, annealed 1 hr at 650°C.

250 ×.

FIG 8—Same alloy as Fig 5, annealed 16 hr at 650°C.

250 ×. All micrographs reduced one-tenth in reproduction.

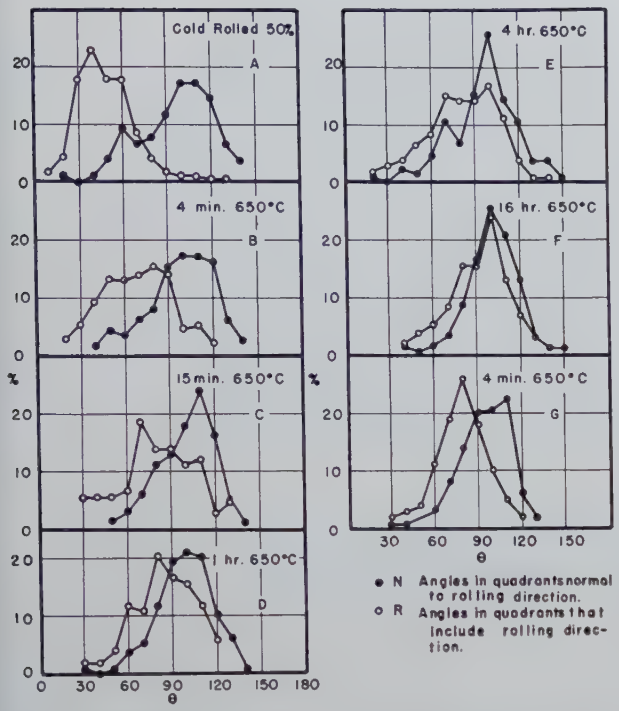

FIG 9—Distribution of angles in α/β bronze with 16 pct tin, grouped in quadrants related to the direction of rolling.

250 angles were measured in each specimen, at a magnification of 1200 ×, except Fig 9-G which was 2500 ×.

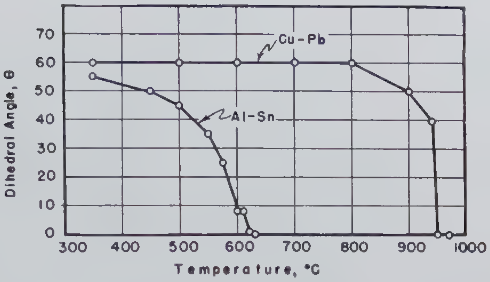

FIG 10—Temperature dependence of dihedral angles in Cu-Pb and Al-Sn alloys.

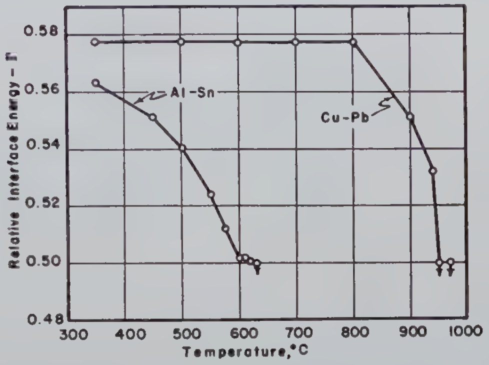

FIG 11—Effect of temperature on relative interface energy, Γ, for Cu-Pb and Al-Sn alloys.

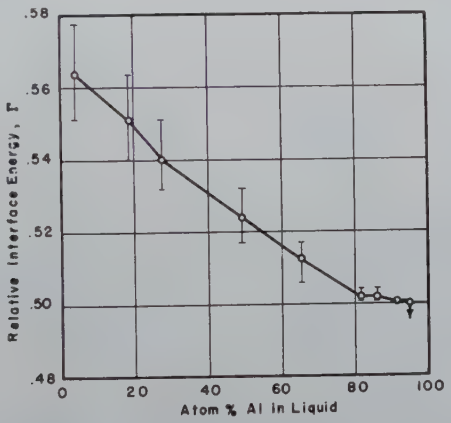

FIG 12—Relative interface energy, Γ, as a function of the composition of the liquid phase in Al-Sn alloys at various temperatures.

surfaces by the long-range geometry prevents equilibrium.* After 1 hr (Fig 9-D) the angles in the longitudinal and normal quadrants are nearly the same, and after 16 hr anneal at 650°C (Fig 9-F) the peaks of the two curves are almost identical, indicating that surface tension forces have entirely overcome the distortion imposed by cold-work. The answer to the question as to whether the mechanism of adjustment is by diffusion or by plastic deformation must await further study.

Effect of Temperature on the Dihedral Angle in a Binary Alloy Containing a Liquid Phase

Fig 10 shows the temperature dependence of the dihedral angle of the liquid phases in a copper-lead alloy with 1 pct lead and in an aluminum-tin alloy with 5 pct tin. Samples of these alloys were first cold-rolled and then annealed at different temperatures for sufficient times to obtain equilibrium. Fig 11 shows values of Γ (the ratio of interphase and intergrain boundary energies) calculated from the dihedral angles.

In the copper-lead system θ is unaffected by temperature up to 800°C, but decreases somewhat at 900 and 930°C and drops sharply to zero at 960°C. In the aluminum-tin alloy θ and Γ decrease with increasing temperature in a more uniform manner. The difference in behavior is easily explained if the constitution diagrams[2] are examined. In the copper-lead system, the composition of the liquid phase in equilibrium with solid copper changes

---

* Equilibrium at a higher magnification (2500 ×) as in Fig 9-G gave a considerably sharper distribution, but still showed a definite difference between those angles near the rolling direction and normal to it. It is possible that on an atomic scale the equilibrium angle is achieved immediately after recrystallization. Samples that have been annealed for a sufficiently long time to allow the particles to acquire smooth, simply curved, outlines show no variation with magnification—provided, of course, that the metallographic preparation and optics are such as to give good resolution of the boundaries.

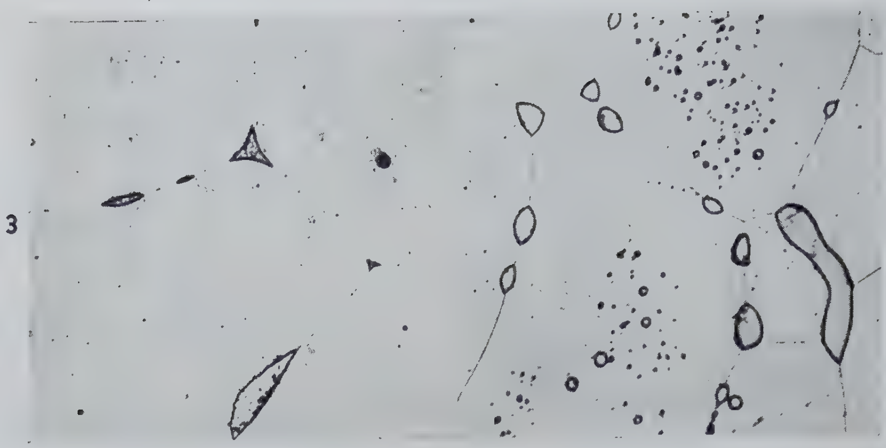

FIG 13 (left)—Microstructure of 94-3-3 Al-Cu-Sn alloy.

Cold-worked 50 pct reduction and annealed 6 hr at 550°C. Etched with 2 pct hydrofluoric acid followed by dilute Keller's etch. 250 ×. Reduced one-tenth in reproduction.

FIG 14 (right)—Microstructure of 95-5 Al-Cd alloy.

Cold-worked 50 pct reduction, annealed 6 hr at 550°C. Etched with 2 pct hydrofluoric acid, followed by dilute Keller's etch. 500 ×. Reduced one-tenth in reproduction.

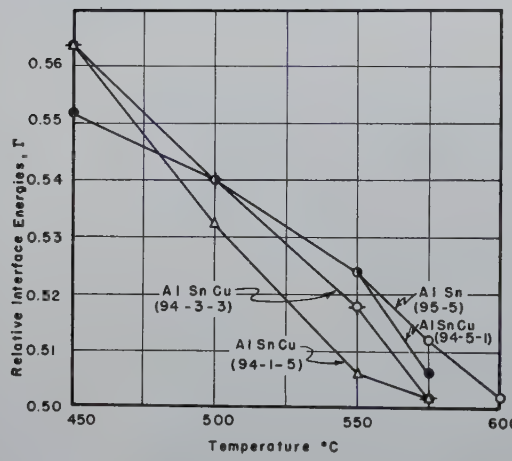

FIG 15—Relative interface energy, Γ, in Al-Sn-Cu alloys as a function of temperature.

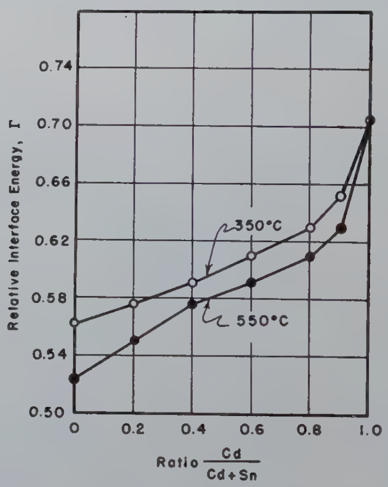

FIG 17—Relative interface energies as a function of composition in Al-Sn-Cd alloys at 350 and 550°C.

(Al constant at 95 pct.)

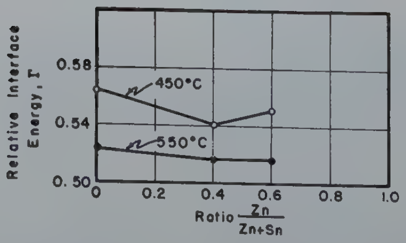

FIG 16—Relative interface energies as a function of composition in Al-Sn-Zn alloys at 450 and 550°C.

(Al constant at 95 pct.)

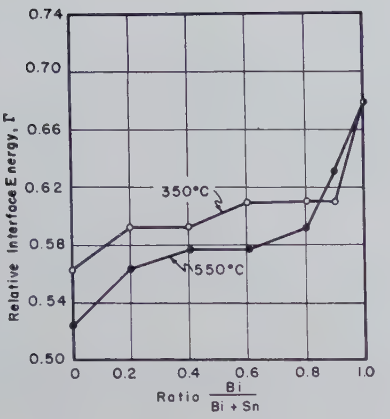

FIG 18—Relative interface energies as a function of composition in Al-Sn-Bi alloys at 350 and 550°C.
(Al constant at 95 pct.)

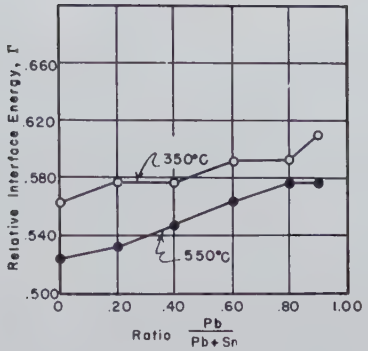

FIG 19—Relative interface energies as a function of composition in Al-Sn-Pb alloys at 350 and 550°C.
(Al constant at 95 pct.)

only from 0.5 to 1.0 pct copper as the temperature rises from 500 to 800°C, and then changes with increasing rapidity to about 7.5 pct copper at the monotectic temperature, 953°C, whereupon it abruptly changes to about 60 pct copper. In the aluminum-tin system the liquid changes continuously and with increasing rapidity from 0.5 to 100 pct aluminum as the temperature is raised from that of the eutectic (229°C) to the melting point of aluminum (660°C). It seems obvious that the major effect of temperature in both alloys is to change the composition of the liquid. Although it would be expected that both $\gamma_{\alpha liq}$ and $\gamma_{\alpha/\alpha}$ would decrease with temperature, though perhaps at different rates, it seems reasonable to attribute most of the change in θ and Γ to the solid/liquid interface rather than to the grain boundary.

If, as in Fig 12, the values of Γ for the aluminum-tin alloys are plotted as a function of the composition of the liquid phase, as read from the liquidus of the constitution diagram,[2] Γ is seen to be a smooth function of composition,* decreasing as the liquid approaches the solid in composition. This is not unexpected.

It has often been supposed that the presence of a liquid phase results in hot-shortness of an alloy. Though extreme brittleness at high temperatures is almost invariably associated with the presence of a liquid, the converse is not necessarily so, for drops of liquid with large dihedral angles are relatively harmless. An alloy will become hot-short immediately above the solidus only if the dihedral angle is nearly zero, causing the liquid to replace a large fraction of the normal grain boundary area and to give rise to sharp notches for stress concentration. The method of determining solidus temperatures by detecting the onset of hot-shortness is an excellent one when θ is zero, but is dangerous to use on alloys where this is not known to be the case.

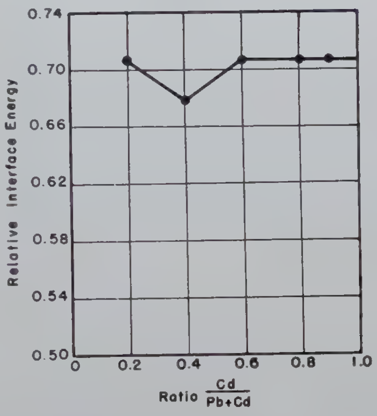

FIG 20—Relative interface energies as a function of composition in Al-Pb-Cd alloys at 350 and 550°C
(Al constant at 95 pct.)

Interface Energies in Ternary Alloys Containing Liquid

It has been shown above that the composition change resulting from variation of solubility with temperature affects the interface energy ratio in a binary two-phase alloy. The change of composition caused by the addition of a third element at a fixed temperature can have a similar influence. The effect of zinc and bismuth added to copper-lead alloys was discussed in an earlier paper.[1] More complete data were obtained with series of ternary alloys of aluminum containing tin and either copper, bismuth, lead, zinc, or cadmium. Except for the copper series, which contained 94 pct aluminum, the alloys investigated contained 95 pct aluminum with the remaining 5 pct divided between tin and the other element in varying proportions. Typical microstructures are shown in Fig 13 and 14.

The alloys containing copper were measured after annealing at several temperatures to show the effect both of temperature and composition (see Fig 15). The other alloys were annealed at 350 and 550°C only (for 16 and for 6 hr respectively) and gave the values of θ and Γ shown in Fig 16 to 20.

Copper and zinc (Fig 15 and 16) are soluble in both the solid and liquid phases in aluminum-tin alloys and they act slightly in the direction of decreasing the value of Γ—whether by modification of the grain boundary energy or of the liquid/solid interface cannot be said. The other elements—cadmium, lead, and bismuth—are virtually insoluble in solid aluminum, and dissolve little aluminum themselves when molten. In their ternary alloys with aluminum and tin it is therefore possible to study the equilibrium angles between an aluminum grain boundary (which, to a first approximation, may be assumed not to change in nature or composition), and the interface between aluminum crystals and liquid that is of varying composition. The data in Fig 17 to 19 show that the energies of the interface between solid aluminum and liquid cadmium, lead,* or bismuth in the binary alloys are all higher than that of the aluminum-tin interface, but that the interface energy is decreased rapidly by the first addition of tin and more slowly as the liquid becomes richer in tin. This parallels closely the variation of surface tension with composition in binary liquid alloys and doubtless arises from a similar cause—the preferential adsorption of the element giving lower interface energy at the interface.†

---

* The vertical lines drawn through the experimental points in Fig 10 represent the range of Γ corresponding to an error of 5° in measuring θ. It is obvious that the smoothness of the curve is to some extent fortuitous.

Summary

Studies have been made of the angles existing at the corners of various microconstituents in alloys after deformation and heat treatment. Liquid phases take relatively short times to reach the angles determined by surface energy equilibrium. Solid phases are slower to adjust, but commercial annealing practice for a bronze gives dihedral angles that are not appreciably changed by longer annealing.

The effect of temperature on the dihedral angle and the relative energies of grain boundary and interphase boundary in copper-lead and aluminum-tin alloys is slight except when the change of temperature produces a change in the composition of the phases in equilibrium. In general, it is predicted that alloys whose constitution diagrams show a nearly vertical liquidus will be substantially unaffected by temperature change, and that alloys with a sloping liquidus will present structures that vary considerably with annealing temperature. The dihedral angle decreases as the composition of the liquid approaches that of the solid. Alloys become hot-short when heated above the solidus *only* if the liquid phase has a small dihedral angle and so replaces a large part of the grain boundary area.

Dihedral angles were measured for a series of ternary alloys of aluminum with tin and other low melting-point elements. If the third element is soluble in both solid and liquid phases the dihedral angle may be decreased (aluminum-tin-copper, aluminum-tin-zinc) but otherwise the ternary alloys possess relative interface energies intermediate between that of aluminum-tin and that of the binary alloy of aluminum with the other component. The first addition to a binary alloy of a third element that itself has a lower interface tension against solid aluminum will cause rapid reduction of interface tension, while further additions are less potent, paralleling the behavior of surface tension in liquid binary alloys.

References

1. C. S. Smith: Grains, Phases, and Interfaces: An Interpretation of Microstructure. *Trans.* AIME (1948) **175**, 15–51. *Metals Tech.* June, 1948 TP 2387.
2. M. Hansen: Der Aufbau der Zweistofflegierungen. (Berlin, Springer, 1936).

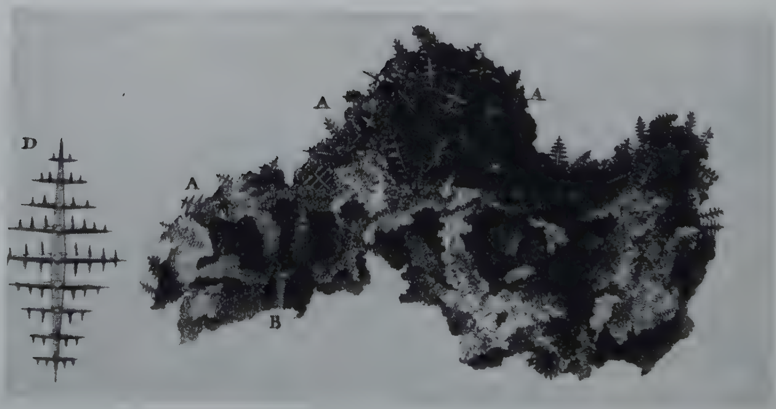

DENDRITES IN CAST BRASS.
Grignon, 1775. (*Courtesy of C. S. Smith*)

---

* The liquid phase in the pure binary alloys of aluminum and lead did not aggregate to a sufficient size to permit θ to be measured, even after annealing for 6 days at 550°C. The alloys with minor additions of cadmium or tin behaved satisfactorily.

† The behavior of the copper-bismuth-lead alloys described in Ref. 1 is not in accord with this, for the Γ curve is convex with increasing bismuth content.

In the ternary Al-Pb-Cd case, there is no variation of Γ with composition (Fig 20).

Preparation and Casting of Beryllium Melts*

J. G. KURA,† J. H. JACKSON,‡ Member, M. C. UDY,§ Member, and L. W. EASTWOOD,‡ Member AIME

Introduction

The melting and casting of any commercial metal depends upon the success with which the problems attendant to the handling of the specific metal are overcome. Common difficulties encountered in the handling of commercial metals are tendencies to burn or oxidize excessively, low fluidity, entrapment of dross, hot cracking, cold embrittlement, cold shuts, and unsoundness caused by gas evolution. Beryllium is not only subject to these same difficulties but is generally more sensitive to them than are the more common metals, thus necessitating more exact founding precautions.

Characteristics of Beryllium

Certain characteristics of beryllium which make it particularly difficult to handle in the plant or laboratory are as follows:

1. The melting point of beryllium is about 2400°F and pouring temperatures vary from 2600 to 2900°F, depending upon the degree of fluidity required. The extreme chemical activity, combined with the high temperatures, makes necessary the use of inert atmospheres, slags, or vacuum for protection during melting and pouring. Furthermore, beryllium tends to react with the melting crucibles, tools, and molds, thus requiring the selection of suitable materials and proper maintenance of these items.

2. The very marked absorption of gas by molten beryllium and the subsequent evolution of gas during solidification causes a great deal of difficulty with unsoundness. Beryllium castings may also be subject to unsoundness as a result of gas formation by chemical reaction with the mold surface during solidification.

3. The very marked chemical affinity between molten beryllium and the normal atmosphere causes the formation of dross. On relatively quiescent melts, this dross forms a very tenacious film which, if carried over to the mold, can cause defects such as the formation of skins or dross in the interior or on the surface of the casting; folds or defects similar to cold shuts may also be found.

4. During the pour and attendant turbulence, the dross may be mixed into the metal and then carried to the casting. There it may be entrapped during freezing and cause internal defects, or it may float to the surface and cause severe dross defects on the cope side of the castings.

5. Solid beryllium is very weak at a temperature near the solidus line; brittleness is also a problem at lower temperatures. Thus, hot and cold cracking must be guarded against.

Scope of the Experimental Work

All of these problems have been given consideration in the work at Battelle. Before the work was started at Battelle, it was customary to melt beryllium in a vacuum furnace or under flux in graphite-lined induction furnaces.

Because of the difficulty of preventing gas unsoundness in beryllium castings, an investigation was undertaken primarily to study this particular problem and, secondarily, to devise methods of overcoming the other difficulties encountered in the founding of beryllium. The objectives of the laboratory work were multifold: 1. To devise a practical method of melting, other than vacuum melting, by means of which consistently sound beryllium castings could be produced. 2. To obtain fundamental data which would promote a better understanding of the causes of gas unsoundness in beryllium. 3. To develop a casting technique which would permit low melt temperatures, minimize dross defects and hot cracking, and eliminate reaction with the mold surface.

Up to the present time, a considerable amount of progress has been made on the first and third objectives, with the result that it can now be safely stated that consistently sound castings can be made by the open-pot melting method, using argon as a protective atmosphere and a proper casting technique. There has been some progress on the second objective of the project, but it cannot yet be safely stated that the problem is completely understood.

Most of the experimental work has been conducted in an enclosed melting and pouring apparatus in which very close control of melting variables has been effected. Findings based on the results of the work conducted in this small experimental apparatus have been applied to large-scale melts which have been made by techniques suitable for duplication on a commercial scale.

Cleveland Meeting, October 1949.
TP 2701 E. Discussion of this paper (2 copies) may be sent to *Transactions* AIME before Dec. 1, 1949. Discussion is tentatively scheduled for publication in May, 1950.
Manuscript received April 28, 1949; revision received July 25, 1949.

* The experimental work described in this paper was sponsored by the Atomic Energy Commission, under Contract W-7405-eng-92 and was issued as AEC D2479.

† Assistant Supervisor, Battelle Memorial Institute, Columbus, Ohio.

‡ Supervisor, Battelle Memorial Institute, Columbus, Ohio.

§ Research Engineer, Battelle Memorial Institute, Columbus, Ohio.

SECRET

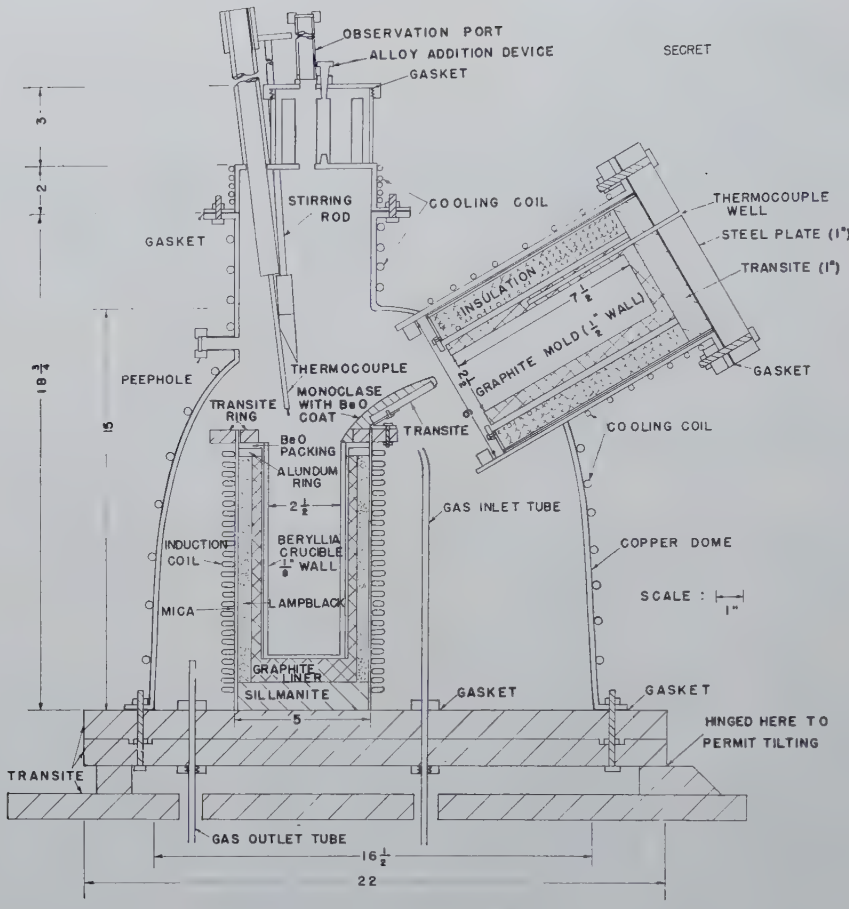

FIG 1—Sectional view of gas atmosphere induction furnace.

The Controlled-atmosphere Furnace

The experimental apparatus for melting and pouring under controlled conditions has been termed the small or controlled gas-atmosphere induction-melting furnace. A sectional view of this furnace is shown in Fig 1. The sketch shows the induction furnace lined with a beryllia crucible and equipped with a graphite mold. Other crucible and mold materials have been investigated in this apparatus, but those mentioned have been selected as the best for the work conducted to date.

As shown in Fig 1, the apparatus consists of a copper dome which fits over the induction furnace. The mold is integral with the dome. This arrangement permits the control of the composition of the ambient atmosphere used during melting and pouring. After putting the dome in place, the charge is melted in the furnace and then cast into the mold by revolving the entire assembly about the axis shown in the lower righthand corner of the drawing. Upon revolving the assembly, the melt pours over the lip of the crucible and into the mold according to the Durville pouring method. This method of pouring is very desirable for easily oxidized or drossy metals because it permits the metal to be poured with a minimum of disturbance of the oxide film and thus prevents the inclusion of dross in the castings. The furnace assembly with the dome installed and in the melting position is shown by Fig 2.

The argon gas used as an atmosphere during melting and pouring is purified and dried, if a low humidity is desired, before it enters the dome. The rate of flow of the gas is closely controlled, its temperature inside the dome measured, and the humidity of the gas that leaves the dome determined. The temperature of the metal throughout the melting cycle is closely controlled, and the temperature of the graphite mold is also closely regulated. The dome is equipped with (1) a cooling coil through which various cooling liquids can be circulated, (2) peepholes for viewing the crucible and mold, and (3) a poking rod and an alloy addition device which permits these operations without opening the dome.

Melting and Casting Large or Small Beryllium Heats

FURNACES AND FURNACE LININGS

The induction furnace is most suitable for the melting of beryllium. Graphite linings for the induction furnace have been used but are not very practical since, at a temperature of about 75° above the melting point of beryllium, the reaction $Be + C \rightarrow Be_2C$ takes place. Since the reaction is exothermic, the utility of a graphite crucible is limited by the necessity of an accurate control of the temperature of the melt.

Magnesia linings for induction furnaces, employed in melting beryllium, have been used in the past with some measure of success. The use of magnesia was abandoned when it was found that the fluxes used in melting beryllium attacked this refractory. Since fluxes are no longer necessary in the melting of beryllium, it may be possible to return to the magnesia lining. This possibility should be investigated.

Large-scale melts have been made most successfully in induction furnaces lined with a graphite-bonded silicon carbide known commercially as Tercod. They are conveniently backed with lampblack for high thermal insulation. Tercod crucibles are available in a variety of sizes and shapes. In the experimental work, they have been used in the melting of heats ranging from about 3 lb up to about 85 lb.

Although Tercod crucibles have been successfully set in the large induction furnace with a silica sand backing, best results have been obtained using a lampblack (Norblack) backing. This material is rammed tightly around the crucible, the coils being protected with a layer of ramming mix next to the coil and a layer of asbestos paper between the ramming mix and the Norblack. With the 80-lb melts, melting time has been cut from 2½ to 1½ hr by the use of the insulating lampblack backing.

The Tercod crucible is ordinarily supplied with a borosilicate glaze. Tercod crucibles, having an alumino-silicate glaze on the outside and little or no glaze on the inside, are said to be available. Up to the present time, the glaze has been removed by melting a cryolite wash in the crucible. The cryolite is then removed by melting a wash heat of beryllium in the crucible. The wash heat may include scrap beryllium such as turnings, sawings, and others. Often, metal containing dross skimmed from previous heats is added to the wash heat which then forms a protective film of beryllium oxide on the inside of the Tercod crucible. Without this protective layer, the Tercod may be attacked by the beryllium.

The Tercod crucible does not appear to be suitable for use in the small gas-atmosphere induction furnace, because under such conditions of melting, the oxide film on the Tercod is not maintained and the melt reacts with the crucible. The use of cryolite for the removal of the glaze is undesirable from a health standpoint because, on subsequently using the crucible for melting beryllium, copious fumes of beryllium fluoride are formed as a result of the reaction between beryllium and the residual cryolite (Na_3AlF_6). It is possible that some means other than that which is used at the present time can be devised for the removal of the glaze and the attainment of a beryllia coating on the Tercod.

The development of beryllia crucibles for use in the small gas-atmosphere induction furnace (Fig 1) has been a step of great importance in the experimental procedure. After a considerable number of trials of various materials, it was found that a beryllia crucible was satisfactory if it was fired by slow heating to 3300°F, and then held at this temperature for 4 hr before slowly cooling to room temperature. Without such treatment, the crucibles fail after each heat because they are subject to considerable dimensional change during the heating and cooling cycle. After firing at 3300°F, the dimensional stability is very satisfactory and crucibles invariably last for 15 to 20 heats and fail through the formation of a skull of beryllium oxide on the inside of the crucible and not through cracking.

The spout of the experimental furnace is lined in such a way that during

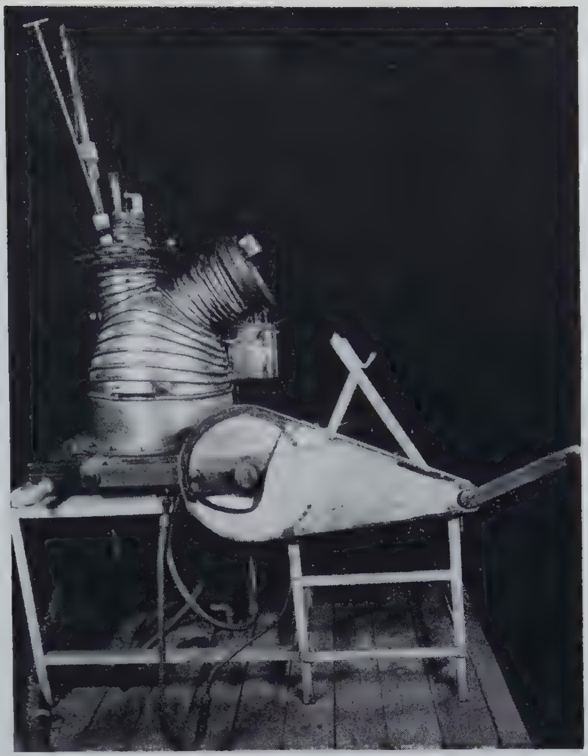

FIG 2—Photograph showing the small controlled-atmosphere induction furnace used to make melts of 1 to 2 lb each.

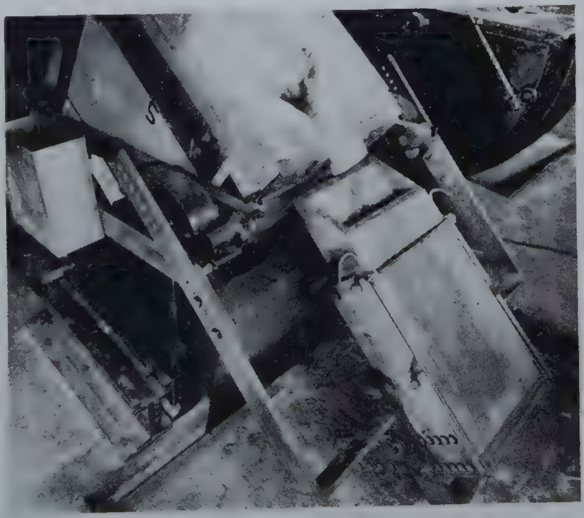

FIG 3—Photograph of the large induction furnace with a graphite mold and tilting mechanism for making the cast 2-in.-round remelting ingots for the furnace illustrated by Fig 1 and 2.

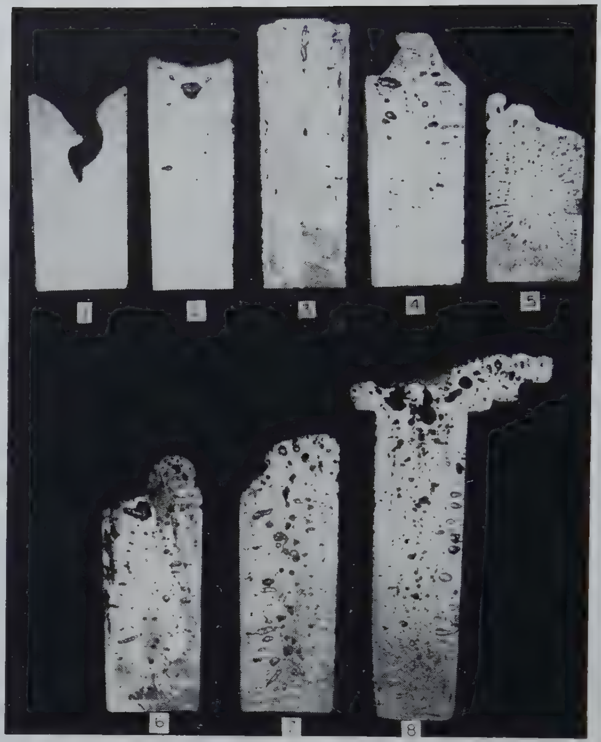

FIG 4—Photograph showing a series of beryllium castings having a considerable range in unsoundness, made in the gas-controlled-atmosphere induction furnace.

the pour the metal contacts only the beryllia refractory.

New beryllia crucibles, even after preheating at 3300°F, are generally unsatisfactory for the melting of beryllium because the first melt made in a new crucible or in a furnace which has not been used for a considerable length of time is often very "gassy." In such instances, the use of a wash heat of beryllium for conditioning the crucible is recommended if sound castings are to be consistently obtained.

One disadvantage of the induction furnace for melting beryllium is that dross is often inductively stirred into the melt and results in dirty castings. When a Tercod crucible is used for the lining, the conductive crucible shields the melt from much of the electromagnetic field which would induce too violent agitation. A further advantage of the Tercod crucible is that it can be heated to a high temperature before the beryllium charge is added to it, thus permitting rapid melting if desired.

The stirring which occurs in the melt prepared in the controlled gas-atmosphere induction furnace (Fig 1) containing a beryllia crucible is of less importance because the use of the inert atmosphere eliminates the dross to a great extent. Furthermore, as shown in Fig 1, the beryllium melt is shielded to some extent from the inductive field by means of a graphite backer for the beryllia crucible.

Although induction heating has been used exclusively in the experimental melting of beryllium, it is conceivable that some other form of heating, such as electrical resistance heating, might be satisfactory. It is unlikely that gas-fired furnaces, unless mixtures other than city gas and compressed air were used, would be suitable because of the high-flame temperatures necessary for the melting operation and the gas absorption from the products of combustion. Arc melting probably would not be desirable because of the possible contamination of the melt by the electrodes.

SELECTION AND PREPARATION OF MELTING STOCK

Beryllium metal stock available for melting in the experimental work has ranged in purity from about 89 pct beryllium up to about 97 pct beryllium. The balance of this material has been, for the most part, fluoride flux remaining in the material from the refining operation. Very often it has also contained about 0.2 pct aluminum and up to 1 pct magnesium. Melting this material by the open-pot method markedly reduces the content of fluoride and magnesium.

In order to prepare 1- to 2-lb charges for the experimental melts, the as-received beryllium is melted in large-scale heats weighing about 85 lb and is cast into 2-in.-diam bars. This melting is conducted in an open pot, using a Tercod-lined induction furnace with a stream of argon directed against the melt surface. The melt is poured in air into graphite molds, 4 bars per mold, using the Durville principle of pouring. Fig 3 shows the mold and apparatus used to prepare the 2-in. bars, the furnace being in a tilted position. The 2-in.-diam bars are cut to lengths weighing about 1.3 lb each. Such a bar makes an ideal material for melting stock in the experimental work because of its uniformity from piece to piece and its uniform surface area. Furthermore, during melting, the solid piece melts down uniformly with no opportunity for bridging which often occurs when lump materials are melted in the small, experimental induction furnace.

It is desirable that the beryllium melting stock, for large or small heats, be as clean as possible and dross should be removed by grinding the surface. The chances of obtaining an unsound heat are greatly minimized by drying the stock thoroughly before melting it. This drying operation can be effectively carried out by holding the material at a temperature of 500 to 800°F for about 12 hr before melting. Naturally, the chance for gas absorption from the surface of the beryllium melting stock is minimized by using pieces as large as practicable.

MELTING TECHNIQUES

Because of the severe chemical reactivity of beryllium, it must be protected from reaction with oxygen and nitrogen during melting. Melting beryllium under a fluoride flux prevents drossing and, in a number of instances, successful castings have been poured by this method. On the other hand, the flux melting method is difficult to use because, during this type of melting, copious fumes evolve from the flux and these fluoride fumes are very toxic. A second disadvantage of this melting method is that the flux is very hygroscopic and, unless it is melted separately and added to the molten beryllium metal, a large quantity of hydrogen may be absorbed from the moisture in the flux. The flux is denser than the molten beryllium and, while it crusts over and is thus mechanically held on

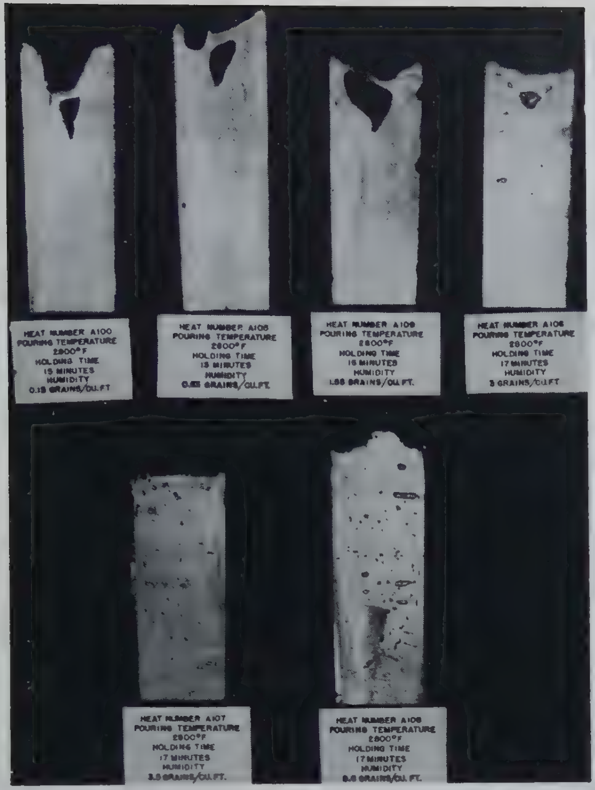

FIG 5—Series of ingots showing the relationship of gas unsoundness to the humidity of the ambient atmosphere.

top of the melt, portions of the flux invariably sink and become entrapped in the metal during the pouring operation. This entrapment of flux occasionally results in flux inclusions in the castings.

Melting under a hydrogen atmosphere has been reported in accounts on the German beryllium industry. This method has not been tried, but melting under an inert atmosphere appears to be, by far, the most practical method for melting beryllium. Inert atmospheres of the argon or helium type are satisfactory. Argon has the advantage that, being denser than air, it forms a better blanket over the surface of the melt than helium which is lighter than air and has a greater tendency to rise. Attempts have been made to use dry nitrogen, but large quantities of beryllium nitride are formed which make this gas undesirable.

Investigations of the gas unsoundness in beryllium castings poured from melts prepared in the small, experimental gas-atmosphere induction furnace have shown that a high degree of purity and of dryness of the protective gas is necessary if sound castings are to be produced. In order to produce argon of high purity for the melting unit, the gas is passed first through copper turnings at 1200°F to remove the bulk of the oxygen present, then through a copper coil which can be refrigerated to a temperature of minus 100°F to remove most of the moisture and, finally, through titanium turnings at 1200°F to remove nitrogen and the last traces of oxygen and water vapor.

Fig 4 illustrates the range of unsoundness which can be obtained in beryllium. Microporosity, such as occurs in copper-base alloys, was not a contributing factor to the unsoundness.

The effect of the moisture content in the argon atmosphere on the soundness of beryllium castings made in the small-scale experimental furnace is shown by Fig 5. For this particular series, it is believed that the other variables were held at values which, excepting for the humidity of the ambient atmosphere, are conducive to a high degree of soundness. The transition from sound to unsound beryllium castings appears to have occurred at a moisture level of about 3 grains per cubic foot. Other series made under similar conditions have indicated that the transition level is considerably lower. In one instance, it appeared to be at about 1.0 grain per cubic foot.

In general, the longer the time that a melt of beryllium is held in the molten state, the more unsound the resultant ingot will be. The effect of increasing the holding time of beryllium melts at the pouring temperature in the gas-atmosphere induction furnace from 4 to 30 min. before pouring is shown in Fig 6. The humidity of the ambient argon atmosphere used for the heats from which these two ingots were poured was less than 1 grain of moisture per cubic foot. The graphite mold was held at a temperature of 300°F and a pouring temperature of 2800°F was employed. This increase in gas unsoundness produced by a prolonged holding at the pouring temperature is typical of some other metals also.

The effect of the length of the holding period at pouring temperature on gas unsoundness should not be confused with the length of time required to melt the metal. The effect of the speed with which the metal is melted and then brought to the pouring temperature has not yet been investigated. Since the rapid melting of beryllium may tend to increase gas unsoundness, it should be emphasized that Fig 6 shows the effect of holding at the pouring temperature. In other words, it is known that, once the metal has reached the pouring temperature, it should be poured without further holding. It does not necessarily follow, however, that the metal should be melted as rapidly as possible. Indeed there is some evidence that slow melting is desirable.

The typical effects of the pouring temperature on the gas unsoundness of beryllium castings are shown in Fig 7. All of these ingots were poured in a graphite mold at 300°F. The heats were made in an argon atmosphere at less than 1 grain of moisture per cubic foot. The tendency to increase gas unsoundness as the casting temperature increases is typical of most metals.

Fig 8 shows a typical example of the occurrence of unsoundness in a casting made from the first melt in a beryllia crucible preheated to 3300°F before using.

MELTING POINT DETERMINATION

The melting point of beryllium, as reported in *Metals Handbook*, is 1285 ±40°C (2345 ±70°F). In the course of the melting of beryllium in the controlled-atmosphere furnace, one melt was allowed to freeze in the crucible and the cooling rate determined by a calibrated platinum, platinum-rhodium thermocouple protected by a beryllium oxide tube. The resultant curve, which is shown in Fig 9, shows a

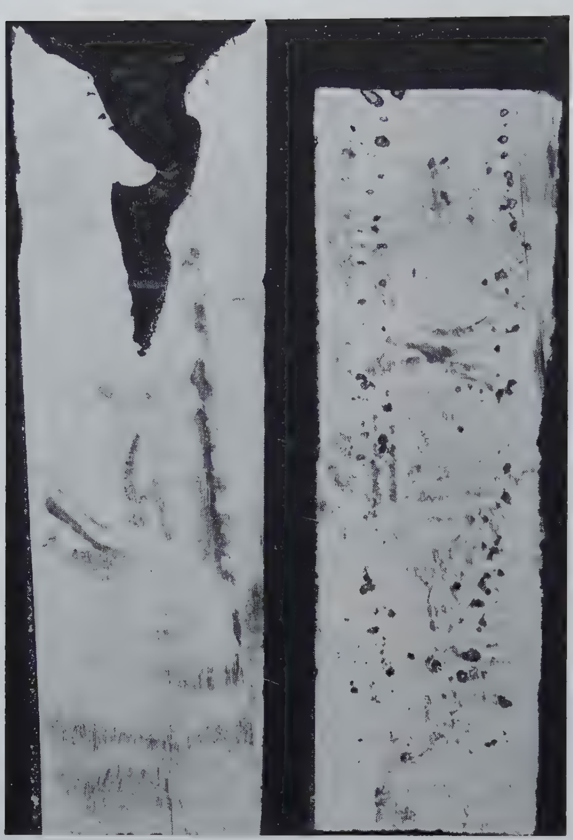

FIG 6—The effect of holding time on the occurrence of gas unsoundness in beryllium.

Pouring temperature 2800°F, mold temperature 300°F.

A-77. Melt poured as soon as the pouring temperature was reached.

A-78. Melt held 30 min. at the pouring temperature before pouring.

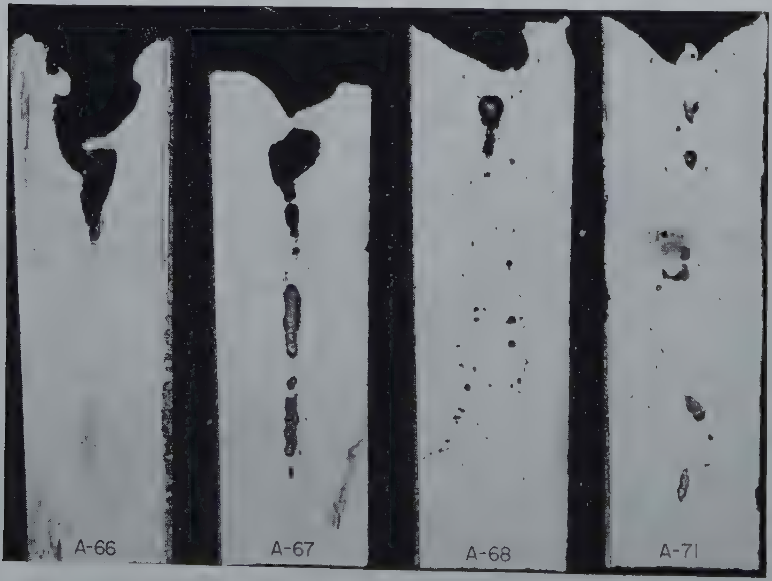

FIG 7—The effect of pouring temperature on the occurrence of gas unsoundness in beryllium.

A-66, held 16 min., poured at 2700°F, mold temp. 300°F.

A-67, held 16 min., poured at 2800°F, mold temp. 300°F.

A-68, held 12 min., poured at 2900°F, mold temp. 300°F.

A-71, held 18 min., poured at 3000°F, mold temp. 300°F.

melting point of 2400°F after some supercooling. This value is near the high limit previously reported. A melting point taken as the maximum temperature after supercooling can be considered only a minimum possibility since it cannot be assured that the maximum temperature after supercooling is anything more than a balance between the heat released on freezing and the heat loss by natural cooling. Thus a value of 2400 +20–10°F seems to be the melting point as determined in this test. The metal was remelted virgin beryllium. By spectrographic analysis it contained 0.10 pct Al, 0.08 pct Si, 0.10 pct Fe, < 0.05 pct Mg, and only traces of other impurities. Carbon was low, as judged by metallographic examination, but no estimate of oxygen content is available.

CASTING PRACTICE

Beryllium static castings can be produced with a minimum of difficulty from gas unsoundness and oxide and dross inclusions if they are poured directly from the furnace using the Durville method, as illustrated by Fig 1, 3, and 10. Ladling of the metal is obviously undesirable because it increases the contact of the metal with the atmosphere, makes higher melt temperatures necessary, and also increases turbulence and attendant included dross. Furthermore, ladles are often a source of gas pickup through unsatisfactory drying. In order to reduce the formation of dross, it is desirable that the molten metal be introduced into the mold with a minimum of turbulence. This can be accomplished by permitting it to run down a slight incline into the mold cavity. Although a mold can be tilted by hand to accomplish this end, the best practice is to design the mold for attachment directly to the furnace so that it tilts or can be separately tilted as the furnace is tilted. Fig 3 and 10 illustrate this technique showing the mold and method of pouring 2-in.-diam ingots and a slab about 2 in. thick and 18 in. square. The ingot mold is tilted by hand, using the special tilting mechanism, thereby permitting several to be poured from the same melt, whereas the slab mold is attached to the furnace and tilts with it, thereby permitting the pouring of one casting per melt. The metal is poured so that it runs down the slightly sloping surface of the riser and, as the furnace is tipped over, the mold is filled without causing undue turbulence. In both instances, the melt is poured direct from the furnace into the inclined mold. The end bells of the ball mill, shown by Fig 11, also illustrate castings made by this method. The end plates are sound, the dark spots being the individual coarse grain revealed by the machining operation.

Centrifugal casting is an ideal method for producing beryllium castings when the size and shape of the casting are suitable. In order to pour a large-diameter casting, ladling metal is often necessary, though direct pouring should always be used if possible. The nature of the centrifugal casting process is such that it tends to reduce or minimize the difficulties with dross formation and gas unsoundness. A rapid pour into the mold is desirable to prevent cold shuts and to minimize the distance of travel of the metal. In the large-diameter castings, it is also desirable to pour the metal into the mold as near as possible to the periphery.

In order to cast an inside vertical wall centrifugally, it is necessary to use a rotating speed that gives a value of centrifugal force at the inside wall of the casting of at least 75 times the force of gravity. Thus the minimum speed of rotation is fixed and is dependent upon the casting diameter. Most of the centrifugal castings have been cast at this speed because it was feared that too high a speed might promote cracking. However, speeds somewhat higher than the minimum showed no harmful effects.

Some of the castings made successfully by centrifugal methods are as follows:

1. A cylinder 2¼-in. od, $\frac{3}{16}$-in. wall, 30 in. long, cast horizontally.
2. A ring 19-in. od, 1-in. wall, 5 in. high, cast vertically.
3. A ring 19-in. od, 7½-in. wall, 5 in. high, cast vertically, using a water-cooled steel mold. This casting after cutting and some machining of the inside surface is shown by Fig 12. The shrinkage on the inside periphery is to be noted.
4. A ring 52-in. od, 2-in. wall, 4 in. high, cast vertically. Fig 13 shows this casting as stripped from the mold.
5. A ball mill 9-in. od, 1½-in. wall, 8 in. long, cast vertically. This casting is illustrated by Fig 11.

A sound, fine-grained molded graphite makes an ideal mold material. It can be used successfully both in static and centrifugal casting. Although successful castings have been made in steel molds coated with acetylene soot, beryllia, or alumina, there is a tendency for beryllium metal to cut steel and, in general, the use of this material is not recommended. Baked, oil-bonded magnesia and zircon-base molds have been used, but the effects of these materials on gas unsoundness are not completely understood and they should be used with caution.

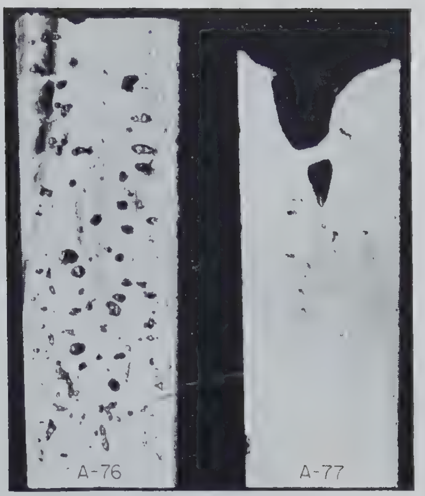

FIG 8—The effect of the use of melting crucible on the occurrence of gas unsoundness in beryllium.

Both castings poured at 2800°F, using a mold temperature of 300°F.

A-76, first heat in the crucible, namely, a wash heat.

A-77, second heat in the crucible.

The extreme tendency for beryllium to hot crack must be guarded against when designing the casting. To accomplish this, the molds must be designed in such a way that the casting is not restricted during its solidification or cooling period. The development of a collapsible mold material for this metal would be very desirable. Meanwhile, small, moderately intricate castings can be made by opening the graphite mold immediately after the casting is solidified so that the metal is subjected to a minimum of restriction as it cools.

All molds should be thoroughly dried before use. A desirable practice is to hold the graphite mold at 1000°F for about 1 hr and then cool it to not lower

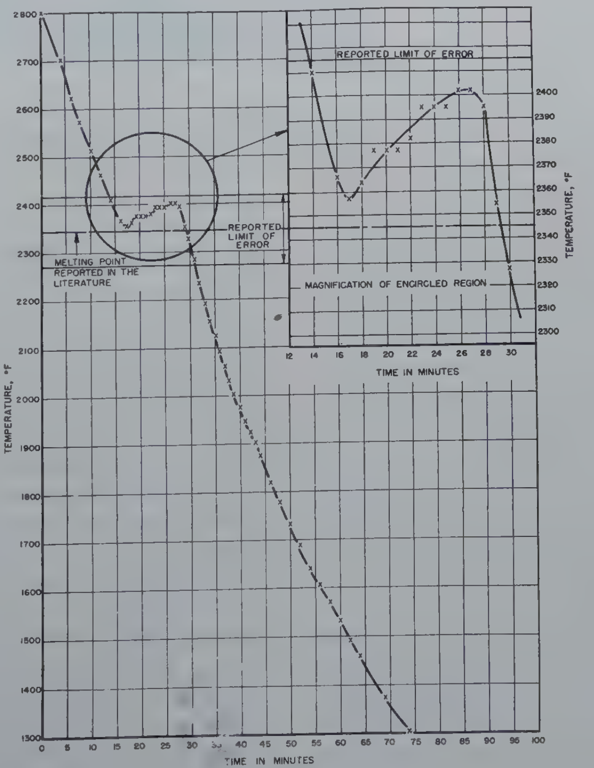

FIG 9—Cooling and solidification curve, Heat No. A-14.

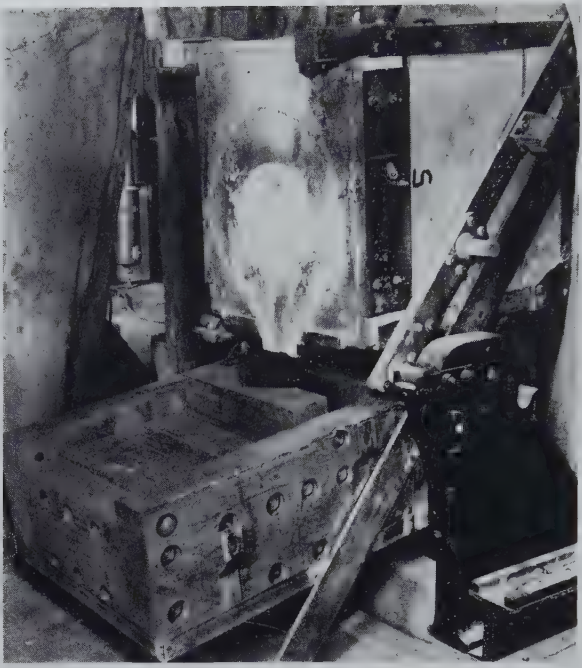

FIG 10—Photograph showing the graphite mold attached to the large induction furnace.

The mold is for a plate 18 inches × 18 inches × 2 inches, which is poured by the Durville method.

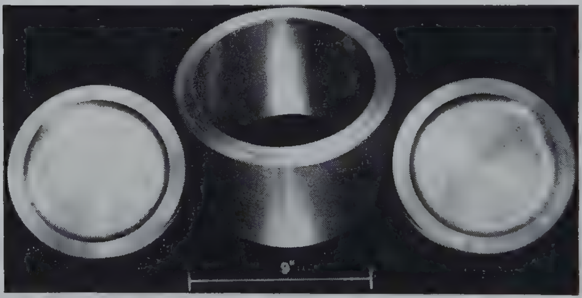

FIG 11—Photograph showing a cylindrical casting and end plates to form a small ball mill approximately 8 in. od.

than 300°F for use. In some instances, where a sufficiently large high-temperature furnace was not available, the molds were preheated to only 600°F and held for 16 hr. Graphite molds should not be allowed to cool below 300°F until all of the castings to be poured into them have been produced. If the mold is held for any length of time at room temperature, it should be reheated to 1000°F (or lower, if the higher temperature is not practicable) before subsequent use.

In the study of graphite as a mold material, it has been observed that the tendency toward gas unsoundness in the casting increases with repeated use of the mold. The reason for this behavior of the graphite is not definitely known, but to insure against the possibility that the re-use of the graphite mold becomes a variable in the experimental studies, no mold is used for more than ten casting operations.

Discussion of Results

Since the experience with the founding of beryllium has not been extensive, it is difficult to evaluate the limitations of the art and science of producing high-quality castings. In this investigation, some consideration has been given to practically all of the founding characteristics of beryllium, and special attention has been given to that problem which has appeared to be the most troublesome, namely, gas unsoundness. The seriousness of the gas unsoundness problem in casting beryllium can be appreciated by observing the range of unsoundness which may be encountered, as shown in Fig 4.

The unsoundness observed in Fig 4 is clearly caused by an evolution of gas during solidification of the metal. The precise type of gas evolution or the particular gas or gases involved is not definitely known. In general, there are two types of gas evolution, as follows: 1. Gas evolved during solidification of the metal because of the very marked decrease in solubility of the gas as the metal changes from liquid to solid. 2. The formation of a relatively insoluble gas by a reaction which occurs between two constituents dissolved in the melt. A typical example of such a phenomenon is the carbon monoxide gas evolved

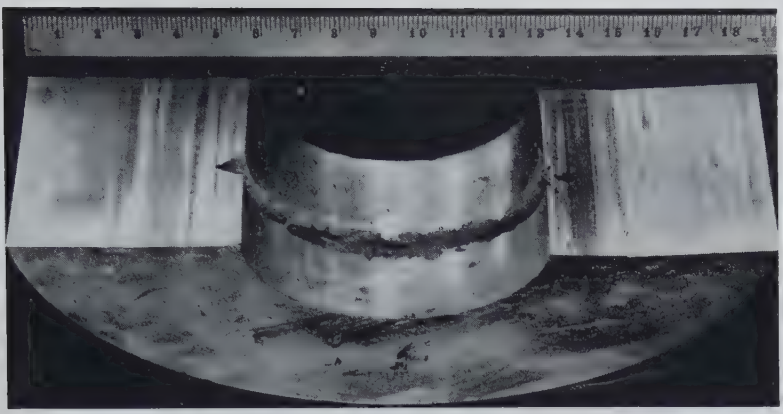

FIG 12—Photograph showing a centrifugal casting 19 in. od, a 7½-in. wall, and 5 in. high.

The casting is shown after it was sawed and some machining done on the inside surface. The shrinkage on the inside periphery is evident.

in a rimming steel ingot as a result of the reaction between dissolved carbon and oxygen. A second example is the formation of steam in copper-base alloys as the result of a reaction between hydrogen and oxygen, or an oxide dissolved in the melt. In both of these instances the gases formed, as a result of the reactions, are relatively insoluble in the solidifying metal and thus precipitate or evolve from the melt.

There are many possibilities of these two types of gas evolution which might occur in beryllium. Hydrogen, carbon monoxide, carbon dioxide, nitrogen, and possibly other gases might evolve from the melt during solidification as Type 1 gas evolution. Type 2 gas evolution could occur as a result of the reaction of hydrogen and oxygen or oxide in the melt to form steam, or the reaction of carbon or carbon monoxide with oxygen or oxide in the melt to form either carbon monoxide or carbon dioxide. If oxygen or beryllium oxide is as insoluble in molten beryllium as is oxygen or the respective oxide in the light alloys, aluminum and magnesium, Type 2 gas evolution may not occur. There have been a few instances in the experimental work where unsound ingots have shown an increased carbon monoxide content. The samples for these tests were selected to include whole gas bubbles, so that evolved as well as dissolved gases would be determined in the vacuum-fusion analyses.

Except for a few instances where carbon monoxide has been found in the unsound ingots, practically all of the gas unsoundness observed in beryllium can be explained by the supposition that hydrogen dissolved in the melt evolves during solidification as a result of decreased solubility. The principal source of hydrogen is, of course, moisture. Experimental proof of the effect of the moisture content in the argon atmosphere on the soundness of beryllium castings made in a small-scale experimental furnace is shown in Fig 5. In addition to this experimental proof of the effect of moisture, there are many indications or circumstantial evidence which place hydrogen, absorbed from moisture, at the head of the list as the main cause of gas unsoundness in beryllium. These are: 1. The necessity for melting a wash heat in a crucible before consistently sound castings can be obtained from it. 2. The necessity, when using the flux method, to melt the flux before it is added to the metal. If the flux is not melted, a considerable amount of hydrogen may be absorbed from the water in the flux. 3. The necessity for drying molds thoroughly before sound beryllium castings are made in them. 4. Melting a charge previously wet with water has produced gas unsoundness in an application where such unsoundness was desired.

In addition, there have been many other indications which have shown that moisture should not be allowed to contaminate any of the tools used in the melting process which are likely to come into contact with the molten beryllium.

Summary and Conclusions

The success with which beryllium castings can be made in the plant or laboratory depends, to a great measure, upon how well certain difficulties attendant to the handling of this metal are overcome. These difficulties, not peculiar to beryllium alone but encountered in the handling of many commercial metals, include a high degree of reactivity with oxygen and nitrogen; this characteristic is accentuated by the high pouring temperatures of 2600–2900°F and results in the formation of dross which, if carried over to the mold, can produce serious casting defects. Another characteristic of the metal is that it is very weak and brittle at high temperatures and, therefore, tends to crack easily when hot. Its low ductility when cold can also result in cracks if the normal contraction of the casting is restrained during cooling. Finally, and perhaps the greatest difficulty encountered has been unsoundness resulting from gas evolution during solidification.

Another characteristic of the metal which must be carefully considered is the apparently extreme toxicity of the fumes evolved during melting and of the dust formed during machining, grinding, sawing, and other procedures.

The problem of gas absorption has been studied by the use of a small, controlled gas-atmosphere induction furnace. It has been found that if reasonable care is taken to prevent the exposure of beryllium to moisture during the melting and casting operations, consistently sound castings can be produced.

The reason for the occurrence of unsoundness is not completely understood but it is apparent from the experimental work that hydrogen picked up from moisture accounts for a major part of the gas which causes the unsoundness.

The results of the present investigation have added considerably to the

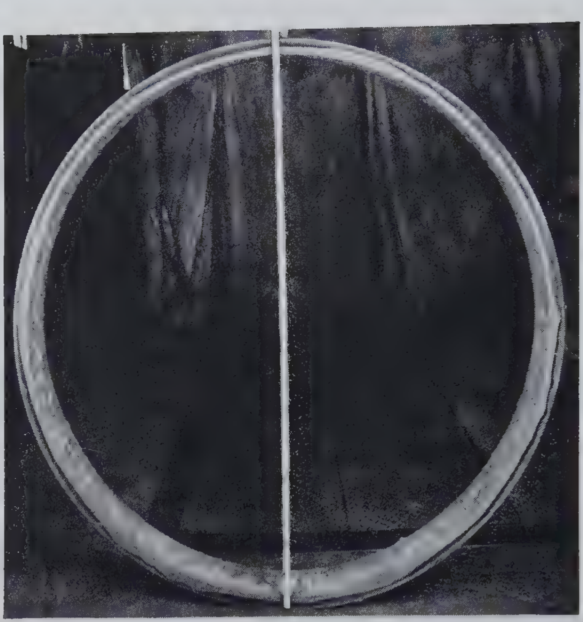

FIG 13—Photograph of a cylindrical casting 52 in. od, with a 2-in. wall, 4 in. high.
This casting is shown as stripped from the mold.

knowledge relating to the proper handling of beryllium in the foundry. Techniques have now been developed which will permit the production of consistently sound beryllium castings from heats weighing up to 80 lb and limited in size only by the melting equipment available for this particular operation.

The following recommendations for the melting and casting of beryllium are based upon observations made in the course of the experimental work, including the preparation of heats weighing up to 80 lb:

1. Melts may be made in thoroughly preheated beryllia or graphite-bonded, silicon carbide crucibles (Tercod). Usually, a wash heat is desirable in a new crucible to insure complete removal of moisture. High-frequency induction heating is the most convenient.
2. The beryllium melting charge should be thoroughly dried out at a temperature between 500 and 800°F. Thereafter, in the melting process, the metal should not be subjected to any atmosphere or material which might be a source of moisture, or gas, particularly hydrogen.
3. No fluxes need be employed, but the metal should be protected from the atmosphere by means of argon of the lowest possible moisture content. This can be accomplished by covering the melting crucible and introducing argon at right angles to the melt surface so that it mushrooms out over the bath. The argon can be satisfactorily dried by passing it through a coiled copper tube held at about minus 100°F.
4. The time that the metal is kept in the molten condition, especially at the pouring temperature, should be held to a minimum, and the casting should be poured as soon as the proper melt temperature has been reached.
5. The maximum temperature should be kept low, preferably less than 2900°F, and the pouring temperature should also be kept at a minimum, consistent with the degree of fluidity necessary to fill the mold cavity completely without cold shuts or misruns.
6. Where possible, the casting should be poured directly from the furnace in order to carry out effectively these recommendations. Ladling, while not desirable, may be useful when pouring centrifugal castings.
7. The mold material should be such that the metal will not react with it. Thoroughly preheated graphite which has not been used for more than ten casting operations appears to be satisfactory, though there are considerable differences among various grades of graphite.
8. Dross entrapment should be avoided. It has been found that this can be accomplished most effectively by introducing the metal into the mold gently by permitting the molten metal to run down a low incline into the cavity, using the Durville method or a modification of it.
9. Any undue restriction to the contraction of the hot casting, such as a fin which would result in cracking, should be prevented by proper design of the mold cavity. As far as is known to date, this means that it is feasible to cast only relatively simple shapes which do not present problems of restriction to contraction. However, the precise limitation on complexity of design has not been established. The development of collapsible molds for beryllium casting is a definite possibility.
10. Beryllium castings having fairly thin sections can be made in a graphite mold if the surface areas are relatively small. The remarkable flowability of beryllium in graphite molds and the reproduction of minute detail in the mold design should not be overlooked.
11. The size of the castings, including the gates and risers, is limited only by the size of the available melting equipment. At the present time at Battelle, the maximum is about 80 lb of beryllium.
12. Within the limitations outlined, both static and centrifugal castings can be satisfactorily made.

Acknowledgments

The authors gratefully acknowledge the contribution of Mr. E. C. Kron, who did some of the earlier work on beryllium, and the guidance of Dr. H. W. Russell and Dr. C. H. Lorig, who provided general supervision of the work.

Metallographic Examination of Beryllium Alloys*

M. C. UDY,† G. K. MANNING,† and L. W. EASTWOOD,† Members AIME

Introduction

Those who have examined beryllium and beryllium-rich alloys under the microscope have noted the results of the difficulties encountered when preparing these materials for examination. Hard constituents are readily chipped and pulled out of the matrix, and the soft ones are easily gouged out or embedded with abrasive or other material. The matrix is easily deformed, which makes it very difficult to remove the effects of scratches. Furthermore, the matrix and some of the constituents are also readily pitted during etching, which makes the structure difficult to develop.

The metallographic techniques designed to avoid these difficulties are neither radically new nor necessarily the best possible procedures. They were developed at Battelle to fill immediate requirements as part of a study of the preparation and pouring of beryllium melts as described in a separate paper.

A part of the research program on the causes of gas unsoundness in beryllium castings entailed a study of the effects of such gases or gas formers as oxygen or oxides, nitrogen or nitrides, and carbon or carbides. These gases or gas formers, if dissolved in the melt, might be an important factor in the study of unsoundness caused by gas evolution in beryllium. Because it was necessary to be able to distinguish these gases or gas formers, if present as alloy constituents, from metallic phases also present as alloy constituents, a series of alloys was prepared with additions of the various possible metallic and nonmetallic constituent formers. It should be emphasized that the constituents referred to as gases or gas formers are important in the study of gases in beryllium only if they form a part of the alloy, that is, if they dissolve in the liquid or solid metal.

During the first part of the development of metallographic techniques, the Massachusetts Institute of Technology, unpublished report (TC 3315, Nov., 1945) by Paul Gordon, describing various microconstituents in beryllium, was quite useful. Of particular interest in this report is the confirmation of one of the conclusions drawn from the present investigation, that is, that a distinct oxide phase apparently does not occur in beryllium.

The Preparation of Metallographic Specimens

GRINDING PROCEDURE

The original specimen is either sawed or cut on an abrasive wheel to a convenient size. For best results, the surface to be polished should not be more than about ¼ in. square, and it is convenient to mount the specimens in bakelite to facilitate handling. Two alternative grinding procedures have been developed. As one alternative, specimens are ground successively on 120-, 240-, and 400-grit, wet-or-dry metallographic discs. The abrasive discs are revolved at 1750 rpm on a conventional pedestal grinder. The coarsest disc (120 grit) is used either wet or dry, and in most instances, it can be eliminated from the procedure. Grinding on the two finer discs (240 and 400 grit) is accompanied by the application of kerosene. The technique consists of holding an oil can, containing kerosene, in one hand and the mounted specimen in the other hand. While the grinding is being done, several drops of kerosene are applied every few seconds close to the center of the disc. Carbon tetrachloride serves at least as well as kerosene as a lubricant; perhaps it is slightly better, but it volatilizes so readily that an additional health hazard is involved. Light oils and water are not satisfactory for the finer grinding operations.

The second procedure is perhaps slightly slower than the first and requires a more careful technique, but it eliminates the use of kerosene. The specimen is first ground wet on a 240-grit disc, followed by dry grinding on a 400-grit disc.

Finer grinding does not appear to be necessary with either of the two alternative procedures.

The pressures used throughout either grinding operation must be *extremely* light, that is, barely sufficient to hold the specimen in contact with the disc; otherwise, flow and chipping are almost certain to occur.

In both procedures, it is essential that the discs be sharp and that they be discarded as they show evidence of becoming dull or loaded. In general, not more than four or five specimens can be ground on a disc before the disc becomes dull enough to warrant discarding it.

Cleveland Meeting, October 1949.
TP 2700 E. Discussion of this paper (2 copies) may be sent to *Transactions* AIME before December 1, 1949. Discussion is tentatively scheduled for publication in May 1950. Manuscript received April 28, 1949.

* The experimental work described in this paper was sponsored by the Atomic Energy Commission, under Contract W-7405-eng-92.

† Research Engineer and Supervisors, respectively, Battelle Memorial Institute, Columbus, Ohio.

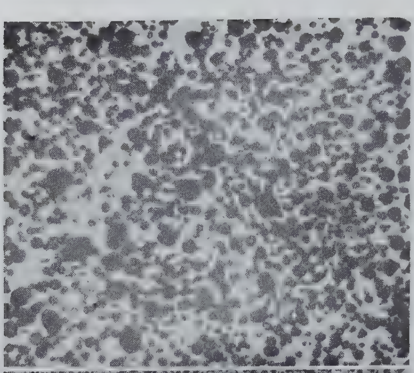

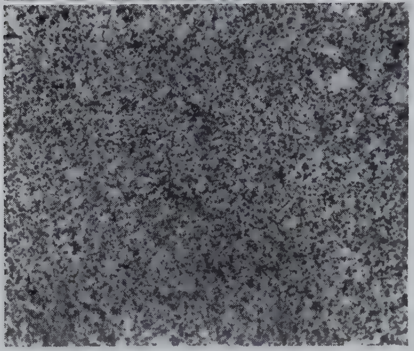

FIG 1 (above)—Heat A-9. Unetched. High carbon from mold reaction.
FIG 2 (below)—Heat A-4. Unetched. High carbon from mold reaction.
× 500. Reduced one-half in reproduction.

Hand grinding of the beryllium alloys has not been successful, even though the grinding is done under kerosene.

The preparation of the specimen may be considered more than half done when a satisfactory fine grind has been obtained. The specimen should be examined at 500 magnification in the ground condition before starting the polishing operation. After some experience, the operator will be able to judge whether or not the grinding has been accomplished without either deforming the surface of the beryllium matrix or breaking out the hard, brittle constituents. If there is evidence that some constituents have been broken out or if there is evidence of flow in the beryllium matrix, it is well to start over again because it is a waste of time to attempt to polish an improperly ground specimen.

POLISHING PROCEDURE

After a proper grind has been obtained on a specimen, the final polishing can be accomplished in a few minutes. Two successful procedures have been developed. With either method, the specimen is slowly counter-rotated on a 4-in. polishing head rotating at 1750 rpm.

The first method is more rapid but less reproducible. The polishing head is covered with worsted serge because the use of longer nap cloths seems to promote pitting and should be avoided. A solution of 5 pct oxalic acid in water is used in conjunction with an abrasive on the polishing cloth. This is an improvement over a more complicated, glycerine-containing solution which was used earlier and which seemed, in some cases, to promote pitting of the specimen. Fine alumina is used sparingly as the abrasive. However, when soft constituents occur, such as those formed by aluminum or tin additions, levigated CP-Fe_2O_3 is better though slower than alumina. When alumina is used as the abrasive, there seems to be a greater tendency for soft constituents to be gouged out. Actual polishing of the specimens apparently requires a proper balance between chemical solution by the oxalic acid on the one hand, with the abrasive action by the alumina on the other. This procedure requires rather careful manual manipulation which can be effected only after considerable practice.

The polishing procedure consists of applying a small amount of abrasive and oxalic acid solution at the beginning of the operation and, as the polishing continues, adding only the oxalic acid solution. As the polishing operation nears completion, the addition of the oxalic acid solution is discontinued and water is added a few drops at a time to keep the wheel slightly moist.

The alternate polishing procedure, slower than the one already described is based on abrasive action alone, and requires less judgment on the part of the operator. It was developed primarily to retain magnesium-rich constituents during the polishing operation. The small-diameter, high-speed wheel is covered with ordinary green billiard cloth, the usefulness of which appears to improve with use. Merck's CP heavy MgO, suspended in 30 pct hydrogen peroxide, is used as the polishing agent. Since this suspension does not "keep" well, it is best to prepare small amounts several times daily. During the polishing operation, a considerable amount of the suspension is used on the wheel, so that, actually, the polishing is done on a layer of MgO rather than on the cloth. The peroxide has two functions. It holds the MgO on the cloth more satisfactorily than does water, and it also appears to inhibit the reaction of water with some of the microconstituents of beryllium, particularly the magnesium-rich phase. Even with this "slower" procedure, polishing can usually be completed within a few minutes.

ETCHING PROCEDURE

No systematic study of etching reagents has been made. However, a number of the common metallographic etchants were tried and, of these, only one appeared to be universally successful on the alloys. This etchant is composed of 10 cc of 48 pct hydrofluoric acid and 90 cc of 190-proof ethyl alcohol. Etching times range from 10 to 30 sec. This etchant outlines and produces many color distinctions to the different alloy phases, and not infrequently develops fine lines in the beryllium matrix which appear to be faults in the lattice structure. The etchant seems to increase in activity after standing for several hours. In general, the other etchants which have been investigated have been found to cause some pitting of the polished surface.

Identification of Constituents

A number of alloys were made especially for metallographic study. In addition, a number of specimens have been included from heats made for other purposes.

Black and white micrographs are included in this paper, and in addition, color transparencies have been prepared of a number of the microstructures. This color photography is of great assistance in preserving and describing the colors of the various constituents. Ansco daylight film was used with a light source consisting of a 6-volt, 18-amp microilluminator, containing a 3200°K ribbon filament. Various combinations of color-correction filters were necessary because of the different reflectivities of the different constituents and, in general, it was difficult to avoid a greenish cast to the background.

No microconstituent has been found which can be identified as an oxide or as a hydride. This, however, does not preclude the possible presence of oxygen (or an oxide) or hydrogen (or a hydride) in liquid or solid solution in the metal, or even as a second phase in the solid metal.

The carbide is a distinctive phase; it is hard, angular, usually gray, and when exposed to the atmosphere, it readily stains, first to all colors of the rainbow and, eventually, to brown.

Fig 1 and 2 are specimens containing a high proportion of carbide, which is the prominent, angular gray constituent. The shadowy, lighter gray phase seen in the background, particularly of Fig 2, is unidentified, but it is probably a silicon-bearing phase. The hydrofluoric etch has no effect on the color of the carbide constituent.

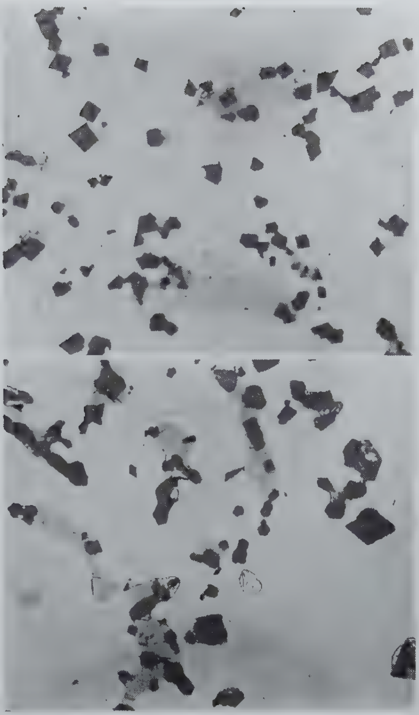

FIG 3 (above)—Heat A-6. Unetched. 1 pct C added.
FIG 4 (below)—Heat A-7. Unetched. 2 pct C added.
× 500. Reduced one-half in reproduction.

Fig 3 and 4 are specimens from heats to which 1 and 2 pct carbon, respectively, were added as graphite. The angular, gray carbide constituent is easily recognizable. The lighter gray constituent (actually a light blue-gray) is a silicon-rich phase, while the bright speckled phase (actually slightly yellow) is an aluminum-rich phase. Fig 3 and 4 should be compared with Fig 1, a high-carbon specimen, and Fig 5, a vacuum-cast material which, in this instance, contains a small amount of carbon in the form of a small quantity of angular, gray carbides. Very little of the light-blue silicon-rich phase is present, but with a relatively greater amount of the yellow speckled aluminum-rich phase. It is of interest that the silicon-rich

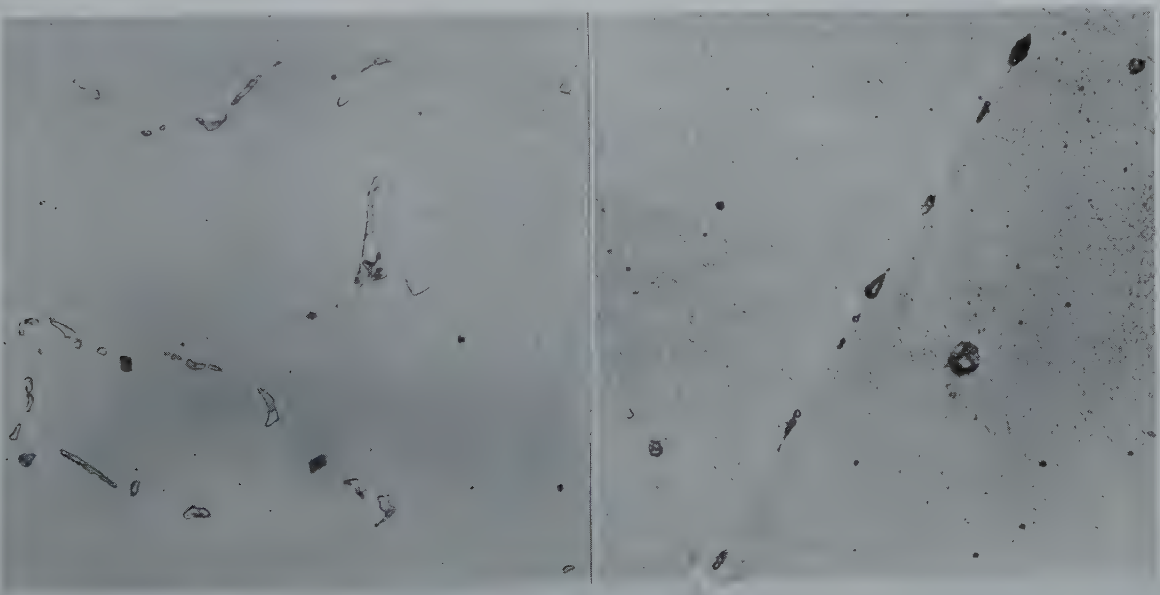

FIG 5 (left)—Vacuum-cast virgin beryllium. Light etch. × 500.
FIG 6 (right)—Heat A-11. Cold worked and deep etched to show grain boundaries. × 500.

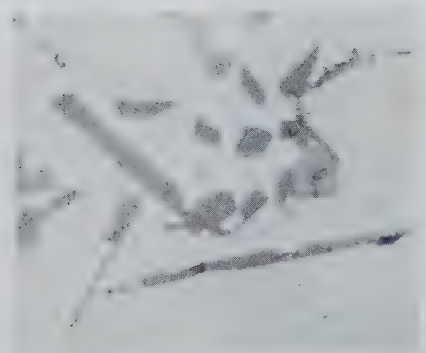

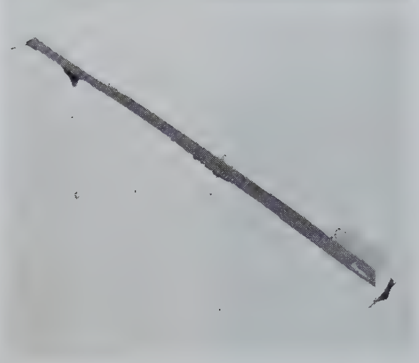

FIG 7 (above)—Heat A-2. Made under nitrogen. Unetched.

FIG 8 (below)—Heat A-2. Isolated nitride needle.

× 500. Reduced one-half in reproduction.

and the aluminum-rich phases can exist in the same "particle" as shown just below the center of Fig 5.

Fig 6 is a photograph of a poorly prepared specimen in which the cold-worked material was not completely removed by the polishing operation. It is of interest, however, that deep etching reveals the individual grains and also delineates the grain boundaries. This treatment is unsatisfactory as a means of revealing "second" phases, however, because the aluminum-rich, silicon-rich, and carbide phases are scarcely recognizable in the figure.

The nitride phase is distinctive. It is also gray, but a darker gray than the carbide, is not affected by the HF etchant, and is usually present in needle-like form. However, in large amounts, it may also have a more massive appearance. Fig 7 is a photograph of a specimen cast from a heat melted under nitrogen and represents a badly segregated part of the ingot. An angular, gray carbide particle is also evident somewhat to the right of the center of the photograph, but other phases are not readily identifiable.

Fig 8 is a photograph of an isolated nitride needle in a portion of the same ingot represented by Fig 7. Associated with the needle are the angular carbide phase, the speckled yellow aluminum-rich phase, and the bluish silicon-rich phase. This latter phase is barely visible in the photograph. Again, the silicon-rich phase and the aluminum-rich phase are seen to occupy the same "particle," about halfway along the top side of the needle. The aluminum-rich phase is also present as an "inclusion" in the nitride and carbide phases. The black areas are holes and a crack is also evident across the lower right-hand corner of the photograph.

One phase found in practically all samples of beryllium studied is an aluminum-rich phase. It has already been noted in the descriptions of the preceding photographs. It is soft and difficult to polish; it is bright yellow and often appears to be speckled. This speckled appearance, revealed by careful polishing, may indicate a eutectic. The HF etch does not affect the color, but does outline the phase which may be present as a grain-boundary constituent or as isolated globules, as shown by Fig 9, a photograph of a 2 pct aluminum alloy. As mentioned before, a light-blue silicon-rich phase is often associated with the bright-yellow aluminum-rich phase. This is noted again in Fig 9, where several areas in the otherwise yellow stringers are occupied by the light-blue phase. It is also possible that the speckled constituent may be the bright-blue, silicon-rich phase, or some other phase attributable to silicon. Only a few carbides are present in the specimen, represented by Fig 9, and they appear about equally abundant in the matrix and in the aluminum phase. In this instance, over-exposure has blackened their appearance considerably as well as darkened the matrix in the photograph.

Fig 10 is a photograph of a heat to which 10 pct silicon has been added. The light-blue phase attributable to silicon is seen in the grain boundaries and as isolated particles. The angular, gray carbide phase is easily recognized, as is the bright-yellow aluminum-rich phase which is associated to some extent with the silicon phase. The light-blue silicon phase is intermediate in hardness between the aluminum-rich phase and the matrix, and is outlined but not stained by the HF etch.

There are probably other phases associated with silicon; one of these is probably illustrated in Fig 11, which is a photograph of a heat that had reacted with a silicon carbide crucible. The triangular-shaped gray phase with a crack running through it is beryllium carbide. The grain-boundary constituent is the light-blue phase previously attributed to silicon. Associated with it are small amounts of the bright-yellowish aluminum-rich phase. The dark, irregularly shaped constituent in the center of the photograph is a hard, dark blue-green constituent whose color is not affected by the HF etchant. It might be silicon carbide, although no positive identification has been made. It also occurs in heats which have had no contact with silicon carbide crucibles, but it always appears to be associated with silicon in some form.

Fig 12 shows a sample to which 10 pct titanium was added. The phase attributable to titanium is slightly pink and generally angular and its color is not affected by the HF etchant. Angular gray carbides are readily identified in the photograph. Aluminum- and silicon-rich phases, if present, have been "absorbed" in the titanium-rich phase. The fine black dots, which seem to be real, have not been identified.

Fig 13 shows a sample to which 10 pct calcium was added. Only two phases other than the matrix appear to be present. One is the angular gray phase previously identified as beryllium carbide, while the second is a light-yellow, generally angular phase present in fairly large amounts which can be

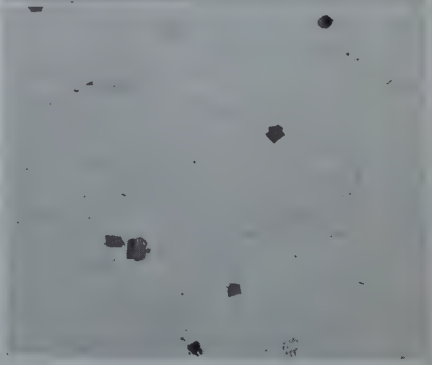

FIG 9 (above)—Heat 162. Unetched. 2 pct Al alloy.

FIG 10 (below)—Heat A-32. Lightly etched. 10 pct Si added.

× 500. Reduced one-half in reproduction.

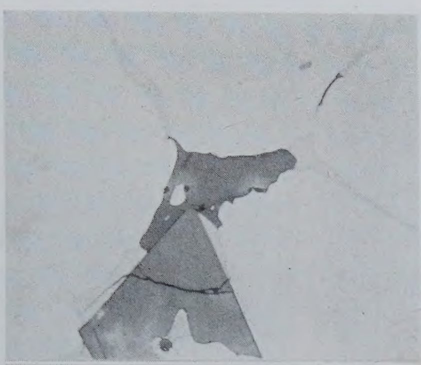

FIG 11 (above)—Heat A-25. Unetched. Melt reacted with silicon carbide crucible.
FIG 12 (below)—Heat A-33. Lightly etched. 10 pct Ti added.
× 500. Reduced one-half in reproduction.

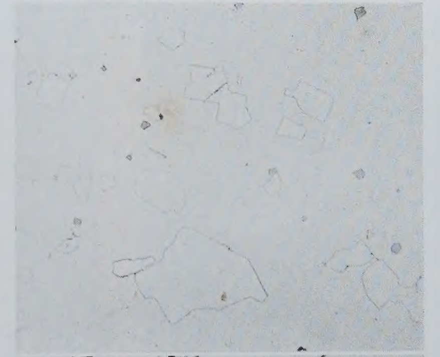

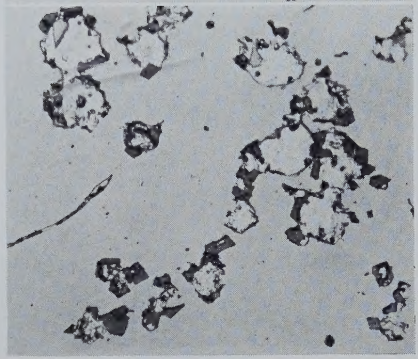

FIG 13 (above)—Heat A-34. Slightly etched. 10 pct Ca added.
FIG 14 (below)—Heat A-35. Unetched. 10 pct Sn added. Segregated area near 2-metal interface.
× 500. Reduced one-half in reproduction.

attributed to the calcium addition.

When tin is added to beryllium, a two-liquid system is formed which causes a two-layer ingot. The heavy tin-rich liquid settles to the bottom and mechanically carries the beryllium carbide along with it. Fig 14 shows a segregated area just above the interface between the two metals. Globules of the tin-rich phase are in evidence, and associated with them are the familiar angular gray carbides. The tin phase is yellow and similar in appearance and polishing characteristics to the aluminum rich phase previously described. It is soft and difficult to polish, as evidenced by the smeary appearance in the photograph. The beryllium layer, away from the interface, is remarkably free of inclusions. The beryllium-rich phase in the tin layer is present as a finely dispersed eutectic resolved only at × 2000 magnification.

Fig 15 and 16 are photographs of a sample to which 10 pct iron was added. Fig 15 shows the sample unetched and the phase attributed to iron appears in the grain boundaries almost entirely and is barely distinguishable from the background. The familiar gray carbides are present in the matrix and only occasionally in the iron-rich material. Other phases, if present, have been "absorbed" in the iron-rich phase. The HF etchant (Fig 16) colors the iron phase to a reddish brown, thus affording a method of distinguishing it from other similar-appearing phases.

Ten per cent manganese was added to the specimen shown in Fig 17. The phase attributable to manganese is very similar in appearance to the iron phase. It appears in the grain boundaries and is slightly more pink than the matrix. The beryllium carbide seems to prefer the grain-boundary location in this alloy. Unlike the iron phase, the manganese phase is not stained by HF but only outlined by it.

Fig 18 shows a specimen to which 6 pct boron was added. The phase attributable to boron appears in the grain boundaries and is colored red, but is stained blue or purple by the HF etchant. The familiar carbides are present, away from the grain boundaries. The yellow aluminum-rich phase also appears as a distinct constituent which, in some locations, is closely associated with the red boron phase.

An attempt was made to produce an oxide phase in beryllium by adding silica to a melt. An increase in the light-blue silicon-rich phase was noted as well as the appearance of small amounts of the dark blue-green phase which has also sometimes been associated with silicon. Any oxide formed, however, either went into solution and remained there, or was insoluble and separated by gravity from the melt.

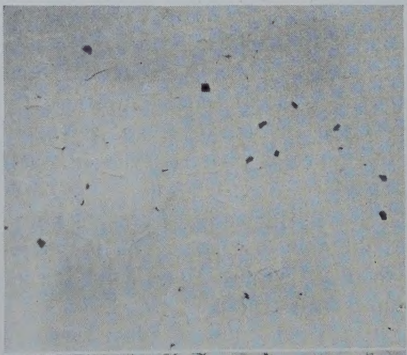

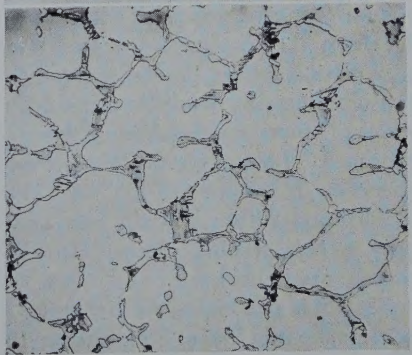

FIG 15 (above)—Heat A-36. Unetched. 10 pct Fe added.
FIG 16 (below)—Heat A-36. Etched. 10 pct Fe added.
× 500. Reduced one-half in reproduction.

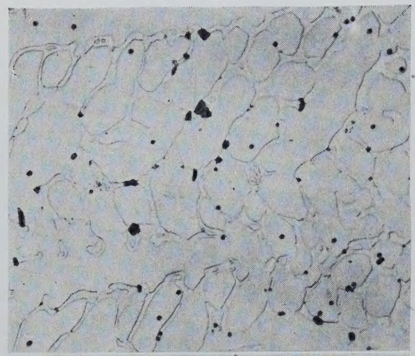

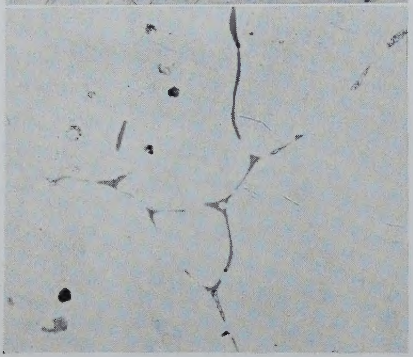

FIG 17 (above)—Heat A-37. Etched. 10 pct Mn added.
FIG 18 (below)—Heat A-39. Unetched. 6 pct B added.
× 500. Reduced one-half in reproduction.

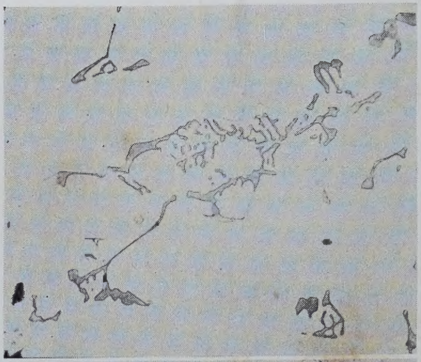

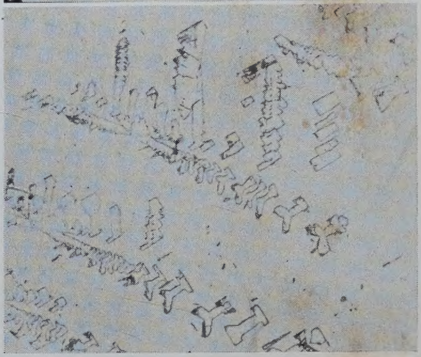

FIG 19 (above)—Heat A-46. Slightly etched. 5 pct Mo added.
FIG 20 (above)—5 pct U alloy. Slightly etched.
× 500. Reduced one-half in reproduction.

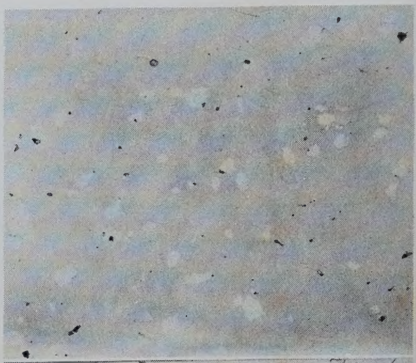

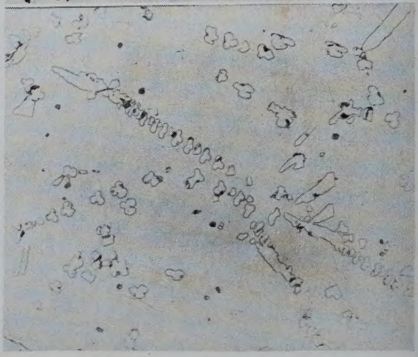

FIG 21 (above)—Melting stock containing 0.75–1.00 Mg. Unetched.
FIG 22 (below)—5 pct Zr alloy. Slightly etched.
× 500. Reduced one-half in reproduction.

Five per cent molybdenum was added to the specimen, represented by Fig 19. Until it is etched, the phase attributable to molybdenum, like the iron-rich phase, appears to be about the color of the matrix. It first stains, on etching, to a chocolate color and then to a black. Carbides were substantially absent in this specimen, but the yellow aluminum-rich phase appears in small amounts.

A 6 pct copper alloy showed no phase attributable to copper. This is indicative of rather high solid solubility of copper in beryllium.

In a 5 pct uranium alloy, the uranium-rich phase was not distinguishable from the matrix in the unetched condition. However, the etchant stained the uranium-rich dendritic phase to a series of colors ranging from yellow to green. A photograph of this etched specimen is shown in Fig 20. The dendritic structure is easily seen and only a few carbides, largely in the matrix, are in evidence.

Materials containing as low as 0.35 pct magnesium have been shown to contain a phase attributable to that material. In some of the early work, this phase was overlooked because it is soft and difficult to maintain during grinding. In addition, it is somewhat reactive to water and may disappear during polishing. Fig 21 shows this phase, believed to be a magnesium-rich constituent, in a specimen containing about 0.75 pct magnesium. It is bright "water white," very soft as compared to the matrix, and readily removed by the HF etch, leaving pits.

Fig 22 shows an alloy to which 5 pct zirconium was added. The phase attributable to zirconium is dendritic in appearance and, until etched, is barely distinguishable from the matrix, but the alcoholic HF etch outlines the phase and stains it a light blue. Further etching has no effect on the color.

Summary

Reasonably satisfactory metallographic techniques have been developed for beryllium and beryllium-rich alloys.

The following phases have been identified:

1. Carbide
2. Nitride
3. Aluminum rich
4. Silicon rich
5. Calcium rich
6. Titanium rich
7. Tin rich
8. Iron rich
9. Manganese rich
10. Boron rich
11. Molybdenum rich
12. Uranium rich
13. Magnesium rich
14. Zirconium rich

No second phase attributable to copper could be found in a 6 pct copper alloy. No phase attributable to oxygen or hydrogen has been found, but this does not preclude their presence in liquid or solid solutions.

Acknowledgments

The work of James Stevens who prepared the specimens and Clarence Barnhart who photographed them is gratefully acknowledged.

copy #1
MASS INST TECH
MAY 1 1951
LINDGREN LIBRARY
LD36-11-47 500

Four typical machine shops report

"LONGER TOOL LIFE"
"BETTER FINISH" } WITH NEW
"FASTER OPERATIONS"

J&L FREE-CUTTING "E"* STEEL

J&L STEEL

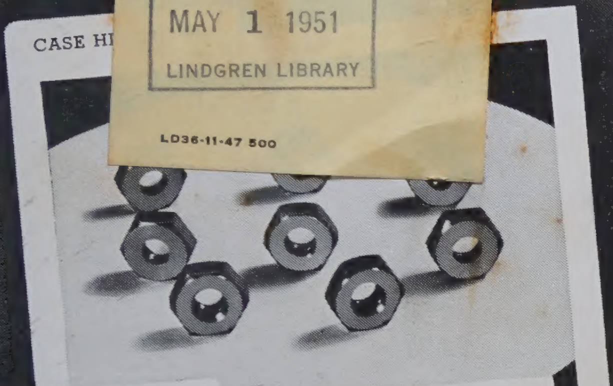
CASE HI

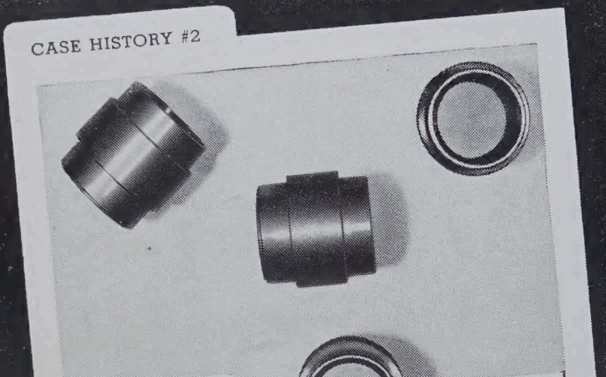
CASE HISTORY #2

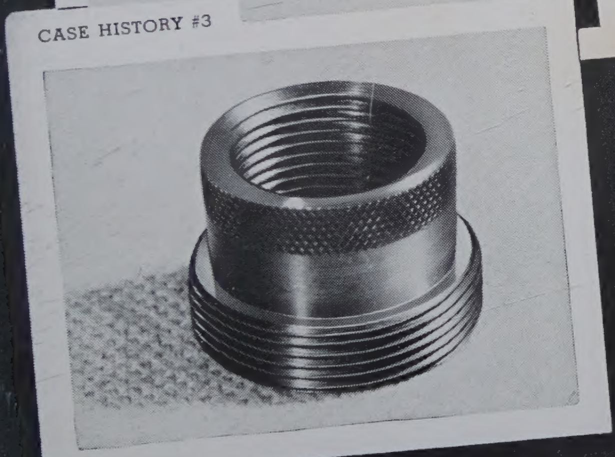
CASE HISTORY #3

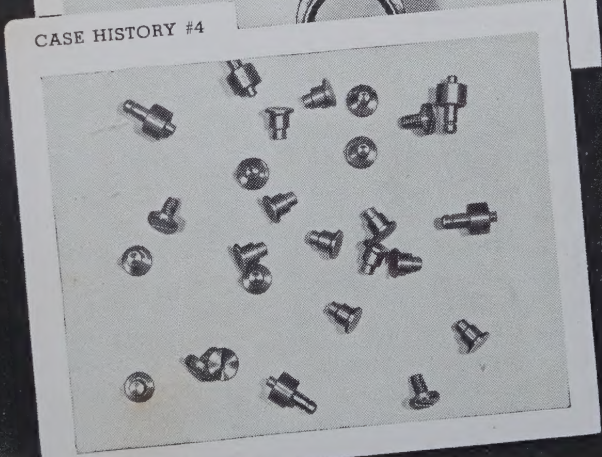
CASE HISTORY #4

Four typical examples, taken from 100 case histories, show superior machinability of J&L "E" Steel.

For 4 years before "E" Steel was publicly announced, this new, free-cutting bessemer screw stock was tried by independent machine shops throughout the metal-working industry.

More than 6,100 tons were tested in over 100 applications!

Here are quotations from 4 typical case histories:

CASE HISTORY #1 ". . . tool life increased 100% at normal speeds . . . better finish . . . shop people liked it."

CASE HISTORY #2 ". . . tool life increased up to 200% . . . uniformity of finish remained constant . . . considerably increased speeds without sacrifice to finish."

CASE HISTORY #3 ". . . tool life increased two to four times . . . we were able to tap 1" full internal pipe thread, almost impossible on regular material."

CASE HISTORY #4 ". . . new steel machines very well . . . finish excellent . . . tool life increased . . . 5 to 10% better production."

You too can get greater economies in your machining operations with new J&L free-cutting "E" Steel. "E" Steel is available in three grades: E-15, E-23 and E-33, each within the composition limits of the standard bessemer screw steels and with similar tensile properties. All standard sizes and shapes are available. For further information write for your copy of our new booklet: "J&L 'E' Steel."

Jones & Laughlin Steel Corporation
445 Jones & Laughlin Building
Pittsburgh 19, Penna.

Please send me a copy of "J&L 'E' Steel."

Name____________________

Company____________________

Address____________________

JONES & LAUGHLIN STEEL CORPORATION

* "E" STEEL IS QUALITY-CONTROLLED FROM OUR OWN MINES THROUGH THE FINISHED PRODUCT

Headquarters for

Laboratory Safety

Laboratories generally are among the safest places to work—partially because the technician's training and intelligence caution him when danger exists. In addition, laboratories have at their command an entirely unique group of safety regulations, apparatus, and chemicals specifically developed to minimize the accident rate.

The development and manufacturing facilities of the Fisher Scientific Co. insure an immediate and comprehensive supply of these items.

- Acid Bottle Carriers
- Coats, Aprons, Gloves
- Radiation Instruments
- Fume Hoods
- Tongs
- Carboys and Tilters
- Stirring Devices
- First Aid Cabinets
- Pipette Fillers
- Safety Shields
- Goggles and Visors
- Respirators
- Protective Creams
- Fire Blankets
- Fire Extinguishers
- Acid Pouring Spouts
- Safety Heating Apparatus
- Desiccator Guards

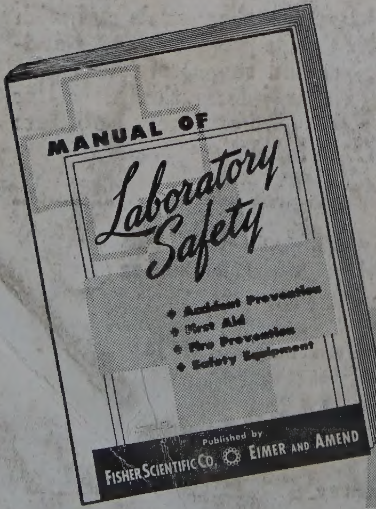

MANUAL OF
Laboratory Safety
• Accident Prevention
• First Aid
• Fire Prevention
• Safety Equipment
Published by
FISHER SCIENTIFIC CO. EIMER AND AMEND

A free copy of this informative and valuable booklet will be sent to you on request. Ask for Manual of Laboratory Safety.

Headquarters for Laboratory Supplies

FISHER SCIENTIFIC CO.
717 Forbes St., **Pittsburgh (19), Pa.**
2109 Locust St., **St. Louis (3), Mo.**

EIMER AND AMEND
Greenwich and Morton Streets
New York (14), New York

In Canada: Fisher Scientific Co., Ltd., 904 St. James Street, Montreal, Quebec